

# **BIOENGINEERED URETHRAL AUGMENTATION**

by

**Donna J. Haworth**

BS, Youngstown State University, 2004

Submitted to the Graduate Faculty of  
Swanson School of Engineering in partial fulfillment  
of the requirements for the degree of  
Doctor of Philosophy

University of Pittsburgh

2009

UNIVERSITY OF PITTSBURGH  
SWANSON SCHOOL OF ENGINEERING

This dissertation was presented

by

Donna J. Haworth

It was defended on

September 17, 2009

and approved by

William de Groat, Distinguished Professor, Department of Pharmacology

Kacey Marra, Assistant Professor, Departments of Bioengineering and Plastic Surgery

Partha Roy, Assistant Professor, Department of Bioengineering

Naoki Yoshimura, Professor, Departments of Urology and Pharmacology

Dissertation Director: David A. Vorp, Professor, Departments of Surgery and Bioengineering

Copyright © by Donna J. Haworth

2009

## **BIOENGINEERED URETHRAL AUGMENTATION**

Donna J. Haworth, PhD

University of Pittsburgh, 2009

Urethral dysfunction is a common complication of many conditions including diabetes mellitus, spinal cord injury, vaginal childbirth, and pelvic trauma. Stress urinary incontinence (SUI) is the involuntary loss of urine due to the inability of the urethral sphincter to maintain a tight seal during the storage phase and is a condition that physically and emotionally affects millions of women. Currently treatments for SUI show limited effectiveness and/or complications. Regenerative medicine techniques may improve function and support of the diseased urethra. We hypothesized that exposure of bone marrow progenitor cells to mechanical stimuli would differentiate these cells to a contractile smooth muscle cell phenotype. This hypothesis was tested with the use of a bioreactor to aid in the differentiation via mechanical and/or chemical stimulation. In addition, an animal model of SUI was used to assess how the structural, functional and mechanical properties of the urethra were affected by placement of the tissue engineered urethral wrap (TEUW) around the native urethra.

Our results indicate that bioreactor culture caused an up-regulation of myosin heavy chain, a contractile smooth muscle cell marker, with the highest expression seen after 10 days of culture with transforming growth factor beta (TGF- $\beta$ ). While some differentiation was observed, bioreactor conditions were not sufficient to create a fully functional TEUW. Exploration of

stimulation regimens similar to what is seen by the urethra may cause further differentiation of these cells towards a smooth muscle phenotype. No differences between in-vivo groups were observed in leak point pressure results, but mechanical and pharmacological assessments indicated that the TEUW provided support to the urethra with responses more similar to controls than to SUI animals. Although ex-vivo results are promising, placement of the TEUW as a full wrap required separation of the urethra from the vagina, which appeared to cause remodeling and possibly scar formation. This separation may have contributed to the discrepancies seen between our in-vivo and ex-vivo data. Continued exploration of the benefits of the TEUW could include an animal model which receives the TEUW as only a partial wrap, attached to only the dorsal urethra, negating the need for tissue separation.

## TABLE OF CONTENTS

<b>NOMENCLATURE.....</b>	<b>XXIX</b>
<b>PREFACE.....</b>	<b>XXXI</b>
<b>1.0 INTRODUCTION.....</b>	<b>1</b>
<b>1.1 LOWER URINARY TRACT ANATOMY AND PHYSIOLOGY .....</b>	<b>1</b>
<b>1.1.1 Urinary Bladder.....</b>	<b>3</b>
<b>1.1.2 Urethra .....</b>	<b>5</b>
<b>1.1.3 Storage and Voiding Reflex .....</b>	<b>10</b>
<b>1.2 STRESS URINARY INCONTINENCE .....</b>	<b>11</b>
<b>1.2.1 Pathophysiology of SUI and Diagnosis .....</b>	<b>11</b>
<b>1.2.2 Current Treatments for SUI.....</b>	<b>14</b>
<b>1.2.3 Animal Models of SUI.....</b>	<b>16</b>
<b>1.2.3.1 Vaginal distension .....</b>	<b>16</b>
<b>1.2.3.2 Neurogenic models .....</b>	<b>18</b>
<b>1.2.3.3 Ovariectomy model.....</b>	<b>19</b>
<b>1.2.4 ECM Changes in SUI .....</b>	<b>20</b>
<b>1.3 TISSUE ENGINEERING FOR THE URETHRA .....</b>	<b>21</b>
<b>1.3.1 Progenitor Cells in Urethral Tissue Engineering .....</b>	<b>22</b>
<b>1.3.2 Previous Approaches in Urethral Tissue Engineering.....</b>	<b>23</b>
<b>1.4 FIBRIN AS A SCAFFOLD MATERIAL.....</b>	<b>25</b>

<b>1.5</b>	<b>GUIDED DIFFERENTIATION OF PROGENITOR CELLS TO SMOOTH MUSCLE CELLS.....</b>	<b>27</b>
1.5.1	Mechanical Stimulation .....	27
1.5.2	Chemical Stimulation .....	29
<b>1.6</b>	<b>BIOMECHANICS OF THE URETHRA .....</b>	<b>31</b>
1.6.1	In-Vivo Studies.....	31
1.6.2	Ex-Vivo Studies.....	32
<b>1.7</b>	<b>HYPOTHESES AND SPECIFIC AIMS .....</b>	<b>34</b>
<b>2.0</b>	<b>EFFECTS OF OVARIECTOMY ON THE MECHANICAL CHARACTERISTICS OF THE FEMALE RAT URETHRA.....</b>	<b>37</b>
<b>2.1</b>	<b>SIGNIFICANCE OF OVARIECTOMY ON URETHRAL FUNCTION....</b>	<b>37</b>
<b>2.2</b>	<b>METHODS.....</b>	<b>38</b>
2.2.1	Animals .....	38
2.2.2	General Surgical Procedures .....	38
2.2.3	Urethral Response During Sneeze.....	41
2.2.4	MIPS .....	41
2.2.5	Biomechanical Testing .....	42
2.2.6	Histology .....	43
2.2.7	Mechanical Characteristics .....	43
2.2.8	Statistics .....	44
<b>2.3</b>	<b>RESULTS .....</b>	<b>45</b>
2.3.1	Urethral Response During Sneeze.....	45
2.3.2	Maximum Intravesical Pressure During Sneeze.....	46
2.3.3	Ex-Vivo Mechanical Analysis.....	47
<b>2.4</b>	<b>DISCUSSION.....</b>	<b>53</b>

<b>3.0</b>	<b>STRAIN DEPENDENCY OF URETHRAL FUNCTIONAL AND MECHANICAL PROPERTIES IN THE RAT.....</b>	<b>58</b>
<b>3.1</b>	<b>MATERIALS AND METHODS.....</b>	<b>59</b>
<b>3.1.1</b>	<b>Animals.....</b>	<b>59</b>
<b>3.1.2</b>	<b>Overview of Experiments.....</b>	<b>59</b>
<b>3.1.3</b>	<b>Surgical Procedures.....</b>	<b>60</b>
<b>3.1.4</b>	<b>Experiment 1: Effects of SUI on Sprague-Dawley and Lewis Rat Leak Point Pressure (LPP). .....</b>	<b>61</b>
<b>3.1.5</b>	<b>Experiment 2: Contribution of the Striated Sphincter to the Continence Mechanism.....</b>	<b>61</b>
<b>3.1.6</b>	<b>Experiment 3: Assessment of Urethral Response During Sneeze .....</b>	<b>62</b>
<b>3.1.7</b>	<b>Experiment 4: Ex-Vivo Biomechanical Analysis .....</b>	<b>62</b>
<b>3.1.8</b>	<b>Experiment 5: Ex-Vivo Functional Analysis.....</b>	<b>63</b>
<b>3.1.9</b>	<b>Histology .....</b>	<b>64</b>
<b>3.1.10</b>	<b>Quantification of Muscle Components .....</b>	<b>65</b>
<b>3.1.11</b>	<b>Geometric Estimation and Mechanical Characteristics .....</b>	<b>65</b>
<b>3.1.12</b>	<b>Statistics.....</b>	<b>66</b>
<b>3.2</b>	<b>RESULTS.....</b>	<b>66</b>
<b>3.2.1</b>	<b>In-Vivo Leak Point Pressure in Continent and SUI Animals.....</b>	<b>66</b>
<b>3.2.2</b>	<b>Urethral Pressure During Sneeze.....</b>	<b>68</b>
<b>3.2.3</b>	<b>Ex-Vivo Mechanical Characteristics .....</b>	<b>69</b>
<b>3.2.4</b>	<b>Ex-Vivo Functional Characteristics of the Middle Urethra of Continent Animals .....</b>	<b>73</b>
<b>3.2.5</b>	<b>Histology.....</b>	<b>76</b>
<b>3.3</b>	<b>DISCUSSION.....</b>	<b>79</b>
<b>4.0</b>	<b>MECHANICAL AND HISTOLOGICAL CHARACTERIZATION OF A TISSUE ENGINEERED URETHRAL WRAP .....</b>	<b>84</b>

4.1	<b>NEED FOR A TISSUE ENGINEERED URETHRAL WRAP</b> .....	84
4.2	<b>MATERIALS AND METHODS</b> .....	86
4.2.1	Cell Source and Culture.....	86
4.2.2	Fabrication and Culture of Tubular Constructs .....	86
4.2.3	Compaction and Viability .....	89
4.2.4	In-Vitro Mechanical Testing.....	89
4.2.5	Histologic Assessment.....	90
4.2.6	Mechanical Characteristics .....	91
4.2.7	Ex-Vivo Studies.....	91
4.2.8	Statistics .....	93
4.3	<b>RESULTS</b> .....	93
4.3.1	TEUW Construct Appearance and Dimensions.....	93
4.3.2	Viability .....	95
4.3.3	Mechanical Characteristics .....	96
4.3.4	Histology .....	100
4.3.5	Ex-Vivo Studies.....	101
4.4	<b>DISCUSSION</b> .....	103
5.0	<b>DESIGN OF AN INDEPENDENT, MULTI-CHAMBER BIOREACTOR FOR TUBULAR CONSTRUCTS</b> .....	106
5.1	<b>METHODS</b> .....	110
5.1.1	Bioreactor Design .....	110
5.1.1.1	Pump .....	110
5.1.1.2	Pulse-dampener and reservoir .....	113
5.1.1.3	Construct-housing chambers .....	118
5.1.1.4	Tees and cannulae .....	121

5.1.1.5	Filling of the bioreactor .....	122
5.1.1.6	Environmental conditions .....	122
5.1.2	System Verification.....	124
5.1.2.1	Flow rate .....	124
5.1.2.2	System sterility and stability .....	124
5.1.2.3	Mounting of constructs.....	125
5.1.3	Statistical Analyses .....	126
5.2	RESULTS .....	127
5.2.1	Bioreactor Fabrication .....	127
5.2.2	Flow Rate.....	129
5.2.3	Sterility and Stability.....	130
5.2.4	Construct Mounting .....	135
5.3	DISCUSSION.....	136
6.0	EFFECTS OF PRESSURE AND THE ADDITION OF TGF-BETA ON THE MECHANICAL AND PHENOTYPIC PROPERTIES OF A TEUW .....	139
6.1	METHODS.....	140
6.1.1	Cell culture and Construct Fabrication.....	140
6.1.2	Dynamic Culture.....	142
6.1.3	Bioreactor Priming .....	143
6.1.3.1	Construct mounting .....	143
6.1.4	Bioreactor culture conditions .....	144
6.1.5	In-Vitro Mechanical Testing.....	145
6.1.6	In-Vitro Functional Testing.....	146
6.1.7	Assessment of ECM and Cell Distribution.....	146
6.1.7.1	Histology and immunofluorescence.....	147

6.1.7.2	Western blotting.....	147
6.1.7.3	Cell counting.....	148
6.1.8	Statistics.....	149
6.2	<b>RESULTS</b> .....	150
6.2.1	System Stability.....	150
6.2.2	In-Vitro Mechanical Testing.....	156
6.2.3	In-Vitro Functional Testing.....	162
6.2.4	Histology.....	164
6.2.5	Western Blots.....	171
6.2.6	Cell Distribution.....	172
6.3	<b>DISCUSSION</b> .....	174
7.0	<b>EFFECTS OF IMPLANTATION OF A TEUW ON THE MECHANICAL AND STRUCTURAL CHARACTERISTICS OF THE NATIVE URETHRA IN A RAT MODEL OF SUI</b> .....	179
7.1	<b>METHODS</b> .....	180
7.1.1	Animals.....	180
7.1.2	Surgical Procedures.....	180
7.1.3	Assessment for V-LPP and Ex-Vivo Functional Properties in SD rats..	184
7.1.3.1	V-LPP.....	184
7.1.3.2	Ex-vivo functional testing.....	184
7.1.4	Assessment for Ex-Vivo Mechanical Properties and Composition in Lewis rats.....	184
7.1.4.1	Ex-vivo mechanical testing.....	184
7.1.4.2	Histology.....	185
7.1.4.3	Western blotting.....	186
7.1.5	Statistics.....	187

7.2	<b>RESULTS</b> .....	188
7.2.1	<b>Assessment of V-LPP and Ex-Vivo Functional Properties for SD Rats.</b>	188
7.2.1.1	<b>V-LPP</b> .....	188
7.2.1.2	<b>Ex-vivo functional testing</b> .....	189
7.2.2	<b>Assessment of Ex-Vivo Mechanical Properties and Composition for Lewis Rats</b> .....	192
7.2.2.1	<b>Ex-vivo mechanical testing</b> .....	192
7.2.2.2	<b>Histology</b> .....	201
7.2.2.3	<b>Western blots</b> .....	207
7.3	<b>DISCUSSION</b> .....	212
8.0	<b>DISCUSSION</b> .....	217
8.1	<b>SUMMARY OF RESULTS</b> .....	217
8.1.1	<b>The Effects of Disease ( Chapter 2.0) and Rat Strain ( Chapter 3.0) on Urethral Function</b> .....	217
8.1.2	<b>The Development ( Chapters 4.0 and 5.0) and Implementation ( Chapter 6.0) of a Novel Bioreactor</b> .....	219
8.1.3	<b>Application of a TEUW for Treatment of SUI (Chapter 7.0)</b> .....	219
8.2	<b>CLINICAL RELEVANCE</b> .....	220
8.3	<b>LIMITATIONS OF METHODOLOGY</b> .....	222
8.4	<b>FUTURE WORK</b> .....	226
	<b>APPENDIX A</b> .....	229
	<b>APPENDIX B</b> .....	232
	<b>APPENDIX C</b> .....	243
	<b>APPENDIX D</b> .....	247
	<b>APPENDIX E</b> .....	253
	<b>APPENDIX F</b> .....	256

<b>APPENDIX G.....</b>	<b>278</b>
<b>APPENDIX H.....</b>	<b>309</b>
<b>BIBLIOGRAPHY .....</b>	<b>338</b>

## LIST OF TABLES

Table 2.1 Compliance and beta stiffness values for control (n=6), sham (n=5) and Ov (n=10) urethras in baseline conditions. Values are shown as average $\pm$ SEM. *p<0.05 compared to corresponding control condition. Red = increasing trends in the proximal portion from control to Ov groups, Green = increasing trends in the middle portion from control to Ov groups and bold = significant differences compared with the corresponding control portion.....	51
Table 2.2 Compliance and beta stiffness values for control (n=6), sham (n=5) and Ov (n=10) urethras in passive conditions. Values are shown as average $\pm$ SEM. *p<0.05 compared to corresponding control condition. Red = increasing trends in the proximal portion from control to Ov groups, Green = increasing trends in the middle portion from control to Ov groups and bold = significant differences compared to the corresponding control portion.....	52
Table 5.1 Summary of bioreactors and their main features.....	109
Table 5.2 Experimental values for flow determination for all chambers. ....	129
Table 5.3 pH values for each chamber at each day of culture. ....	133
Table 5.4 pCO <sub>2</sub> values (mmHg) for each chamber at each day of culture. ....	133
Table 5.5 pO <sub>2</sub> values (mmHg) for each chamber at each day of culture. ....	134
Table 5.6 HCO <sub>3</sub> <sup>-</sup> (mmol/L) values for each chamber at each day of culture.....	134

Table 6.1 Experimental bioreactor culture conditions and experimental number. SF = spinner flask culture, Mo = minimal pressure and flow and T = addition of TGF- $\beta$  to the culture media. Time points are indicative of time in addition to an initial 5 days of spinner flask culture for compaction of the construct..... 145

Table 6.2 Compliance ( $\text{mmHg}^{-1}$ ) at various pressure ranges and beta stiffness for constructs cultured under T0 (n=3), SF-5 day (n=3), Mo-5 day (n=8), MoT-5 day (n=6), SF-10 day (n=4), Mo-10 day (n=7) and MoT-10 day (n=4). Values shown as average  $\pm$  SEM. \* $p < 0.05$  and values most similar to the native urethra are shaded gray. .... 160

Table 6.3 Graded representation of smooth muscle marker expression for constructs cultured under T0, SF-5 day, Mo-5 day, MoT-5 day, SF-10 day, Mo-10 day, MoT-10 day, and dedifferentiation and their comparison to the native urethra. .... 170

## LIST OF FIGURES

Figure 1.1 The lower urinary tract anatomy. Reproduced from Drake <i>et al.</i> , (2005) [6].	2
Figure 1.2 Movat's pentachrome staining of a cross-section of a female, Sprague-Dawley rat bladder. Tissue section courtesy of Silvia Wognum-Enders.	4
Figure 1.3 Cross-section of the human urethra. Reproduced from Brading <i>et al.</i> , (2001) [14].	5
Figure 1.4 Female urethral support structures. Reproduced from DeLancey(1994) [18].	7
Figure 1.5 Innervation of the bladder and urethra. Reproduced from Wein (2007) [8]	9
Figure 2.1 Schematic of the experimental design.	40
Figure 2.2 Active urethral response to sneeze (A-URS) and urethral baseline pressure (UBP) for control (n=7), sham (n=12) and Ov (n=12) groups. Values are shown as average $\pm$ SEM. *p<0.05.	45
Figure 2.3 MIPS results for control (n=6), sham (n=6) and ovariectomy (n=8) groups. Values are shown as average $\pm$ SEM. *p<0.05.	46
Figure 2.4 MIPS results for ovariectomy (n=8) animals that did (n=5) and did not (n=3) leak. Values are shown as average $\pm$ SEM.	47
Figure 2.5 Baseline pressure-diameter curves for (A) proximal, (B) middle and (C) distal portions of control (n=6), sham (n=5) and Ov (n=10) urethras. Values shown as average $\pm$ SEM.	49

Figure 2.6 Passive pressure-diameter curves for (A) proximal, (B) middle and (C) distal portions of control (n=6), sham (n=5) and Ov (n=10) urethras. Values shown as average  $\pm$  SEM. .... 50

Figure 3.1 Vertical leak point pressure (V-LPP) for both Lewis (n=3) and Sprague-Dawley (n=2) rats in both Continent and SUI states. Data shown as average  $\pm$  SEM, \*p<0.05. .... 67

Figure 3.2 Supine leak point pressure (Su-LPP) for both Lewis (n=7) and Sprague-Dawley (n=4) rats before and after injection with alpha-bungarotoxin (333  $\mu$ g/kg, i.v.). Data shown as average  $\pm$  SEM, \*p<0.05. .... 67

Figure 3.3 Urethral pressure response (A-URS) during sneeze, urethral baseline pressure (UBP) and change in abdominal pressure ( $\Delta P_{abd}$ ) for both Lewis (n=8) and Sprague-Dawley (n=10) rats. Data shown as average  $\pm$  SEM, \*p<0.05. .... 68

Figure 3.4 Baseline pressure-diameter curves from the (A) proximal, (B) middle and (C) distal urethral portions of continent Lewis (n=4) and Sprague-Dawley (n=6) rats. Data shown as average  $\pm$  SEM, \*p<0.05. NID = normalized inner diameter. .... 70

Figure 3.5 Passive pressure-diameter curves from the (A) proximal, (B) middle and (C) distal urethral portions of continent Lewis (n=4) and Sprague-Dawley (n=6) rats. Data shown as average  $\pm$  SEM, \*p<0.05. NID = normalized inner diameter. .... 71

Figure 3.6 Baseline and passive compliance values for the proximal and middle urethral portions of continent Lewis (n=4) and Sprague-Dawley (n=6) rats. Data shown as average  $\pm$  SEM, \*p<0.05. .... 72

Figure 3.7 Middle urethral response of all three continent Lewis and Sprague-Dawley rats tested to various agonists and antagonists (100  $\mu$ M N $\omega$ -nitro-L-arginine, 40  $\mu$ M phenylephrine, 5 mM acetylcholine and 3 mM EDTA). Data was measured at 1 Hz

with 30 minute equilibrations at each condition. “Time” represents the seconds into the initiation of the measurements when data was obtained. Outer diameter measurements were normalized to the initial outer diameter at 0 mmHg. .... 74

Figure 3.8 Percent outer diameter change of the middle urethra of continent Lewis (n=3) and Sprague-Dawley (n=3) rats to various agonists and antagonists (100  $\mu$ M N $\omega$ -nitro-L-arginine, 40  $\mu$ M phenylephrine, 5 mM acetylcholine and 3 mM EDTA) with respect to 8 mmHg (A) and the equilibrated previous condition (A). Data was measured at 1 Hz with 30 minute equilibrations at each condition. Outer diameter measurements were normalized to the initial outer diameter at 0 mmHg..... 75

Figure 3.9 Masson’s trichrome staining of proximal, middle and distal portions of continent Lewis and SD urethras. Images are representative and taken at 4x. Red = muscle, blue/green = collagen, black = nuclei..... 77

Figure 3.10 Percent of the total cross-sectional area staining positive for (A) smooth muscle actin or (B) fast twitch skeletal muscle and (C) total cross-sectional area of both the Lewis (n=7) and Sprague-Dawley (n=4-7) urethra. Data shown as average  $\pm$  SEM, \*p<0.05..... 78

Figure 4.1 Fabrication of TEUWs. (A) Mold comprised of a rubber stopper, glass sheath and Teflon® mandrel used to create the tubular construct. (B) Fibrin-cell mixture following gelation in the mold. (C) Tubular construct on mandrel following removal of the glass sheath. (D) Tubular construct after being completely removed from the mold. (E) End view of a section of the tubular construct. Constructs fabricated with  $1.00 \times 10^6$  cells/mL following gelation (D), and spinner flask culture for either 3 (F) or 5 (G) days. Scale is in cm. .... 88

Figure 4.2 Average compaction, calculated at a percentage of the initial volume for constructs fabricated from  $7.50 \times 10^5$ ,  $1.00 \times 10^6$ , or  $1.25 \times 10^6$  cells/mL for 3 (n=3) or 5 (n=4) days. Overall is the overall average compaction from all seeding densities and culture durations. Data shown as average  $\pm$  SEM, \*p<0.05..... 94

Figure 4.3 Average estimated total cells from the MTT assay for constructs fabricated from  $7.50 \times 10^5$ ,  $1.00 \times 10^6$ , or  $1.25 \times 10^6$  cells/mL for 3 (n=3) or 5 (n=4) days. Data shown as average  $\pm$  SEM. No statistically significant differences were found between any groups. .... 95

Figure 4.4 Average burst pressure values for constructs fabricated from  $7.50 \times 10^5$ ,  $1.00 \times 10^6$ , or  $1.25 \times 10^6$  cells/mL for 3 (n=3) or 5 (n=4) days. Data shown as average  $\pm$  SEM. .. 96

Figure 4.5 Average pressure-diameter curves for constructs fabricated from  $7.50 \times 10^5$ ,  $1.00 \times 10^6$ , or  $1.25 \times 10^6$  cells/mL for 3 (n=3) or 5 (n=4) days, where NID is the diameter normalized to the diameter at 0 mmHg. Data shown as average  $\pm$  SEM. .... 98

Figure 4.6 Average stepwise compliance curves for constructs fabricated from  $7.50 \times 10^5$ ,  $1.00 \times 10^6$ , or  $1.25 \times 10^6$  cells/mL for 3 (n=3) or 5 (n=4) days. Data shown as average  $\pm$  SEM. .... 99

Figure 4.7 Average beta stiffness values for constructs fabricated from  $7.50 \times 10^5$ ,  $1.00 \times 10^6$ , or  $1.25 \times 10^6$  cells/mL for 3 (n=3) or 5 (n=4) days. Data shown as average  $\pm$  SEM.100

Figure 4.8 Representative H&E sections from constructs fabricated from  $7.50 \times 10^5$  (A,D),  $1.00 \times 10^6$  (B,E), or  $1.25 \times 10^6$  (C,F) cells/mL for 3 (A-C) or 5 (D-F) days. Images taken at 10x, L indicates the lumen of each construct. .... 101

Figure 4.9 Pictures of a healthy, unwrapped urethra (A), a wrapped urethra (B) and a wrapped urethra under pressure. Arrows indicate sutures. .... 102

Figure 4.10 Average compliance values for dysfunctional urethras with and without a TEUW around the proximal portion of the urethra (n=2). Data shown as average  $\pm$  SEM. .... 103

Figure 5.1 The Masterflex<sup>®</sup> L/S pump (A) with L/S<sup>®</sup> Multichannel Pump Head (B) and two-stop L/S 16 pharmed tubing (C) was controlled by the Masterflex controller/dispenser (D). .... 112

Figure 5.2 Solidworks<sup>®</sup> drawing of the (A) cap and (B) base of the pulse dampener. Dimensions in inches..... 114

Figure 5.3 Pictures of the bioreactor pulse-dampener as separate components from the top (A), with lid in place from the side (B) and with lid in place from the top (C). Scale in inches..... 115

Figure 5.4 Solidworks<sup>®</sup> drawing of the (A) cap and (B) base of the reservoir. Dimensions in inches..... 116

Figure 5.5 Pictures of the bioreactor reservoir as separate components from the top (A), with lid in place from the side (B) and with lid in place from the top (C). Scale in inches. 117

Figure 5.6 Solidworks<sup>®</sup> drawing of the top and side views of the chamber lid (A) and base (B). Dimensions in inches..... 119

Figure 5.7 Pictures of the bioreactor construct-housing chamber as separate components from the top (A), with lid in place from the top (B) and with lid in place from the side (C). Scale in inches. .... 120

Figure 5.8 Side (A) and top (B) images of a stainless steel tees used in the bioreactor. The cannulae on which the construct is mounted (C) is attached to the male luer of the stainless steel tees (D). .... 121

Figure 5.9 Photographs of the entire filling apparatus (A), the reservoir to the manifold (B) and the manifold to the chambers (C).....	123
Figure 5.10 Images depicting the process of mounting a construct onto the cannulae. The guide is threaded through one cannula (A), the construct and then another cannula (B). The guide is then placed into the clamp assembly (C-D). Scale in inches.....	126
Figure 5.11 A picture of the entire bioreactor system assembled on a cell culture incubator tray. Stars represent injection ports and pluses represent ports for pressure transducers.	128
Figure 5.12 Average flow rates for each chamber (n=3) in the bioreactor circuit. Values are shown as average $\pm$ SEM. ....	130
Figure 5.13 Average environmental conditions for each chamber over the culture duration. Values shown as average $\pm$ SEM. ....	131
Figure 5.14 Average environmental conditions across all chambers for each day of culture. Values shown as average $\pm$ SEM. Dotted lines indicate an acceptable range for each parameter as determined in Appendix E.....	132
Figure 5.15 Mounting of a construct. The lumen of the construct was located with forceps (A), the guide was passed through the lumen of the construct (B) and the other cannula was added (C). The construct was then sutured to the cannula (D-E). Flow through the construct, without leaking at the suture sites, was observed (F).....	136
Figure 6.1 Passage of cells for construct fabrication for utilization in the bioreactor.....	141
Figure 6.2 Schematic of cell culture to produce independent constructs. ....	142
Figure 6.3 Intraluminal pressure measurements for constructs cultured under Mo-5 day (n=8), MoT-5 day (n=6), Mo-10 day (n=7) and MoT-10 day (n=4) show that all values fall	

within an acceptable range of $5 \pm 2$ mmHg (dotted lines). Values shown as average $\pm$ SEM. *p<0.05.....	151
Figure 6.4 Environmental pH values for constructs cultured under Mo-5 day (n=8), MoT-5 day (n=6), Mo-10 day (n=7) and MoT-10 day (n=4) show that all values fall within an acceptable range (dotted lines). Values shown as average $\pm$ SEM. *p<0.05.....	152
Figure 6.5 Environmental pCO <sub>2</sub> conditions for constructs cultured under Mo-5 day (n=8), MoT-5 day (n=6), Mo-10 day (n=7) and MoT-10 day (n=4) show that all values fall within an acceptable range (dotted lines). Values shown as average $\pm$ SEM. *p<0.05.....	153
Figure 6.6 Environmental pO <sub>2</sub> conditions for constructs cultured under Mo-5 day (n=8), MoT-5 day (n=6), Mo-10 day (n=7) and MoT-10 day (n=4). Values shown as average $\pm$ SEM. *p<0.05.....	154
Figure 6.7 Environmental HCO <sub>3</sub> <sup>-</sup> conditions for constructs cultured under Mo-5 day (n=8), MoT-5 day (n=6), Mo-10 day (n=7) and MoT-10 day (n=4) show that all values fall within an acceptable range (dotted lines). Values shown as average $\pm$ SEM. *p<0.05.....	155
Figure 6.8 Pressure-diameter curves for constructs cultured under T0 (n=3), SF-5 day (n=3), Mo-5 day (n=8), MoT-5 day (n=6), SF-10 day (n=4), Mo-10 day (n=7) and MoT-10 day (n=4). Values shown as average $\pm$ SEM. *p<0.05 between groups at the indicated pressure. ....	157
Figure 6.9 Step-wise compliance curves for constructs cultured under T0 (n=3), SF-5 day (n=3), Mo-5 day (n=8), MoT-5 day (n=6), SF-10 day (n=4), Mo-10 day (n=7) and MoT-10 day (n=4). Values shown as average $\pm$ SEM. *, <sup>+</sup> p<0.05 between groups at the indicated pressure.....	158

Figure 6.10 Burst pressure for constructs cultured under T0 (n=3), SF-5 day (n=3), Mo-5 day (n=8), MoT-5 day (n=6), SF-10 day (n=4), Mo-10 day (n=7) and MoT-10 day (n=4). Values shown as average  $\pm$  SEM..... 161

Figure 6.11 Outer diameter response of an Mo-5 day construct to various agonists and antagonists (N $\omega$ -nitro-L-arginine (NOSi), phenylephrine (PE), acetylcholine (Ach) and EDTA). Data was measured at 10 Hz with 15 minute equilibrations at each condition. “Time” represents the seconds into the initiation of the measurements when data was obtained. Outer diameter measurements were normalized to the initial outer diameter at 0 mmHg ..... 163

Figure 6.12 Representative trichrome staining for constructs cultured under T0, SF-5 day, Mo-5 day, MoT-5 day, SF-10 day, Mo-10 day, MoT-10 day, and Mo-SF. Images taken with a 4x objective and the native urethra served as a positive control. Red = fibrin, blue/green = collagen, black = nuclei..... 165

Figure 6.13 Representative picrosirius red staining for constructs cultured under T0, SF-5 day, Mo-5 day, MoT-5 day, SF-10 day, Mo-10 day, MoT-10 day, and Mo-SF. Images taken with a 4x objective and the native urethra served as a positive control. Red = organized and mature collagen, green = unorganized or immature collagen. Arrows indicate the lumen of the construct..... 166

Figure 6.14 Representative  $\alpha$ -SMA staining for constructs cultured under T0, SF-5 day, Mo-5 day, MoT-5 day, SF-10 day, Mo-10 day, MoT-10 day, and dedifferentiation. Images taken with a 10x objective and the native urethra served as a positive control. Blue = nuclei, green =  $\alpha$ -SMA. Arrows indicate the lumen. Remaining Sections shown in Appendix H..... 167

Figure 6.15 Representative CALP staining for constructs cultured under T0, SF-5 day, Mo-5 day, MoT-5 day, SF-10 day, Mo-10 day, MoT-10 day, and dedifferentiation. Images taken with a 10x objective and the native urethra served as a positive control. Blue = nuclei, green = CALP. Arrows indicate the lumen. .... 168

Figure 6.16 Representative MHC staining for constructs cultured under T0, SF-5 day, Mo-5 day, MoT-5 day, SF-10 day, Mo-10 day, MoT-10 day, and dedifferentiation. Images taken with a 10x objective and the native urethra served as a positive control. Blue = nuclei, green = MHC. Arrows indicate the lumen. Remaining Sections shown in Appendix H. .... 169

Figure 6.17 Western blot stained for MHC (A) and the white light molecular weight standard (B) for constructs cultured under T0, SF-5 day, SF-10 day, Mo-5 day, MoT-5 day and Mo-10 day culture conditions..... 171

Figure 6.18 Cell aggregation on inner vs outer portions for constructs cultured under T0, SF-5 day, Mo-5 day, MoT-5 day, SF-10 day, Mo-10 day, MoT-10 day, and Mo-SF. Values are shown as experimental average  $\pm$  SEM. \* $p < 0.05$  between inner and outer portions within a culture condition..... 173

Figure 7.1 Schematic of the test groups and procedures each receives. .... 182

Figure 7.2 Images of one representative implantation of a TEUW showing tissue separation (A), placement of TEUW around the proximal urethra (B) and TEUW sutured around the urethra (C). Scale in centimeters, arrows indicate 10-0 suture locations..... 183

Figure 7.3 SD leak point pressure values for sham continent (SC), sham SUI (SS) and rat TEUW (RT) groups. Values shown as average  $\pm$  SEM. .... 188

Figure 7.4 Representative sprague-dawley outer diameter reponse of the middle urethra of sham continent (A), sham SUI (B) and rat TEUW (C) groups to various agonists and antagonists (NOSi, PE, Ach and EDTA). Data was measured at 1 Hz with 30 minute equilibrations at each condition. Outer diameter measurements were normalized to the initial outer diameter at 0 mmHg. All plots are available in Appendix G. .... 190

Figure 7.5 Outer diameter change of the middle urethra for SD rats of sham continent (SC, n=6), sham SUI (SS, n=6) and rat TEUW (RT, n=4) groups to various agonists and antagonists (NOSi, PE, Ach and EDTA) with respect to 8 mmHg (A) and the equilibrated previous condition (A). Data was measured at 1 Hz with 30 minute equilibrations at each condition. Outer diameter measurements were normalized to the initial outer diameter at 0 mmHg. Values shown as average  $\pm$  SEM. \*,<sup>¥</sup>p<0.05 compared to SC..... 191

Figure 7.6 Baseline pressure-diameter curves for the proximal, middle and distal urethra of sham continent (SC; n=5), sham SUI (SS; n=6) and rat TEUW (RT; n=7) groups. Data shown as average  $\pm$  SEM..... 193

Figure 7.7 Passive pressure-diameter curves for the proximal, middle and distal urethra of sham continent (SC; n=5), sham SUI (SS; n=6) and rat TEUW (RT; n=7) groups. Data shown as average  $\pm$  SEM, \*,<sup>+</sup>p<0.05 compared to Sham Continent. .... 194

Figure 7.8 Baseline step-wise compliance curves for the proximal, middle and distal urethra of sham continent (SC; n=5), sham SUI (SS; n=6) and rat TEUW (RT; n=7) groups. Data shown as average  $\pm$  SEM, \*,<sup>+</sup>p<0.05 compared to Sham Continent and <sup>\$</sup>p<0.05 compared to Sham SUI at the designated pressure. .... 195

Figure 7.9 Passive step-wise compliance curves for the proximal, middle and distal urethra of sham continent (SC; n=5), sham SUI (SS; n=6) and rat TEUW (RT; n=7) groups. Data shown as average  $\pm$  SEM, \*,<sup>+</sup>p<0.05 compared to Sham Continent at the designated pressure..... 196

Figure 7.10 Baseline compliance values for the proximal, middle and distal urethra of sham continent (SC; n=5), sham SUI (SS; n=6) and rat TEUW (RT; n=7) groups. Data shown as average  $\pm$  SEM, \*,<sup>+</sup>p<0.05 compared to Sham Continent. .... 197

Figure 7.11 Passive compliance values for the proximal, middle and distal urethra of sham continent (SC; n=5), sham SUI (SS; n=6) and rat TEUW (RT; n=7) groups. Data shown as average  $\pm$  SEM, \*,<sup>+</sup>p<0.05 compared to Sham Continent. .... 198

Figure 7.12 Baseline and passive beta stiffness values for the proximal, middle and distal urethra of sham continent (SC; n=5), sham SUI (SS; n=6) and rat TEUW (RT; n=7) groups. Values shown as average  $\pm$  SEM. .... 200

Figure 7.13 Representative trichrome staining for proximal, middle and distal portions of sham continent (SC), sham SUI (SS) and rat TEUW (RT) urethras. Images taken with a 4x objective. Red = muscle, blue/green = collagen, black = nuclei. The vagina is located with a V, where visible. All images are available in Appendix H..... 202

Figure 7.14 Representative picrosirius red staining for proximal, middle and distal portions of sham continent (SC), sham SUI (SS) and rat TEUW (RT) urethras. Images taken with a 4x objective. Red = mature collagen, green = immature collagen. All images are available in Appendix H. .... 203

Figure 7.15 Representative  $\alpha$ -smooth muscle actin staining for proximal, middle and distal portions of sham continent (SC), sham SUI (SS) and rat TEUW (RT) urethras.

Images taken with a 4x objective. Green = calponin, blue = nuclei. All images are available in Appendix H .....	204
Figure 7.16 Representative calponin staining for proximal, middle and distal portions of sham continent (SC), sham SUI (SS) and rat TEUW (RT) urethras. Images taken with a 4x objective. Green = calponin, blue = nuclei. All images are available in Appendix H.....	205
Figure 7.17 Representative myosin heavy chain staining for proximal, middle and distal portions of sham continent (SC), sham SUI (SS) and rat TEUW (RT) urethras. Images taken with a 4x objective. Green = MHC, blue = nuclei. All images are available in Appendix H .....	206
Figure 7.18 Western blot results for $\alpha$ -SMA. Blots from n=2 rats per group (A) were quantified by densitometry and reported as changes in $\alpha$ -SMA levels in urethral portion (P=proximal, M=middle, D=distal) relative to sham continent (SC) animals (B). The dotted line in (B) represents no change. ....	207
Figure 7.19 Western blot results for calponin. Blots from n=2 rats per group (A) were quantified by densitometry and reported as changes in calponin levels in urethral portion (P=proximal, M=middle, D=distal) relative to sham continent (SC) animals (B). The dotted line in (B) represents no change. ....	208
Figure 7.20 Western blot results for MHC. Blots from n=2 rats per group (A) were quantified by densitometry and reported as changes in MHC levels in urethral portion (P=proximal, M=middle, D=distal) relative to sham continent (SC) animals (B). The dotted line in (B) represents no change. ....	210

Figure 7.21 Western blot results for PGP 9.5. Blots from n=2 rats per group (A) were quantified by densitometry and reported as changes in PGP 9.5 levels in urethral portion (P=proximal, M=middle, D=distal) relative to sham continent (SC) animals (B). The dotted line in (B) represents no change. .... 211

## NOMENCLATURE

SUI – stress urinary incontinence

ECM – extracellular matrix

PMC – pontine micturition center

ISD – intrinsic sphincter dysfunction

VD – vaginal distension

Ov – ovariectomy

MDSC – muscle derived stem cells

LPP – leak point pressure

PGP 9.5 – protein gene product 9.5

H&E – hematoxylin and eosin

TEU – tissue engineered urethra

SMC – smooth muscle cell

MSC – mesenchymal stem cell

BMPC – bone marrow progenitor cell

TEUW – tissue engineered urethral wrap

BMSC – bone marrow stem cell

PSR – picrosirius red

PBS – phosphate buffered saline

TGF- $\beta$  – transforming growth factor beta

ID = inner diameter

OD = outer diameter

$\alpha$ -SMA – smooth muscle alpha actin

CALP – calponin

MHC – myosin heavy chain

SKEL – skeletal muscle

SC – sham continent

SS – sham SUI

RT – rat TEUW

V-LPP – vertical leak point pressure

MIPS – maximum intravesical pressure during sneeze

UBP – urethral baseline pressure

URS – urethral response to sneeze

P-D – pressure diameter

SD – Sprague-dawley

Mo – minimal mechanical stimulation

MoT – minimal mechanical stimulation in the presence of TGF- $\beta$

BT – bovine TEUW

Cont - continent

## PREFACE

The five years spent working towards my doctorate in Bioengineering has been the most mentally and emotionally challenging time in my life. I am proud of what I have accomplished in this time and acknowledge that it would not have been possible without the unending support, love, help and guidance of numerous people, which I would like to acknowledge.

I would first like to thank my advisor, Dr. David Vorp, for allowing me the opportunity to join his laboratory in which I have grown as a scientist and a person. Thank you for your mentorship, guidance, and especially your patience as my project took many tangents over the years. Thank you for also being a friend as well as a wonderful mentor.

Dr. Yoshimura and the Urology Research Department, thank you for accepting me into your laboratory and for sharing your wealth of knowledge. Thank you to Dr. Takeya Kitta, Dr. Yasu Kaiho, Dr. Minoru Miyazato, Dr. Masa Yano, Dr. Akira Furuta, and Dr. Dae Kyung Kim for your patience and helping me with and teaching me all of the surgical procedures for my project. Dr. Michael Chancellor, thank you for your guidance and support with my project and for allowing me to shadow you in the clinic, it was an amazing experience that I will never forget. Vickie Erickson and Steve Coleman, thank you for your help with ordering animals, scheduling microscope and surgery time and for your support and friendship.

I would also like to thank Dr. Harvey Borovetz for providing me with the opportunity to be a part of the Bioengineering Department here at the University of Pittsburgh. Your dedication

to this department and the students cannot be matched. Thank you for your support both academically and personally, I look forward to finally meeting you for that 5 am run.

Douglas Chew, your dedication to science and education is contagious, and I thank you for all of the wonderful projects and opportunities that you have brought into my life. I cannot thank you enough for your endless support and guidance both in my research and as a friend and for helping me to grow as a scientist.

To my fellow lab mates in the Vascular Bioengineering Laboratory (past and present), thank you for sharing your knowledge, your support and for making these past five years so enjoyable. Melissa Morgan, I cannot thank you enough for all of your help with my bioreactor and testing systems and everything else that you helped me with and for letting Yoda babysit my bioreactor system. Deb Cleary and Chris Rovensky, thank you for the countless hours of counting nuclei. Vivian Allahyari, Margaret Stevenson, and Brian Morelli, thank you for the hours you spent in the dark imaging all of that immunofluorescence. Robert Dulabon, Garret Viglione and Joseph Muthu, thank you for your assistance with testing all of those urethral and construct specimens late into the night. I would also like to thank Dr. Rachelle Prantil-Baun and Dr. Timothy Maul for being my mentors. I know that I often frustrated you, but I am glad that it has brought us as close as it did. Rachelle, thank you for sharing your knowledge of the urethra and biomechanics, I would have been lost without you. Tim, you put up with a lot of questions and taught me an amazing amount about all aspects of bioengineering. Thank you for always going above and beyond, even when you were no longer in our laboratory, you have been an amazing friend.

On a personal note, I would like to thank my family (mom, dad, Elaine, Jesse, Samantha, Marie and Denny). You are the best support system anyone could ask for. Thank you for always

encouraging me and supporting my love of science even when you had no idea what I was talking about. Also, thank you for being so understanding and for always believing in me. Most of all, I want to thank my fiancé, Mike Ward. You have been my rock over the past five years, and I could not have done this without you. Thank you for staying with me when I tested late, for bringing me dinner, proof reading and listening to me practice my presentations. Thank you for being so understanding of the long hours and for keeping me balanced. Your unending love and support has meant the world to me.

Finally, I would like to acknowledge the funding sources that have made this research possible. This work was funded by NIBIB 5T32EB001026, NIBIB R21 EB006318, NIH DK067226, NIH AR049398 and NIH DK055387.

## 1.0 INTRODUCTION

Urethral dysfunction is a common complication of diabetes mellitus, spinal cord injury, vaginal childbirth and pelvic trauma. The most common urethral dysfunction is urinary incontinence, where there is an involuntary loss of urine. Stress urinary incontinence (SUI) [1] is the most common type of urinary incontinence. It is defined as an involuntary loss of urine due to the inability of the urethral sphincter to maintain a tight seal during the storage phase and is a condition that physically and emotionally affects 25 million American women annually [2]. This condition is emotionally draining and may cause social isolation.

### 1.1 LOWER URINARY TRACT ANATOMY AND PHYSIOLOGY

The lower urinary tract, consisting of the bladder and urethra (**Figure 1.1**), function over three phases: continence, transition, and urination, where the forces of continence and urination are believed to oppose each other [3]. The filling and emptying of the bladder is the result of reverse-order pressure in the bladder and urethra. That is, the urinary (bladder) pressure is low and the urethral pressure is high during bladder filling, which reverses when the bladder empties [4]. The bladder acts as a reservoir for urine storage and as a pump for micturition. Once the bladder reaches capacity, stretch receptors within the detrusor muscle are activated and initiate a voiding reflex. Voiding occurs as the urethra relaxes and the detrusor muscle contracts, allowing

urine to flow out of the body [5]. The urethra maintains a tight seal during bladder filling and relaxes during micturition. The following sections describe the anatomy and neural control of the bladder and urethra.

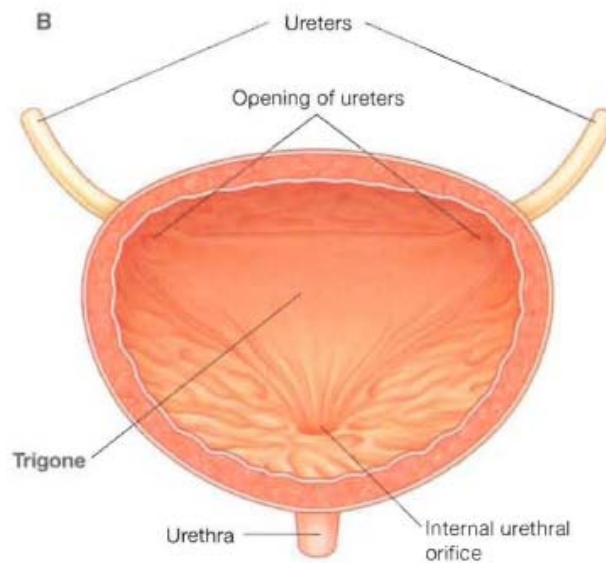


**Figure 1.1** The lower urinary tract anatomy. Reproduced from Drake *et al.*, (2005) [6].

### 1.1.1 Urinary Bladder

The urinary bladder is a hollow organ composed mainly of smooth muscle layers and an inner lining of epithelial cells. The main function of the bladder is to store urine as it is transported from the kidney to the bladder by the ureters. The maximum volume of the bladder is 700-800 mL [7]. The bladder can be divided into 3 main portions: the urothelium, the detrusor and the trigone (**Figure 1.1**). The urothelium (**Figure 1.2**) is a stratified epithelium consisting of a layer of umbrella cells and an underlying basal layer. There may be several layers of transitional cells between the two main layers [8]. The human detrusor (**Figure 1.2**) is composed of three layers of bundles of smooth muscle organized in alternating longitudinally and circumferentially oriented layers and is responsible for contraction of the bladder during voiding [9]. The trigone is a triangular area formed by the ureters and urethra at the base of the bladder and is responsible for maintaining continence during filling and for opening the urethra during voiding [10].

The bladder is autonomically controlled by both parasympathetic and sympathetic nerves (see **Section 1.1.3**). Parasympathetic signals travel between the bladder and the sacral portion of the spinal cord via the pelvic nerve. Sympathetic signals travel between the bladder and thoracic-lumbar portion of the spinal cord via the hypogastric nerves [11].

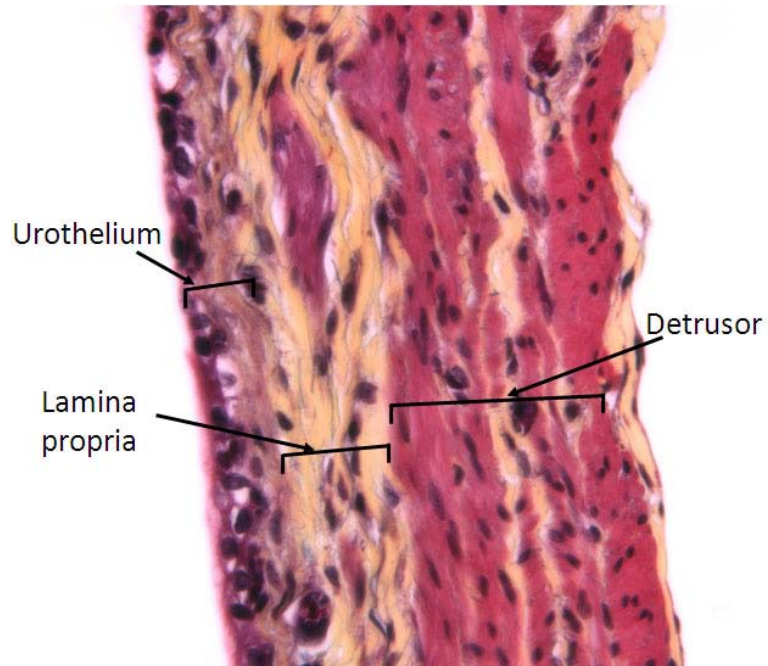


**Figure 1.2** Movat's pentachrome staining of a cross-section of a female, Sprague-Dawley rat bladder. Tissue section courtesy of Silvia Wognum-Enders.

### 1.1.2 Urethra

The human urethra is approximately 6 mm in diameter with a length of 4 cm in females and 20 cm in males, with the main purpose of preventing urine leakage during bladder filling [12, 13]. It is composed of several layers and cell types contained in a dense connective tissue (**Figure 1.3**).

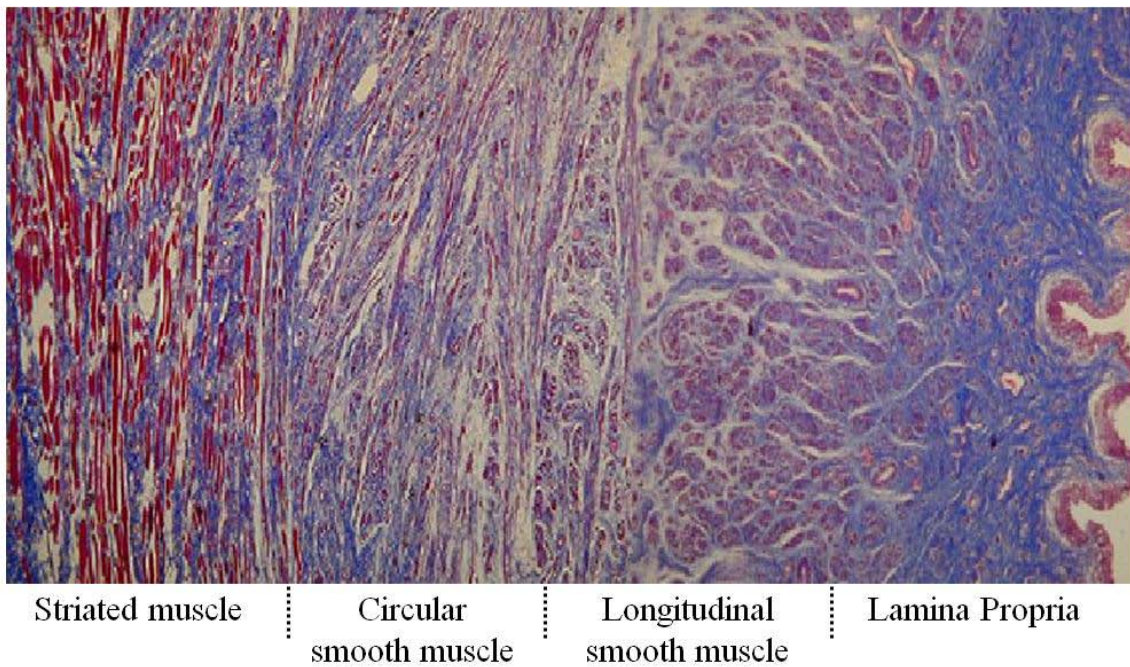


**Figure 1.3** Cross-section of the human urethra. Reproduced from Brading *et al.*, (2001) [14].

The inner most layer of the urethra consists of a lumen covered with urothelial cells, which is continuous with the bladder urothelium and whose main function is to protect the underlying layers from urine. The next layer, the lamina propria, is composed of both mucosal and submucosal layers. The submucosal layer contains numerous blood vessels, longitudinally-oriented smooth muscle cells and elastic fibers and contributes to the tight seal of the urethra during contraction. The mucosal layer contains glands, whose secretions most likely contribute to coaptation and continence. Surrounding the lamina propria is a layer of longitudinally-oriented smooth muscle, whose role is unclear but whose contraction may aid in urethral shortening and funneling of the urethra during voiding. Surrounding the longitudinal smooth muscle is a layer of circumferentially-oriented smooth muscle, which aids in the maintenance of urethral pressure during storage and contributes to the resting tone of the urethra. The outermost layer of the urethra is composed of a layer of striated muscle cells, which is believed to be responsible for continuous urethral pressuring during bladder filling and increased contractions during increases in bladder pressure [15]. The urethra contains two sphincters - the internal (located at the bladder neck and composed of mostly smooth muscle) and external (located at the external meatus and composed of mostly striated muscle) - which are responsible for maintaining involuntary and voluntary urethral control, respectively [12]. The urethra also contains a large amount of extracellular matrix (ECM). The main ECM component in the urethra is collagen, which is circumferentially-oriented and provides structural support to the tissue [16]. The urethra also contains some longitudinally-oriented elastin, which is generally localized around the muscle fibers, but whose role in the continence mechanism remains unclear [17].

The urethra's ability to maintain continence is composed of several mechanisms. One mechanism is the support of the surrounding structures including the pelvic floor muscles and the

surrounding organs (the vagina in the female and the prostate in the male) during increased abdominal pressure by pressing the urethra closed (**Figure 1.4**) [15]. There is also a large degree of innervation by both the autonomic and somatic nervous systems which control the activity of the internal and external urethral sphincters [13].

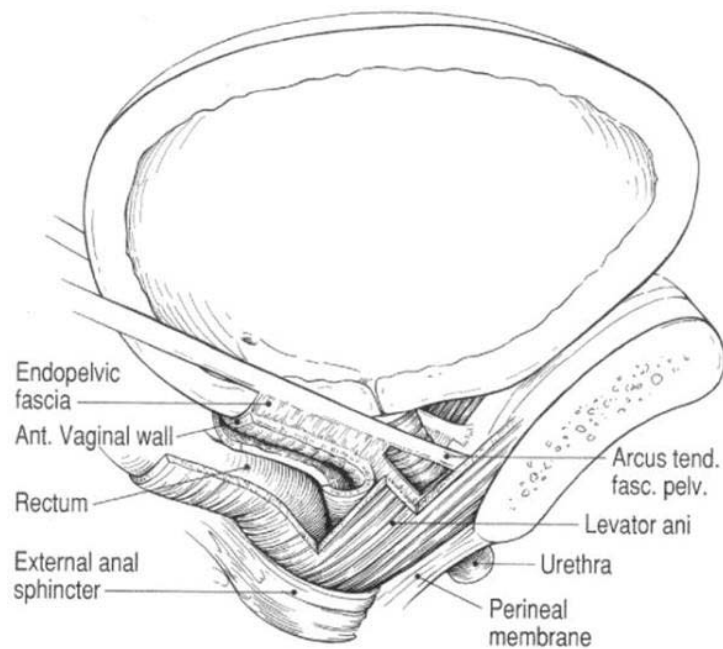


**Figure 1.4** Female urethral support structures. Reproduced from DeLancey(1994) [18].

The urethra is innervated by parasympathetic, sympathetic and somatic nerves (**Figure 1.5**). Sympathetic signals via the hypogastric nerve innervate the proximal urethra and bladder neck through  $\alpha_1$ -adrenergic and  $\beta$ -adrenergic receptors, respectively. Parasympathetic signals via the pelvic nerve innervate the urethral smooth muscle (both circumferential and longitudinal) through cholinergic, peptidergic and nitrenergic receptors, as well as the bladder smooth muscle via muscarinic receptors [19-21]. The pudendal nerve (somatic) innervates the striated muscle of the external urethral sphincter, providing voluntary urethral continence [22].

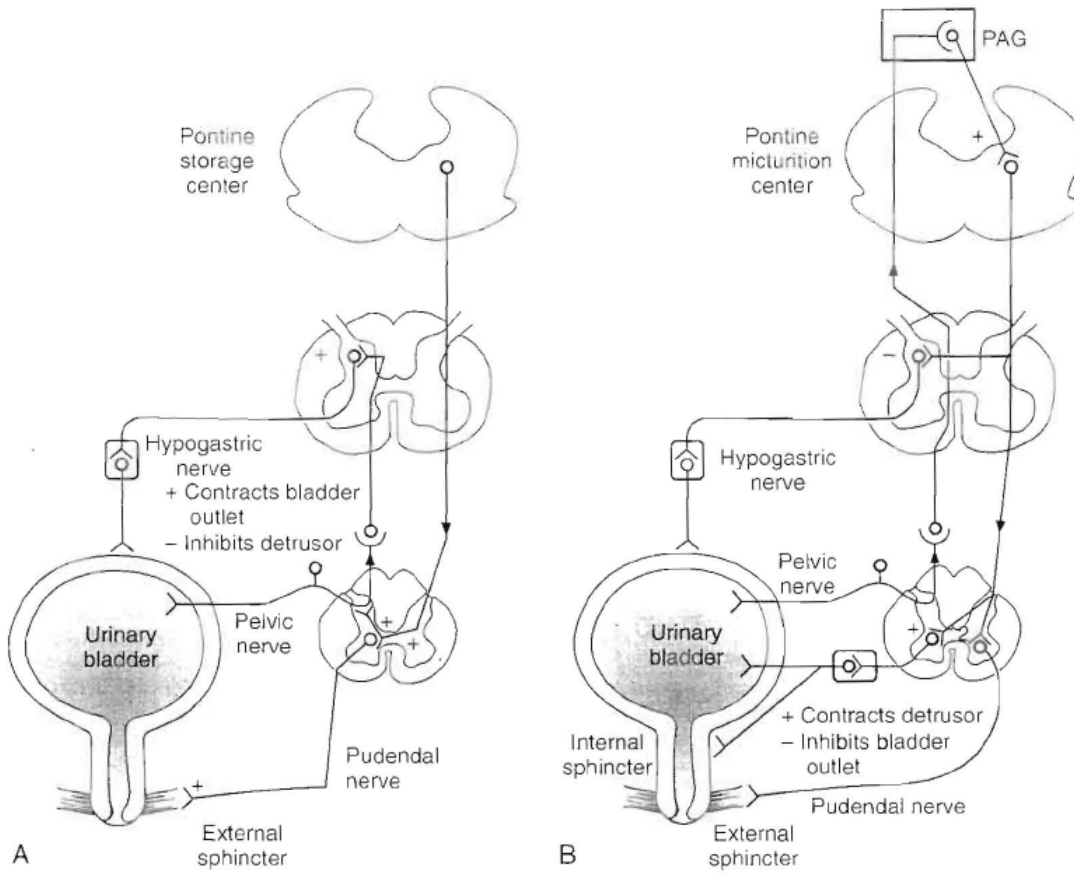


**Figure 1.5** Innervation of the bladder and urethra. Reproduced from Wein (2007) [8]

### 1.1.3 Storage and Voiding Reflex

Storage and micturition are dependent on both the bladder and urethra. The storage and voiding reflex of the bladder (smooth muscle) and urethra (smooth and striated muscle) is under neural control by both the autonomic and somatic nervous systems (**Figure 1.5**). Three main pathways control these organs. The sacral parasympathetic pathway provides contraction of the bladder and relaxation of the urethra and serves as the primary activator of storage and micturition reflexes in the sacral spinal cord. The thoracolumbar sympathetic and sacral somatic pathways provide contraction of the urethra [23].

During storage, as urine is transported to the bladder, pressure within the bladder increases. During this process continence is maintained by excitatory inputs from sacral afferent pathways activating the sympathetic and somatic efferent nerves to the urethra, while parasympathetic input to the bladder is dormant [23]. Storage is maintained by sympathetic inhibition of parasympathetic ganglion efferent signaling and sympathetic stimulation of  $\beta$ -adrenergic receptors in the bladder (relaxation) and  $\alpha$ -adrenergic receptors in the urethra (contraction). Afferent input from the bladder signals the pudendal nerve to contract the striated sphincter to maintain urethral closure [24].

As bladder filling progresses, eventually a threshold is reached and stretch receptors activate voiding by sending afferent signals via the pelvic nerve to the sacral portion of the spinal cord [11]. During micturition, the pontine micturition center (PMC), located in the rostral brainstem, activates the parasympathetic excitatory input to the bladder via the pelvic nerve and inhibits the sympathetic and somatic signals to the urethra via the hypogastric and pudendal nerves, respectively [23, 24]. The PMC is responsible for bladder emptying via sustained contraction of the detrusor and relaxation of the striated sphincter [24]. The PMC receives input

from the cerebellum which synchronizes contraction of the bladder with relaxation of the striated sphincter [24]. First, bladder contraction is activated by parasympathetic activation of cholinergic receptors in the detrusor. Simultaneously, the sympathetic and somatic innervation of the urethra is inhibited creating an open conduit to the outside of the body [24].

## **1.2 STRESS URINARY INCONTINENCE**

Continence is maintained by a coordinated response between the bladder, urethra, pelvic muscles and connective tissues. Urinary incontinence is the result of a disturbance in the storage and or micturition functions of the lower urinary tract [25]. Stress urinary incontinence [1] is the involuntary leakage of urine with increases in abdominal pressure caused from laughing, sneezing, and coughing but in the absence of a bladder contraction. Although SUI affects both men and women, it is more common in the female population. SUI is the most common type of urinary incontinence [26] costing the US more than \$26 billion annually [27]. It affects women not only physically, but psychologically as well. Due to the embarrassing nature of SUI (causing odor, wetness, and discomfort), many sufferers experience decreased self-esteem, and avoid social settings and discussing the problem with their physician [28].

### **1.2.1 Pathophysiology of SUI and Diagnosis**

SUI occurs when abdominal pressures exceed the urethral closure pressure, resulting in urine leakage [29]. Urethral pressure is influenced by many things including the surrounding structures such as the vagina and the pelvic floor, the urethral smooth and striated muscle, and

neural and vascular innervation of the urethra [29]. The main factors contributing to SUI are thought to be urethral hypermobility, where the urethra is lacking support from its surrounding structures and unable to withstand high intravesicle pressures [30], and intrinsic sphincter deficiency (ISD), where a weak urethral sphincter is incapable of preventing urine flow with increased abdominal pressures [31]. Stress incontinence can be classified as one of three types: 1.) urethral hypermobility; 2.) intermediate; 3.) ISD, with severity increasing from type 1-3. Major causes of SUI include pelvic nerve damage, muscle weakness or damage, or damage to the supporting structures of the bladder and urethra, which can be a result of natural childbirth, hormonal deficiency, increased age and obesity [32, 33].

Vaginal delivery is the most common risk factor of SUI. Anatomically, the female urethra lies directly on top of the vagina, making it susceptible to injury during vaginal delivery. It is believed that during this process, neural, muscular and connective tissue injury occurs. It has previously been shown that urethral closure pressure decreases as an effect of damage to the pelvic and/or pudendal nerves during vaginal delivery [34]. Since it is common for SUI to develop later in life following vaginal delivery, it is thought to be related to ischemia and decreased blood flow, which has been confirmed in an animal model [35]. It has also been shown that changes in hormone levels, following menopause can lead to an increased risk of SUI [36]. Estrogen has been shown to maintain neuronal stability. As estrogen levels decrease following menopause, nerves that were damaged by vaginal distension may no longer be able to remain stable and could therefore contribute to the late onset of SUI [37].

Urethral hypermobility is due to a decreased support of the proximal portion of the urethra. This lack of support alters the transmission of pressure to the urethra and results in incontinence. These alterations in pressure transmission are thought to be due to a change in the

anatomical position of the urethra and/or a loss of integrity of the pubourethral ligament and endopelvic fascia, which compose the connective tissue support of the urethra [38]. Hypermobility is detected by a Q-tip test in which a cotton swab is inserted into the urethra and the patient is asked to strain. The angular change in the Q-tip between rest and strain is used to determine the degree of hypermobility of the urethra [39]. If it is determined that hypermobility is present, a support device may be implanted to provide structural support to aid the urethra in maintaining continence [40].

ISD is the most severe form of incontinence, where the urethra is unable to maintain its seal and leakage occurs. ISD can accompany urethral hypermobility, but can be present without it [38]. The simplest test for ISD is that for Valsalva leak point pressure. This test is performed with the patient in the vertical position by first inserting a 10-Fr microtip pressure transducer catheter to measure bladder pressure and an anal probe to measure abdominal pressure. The bladder is then filled to half of capacity (~200 mL) with saline or a contrast agent, and the patient is then asked to make an expulsive effort against a closed glottis until leakage is observed. This is repeated several times and the lowest pressure is taken as the Valsalva leak point pressure. Values of 60 cmH<sub>2</sub>O or less indicate ISD, while values near 90 cmH<sub>2</sub>O are associated with urethral hypermobility [41].

In addition to the above mentioned detection methods for hypermobility and ISD, SUI can be diagnosed in several other ways. Some physicians rely solely on a questionnaire or diary and a cough stress test in the office. This requires the patient to keep detailed records of such things as liquid consumption, voiding volumes and number of accidents. Further evaluation can include urodynamics, which allows measurement of urethra and bladder physiologic functions simultaneously during filling and emptying [29]. Numerous studies have been performed on the

validity and reproducibility of the different ways to diagnose SUI, but there is no gold standard at this time.

### **1.2.2 Current Treatments for SUI**

Currently there are several options for the treatment of SUI. These options include non-invasive, surgical or pharmacological treatments. Although there is no preferred treatment of SUI, each available treatment has both benefits and limitations.

Non-invasive treatments rely heavily on patient compliance. Such treatments include keeping a diary of fluid intake and voiding, behavioral changes such as weight loss, monitoring fluid intake and developing a regular voiding schedule. Other non-invasive treatments include strengthening of the pelvic floor muscles with Kegel exercises. Pelvic floor training can increase the likeliness of being cured of SUI by a factor of seven. Many women, however, either do not perform the exercises correctly or do not adhere to the strict regimen required to see results [25]. These non-invasive treatments are generally used as a first measure of treatment, but due to patient non-compliance, additional treatment is generally required [25, 29, 42].

There are over 160,000 surgical treatments for SUI performed in the United States [43]. The most common surgical treatments for SUI include the injection of a bulking agent, colposuspension or sling placement. Injection of a bulking agent into the urethra is the least invasive of the surgical treatments available. An agent such as collagen, fat or silicone is injected into the periurethral tissue at the proximal urethra to provide support to the urethra and aid in maintenance of closure. Success rates for bulking agents are 75% with a cure rate of 50%. These agents, however, tend to dissipate over time requiring additional procedures [25, 38, 42].

Retropubic urethropexy (colposuspension) is thought of as the optimal surgical treatment for SUI with the most long-term results [25]. The colposuspension lifts the bladder neck by suturing it either to the Cooper's ligament or the peristeam of the pubic symphysis via a suprapubic incision. These procedures have a reputable cure rate up to 8 years (90%), but this decreases to 55-69% by 10 years [25]. There is also a relatively high (~25%) rate of complication with this procedure. Pubovaginal sling procedures require placement of a strip of polymer or tissue under the urethra to hold it up. The ends of the strip are then anchored in the body, generally to the pubic symphysis. Slings have similar success and complication rates to the colposuspension with less long-term data [25]. Although a range of materials have been used for the slings, naturally occurring materials have a greater success rate. Synthetic materials tend to have an increased rate of complications, such as erosion of the urethra and/or vagina [25]. It is thought that complication rates are high due to overtightening of the sling or overlifting of the bladder neck in these procedures causing retention and other complications. Although these surgical treatments have decent success rates, they are limited in that they only focus on treating urethral hypermobility.

There are several pharmacological treatments prescribed for SUI. Alpha-adrenergic agonists, such as ephedrine and midodrine, can act on  $\alpha$ -adrenergic receptors at the bladder neck and proximal urethra to increase smooth muscle contraction. Tricyclic antidepressants, such as doxepin and imipramine hydrochloride, have been shown to increase urethral resistance and decrease bladder contractility, although the exact mechanism is unknown. Beta-adrenergic antagonists, such as propranolol, amplify an  $\alpha$ -adrenergic response. Serotonin and norepinephrine reuptake inhibitors, such as duloxetine hydrochloride, subdue parasympathetic activity and enhance both sympathetic and somatic activity increasing bladder relaxation and

urethral resistance [44, 45]. Although early studies indicate that such drugs would be beneficial to those with SUI, systemic effects and lack of long-term data have prevented any drug from receiving FDA approval for SUI.

### **1.2.3 Animal Models of SUI**

SUI can develop as a result of various bodily changes or traumas including obesity, nerve damage, vaginal child birth and age. In order to identify the mechanism of how each factor contributes to SUI and assess possible treatments for it, a reproducible animal model is necessary. As there are many factors that can lead to SUI, independently or collaboratively with others, various models of SUI are needed. There are several SUI models regularly used to assess how specific factors contribute to the onset of SUI, each with its own limitations. The most common models include vaginal distension, hormone deficiency and neurogenic models.

#### **1.2.3.1 Vaginal distension**

Vaginal delivery is one of the most common risk factors for SUI. As a baby is delivered through the vaginal canal, the surrounding organs, structures and nerves are distorted and serious trauma occurs [35, 46]. As the urethra lies on top of the vagina and is connected to it via connective tissue, nerves and blood vessels, it could be at risk for hypoxia and loss of innervation during the trauma of child birth. This trauma contributes to both an acute and delayed onset of SUI in a rat model, with the risk of SUI increasing with increased vaginal deliveries [36]. Therefore, a model of vaginal distension (VD) has been implemented for animal studies to determine the mechanism of the development of SUI [47-49]. Models that simulate the mechanical trauma of childbirth

include intravaginal balloon inflation with [49, 50] and without [32, 35, 46, 51] ovariectomy to address how hormonal changes affect damage caused by VD (see **Section 1.2.3.3**).

VD is performed on anesthetized animals by first inserting a balloon catheter into the vagina of the animal. The balloon is then inflated to a volume representative of the size of a pup from the desired model. The catheter is generally left in place for at least 4 hours [35, 46]. Models including ovariectomy with VD better simulate what happens in humans. In this procedure, anesthetized animals are subjected to ligation of the fallopian tubes and the ovarian branch of the uterine artery, followed by removal of the ovaries (see **Section 1.2.3.3**). Three days post ovariectomy, animals are subjected to vaginal distension [50]. Animals have been assessed at various time points, from hours to days to weeks, following VD. From these studies, it has been established that VD in a rat model causes an acute decrease in urethral resistance [32, 46, 48, 49, 51], which tends to return to normal over time [47], decreased mid-urethral innervation [46, 52] and bloodflow [35], and increased smooth muscle hypoxia [35] and urethral compliance [53, 54].

VD studies have shown that the severity of SUI is dependent on both the duration and degree of distension. Numerous studies have shown that VD decreases leak point pressure in a rat model [48, 51]. It has also been shown that VD has a large effect on the striated sphincter, decreasing urethral response to sneeze [48] and causing hypoxia of the urethral cells [35]. Longer durations of VD in a rat model caused a lower leak point pressure and more muscular damage than shorter durations [51]. It has also been demonstrated that VD causes striated sphincter necrosis as well as decreased ganglion and nitric oxide synthase in the vaginal neural plexus [32]. Although these models can produce SUI by vaginal birth simulation, they are only accurate for acute studies due to the rapid healing of this model [55].

### 1.2.3.2 Neurogenic models

The urethra is a highly innervated structure (see **Sections 1.1.2** and **1.1.3**) and the maintenance of continence is controlled by complex circuitry allowing communication between the bladder, urethra and spinal cord. Thus, damage to any of these nerves could lead to incontinence. It is known that the pudendal nerve, innervating the striated sphincter of the urethra, is damaged during childbirth and that this nerve trauma can lead to SUI [56]. It has been reported that women with SUI tend to have some degree of denervation of the pelvic floor muscles as well as pudendal nerve neuropathy [57]. Thus, neurogenic models of SUI are important to assess to determine how denervation of various nerves contributes to SUI. There are several neurogenic models including pelvic nerve transection and pudendal nerve crush [46, 47, 56] or transection [43, 47, 58].

Transection of the pelvic nerves, which innervate the bladder and proximal urethra, creates an SUI model by abolishing tonic urethral continence mechanisms activated in the afferent pathways of the pelvic nerve [59]. However, micturition signals are also mediated by the efferent pathways of the hypogastric and pudendal nerves [60]. Hence this is a somewhat incomplete model of SUI.

Pudendal nerve crush or transection (the chosen model for this work) [46, 47, 56] was developed as a model of SUI based on a report that women with SUI may also have pudendal nerve damage possibly caused by vaginal distension during childbirth [46]. Direct damage to the pudendal nerve has been shown to significantly decrease leak point pressure [56, 61] with decreased amplitude of urethral contraction, voided volume and atrophy of the striated muscle [61]. Models in which the external urethral sphincter is denervated in order to create an SUI model have been used to test slings [62, 63] and stem cell injections [64, 65], which were placed

proximal to the denervated portion of the urethra. It has also been shown that transection of the sciatic nerve proximal to its branching into the pudendal nerve causes proximal urethral atrophy with decreased smooth muscle cell (SMC) contractility and abolished striated muscle contractility [64]. The pudendal nerve transection model results in a weakened proximal urethra while simulating the nerve injury that may occur with childbirth (one of the primary contributors to SUI). Neurogenic models are able to supply a more chronic model of SUI, but do not portray any of the pathophysiology that accompanies most cases of SUI.

### **1.2.3.3 Ovariectomy model**

Although the trauma of vaginal delivery significantly contributes to the development of SUI, it is generally not evident until many years later. In fact, symptoms of SUI do not appear until years later, generally following menopause [36]. It has been reported that over 50% of women over the age of 60 are afflicted with urinary incontinence [66], with SUI being the second leading cause of bladder overactivity in causes of urinary leakage in elderly females [36]. During menopause there is a permanent loss of ovarian follicular activity [67]. This means that a woman's menstrual cycle ceases and there is a decrease in levels of estrogen and progesterone [67]. There is a strong belief that this hormone deficiency contributes to the severity and emergence of SUI. An ovariectomy (Ov) animal model was developed to simulate menopause. In this model, animals are subjected to bilateral removal of the ovaries and are studied at various time points following the procedure [36]. It is common to assess this model in the presence of other procedures such as VD or pudendal nerve crush to better simulate the conditions of the population most affected by SUI [47]. Although previous studies have not shown a strong effect of Ov on continence rates, it has increased incontinence when used in conjunction with VD [47].

#### 1.2.4 ECM Changes in SUI

The urethral ECM is composed of collagen (types I and III) and elastin [68]. The ECM provides resistance to increased tension and structural recovery from the tension. Collagen, which provides structural resistance to the tissue, comprises ~30% of the urethral ECM and is produced mainly by fibroblasts [52]. Globally, the collagen fibers are circumferentially oriented. Elastin allows the urethra to undergo elastic deformation and helps it to retain its shape during micturition [68], but is present in smaller quantities than collagen [17]. Elastin is oriented longitudinally in the urethra and is localized to muscle fibers [17, 69]. There have been contradicting reports on how SUI affects the ECM content of the urethra and periurethral tissues. One study reports that nulliparous, incontinent females had significantly less collagen in periurethral tissue [70], while another reports that incontinent women at reproductive age had ~30% more collagen in periurethral tissues [71]. A study in rats showed that following natural childbirth and/or simulated childbirth, there was an immediate, significant increase in collagen compared to controls [68]. These studies did not assess the degree of incontinence in these animals. Another study showed that VD caused a decrease in collagen content of the middle urethra and increase in whole-urethra elastin content in a rat model of SUI [53]. Although the results of these studies are inconsistent, it is clear that there is an alteration in the remodeling of the urethra and its surrounding structures during SUI. These alterations in the structural proteins of the urethra may be one of the main contributors to the inability of the urethra to maintain a tight seal. Therefore, a urethral treatment which provides both structural support and a foundation for cell growth and ECM production, such as the TEUW, may provide more directed remodeling, and a more effective treatment.

### 1.3 TISSUE ENGINEERING FOR THE URETHRA

Although the exact definition of tissue engineering may have changed over the years, it is basically the application of both engineering and life science principles to the development of biologically-based replacements for the repair, maintenance or enhancement of normal tissue or organ function [72]. Tissue engineering includes the use of cells and/or scaffolds [73].

The cells used in tissue engineering can be divided into two main types: adult or terminally differentiated cells and stem or progenitor cells [73]. Adult cells are generally isolated from a small tissue biopsy and grown in culture. However, adults cells tend to grow slowly and if they are isolated from the area needing repair, could yield only diseased cells [74]. Stem cells can be isolated from various areas (bone marrow, blood, the embryo), grow quickly and have the ability to differentiate into various cell types [72, 75]. Both types of cells can come from various sources such as: from the person they are to be used on (autologous), from a donor of the same species (allogenic), from a genetically identical donor (syngeneic) or from a different species (xenogenic) [72].

The scaffold is used to serve as an artificial ECM, providing a 3-D environment for the cells to adhere, grow and organize a new tissue [74]. Just as there are numerous types and sources of cells, the same applies for scaffolds. Scaffolds are generally divided into those that are biologically or synthetically derived [74]. Biological scaffolds, such as collagen, fibrin and ECM, provide natural, inherently friendly environments for the cells and degrade into natural bi-products that can easily be processed in the body [72, 74, 76]. Synthetic scaffolds for tissue engineering can be developed from a variety of polymers and are generally divided into degradable, degrade into naturally occurring monomers, which can be processed by the body, or non-degradable. The choice of a degradable or non-degradable polymer with or without cells,

generally depends on the body area of interest and its naturally occurring mechanical and functional properties [72].

### **1.3.1 Progenitor Cells in Urethral Tissue Engineering**

Although several reviews of urologic tissue engineering give an overview of the potentials of stem cell usage [77-79] there have been no reports, to our knowledge, of constructs seeded with them for urethral augmentation. A small number of previous studies have been performed on the use of progenitor cells for treatment of urethral dysfunction [80, 81].

Several groups have performed studies to investigate the abilities of stem cell injections to augment the in-vivo function of the lower urinary tract [64, 65, 81-85]. In one series of studies, muscle derived stem cells (MDSCs) were injected into the lateral walls of the mid-urethra in ISD [81] and SUI [65] Sprague-Dawley rat models. In the ISD study [81], rats were divided into three groups: those undergoing urethral cauterization and injection of MDSCs a week later, those undergoing cauterization and injection of saline a week later, and a sham group where the urethra was exposed but not cauterized. Cystometry, leak point pressure (LPP), H&E, fast myosin heavy chain, anti-protein gene product (PGP), and LacZ were assessed at 2, 4, and 6 weeks post-injection. Cystometry showed that cauterization did not damage bladder function. LPP results revealed an improved urethral closure function for the MDSC-injected group when compared to the saline-injected controls, returning to a baseline by 6 weeks. Histology showed that the saline-injected urethra had disruptions in the striated muscle layer, while those receiving MDSCs did not.  $\beta$ -galactodidase was expressed within the wall of the MDSC-injected urethras, suggesting the injected cells remained at the site of injury. PGP staining revealed more nerves in this group than the saline-injected urethras, suggesting increased innervation to the tissue.

In the SUI study [65], three experimental groups were again utilized: a sham, an SUI (via urethral sciatic nerve transaction) group with saline injection, and an SUI group with MDSC injection. LPP measurements and H&E were performed at 1 and 4 weeks post-injection. At 4 weeks, MDSC-injected cells demonstrated increased dorsolateral skeletal muscle masses with variable orientation at the injection site, while the saline-injected group became atrophic. LPP measurements showed improved urethral closing function in the MDSC-injected urethras compared to the saline-injected and even the sham controls at both time points. A short term study was also performed in which the time points were 14 days, and these results match those of the long term study [64].

While intriguing, this method of urethral augmentation is still under development and is unproven. For example, cell fate following injection, in terms of remaining localized to the point of injection and their terminal differentiation status, remains unclear.

### **1.3.2 Previous Approaches in Urethral Tissue Engineering**

The concept of a tissue engineered urethra (TEU) is one that has gained recent interest. Unfortunately, several common limitations have persisted that have hampered progress of this technology. The earliest forms of tissue engineering applications for the urethra were based on the use of native tissues, including genital and extragenital skin flaps, mucosal grafts generated from both bladder and buccal sub-mucosa, tunica vaginalis, and peritoneal grafts [86]. Due to the high rate of complications resulting from the use of these native tissue materials such as hair growth, graft shrinkage, stricture and stone formation in addition to donor site morbidity, pain, immobilization of the lower abdominal incision, bladder spasm, hematuria, and post-operative voiding frequency [86-88], the focus was turned toward the use of synthetic materials. Silicone

grafts were the most common early synthetic prosthesis for urethral use [78], followed soon after by Teflon and Dacron [86]. These early synthetic materials were generally accompanied by erosion, dislodgement, fistula, stenosis, extravasation, and calcification [86].

Collagen has served as a scaffold for urethral reconstruction quite successfully in animal models over the years [89-92]. It has excellent biocompatibility and is amenable to cellular remodeling. Collagen is however, limited by its mechanical strength [78]. Non-seeded materials may be adequate for repair of small areas. However, if total urethral replacement is required, seeding the material with urothelial and SMCs may be necessary to prevent graft contraction and shrinkage [87, 93]. In one study, acellular collagen was isolated from donor porcine bladder to be used in an onlay fashion as a urethral replacement in a hypospadias model. The study revealed that cell infiltration and angiogenesis was present within two weeks of the onlay placement. Within two months of the onlay, muscle fibers were present in the construct and there were no incidences of scarring, stricture or shrinkage out to six months. It was observed, however, that an unseeded construct was only beneficial in an onlay fashion over a small area and that a larger replacement, such as a tubular segment of the urethra, requires seeding of the construct to initiate infiltration of native urethral cells and to prevent contracture of the construct [86, 90, 92].

In addition to naturally occurring biomaterials, several biocompatible polymers have been developed for urologic applications [74]. For example, a polyglycolic acid polymer scaffold coated with poly-L-lactic acid and seeded with chondrocytes has been shown to be elastic and capable of withstanding high pressures [77]. Additionally, a non-woven mesh of polyglycolic acid demonstrated re-epithelialization of the implantation site and degradation of the polymer after 14 days with no complications to voiding or structure [92]. Furthermore, the

development of a polyglactin-fiber mesh tubes coated with polyhydroxybutyric acid and hyaluronan benzyl ester have shown complete regeneration of the urethral epithelium and of the adjacent connective tissue [86].

While promising, all of these studies have been tested in a male animal model. The male urethra is divided into three portions: (1) the prostatic urethra, which begins at the urinary bladder and is the continence maintaining portion of the male urethra, (2) the membranous urethra, which passes through the pelvic floor muscles, and (3) the spongy urethra, which passes through the penis to the urethral orifice [7]. The above approaches have focused on regeneration of the conduit and non-functional (membranous and spongy) portions of the male urethra, providing no evidence that they are capable of contributing to continence.

#### **1.4 FIBRIN AS A SCAFFOLD MATERIAL**

Fibrin is a natural biomaterial that is a main component of blood clots and aids in the regulation of wound healing. Fibrin forms as part of the coagulation cascade when fibrinogen comes into contact with thrombin [76]. Fibrin naturally contains binding sites for both smooth muscle and endothelial cells [94] as well as several important growth factors (e.g., FGF-2 and VEGF) allowing cells to maintain cell function and contribute to tissue remodeling [76] and myogenesis [95]. Fibrin also supports cell migration, proliferation and extracellular matrix (ECM) production [95]. Since fibrin is naturally formed within the body, it can be formed from autologous fibrinogen, which can be isolated from the blood and therefore avoid a potential allergic reaction from animal sources like collagen [96].

In tissue engineering, fibrin is generally utilized in a cell entrapment technique in which constructs are created by suspending cells within a fibrinogen solution, adding thrombin and gelling the mixture within a mold [94]. This produces a highly efficient seeding density and homogeneous cell distribution [94]. Concentrations of fibrinogen, thrombin, calcium and clotting time all contribute to the structure of fibrin and its mechanical properties [76]. For example, Rowe, *et al.*, reported that fibrin fiber diameter, construct compaction, material modulus and tensile strength all increased with decreasing thrombin concentration [76]. Its degradation and hence remodeling can be controlled by aprotinin or aminohexanoic acid, which are fibrinolytic inhibitors [94]. However, they have been reported to alter mechanical strength and vascular reactivity [96].

Fibrin has been used in numerous tissue engineering applications, specifically for vascular applications [94, 97-100]. Ross *et al.*, performed studies in which smooth muscle cells were seeded into fibrin constructs and cultured. They found that as the fibrin was degraded, collagen and elastin fibers replaced it. They also showed increased mechanical properties with increased culture duration as collagen and elastin were replacing the fibrin [100]. Yao *et al.*, performed studies in which they implanted fibrin constructs into the jugular vein of lambs with patency up to 15 weeks. These constructs were highly remodeled and had adequate mechanical strength due to the presence of large amounts of collagen and elastin [94].

## **1.5 GUIDED DIFFERENTIATION OF PROGENITOR CELLS TO SMOOTH MUSCLE CELLS**

As described in **Section 1.2**, there is damage to both the muscular and ECM components of the urethra in urethral dysfunctions such as SUI. Due to the alterations seen in the urethral tone and compliance of the proximal urethra in SUI [53, 54, 101], a therapy which targets the contractile deficiency of the smooth muscle in that portion may increase urethral resistance and eliminate incontinence. A cell-based therapy is therefore a logical treatment for SUI. Since cells are a product of their environmental cues [102], smooth muscle cells for urethral therapy should be isolated from the lower urinary tract. However, utilizing a biopsy from an already damaged area may not produce the most effective treatment [74]. Therefore, the use of stem cells is an attractive option. Stem cells allow for an autologous therapy, while providing a cell type that is capable of differentiating into a variety of other cell types [72, 75] with mechanical and/or chemical cues similar to the environment in which they will be placed.

### **1.5.1 Mechanical Stimulation**

The role of biomechanical forces in progenitor cell differentiation has been largely ignored. Therefore, the powerful potential of this stimulus may have gone underutilized in the field of urologic tissue engineering. There are several reports evaluating the effect of biomechanical forces on progenitor cell differentiation to smooth muscle cells in-vitro [103-105].

Our laboratory previously reported that rat BMPCs in monolayer were responsive to cyclic uniaxial strain, suggesting that cyclic uniaxial strain guides BMPC differentiation to a SMC lineage [103]. Decreased proliferation, increased alignment perpendicular to the direction

of strain and expression of both  $\alpha$ -SMA and h1-calponin resulted from exposure to 10% strain at 1 Hz for 7 days [103]. Other studies published at approximately the same times, showed similar results [104, 105].

Park *et al.* exposed mesenchymal stem cells (MSCs) to both uniaxial and equiaxial strain. They reported increased  $\alpha$ -SMA and collagen production and cell alignment perpendicular to the direction of strain when exposed to uniaxial strain (10%, 1Hz), and decreased  $\alpha$ -SMA when exposed to equiaxial strain (10%, 1Hz) [104]. Kobayashi *et al.* exposed BMPCs to cyclic shear stress (0.6/1.2 L/min at a pressure of 10mmHg), cyclic hydrostatic pressure (120/60mmHg, at a flow of 0.1L/min), and the combination of both shear and pressure stimulation. They reported that pressure or combined stimulation upregulated smooth muscle  $\alpha$ -actin and smooth muscle myosin heavy chain [105].

Additional reports include a study by Huang *et al.*, which found that seeding of embryonic stem cells onto a segmented polyurethane matrix and culturing them in a perfusion system under pulsatile conditions produced differentiation of the cells lining the lumen to endothelial cells with those deeper in the matrix to cells expressing smooth muscle actin [106]. Also, a study on mouse embryonic fibroblasts by Kim-Kaneyama *et al.*, found that uni-axial stretch causes Hic-5 to relocalize to stress fibers, regulating the contractile ability of cells within the stress fibers [107].

Additional studies by our laboratory show that rat BMPCs, obtained from the Tulane Center for Genetics (utilized in the work described in **Chapters 2.0 - 7.0** ), stimulated in monolayer with cyclic uniaxial stretch (10%, 1Hz) for 5 days express smooth muscle alpha actin, calponin, and myosin heavy chain (MHC) while unstrained control cells remained negative

for these markers. Our laboratory also noted that these cells are positive for Flk-1, a homologue of vascular endothelial growth factor receptor 2 (VEGFR2) [108-111].

Three-dimensional studies, utilizing a Flexcell<sup>TM</sup> Tissue-Train<sup>TM</sup> and the same Tulane BMPCs, showed that exposure to 10% longitudinal cyclic stretch at 1Hz for 6 days increased stress filament area per cell and caused alignment of cells parallel to the direction of the stress/strain over static and constrained (but not cyclically stretched) controls [102]. An increased expression of SMA and calponin was seen in both the constrained and cyclically stretched samples [102]. These studies clearly highlight the important potential of mechanical stimulation in guiding progenitor cell differentiation to SMCs.

### **1.5.2 Chemical Stimulation**

As our knowledge of growth factors, cytokines and other bioactive molecules that mediate cell phenotype in-vivo has increased, conditions have been identified that can be utilized to guide the in-vitro differentiation of progenitor cells to various cell types [112-117]. It has been shown that BMPCs can differentiate into SMC using biochemical stimulation. Arakawa *et al.*, [117] observed that a clonal cell line isolated from bone marrow could differentiate into smooth muscle when grown in the presence of 2-mercaptoethanol and ascorbic acid. The cells were positive for SMC-specific genes, including h1-calponin, h-caldesmon and myosin heavy chain. They further observed that ascorbic acid was a potent factor inducing the expression of h1-calponin, a marker for contractile SMC phenotype. Another study has shown the ability of embryonic derived stem cells to differentiate into smooth muscle when cultured in high concentrations of retinoic acid and dibutyryl cAMP [118]. These embryonic cells were positive for myosin heavy chain, contained typical ion channels (Ca<sup>2+</sup>-activated maxi K<sup>+</sup>, delayed-rectifier K<sup>+</sup>, and

dihydropyridine-sensitive (L-type)  $\text{Ca}^{2+}$  channels) and responded to specific agonists with an increased  $\text{Ca}^{2+}$  influx. Furthermore, the growth factors PDGF [119-122], TGF- $\beta$  [122-126], and VEGF [127, 128] are known to play pivotal roles in smooth muscle differentiation and migration. In particular, VEGF is an important molecule during development of the vascular system, and it is also known that bone marrow derived progenitor cells express the functional VEGF receptor, VEGFR1 (FLK-1/KDR) [129, 130], possibly suggesting that they, too, can respond to VEGF stimulation.

TGF- $\beta$  is a cytokine thought to play a vital role in vascular development and SMC differentiation [123]. The role of TGF- $\beta$  in differentiation of various cell types to contractile smooth muscle cells has been studied. It has been reported that neural crest cells cultured in TGF- $\beta$  show expression of both  $\alpha$ -SMA and calponin [124, 131], but no functional studies were performed. Another study showed that adipose derived stem cells significantly up-regulated expression of both  $\alpha$ -SMA and h1-calponin when cultured in media supplemented with TGF- $\beta$ . It has previously been shown that culture of human mesenchymal stem cells in the presence of TGF- $\beta$  causes in an up-regulation of  $\alpha$ -SMA and calponin after 14 days in culture and decreased proliferation [132]. The regulatory roles that TGF- $\beta$  plays in cell proliferation, differentiation, migration and production of ECM [133], make it an exceptional candidate for use in the differentiation of BMPCs to SMCs.

Utilization of a bioreactor system which exposes constructs containing cells to mechanical and/or chemical stimuli can enhance the differentiation of stem cells to various phenotypes, including that of a contractile smooth muscle cell. Due to the decrease in urethral resistance that accompanies SUI (see **Section 1.2**), a cell-based therapy which took advantage of

differentiation capabilities of a bioreactor could provide a functional therapy capable of providing immediate relief from SUI.

## **1.6 BIOMECHANICS OF THE URETHRA**

The urethra is a complex structure composed of various cell types as well as extracellular matrix, and both neuronal and vascular innervation (see **Section 1.1.2**). To better understand the pathological progression of urethral dysfunctions, such as SUI, it is important to understand how each of these components contributes to healthy urethral function and how they are altered in the diseased state. Understanding the mechanical contribution of each of these components will aid in the development of new treatment methods, which can better target the damaged component.

The urethra is a soft tissue composed of both active (contractile muscle) and passive (ECM, urothelium, etc.) components. These components are mainly circumferentially-oriented to provide a strong force in response to increased intraluminal pressures and prevent urine leakage. The urethra, like all soft tissues, is viscoelastic and its elasticity depends on the rate of load, where the muscular components provide long-term stability [16]. Although there is limited information regarding the mechanical characterization of the urethra, some studies have attempted to explore the mechanical contributions of the urethral components.

### **1.6.1 In-Vivo Studies**

An early study of healthy urethral biomechanics assessed changes in diameter with increases in intravesicle pressure. Anesthetized, female, mongrel dogs were assessed for urethral

displacement at the proximal, middle and distal portions of the urethra as the bladder was filled. The proximal and middle portions had greater compliance and resistance to flow than the distal portion [134]. Other studies have used a probe, composed of a balloon attached to a catheter, which is inserted into the urethra to conduct inflation studies. Measurements of intraurethral pressure and cross-sectional area are used to measure the rigidity of the urethra. These studies showed increased rigidity in the middle and distal portions compared to the proximal portion of the urethra in young healthy women [135, 136]. In a comparison of healthy and SUI women, investigators found that the proximal and middle portions of the urethra had decreased response to incidents of stress, indicating their importance to maintaining continence [137].

Although in-vivo studies are ideal as the tissue is behaving in its native environment, they are limited by the investigative techniques with which they are conducted. Insertion of a catheter or probe into the urethra changes the shape of the lumen and therefore the pressure distribution to maintain continence, yielding inaccurate readings. It has also been reported that these measurements are dependent on the size of the catheter/probe used as well as the position of the transducer along the length and circumference of the urethra [138, 139].

### **1.6.2 Ex-Vivo Studies**

Until recently, there had only been one ex-vivo study of the mechanical properties of the urethra. The first study assessed an intact urethral specimen for anisotropy. The urethra from a female mongrel dog was isolated and mounted into a system where it was placed under static pressure and length was measured. The study reported that the circumferential components were stronger than the longitudinal ones, making the urethra anisotropic [140]. This study, however, failed to

maintain in-vivo length and reported that samples retracted an average of 4.7% following isolation, which could contribute to the tissues response to increases in pressure.

More recently, several studies from our laboratory have assessed the ex-vivo biomechanical characteristics of the urethra in both a healthy and various diseased states [53, 54, 101, 141, 142]. These studies all used a modified ex-vivo system to assess pressure-diameter relationships at various locations along the length of a rat urethra [53, 101, 142, 143]. A study on healthy urethras reported that the proximal portion of the tissue was the most compliant at low pressures, followed by middle and distal portions, respectively. This study also reported on the presence of smooth muscle tone, both smooth and striated muscle contraction and relaxation in response to various chemical agents [142]. Further studies explored the biomechanical contributions of each muscle component to urethral function at the middle portion of the urethra. It was reported that the striated muscle only contributed one third of that of the smooth muscle to force generation and acted for a shorter period of time [143]. Another study assessing the affects of VD on urethral biomechanics reported that VD increased compliance of the proximal urethra, stiffness of the distal portion and altered basal tone [54]. Diabetes, induced by streptozotocin, increased stiffness and altered urethral response to contractile or relaxation agents [101].

It has been well established that an ineffective continence mechanism is accompanied by damage to both the muscular and ECM components of the urethra in **Sections 1.2** and **1.6**. This damage alters the mechanical properties of the urethra, decreasing its ability to contract and resist increases in pressure. Therefore, the most effective treatment would be one that targeted both the functional and structural damages by providing both support and contraction to the urethra. The use of autologously derived fibrinogen, thrombin and stem cells to create a 3-D support for the urethra would allow the entrapped cells to produce their own ECM and to become

integrated with the native urethra and provide structural support. Utilization of mechanical and/or biochemical stimulation within a bioreactor could enhance the orientation of cells as well as collagen production and even differentiation to a contractile smooth muscle phenotype to provide functional support to the urethra as well.

## 1.7 HYPOTHESES AND SPECIFIC AIMS

While efforts have been made to find a treatment for SUI, the current treatments are only satisfactory for short times, or can dissipate due to re-absorption into the body over time. To address this we developed a tissue engineered urethral wrap (TEUW) from fibrin and bone marrow progenitor cells, to provide mechanical and functional support to the diseased urethra. This study utilizes both a custom-designed bioreactor culture system, to provide chemical and/or mechanical stimulation to 3-D TEUWs, as well as an ex-vivo testing system, to determine the mechanical properties of TEUWs following bioreactor culture and/or urethral samples following implantation of a TEUW. Biomechanical data were compared to micro-structural and immunohistochemical analyses. The hypotheses and specific aims corresponding are as follows:

**Hypothesis 1:** A living, functional, smooth muscle-populated tubular construct can be fabricated in-vitro by mechanically and/or biochemically stimulating bone marrow derived progenitor cells (BMPCs) within a natural biological matrix.

**Specific Aim 1** (addresses **Hypothesis 1**): To fabricate a living, functional smooth muscle populated tubular construct from BMPCs and a natural biological matrix that is suitable for implantation as a TEUW. This will be achieved by determining the in-vitro stimulation

regimen - chosen from carefully-chosen combinations of mechanical strain and biochemicals - that yield optimal histological, functional and biomechanical properties.

**Hypothesis 2:** A TEUW can be successfully implanted and will reverse the short-term changes in mechanical and functional properties of the urethra found in a rat model of SUI.

**Specific Aim 2** (addresses **Hypothesis 2**): To assess a TEUW composed of the BMPC-derived SMC-populated constructs from Specific Aim 1. Assessments will include both in-vitro and in-vivo analyses, using histological, functional, biomechanical and immunological endpoints. Results will be compared with normal and diseased native urethra, as well as a TEUW constructed using isolated urethral SMCs.

In order to appropriately develop our TEUW, changes to urethral properties due to common risk factors were first assessed (**Chapter 2.0**). To differentiate the stem cells within our TEUWs, an appropriate seeding density and compaction culture duration were determined (**Chapter 4.0**) prior to development of a bioreactor capable of providing the desired mechanical and/or chemical stimuli (**Chapter 5.0**) for differentiation of BMPCs to contractile SMCs in 3-D. In order to verify that the TEUW is capable of acting as a urethral support both structurally and functionally, an analysis of its mechanical and phenotypic properties was necessary (**Chapter 6.0**). Next, verification of our in-bred animal model was necessary and performed against a commonly used out-bred rat strain (**Chapter 3.0**). To understand the structural and functional effect of the TEUW on the native urethra, in-vivo studies were performed and specimens analyzed mechanically to provide insight into the contribution of the TEUW to the native tissue as well as how the diseased tissue differs from that of controls (**Chapter 7.0**). Distinguishing

which components are most influenced may help to provide insights to using a TEUW as a treatment for SUI.

## **2.0 EFFECTS OF OVARIECTOMY ON THE MECHANICAL CHARACTERISTICS OF THE FEMALE RAT URETHRA**

### **2.1 SIGNIFICANCE OF OVARIECTOMY ON URETHRAL FUNCTION**

There are many contributing factors to the onset of SUI. Seventy percent of women report symptoms of SUI following menopause [144]. Menopause causes many changes to a woman's body, including decreased levels of estrogen and progesterone. Estrogen provides increased periurethral resistance and  $\alpha$ -adrenoreceptor activity in the urethral smooth muscle through the large number of receptors in the proximal urethra [145]. Following estrogen deficiency from menopause, it is common for women to develop urinary disorders such as frequency, urgency and incontinence [36, 144]. Although estrogen plays an important role in the maintenance of continence, the use of hormone therapy as a treatment for SUI has shown mixed results [36].

In order to better assess the role of estrogen in urinary continence, an ovariectomized animal model is used. The ovariectomy model causes estrogen deficiency by the bilateral removal of the ovaries. While numerous studies have assessed the effects of estrogen deficiency or therapy on the LPP, voiding pattern and innervations of the ovariectomized urethra with and without VD [36, 49, 50], none have assessed the effects on the mechanical properties of the urethra.

Assessment of the urethral closure mechanisms in-vivo as well as the biomechanical characteristics following ovariectomy can provide insight on the role of estrogen in maintaining continence and aid in the development and initiation of new and better treatments for urinary dysfunction following menopause.

## 2.2 METHODS

### 2.2.1 Animals

Adult, female, virgin Sprague-Dawley rats (200-250 g) (Hilltop Lab Animals, Inc., Scottsdale, PA) were used in this study. Animals were housed at the University of Pittsburgh under the supervision of the Department of Laboratory Animal Resources. The policies and procedures for the animal studies are in accordance with those detailed in the Guide for the Care and Use of Laboratory Animals, published by the US Department of Health and Human Services. Procedural protocols were approved by the University of Pittsburgh's Institutional Animal Care and Use Committee.

### 2.2.2 General Surgical Procedures

Animals were divided into three groups (**Figure 2.1**): ovariectomy (Ov), sham and control. At day 0, under 4% isoflurane anaesthetic, Ov animals received a midline incision and two longitudinal muscle incisions through which the fallopian tubes and ovarian branch of the uterine artery were exposed and ligated, followed by removal of both ovaries [50]. Sham animals

received the incisions and manipulation of the internal space without ovary removal and controls received no procedures at all.

Six weeks later (**Figure 2.1**), animals were assessed for urethral response to sneeze (see **Section 2.2.3**), maximum intravesical pressure during sneeze (MIPS; see **Section 2.2.4**), and urethral ex-vivo mechanical properties (see **Section 2.2.5**). Rats were anesthetized by 4% isoflurane inhalation, and the bladder was exposed via a midline incision. Ligation of both ureters was performed to prevent migration of urine into the bladder, which could alter intravesical pressure readings. The colon was cleared of feces through a small incision. Following all surgical procedures, isoflurane anesthetic was discontinued and replaced with urethane anesthetic (1.2 g/kg, subcutaneous, Sigma, St. Louis, Mo.). Additional doses of anesthetic were administered intravenously, as required, during experimentation.

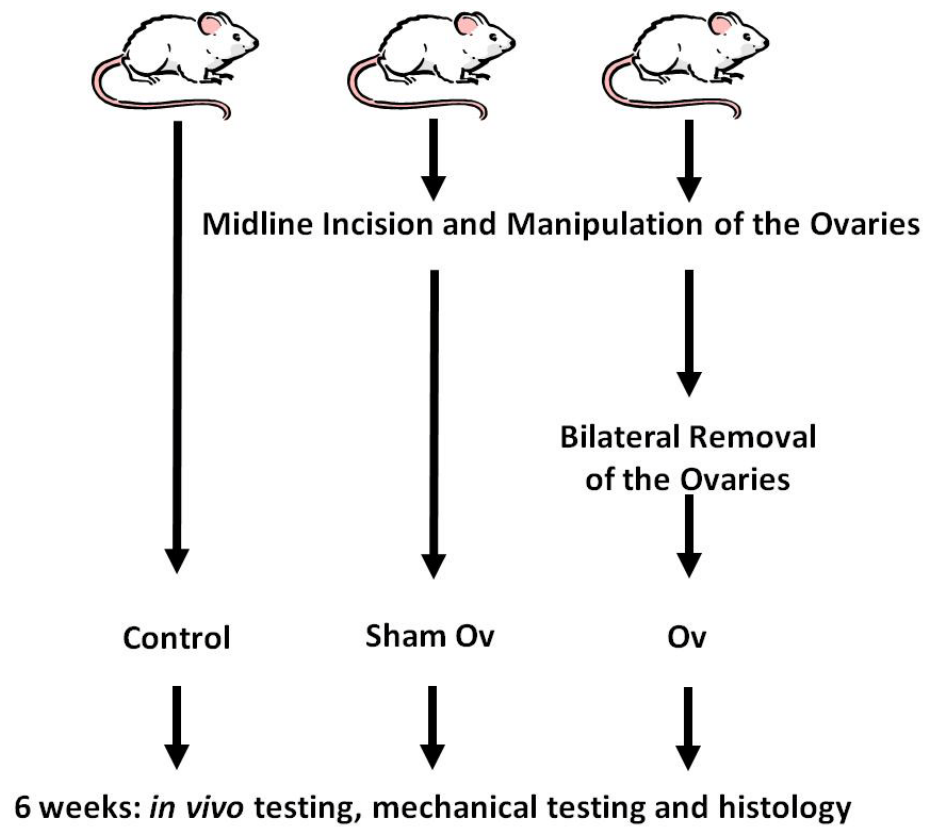


**Figure 2.1** Schematic of the experimental design.

### 2.2.3 Urethral Response During Sneeze

All groups were subjected to sneeze testing as previously reported [146, 147]. Briefly, bladders were manually emptied by compression and a catheter, with a side-mounted microtransducer, (SPR-524, Millar Instruments, Houston, TX) was inserted into the urethra via the external orifice. The sensor was positioned at the middle urethra on the inner urethral surface, based on previous studies. To evaluate the intensity of the induced sneeze, which varied with each sneeze event, pressure increases in abdominal pressure ( $P_{abd}$ ) during sneezing were also measured via an intra-abdominal balloon catheter. The sneeze reflex was induced by inserting a cut whisker into the animal's nostril. Prior to and following initiation of the sneeze, urethral baseline pressure (UBP) and  $P_{abd}$  were measured in  $\text{cmH}_2\text{O}$ . During sneeze, amplitude of the urethral pressure response (A-URS) and  $P_{abd}$  were measured in  $\text{cmH}_2\text{O}$ . The average of at least 10 measurements was taken as the value of each metric for individual rats.

### 2.2.4 MIPS

All groups were subjected to MIPS testing as previously reported [148]. Briefly, a catheter (PE-90) connected to a pressure transducer (Transbridge 4M, World Precision Instruments, Sarasota, FL) was inserted into the bladder to measure intravesicle pressure. While in the supine position, bladders were emptied by manual pressure and filled with 0.4 mL of saline solution containing Evans blue (100  $\mu\text{g}/\text{mL}$ ; Sigma, St. Louis, MO). Intravesical and abdominal pressures were recorded at 400 Hz with data acquisition software (Chart, AD Instruments) on a computer equipped with an analog-to-digital converter (Power Lab, AD Instruments). Sneezing was induced by inserting a cut whisker into the nostril of the animal at least 50 times to achieve

intravesical pressures large enough to cause leakage. The maximum intravesical pressure during sneeze was recorded. If leakage occurred, the lowest pressure to cause leakage was recorded.

### **2.2.5 Biomechanical Testing**

Following MIPS measurements, the urethra was excised and tested as previously described by our group [54, 142, 143]. Briefly, PE-50 tubing (Becton-Dickson, Franklin Lakes, NJ), was inserted through the urethra into the dome of the bladder. The bladder dome, as well as the external urethral meatus, was ligated to the catheter with 4-0 silk suture (Syneture, Mansfield, MA). The ureters were ligated and served as anatomical landmarks for the maintenance of in vivo length during mechanical testing. The urethra was then separated from the surrounding tissues and placed in cold, oxygenated Media 199 (Sigma-Aldrich, St. Louis, MO), containing antibiotic/antimycotic and L-glutamine (Invitrogen, Carlsbad, CA) to prevent hypoxia of the tissue.

The urethra was mounted onto stainless steel cannulae within a bathing chamber filled with Media 199 and kept at physiologic conditions via a circulation loop and gaseous mixture of 95% O<sub>2</sub> and 5% CO<sub>2</sub>. A calibrated hydrostatic reservoir was used to increase intraluminal pressure from 0-20 mmHg in 2 mmHg increments. Outer diameter and pressure were continuously measured during over the duration of the experiments. Due to the heterogeneity of the urethra, measurements were taken at proximal, middle, and distal segments along its length [54, 142]. Samples were assessed in both baseline (without pharmacological agents) and passive (3 mM EDTA) conditions.

## 2.2.6 Histology

Following each experiment, urethras were placed into 4% paraformaldehyde (Fisher, Pittsburgh, PA) followed by 30% sucrose. Urethras were divided into proximal, middle, and distal portions, each portion was cut in half, and each half processed into 10  $\mu\text{m}$  paraffin or frozen sections. Paraffin sections were dewaxed, rehydrated with an ethanol series, and stained with Lillie's-modified Masson's trichrome, hematoxylin and eosin (H&E), and picosirius red (PSR).

## 2.2.7 Mechanical Characteristics

Inner diameters of tested urethras were estimated for proper calculation of various mechanical parameters [54]. Paraffin sections stained for Lillie's-modified Masson's trichrome were imaged as described above and used for thickness assessment.

Images were imported to Scion Imaging software (version 4.0.3.2, Scion, Frederick, MD) for quantification of the specimen radial thickness (50 to 60 measurements per cross-section). The average of thickness measurements from 3 to 4 cross-sections per specimen was used as the thickness for that specimen. Assuming incompressibility and constant length during testing, the inner diameter at zero pressure was calculated by subtracting twice the average thickness from the measured outer diameter. The inner radius at all other pressures was calculated as [53]:

$$R_{i,P} = \sqrt{R_{o,P}^2 - R_{o,P0}^2 + R_{i,P0}^2} \quad (1)$$

Here,  $R_{i,P}$  and  $R_{o,P}$  are the inner and outer radii at any applied pressure,  $P$ , and  $R_{i,P0}$  and  $R_{o,P0}$  are the inner and outer radii at zero pressure. Compliance ( $C$ ), a measure of the distensibility of a tube, was calculated from measurements within 0 to 20 mmHg as [53]:

$$C = \frac{ID_{\max} - ID_{\min}}{ID_{\max} (P_{\max} - P_{\min})} \quad (2)$$

where  $ID_{\max}$  is the inner diameter at maximum pressure ( $P_{\max}$ ), and  $ID_{\min}$  is the inner diameter at minimum pressure ( $P_{\min}$ ) [53]. As compliance is a linear measure and our pressure diameter curves are non-linear, it was calculated over each applied pressure increment. To assess the mechanical properties over the full range of intraluminal pressures, beta stiffness ( $\beta$ ) was calculated as:

$$\beta = \frac{\ln\left(\frac{P}{P_{10}}\right)}{\left(\frac{ID}{ID_{10}} - 1\right)} \quad (3)$$

where  $P_{10}=10$  mmHg (the midpoint) and  $ID_{10}$  is the corresponding inner diameter diameter [53].

### 2.2.8 Statistics

Data is represented as the average  $\pm$  standard error of the mean. Excessively large sneezes, which induced increases in  $P_{\text{abd}}$  greater than two standard deviations above the average, or very small sneezes, which induced increases in  $P_{\text{abd}}$  less than 3 cmH<sub>2</sub>O, were excluded from data analyses. The values of the A-URS and UBP as well as increases in  $P_{\text{abd}}$  during sneezing were averaged in each rat. The average of each group of animals was then calculated from the averaged value in each rat. Statistical comparisons were performed using a Student's t-test. Significance was detected at p-values less than 0.05.

## 2.3 RESULTS

### 2.3.1 Urethral Response During Sneeze

Ov rats had a significantly lower A-URS and UBP than both control and sham groups, which had similar A-URS and UBP values (**Figure 2.2**). The  $\Delta P_{abd}$  was similar for all groups [149].

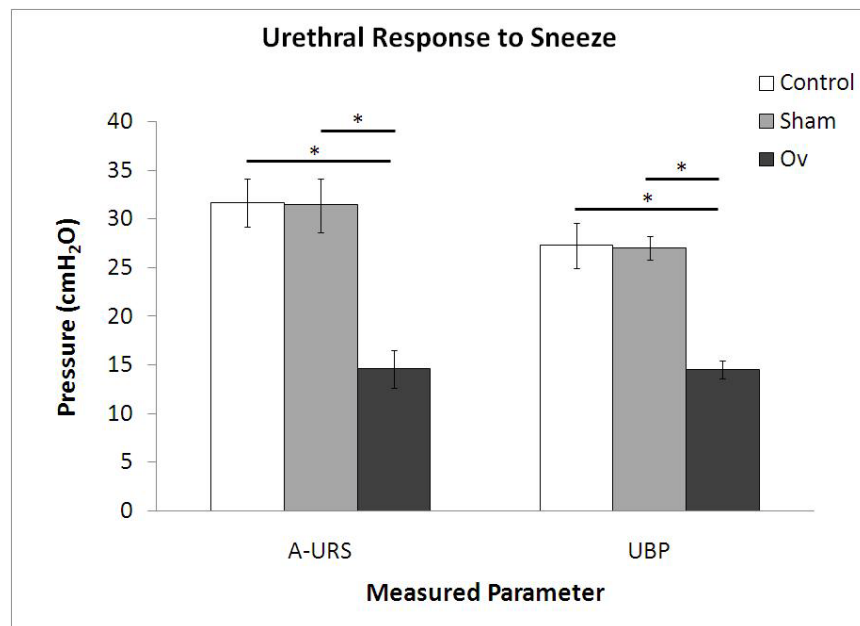


**Figure 2.2** Active urethral response to sneeze (A-URS) and urethral baseline pressure (UBP) for control (n=7), sham (n=12) and Ov (n=12) groups. Values are shown as average  $\pm$  SEM. \*p<0.05.

### 2.3.2 Maximum Intravesical Pressure During Sneeze

Animals receiving ovariectomy had a significantly lower MIPS than controls (**Figure 2.3**) [149]. Although the Ov animals had a lower MIPS than shams (**Figure 2.3**), they did not quite reach significance ( $p = 0.07$ ) [149]. During sneeze, no animals from either the control or sham groups had visible leakage from the urethral orifice, however, five out of the eight (62.5%) Ov animals did leak during sneeze. The Ov animals that leaked had an average MIPS of  $71.5 \pm 8.18$  cmH<sub>2</sub>O, while those that did not had an average of  $65.7 \pm 3.25$  cmH<sub>2</sub>O (**Figure 2.4**,  $p=0.62$ ) [149].

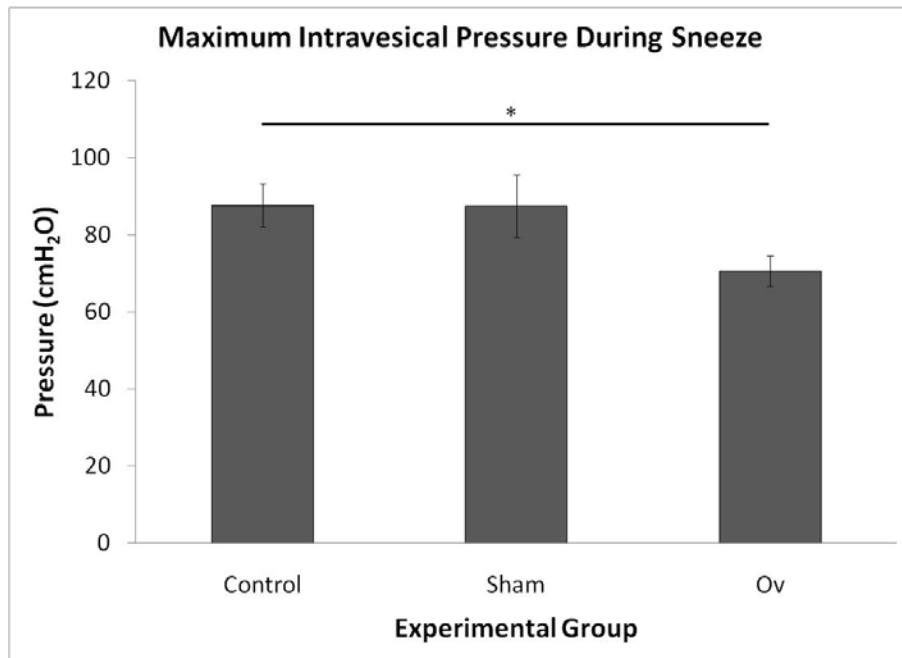


**Figure 2.3** MIPS results for control (n=6), sham (n=6) and ovariectomy (n=8) groups. Values are shown as average  $\pm$  SEM. \* $p < 0.05$ .

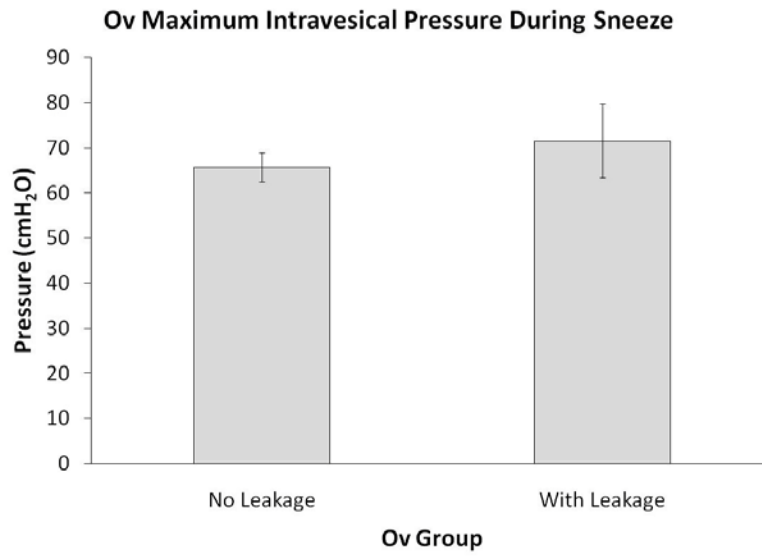


**Figure 2.4** MIPS results for ovariectomy (n=8) animals that did (n=5) and did not (n=3) leak. Values are shown as average  $\pm$  SEM.

### 2.3.3 Ex-Vivo Mechanical Analysis

Pressure-diameter curves show a trend towards an increasing compliance in the proximal and middle urethral portions with a gradient from controls to Ov animals in both the baseline and passive states (**Figure 2.5A-B**, **Figure 2.6A-B**). Control and Ov distal portions had similar pressure-diameter curves, shifted to the right of the sham group (**Figure 2.5C**, **Figure 2.6C**), indicating that they are more compliant than the sham group. An increasing gradient in baseline compliance from control to Ov rats in the proximal (low and overall pressure ranges) and middle (low, middle and overall pressure ranges) portions of the urethra is shown in **Table 2.1**. There is also an increasing gradient in passive compliance from control to Ov rats in the proximal (low, middle and overall pressure ranges) and middle (low and overall pressure ranges) portions of the urethra, with a decreasing gradient in both the proximal and middle portions at high pressure

ranges (**Table 2.2**). The sham distal urethra had compliance values significantly lower than the control urethra at both low (0-6 mmHg) and overall (0-20 mmHg) pressure ranges in the passive state (**Table 2.2**). Beta stiffness for the proximal portion of the Ov urethra in the baseline state was significantly lower than the corresponding control portion (**Table 2.1**). There were no significant differences between the sham and Ov groups, although there is a clear trend towards the Ov group having a larger compliance value than the control and sham groups.

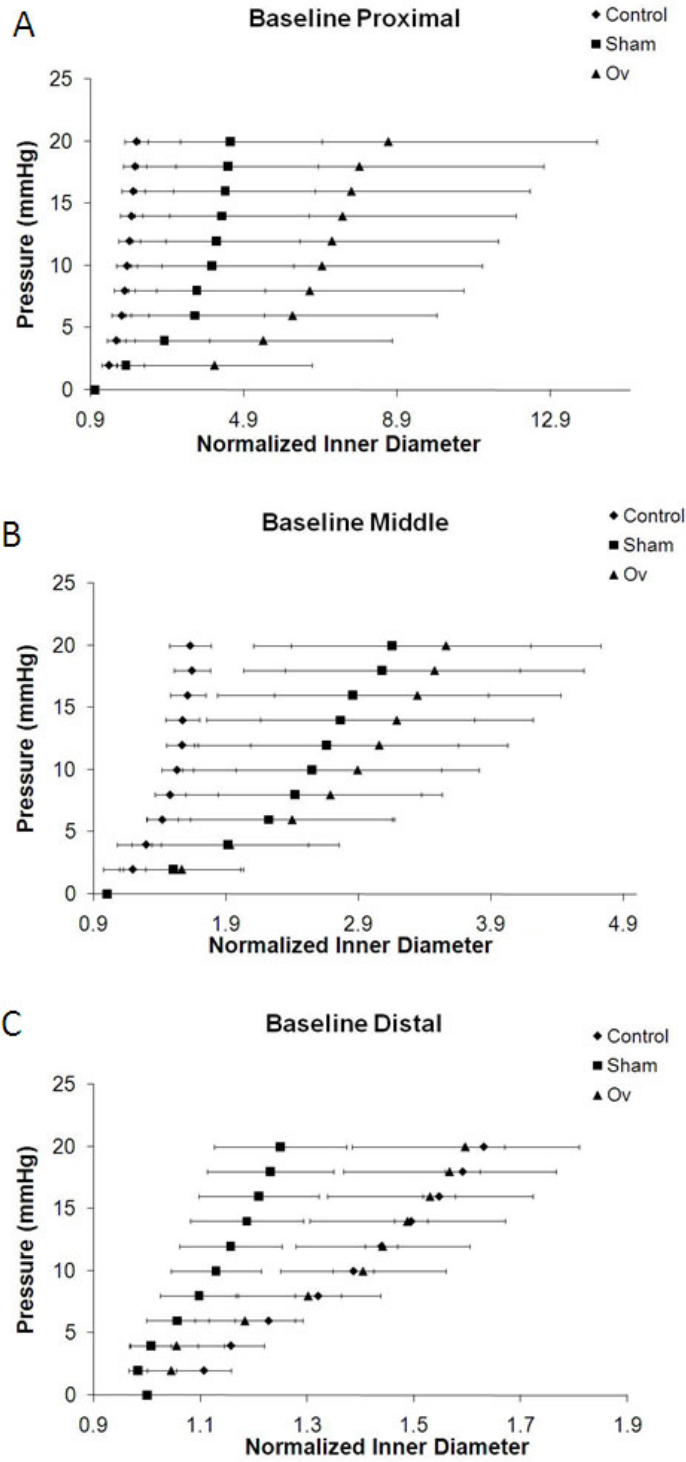


**Figure 2.5** Baseline pressure-diameter curves for (A) proximal, (B) middle and (C) distal portions of control (n=6), sham (n=5) and Ov (n=10) urethras. Values shown as average  $\pm$  SEM.

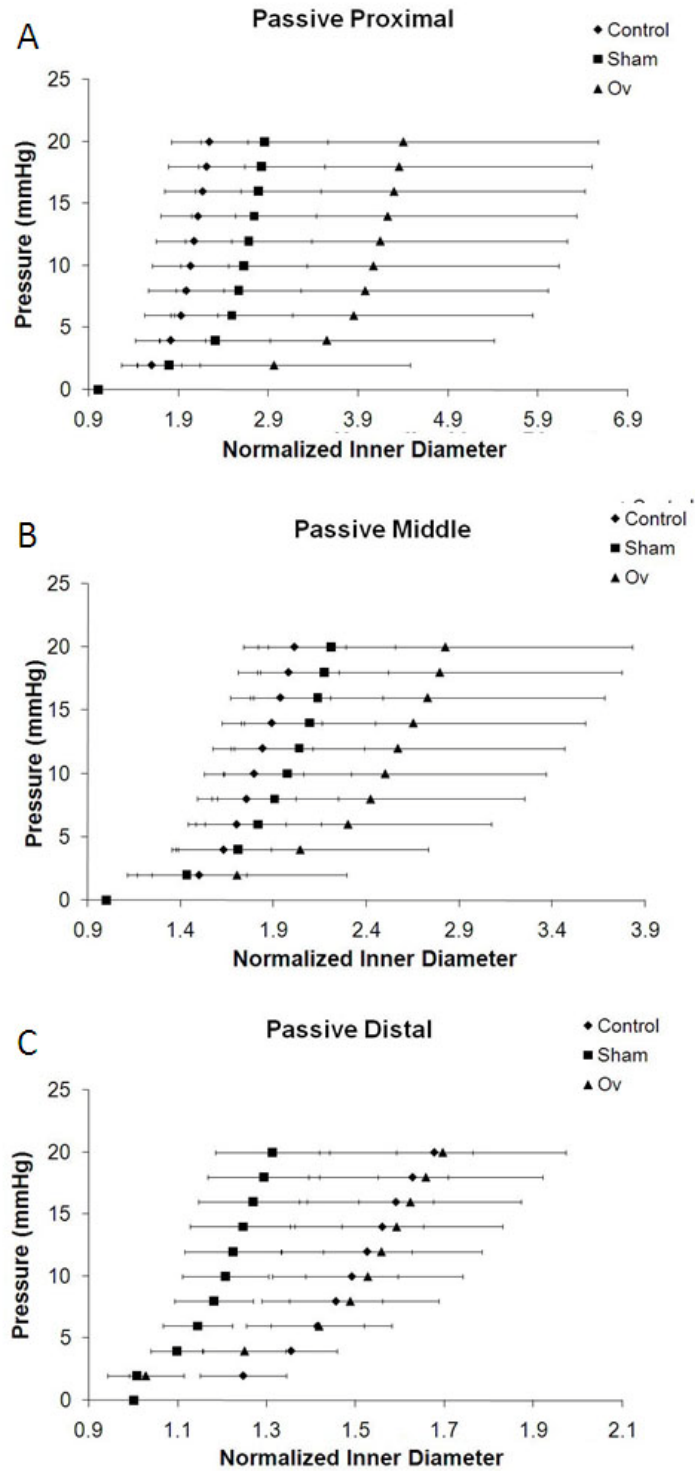


**Figure 2.6** Passive pressure-diameter curves for (A) proximal, (B) middle and (C) distal portions of control (n=6), sham (n=5) and Ov (n=10) urethras. Values shown as average  $\pm$  SEM.

**Table 2.1** Compliance and beta stiffness values for control (n=6), sham (n=5) and Ov (n=10) urethras in baseline conditions. Values are shown as average  $\pm$  SEM. \*p<0.05 compared to corresponding control condition. Red = increasing trends in the proximal portion from control to Ov groups, Green = increasing trends in the middle portion from control to Ov groups and bold = significant differences compared with the corresponding control portion.

Baseline Compliance x 100 (mmHg <sup>-1</sup> )		Low Pressure (0-6 mmHg)	Middle Pressure (6-12 mmHg)	High Pressure (12-20 mmHg)	Overall Pressure (0-20 mmHg)	Beta Stiffness
Control	Proximal	11.80 $\pm$ 4.22	1.95 $\pm$ 0.53	1.20 $\pm$ 0.23	5.46 $\pm$ 1.53	8.04 $\pm$ 2.17
	Middle	6.97 $\pm$ 1.93	1.80 $\pm$ 0.28	0.51 $\pm$ 0.80	3.15 $\pm$ 0.79	5.81 $\pm$ 1.13
	Distal	3.79 $\pm$ 1.06	3.10 $\pm$ 1.01	1.67 $\pm$ 0.29	3.15 $\pm$ 0.19	6.11 $\pm$ 1.12
Sham	Proximal	20.36 $\pm$ 15.45	4.04 $\pm$ 1.77	2.78 $\pm$ 1.46	10.75 $\pm$ 5.24*	5.76 $\pm$ 1.14
	Middle	20.36 $\pm$ 15.45	4.04 $\pm$ 1.77	2.78 $\pm$ 1.46	10.75 $\pm$ 5.24	4.54 $\pm$ 1.00
	Distal	0.94 $\pm$ 0.97	1.49 $\pm$ 0.57	0.94 $\pm$ 0.26	1.25 $\pm$ 0.62	10.30 $\pm$ 2.47
Ov	Proximal	86.24 $\pm$ 65.63	3.26 $\pm$ 0.48	1.49 $\pm$ 0.30	35.60 $\pm$ 25.83	3.66 $\pm$ 0.70*
	Middle	23.29 $\pm$ 13.47	4.48 $\pm$ 1.01	1.89 $\pm$ 0.34	12.79 $\pm$ 6.12	4.43 $\pm$ 0.82
	Distal	3.06 $\pm$ 1.64	3.40 $\pm$ 1.20	1.13 $\pm$ 0.26	2.98 $\pm$ 1.12	7.30 $\pm$ 1.54

**Table 2.2** Compliance and beta stiffness values for control (n=6), sham (n=5) and Ov (n=10) urethras in passive conditions. Values are shown as average  $\pm$  SEM. \*p<0.05 compared to corresponding control condition. Red = increasing trends in the proximal portion from control to Ov groups, Green = increasing trends in the middle portion from control to Ov groups and bold = significant differences compared to the corresponding control portion.

Passive Compliance x 100 (mmHg <sup>-1</sup> )		Low Pressure (0-6 mmHg)	Middle Pressure (6-12 mmHg)	High Pressure (12-20 mmHg)	Overall (0-20 mmHg)	Beta Stiffness
Control	Proximal	15.41 $\pm$ 6.80	1.38 $\pm$ 0.31	1.17 $\pm$ 0.28	6.20 $\pm$ 2.12	9.22 $\pm$ 2.73
	Middle	11.68 $\pm$ 4.37	1.45 $\pm$ 0.26	1.24 $\pm$ 0.35	5.06 $\pm$ 1.38	8.52 $\pm$ 1.33
	Distal	6.90 $\pm$ 1.76	1.39 $\pm$ 0.28	1.31 $\pm$ 0.23	3.39 $\pm$ 3.39	8.72 $\pm$ 1.57
Sham	Proximal	24.79 $\pm$ 11.28	1.59 $\pm$ 0.44	1.13 $\pm$ 0.43	9.27 $\pm$ 3.53	6.40 $\pm$ 1.54
	Middle	13.62 $\pm$ 5.64	2.20 $\pm$ 0.85	1.21 $\pm$ 0.35	6.06 $\pm$ 1.71	7.39 $\pm$ 1.70
	Distal	2.40 $\pm$ 1.30*	1.07 $\pm$ 0.58	0.86 $\pm$ 0.20	1.56 $\pm$ 0.64*	4.07 $\pm$ 5.48
Ov	Proximal	47.46 $\pm$ 28.24	1.95 $\pm$ 0.00	0.98 $\pm$ 0.31	17.00 $\pm$ 9.25	6.42 $\pm$ 0.91
	Middle	23.74 $\pm$ 12.24	1.50 $\pm$ 0.29	1.11 $\pm$ 0.29	9.82 $\pm$ 4.80	8.19 $\pm$ 1.91
	Distal	6.95 $\pm$ 2.48	1.37 $\pm$ 0.34	0.99 $\pm$ 0.19	3.48 $\pm$ 1.21	9.32 $\pm$ 2.02

## 2.4 DISCUSSION

Mid-urethral response to sneeze was significantly affected by ovariectomy. Ov rat UBP and A-URS were significantly lower than both control and sham groups (**Figure 2.2**), indicating changes to either the neural or muscular components [148]. Ov MIPS values were also significantly lower than controls (**Figure 2.3**), with over 60% of Ov rats leaking during sneeze, while neither control nor sham animals leaked. Both proximal and middle portions of the Ov urethra showed trends towards an increased compliance over both control and sham groups in both the baseline and passive states (**Figure 2.5** and **Figure 2.6**), although not significantly.

Previous studies showed no effects of ovariectomy on urethral function up to four weeks following creation of the model [37, 49, 50]. However, we have assessed both short (3 weeks) and longer (6 weeks) time points and found that although the urethral response to sneeze may be impaired early on, SUI is not induced until later [149]. Sievert *et al.*, assessed urethral leakage during stress and reported that delivery alone or delivery followed by Ov (4 weeks postpartum) produced the same number of incontinent animals (16.7%) 8 weeks postpartum [49]. Our laboratory has reported that although there was a decreased urethral response in virgin rats 3 weeks following ovariectomy, there was 0% incontinence [149], indicating that the trauma of vaginal delivery and/or distension is the main short-term contributor to SUI. While Sievert *et al.*, reported an increased percentage of incontinence with the addition of vaginal distension immediately following delivery (58.3%) or vaginal distension plus Ov (4 weeks postpartum; 72.7%) [49], our laboratory has shown incontinence in over 60% of virgin rats 6 weeks following ovariectomy [149], showing the isolated effects of estrogen deficiency on urethral function and maintenance of continence.

To our knowledge, there have been no other reports on the ex-vivo biomechanical effects of ovariectomy on the urethra. However, there have been several reports on how SUI [53, 54] and diabetes [101] alter urethral biomechanics. Knowledge of how various conditions alter the mechanical properties of the urethra can provide valuable information for the development of new and effective treatments. Although we expected to see no difference between sham and control groups, the trend towards an increased compliance in proximal and middle urethral portions of shams (**Table 2.1** and **Table 2.2**) could be due to damage of the pudendal nerve during internal manipulation to create the sham ovariectomy model, which has previously been reported [150]. As pudendal nerve transaction/crush is a commonly used model of SUI [56, 61, 147], it is possible that damage during sham surgeries contributed to increased urethral compliance.

The gradient of increasing compliance from controls to Ov animals in the baseline state (**Table 2.1**) indicates that the muscular components of the urethra have been compromised. Since it has previously been reported that estrogen levels do not influence the size of urethral muscle fibers [151], the increase in compliance following ovariectomy may be a result of altered contractile machinery. Sievert *et al.*, reported decreased urethral levels of caveolin-1 (in smooth muscle) and -3 (in striated muscle) following delivery and ovariectomy compared to virgins [49]. Caveolins are membrane proteins thought to be restricted to muscle tissues and to contribute to calcium homeostasis [152]. Caveolins are involved in several signalling pathways and a defect in the caveolin gene can result in muscular dystrophy [152]. While, Sievert *et al.*, observed a similar decrease of caveolin-1 in animals receiving vaginal dilation or vaginal dilation and ovariectomy following delivery, the level of caveolin-3 was lowest in animals which received only ovariectomy following delivery [49], indicating that the trauma of vaginal distension may

damage the contractile ability of urethral smooth muscle, while estrogen deficiency damages the striated sphincter, which provides the main mechanism for maintaining continence. It is also possible that the trauma of childbirth activates a repair mechanism that altered hormone levels alone do not.

The gradient increase in low pressure compliance from shams to Ov animals in the passive state in this study is similar to trends seen in the comparison of control and vaginally distended rats [53]. The study of vaginal distension also reported significantly more collagen in the middle portion of the diseased urethra per cross-sectional area via trichrome staining, but significantly less from a biochemical assay. The study also reports significantly more elastin in the vaginally distended urethra than in controls [53], all of which could contribute to the changes in mechanical properties. Previous studies have reported decreases in the number of blood vessels within the submucosal layer of the urethra and collagen-I, which provides structural support and rigidity to the urethral wall, following ovariectomy [145, 153]. Increased collagen-III, which provides elasticity to the urethra, has also been reported following ovariectomy [153]. These changes in extracellular proteins are further supported by the increased passive compliance in Ov animals seen in **Table 2.2**. The large amount of variability in ovariectomy mechanical data could be a result of the variable leakage response to sneeze. SUI has previously been shown to increase urethral compliance [53] making it plausible that the high variability of SUI in Ov rats also causes a large variability in the mechanical properties of those urethras.

Although this study provided evidence that estrogen deficiency alone has a large role in proper urethral function and the maintenance of continence, further analyses should be performed. This study was designed to focus solely on the effect of estrogen on urethral response, and we acknowledge that utilizing virgin rats limits our correlation to human clinical

relevance. Increasing the n value for sham animals could decrease data variability and help to more clearly identify differences in mechanical behaviour. Further studies, assessing the same urethral responses, in retired breeders, are currently underway. An assessment of pudendal nerve damage, such as staining for a neuronal marker such as PGP 9.5 in the middle urethra, in sham rats could also be performed to explain the large amount of variability in our mechanical data. Quantification of the urethral ECM and muscular components at both 3 and 6 weeks following ovariectomy would also provide further support of the differences in mechanical properties seen in this study. Another limitation of this work could be a lack of uniformity in the thickness measurements around the circumference of the urethra, which were used to calculate all mechanical parameters. We did see a minimal variation in thickness measurements within each section and portion. For example, thickness measurements from a Sham urethra were as follows: one proximal tissue section had an average thickness of  $0.2523 \pm 0.0333$  mm, while an average of the proximal portion (from four tissue sections) was  $0.2401 \pm 0.0043$  mm. The average for the middle portion was  $0.3590 \pm 0.0016$  mm and  $0.3623 \pm 0.0070$  mm for the distal portion

Although many factors such as childbirth and nerve injury contribute to the development of SUI, symptoms may not appear until years following the injury. The prevalence of SUI increases with age and onset commonly occurs following menopause, indicating a potential hormonal role in the continence maintaining mechanism. Estrogen has been shown to significantly contribute to the stability and regrowth of neuronal fibers [150], and loss of estrogen is associated with a higher incidence of SUI [36, 37, 49]. Therefore, it is possible that estrogen aids the body in compensating for a damaged continence mechanism. Since differences in urethral function following ovariectomy are observed without urethral trauma, the role of estrogen in urinary continence warrants further analysis.

This work provides evidence that estrogen deficiency alone affects both the smooth and striated muscle response under stress conditions. We have also shown that muscular and extracellular matrix components are less resistant to increases in pressure in both the proximal and middle portions of the ovariectomy urethra, indicating that estrogen plays an important role in the continence mechanism. Knowing how the mechanical properties of the urethra change following menopause may aid in the development of preventative treatments for SUI in premenopausal women.

### **3.0 STRAIN DEPENDENCY OF URETHRAL FUNCTIONAL AND MECHANICAL PROPERTIES IN THE RAT**

Over the past decade therapies and various treatments for stress urinary incontinence [154] have emerged, including injection of bulking agents [29], placement of synthetic slings [154], electrical stimulation [155] and the injection of stem cells [64, 156-158]. As technology advances and more cell-based therapies are developed, it is imperative that these treatments are tested in an appropriate animal model.

To date, the majority of lower urinary tract studies have been performed in the Sprague-Dawley (SD) rat [35, 54, 64, 141, 148], since the structure of the rat urethra is very similar to that of humans [159]. This out-bred, all-purpose strain is used in many areas of research [160]. However, as cellular treatments progress, a new model may be more appropriate for the initial validation of the treatment. Utilization of in an in-bred animal would allow for fine tuning of the therapy in a more controlled in-vivo study, without increased variability from genetic variation, or immune responses by the test animal. The Lewis rat, an in-bred strain, is generally used in immunological and stem cell research studies and could serve as a better model for investigating possible stem cell therapies to be used in the lower urinary tract [160]. To this end, the lower urinary tract properties and response to urethral dysfunction would need to be verified in the Lewis rat.

The purpose of this portion of the dissertation work was to verify the Lewis rat as a model of SUI by pudendal nerve transection for cellular based thereapies, by comparing it to the commonly used SD rat.

## **3.1 MATERIALS AND METHODS**

### **3.1.1 Animals**

Adult, female, SD and Lewis rats (200-250 g) (Hilltop Lab Animals, Inc., Scottdale, PA) were used in this study. Animals were housed at the University of Pittsburgh under the supervision of the Department of Laboratory Animal Resources. The policies and procedures for the animal studies are in accordance with those detailed in the *Guide for the Care and Use of Laboratory Animals*, published by the US Department of Health and Human Services. Procedural protocols were approved by the University of Pittsburgh's Institutional Animal Care and Use Committee.

### **3.1.2 Overview of Experiments**

Five types of experiments were performed. *Experiment 1* evaluated, in SD and Lewis rats, the effects of SUI induced by bilateral pudendal nerve transection on the leak point pressure (LPP), a common in-vivo measure of urethral function [146, 157]. *Experiment 2* compared the contribution of the striated sphincter to the continence mechanism in SD and Lewis rats using a specific inhibitor of skeletal muscle activity. *Experiment 3* assessed common functional indices of the urethra during sneezing in continent SD and Lewis rats. *Experiment 4* utilized our ex-vivo

urethral testing system [54, 141, 142] to assess the mechanical properties of SD and Lewis urethras. *Experiment 5* evaluated the ex-vivo functional response of both SD and Lewis urethras to smooth and striated muscle agonists. Each experiment, as well as methodology common to them, are detailed below.

### 3.1.3 Surgical Procedures

The SUI group for each strain in *Experiment 1* was created by anesthetizing the animal with 4% isoflurane, and then transecting the pudendal nerves bilaterally using aseptic, surgical techniques [147]. Since this common model for SUI [161, 162] utilizes complete transection of the nerve, it provides an immediate effect. However, animals were assessed one week following nerve transection.

For all experiments, rats were anesthetized by isoflurane inhalation, and the bladder was exposed via a midline incision. Ligation of both ureters was performed to prevent flow of urine into the bladder, which could alter intravesical pressure readings. The colon was cleared of feces through a small incision. Following all surgical procedures, isoflurane anesthetic was discontinued and replaced with urethane anesthetic (1.2 g/kg, subcutaneous, Sigma, St. Louis, Mo.). Additional doses of anesthetic were administered intravenously, as required, during experimentation.

For *Experiments 1 and 2*, a catheter (PE-90) was inserted into the bladder dome for recording of intravesical pressure and then the spinal cord was transected at the T9-T10 level after laminectomy. A sterile sponge (Gelfoam, Upjohn, Kalamazoo, Mich.) was placed between the cut ends of the spinal cord and the overlying muscle and skin were sutured closed. Spinal transection eliminates the voiding reflex mediated by spinobulbospinal pathways, but still allows

spinal urethral contractile reflexes via sympathetic and somatic nerves to remain active during bladder filling. In addition, for *Experiment 2*, catheters were placed in the carotid artery (PE-50) to measure blood pressure, in the jugular vein (PE-10) for administration of intravenous drugs, and in the trachea (PE-160) for artificial respiration. A small balloon-catheter was inserted into the abdominal cavity via the rectum and connected to a pressure transducer to record abdominal pressures ( $P_{abd}$ ) during *Experiment 3*.

#### **3.1.4 Experiment 1: Effects of SUI on Sprague-Dawley and Lewis Rat Leak Point Pressure (LPP).**

Continent and SUI rats from each strain were compared. One week following creation of the SUI model, the LPP was assessed in each animal using the vertical tilt table method (V-LPP) [64]. Briefly, rats were mounted onto the tilt table, and the bladder catheter was attached to a pressure reservoir and a pressure transducer (BLPR, World Precision Instruments, Sarasota, Fla.) via a 3-way stopcock. Intravesical pressure was increased in 2 cmH<sub>2</sub>O increments until leakage was visible, while data was recorded with Chart<sup>TM</sup> software (AD Instruments, Castle Hill, NSW, Australia) on a computer with a PowerLab<sup>®</sup> analog-to-digital converter. The measure was repeated a minimum of 2 times. The average of the measurements was taken as the V-LPP for that animal.

#### **3.1.5 Experiment 2: Contribution of the Striated Sphincter to the Continence Mechanism**

Continent SD and Lewis rats were prepared and tested for LPP as described above, but in the supine position (Su-LPP) as vertical positioning caused a significant decrease in blood pressure

following intravenous injections of alpha-bungarotoxin, a neuromuscular blocking agent. Following initial Su-LPP testing, animals were injected with divided doses of 333  $\mu\text{g}/\text{kg}$  alpha-bungarotoxin dissolved in sterile saline at 10 minute intervals, and tested for Su-LPP again. Animal respiration was maintained by a ventilator (3.5 mL/stroke, 80 strokes/min) following injection of alpha-bungarotoxin [163].

### **3.1.6 Experiment 3: Assessment of Urethral Response During Sneeze**

Continent SD and Lewis rats were subjected to sneeze testing as previously reported [148] and as described in **Section 2.2.3**. Briefly, bladders were emptied and a catheter with a side-mounted microtransducer, (SPR-524, Millar Instruments, Houston, TX) was inserted into the urethra via the external orifice. The sensor was positioned at the middle urethra on the inner urethral surface, based on previous studies [146]. The sneeze reflex was induced by inserting a cut whisker into the animal's nostril [148]. Prior to and following initiation of the sneeze, urethral baseline pressure (UBP) and abdominal pressure ( $P_{\text{abd}}$ ) were measured in  $\text{cmH}_2\text{O}$  [148]. During sneeze, amplitude of the urethral pressure response (A-URS) and  $P_{\text{abd}}$  were measured in  $\text{cmH}_2\text{O}$  [148]. The average of at least 10 measurements of each metric was taken as the value for individual rats [146, 148].

### **3.1.7 Experiment 4: Ex-Vivo Biomechanical Analysis**

Following LPP measurements, the urethra was excised and tested as previously described by our group [54, 141, 142] (see **Section 2.2.5**). Briefly, PE-50 tubing (Becton-Dickson, Franklin Lakes, NJ), was inserted through the urethra into the dome of the bladder. The bladder dome, as

well as the external urethral meatus, was ligated around the catheter with 4-0 silk suture (Syneture, Mansfield, MA). The ureters were ligated and served as anatomical landmarks for the maintenance of in-vivo length during mechanical testing. The urethra was then separated from the surrounding tissues and placed in cold, oxygenated media 199 (Sigma-Aldrich, St. Louis, MO), containing antibiotic/antimycotic and L-glutamine (Invitrogen, Carlsbad, CA) to prevent hypoxia of the tissue. Tissue was transported to our testing facility on ice.

The urethra was mounted onto stainless steel cannulae within a bathing chamber filled with media 199 and kept at physiologic conditions via a circulation loop and gaseous mixture of 95% O<sub>2</sub> and 5% CO<sub>2</sub>. A hydrostatic reservoir was used to increase intraluminal pressure from 0-20 mmHg in 2 mmHg increments. Outer diameter and pressure were continuously measured over the duration of the experiments. Due to the heterogeneity of the urethra, measurements were taken at proximal, middle, and distal segments along its length [54, 142]. Samples were assessed in both baseline (without pharmacological agents) and passive (in the presence of 3 mM EDTA) conditions.

### **3.1.8 Experiment 5: Ex-Vivo Functional Analysis**

Urethras isolated from continent animals (see **Section 2.2.5**) from each strain were mounted in our ex-vivo testing system as described in **Section 2.2.5**, and subjected sequentially to: 0 mmHg and 8 mmHg intraluminal pressures, N $\omega$ -nitro-L-arginine (100  $\mu$ M; to remove endogenous nitric oxide synthase activity), phenylephrine (40  $\mu$ M; to assess smooth muscle contraction), acetylcholine (5 mM; to assess striated muscle contraction) and EDTA (3 mM; to inhibit muscular response) as previously described [141]. Each stimulus was followed by a 30 minute

equilibration period, and the outer diameter of the middle portion of the urethra was continuously recorded at 1 Hz.

### **3.1.9 Histology**

Following each experiment, urethras were placed into 4% paraformaldehyde (Fisher, Pittsburgh, PA) followed by 30% sucrose. Urethras were divided into proximal, middle, and distal portions, each portion was cut in half, and each half processed into 10  $\mu\text{m}$  paraffin or frozen sections.

Paraffin sections were dewaxed, rehydrated with an ethanol series, and stained with Lillie's-modified Masson's trichrome, hematoxylin and eosin (H&E), and picosirius red (PSR). Frozen sections were stained for alpha-smooth muscle actin [164] and fast-twitch striated muscle (SKEL; Sigma-Aldrich, St. Louis, MO). Sections were permeabilized with 0.1% (v/v) Triton-X-100 in phosphate buffered saline (PBS) for 15 minutes and then blocked in PBS containing 0.02% (w/v) bovine serum albumin (Fraction V; Sigma-Aldrich, St. Louis, MO) and 0.015% (w/v) glycine (Sigma-Aldrich, St. Louis, MO) for 45 minutes. Sections were incubated with a primary antibody against either SMA (clone 1A4; Sigma-Aldrich, St. Louis, MO; 1:500 in blocking solution) or SKEL (clone NOQ7.5.4D; Sigma-Aldrich, St. Louis, MO; 1:250 in blocking solution) for 1 hour in a humidification chamber at room temperature. Unbound primary antibody was removed from sections by multiple washes with PBS. Next, sections were incubated with an Alexa 488-conjugated secondary antibody (Invitrogen, Carlsbad, CA; 1:500 in blocking solution) for 1 hour at room temperature in a humidification chamber. All sections were counterstained with DAPI for nuclear visualization and mounted with gelvatol. Sections were imaged with a color, digital camera (QImaging, Surrey, BC, Canada) on an E800 Nikon

Eclipse microscope (Nikon, Melville, NY) using NIS Elements BR 3.0 software (Nikon, Melville, NY).

### **3.1.10 Quantification of Muscle Components**

Frozen sections stained for SMA and SKEL were used to quantify the cross-sectional area of smooth and striated muscle in each portion of the urethra. Total cross-sectional area was determined for each section using the NIS-Elements BR 3.0 software (Nikon, Melville, NY) area tool. The luminal and external circumference were manually outlined, and the difference between those areas was taken as the total cross sectional area. The total area stained positive for either SMA or SKEL was calculated using the NIS-Elements BR 3.0 software (Nikon, Melville, NY) thresholding tool, which calculates the total area of fluorescence within a set intensity range. The intensity range was manually adjusted for each section such that only the visible fluorescence was incorporated into the measurement. The sum of the area associated with each fluorescent element was taken as the total positive area. The average percent of total area positively stained for each antibody is reported.

### **3.1.11 Geometric Estimation and Mechanical Characteristics**

Inner diameters of tested urethras were estimated for proper calculation of various mechanical parameters [54] (see **Section 2.2.7**). Paraffin sections stained with Lillie's-modified Masson's trichrome were imaged as described above and used for thickness assessment as previously described [54] (see **Section 2.2.7**).

Compliance, a linear measure of the distensibility of a tube, was calculated for each applied pressure increment as previously described [54] (see **Section 2.2.7**).

### **3.1.12 Statistics**

Data are represented as the average  $\pm$  standard error of the mean. Statistical comparisons were performed using a Student's t-test. For the alpha-bungarotoxin studies, a paired Student's t-test was used. Significance was detected at p-values less than 0.05.

## **3.2 RESULTS**

### **3.2.1 In-Vivo Leak Point Pressure in Continent and SUI Animals**

SUI SD animals had a significantly lower V-LPP than continent SD controls, but this difference was not detected in the Lewis rat (**Figure 3.1**). The continent and SUI Lewis rat also had a significantly lower V-LPP than the continent SD rat (**Figure 3.1**). In the supine position, which was necessary to test the effect of alpha-bungarotoxin, the continent SD rat maintained a significantly higher LPP than that of the Lewis rat (**Figure 3.2**). The injection of alpha-bungarotoxin (333  $\mu\text{g}/\text{kg}$ , i.v.) significantly decreased Su-LPP in the SD rat, but did not alter Su-LPP in the Lewis rat (**Figure 3.2**).

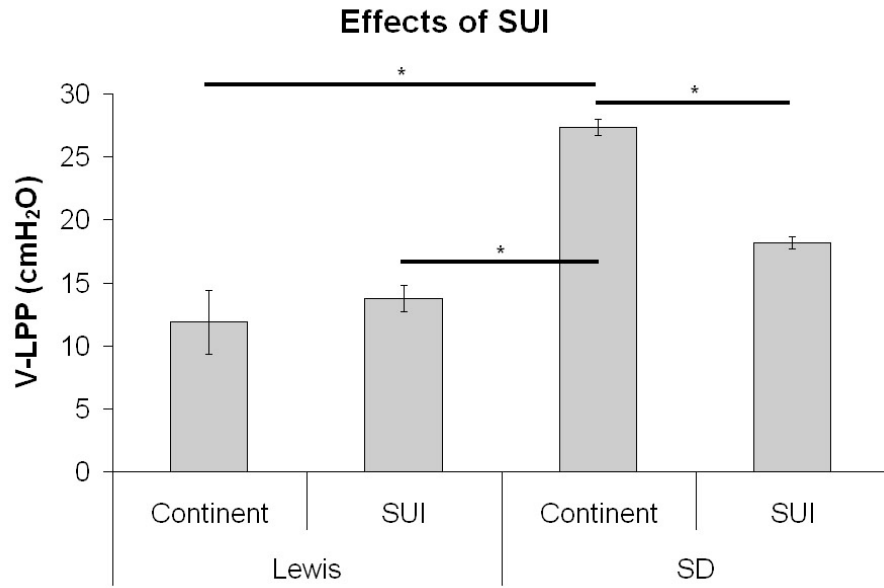


**Figure 3.1** Vertical leak point pressure (V-LPP) for both Lewis (n=3) and Sprague-Dawley (n=2) rats in both Continent and SUI states. Data shown as average  $\pm$  SEM, \*p<0.05.

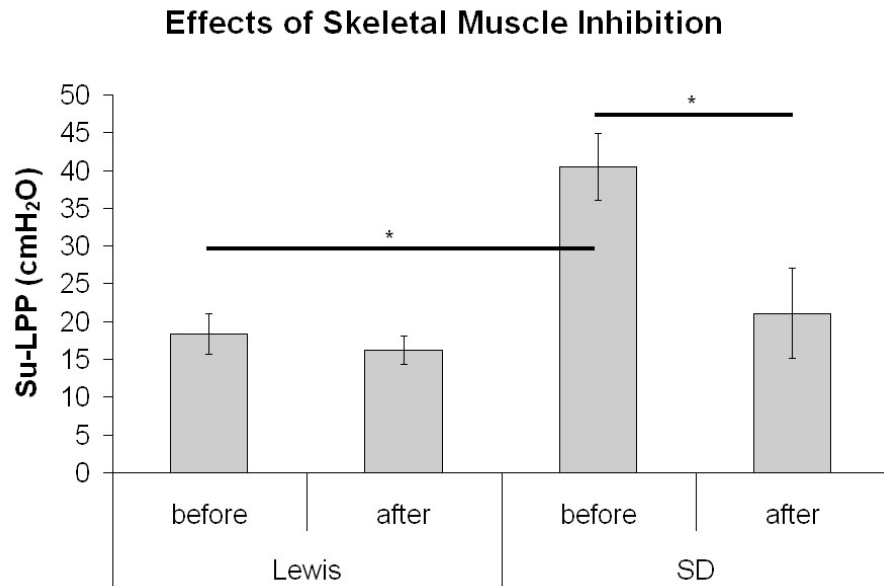


**Figure 3.2** Supine leak point pressure (Su-LPP) for both Lewis (n=7) and Sprague-Dawley (n=4) rats before and after injection with alpha-bungarotoxin (333  $\mu$ g/kg, i.v.). Data shown as average  $\pm$  SEM, \*p<0.05.

### 3.2.2 Urethral Pressure During Sneeze

In the supine position the Lewis rats had a significantly lower urethral baseline pressure than the SD rats prior to and during sneeze (**Figure 3.3**). However, there was no difference between the two strains of rats in the peak urethral pressure response or the peak abdominal pressure response during sneeze.

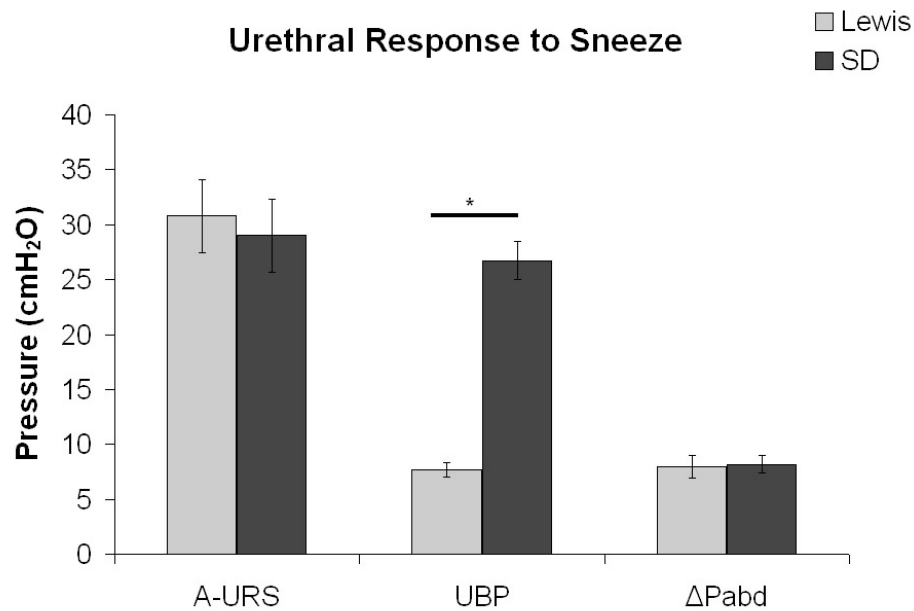


**Figure 3.3** Urethral pressure response (A-URS) during sneeze, urethral baseline pressure (UBP) and change in abdominal pressure ( $\Delta P_{abd}$ ) for both Lewis (n=8) and Sprague-Dawley (n=10) rats. Data shown as average  $\pm$  SEM,

\*p<0.05.

### 3.2.3 Ex-Vivo Mechanical Characteristics

Pressure-diameter (P-D) curves obtained from ex-vivo mechanical testing of the urethras in their baseline conditions are shown in **Figure 3.4**. In the proximal urethra the P-D curve for SD rats was shifted to the right of the curve for Lewis rats; representing a slightly larger compliance with increasing pressure in SD rats (**Figure 3.4A**). The Lewis middle urethra showed a larger distension at low pressures, indicating an increased compliance compared to the SD mid-urethra (**Figure 3.4B**). There were no detectable differences between strains in the distal portion (**Figure 3.4C**).

In the passive state, the P-D curves for both the proximal and middle portions of the Lewis urethra were shifted to the right of the curves for SD rats, while the curves for the distal portion were shifted to the left (**Figure 3.5A-C**). Calculated compliance values were greater in the Lewis urethra at low pressures in the middle portion in the baseline state as well as in the proximal and middle portions in the passive state (**Figure 3.6**). The passive, distal, SD urethra was more compliant than the corresponding Lewis urethra, although not significantly (data not shown).

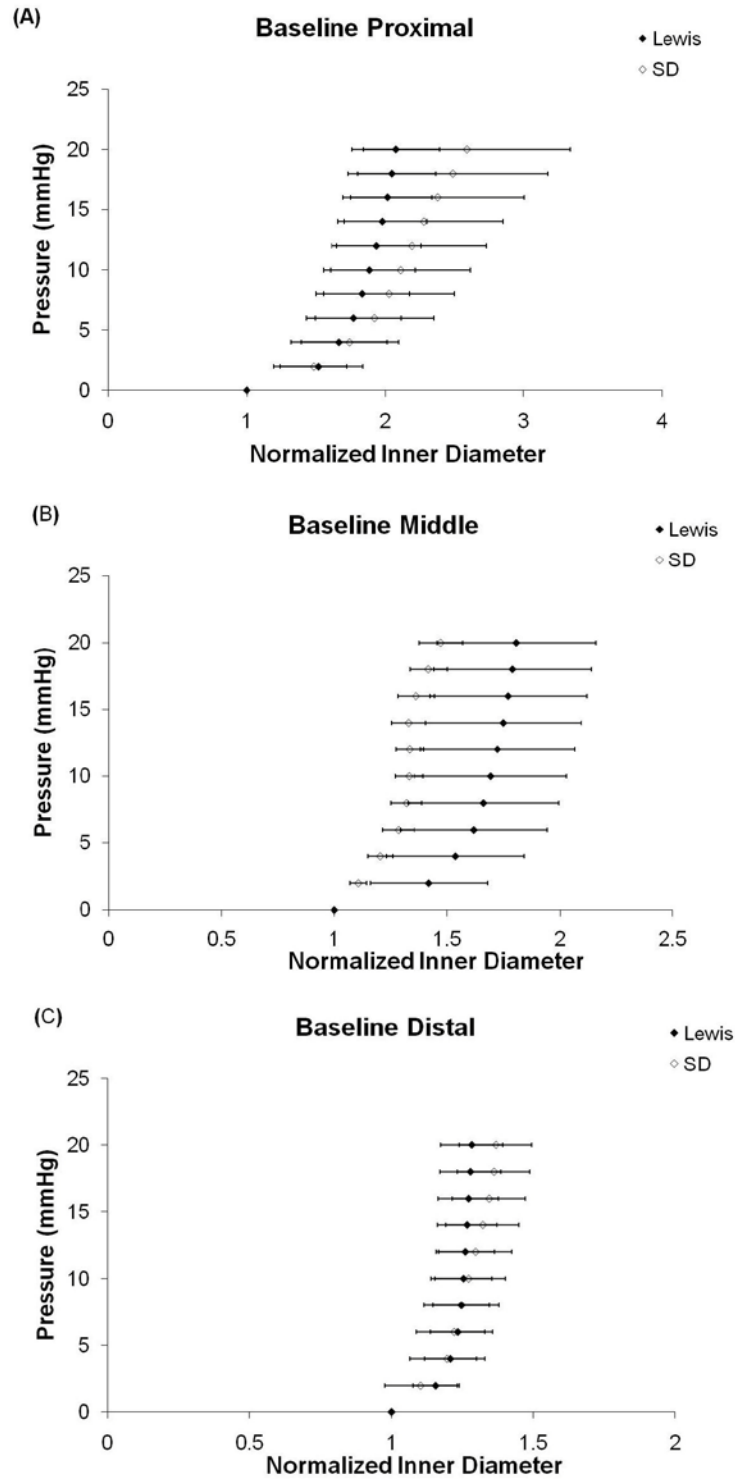


**Figure 3.4** Baseline pressure-diameter curves from the (A) proximal, (B) middle and (C) distal urethral portions of continent Lewis (n=4) and Sprague-Dawley (n=6) rats. Data shown as average  $\pm$  SEM, \*p<0.05. NID = normalized inner diameter.

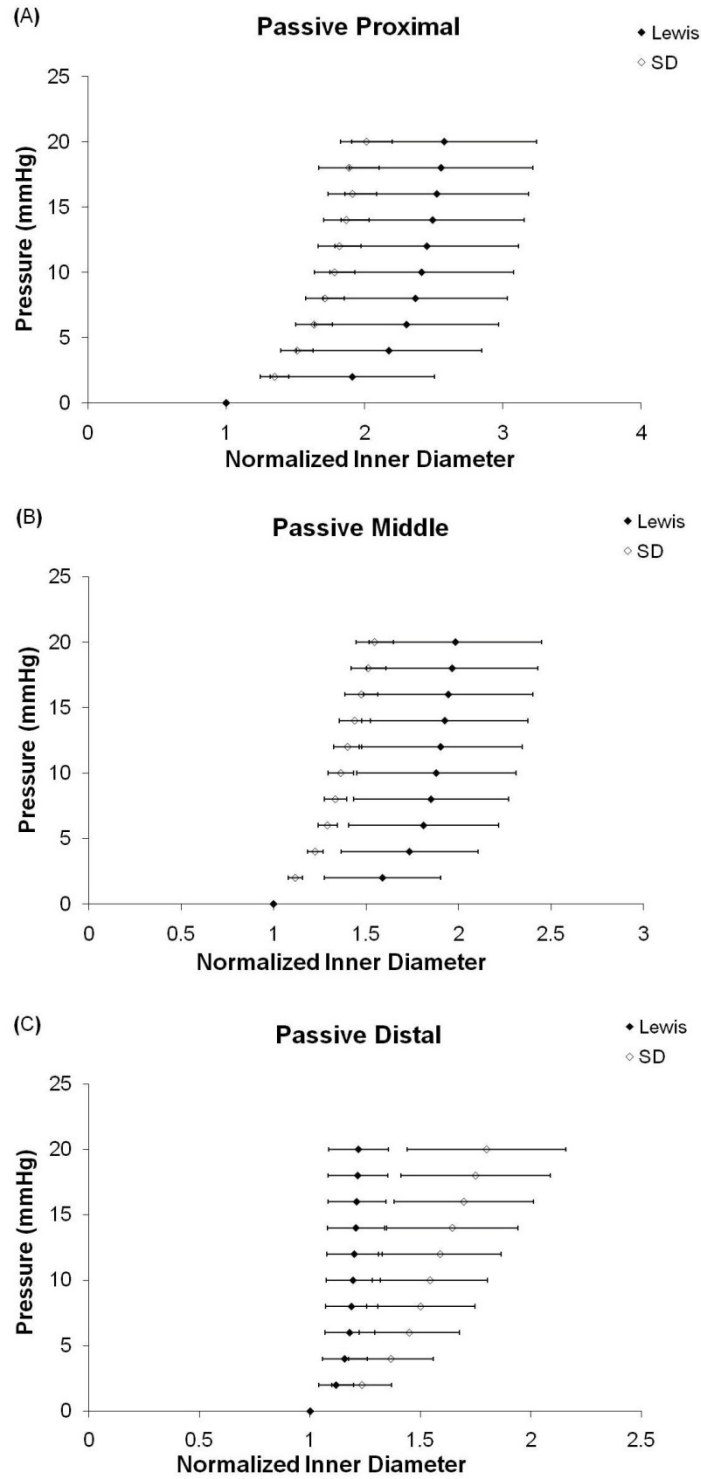


**Figure 3.5** Passive pressure-diameter curves from the (A) proximal, (B) middle and (C) distal urethral portions of continent Lewis (n=4) and Sprague-Dawley (n=6) rats. Data shown as average  $\pm$  SEM, \*p<0.05. NID = normalized inner diameter.

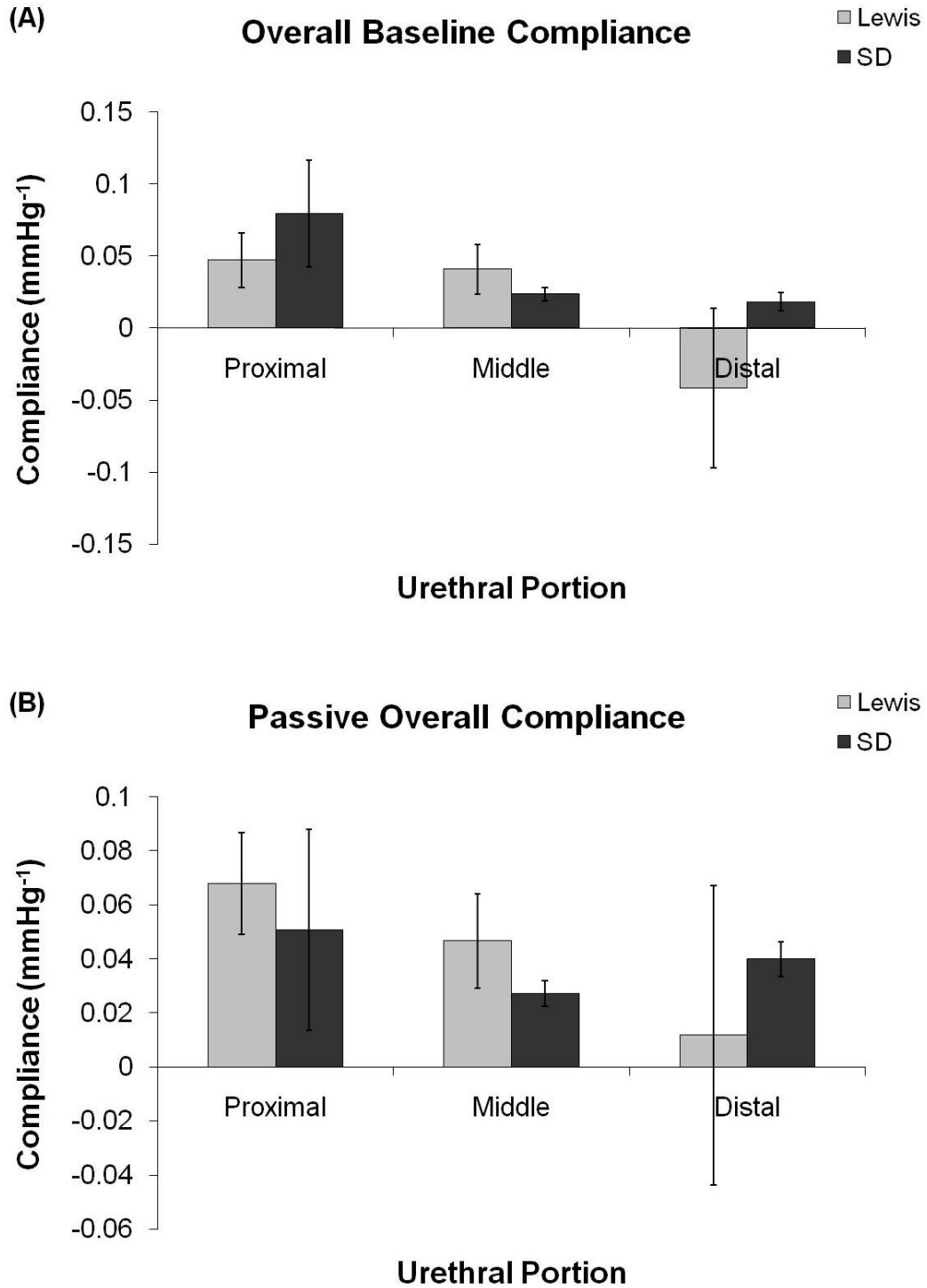


**Figure 3.6** Baseline and passive compliance values for the proximal and middle urethral portions of continent Lewis (n=4) and Sprague-Dawley (n=6) rats. Data shown as average  $\pm$  SEM, \*p<0.05.

### 3.2.4 Ex-Vivo Functional Characteristics of the Middle Urethra of Continent Animals

Diameter profiles for SD urethras showed a distinct response to each drug, while Lewis urethras tended to drift without a clear response (**Figure 3.7**). In SD urethras (n=3) N $\omega$ -nitro-L-arginine (100  $\mu$ M, a NOSi), did not elicit a consistent change in outer diameter; whereas phenylephrine (PE, 40  $\mu$ M) and acetylcholine (5 mM) both produced a contraction. Subsequent addition of EDTA completely reversed the contractile response (**Figure 3.7**). Lewis urethras, which exhibited a large increase in outer diameter in response to an 8 mmHg pressure, appeared to be unresponsive to any drugs tested (**Figure 3.7**). Peak response was calculated with respect to the initial pressure increase (**Figure 3.8A**) as well as with respect to the equilibrated diameter from the previous condition (**Figure 3.8B**). With respect to 8 mmHg and the previous condition, the SD urethra had a greater response to both PE and Ach, although not significantly. The Lewis urethra had a much larger change in outer diameter than the SD urethra to 8 mmHg (**Figure 3.8B**), confirming our mechanical data (**Section 3.2.3**), which showed a trend towards an increased compliance in the middle urethra of the Lewis rat.

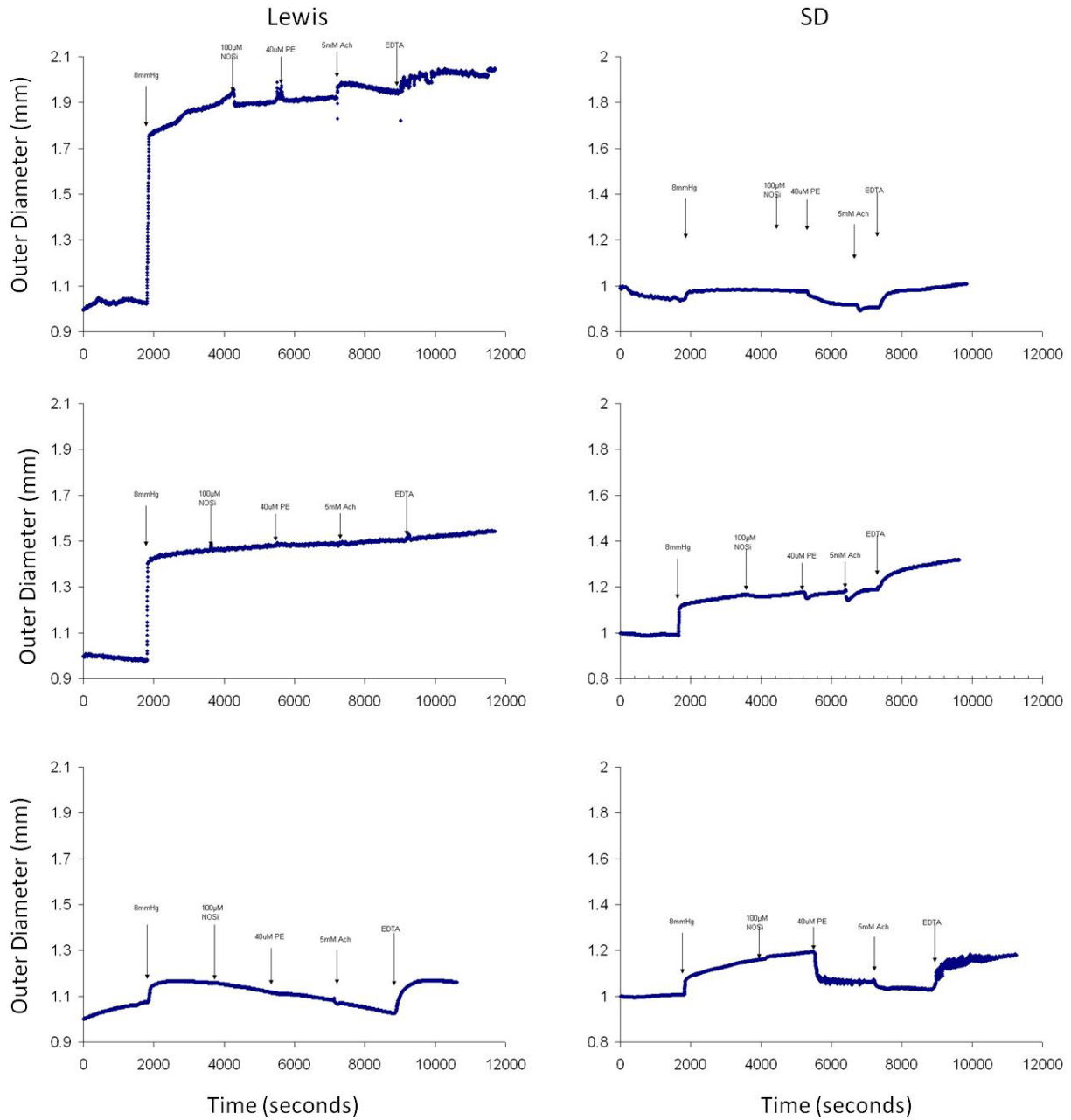


**Figure 3.7** Middle urethral response of all three continent Lewis and Sprague-Dawley rats tested to various agonists and antagonists (100 µM N $\omega$ -nitro-L-arginine, 40 µM phenylephrine, 5 mM acetylcholine and 3 mM EDTA). Data was measured at 1 Hz with 30 minute equilibrations at each condition. “Time” represents the seconds into the initiation of the measurements when data was obtained. Outer diameter measurements were normalized to the initial outer diameter at 0 mmHg.

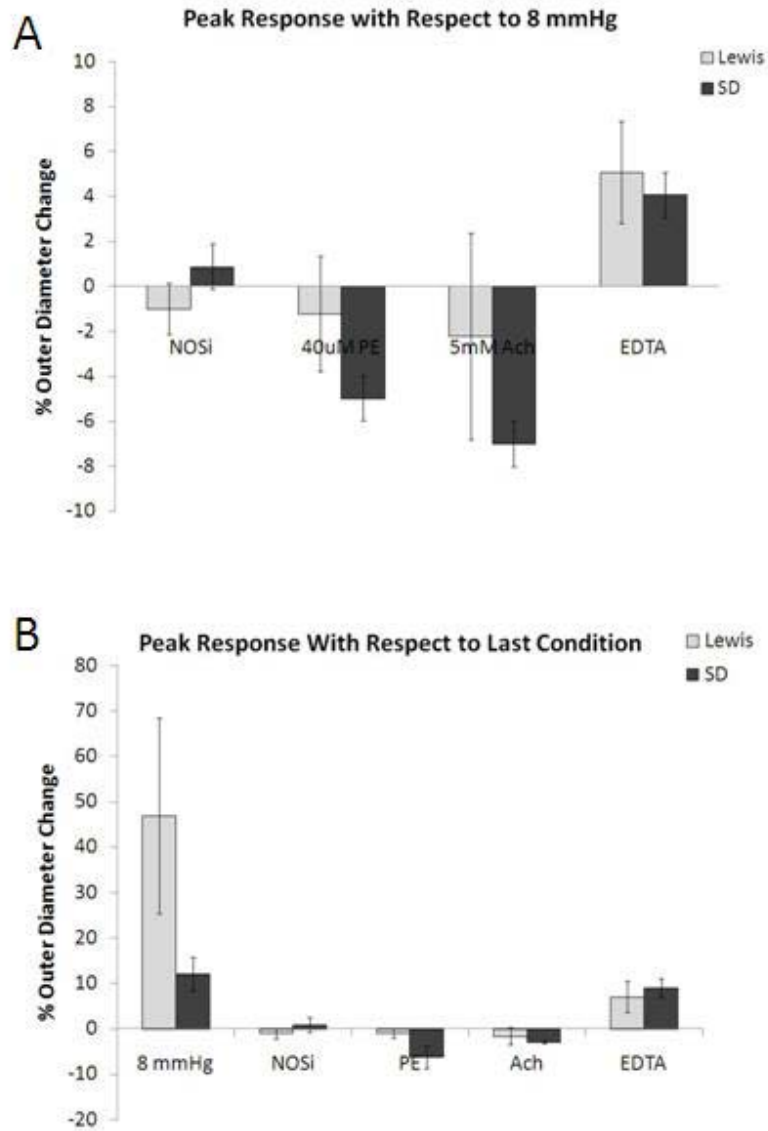


**Figure 3.8** Percent outer diameter change of the middle urethra of continent Lewis (n=3) and Sprague-Dawley (n=3) rats to various agonists and antagonists (100  $\mu$ M N $\omega$ -nitro-L-arginine, 40  $\mu$ M phenylephrine, 5 mM acetylcholine and 3 mM EDTA) with respect to 8 mmHg (A) and the equilibrated previous condition (B). Data was measured at 1 Hz with 30 minute equilibrations at each condition. Outer diameter measurements were normalized to the initial outer diameter at 0 mmHg.

### 3.2.5 Histology

Qualitatively, it appeared that the SD urethra had greater overall muscularity than the Lewis urethra, which appeared to have a greater amount of extracellular matrix via Masson's trichrome staining (**Figure 3.9**). Semi-quantification revealed that all portions of the Lewis urethra have a higher percentage of smooth muscle than the SD urethra (**Figure 3.10A**), while all portions of the SD urethra contain a higher percentage of fast-twitch striated muscle than the Lewis urethra, with proximal and distal portions being significantly different (**Figure 3.10B**). It was also observed that the SD rats had a larger total cross-sectional area in all three portions of the urethra, than the Lewis rat (**Figure 3.10C**).

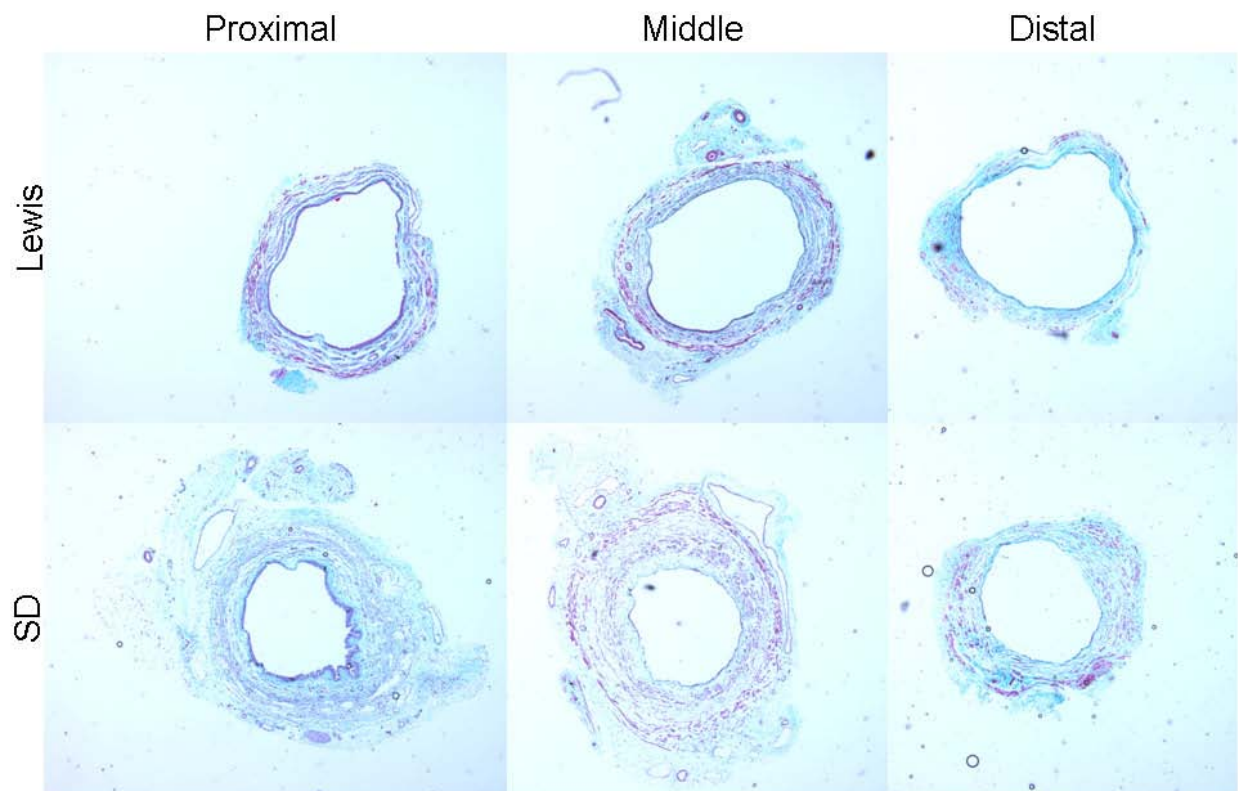


**Figure 3.9** Masson's trichrome staining of proximal, middle and distal portions of continent Lewis and SD urethras.

Images are representative and taken at 4x. Red = muscle, blue/green = collagen, black = nuclei.

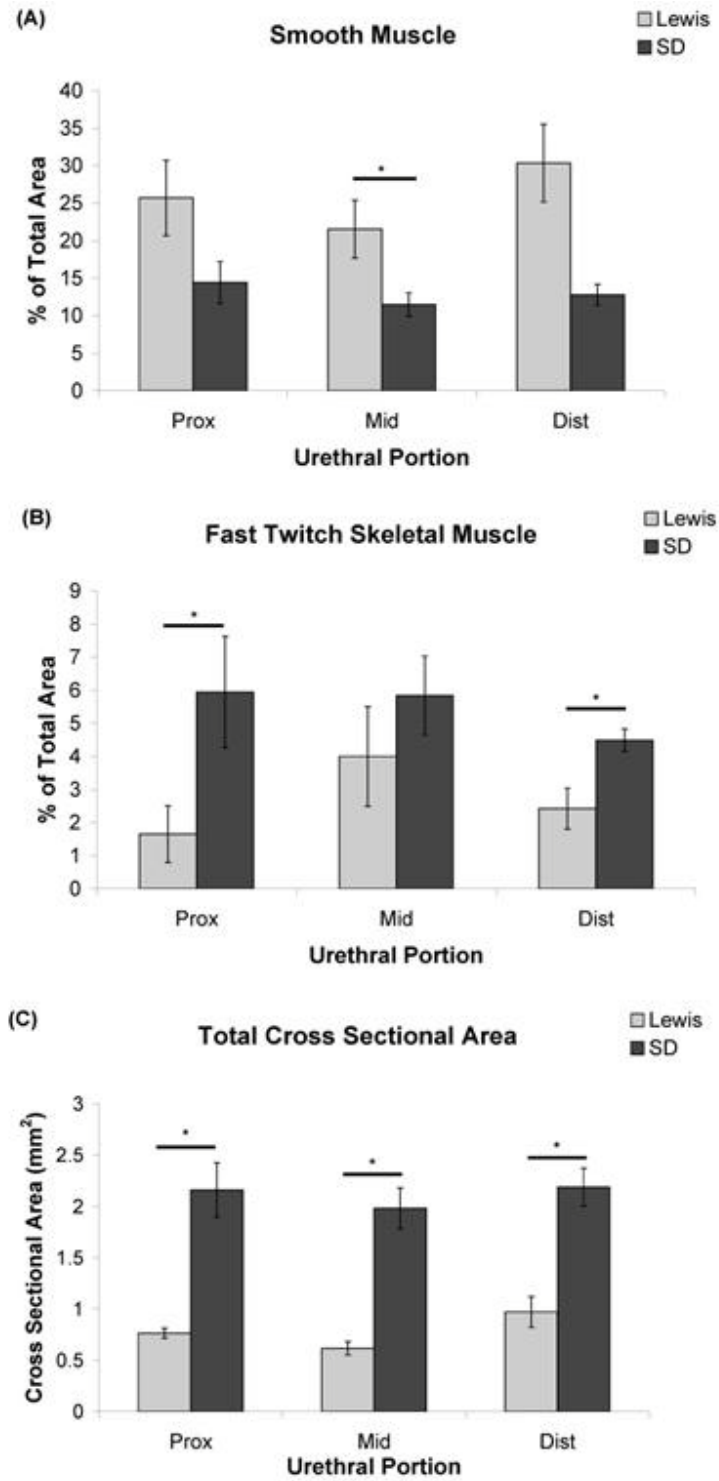


**Figure 3.10** Percent of the total cross-sectional area staining positive for (A) smooth muscle actin or (B) fast twitch skeletal muscle and (C) total cross-sectional area of both the Lewis (n=7) and Sprague-Dawley (n=4-7) urethra.

Data shown as average  $\pm$  SEM, \*p<0.05.

### 3.3 DISCUSSION

In-vivo and ex-vivo experiments revealed that the normal properties of the urethra and the response of the urethra to bilateral pudendal nerve transection are markedly different in the Lewis and SD rats. Lewis rats exhibited a significantly lower LPP and intraurethral baseline pressure in-vivo (**Figure 3.3**) and higher compliance (**Figure 3.4**) at the middle urethra in-vitro compared to the measurements in SD rats. In addition Lewis rat LPP was unaffected by pudendal nerve transection, whereas LPP was significantly reduced by nerve transection in SD rats (**Figure 3.1**). Injection of alpha-bungarotoxin also had no effect on LPP in Lewis rats, while significantly decreasing the LPP in SD rats (**Figure 3.2**), indicating a greater contribution of striated muscle to the maintenance of continence in the SD rat, compared to the Lewis rat. The SD rat urethra in comparison to the Lewis rat urethra had a larger cross sectional area at all three segmental levels and had a muscular layer that exhibited a significantly greater proportion of striated versus smooth muscle (**Figure 3.10**). These functional, morphological and mechanical differences suggest that the Lewis rat has a lower level of intrinsic and neurally mediated contractile activity of the urethral muscle; and therefore is not a useful model for SUI induced by neural injury or neurogenic disorders.

To our knowledge, only one other publication [160] has described the properties of the urethra in the Lewis rat. In this study, LPP was measured in normal animals and in the vaginal distension model of SUI. It was reported that vaginal distension, an acute model of SUI, did result in a significant decrease in LPP, but almost the same decrease in LPP occurred in the sham group. In addition the Lewis rats had a noticeably lower LPP compared to SD rats [160].

In our current study, we chose a chronic model of SUI: bilateral pudendal nerve transection [146, 162]. The pudendal nerve innervates the external urethral striated sphincter and

plays a major role in maintaining continence [165]. Following nerve transection, there is a significant decrease in the pressure required to induce urine leakage that persists for 6 weeks [162] in contrast to the rapid recovery that occurs in the vaginal distension model [146, 162, 166]. Lewis rats were unaffected by pudendal nerve transection and had significantly lower LPP values than those in SD rats (**Figure 3.1**), which are in agreement with LPP values previously published in SD rats [46, 64, 146]. However, these results vary from reports that SUI, due to vaginal distension, significantly lowers LPP in both strains [51, 160].

The unaltered LPP following alpha-bungarotoxin in the Lewis rats (**Figure 3.2**) indicates that the striated sphincter does not contribute to urethral outlet resistance or the maintenance of continence under the conditions of our experiments. This contrasts with the prominent lowering of LPP by alpha-bungarotoxin in the SD rat in the same experimental model (see also a previous report [167]). The more abundant striated muscle in the SD rat (**Figure 3.10**) is consistent with the greater contribution of the striated sphincter to LPP in this strain. In addition it is probable that the reflex activation of the striated sphincter muscle is lower in Lewis rats than in SD rats because transection of the pudendal nerve, which innervates and activates the striated sphincter, did not affect LPP in the Lewis rat but significantly reduced it in the SD rat.

Although LPP was lower in the continent Lewis rat due to insignificant contribution of striated muscle to the urethral continence reflex induced by passive intravesical pressure increases, as compared to the continent SD rat, midurethral pressure responses to sneeze measured by microtransducer-tipped catheters were not different in Lewis and SD rats while UBP in Lewis rats was significantly lower than SD rats (**Figure 3.3**). As reported previously, sneeze-induced urethral closure mechanisms are mediated by somatic nerve-induced reflex contractions of external urethral sphincter and pelvic floor striated muscles, and directly induced by sneeze

without intravesical pressure increases [15, 19]. Thus the striated muscle-mediated urethral continence reflex induced by strong, phasic stimuli such as sneeze seems to be still maintained in the Lewis rat.

Because smooth muscle represents a greater proportion of the muscle mass in the Lewis rat urethra, it might be expected that smooth muscle activity would make a greater contribution to the continence mechanism. However, the lower UBP indicates a decreased activity of the urethral smooth muscle in the Lewis rat compared to SD (**Figure 3.3**), and may explain the increased compliance of the Lewis urethra compared to the SD urethra (**Figure 3.4**). This decreased smooth and striated muscle activity was confirmed in ex-vivo studies showing a clear response of the SD urethra to various agents, while it appeared that the Lewis urethra did not respond (**Figure 3.7**). Quantification of the tissue response, showed an increased contraction of the SD urethra in response to PE and Ach, although not significantly greater than the Lewis urethra (**Figure 3.8**). Although the inconsistent drift of the Lewis urethra during testing, could be introducing a response independent of the agents.

There are many possible reasons for the differences found in urethral function between these animals. First, receptor expression in the smooth and/or striated muscle cells could be lower, thereby diminishing the response to contractile agents. Second the Lewis rats may have an increased sensitivity to the anesthetic used in the in-vivo experiments which would reduce reflex activity of the sphincter. However no obvious differences in the depth of anesthesia were observed in the two strains. Furthermore the same dose of anesthetic was used in experiments in another laboratory when SUI induced by vaginal distension reduced LPP in the Lewis rat [160]. The vaginal distension model used in the latter studies may produce a more extensive injury to

smooth muscle and blood vessels as well as nerves in the urethra and therefore produce a larger change in LPP.

Although this study systematically attempted to determine the cause of differences in urethral function between these strains, further studies are needed to address this issue. Increasing the number of studies for the pharmacological endpoints may reveal a more concrete difference in the urethras response to various agents. A better understanding of the neural control of the urethra could be obtained by quantifying the density and type of innervation of the urethra in the two strains by using immunohistochemistry to identify cholinergic and adrenergic nerves. In addition assessing the expression of various transmitter receptors using molecular techniques and the effects of electrical stimulation of nerves could be useful. All of our work was performed in anesthetized animals, therefore assessing micturition frequency and volume in a metabolic cage [168] or performing awake cystometry [169] might eliminate any functional differences as a result of anesthesia although the LPP measurements are technically difficult to perform in awake conditions.

Studies in Sprague-Dawley rats have provided considerable insight into the function of the lower urinary tract. This out-bred, all-purpose animal has yielded an abundance of information on factors which contribute to and therapies that provide relief from many urethral disorders. However, as stem-cell therapies continue to develop for urethral dysfunctions, an in-bred strain with less genetic variation may be more suitable for initial validation of these therapies to avoid rejection issues. Due to differences between SD and Lewis rats in regard to inflammatory responses [170], adaptive behavior [171], and response to pharmacological agents [172], the mechanisms contributing to the differences in urethral properties in these two strains warrant further investigation.

In summary, this work has provided strong evidence that functional and mechanical characteristics of the urethra are markedly different in Lewis and SD rats. We have also shown that pudendal nerve transection is not an appropriate model of chronic SUI in the Lewis rat.

## **4.0 MECHANICAL AND HISTOLOGICAL CHARACTERIZATION OF A TISSUE ENGINEERED URETHRAL WRAP**

### **4.1 NEED FOR A TISSUE ENGINEERED URETHRAL WRAP**

Urethral dysfunction commonly accompanies many conditions and diseases including spinal cord injury and diabetes. One consequence of urethral dysfunction is urinary incontinence. Urinary incontinence is a condition in which urine leakage occurs due to an inability of the lower urinary tract to maintain continence [25]. One of the most predominant forms of urinary incontinence is SUI [25], which is an involuntary loss of urine that occurs in the absence of a bladder contraction but in the presence of an increase in abdominal pressure, generally caused by laughing, coughing, or sneezing. SUI is associated with a weak urethral sphincter, which is incapable of preventing urine flow [173].

Currently there are several treatments for SUI including muscle therapy, injection of bulking agents, and surgical treatments. However, each of these treatments is accompanied by additional complications or may dissipate by re-absorption into the body over time, requiring additional or multiple treatments [25, 29, 42]. The inability of current treatments to provide long-lasting and worry-free relief from SUI requires a new approach for treatment.

The trauma to the urethra and its surrounding organs and supportive structures during vaginal childbirth, resulting in SUI, can be detrimental to both organ function and support. It has

previously been shown in a rat model, that in the presence of SUI, the urethra and surrounding structures experience varying degrees of hypoxia, atrophy, and denervation [35, 52, 174]. This breakdown of urethral composition is what most likely leads to the significant decreases in intravesicle pressure required to cause urine leakage in SUI [46, 165]. Previous studies from our group have shown altered mechanical properties of the urethra in a rodent model of SUI, particularly in the proximal portion [54]. These studies showed that SUI results in increased compliance in the proximal portion of the urethra at low pressures compared to healthy controls. Beta stiffness values for SUI specimens decreased in the proximal portion, but increased in the middle portion of the urethra compared to controls. A decrease in muscular tone as well as a disruption of urethral extracellular matrix in this model of SUI may contribute to an inability of the urethra to resist deformation due to increases in intraluminal pressures [54].

Regenerative medicine poses many possible, cellular-based approaches to treat the structural and functional complications of SUI. Some investigators have been exploring the injection of muscle-derived stem cells directly into the urethra [64, 157, 158, 175]. We believe that the mechanical and structural damages that accompany SUI render tissue engineering a possible solution for the urethra. Cell injection alone may require significant time for the cells to become acclimated to their new environment and begin to work towards returning function. The use of a biomaterial can provide a temporary matrix for the cells and acutely enhance any biological and mechanical benefits of the therapy [176].

The new therapy we propose for urethral dysfunction is to fabricate a tissue engineered urethral wrap (TEUW) utilizing fibrin and bone marrow progenitor cells (BMPCs), allowing for both an autologous matrix and cell source. The TEUW can be placed around the native, diseased urethra in a cuff-like fashion and will acutely act as a bulking agent, to prevent overexpansion of

the urethra, and chronically provide improved functionality to the diseased tissue. The goals of this work were to develop a TEUW with mechanical properties similar to that of the native urethra, and to show proof of concept that the TEUW is able to provide resistance to increased dilation of the urethra, under increased intraluminal pressures.

## 4.2 MATERIALS AND METHODS

### 4.2.1 Cell Source and Culture.

Male, Lewis rat bone marrow progenitor cells (BMSCs), obtained from the Tulane Center for Gene Therapy [177], were cultured in complete media ( $\alpha$ -modified Eagle's medium ( $\alpha$ -MEM; 12561-072; Invitrogen, Carlsbad, CA) supplemented with 20% fetal bovine serum (FBS; lot selected; Atlanta Biologicals, Atlanta, GA), 1% antibiotic/antimycotic (Invitrogen, Carlsbad, CA), and 2 mM L-glutamine (Invitrogen, Carlsbad, CA)) at 37°C and with humidified air containing 5% CO<sub>2</sub>. Media was changed every 48 hours, and cells were grown to ~80% confluence.

### 4.2.2 Fabrication and Culture of Tubular Constructs

Tubular constructs were fabricated (**Figure 4.1**) by first positioning a Teflon<sup>®</sup> mandrel concentrically within a glass sheath (**Figure 4.1A**). A mixture containing 3 mg/mL bovine fibrinogen (Sigma-Aldrich, St. Louis, MO) with 0.5 units/mg bovine thrombin (Sigma-Aldrich, St. Louis, MO) and  $0.75 \times 10^6$ ,  $1.00 \times 10^6$ , or  $1.25 \times 10^6$  cells/mL in serum-free  $\alpha$ -MEM was

poured around the mandrel and incubated at 37°C and 5% CO<sub>2</sub> for 45 minutes (**Figure 4.1B**). Following incubation, tubular constructs were removed from the mold (**Figure 4.1C-E**) and placed into a dynamic spinner flask culture, containing complete media, supplemented with 0.3 mM ascorbic acid and 0.1 g/mL (puriss grade) aminohexanoic acid (Sigma-Aldrich, St. Louis, MO). Constructs were maintained in spinner flask culture for either 3 or 5 days. Constructs were then assessed for geometric dimensional changes (compaction) and viability, mechanically tested, and histologically assessed.

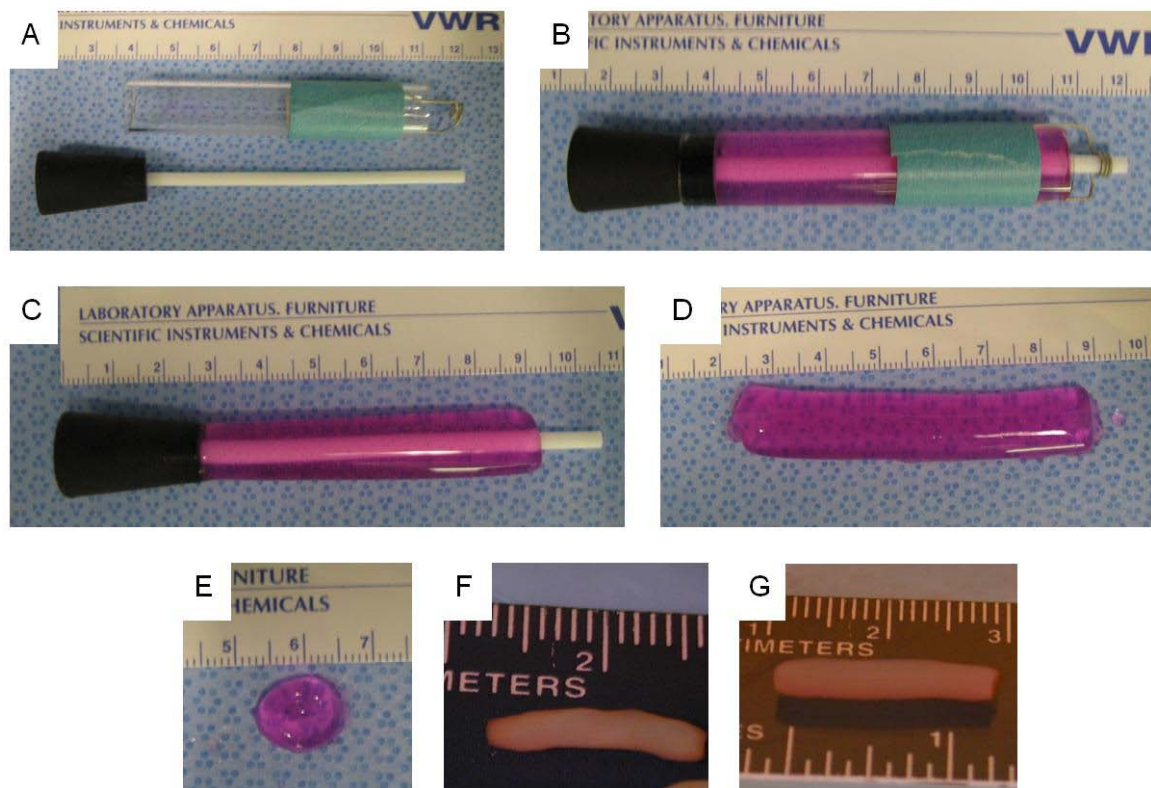


**Figure 4.1** Fabrication of TEUWs. (A) Mold comprised of a rubber stopper, glass sheath and Teflon® mandrel used to create the tubular construct. (B) Fibrin-cell mixture following gelation in the mold. (C) Tubular construct on mandrel following removal of the glass sheath. (D) Tubular construct after being completely removed from the mold. (E) End view of a section of the tubular construct. Constructs fabricated with  $1.00 \times 10^6$  cells/mL following gelation (D), and spinner flask culture for either 3 (F) or 5 (G) days. Scale is in cm.

### 4.2.3 Compaction and Viability

Initial construct length was determined from the dimensions of the mold. Following culture, construct length was measured with calipers, unloaded outer diameter via a He-Ne laser micrometer and inner diameter via histology. Compaction was determined as a percentage of the original volume of the construct.

Viability of cells within the construct was assessed using the 3-(4,5-Dimethylthiazol-2-yl)-2,5-diphenyltetrazolium bromide (MTT) assay [102]. First, construct length was measured and a small ring of the construct was removed and its length was measured. The ring was cut into 4 equal sections, and each was placed in an individual well of a 96-well plate containing 200  $\mu\text{L}$  of media and 20  $\mu\text{L}$  of MTT solution (Sigma-Aldrich, St. Louis, MO). The plate was incubated for 4 hours at 37°C, 5%  $\text{CO}_2$ . Following incubation, the solution was removed from each well and was replaced with 200  $\mu\text{L}$  of 4 nM HCl in isopropanol. The plate was stored at 4°C overnight. The following day, 100  $\mu\text{L}$  from each well was moved to a clean well and the plate was read on a spectrophotometer at 530 nm. Absorbance values were converted to cell number based on a standard curve generated with cells from 2D culture. Total cell number for each construct was determined by the calculated cell number from the MTT assay and the dimensions of the construct, assuming a homogeneous distribution.

### 4.2.4 In-Vitro Mechanical Testing

Mechanical testing was performed as previously described by our group [53, 54, 101, 142, 143] and described in **Section 2.2.5**. Briefly, constructs were mounted on stainless steel tees in a bathing chamber and maintained in a physiologic environment via a circulation loop. In order to

remove viscoelastic effects, constructs were preconditioned by changing intraluminal pressures from 0 to 8 mmHg every 10 s for 10 cycles with a fluid reservoir. Preconditioning was followed by mechanical testing, which consisted of increasing the intraluminal pressure from 0 to 20 mmHg in 2 mmHg steps, while simultaneously recording the outer diameter and intraluminal pressure of the construct [142]. Following this, burst pressure was determined by increasing the intraluminal pressure until failure of the construct [178].

#### **4.2.5 Histologic Assessment**

Following mechanical testing, specimens were fixed in 4% paraformaldehyde (Fisher, Pittsburgh, PA), cut in half and processed for both paraffin and frozen sections in 10  $\mu$ m sections. Paraffin sections were stained with Lillie's-modified Masson's trichrome, hematoxylin and eosin (H&E), and picosirius red (PSR). Frozen sections were stained for alpha-smooth muscle actin ( $\alpha$ -SMA) and actin filaments (Sigma-Aldrich, St. Louis, MO). Sections were permeabilized with 0.1% Triton-X-100 in phosphate buffered saline (PBS) for 15 minutes. Sections were then blocked in PBS containing 0.02% (w/v) bovine serum albumin (Fraction V, Sigma-Aldrich, St. Louis, MO) and 0.015% (w/v) glycine (Sigma-Aldrich, St. Louis, MO) for 45 minutes. Sections were incubated with a primary antibody against  $\alpha$ -SMA (clone 1A4; Sigma-Aldrich, St. Louis, MO) (1:500 in blocking solution) for 1 hour in a humidification chamber at room temperature. Unbound primary antibody was removed from sections by multiple washes with PBS. Next, sections were incubated with an Alexa 488-conjugated secondary antibody (Invitrogen, Carlsbad, CA) (1:500 in blocking solution) for 1 hour at room temperature in a humidification chamber. Additional sections were incubated with Alexa 488-conjugated phalloidin (Sigma-Aldrich, St. Louis, MO) (1:250 in PBS) for visualization of f-actin filaments.

All sections were counter-stained with DAPI for nuclear visualization, and mounted with gelvatol. Sections were imaged on a color digital camera (Olympus, Dulles, VA) on a BX45 Olympus microscope (Olympus, Dulles, VA) using MagnaFire software (Olympus, Dulles, VA).

#### **4.2.6 Mechanical Characteristics**

The TEUWs were relatively thick, necessitating a determination of their inner diameter for proper calculation of various mechanical parameters. Paraffin sections stained for Lillie's-modified Masson's trichrome were imaged as described above and used for thickness assessment as described in **Section 2.2.7**.

#### **4.2.7 Ex-Vivo Studies**

To show that our TEUW is capable of providing bulking support to the native urethra upon implantation, preliminary ex-vivo studies were performed. Adult, female, Sprague-Dawley rats (200-250 g) (Hilltop Lab Animals, Inc., Scottdale, PA) were used in the proof-of-concept assessment. Animals were housed at the University of Pittsburgh under the supervision of the Department of Laboratory Animal Resources. The policies and procedures for the animal studies are in accordance with those detailed in the *Guide for the Care and Use of Laboratory Animals*, published by the US Department of Health and Human Services. Procedural protocols were approved by the University of Pittsburgh's Institutional Animal Care and Use Committee.

The SUI group was created by first anesthetizing the animal with 4% halothane, and then creating a bilateral pudendal nerve transection using aseptic, surgical techniques [147]. Continent animals served as controls. Two weeks after the initial procedures, animals were

anesthetized with urethane (1.2 g/kg), and the urethras were excised as previously described by our group [53, 54]. Briefly, PE-50 tubing (Becton-Dickson, Franklin Lakes, NJ), was inserted through the urethra into the dome of the bladder. The dome of the bladder, as well as the external urethral meatus, was ligated to the catheter with 4-0 silk suture (Syneture, Mansfield, MA). The ureters were ligated and served as anatomical landmarks for the maintenance of *in-vivo* length during mechanical testing. The urethra was then separated from the surrounding tissues and placed in oxygenated media 199 (Sigma-Aldrich, St. Louis, MO), containing antibiotic/antimycotic and L-glutamine (Invitrogen, Carlsbad, CA), to prevent hypoxia of the tissue. Tissue was transported to our testing facility on ice.

Urethras were then fitted with a TEUW, which contained  $1.00 \times 10^6$  cells/mL and had been cultured for 5 days in spinner flask. The TEUW was cut along the longitudinal axis and placed around the native urethra, in a cuff-like fashion. The construct was closed around the urethra by interrupted stitches with 10-0 nylon suture (AROSurgical, Newport Beach, CA). Urethra-TEUW specimens were mounted into the testing system and mechanically tested as described above. Because the urethra is not homogeneous along its length, proximal, middle and distal segments were assessed individually [54, 141]. Following testing of the urethra in the presence of the TEUW, the TEUW was carefully removed, and the urethra was tested again. This testing order was necessary due to the ex-vivo placement of the TEUW requiring use of a dissection microscope and the desire to minimize handling of the tissue, which could cause differences in mechanical characteristics.

#### 4.2.8 Statistics

Data is represented as the average  $\pm$  standard error of the mean. Statistical comparisons were performed using the software package SPSS (version 16.0, SPSS, Inc., Chicago, IL). For comparisons between groups, a one-way ANOVA was used with the factor being either time or seeding density. Post-hoc testing was performed with a Bonferroni or Games-Howell test. Significance was detected at p-values less than 0.05.

### 4.3 RESULTS

#### 4.3.1 TEUW Construct Appearance and Dimensions

Following dynamic culture, constructs had an opaque, tissue-like appearance and maintained an open lumen (**Figure 4.1F-H**). Constructs were easy to handle and capable of being mounted with 4-0 silk suture onto stainless steel cannulae. Further tests showed that constructs were able to be sutured with 10-0 nylon suture without damage (data not shown).

All constructs compacted to a great extent in all dimensions over their culture duration. The average compaction (**Figure 4.2**) for all constructs, regardless of density or culture duration, was 98.2%. Constructs composed of  $1.25 \times 10^6$  cells/mL compacted significantly more ( $p=0.02$ ) at 5 days ( $1.27 \pm 0.13\%$ ) than 3 days ( $2.07 \pm 0.23\%$ ). There were no other significant differences in compaction detected between time points or between seeding densities at  $0.75 \times 10^6$  or  $1.00 \times 10^6$  cells/mL. Values for all experiments can be found in **Appendix D**.

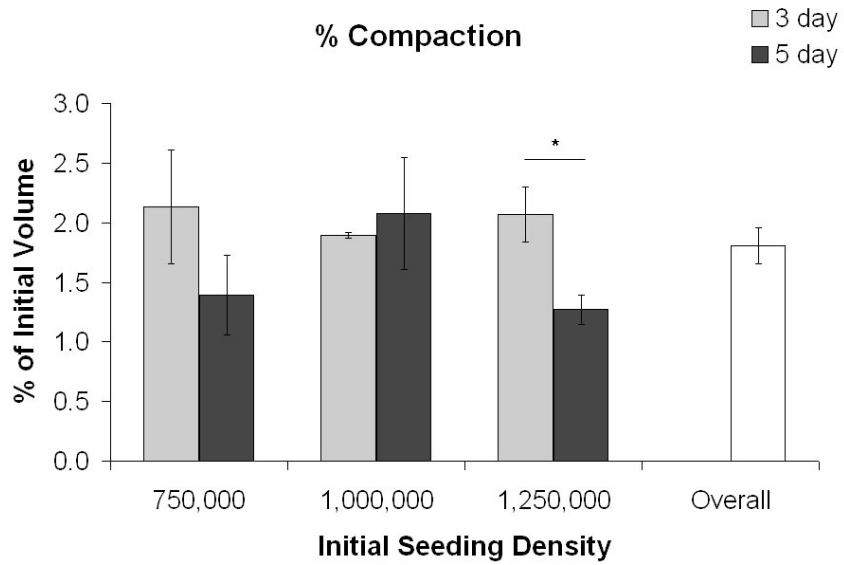


**Figure 4.2** Average compaction, calculated at a percentage of the initial volume for constructs fabricated from  $7.50 \times 10^5$ ,  $1.00 \times 10^6$ , or  $1.25 \times 10^6$  cells/mL for 3 (n=3) or 5 (n=4) days. Overall is the overall average compaction from all seeding densities and culture durations. Data shown as average  $\pm$  SEM, \*p<0.05.

### 4.3.2 Viability

MTT results showed a trend towards a decrease in cell density with increased culture duration for all seeding densities (**Figure 4.3**). There were no statistically significant differences in viability between seeding densities at either 3 or 5 days or between time points within a given seeding density.

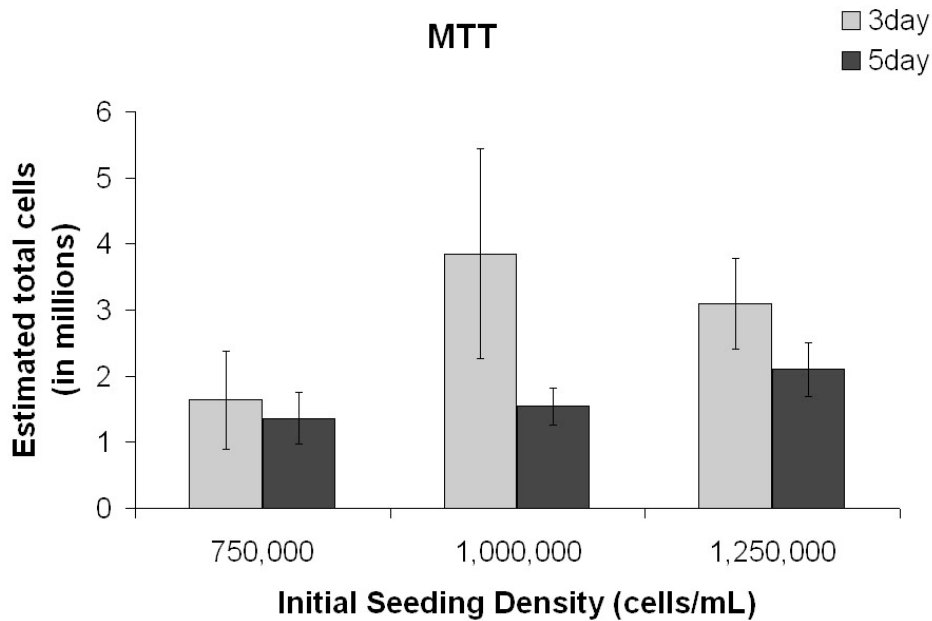


**Figure 4.3** Average estimated total cells from the MTT assay for constructs fabricated from  $7.50 \times 10^5$ ,  $1.00 \times 10^6$ , or  $1.25 \times 10^6$  cells/mL for 3 (n=3) or 5 (n=4) days. Data shown as average  $\pm$  SEM. No statistically significant differences were found between any groups.

### 4.3.3 Mechanical Characteristics

Burst pressure results revealed a trend towards increased burst strength with increased culture duration for all seeding densities (Figure 4.4). However, there was no obvious correlation to seeding density for either culture duration. No significant differences were detected between any groups.

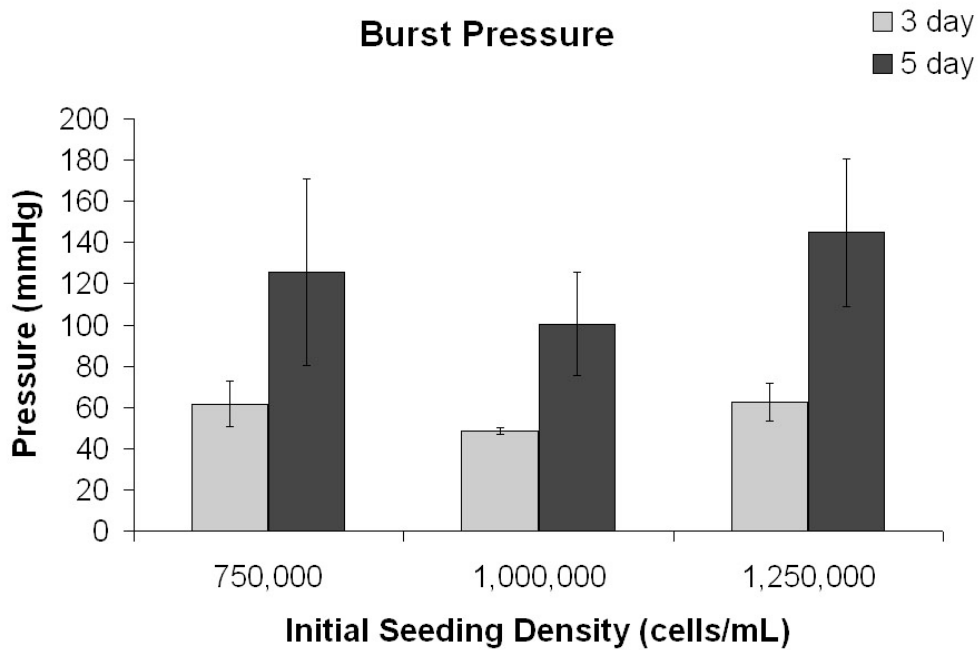
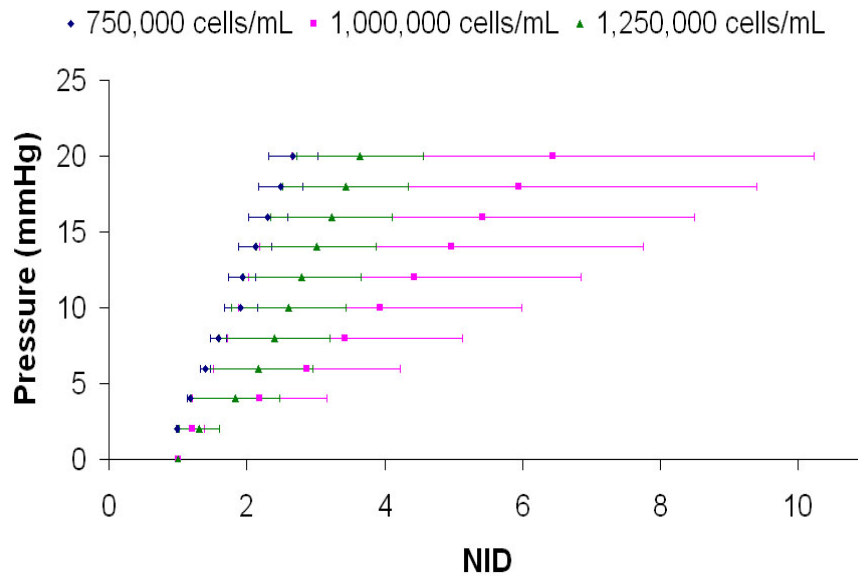


**Figure 4.4** Average burst pressure values for constructs fabricated from  $7.50 \times 10^5$ ,  $1.00 \times 10^6$ , or  $1.25 \times 10^6$  cells/mL for 3 (n=3) or 5 (n=4) days. Data shown as average  $\pm$  SEM.

Pressure-diameter curves were non-linear, typical of native soft tissues, for all seeding densities at both culture durations (**Figure 4.5**). The slopes of the pressure-diameter curves decreased with increased culture for  $0.75 \times 10^6$  and  $1.25 \times 10^6$  cells/mL, but increased for  $1.00 \times 10^6$  cells/mL. All curves showed an initial resistance to pressure increases, which was maintained best by  $0.75 \times 10^6$  at 3 days. At 5 days, curves were similar for all constructs. This trend can also be visualized in the stepwise compliance curves (

**Figure 4.6**), where it is obvious that as pressure increased, compliance values seemed to approach a threshold value at higher pressures. Constructs composed of both  $1.00 \times 10^6$  and  $1.25 \times 10^6$  cells/mL were more compliant at 3 days compared to 5 days at low pressures, while the inverse was true for  $0.75 \times 10^6$  cells/mL constructs. At 3 days  $1.00 \times 10^6$  cells/mL and at 5 days  $0.75 \times 10^6$  cells/mL constructs were the most compliant at low pressures, while the remaining constructs were very similar to each other at 3 days,  $1.25 \times 10^6$  was more compliant than  $1.00 \times 10^6$  cells/mL at 5 days. Beta stiffness (**Figure 4.7**) values showed a consistent decreasing trend with increased culture duration for all seeding densities.

### 3 day Pressure-Diameter



### 5 day Pressure-Diameter

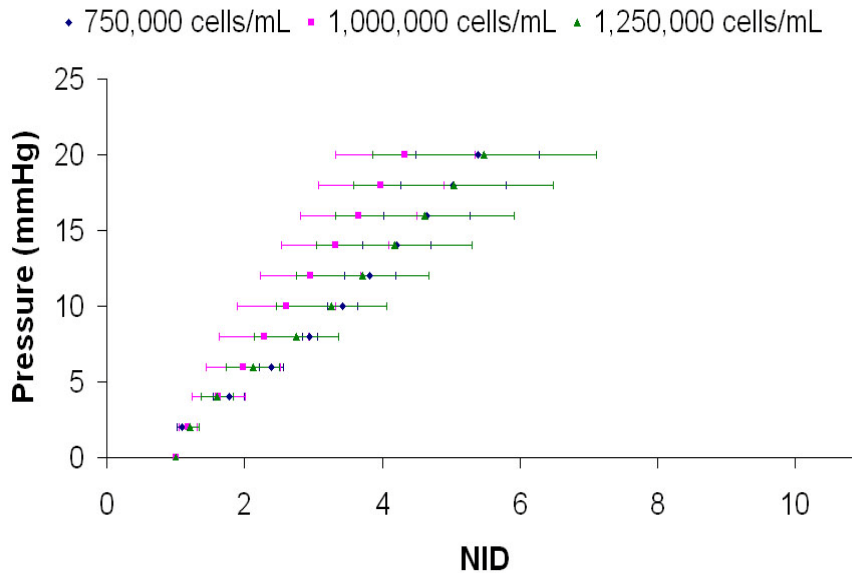


**Figure 4.5** Average pressure-diameter curves for constructs fabricated from  $7.50 \times 10^5$ ,  $1.00 \times 10^6$ , or  $1.25 \times 10^6$  cells/mL for 3 ( $n=3$ ) or 5 ( $n=4$ ) days, where NID is the diameter normalized to the diameter at 0 mmHg. Data shown as average  $\pm$  SEM.

## Stepwise Compliance

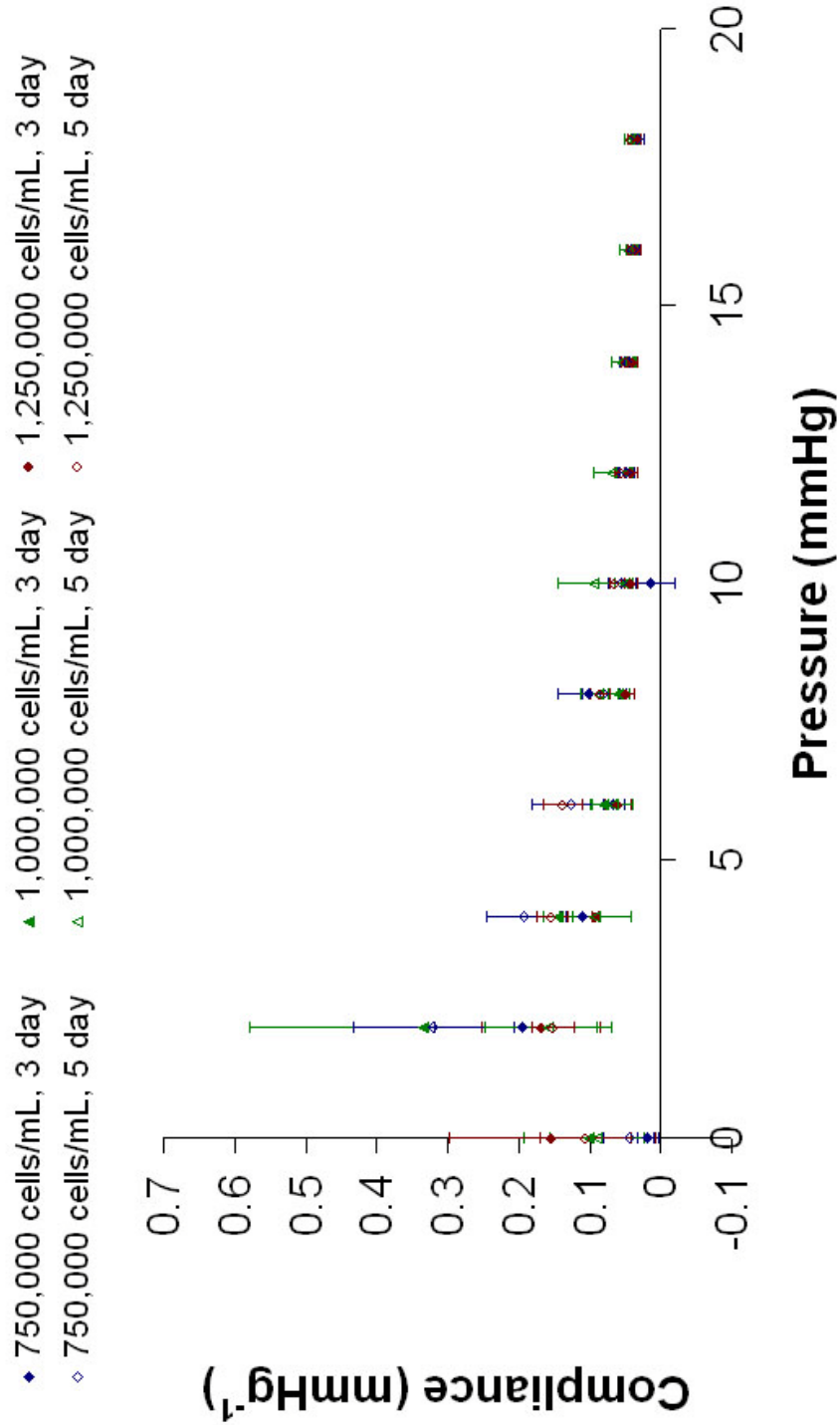


**Figure 4.6** Average stepwise compliance curves for constructs fabricated from  $7.50 \times 10^5$ ,  $1.00 \times 10^6$ , or  $1.25 \times 10^6$  cells/mL for 3 (n=3) or 5 (n=4) days. Data shown as average  $\pm$  SEM.

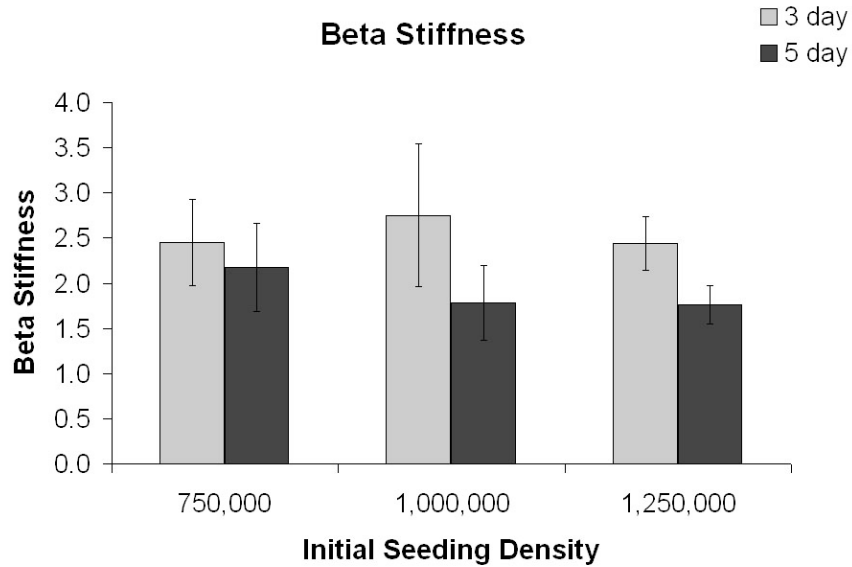


**Figure 4.7** Average beta stiffness values for constructs fabricated from  $7.50 \times 10^5$ ,  $1.00 \times 10^6$ , or  $1.25 \times 10^6$  cells/mL for 3 (n=3) or 5 (n=4) days. Data shown as average  $\pm$  SEM.

#### 4.3.4 Histology

H&E staining showed a homogeneous distribution of cells through the thickness of all constructs (**Figure 4.8A-F**). No differences in cell distribution or density were qualitatively detected between any groups. Both trichrome and PSR staining were negative (data not shown), indicating that no collagen was produced for any seeding density during either 3 or 5 days of dynamic culture. Staining for  $\alpha$ -sma was also negative for all conditions, indicating that dynamic culture within a spinner flask is not enough to stimulate differentiation of these BMPCs to smooth muscle cells.

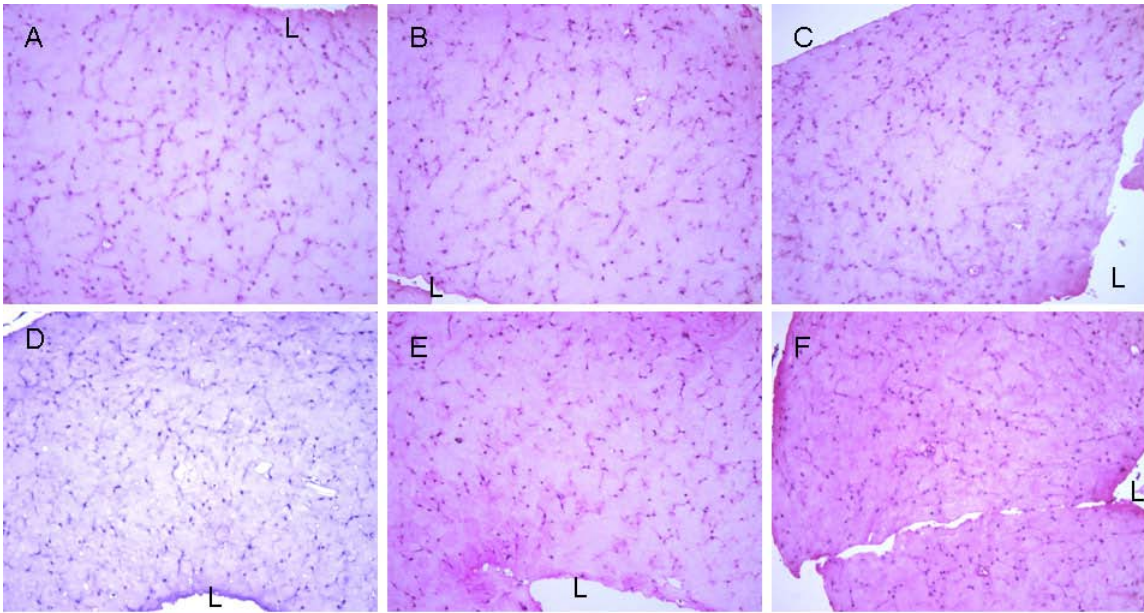


**Figure 4.8** Representative H&E sections from constructs fabricated from  $7.50 \times 10^5$  (A,D),  $1.00 \times 10^6$  (B,E), or  $1.25 \times 10^6$  (C,F) cells/mL for 3 (A-C) or 5 (D-F) days. Images taken at 10x, L indicates the lumen of each construct.

### 4.3.5 Ex-Vivo Studies

Placement of the TEUW around the diseased urethra (**Figure 4.9**) decreased compliance compared to the urethra alone (**Figure 4.10**). The TEUW was able to provide some mechanical support to the diseased tissue, minimizing dilation of the proximal portion upon increases in intraluminal pressures.

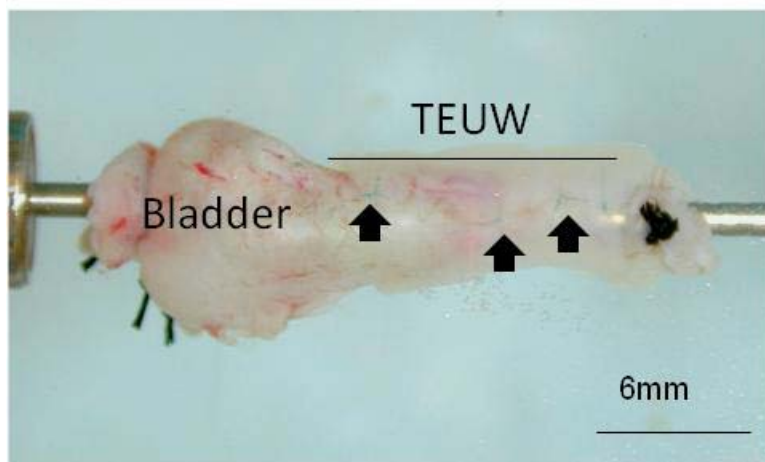
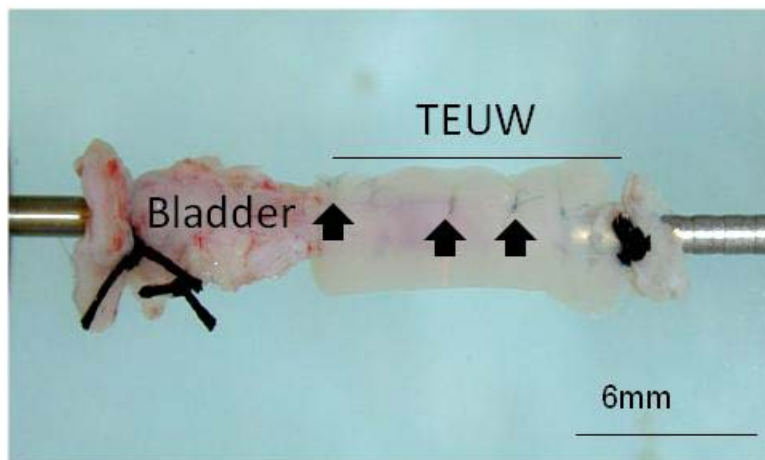
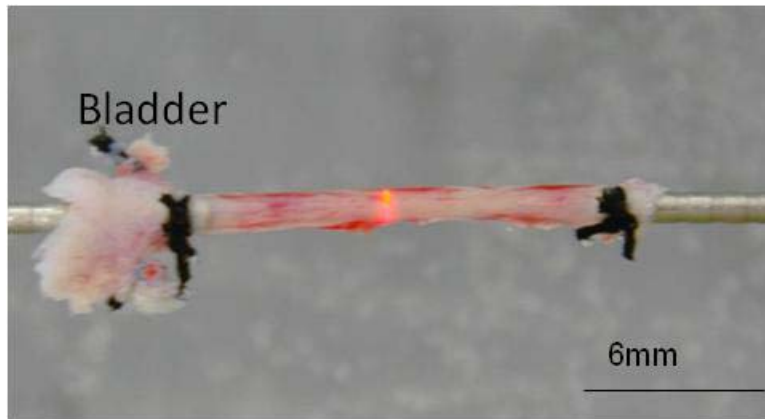


**Figure 4.9** Pictures of a healthy, unwrapped urethra (A), a wrapped urethra (B) and a wrapped urethra under pressure. Arrows indicate sutures.

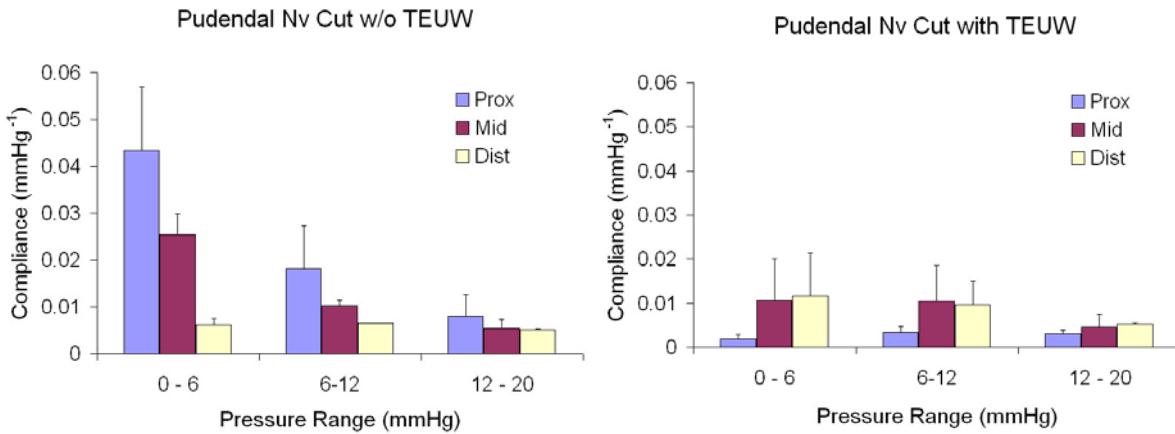


**Figure 4.10** Average compliance values for dysfunctional urethras with and without a TEUW around the proximal portion of the urethra (n=2). Data shown as average  $\pm$  SEM.

#### 4.4 DISCUSSION

We have demonstrated that a tissue engineered urethral wrap, composed of fibrin and bone marrow progenitor cells, may provide support to the diseased urethra. Mechanical properties show burst pressures greater than typical peak intraurethral pressures (~40 mmHg in the rat [179]), while maintaining compliance values similar to those of a healthy urethra [142]. Ex-vivo testing provides proof-of-concept that when placed around a dysfunctional urethra, the TEUW lends structural support, decreasing the compliance of the tissue by not allowing it to distend as much as it would in its diseased state, allowing urine leakage.

Current treatments for urethral dysfunction include the use of bulking agents, which dissipate over time; implantation of synthetic materials, which can cause erosion of the surrounding tissues [154], or use of urogenital tissue, which are limited in source and may cause

fistula or stricture formation [180]. Many tissue engineering approaches attempt to replace the damaged or diseased portion of the urethra, which may also lead to fistula or stenosis [181] and requires the replacement to withstand contact with urine as well as urethral pressures during micturition. Our approach is based on augmenting the diseased tissue, while keeping it intact. In using fibrin, the TEUW can degrade as the stem cells provide structural and biological support to the tissue.

We observed a homogeneous cell distribution for all densities at both culture durations, which is typically seen in fibrin gels [96]. Our mechanical characteristics agree with those in the literature showing that mechanical properties increase with increasing compaction [97]. The inverse trend seen between cell viability and burst pressure disagrees with what has been reported previously for smooth muscle cells in fibrin [97]. This may be a result of the interaction between the BMPCs and fibrin during culture. These BMPCs are highly proliferative and compaction of the constructs may be impeding this proliferation via contact inhibition. The compaction seen in our constructs (1.81% of initial volume) is slightly greater than that published on fibrin gels containing smooth muscle cells (~3-4%) [94, 97, 182]. This difference could be a result of many factors including the concentrations of fibrin and/or thrombin [97] and the difference in the reaction of the cell type to the fibrin substrate.

We believe that the lack of collagen production for constructs was due to our short culture durations. Most in-vitro studies showing collagen production in fibrin involved culture for 2 or more weeks and used smooth muscle cells or fibroblasts, which tend to produce large amounts of collagen naturally [94, 100, 182]. We do believe that following implantation the body will act as a bioreactor and stimulate collagen production in-vivo, either by the BMPCs or by host cells that migrate into the TEUW.

Limitations of the current study include use of the MTT assay for cell viability. Most metabolic viability assays, including the MTT assay, were developed for 2D cultures. The three-dimensional nature of our constructs presents many challenges in using this assay. It may be more difficult for the reagents to diffuse through the matrix to reach the cells and the metabolic activity of cells in 3D may be very different than in 2D [183]. Other assays such as cell counting from histologic sections may have been more appropriate. Additional mechanical testing, including tensile tests, would have been beneficial in determining the ultimate mechanical properties of these constructs. Although we utilized ascorbic acid in the culture media to enhance collagen production other methods such as the addition of TGF- $\beta$  or use of mechanical stimulation may have been more beneficial (**Chapter 6.0**) [94, 100, 102].

This study has laid a foundation for further development of the TEUW for urethral dysfunction. We have developed a wrap with appropriate mechanical properties to provide support to the diseased urethra, and have shown that the TEUW is capable of decreasing the compliance of a diseased urethra. The TEUW shows promise for an autologous therapy to provide support to the urethra. We believe that our future studies will continue to show the short and long term benefits of the TEUW to urethral function.

## 5.0 DESIGN OF AN INDEPENDENT, MULTI-CHAMBER BIOREACTOR FOR TUBULAR CONSTRUCTS

As tissue engineering and regenerative medicine continue to grow and expand so does bioreactor technology. Bioreactors have been used for decades for the culture and rapid expansion of microbes or mammalian cells, but the expansion to culture of 3-D structures required the expansion of concepts and design [184]. Today, bioreactors are generally utilized to increase diffusion of nutrients from media to cells within a matrix as well as to provide stimuli to those cells to enhance maintenance of, or differentiation to, a desired phenotype. A variety of bioreactors have been implemented [180, 184, 185] and some commercialized [186-188] to provide mechanical stimulation to constructs, with the majority of bioreactors designed for the culture of bone/cartilage replacements or vascular grafts [184, 189, 190] as reviewed below and summarized in **Table 5.1**.

One bioreactor utilized compression loading of multiple samples simultaneously within a petri dish by paddles within static bathing media to enhance cell alignment for cartilage engineering [191]. Another cartilage bioreactor utilized biaxial strain, delivered by a piezoelectric stamp, to stimulate osteoblasts within a collagen gel [192]. This system utilized open loop circulation, where the constructs were continuously exposed to fresh media for the 1 to 3 week culture period, and allowed for the stimulation of four independent constructs at a time [192]. A bioreactor for the development of bladder tissue utilized a pressure system where a

sheet of ECM seeded with cells was clamped between two chambers and exposed to pressure, which was controlled by a closed-loop feedback system, on one side [193]. Due to the short duration of these experiments (18 hours), no media circulation was utilized [193].

In contrast to cartilage tissue engineering, vascular or tubular tissue engineering tends to utilize one of two culture methods, perfusion or rotation. One study assessed the difference between rotation and perfusion culture with two custom made systems, which can be run within a standard incubator and culture one construct at a time [194]. The rotating bioreactor consisted of a cylinder filled with media, in which the construct was immersed, which was placed on a variable speed rotator to provide mixing of the culture media for enhanced oxygen and nutrient uniformity [194]. The perfusion bioreactor utilized a continuous flow, closed-loop circulation, which provided pulsatile flow and shear stress to the lumen of the mounted construct [194]. Other perfusion bioreactors for the delivery of pulsatile flow have also been developed [106, 185, 195-197]. Some allow for only one construct [196, 197] to be cultured at a time with [197] or without [196] media changes over the culture duration, while others allow for the simultaneous culture of multiple constructs, which share bathing and/or luminal media [106, 185, 195]. In addition, BOSE<sup>®</sup> and Tissue Growth Technologies (TGT) have developed several versatile, commercially available bioreactors including ones for compression, tension or perfusion with or without tension or compression, all of which are computer controlled and allow for culture of one or multiple constructs simultaneously and independently [186, 188].

However, these bioreactors have several shortcomings, including their large size [198, 199], which requires them to be run on a bench top while maintaining appropriate gas and temperature conditions and also to utilize a large volume of media, increasing experimental cost. Another limitation of these bioreactors is the number of constructs they can culture at one time.

If they are built to accommodate multiple constructs, the constructs generally share media, generating replicates instead of independent experiments. The independent culture of constructs is needed to limit cross-contamination of shared media between constructs by cells within one of the constructs. Although the commercially available systems provide independent culture, they tend to be quite expensive.

Development of a compact, multi-chamber bioreactor capable of accommodating up to four independently cultured constructs reduces experimental cost by decreasing required media volumes and eliminates additional means of temperature and gas regulation as it can be run within a standard cell culture incubator. The separation of each unit allows various culture conditions to be run simultaneously and prevents cross-contamination between constructs. The goal of this work was to design a space- and cost-efficient bioreactor for the perfusion of multiple tubular constructs, for augmentation of the urethra, under minimal pressure and flow.

**Table 5.1** Summary of bioreactors and their main features.

	Number of Constructs	Media Volume	Constructs Share Media	Media Change/ Monitoring	In Incubator	Feedback Control	Type(s) of Stimulus
Punchard <i>et al.</i> , 2007 [196]	1	NA	NA	No/No	Yes	No	Pulsatile Flow
Xu <i>et al.</i> , 2005 [197]	1	NA	NA	Yes/No	Yes	Yes	Pulsatile Flow
BOSE® [186]	1 and up	NA	No	Yes/Yes	Yes	Yes	Pulsatile, Compression and Tension
TGT [188]	1-6	NA	No	Yes/Yes	Yes	Yes	Pulsatile, Compression and Tension
Huang <i>et al.</i> , 2005 [106]	3	250 mL	Yes	No/No	Yes	No	Pulsatile Flow
Hahn <i>et al.</i> , 2007 [195]	3	NA	Yes	No/No	Yes	No	Pulsatile Flow
Williams <i>et al.</i> , 2004 [185]	1 and up	1000 mL	Yes	Yes/No	Yes	No	Pulsatile Flow
Au-yeng <i>et al.</i> , 2009 [191]	4	7 mL	Yes	Yes/No	Yes	No	Compression
Meyer, <i>et al.</i> , 2005 [192]	4	NA	No	Yes/No	Yes	No	Biaxial Strain
Arrigoni <i>et al.</i> , 2008 [194]	1	100 mL	NA	No/No	Yes	No	Pulsatile Flow or Rotation
Wallis <i>et al.</i> , 2008 [193]	1	NA	NA	No/No	Yes	Yes	Pressure
Altman <i>et al.</i> , 2002 [198]	24	NA	No	Yes/Yes	No	Yes	Rotational Strain

## 5.1 METHODS

### 5.1.1 Bioreactor Design

One design constraint for the bioreactor was limiting the size of the entire system to that of a standard incubator tray (18 x 18 in). Another was minimizing the volume required for each circuit. Easy access for sampling to measure environmental conditions (pH, pCO<sub>2</sub>, pO<sub>2</sub> and pressure) for each circuit was desired. Each circuit was designed to include a pump (**Section 5.1.1.1**) to control flow, a culture chamber (**Section 5.1.1.3**) to house the constructs, a pulse-dampener (**Section 5.1.1.2**) to remove pulsatility from the flow and a reservoir (**Section 5.1.1.2**) for media overflow. All components were designed in SolidWorks<sup>®</sup> 2007 (CADventure, Willoughby, OH) and fabricated at the University of Pittsburgh's Department of Cell Biology and Physiology Machine Shop. All ports and fittings were purchased from McMaster-Carr (McMaster-Carr, Robbinsville, NJ). Bioreactor components were sterilized by autoclave or ethylene oxide (Anderson Products, Inc., Haw River, NC). Each component of the chambers, pulse-dampener and reservoir was fabricated by milling them out of a solid block of Plexiglas. Helicoils were used for all components in each of the screw-holes to prevent stripping with repeated assembly and disassembly.

#### 5.1.1.1 Pump

The pump for this system was a Masterflex<sup>®</sup> L/S pump (Model 77300-50, Cole-Parmer, Vernon Hills, IL) (**Figure 5.1A**). The pump head chosen for this system was the L/S<sup>®</sup> Multichannel Pump Head for L/S pump tubing (Model EW-07535-04, Cole-Parmer, Vernon Hills, IL) (**Figure 5.1B**), with a flow range of 0.045 – 280 mL/min. This pump head utilizes six

roller heads for low-pulsation flow and is stackable if additional circuits were required. It is made of stainless steel and anodized aluminium and is able to run within an incubator environment. Two-stop pharmed tubing is required for use in this head, L/S 16 pharmed tubing (Model 96114-16 Masterflex, Cole-Parmer, Vernon Hills, IL) was chosen based on our desired flow rates (**Figure 5.1C**). A Masterflex controller/dispenser (Model 77300-70, Cole-Parmer, Vernon Hills, IL) (**Figure 5.1D**) was used to control the pump. The controller was programmed for the pump head and tubing used in order to yield desired flow rates.

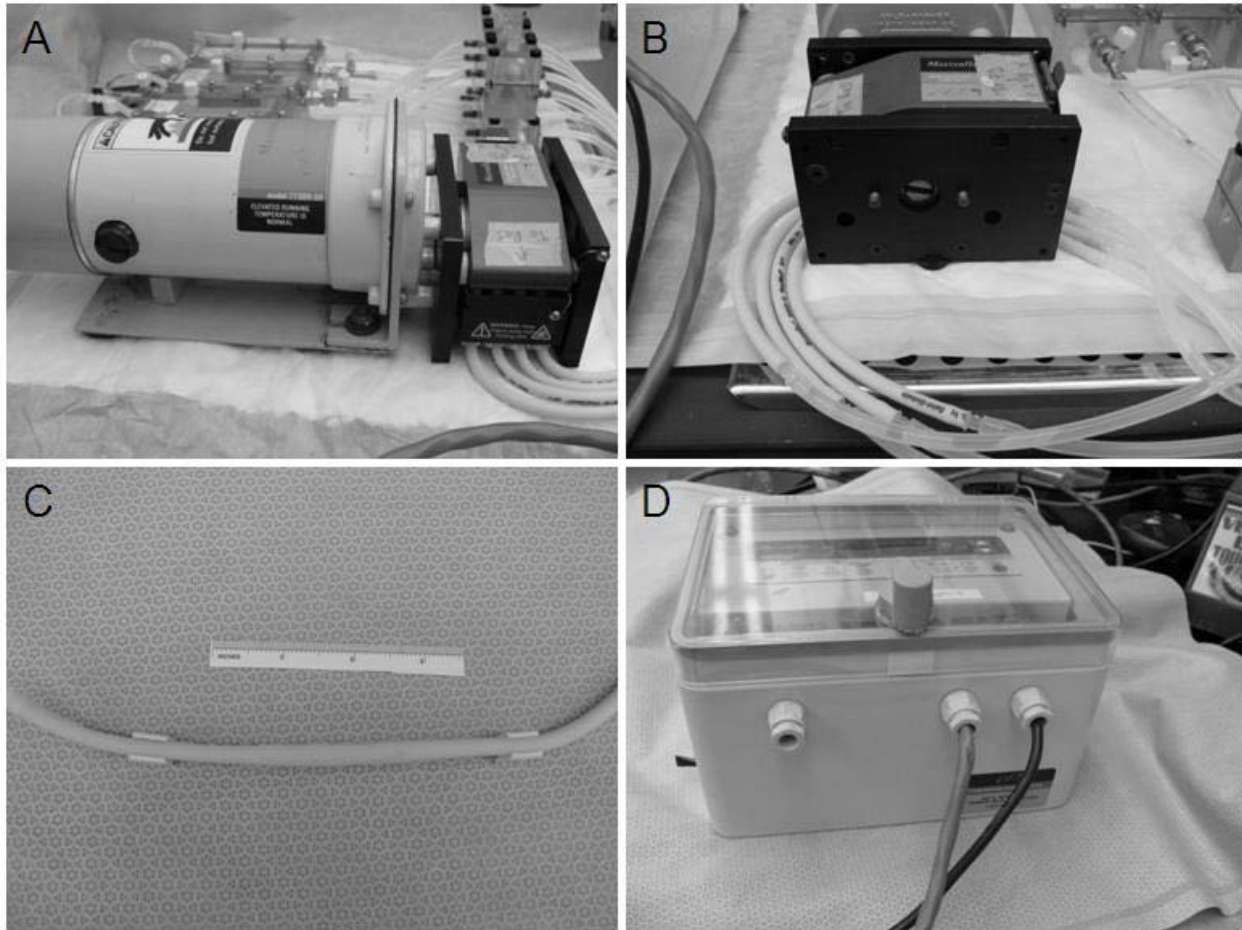


**Figure 5.1** The Masterflex® L/S pump (A) with L/S® Multichannel Pump Head (B) and two-stop L/S 16 pharmed tubing (C) was controlled by the Masterflex controller/dispenser (D).

### 5.1.1.2 Pulse-dampener and reservoir

The pulse-dampener was custom-designed as four independent chambers within one block unit (**Figure 5.2** and **Figure 5.3**). The unit is composed of a cap, rubber gasket and base. The pulse-dampener cap unit (**Figure 5.2A** and **Figure 5.3A**) consists of four hemispheres, each with a radius of 0.5 in. The pulse-dampener base unit (**Figure 5.2B** and **Figure 5.3B**) consists of four cylinders, each with a radius of 0.5 in and a height of 0.75 in with both in- and out-flow ports on each pulse-dampener. Each chamber can hold a total volume of 14 mL. The three components are held together by compression with sixteen one-inch long thumb screws.

The reservoir (**Figure 5.4** and **Figure 5.5**) is a modified version of the pulse-dampener, where each hemisphere in the cap unit has a radius of 0.53 (**Figure 5.4A** and **Figure 5.5A**) and each cylinder in the base unit has a radius of 0.53 in and a height of 0.75 in (**Figure 5.4B** and **Figure 5.5A**). Each chamber therefore holds a volume of 16 mL. The reservoir unit is also equipped with female luers on the outer side, one at the center of each dome in the cap unit. These luers accommodate a double ended male luer with a 0.2  $\mu\text{m}$  syringe filter (Corning, Inc, Corning, NY) to aid in gas exchange during culture. However, most gas exchange occurs via silicone tubing (ID = 0.125 in, OD = 0.250 in, wall = 0.063 in; Masterflex, Cole Parmer Instrument Co., Vernon Hills, IL).

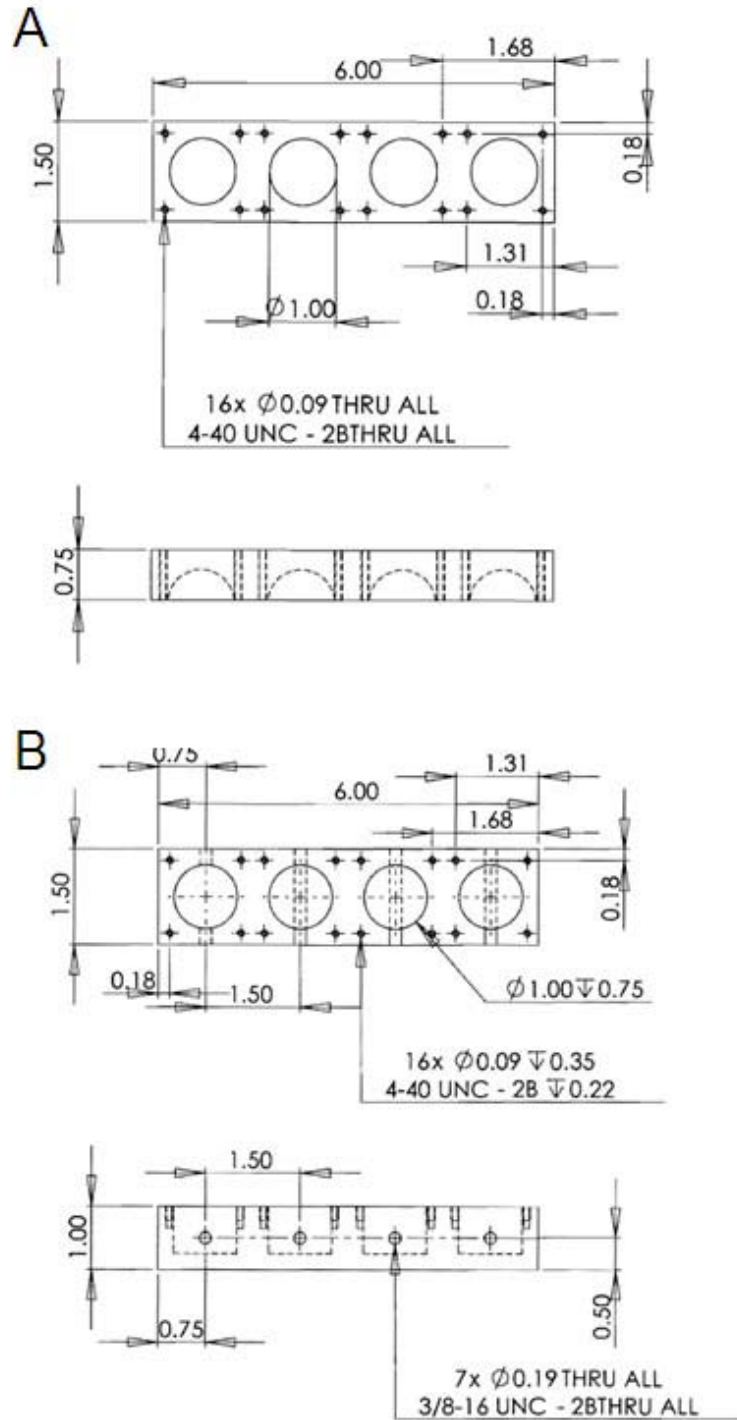


**Figure 5.2** Solidworks<sup>®</sup> drawing of the (A) cap and (B) base of the pulse dampener. Dimensions in inches.

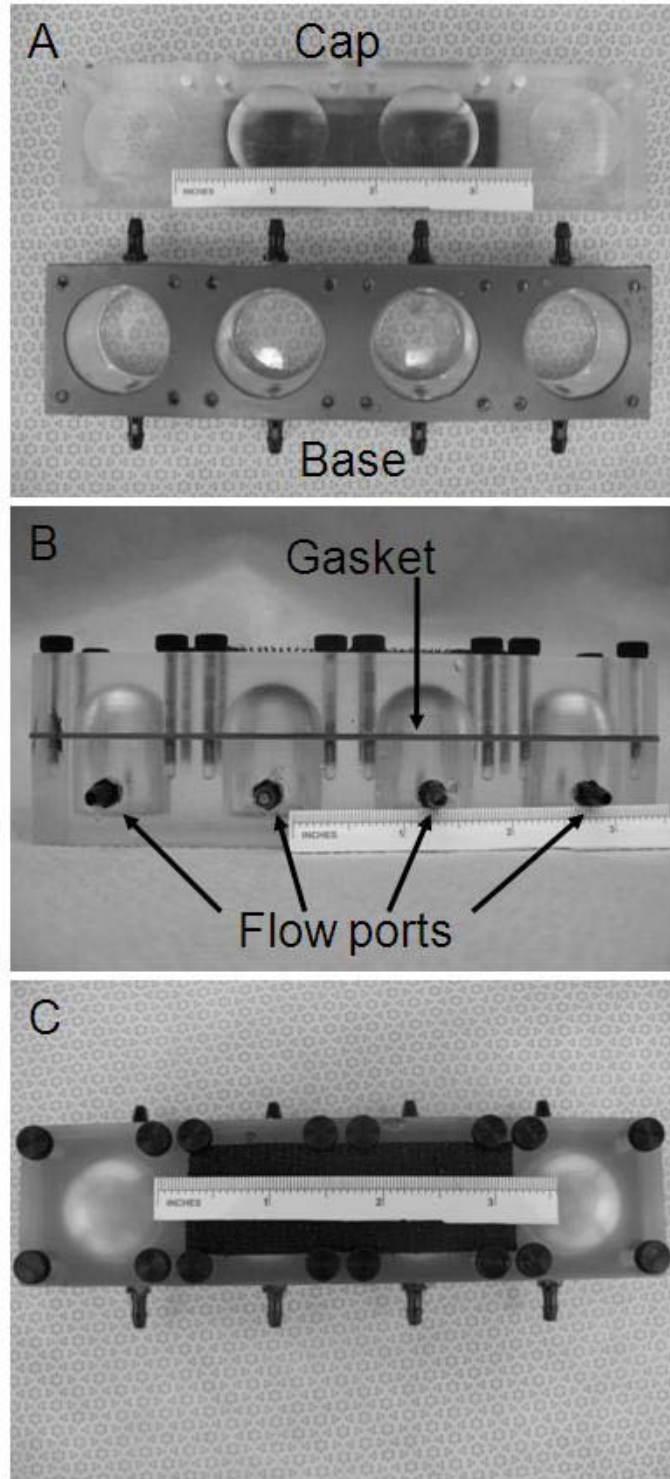


**Figure 5.3** Pictures of the bioreactor pulse-dampener as separate components from the top (A), with lid in place from the side (B) and with lid in place from the top (C). Scale in inches.

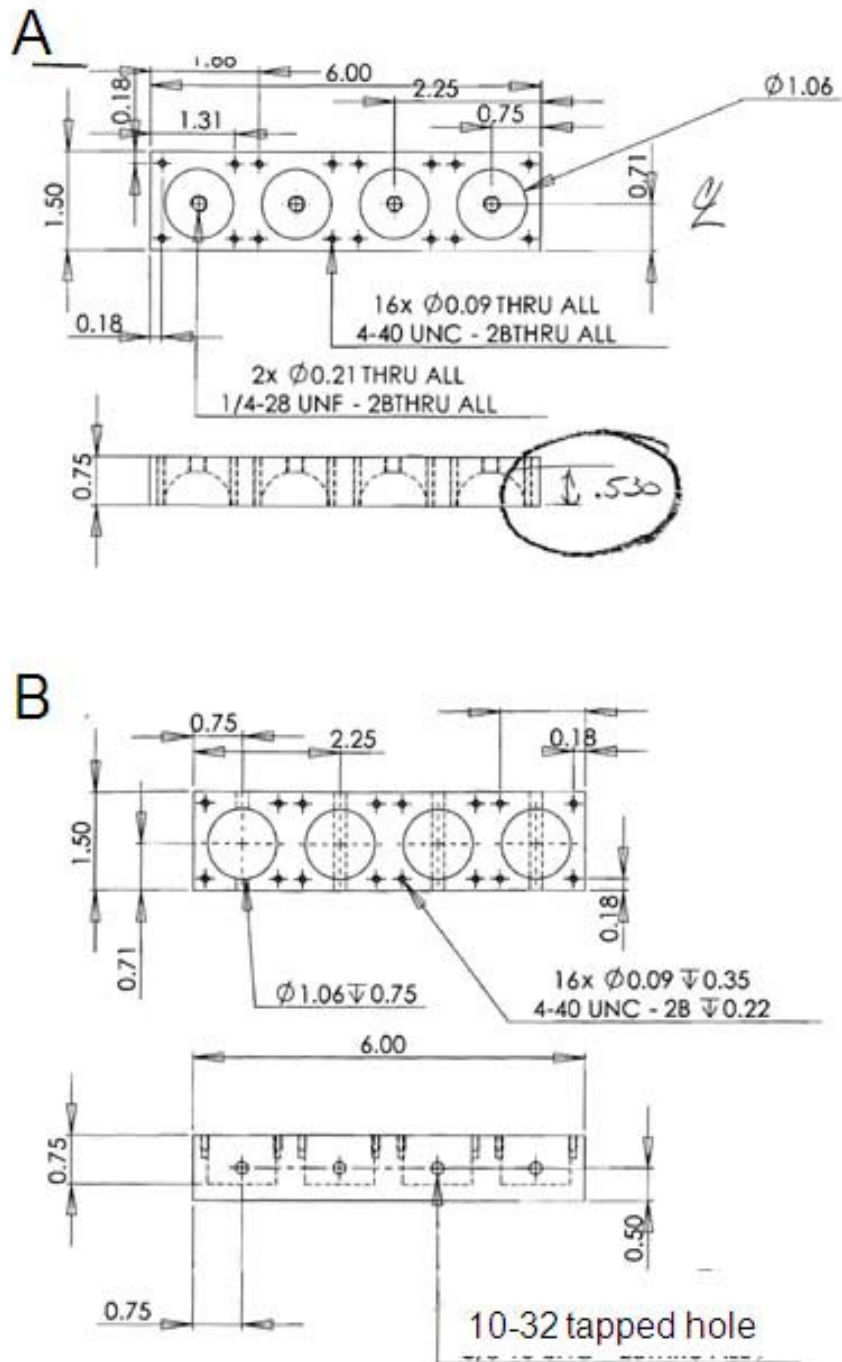
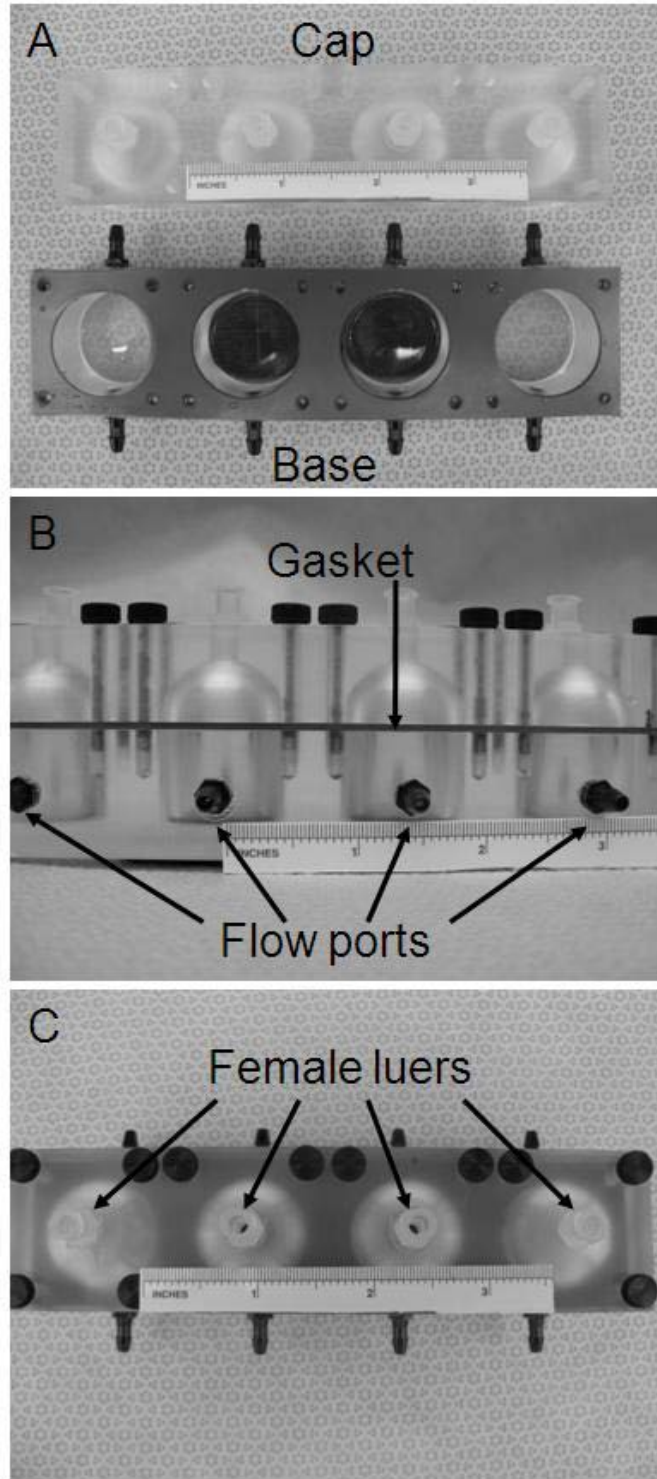


Figure 5.4 Solidworks® drawing of the (A) cap and (B) base of the reservoir. Dimensions in inches



**Figure 5.5** Pictures of the bioreactor reservoir as separate components from the top (A), with lid in place from the side (B) and with lid in place from the top (C). Scale in inches.

### 5.1.1.3 Construct-housing chambers

Each culture chamber is comprised of a lid, base and rubber gasket (**Figure 5.6** and **Figure 5.7**). The lid (**Figure 5.6A** and **Figure 5.7A**) is a solid piece of Plexiglas<sup>®</sup> with a female luer port to accommodate an injection port for media sampling and addition of chemical agents to the culture. Each construct-housing chamber (**Figure 5.6B** and **Figure 5.7A**) is outfitted with two ports for media inflow and outflow and two one-quarter inch swageloks<sup>®</sup> for the stainless steel tees described in **Section 5.1.1.4**. The volume of the construct housing chamber is 149 mL. The three pieces are compression-fit with eight half-inch thumb screws. The construct-housing chambers were designed for luminal flow to enter the constructs from the pulse-dampener and exit to the bathing chamber. Media from the bathing chamber then flowed into the reservoir to be re-circulated through the system.

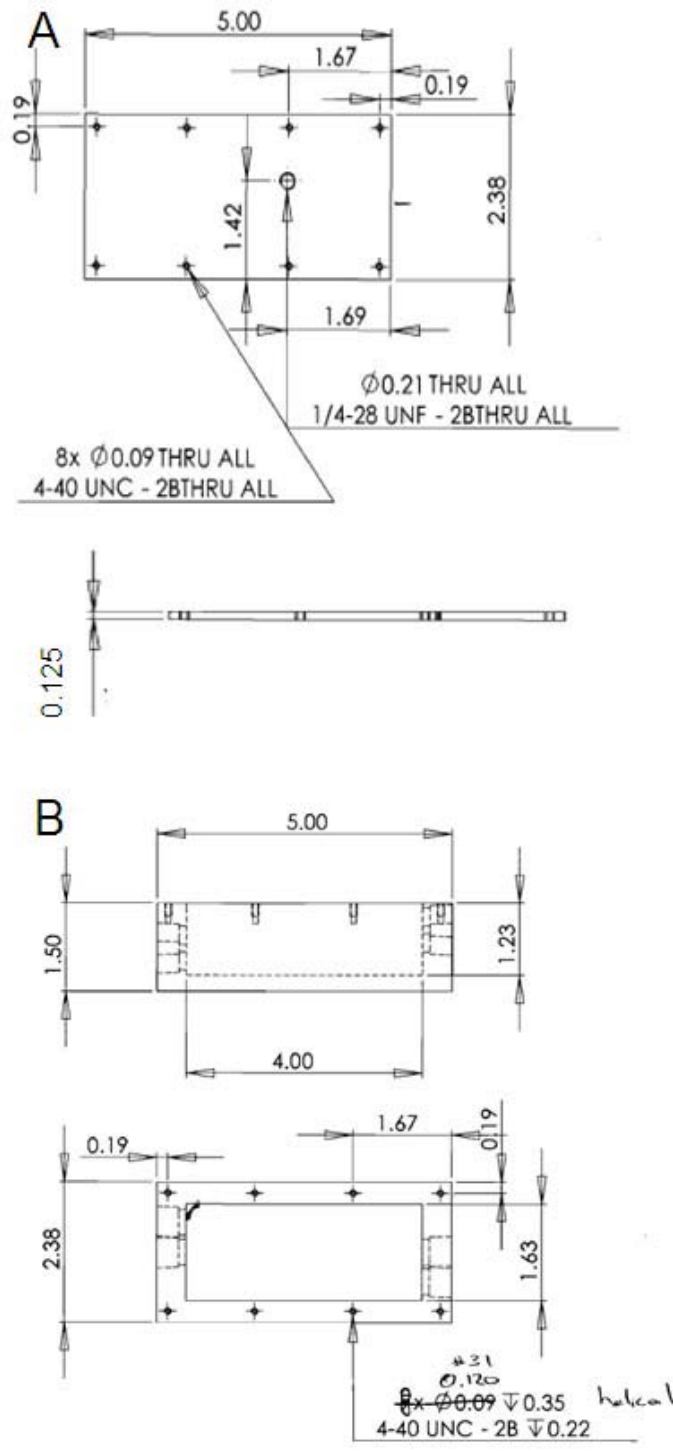


**Figure 5.6** Solidworks® drawing of the top and side views of the chamber lid (A) and base (B). Dimensions in inches.

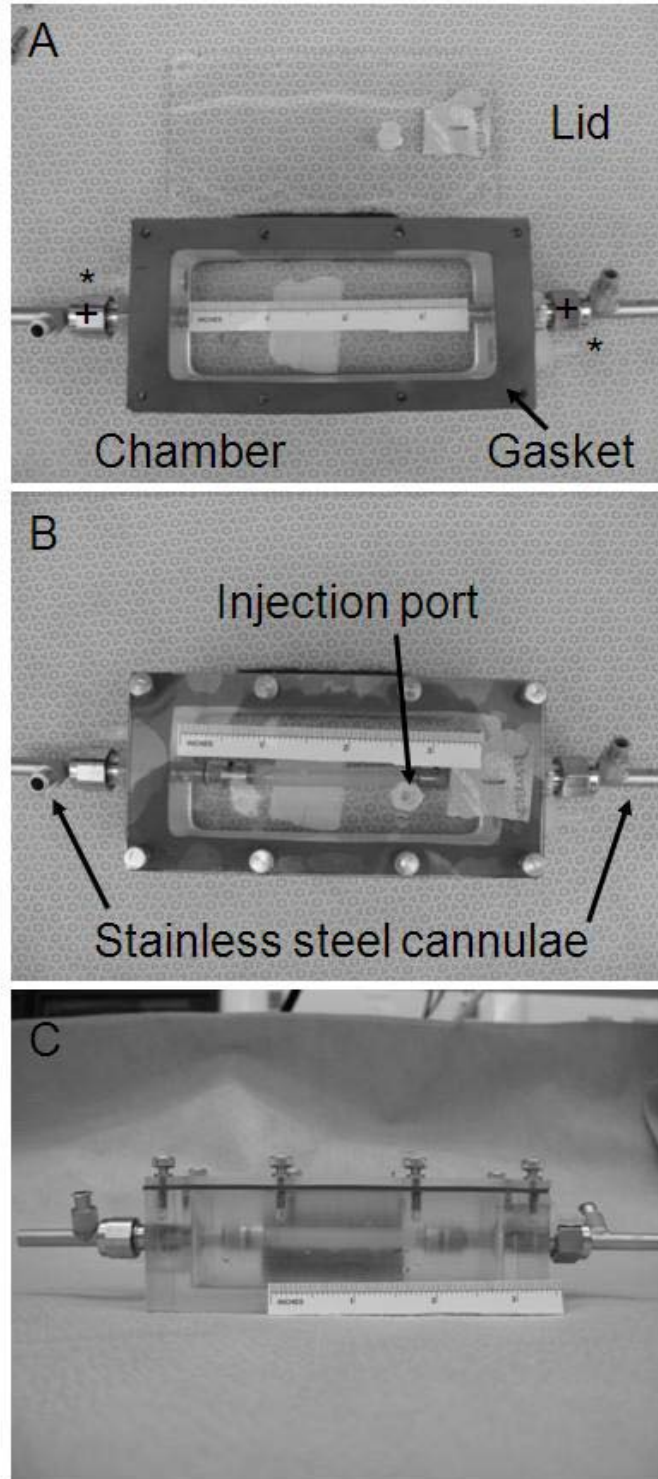


**Figure 5.7** Pictures of the bioreactor construct-housing chamber as separate components from the top (A), with lid in place from the top (B) and with lid in place from the side (C). Scale in inches.

#### 5.1.1.4 Tees and cannulae

Each construct-housing chamber is equipped with two tees, which are comprised of several parts. A three inch long piece of stainless steel tubing, with inner and outer diameters of 0.12 and 0.25 inches, respectively, had the proximal end bored and threaded. The end was then fitted with a male luer attached to a screw and a rubber gasket (**Figure 5.8A-B**). The stainless steel tubing was also fitted with a female luer perpendicular to the long axis of the tubing and 0.75 inches from its distal end (**Figure 5.8A-B**). Tubular constructs are mounted onto cannulae (ID = 0.024 in, OD = 0.036 in, L = 1 in; Becton Dickson; Sandy, UT) cut to a length of 0.5 in (**Figure 5.8C**), which are then mounted onto the proximal stainless steel tees via luer fittings (**Figure 5.8D**).

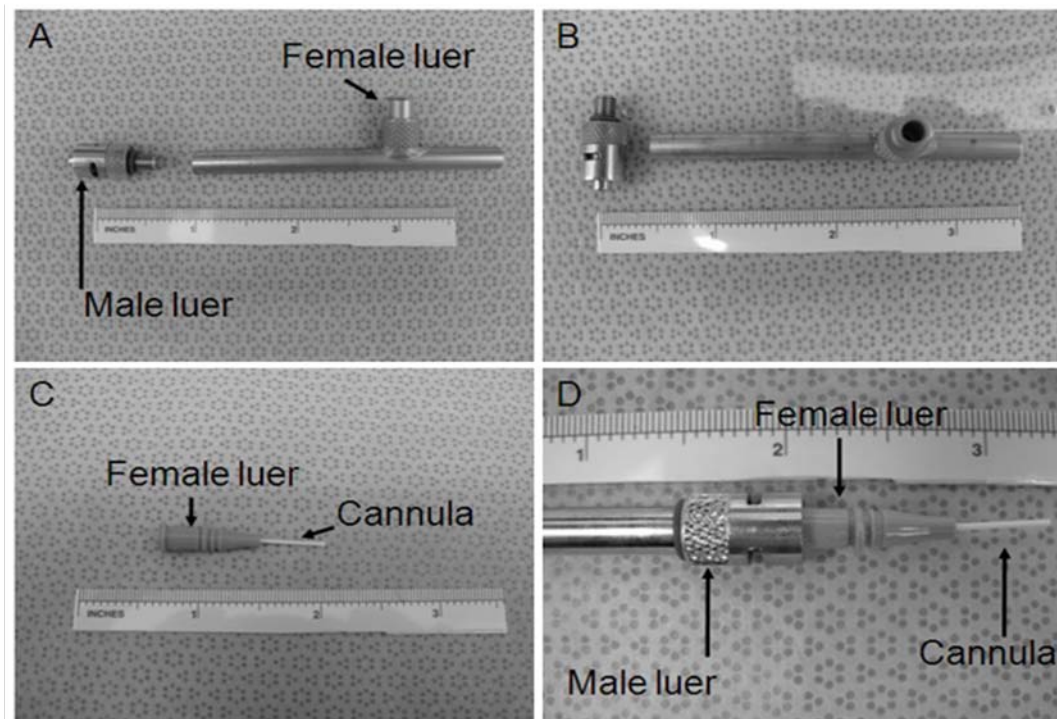


**Figure 5.8** Side (A) and top (B) images of a stainless steel tees used in the bioreactor. The cannulae on which the construct is mounted (C) is attached to the male luer of the stainless steel tees (D).

#### **5.1.1.5 Filling of the bioreactor**

A system consisting of a 60 mL syringe (Becton-Dickinson, Franklin Lakes, NJ), a manifold (Medtronic, Minneapolis, MN), pigtails (Becton-Dickinson, Franklin Lakes, NJ), and male-to-male luers (Argon Medical Devices, Athens, TX) was utilized to fill the system by gravity. The system (**Figure 5.9A**) was assembled by removing the plunger from the syringe, which was placed on a ring stand. The syringe was attached to a five port manifold by a pigtail (**Figure 5.9B**). The manifold ports were each attached to a pigtail which was connected to the female luer on the construct-housing chamber lid by a male-to-male luer (**Figure 5.9C**). Media was poured into the syringe and flowed into the construct-housing chambers by gravity. Each chamber was filled until the level of media reached its distal outflow port.

#### **5.1.1.6 Environmental conditions**

Since the bioreactor is run within a cell culture incubator, temperature and gas concentration are automatically regulated. The main mechanism of gas exchange between the bioreactor and incubator was silicone tubing (ID = 0.125 in, OD = 0.063 in; Masterflex; Cole-Parmer, Vernon Hills, IL). As stated in **Section 5.1.1.3**, each chamber is equipped with an injection port. This port was used to take media samples for measurement of pH, pCO<sub>2</sub>, and pO<sub>2</sub> via a blood gas analyzer (ABL5<sup>TM</sup>, Radiometer Medical A/S, Copenhagen, Denmark). The female luers on the stainless steel tubing described in **Section 5.1.1.4** served as the attachment site for pressure transducers (Edwards Life Sciences, Irvine, CA), which were used to monitor proximal and distal intraluminal pressures during culture. Pressure transducers were zeroed to the atmosphere then opened to the system and allowed to stabilize prior to each measurement.

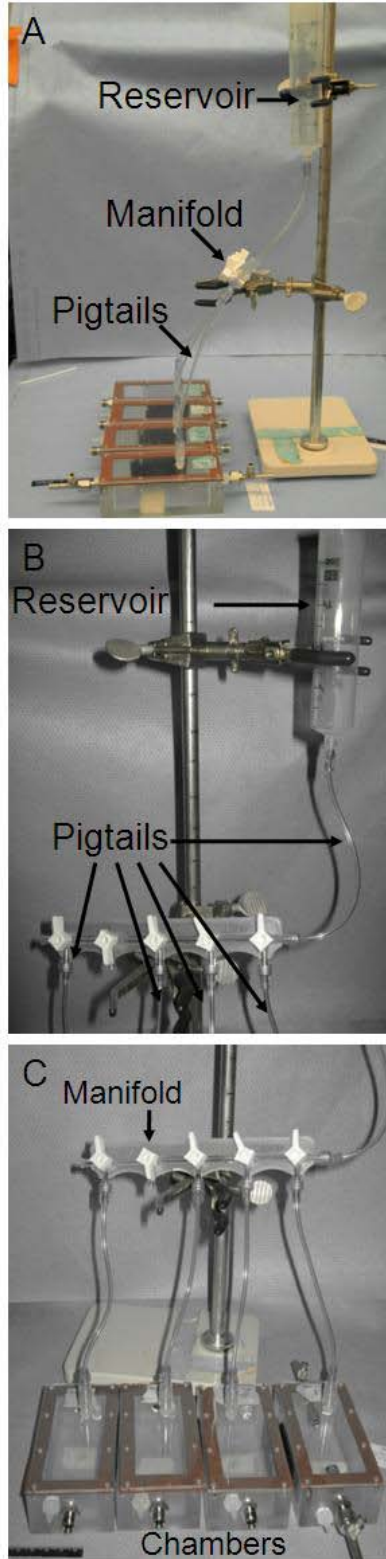


**Figure 5.9** Photographs of the entire filling apparatus (A), the reservoir to the manifold (B) and the manifold to the chambers (C).

## 5.1.2 System Verification

### 5.1.2.1 Flow rate

Flow rate was determined by assembling the system on an incubator tray on the bench top. The system was filled with deionized water, and the pump was turned on. Once all air was removed from the circuit, the system was allowed to equilibrate for ten minutes. Following equilibration, the tubing connected to the distal stainless steel cannula was separated from the chamber. The fluid exiting the cannula was collected in a graduated cylinder for 20 seconds and the volume was recorded. This process was performed for each circuit and repeated twice. The average for each chamber was multiplied by three and taken as the flow rate (mL/min) for each chamber for the designated pump settings. Values across chambers were compared to evaluate uniformity of flow.

### 5.1.2.2 System sterility and stability

Stability of the system was assessed by sterilizing the system and assembling in a cell culture laminar flow hood with sterile gloves. The system was filled with complete media (as defined in **Section 4.2.1**) and run in the cell culture incubator for 5 days. Environmental conditions were monitored for the duration of the experiment as described in **Section 5.1.1.6**. A first assessment of system sterility was the opaqueness of the media. ABL readings for pH, pCO<sub>2</sub>, pO<sub>2</sub> and HCO<sub>3</sub><sup>-</sup> were averaged both for each chamber over the entire culture duration and across all chambers each day. Values were compared to control media contained in a vented conical tube within the same incubator as the bioreactor system.

### 5.1.2.3 Mounting of constructs

Mounting of fibrin constructs (see fabrication in **Section 4.2.2**) was assessed on the bench top. One cannula was placed onto the stylet for a spinal needle (Becton Dickson; Sandy, UT) (**Figure 5.10A**) and guided through the lumen of the construct. Another cannula was placed on the stylet (**Figure 5.10B**). The stylet was then mounted into a clamp assembly (**Figure 5.10C-D**). Cannulae were adjusted so that they were ~1 – 1.5 mm inside each end of the construct. The construct was then tied to the cannulae with 4-0 silk suture (Syneture, Mansfield, MA). The stylet was removed and a 3 mL syringe of blue dye was attached to one of the cannula and gently depressed until flow through the construct was visible. The assembly was observed for leakage at the suture line.

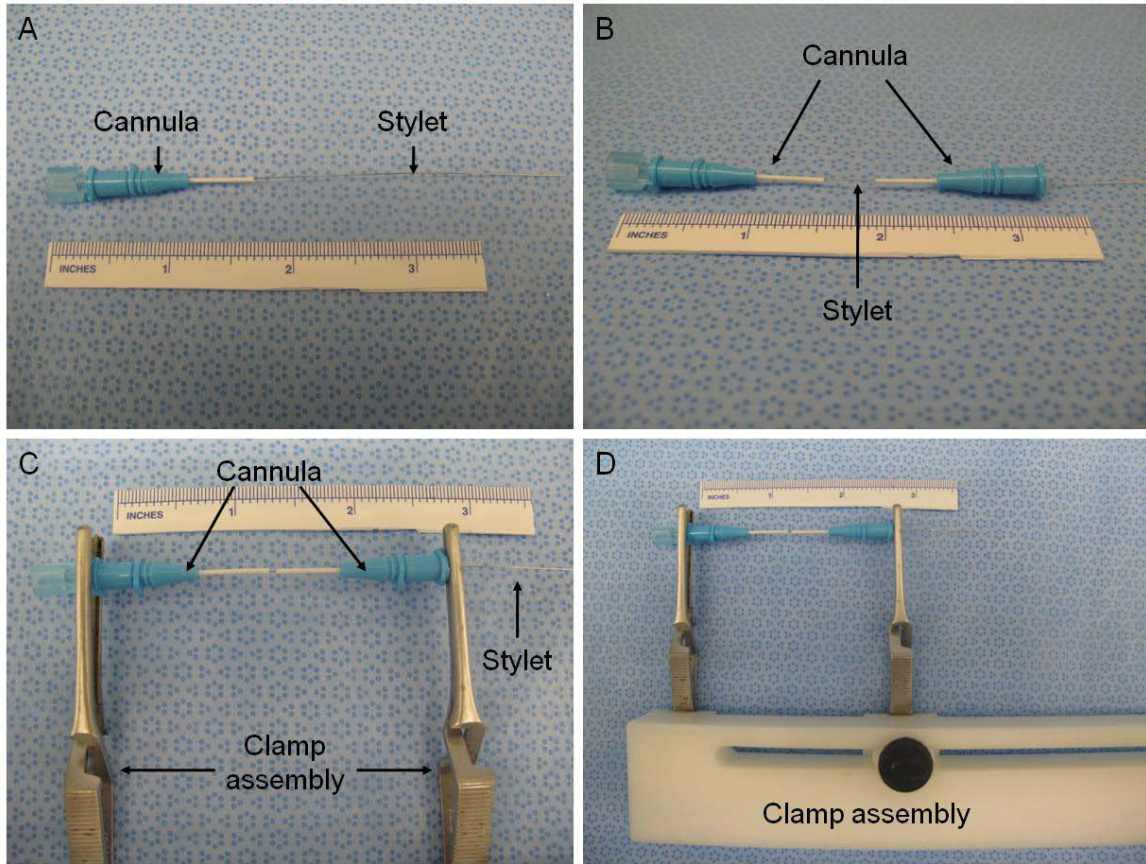


**Figure 5.10** Images depicting the process of mounting a construct onto the cannulae. The guide is threaded through one cannula (A), the construct and then another cannula (B). The guide is then placed into the clamp assembly (C-D). Scale in inches.

### 5.1.3 Statistical Analyses

Data is represented as the average  $\pm$  standard error of the mean. Flow rates were averaged for each chamber. Environmental conditions were averaged for each chamber over the entire culture period as well as across chambers at each day of culture. Bioreactor values were compared to those of media housed within a vented conical tube kept in the same incubator as the bioreactor. Statistical comparisons were performed using a Student's t-test. Significance was detected at p-values less than 0.05.

## 5.2 RESULTS

### 5.2.1 Bioreactor Fabrication

The entire system was able to fit on a standard cell culture incubator tray when assembled (**Figure 5.11**) and required only 500 mL of media for the culture of four independent constructs. As all of the components are sealed by compression, there is a pressure threshold, above which, leaking will occur. However, all of our experiments were performed at low pressures, well below the threshold of leaking (~40 mmHg).

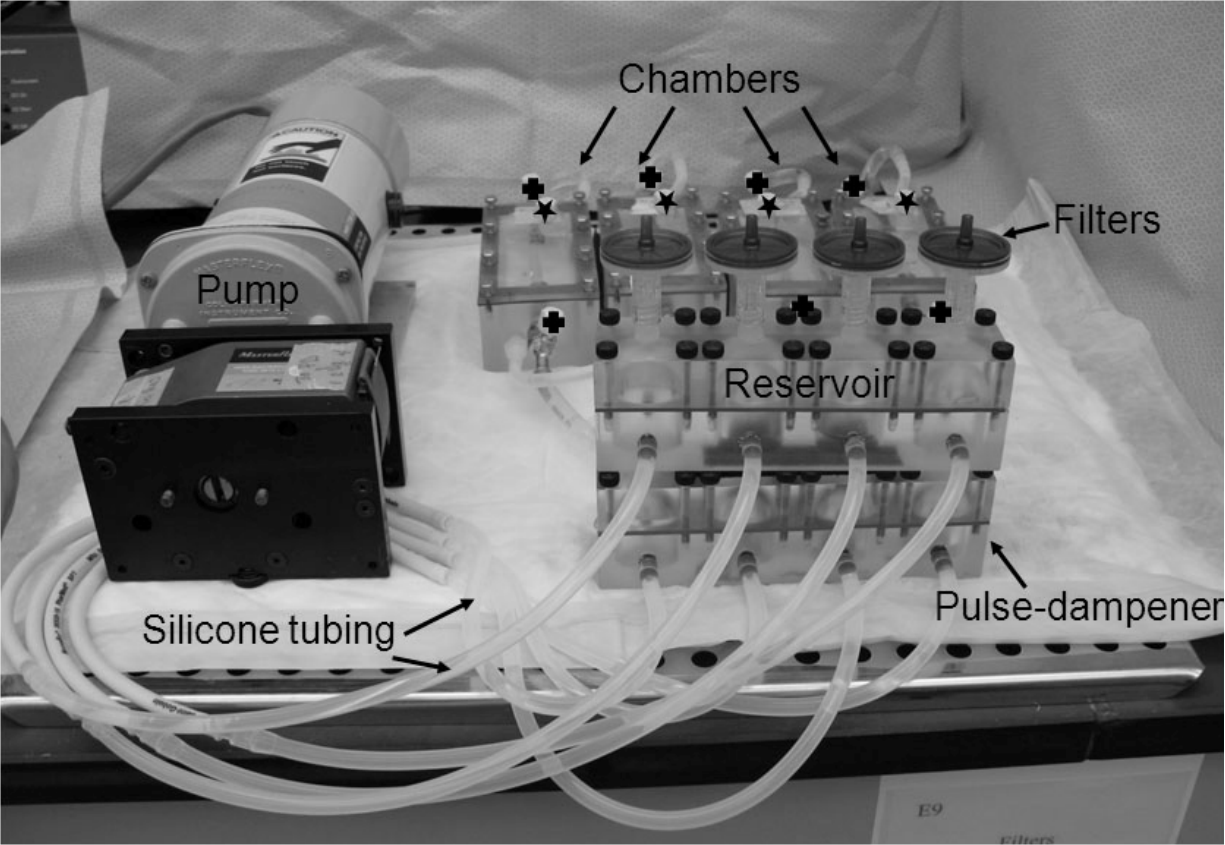


**Figure 5.11** A picture of the entire bioreactor system assembled on a cell culture incubator tray. Stars represent injection ports and pluses represent ports for pressure transducers.

## 5.2.2 Flow Rate

A minimal average intraluminal flow rate of 3.6 mL was obtained for each of the four chambers (n=3) as seen in Table 5.2. The average flow rate for each chamber was 3.6 mL (**Figure 5.12**). There were no significant differences between flow rates from any of the chambers.

**Table 5.2** Experimental values for flow determination for all chambers.

	<b>Run 1</b> mL/min	<b>Run 2</b> mL/min	<b>Run 3</b> mL/min	<b>Average</b> mL/min	<b>SEM</b> mL/min
Chamber 1	3.6	3.6	3.6	3.6	0
Chamber 2	3.6	3.6	3.6	3.6	0
Chamber 3	3.6	3.6	3.6	3.6	0
Chamber 4	3.6	3.6	3.6	3.6	0

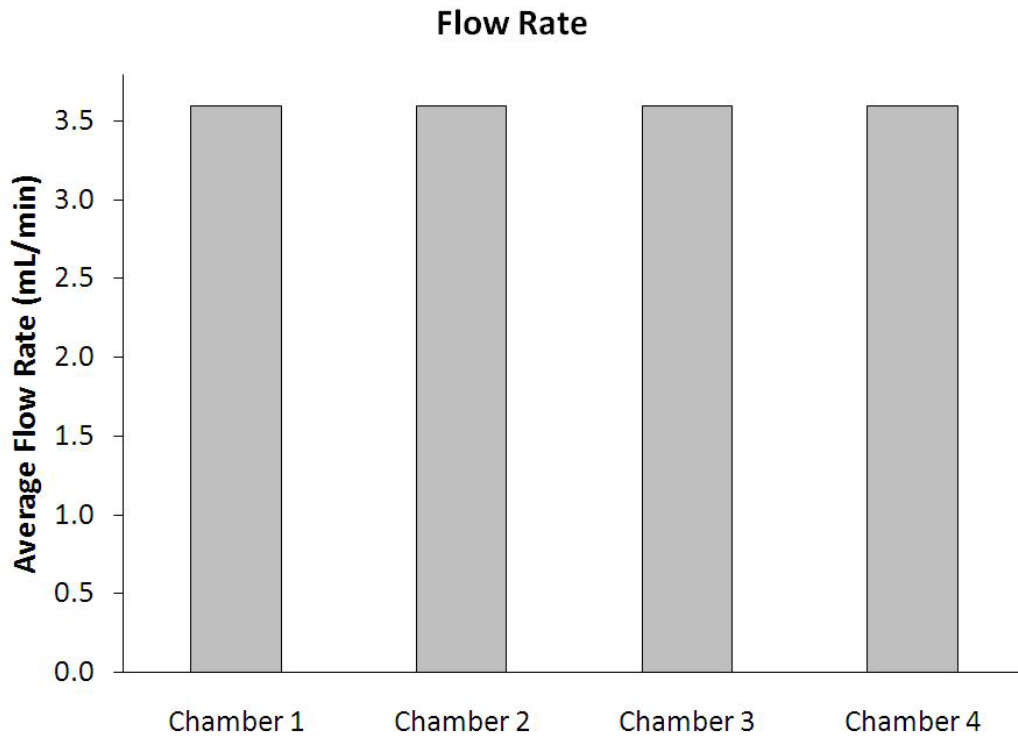


**Figure 5.12** Average flow rates for each chamber (n=3) in the bioreactor circuit. Values are shown as average  $\pm$  SEM.

### 5.2.3 Sterility and Stability

The media in each chamber was clear and lacked cloudiness for the duration of the experiment, indicating no visible signs of contamination. There were no significant differences between any chamber of the bioreactor and the conical tube for any environmental condition (**Figure 5.13** and **Figure 5.14**). Measurements are relatively uniform across chambers and timepoints (**Table 5.3**, **Table 5.4**, **Table 5.5**, and **Table 5.6**), with no significant differences detected. Error bars for each condition are small, indicating minimal variation within each chamber over the culture duration.

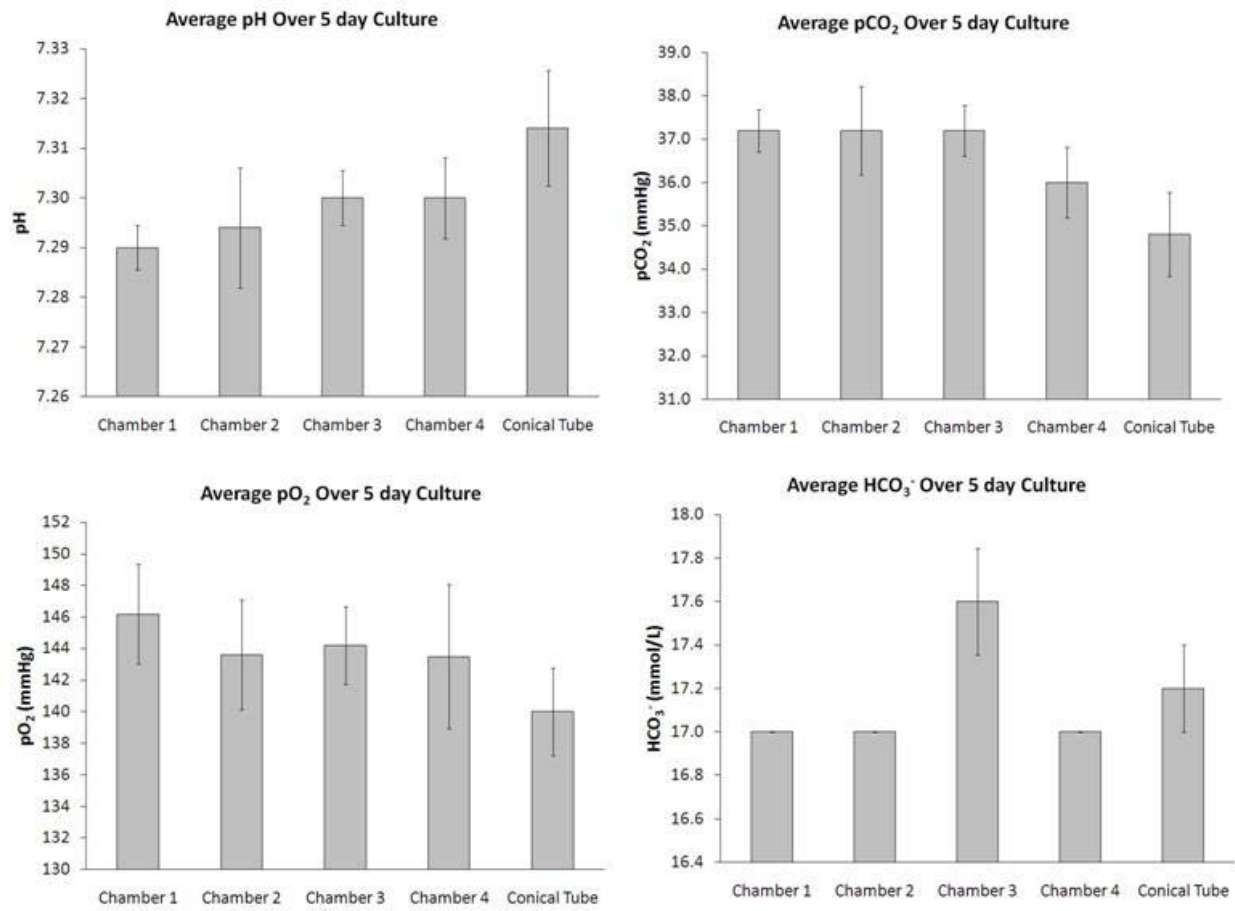


**Figure 5.13** Average environmental conditions for each chamber over the culture duration. Values shown as average  $\pm$  SEM.

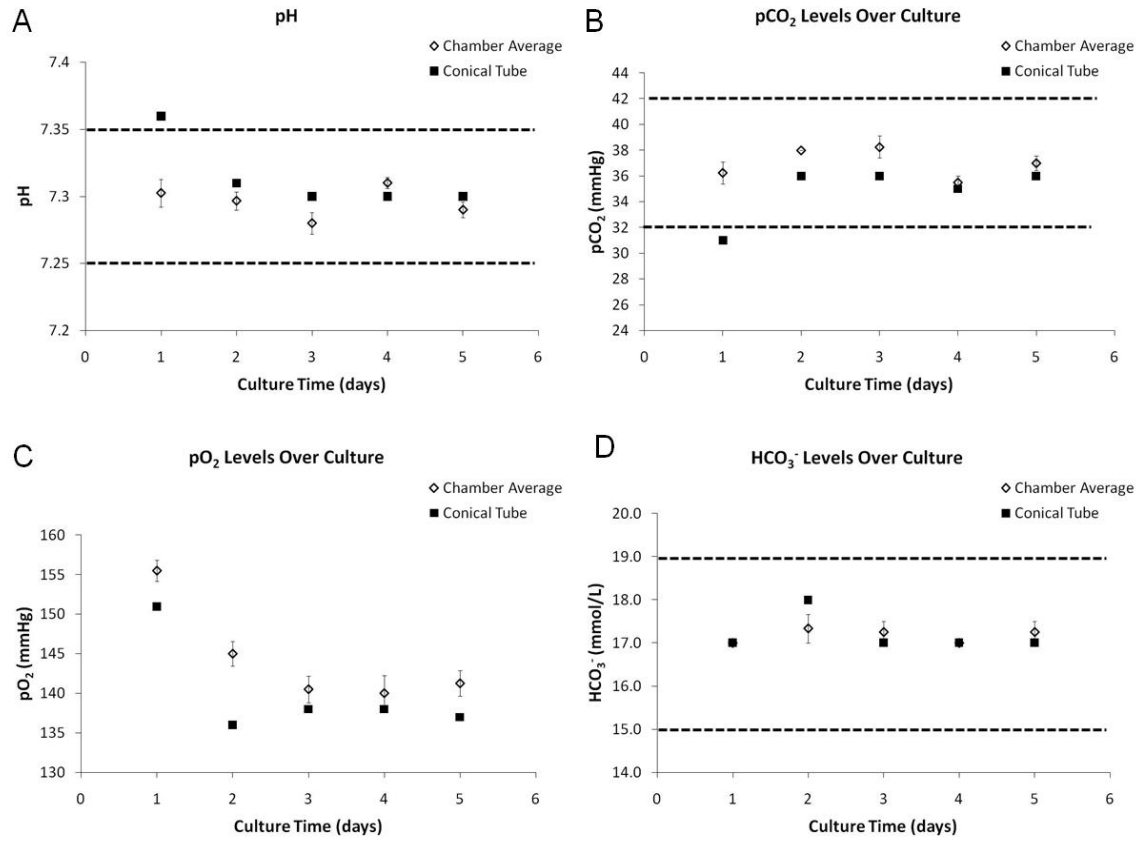


**Figure 5.14** Average environmental conditions across all chambers for each day of culture. Values shown as average  $\pm$  SEM. Dotted lines indicate an acceptable range for each parameter as determined in **Appendix E**.

**Table 5.3** pH values for each chamber at each day of culture.

	Day 1	Day 2	Day 3	Day 4	Day 5
Chamber 1	7.30	7.29	7.28	7.30	7.28
Chamber 2	7.33	7.29	7.26	7.31	7.28
Chamber 3	7.30	7.31	7.28	7.31	7.30
Chamber 4	7.28		7.30	7.32	7.30
Conical Tube	7.36	7.31	7.30	7.30	7.30

**Table 5.4** pCO<sub>2</sub> values (mmHg) for each chamber at each day of culture.

	Day 1	Day 2	Day 3	Day 4	Day 5
Chamber 1	36	38	38	36	38
Chamber 2	34	38	40	36	38
Chamber 3	37	38	39	36	36
Chamber 4	38		36	34	36
Conical Tube	31	36	36	35	36

**Table 5.5** pO<sub>2</sub> values (mmHg) for each chamber at each day of culture.

	Day 1	Day 2	Day 3	Day 4	Day 5
Chamber 1	158	144	145	145	139
Chamber 2	157	143	137	141	140
Chamber 3	152	148	141	140	140
Chamber 4	155		139	134	146
Conical Tube	151	136	138	138	137

**Table 5.6** HCO<sub>3</sub><sup>-</sup> (mmol/L) values for each chamber at each day of culture.

	Day 1	Day 2	Day 3	Day 4	Day 5
Chamber 1	17	17	17	17	17
Chamber 2	17	17	17	17	17
Chamber 3	17	18	18	17	18
Chamber 4	17		17	17	17
Conical Tube	17	18	17	17	17

#### 5.2.4 Construct Mounting

Constructs were easy to handle and mount. In order to easily thread the guide through the lumen of the construct, it was necessary to open the lumen by gently guiding the construct onto the end of a pair of Dumont #2 Laminectomy Forceps (Fine Science Tools, Inc., Foster City, CA) (**Figure 5.15A**). The stylet was then easily threaded through the lumen of the construct (**Figure 5.15B**). The construct was strong enough to be tied securely to the cannulae with suture without tearing (**Figure 5.15D-E**). Following initialization of flow through the mounted construct, liquid was visible exiting the opposite cannula (**Figure 5.15F**). There was no observed leakage at either suture site.

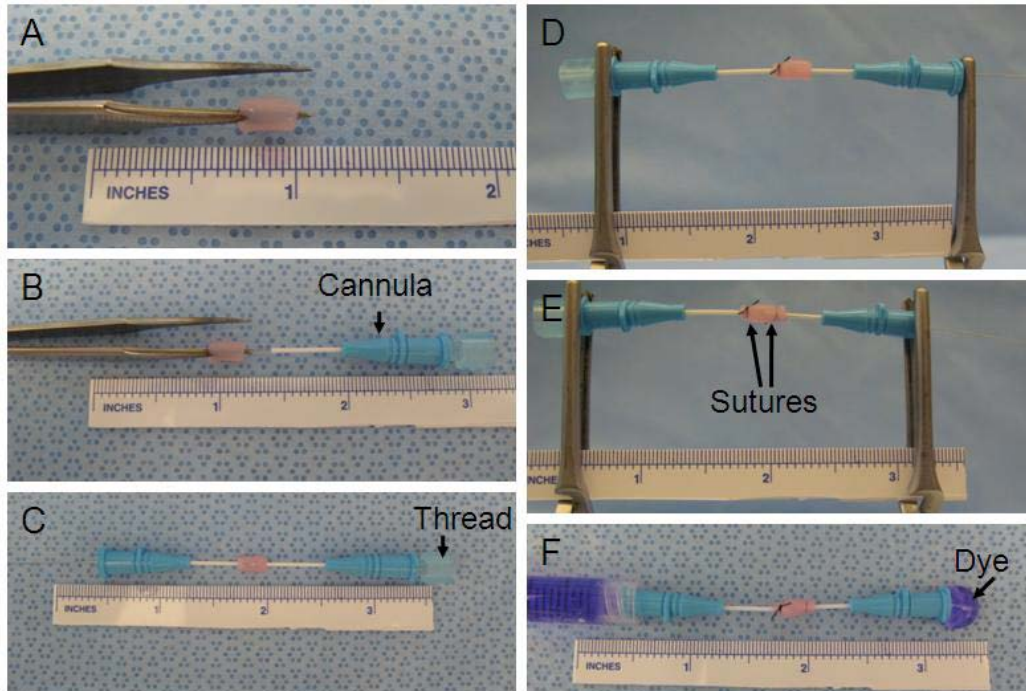


**Figure 5.15** Mounting of a construct. The lumen of the construct was located with forceps (A), the guide was passed through the lumen of the construct (B) and the other cannula was added (C). The construct was then sutured to the cannula (D-E). Flow through the construct, without leaking at the suture sites, was observed (F).

### 5.3 DISCUSSION

We have designed, fabricated and tested a novel, independent, multi-chamber bioreactor for the culture of tubular constructs. Our system is compact and, when assembled, fits on a standard cell culture incubator tray. The compact size and use of silicone tubing and filters for gas exchange allows the system to be run within a standard cell culture incubator, negating the need for exogenous temperature and gas regulation. The system requires a minimal volume of media (500 mL for four constructs) and is able to accommodate constructs of various lengths and diameter. The entire system remained stable (**Figure 5.13** and **Figure 5.14**) over a 5 day culture

period and constructs were easily mounted onto cannulae (**Figure 5.15**) and into the system. The independence of each chamber allows for simultaneous culture of various mechanical and/or chemical conditions.

The development of bioreactors has enhanced the field of tissue engineering by providing tools to expose 3-D constructs to stimuli which enhance the formation of tissue-equivalents. Bioreactors are designed to control the culture environment, diffusion of nutrients and appropriate, tissue-dependent stimuli [184, 189]. Our bioreactor meets all of these criteria. Our system is run within a cell culture incubator, which has well controlled temperature and gas parameters, allowing us to maintain tight control of environmental (pH, pCO<sub>2</sub> and pO<sub>2</sub>) conditions over a 5 day culture period (**Figure 5.13** and **Figure 5.14**). The minimal variation seen over the culture period and lack of significant differences between the bioreactor and conical tubes, indicate that the bioreactor maintains a stable culture environment. To address possible diffusion limitations, our bioreactor allows for intraluminal flow through the construct as well as flow of bathing media on the outer surface of the tubular constructs, allowing for nutrient diffusion from both directions. Our system also allows us to assess the effects of varying intraluminal pressures or flow with or without the addition of chemical stimulation.

Previously developed bioreactors have established the importance of mechanical and chemical factors in the mechanical integrity of the construct as well as cell proliferation, migration and differentiation [99, 180, 189, 200]. However, most bioreactors lack independence [185, 199, 201] or are of a large size [198, 199], necessitating a large volume of media and/or exogenous sources of temperature and gas regulation. The independence of our system allows us to compare four constructs, each cultured under various conditions simultaneously. This independent system also prevents cross-contamination and communication between constructs.

The compact size of our system minimizes the volume of media required as well as allows it to be run in an incubator, reducing experimental costs.

While our bioreactor system is both cost- and space-efficient, it is limited in several ways. Since the system was designed for low pressure experiments, the pulse-dampener, reservoir and chambers are sealed only by compression, limiting the internal pressures it can withstand without leaking. Modifications to the components, such as inclusion of a sunken o-ring in both the lid and base, or lids with a lip that protruded into the base and sealed with an o-ring, could allow for higher pressurization. Although the cannulae are adjustable to accommodate various length constructs, the size of the chambers restricts the maximum length of constructs which can be mounted in the system. The pressure transducers used in this system are clinical grade with an error of  $\pm 2$  mmHg. As this is designed as a low pressure bioreactor, an error of 2 mmHg is quite large. More sensitive pressure transducers would allow tighter control of intraluminal pressures. Pressures can be adjusted manually by a screw clamp, but the lack of an internal feedback system does not protect against pressure spikes or drops that may occur.

This study has resulted in the development of a bioreactor for the culture of tubular constructs under minimal pressure and flow. We have developed a compact and stable bioreactor for the mechanical and chemical stimulation of constructs to be used as a TEUW.

## **6.0 EFFECTS OF PRESSURE AND THE ADDITION OF TGF-BETA ON THE MECHANICAL AND PHENOTYPIC PROPERTIES OF A TEUW**

The importance of environmental (mechanical and chemical) cues on cell phenotype has been well documented [126, 202]. Studies indicate that progenitor cells can be differentiated toward a SMC-like phenotype via mechanical (refer to **Section 1.5.1**) and/or chemical (refer to **Section 1.5.2**) stimulation. Bioreactors can be utilized to expose cellular constructs to these environmental cues for regenerative medicine therapies. The ability to pre-condition cells to the environment that they will be exposed to could enhance their function upon implantation and lead to a faster recovery.

Regenerative medicine techniques, applied to the native urethra, may aid in improving urethral function and alleviate a number of conditions associated with lower urinary track dysfunction. Implementation of a bioreactor for the differentiation of stem cells to SMCs via mechanical and or chemical stimulation, similar to that of the lower urinary tract, could provide both a structural and functional treatment for urethral dysfunctions such as SUI.

The function and structure of the urethra expose it to intraluminal pressures, which in turn cause circumferential, radial and longitudinal deformations of the tissue. These deformations can be best replicated, for tissue engineering purposes, in a perfusion bioreactor similar to those used for the development of tissue engineered vascular grafts [106, 185, 192, 195-197] (recall **Table 5.1**). These studies have shown how increases in intraluminal flow and

pressures can differentiate cells towards a SMC phenotype and develop a more suitable graft for tissue replacement than constructs cultured statically. It has been reported that TGF- $\beta$  plays a pivotal role in smooth muscle cell development and differentiation [123, 133]. Previous studies (recall **Section 1.5.2**) have shown the promise of TGF- $\beta$  for the differentiation of stem cells towards a SMC phenotype with and without mechanical stimulation [124, 131, 203], making it an attractive option to aid in BMPC differentiation within a perfusion bioreactor.

The goal of this work was to utilize a custom built bioreactor system (**Chapter 4.0**) for the differentiation of BMPCs to SMCs by mechanical and/or chemical stimulation for use as a treatment for SUI.

## 6.1 METHODS

### 6.1.1 Cell culture and Construct Fabrication

Adult bone marrow derived progenitor cells were cultured according to **Section 4.2.1**. Briefly, cells were plated on T-175 flasks at 200 cells/cm<sup>2</sup> and cultured in complete media. Media was changed every other day and cells were grown to ~80% confluence. In order to fabricate independent constructs, we used a tiered method for culturing the cells. One flask of cells (Flask 1) was passed into four separate flasks (Flasks 1A-1D). Each of the four flasks was passed into four flasks (*i.e.*, A.1, A.2, A.3 and A.4) (**Figure 6.1**). Each set these of flasks was trypsinized and combined into one conical tube, yielding four separate conical tubes of cells (A-D). Each tube was then used to fabricate a construct (**Figure 6.2**) as described in **Section 4.2.2**. Briefly, molds were assembled by inserting a mandrel into a stopper and placing the combination inside

of a glass sheath. The cell-fibrin mixture ( $1 \times 10^6$  cells/mL) was placed in the annular space of the mold then into a cell culture incubator to gel.

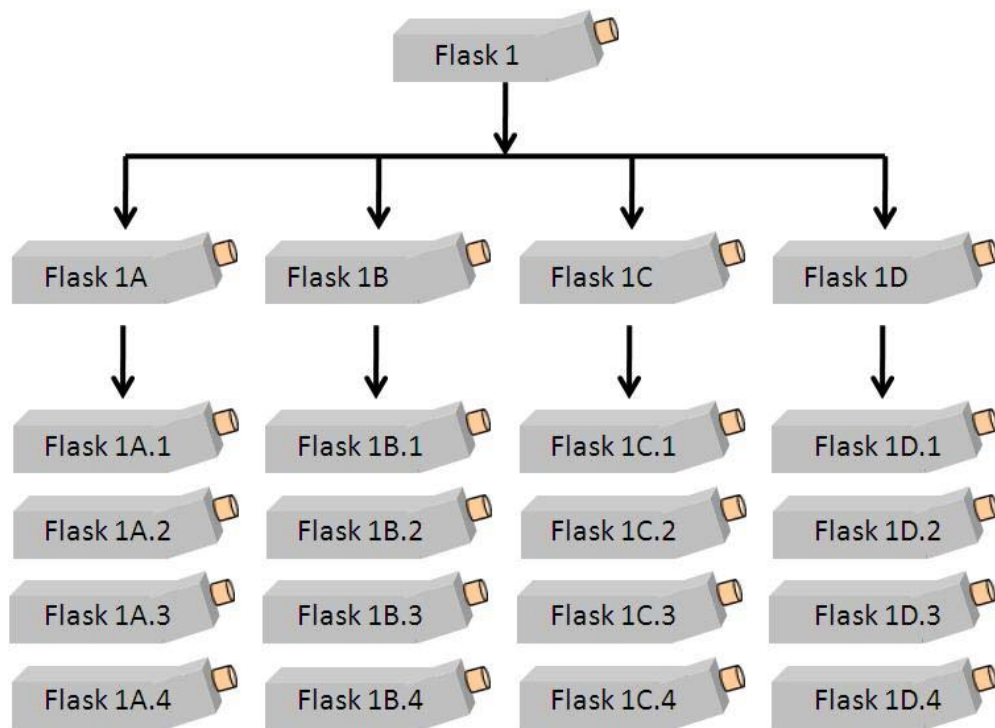


**Figure 6.1** Passage of cells for construct fabrication for utilization in the bioreactor.

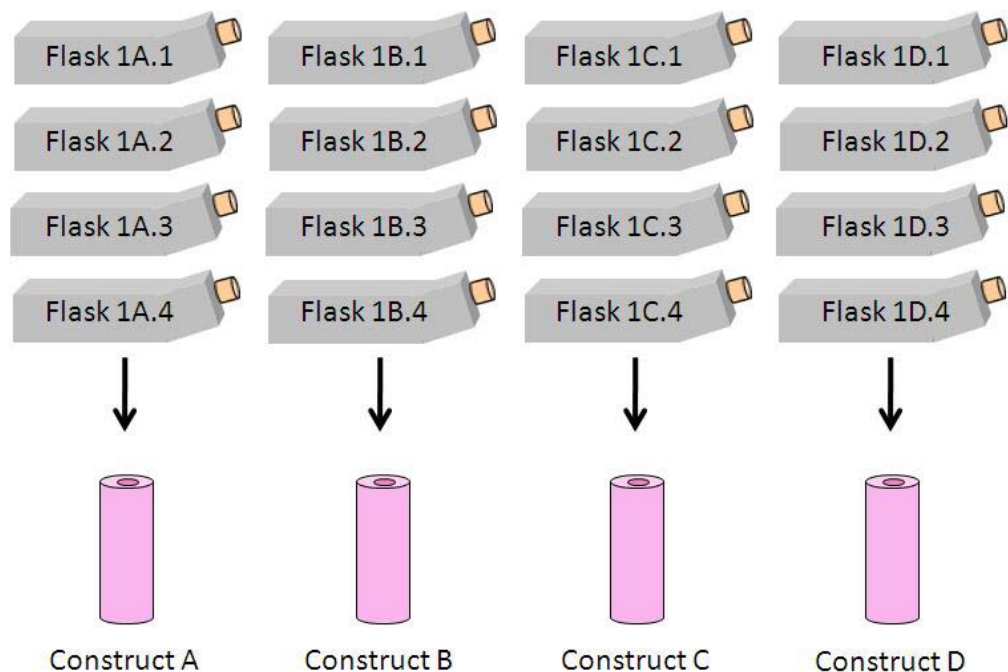


**Figure 6.2** Schematic of cell culture to produce independent constructs.

### 6.1.2 Dynamic Culture

Following gelation, constructs were removed from the molds and each construct was placed into its own spinner flask containing complete media (as defined in **Section 4.2.1**) supplemented with aminohexanoic (0.1 g/mL) and ascorbic (0.3 mM) acids (Sigma-Aldrich, St. Louis, MO) to prevent fibrin degradation and enhance collagen production, respectively. Constructs were cultured in spinner flasks for 5 days.

### **6.1.3 Bioreactor Priming**

The bioreactor was primed twenty-four hours prior to implantation of constructs to equilibrate the culture media. The bioreactor components (see **Section 5.1.1**) were assembled in a sterile manner, filled with ~500 mL of complete media (as defined in **Section 4.2.1**) and placed into the cell culture incubator. The system was run overnight to eliminate any air within the system lines and to stabilize in the culture environment. Before mounting of the constructs into the bioreactor, a media sample was taken from each chamber of the bioreactor and analyzed on the ABL-5 (Radiometer Medical A/S, Copenhagen, Denmark) for pH, pCO<sub>2</sub>, pO<sub>2</sub> and HCO<sub>3</sub><sup>-</sup>.

#### **6.1.3.1 Construct mounting**

Following compaction, constructs were mounted onto cannulae as described in **Section 5.1.1.4**. Briefly, constructs were first measured for initial length and then one cannula was placed onto the stylet from a spinal needle. The stylet was gently passed through the lumen of the construct and another cannula was placed onto the guide (**Figure 5.15**). The construct was mounted onto the cannulae with 4-0 silk suture (Syneture, Mansfield, MA). The stylet prevented the mounting from closing off the lumen of the cannulae. Once secure, the suture-to-suture length was measured. The stylet was removed, and the construct was bathed in media. After all constructs were mounted, the bioreactors were removed from the incubator and placed into the laminar flow hood. The mounted constructs were then inserted onto the stainless steel tees in each bioreactor chamber via luer fittings. If needed, additional complete media was added to the chamber to completely cover the construct. Construct media supplements were also added to prevent degradation of the fibrin and to enhance the production of collagen within the constructs, respectively. The stainless steel tees were adjusted so that the suture-to-suture length equalled

that of the initial end-to-end construct length, inducing a longitudinal stretch of ~10%. This process was repeated for the three remaining chambers. Once all constructs were mounted, the bioreactor was returned to the incubator and connected to the pressure monitor and pump controller.

#### **6.1.4 Bioreactor culture conditions**

Constructs exposed to only the initial 5 days of compaction in spinner flask culture served as time zero (T0) controls and were compared to constructs exposed to an additional: 5 (SF-5 day) or 10 (SF-10 day) days of spinner flask culture, 5 days at minimal pressure and flow with (MoT-5 day) and without (Mo-5 day) TGF- $\beta$  (10 ng/mL; R&D Systems, Inc, Minneapolis, MN) or 10 days at minimal pressure and flow with (MoT-10 day) or without (Mo-10 day) TGF- $\beta$  (**Table 6.1**). Once a day, media samples from each chamber were measured for pH, pCO<sub>2</sub>, pO<sub>2</sub> and HCO<sub>3</sub><sup>-</sup> on the ABL-5 (Radiometer Medical A/S, Copenhagen, Denmark). Twice a day, proximal and distal pressure measurements were taken. Due to the short length of the construct and the small inner diameter changes under low pressure, the pressure change should be linear. Therefore, the average of the proximal and distal measurements was used as the pressure within the construct. The two daily measurements were averaged and used as the average daily pressure within the construct. Following the experimental culture period, the constructs were assessed for mechanical properties, functional properties and cell distribution and phenotype as described in **Sections 6.1.5, 6.1.6 and 6.1.7**, respectively.

**Table 6.1** Experimental bioreactor culture conditions and experimental number. SF = spinner flask culture, Mo = minimal pressure and flow and T = addition of TGF- $\beta$  to the culture media. Time points are indicative of time in addition to an initial 5 days of spinner flask culture for compaction of the construct.

	<b>SF</b>	<b>Mo</b>	<b>MoT</b>
<b>5 day</b>	n = 3	n = 8	n = 6
<b>10 day</b>	n = 4	n = 7	n = 4

To assess the stability of the cellular phenotype following bioreactor culture, a set of constructs were subjected to Mo-5 day conditions then removed from the cannulae and placed into spinner flask culture for an additional 5 days and referred to as Mo-SF. Constructs were then assessed for cell phenotype as described in **Section 6.1.7.1**.

### **6.1.5 In-Vitro Mechanical Testing**

Following bioreactor culture, constructs were mechanically assessed as described in **Section 2.2.5**. Briefly, constructs were removed from the stainless steel cannulae in the bioreactor, mounted onto stainless steel cannulae (the same type used in the bioreactor) in a bathing chamber filled with sterile saline and de-aired. The distal end was clamped, and the construct was preconditioned with ten cycles of pressure changes from 0 mmHg to 8 mmHg. Following preconditioning, intraluminal pressure was incrementally increased from 0 mmHg to 20 mmHg in 2 mmHg steps. Outer diameter and intraluminal pressure was recorded at 10 Hz (see **Section 4.2.4**). Immediately following mechanical testing, intraluminal pressure was increased until

construct failure. Constructs were then removed from their cannulae and placed into 4% paraformaldehyde.

### **6.1.6 In-Vitro Functional Testing**

To assess differentiation of BMPCs to contractile smooth muscle cells following bioreactor culture, a select group of constructs, based on SMC marker expression, were subjected to functional testing. Constructs were removed from the bioreactor and mounted into a bathing chamber filled with Media 199 (Sigma-Aldrich, St. Louis, MO). Constructs were sequentially subjected to 0 mmHg and 8 mmHg intraluminal pressures, N $\omega$ -nitro-L-arginine (100  $\mu$ M; to remove endogenous nitric oxide synthase activity), phenylephrine (40  $\mu$ M; to assess smooth muscle contraction), acetylcholine (5 mM; to assess any striated muscle contraction) and EDTA (3 mM; to inhibit muscular response) as previously described in our testing protocols for the urethra [141]. Each stimulus was followed by a 15 minute equilibration period, and the outer diameter of the middle portion of the urethra was continuously recorded at 10 Hz.

### **6.1.7 Assessment of ECM and Cell Distribution**

Constructs were histologically assessed for structure and collagen by H&E, Lillie's modified Masson's trichrome and picrosirius red (see **Section 6.1.7.1**). Differentiation of the BMSCs was assessed by immunofluorescence staining (**Section 6.1.7.1**) and western blotting (**Section 6.1.7.2**) for the smooth muscle markers alpha smooth muscle actin ( $\alpha$ -SMA), calponin (CALP) and myosin heavy chain (MHC).

### **6.1.7.1 Histology and immunofluorescence**

Constructs were processed and stained as described in **Section 4.2.5**. Briefly, constructs were fixed in 4% paraformaldehyde for 24 hours then transferred to 30% sucrose, cut in half and processed for both frozen and paraffin 10  $\mu\text{m}$  sections. Paraffin sections were dewaxed, rehydrated and stained for H&E, Lillie's modified Masson's trichrome and PSR. Sections were imaged on a color digital camera (Model 1KH027799; Olympus, Dulles, VA) on a BX45 Olympus microscope (Olympus, Dulles, VA) using MagnaFire software (version 2.1; Olympus).

Frozen sections were permeabilized, blocked, and stained with primary antibodies for the smooth muscle cell markers  $\alpha$ -SMA (clone 1A4; Sigma-Aldrich, St. Louis, MO), (1:250 in blocking solution), CALP (DAKO, Glostrup, Denmark), (1:250 in blocking solution) and MHC (clone 1C10; DAKO), (1:400 in blocking solution). Markers were fluorescently tagged with an Alexa 488-conjugated secondary antibody (Invitrogen, Carlsbad, CA), (1:500 in blocking solution). All frozen sections were counter-stained with DAPI for nuclear visualization, and mounted with gelvatol. Immunofluorescence was imaged with a color, digital camera (QImaging, Surrey, BC, Canada) on an E800 Nikon Eclipse microscope (Nikon, Melville, NY) using NIS Elements BR 3.0 software (Nikon, Melville, NY).

### **6.1.7.2 Western blotting**

To quantify differentiation of the cells to a smooth muscle cell phenotype, western blotting was performed. Following culture, constructs were rinsed with sterile phosphate buffered saline and placed into an empty, pre-weighed 1.5mL tube (Bel-Art Products, Pequannock, NJ) and were snap frozen in liquid nitrogen followed by storage in a  $-80^{\circ}\text{C}$  freezer. Samples were ground in the micro-tubes with matching pestles (Bel-Art Products) on dry ice. A lysate buffer (1% Triton X-100, 1 M Tris-HCl, 5 M NaCl, 0.05% Brij 35, and 1 M  $\text{NaN}_3$  in

ultrapure water) supplemented with protease inhibitor and EDTA (Roche Diagnostics, Mannheim, Germany), 2 mM serine protease inhibitor (PMSF; Sigma-Aldrich, St. Louis, MO) and 5 µg/mL cysteine protease inhibitor in water (E-64; AG Scientific Inc., San Diego, CA) was used to lyse all cells within the powdered construct. Lysates were sonicated and microcentrifuged at 13,000 rpm for 10 minutes. Supernatants were collected and total protein concentrations were determined by the BCA assay (Pierce, Rockford, IL).

Samples were loaded at 16 µg per well and resolved by electrophoresis on 4-15% Tris-HCl gradient gels (Bio-Rad Laboratories, Hercules, CA) at 200 V. Total protein was separated by SDS-PAGE and electro-transferred to nitrocellulose membranes (Bio-Rad Laboratories, Hercules, CA) in a cold Tris-glycine buffer (Pierce) at 100 V for 1 hour. To ensure equal loading, membranes were stained with Ponceau-S for 30 minutes and rinsed with water to visualize total protein content. Membranes were then blocked with non-fat, powdered milk blocking buffer (5% v/v) and incubated with primary antibody for the same smooth muscle markers ( $\alpha$ -SMA (1:1,000), CALP (1:500) or MHC (1:500)) used in immunofluorescence (**Section 6.1.7.1**) overnight at 4°C. Membranes were then labeled with horse radish peroxidase goat-anti-mouse conjugated secondary antibody (1:10,000, Thermo Scientific, Rockford, IL) at room temperature for 1 hour. Protein bands were detected and imaged using Supersignal West Femto Luminal Enhancer Solutions (Thermo Scientific, Rockford, IL) on a Kodak Molecular Imaging Station (v.4.5.0, Kodak, Rochester, NY).

### **6.1.7.3 Cell counting**

Cell aggregation toward the inner or outer construct surface under our various culture conditions was assessed by regional nuclei counts. Cell counting was performed on DAPI images taken with a 10x objective as described in **Section 6.1.7.1**. Two fields of view were

imaged for each section with four sections stained per primary antibody (12 sections per antibody and 24 total fields of view). Each field of view allowed for visualization of both the lumen and outer edge. Images were imported into ImageJ software (National Institute of Health, Bethesda, MD) and thresholded for analysis. The threshold was adjusted for each image so that individual nuclei were clearly visible with minimal background. The lumen and outer edge of the construct were distinguished, and the area to be measured (the outer or lumen half of the construct) was outlined. Automated nuclear counts in the outlined area were obtained by specifying the circularity of the pixels (0.83-1.00, as determined by comparing computer and hand-counted values for several test sample areas). All 24 values were averaged for both the lumen and outer halves for each experiment and taken as the values for that experiment. Averages were used to calculate inner and outer percentages of total cells per field of view. Experimental values were averaged for each condition and compared.

### **6.1.8 Statistics**

Data is represented as the average  $\pm$  standard error of the mean. Statistical comparisons were performed using the software package SPSS (version 16.0, SPSS, Inc., Chicago, IL). For comparisons between groups, a one-way ANOVA was used with the factor being either time or culture conditions. Post-hoc testing was performed with a Gabriel or Games-Howell test (for normally distributed data), or the Kruskal-Wallis test, followed by a Monte-Carlo test between groups (for non-parametric data). Pressure-diameter data was analyzed using repeated measures ANOVA with a post-hoc Bonferroni test to detect overall differences in the curves between culture conditions. Significance was detected at p-values less than 0.05.

## 6.2 RESULTS

### 6.2.1 System Stability

Parameter stability during culture can be seen in **Figure 6.3 - Figure 6.7**, where dotted lines indicate an acceptable parameter range (**Appendix E**) as determined from ABL-5 readings of control media or a target pressure of 5 mmHg. Pressure values (**Figure 6.3**) were relatively stable over both 5 and 10 day culture durations. Although some pressures were slightly higher than the acceptable pressure range, they were not significantly different than those within the range. The remaining parameters were close to or within their acceptable range for all conditions over the culture duration. There was a significant difference in pH values (**Figure 6.4**) between Mo-5 day and MoT-5 day at day 3 and between Mo-10 day and MoT-10 day at day 2, in pCO<sub>2</sub> values between Mo-10 day and MoT-10 day at day 7 (**Figure 6.5**); and in HCO<sub>3</sub><sup>-</sup> values between Mo-10 day and MoT-10 day at day 0 (**Figure 6.7**), but all values were within or close to the acceptable range for each parameter and not considered biologically significant.

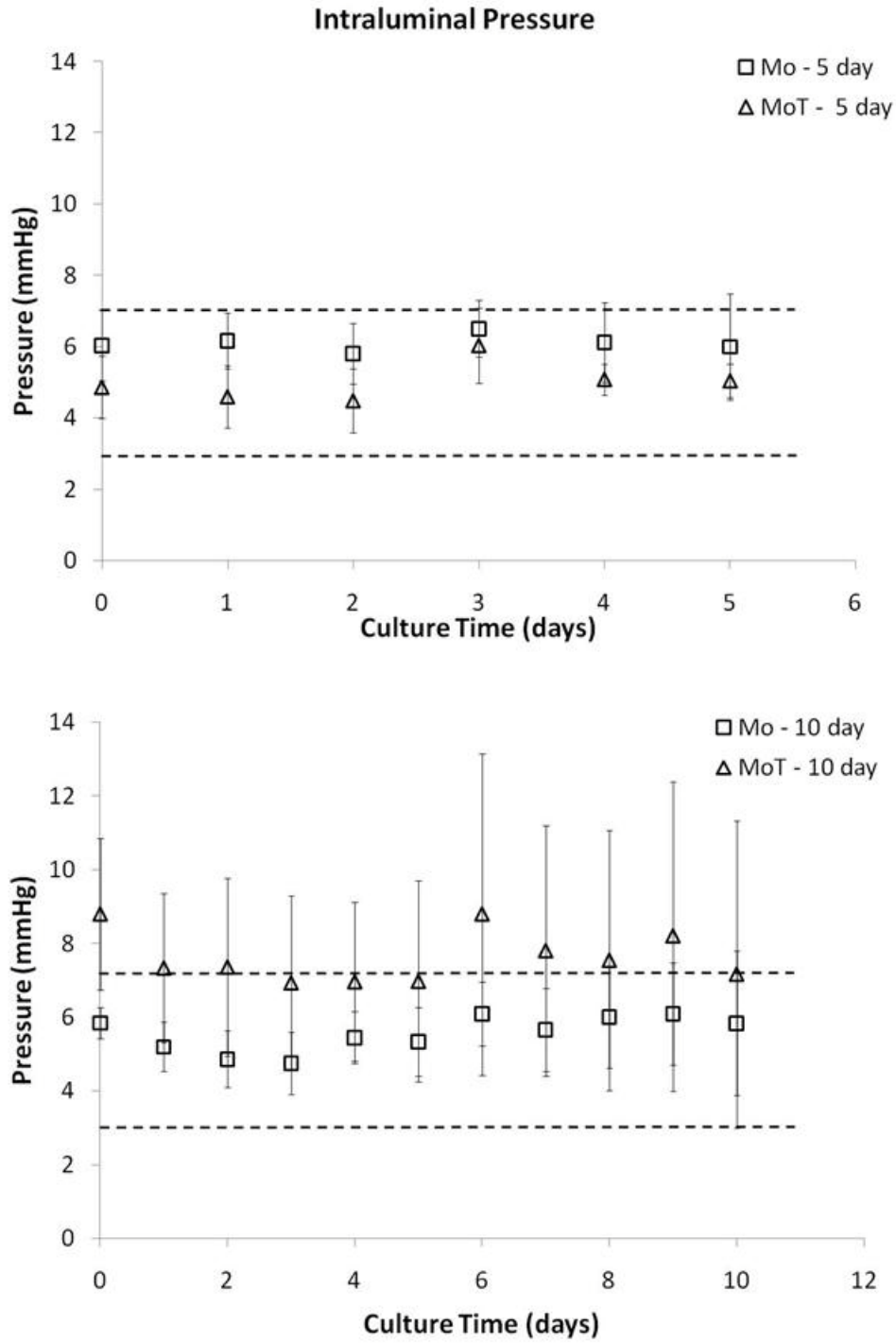


**Figure 6.3** Intraluminal pressure measurements for constructs cultured under Mo-5 day (n=8), MoT-5 day (n=6), Mo-10 day (n=7) and MoT-10 day (n=4) show that all values fall within an acceptable range of  $5 \pm 2$  mmHg (dotted lines). Values shown as average  $\pm$  SEM. \*p<0.05.

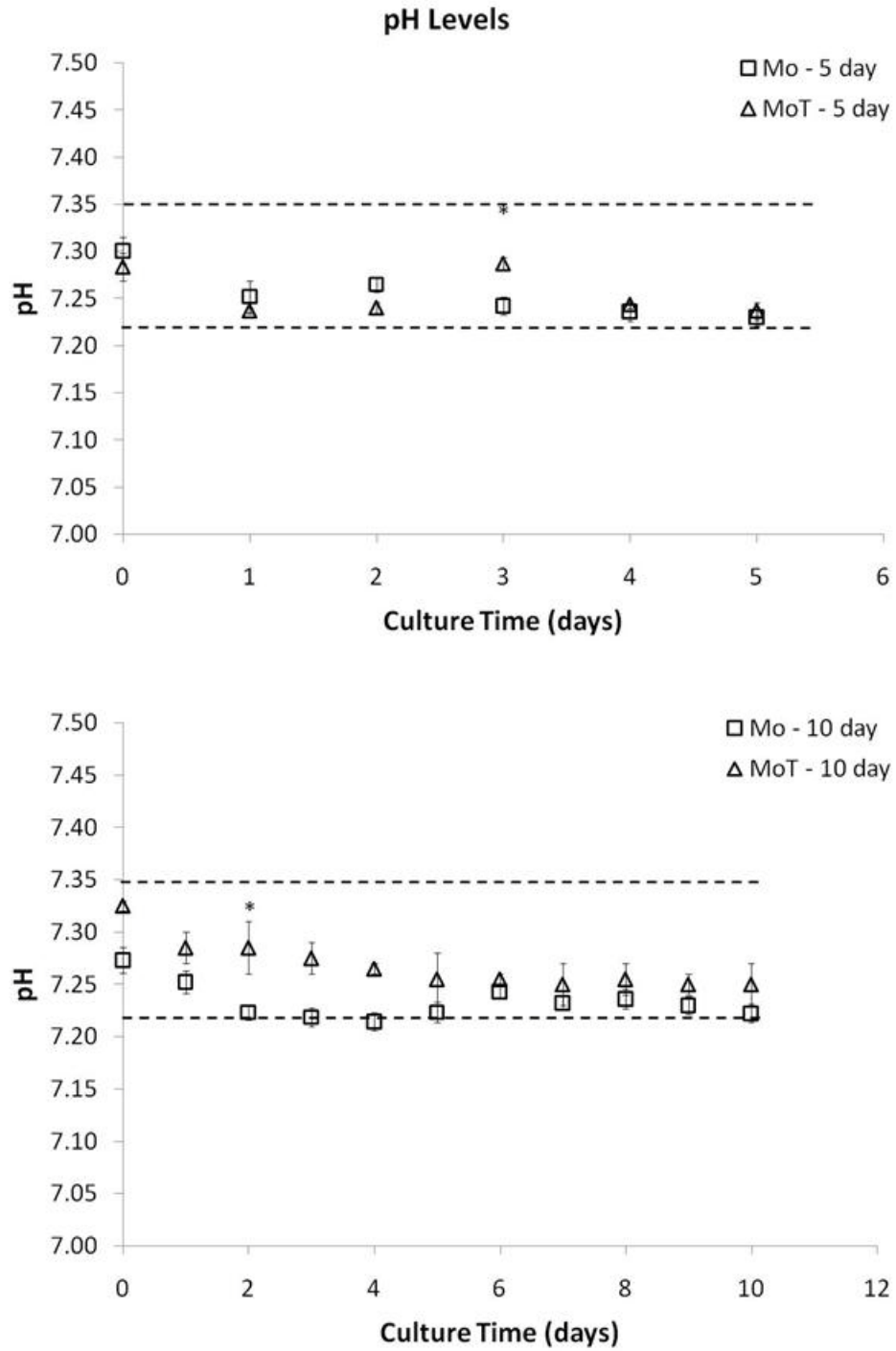


**Figure 6.4** Environmental pH values for constructs cultured under Mo-5 day (n=8), MoT-5 day (n=6), Mo-10 day (n=7) and MoT-10 day (n=4) show that all values fall within an acceptable range (dotted lines). Values shown as average  $\pm$  SEM. \*p<0.05.

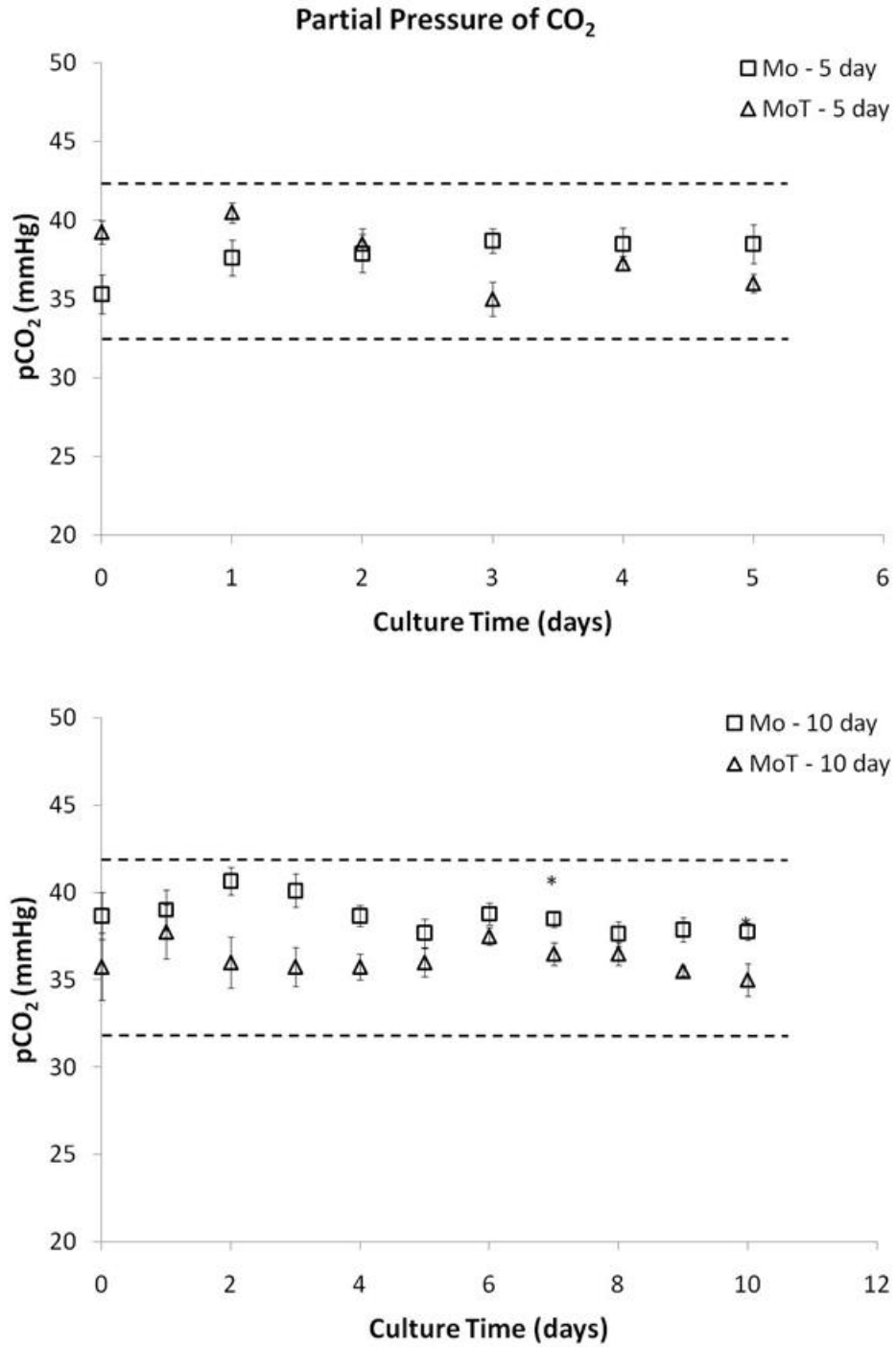


**Figure 6.5** Environmental pCO<sub>2</sub> conditions for constructs cultured under Mo-5 day (n=8), MoT-5 day (n=6), Mo-10 day (n=7) and MoT-10 day (n=4) show that all values fall within an acceptable range (dotted lines). Values shown as average ± SEM. \*p<0.05.

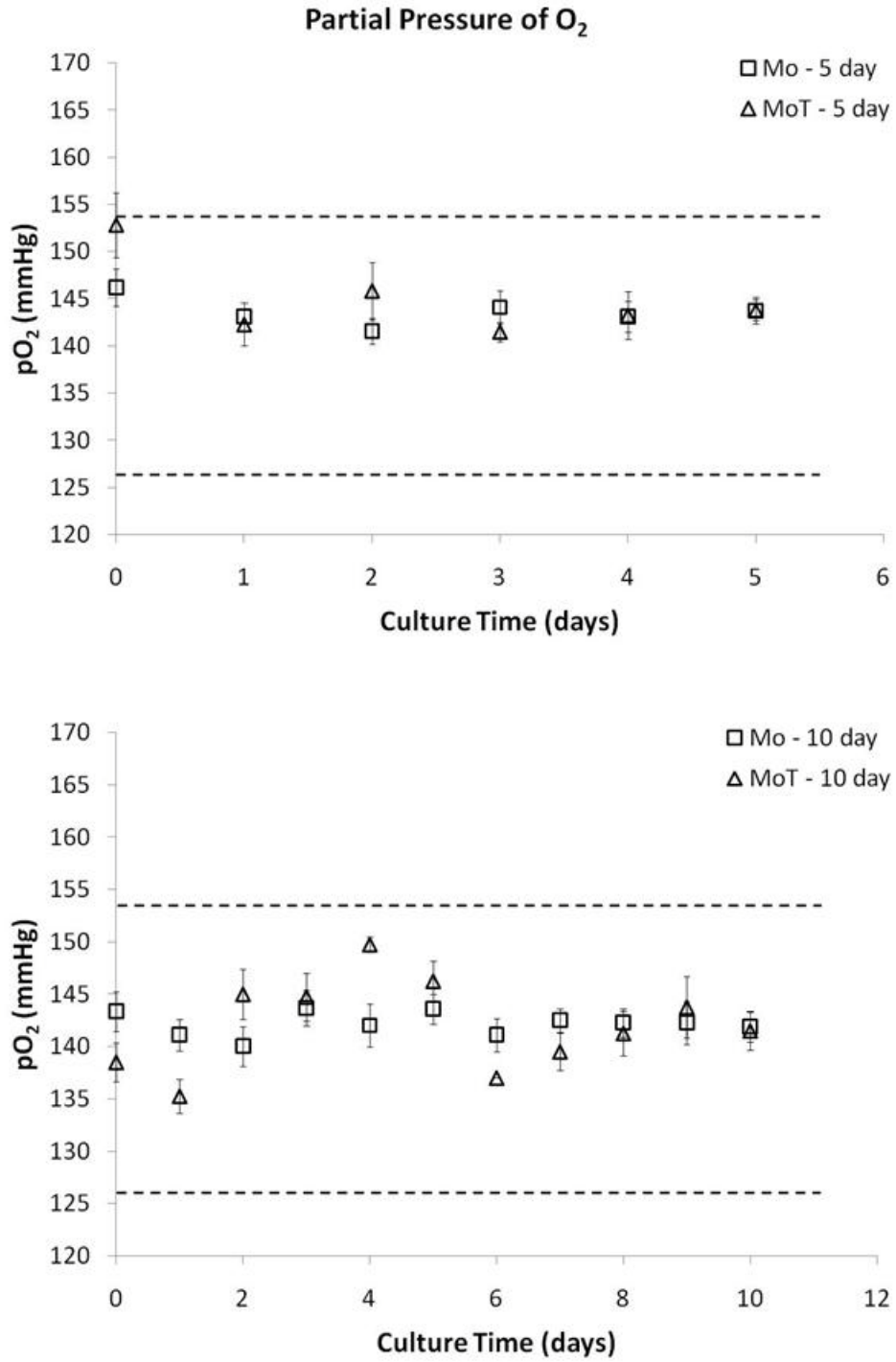


**Figure 6.6** Environmental pO<sub>2</sub> conditions for constructs cultured under Mo-5 day (n=8), MoT-5 day (n=6), Mo-10 day (n=7) and MoT-10 day (n=4). Values shown as average ± SEM. \*p<0.05.

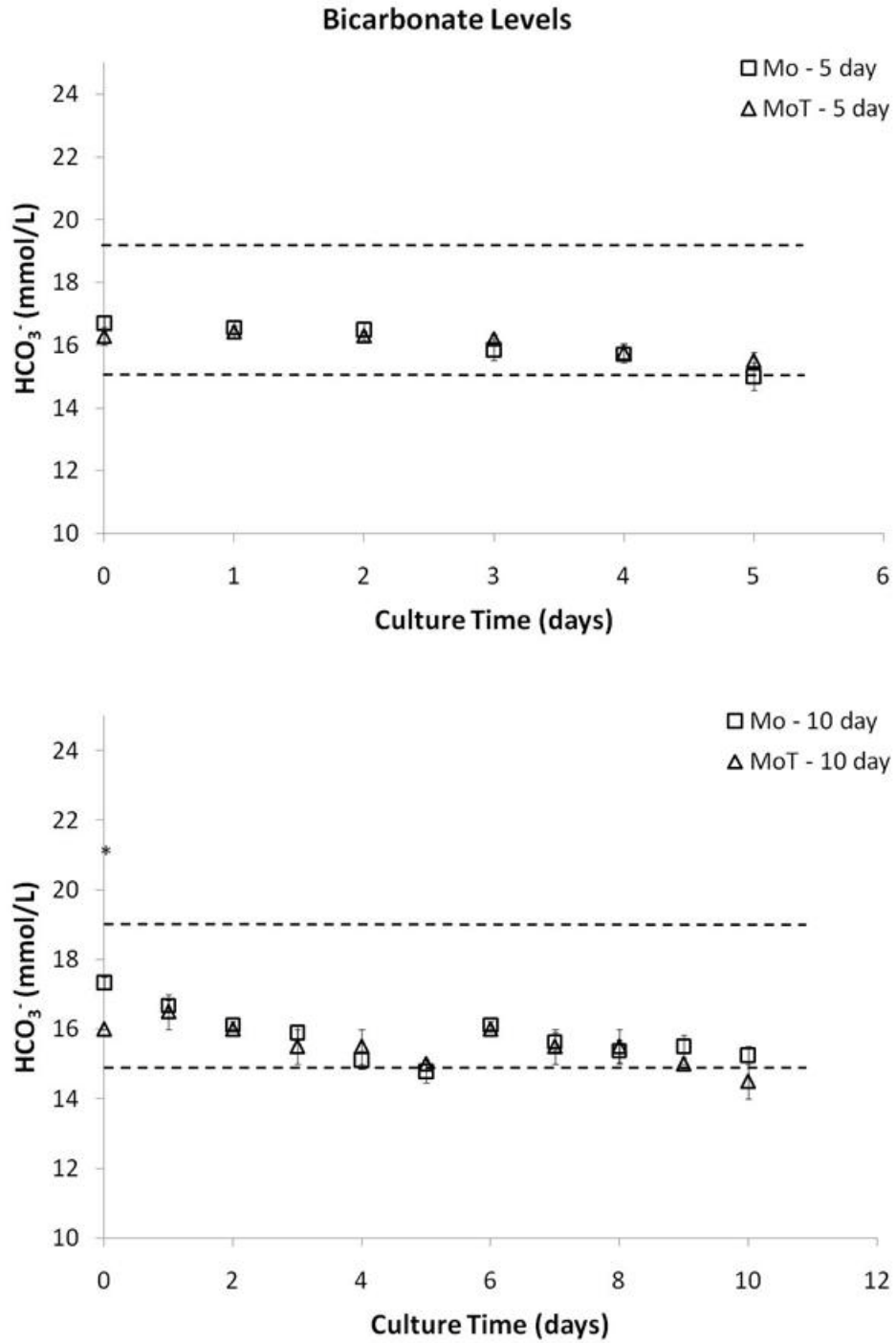


**Figure 6.7** Environmental  $\text{HCO}_3^-$  conditions for constructs cultured under Mo-5 day (n=8), MoT-5 day (n=6), Mo-10 day (n=7) and MoT-10 day (n=4) show that all values fall within an acceptable range (dotted lines). Values shown as average  $\pm$  SEM. \*p<0.05.

## 6.2.2 In-Vitro Mechanical Testing

Pressure-diameter (P-D) results (**Figure 6.8**) were similar for most groups, with Mo-10 indicating a decreased compliance from the rest. There is a visible trend of P-D curves shifting to the left (decreased compliance) with increased bioreactor culture duration. The only significant difference was detected at 4 mmHg between Mo-5 day and Mo-10 day and the largest variability was seen in SF-5 day and SF-10 day constructs. No overall significant differences in pressure-diameter curves between culture conditions were found. Step-wise compliance (**Figure 6.9**) shows the largest spread in data at low pressures (0-6 mmHg), with 10 day cultures having lower compliance values than 5 day cultures, with T0 falling between 5 and 10 day constructs. Significant differences were found at 18 mmHg between SF-10 day and Mo-5 day, as well as between SF-10 day and Mo-10 day.

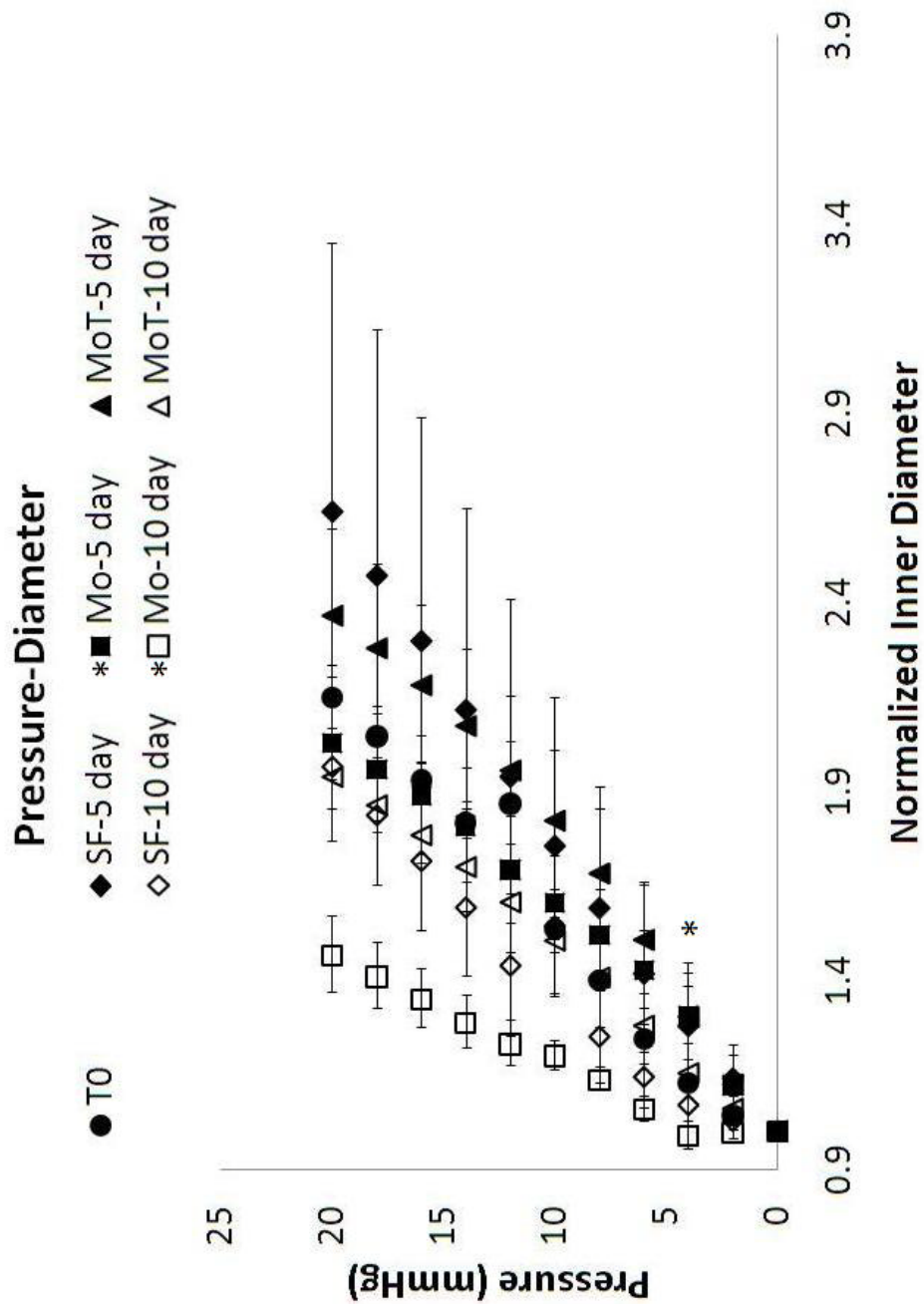


**Figure 6.8** Pressure-diameter curves for constructs cultured under T0 (n=3), SF-5 day (n=3), Mo-5 day (n=8), MoT-5 day (n=6), SF-10 day (n=4), Mo-10 day (n=7) and MoT-10 day (n=4). Values shown as average  $\pm$  SEM. \*p<0.05 between groups at the indicated pressure.

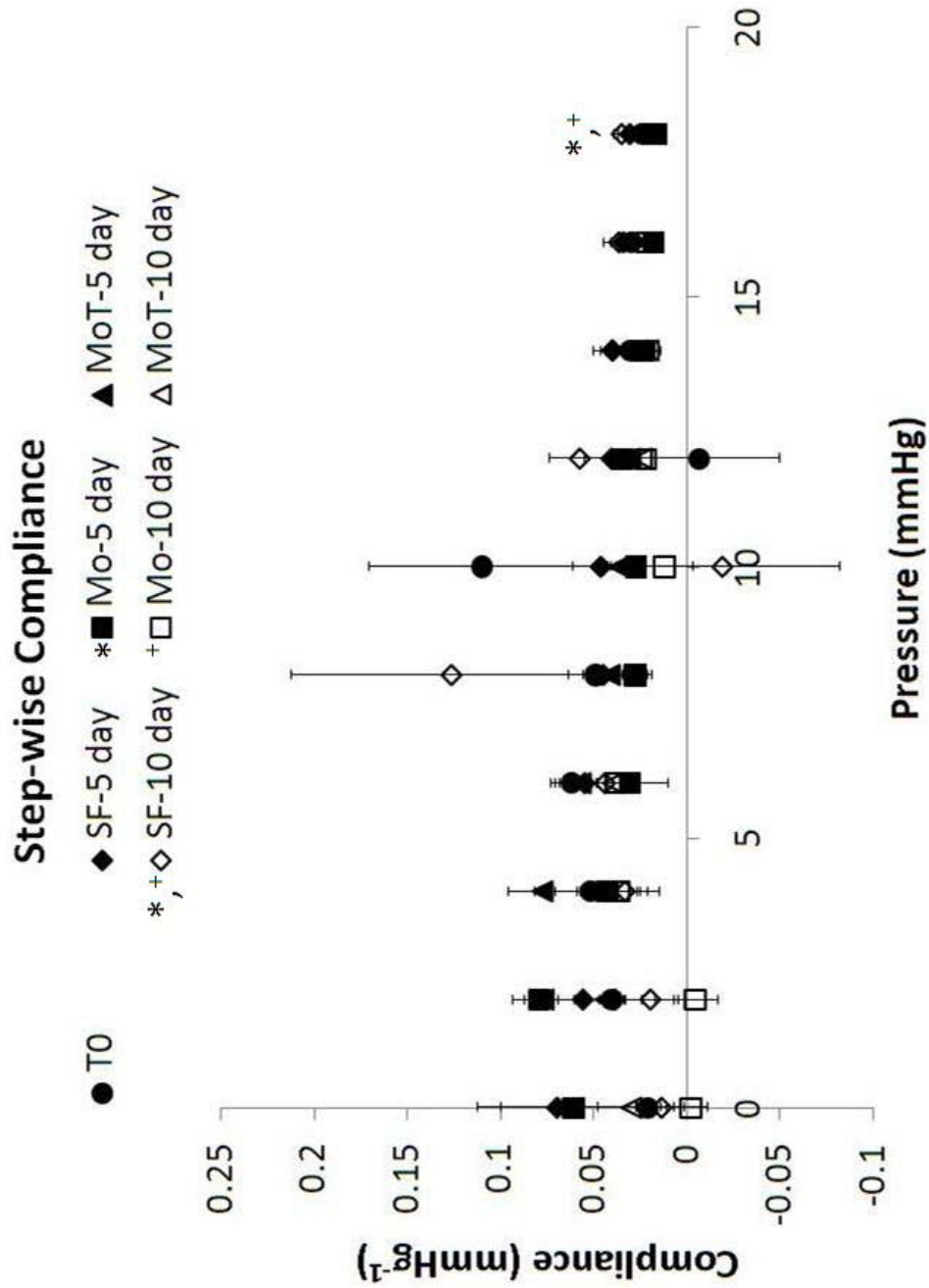


**Figure 6.9** Step-wise compliance curves for constructs cultured under T0 (n=3), SF-5 day (n=3), Mo-5 day (n=8), MoT-5 day (n=6), SF-10 day (n=4), Mo-10 day (n=7) and MoT-10 day (n=4). Values shown as average  $\pm$  SEM.

\*,+p<0.05 between groups at the indicated pressure.

Compliance values calculated over specific pressure ranges (**Table 6.2**) show that at low pressure (0-6 mmHg) TGF- $\beta$  increases construct compliance. Culture duration also appears to influence the mechanical properties of TGF- $\beta$  stimulated constructs where 5 day culture increases compliance from T0, but 10 day culture decreases it. There was a significant difference between MoT-5 and Mo-10. Middle pressure (6-12 mmHg) compliance decreased with culture duration (10 day < 5 day < T0), but addition of TGF- $\beta$  increased compliance at both 5 and 10 days, but with no effect of culture time. SF-5 and -10 cultures had the highest high pressure (12-20 mmHg) compliance at each time point, with MoT-10 having the highest compliance, but also the largest variability.

Beta stiffness values (**Table 6.2**) increased with increased culture duration, especially when cultured in the bioreactor for 10 days.

**Table 6.2** Compliance ( $\text{mmHg}^{-1}$ ) at various pressure ranges and beta stiffness for constructs cultured under T0 (n=3), SF-5 day (n=3), Mo-5 day (n=8), MoT-5 day (n=6), SF-10 day (n=4), Mo-10 day (n=7) and MoT-10 day (n=4). Values shown as average  $\pm$  SEM. \* $p < 0.05$  and values most similar to the native urethra are shaded gray.

<b>Compliance x 100</b>	<b>Low Pressure (0-6 mmHg)</b>	<b>Middle Pressure (0-12 mmHg)</b>	<b>High Pressure (12-20 mmHg)</b>	<b>Overall Pressure (0-20 mmHg)</b>	<b>Beta Stiffness</b>
<b>T0</b>	4.08 $\pm$ 0.63	8.31 $\pm$ 1.87	2.13 $\pm$ 1.50	5.74 $\pm$ 0.42	2.42 $\pm$ 0.26
<b>SF-5 day</b>	6.94 $\pm$ 4.00	5.50 $\pm$ 1.99	4.16 $\pm$ 1.35	8.19 $\pm$ 3.55	3.68 $\pm$ 1.70
<b>Mo-5 day</b>	7.09 $\pm$ 1.73	3.01 $\pm$ 0.41	2.49 $\pm$ 0.41	5.13 $\pm$ 0.86	4.27 $\pm$ 0.55
<b>MoT-5 day</b>	8.44 $\pm$ 2.39*	4.96 $\pm$ 0.73	2.65 $\pm$ 0.33	6.82 $\pm$ 1.14	3.19 $\pm$ 0.63
<b>SF-10 day</b>	2.39 $\pm$ 1.40	4.06 $\pm$ 1.11	4.82 $\pm$ 0.99	4.83 $\pm$ 1.00	2.88 $\pm$ 0.20
<b>Mo-10 day</b>	0.96 $\pm$ 0.55*	2.81 $\pm$ 1.02	2.32 $\pm$ 0.39	2.33 $\pm$ 0.50	5.51 $\pm$ 0.94
<b>MoT-10 day</b>	2.52 $\pm$ 1.41	4.22 $\pm$ 2.53	4.17 $\pm$ 3.24	4.66 $\pm$ 2.61	5.95 $\pm$ 1.74

Burst pressure results (**Figure 6.10**) showed no significant differences between any groups. Additional SF culture over T0 had no effect on burst pressure. However, Mo culture tended to decrease burst pressure, with increased culture causing larger decreases. The addition of TGF- $\beta$  (MoT) increased burst pressure over Mo alone at both 5 and 10 days.

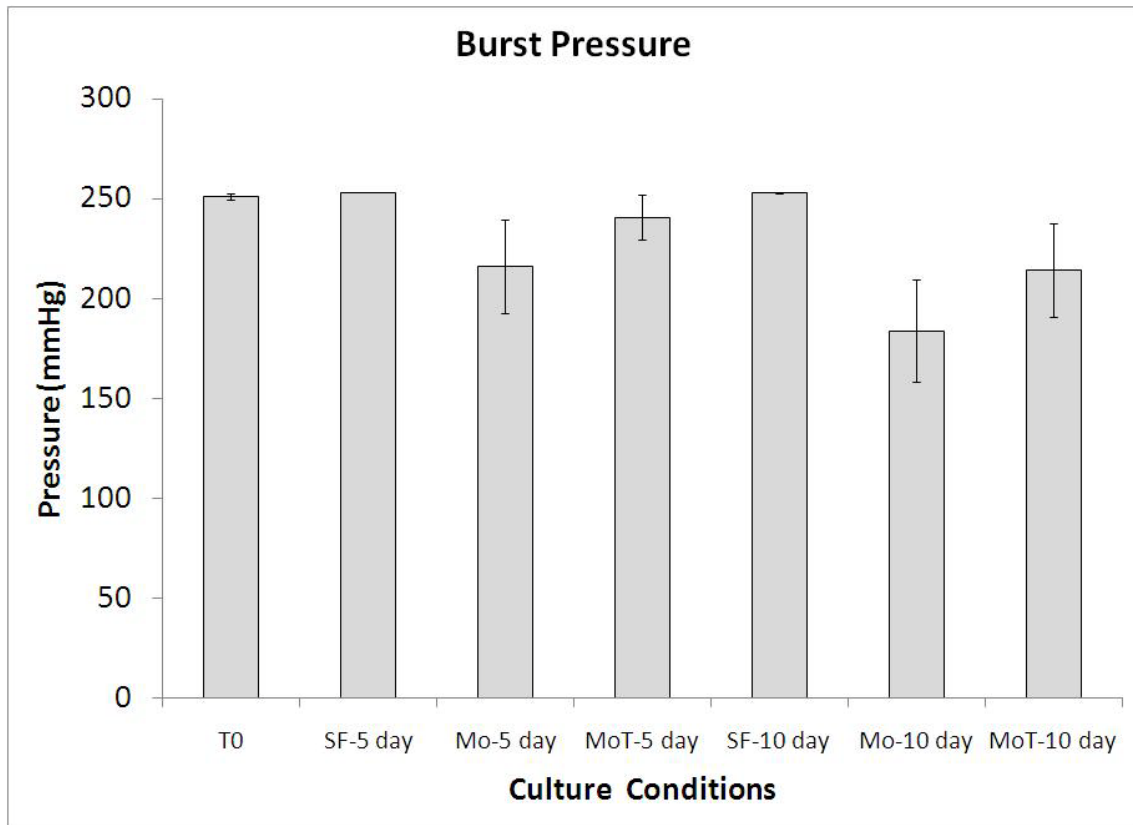


**Figure 6.10** Burst pressure for constructs cultured under T0 (n=3), SF-5 day (n=3), Mo-5 day (n=8), MoT-5 day (n=6), SF-10 day (n=4), Mo-10 day (n=7) and MoT-10 day (n=4). Values shown as average  $\pm$  SEM.

### **6.2.3 In-Vitro Functional Testing**

The construct showed an increase in diameter in response to an 8 mmHg increase in pressure, but showed no contractile response (decrease in diameter) to any agent added (**Figure 6.11**). Extraneous variations in diameter were due to an accidental bump of the pressure reservoir during testing. There was an increase in diameter between Ach and EDTA, possibly due to the long duration of an increased intraluminal pressure or creep failure. The final diameter increase was due to bursting of the construct.

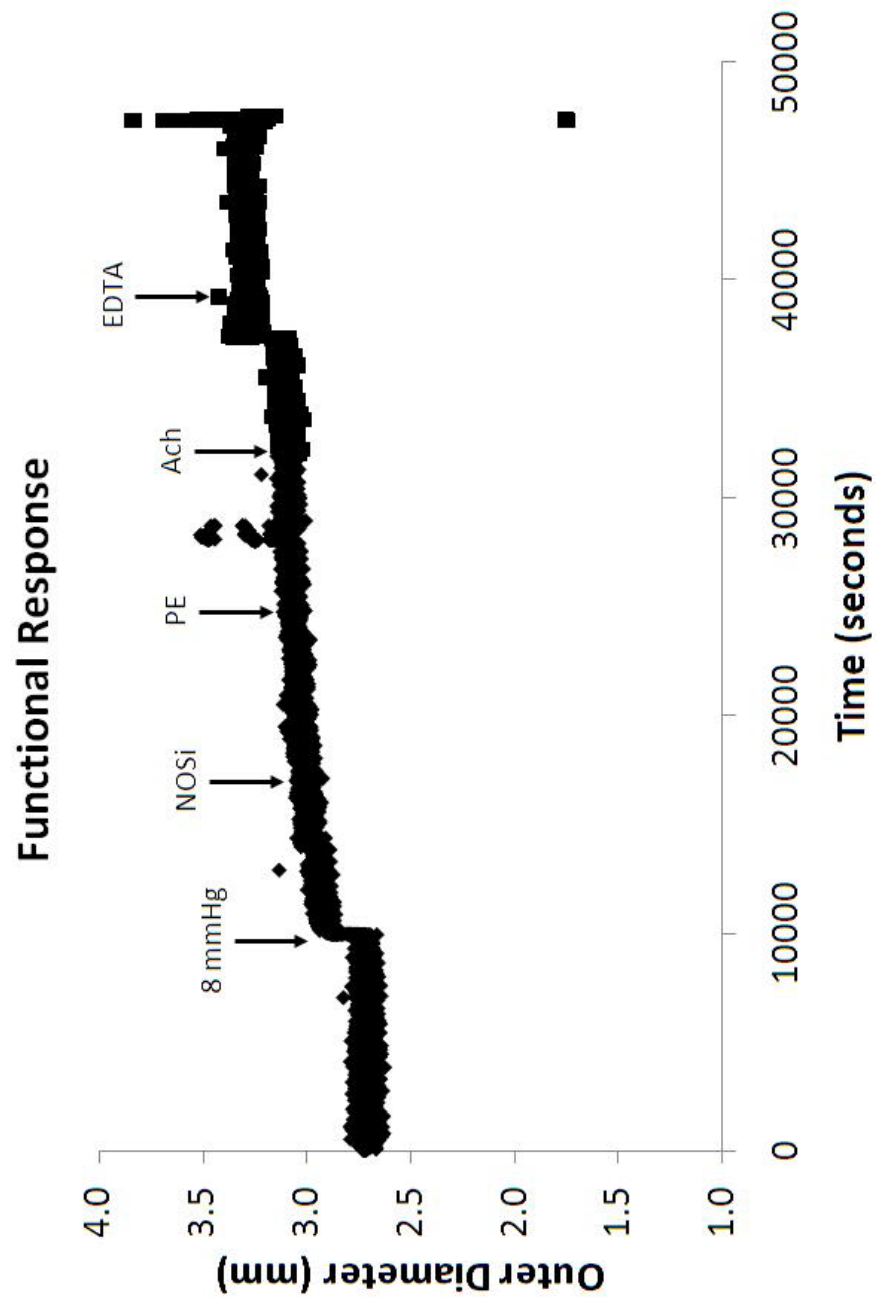


**Figure 6.11** Outer diameter response of an Mo-5 day construct to various agonists and antagonists (N $\omega$ -nitro-L-arginine (NOSi), phenylephrine (PE), acetylcholine (Ach) and EDTA). Data was measured at 10 Hz with 15 minute equilibrations at each condition. “Time” represents the seconds into the initiation of the measurements when data was obtained. Outer diameter measurements were normalized to the initial outer diameter at 0 mmHg

## 6.2.4 Histology

Lillie's modified Masson's trichrome (**Figure 6.12**) and PSR (**Figure 6.13**) staining showed no distinct collagen production within constructs under any culture condition, although Mo-10 showed very faint positive staining in PSR, which could be collagen or background. The fibrin showed a strong autofluorescence. Detection of positive staining was based on image comparison to a primary delete for each condition for IF analysis, since all culture conditions stained positive for  $\alpha$ -SMA (**Figure 6.14**), including the Mo-SF constructs, but none were positive for CALP (**Figure 6.15**). Only constructs cultured in the bioreactor, with or without TGF- $\beta$ , had some positive staining for MHC (**Figure 6.16**), with Mo-5 and MoT-10 conditions showing a more homogeneous expression. Although bioreactor culture shows some positive MHC staining, it lacks the intensity and structure seen in the native urethra. The Mo-SF construct (Mo-5 day followed by 5 days in SF) was negative for MHC. A summary of graded smooth muscle marker results is available in **Table 6.3**, showing that constructs culture in the bioreactor with or without TGF- $\beta$  for either 5 or 10 days had the greatest differentiation towards a smooth muscle phenotype.

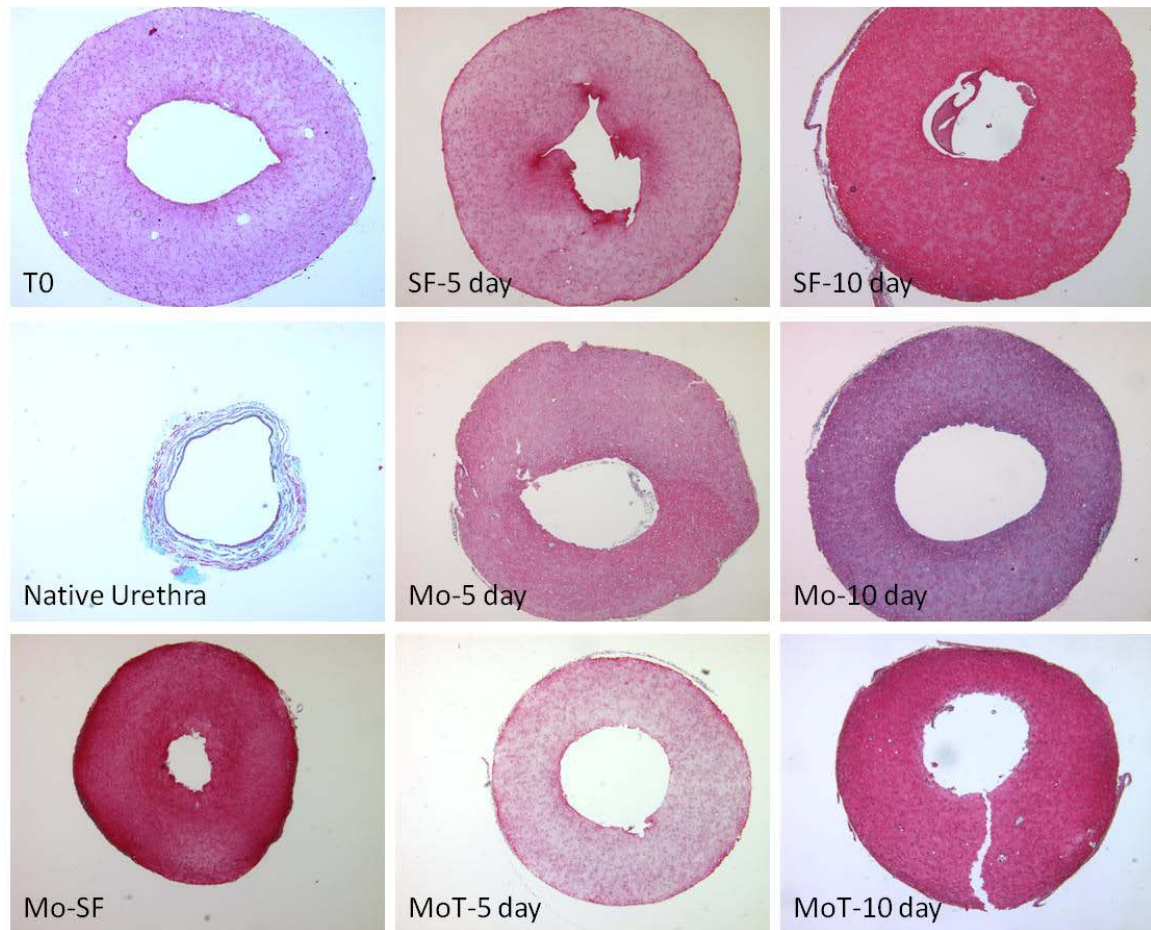


**Figure 6.12** Representative trichrome staining for constructs cultured under T0, SF-5 day, Mo-5 day, MoT-5 day, SF-10 day, Mo-10 day, MoT-10 day, and Mo-SF. Images taken with a 4x objective and the native urethra served as a positive control. Red = fibrin, blue/green = collagen, black = nuclei.

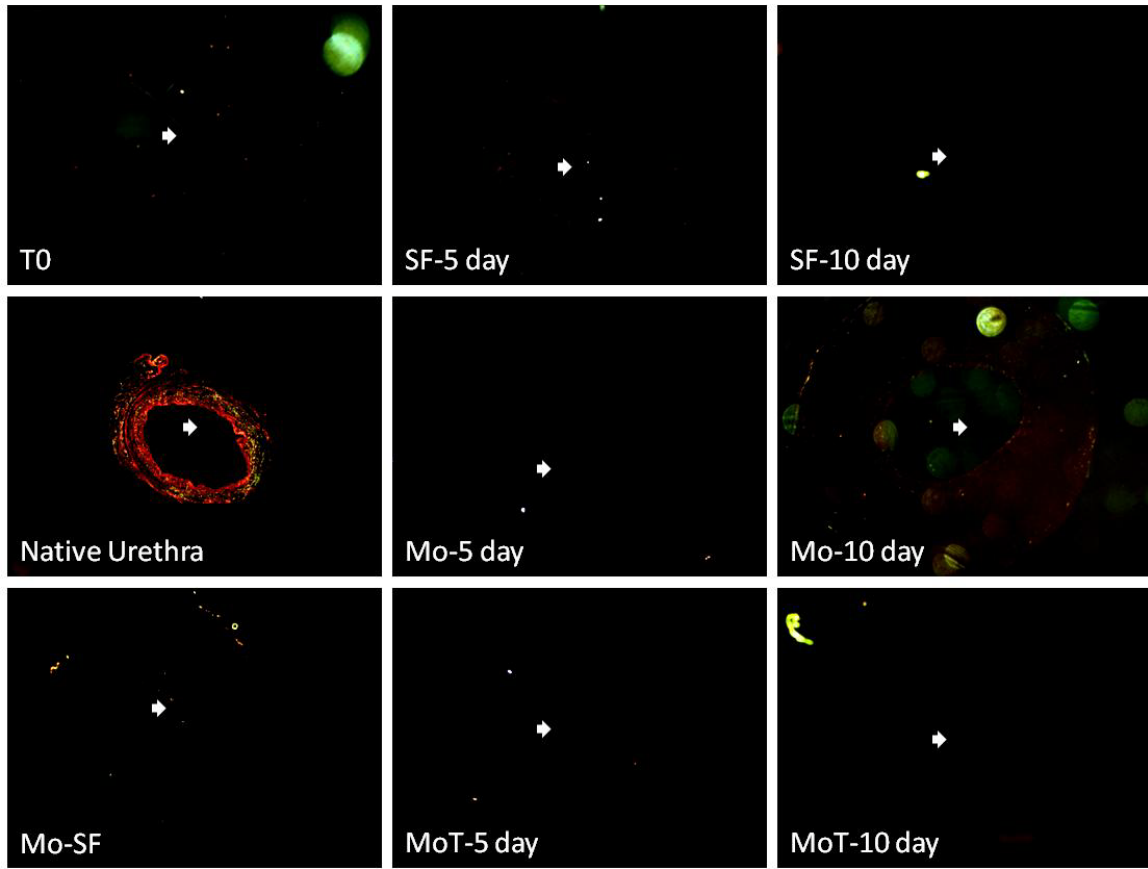


**Figure 6.13** Representative picosirius red staining for constructs cultured under T0, SF-5 day, Mo-5 day, MoT-5 day, SF-10 day, Mo-10 day, MoT-10 day, and Mo-SF. Images taken with a 4x objective and the native urethra served as a positive control. Red = organized and mature collagen, green = unorganized or immature collagen.

Arrows indicate the lumen of the construct.

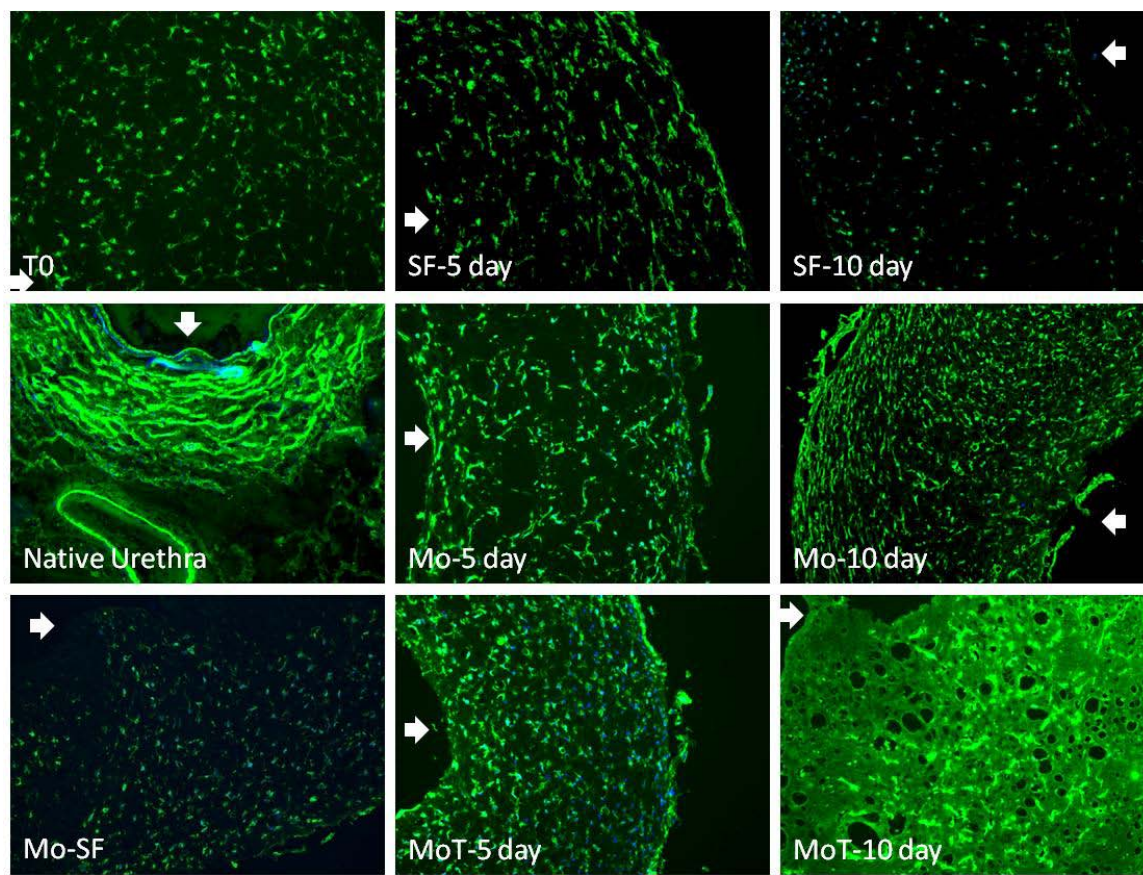


**Figure 6.14** Representative  $\alpha$ -SMA staining for constructs cultured under T0, SF-5 day, Mo-5 day, MoT-5 day, SF-10 day, Mo-10 day, MoT-10 day, and dedifferentiation. Images taken with a 10x objective and the native urethra served as a positive control. Blue = nuclei, green =  $\alpha$ -SMA. Arrows indicate the lumen. Remaining Sections shown in **Appendix H**.

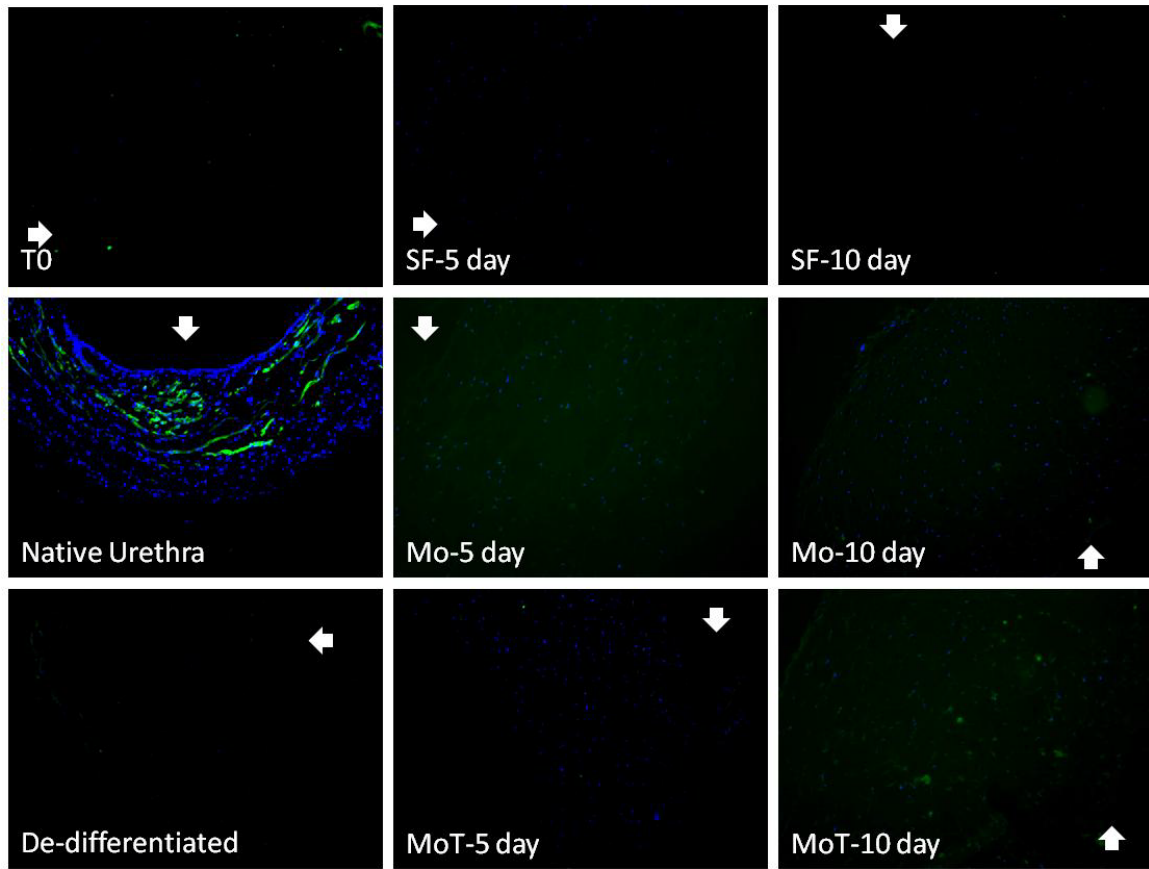


**Figure 6.15** Representative CALP staining for constructs cultured under T0, SF-5 day, Mo-5 day, MoT-5 day, SF-10 day, Mo-10 day, MoT-10 day, and dedifferentiation. Images taken with a 10x objective and the native urethra served as a positive control. Blue = nuclei, green = CALP. Arrows indicate the lumen.

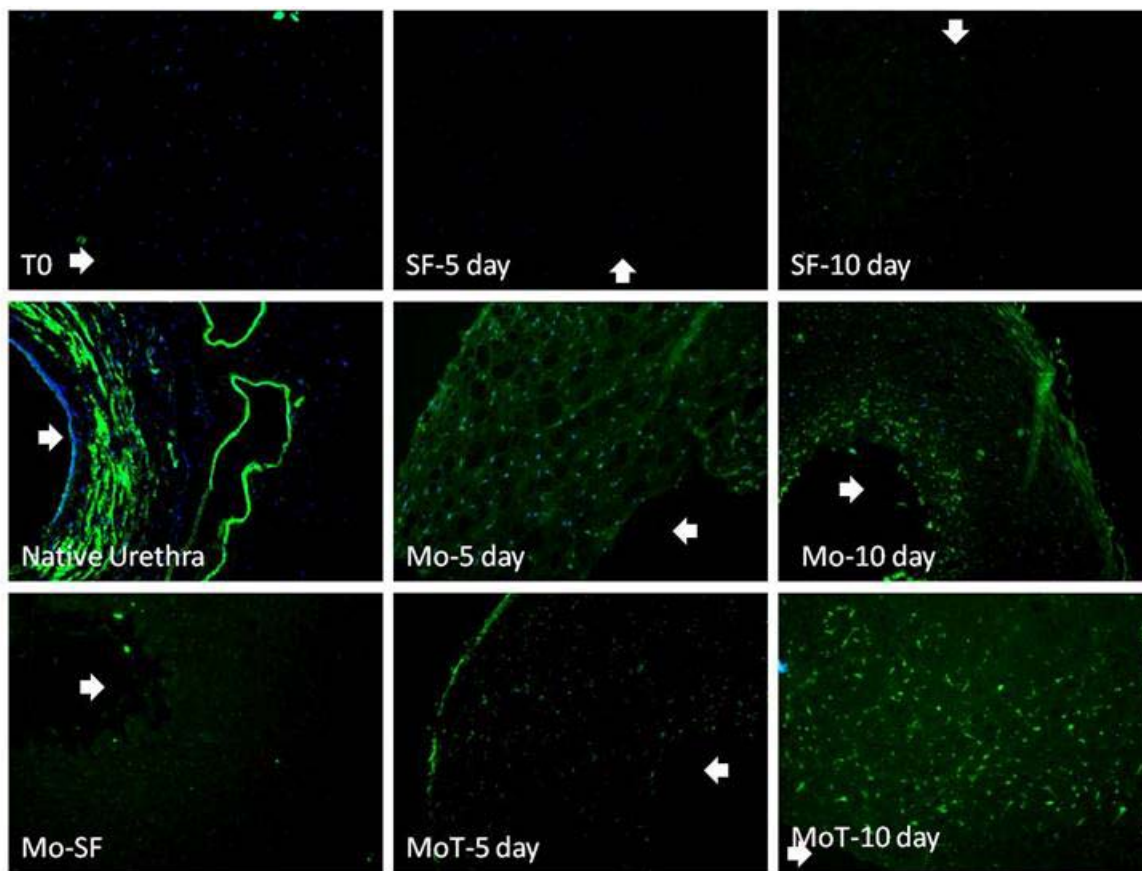


**Figure 6.16** Representative MHC staining for constructs cultured under T0, SF-5 day, Mo-5 day, MoT-5 day, SF-10 day, Mo-10 day, MoT-10 day, and dedifferentiation. Images taken with a 10x objective and the native urethra served as a positive control. Blue = nuclei, green = MHC. Arrows indicate the lumen. Remaining Sections shown in **Appendix H**.

**Table 6.3** Graded representation of smooth muscle marker expression for constructs cultured under T0, SF-5 day, Mo-5 day, MoT-5 day, SF-10 day, Mo-10 day, MoT-10 day, and dedifferentiation and their comparison to the native urethra.

	<b>SMA</b>	<b>CALP</b>	<b>MHC</b>
T0	+++	-	-
SF-5 day	+++	-	-
Mo-5 day	+++	-	+
MoT-5 day	+++	-	+
SF-10 day	++	-	-
Mo-10 day	+++	-	+
MoT-10 day	+++	-	++
Mo-SF	+++	-	-
Native Urethra	+++	+++	+++

## 6.2.5 Western Blots

Although we were able to isolate a large amount of protein from our constructs, it is believed that the majority of it is fibrin. The large amount of fibrin in these constructs made it challenging to detect the small amounts (in comparison to fibrin) of  $\alpha$ -SMA and MHC that were observed in our immunofluorescence results (Section 6.2.4). Although blots for both  $\alpha$ -SMA and CALP were blank (Appendix B), an intense band near 75 kDa was visible on MHC blots (Figure 6.17).

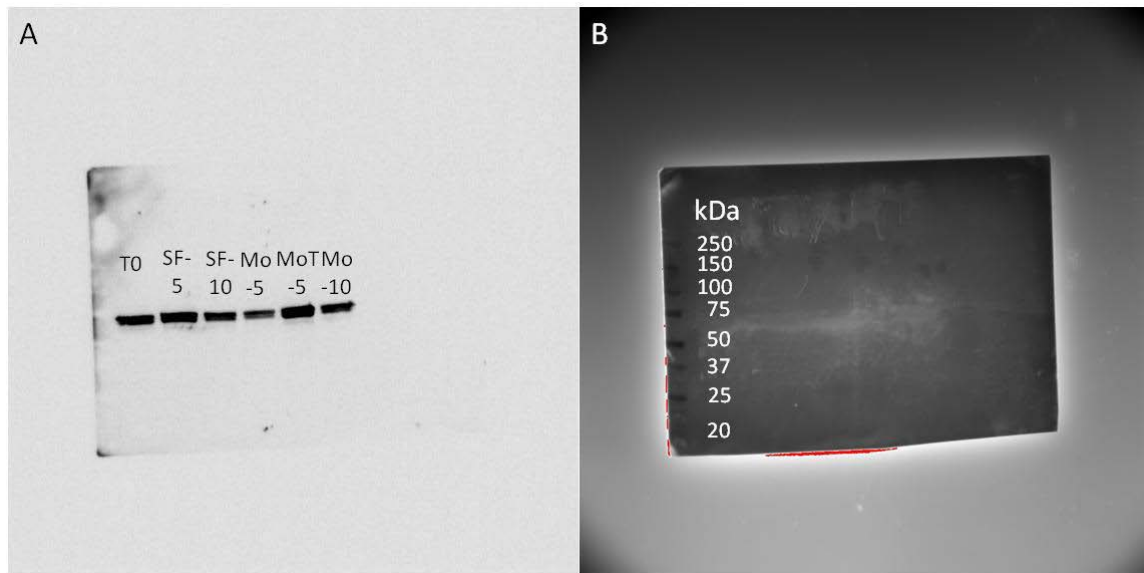


**Figure 6.17** Western blot stained for MHC (A) and the white light molecular weight standard (B) for constructs cultured under T0, SF-5 day, SF-10 day, Mo-5 day, MoT-5 day and Mo-10 day culture conditions.

## 6.2.6 Cell Distribution

Analysis of cellular distribution indicated that there was a greater aggregation of cells towards the outer surface than the lumen for all culture conditions (**Figure 6.18**). Only T0 and Mo-5 conditions had aggregation percentages closest to 50% in each half of the construct. The addition of TGF- $\beta$  for 5 or 10 days in the bioreactor caused a greater aggregation towards the outer edge with Mo-10 having lower percentages than the T0 control. Although not significantly significant, there was a very strong trend ( $p=0.06$ ) for aggregation towards the outer surface in Mo-SF constructs.

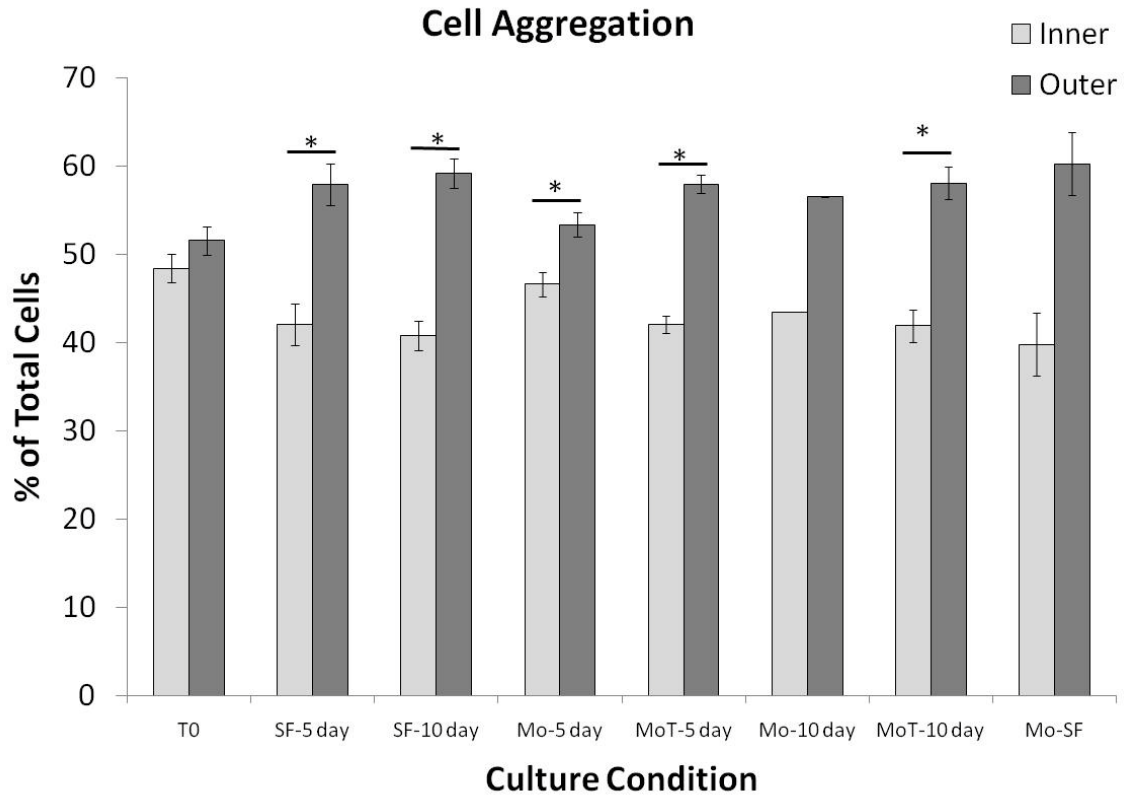


**Figure 6.18** Cell aggregation on inner vs outer portions for constructs cultured under T0, SF-5 day, Mo-5 day, MoT-5 day, SF-10 day, Mo-10 day, MoT-10 day, and Mo-SF. Values are shown as experimental average  $\pm$  SEM.

\* $p < 0.05$  between inner and outer portions within a culture condition.

### 6.3 DISCUSSION

The bioreactor system was relatively stable over both 5 and 10 day culture durations (**Figure 6.3- Figure 6.7**). Although a few points fell outside of the acceptable range, they were still next to the line and not biologically significant. Pressure-diameter curves indicated that compliance decreased with culture duration (shifted to the left of 5 day cultures), with Mo-10 day being the least compliant (**Figure 6.8**). This is easily seen in **Figure 6.9** with 5 day bioreactor cultures with and without TGF- $\beta$  having the highest compliance, with the greatest variation in compliance occurring at lower pressures. Compliance values calculated over low (0-6 mmHg), middle (6-12 mmHg) and high (12-20 mmHg) pressure ranges showed that compared to T0 conditions, all 5 day cultures increased low pressure compliance and 10 day cultures decreased it (**Table 6.2**). Although there was no significant difference between groups when tested for burst pressure, constructs exposed to bioreactor culture tended to have lower burst pressures than spinner flask controls (**Figure 6.10**). Constructs cultured with TGF- $\beta$  showed less of a decrease in burst pressure from spinner flask controls than those cultured without it. Bioreactor culture increased differentiation towards a smooth muscle phenotype, staining positive for myosin heavy chain (**Figure 6.16**). There was an aggregation of cells towards the outer edge of all constructs (**Figure 6.18**), indicating inadequate nutrient diffusion at the luminal surface. An increased luminal flow rate could possibly reduce this outer edge aggregation. Although there is a statistically significant aggregation towards the outer edge, it is only a 10% difference from equilibrium, which could arguably be biologically insignificant. Although cell aggregation could have also been assessed along the longitudinal axis, the small size of our construct and division of it for both paraffin and frozen sections (**Section 6.1.7.1**) prevented us from assessing aggregation along the longitudinal axis. Aggregation could have also been assessed in the

circumferential direction by dividing the circular cross-section into quadrants. However, our radial assessments were made on images that were  $\sim 1/4$  of the total cross-sectional area and randomly taken around the circumference. Due to the minimal variability seen in the error bars of our radial assessment (**Figure 6.18**), we feel that there would be only a minimal variation in the circumferential assessment as well.

Although the TEUW is designed to augment, not replace, the diseased urethra, mechanical properties that differ greatly from that of a healthy urethra could be detrimental. A TEUW that provides either not enough support to be beneficial or too much, causing urinary retention would not provide an ideal treatment. In comparing the compliance values of our constructs to those previously reported for the native urethra [53] we found that T0 was most similar to the native urethra at low ( $0.04 \pm 0.01$  vs  $0.05 \pm 0.01$  mmHg<sup>-1</sup>) and high ( $0.03 \pm 0.02$  vs  $0.01 \pm 0.02$  mmHg<sup>-1</sup>) pressure ranges, while Mo-10 day was most similar to middle ( $0.02 \pm 0.01$  vs  $0.01 \pm 0.00$  mmHg<sup>-1</sup>) pressure compliance (**Table 6.2**). However, there was a lack of collagen production in our constructs even with ascorbic acid and TGF- $\beta$  media supplements (**Figure 6.12** and **Figure 6.13**). Previous studies have reported an increase in collagen production in response to mechanical stimulation with or without TGF- $\beta$  [94, 100, 102, 203, 204]. However, these reports tend to have longer culture durations (1 to 5 weeks), more rigorous mechanical stimulation regimens and many use smooth muscle cells, which tend to readily produce collagen, especially in the presence of TGF- $\beta$  [205]. We do feel that implantation will enhance the remodelling of the constructs and initiate collagen production as the body acts as the ultimate bioreactor exposing the constructs to many additional stimuli. An increase in collagen would provide more mechanical strength and decrease compliance values.

The enhanced differentiation of BMPCs to a smooth muscle cell phenotype, as seen by the expression of  $\alpha$ -SMA in **Figure 6.14** and MHC in **Figure 6.16**, in the presence of mechanical stimulation with or without the addition of TGF- $\beta$  agrees with work previously reported with the same BMPCs cultured in a Flexcell<sup>TM</sup> Tissue-Train<sup>TM</sup> system [102, 203]. These studies showed that cells within a micro-scale 3-D environment express the smooth muscle cell markers  $\alpha$ -SMA and h-calponin when exposed to either mechanical stimulation with [203] or without [102] TGF- $\beta$ . The lack of calponin expression in this work (**Figure 6.15**) could be a result of a low sensitivity of the antibody to the 29 kDa form of calponin found in the lower urinary tract. Although we see positive staining in the native urethra (**Figure 6.15**), it is not as intense or uniform as the  $\alpha$ -SMA (**Figure 6.14**) or MHC (**Figure 6.16**) staining. Since the constructs only express a small amount of MHC, it is likely that the calponin staining is too weak to detect. Although we see  $\alpha$ -SMC expression under all culture conditions, we only see fully contractile smooth muscle cell markers with and without TGF- $\beta$  at both 5 and 10 days (**Table 6.3**). It appears that TGF- $\beta$  has a greater effect on differentiation at longer culture durations. Qualitatively there is more positive staining for MHC with TGF- $\beta$  than without in 10 day cultures (**Figure 6.16** and **Table 6.3**), indicating that MoT-10 day shows the greatest degree of differentiation towards a SMC phenotype. However, MHC expression was not confirmed by western blot results, which showed only a 75 kDa band and is most likely the product of degradation (**Figure 6.17**). The lack of contractile response to muscular agonists (**Figure 6.11**), non-homogeneous MHC expression (**Figure 6.16**) and lack of cell organization (**Figure 6.12**) indicate that while some differentiation of the BMPCs to contractile SMCs has occurred, it was not sufficient to create a fully contractile TEUW. While the contribution of TGF- $\beta$  to smooth muscle differentiation has been reported [123, 126, 203], it has also been shown to increase

mechanical properties [94, 100, 204]. As we saw with a trend towards an increase in burst pressure in the presence of TGF- $\beta$  (**Figure 6.10**), others have reported an increased modulus [100, 204] and tensile strength [100].

While this work shows the benefit of bioreactor culture with and without TGF- $\beta$  to enhance BMPC differentiation towards a smooth muscle cell phenotype, further analyses are necessary. This study focussed on minimal mechanical stimulation with and without TGF- $\beta$ , but additional studies assessing the effects of mechanical stimuli more similar to that seen by the native urethra (steps to gradually increase pressure or short bursts of increased pressure) would also be beneficial. Perhaps a more rigorous stimulus would decrease the loss of MHC seen in immunofluorescence following Mo-SF culture (**Figure 6.16**), enhance cell orientation in the circumferential direction and increase functional response to contractile agonists. Pre-conditioning of BMPCs in mono-layer with mechanical stimulation prior to incorporation within the TEUW could also benefit the mechanical properties and differentiation caused by the bioreactor. The use of different pressure transducers designed for a low pressure environment would also reduce the variability seen in **Figure 6.3**. A more rigorous control system which continuously measures and records media composition and intraluminal pressures would provide a more thorough assessment of system stability. Also, the inclusion of a feedback loop and/or pressure relief valves would provide more control over the mechanical stimulation and prevent variations due to unexpected pressure increases during culture. An increase in  $n$  value for several groups could also aid in changing the trends to significant differences. Although we were unable to confirm the expression of our smooth muscle markers by western blot, further studies utilizing immuno-precipitate may concentrate the amounts of  $\alpha$ -SMA and MHC enough for detection.

This study has laid the groundwork for differentiation of BMPCs within a fibrin matrix by a bioreactor for urethral augmentation. We show how bioreactor culture enhances smooth muscle cell marker expression while maintaining mechanical integrity. We believe that further studies will enhance the work presented here and lead to a new, mechanical and functional support for the diseased urethra.

## **7.0 EFFECTS OF IMPLANTATION OF A TEUW ON THE MECHANICAL AND STRUCTURAL CHARACTERISTICS OF THE NATIVE URETHRA IN A RAT MODEL OF SUI**

SUI is an emotionally and physically debilitating disease that affects millions of women annually [2], with a large number of un-diagnosed women due to the embarrassing nature of the disease. While the development and onset of SUI can be caused by many factors including increased age, vaginal delivery, prolonged stages of labor and menopause, the main mechanisms of SUI are inadequate support of the urethra by surrounding tissues/structures and/or a neuromuscular defect [38, 206], which lead to an ineffective closure mechanism. Although numerous treatments for SUI are available, most require strict patient compliance, dissipate over time, or are accompanied by additional complications [29, 38].

While tissue engineering has explored various treatments for urethral repair (refer to **Section 1.3**), most have focused on the replacement of a non-functional portion of the tissue in a male animal model. The most promising results have developed from the injection of MDSCs into the urethra for treatment of SUI [80, 81, 85, 175]. Although the MDSCs have shown improvements in LPP and contraction [80, 81, 85, 157, 175], no long-term assessments of their location following injection have been performed. Several studies have shown in a rat model of SUI that in addition to a damaged muscular component, the ECM is also damaged [35, 51] (**Chapter 2.0**). Therefore, we believe that a 3-D, cell-based therapy could provide both a

mechanical and functional support to the diseased urethra to repair both the damaged muscle and ECM components. Placement of a TEUW around the proximal portion of the urethra could provide both a mechanical support, to prevent overdistension of the diseased urethra during increases in intraluminal pressures, as well as a functional component via cells to aid in urethral contraction to maintain continence, providing relief from SUI.

## 7.1 METHODS

### 7.1.1 Animals

Adult female Lewis and SD rats (250-300 g) (Hilltop Lab Animals, Inc., Scottsdale, PA) were used in this study. Animals were housed at the University of Pittsburgh under the supervision of the Department of Laboratory Animal Resources. The policies and procedures for the animal studies are in accordance with those detailed in the Guide for the Care and Use of Laboratory Animals, published by the US Department of Health and Human Services. Procedural protocols were approved by the University of Pittsburgh's Institutional Animal Care and Use Committee.

### 7.1.2 Surgical Procedures

Animals were divided into three groups per strain: sham continent (SC), sham SUI (SS) and rat TEUW (RT) (**Figure 7.1**). All initial (day 0) procedures were performed under 4% isoflurane anaesthetic. SC animals received a midline incision and separation of the proximal urethra from the underlying vagina (**Figure 7.2A**). Separation of the urethra and the vagina on both sides was

initiated by using cautery (Bovie<sup>®</sup> AARON Medical, St. Petersburg, FL). A pair of Moria Iris Forceps (Fine Science Tools, Foster City, CA) was then used to completely separate the tissues, creating a 5 mm long separation (**Figure 7.2A**).

SS animals received the incision, separation of urethra and vagina as well as a bilateral pudendal nerve transection as described in **Section 3.1.3** to induce SUI.

RT animals received the tissue separation and nerve transection, but also received placement of a TEUW composed of  $5 \times 10^6$  BMPCs embedded in rat fibrin around the proximal portion of the urethra (**Figure 7.2B-C**). TEUWs were fabricated as described in **Section 4.2.2**, but were made with rat fibrinogen (3 mg/mL; Sigma-Aldrich, St. Louis, Mo) instead of bovine fibrinogen to decrease an acute inflammatory response seen in preliminary studies (**Appendix F**). Following fabrication, constructs were cultured in a spinner flask for 5 days prior to implantation (**Section 4.2.2**). For implantation, constructs were cut to a length of 5 mm and opened along the longitudinal axis. The construct was then wrapped around the proximal portion of the urethra in a cuff-like fashion (**Figure 7.2B**) and closed around the urethra with 10-0 nylon suture (ARO-Surgical) (**Figure 7.2C**).

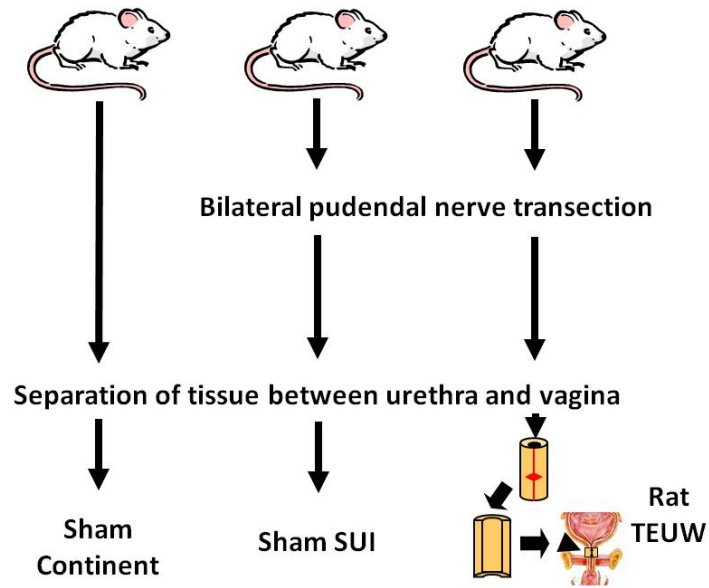


**Figure 7.1** Schematic of the test groups and procedures each receives.

Three weeks following initial procedures, SD rats were assessed for V-LPP (see **Section 3.1.4**) and urethral ex-vivo functional properties (see **Section 3.1.8**). Lewis rats were assessed for urethral ex-vivo mechanical properties (see **Section 2.2.5**), histology and western blotting. Studies were divided between the two rat strains due to differences reported in **Chapter 3.0** and the preliminary work that had been performed in Lewis rats (**Appendix F**).

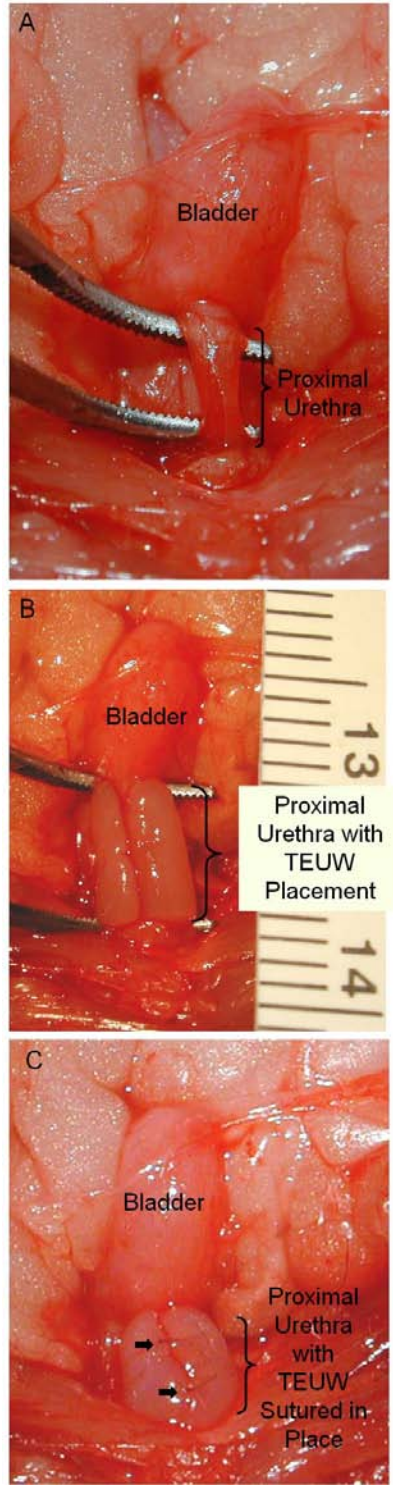


**Figure 7.2** Images of one representative implantation of a TEUW showing tissue separation (A), placement of TEUW around the proximal urethra (B) and TEUW sutured around the urethra (C). Scale in centimeters, arrows indicate 10-0 suture locations.

### **7.1.3 Assessment for V-LPP and Ex-Vivo Functional Properties in SD rats**

#### **7.1.3.1 V-LPP**

Three weeks following procedures, SD rats were assessed for V-LPP as described in **Section 3.1.4**. Briefly, V-LPP was assessed by transecting the spinal cord at the T9-T10 level, ligating both ureters and clearing the colon of feces. A catheter was implanted into the bladder dome and attached to both a pressure reservoir and pressure transducer. Animals were mounted in the vertical position and intravesicle pressure was increased incrementally until leakage from the urethral orifice was visible [64].

#### **7.1.3.2 Ex-vivo functional testing**

Following V-LPP, urethras were excised and mounted into a bathing chamber as described in **Section 2.2.5**. Functional testing was performed as described in **Section 3.1.8**. Briefly, urethras were exposed sequentially to 0 mmHg and 8 mmHg intraluminal pressures, N $\omega$ -nitro-L-arginine (100  $\mu$ M; to remove endogenous nitric oxide synthase activity), phenylephrine (40  $\mu$ M; to assess smooth muscle contraction), acetylcholine (5 mM; to assess striated muscle contraction) and EDTA (3 mM; to inhibit muscular response) while measuring the outer diameter of the middle portion of the urethra [141].

### **7.1.4 Assessment for Ex-Vivo Mechanical Properties and Composition in Lewis rats**

#### **7.1.4.1 Ex-vivo mechanical testing**

Ex-vivo mechanical testing was performed as described in **Section 3.1.7**. Briefly, the urethra was isolated and mounted into our ex-vivo testing system. The tissue was preconditioned

at 0 to 8 mmHg to remove viscoelastic effects and then subjected to incremental increases in intraluminal pressure from 0 to 20 mmHg, while measuring outer diameter [54, 142]. The tissue was assessed at various positions (proximal, middle and distal) along its length. After testing, tissues were assessed for histology as described in **Section 7.1.4.2**

#### **7.1.4.2 Histology**

The tissue was processed and stained as described in **Section 3.1.9**. Briefly, the tissue was fixed in 4% paraformaldehyde for 24 hours then transferred to 30% sucrose, and cut into proximal, middle and distal segments. Each segment was cut in half and processed for both frozen and paraffin 10  $\mu$ m sections. Paraffin sections were dewaxed, rehydrated and stained for H&E, Lillie's modified Masson's trichrome and PSR. Sections were imaged on a color digital camera (Olympus, Dulles, VA) on a BX45 Olympus microscope (Olympus, Dulles, VA) using MagnaFire software (Olympus, Dulles, VA).

Frozen sections, assessed for IF, were permeabilized, blocked, and stained with primary antibodies for the smooth muscle cell markers  $\alpha$ -SMA (clone 1A4; Sigma-Aldrich, St. Louis, MO), (1:250 in blocking solution), CALP (DAKO, Glostrup, Denmark), (1:250 in blocking solution) and MHC (clone 1C10; DAKO), (1:400 in blocking solution) followed by Alexa 488-conjugated secondary antibody (Invitrogen, Carlsbad, CA) (1:500 in blocking solution). All frozen sections were counter-stained with DAPI for nuclear visualization, and mounted with gelvatol. Immunofluorescence was imaged with a color, digital camera (QImaging, Surrey, BC, Canada) on an E800 Nikon Eclipse microscope (Nikon, Melville, NY) using NIS Elements BR 3.0 software (Nikon, Melville, NY).

### 7.1.4.3 Western blotting

To quantify changes in protein levels due to treatment, western blotting was performed as described in **Section 6.1.7.2**. Briefly, urethras were isolated and rinsed with sterile phosphate buffered saline. Urethras were then separated into proximal, middle and distal segments and each was placed into a pre-weighed tube and snap frozen. Samples were ground on dry ice and a lysed in buffer (see **Section 6.1.7.2**). Lysates were sonicated and microcentrifuged, then supernatants were collected. Total protein concentrations were determined by the BCA assay (Pierce, Rockford, IL). Samples were loaded at 16  $\mu$ g per well and resolved by electrophoresis on 4-15% Tris-HCl gradient gels (Bio-Rad Laboratories, Hercules, CA) at 200 V. Total protein was separated by SDS-PAGE and electro-transferred to nitrocellulose membranes (Bio-Rad Laboratories). To ensure equal loading, membranes were stained with Ponceau-S to visualize total protein content. Membranes were then blocked with milk blocking buffer and incubated with primary antibody for the same smooth muscle markers ( $\alpha$ -SMA (1:1,000), CALP (1:500) and MHC (1:500)) used in immunofluorescence (**Section 6.1.7.1**) as well as PGP 9.5 (1:1,000), which is a general neuronal marker, overnight at 4°C. Smooth muscle marker membranes were then labeled with horse radish peroxidase goat-anti-mouse conjugated secondary antibody (1:10,000, Thermo Scientific, Rockford, IL) and PGP 9.5 membranes were labeled with horse radish peroxidase goat-anti-rabbit conjugated secondary antibody (1:10,000, Thermo Scientific, Rockford, IL) at room temperature for 1 hour. Protein bands were detected and imaged using Supersignal West Femto Luminal Enhancer Solutions (Thermo Scientific, Rockford, IL) and the Kodak Molecular Imaging Station (v.4.5.0, Kodak, Rochester, NY). All three urethral portions from each experimental condition were run together on each gel. Densitometry results were

analyzed within each gel as a fold difference from the respective portion of the sham continent group.

### **7.1.5 Statistics**

Data is presented as the average  $\pm$  standard error of the mean. Statistical comparisons were performed using the software package SPSS (version 16.0, SPSS, Inc., Chicago, IL). For comparisons between groups, a one-way ANOVA was used. Post-hoc testing was performed with a Gabriel or Games-Howell test (for normally distributed data), or the Kruskal-Wallis test, followed by a Monte-Carlo test between groups (for non-parametric data). Pressure-diameter data was analyzed using repeated measures ANOVA with a post-hoc Bonferroni test to detect overall differences in the curves between experimental conditions. Significance was detected at p-values less than 0.05.

## 7.2 RESULTS

### 7.2.1 Assessment of V-LPP and Ex-Vivo Functional Properties for SD Rats

#### 7.2.1.1 V-LPP

SD V-LPP values (**Figure 7.3**) show a trend of pudendal nerve transection lowering LPP in the SS group compared to SC. A similar decrease is visible in the RT group, indicating the neither pudendal nerve transection nor placement of the TEUW had a significant effect on LPP.

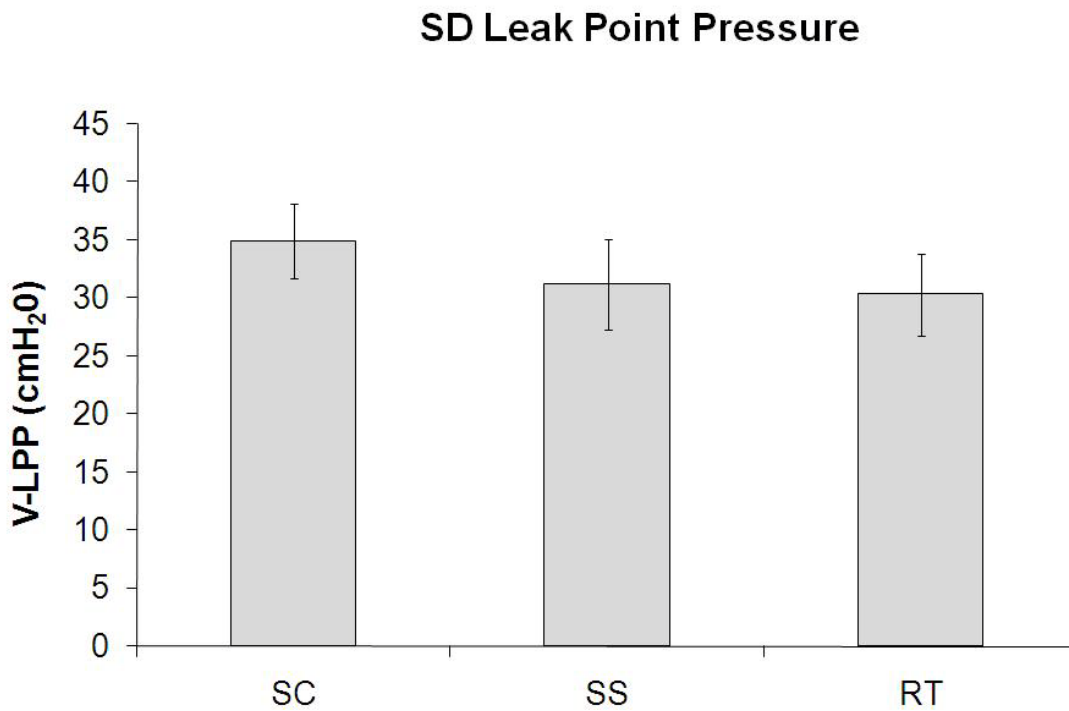


**Figure 7.3** SD leak point pressure values for sham continent (SC), sham SUI (SS) and rat TEUW (RT) groups.

Values shown as average  $\pm$  SEM.

### 7.2.1.2 Ex-vivo functional testing

All urethras showed a distinct response to the initial increase in pressure and to each chemical agent, excluding N $\omega$ -nitro-L-arginine [199] (**Figure 7.4**). Each response was quantified with respect to the equilibrated diameter at both 8 mmHg and the prior condition (**Figure 7.5**). With respect to 8 mmHg (**Figure 7.5A**), it appears that the rat TEUW group had responses more similar to the sham continent group than did the sham SUI group for all stimuli except EDTA. The sham SUI group had a significantly greater response than sham continent animals to phenylephrine (PE), while the rat TEUW response was significantly lower than that of the sham SUI group (**Figure 7.5A**). Quantification of each response with respect to equilibrium prior to each stimulus shows a similar trend with the rat TEUW animals being most similar to sham continent animals (**Figure 7.5B**). Sham SUI animals had a significantly greater contraction in response to PE than sham continent animals.

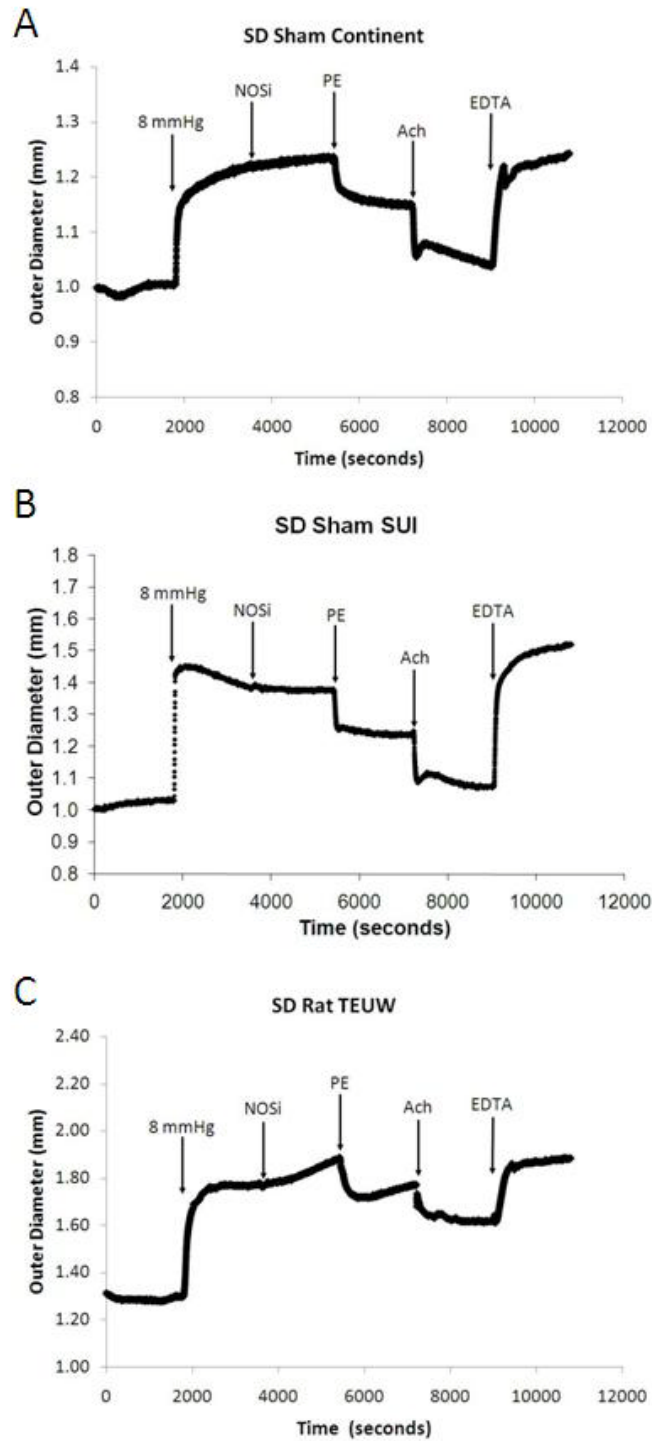


**Figure 7.4** Representative sprague-dawley outer diameter reponse of the middle urethra of sham continent (A), sham SUI (B) and rat TEUW (C) groups to various agonists and antagonists (NOSi, PE, Ach and EDTA). Data was measured at 1 Hz with 30 minute equilibrations at each condition. Outer diameter measurements were normalized to the initial outer diameter at 0 mmHg. All plots are available in **Appendix G**.

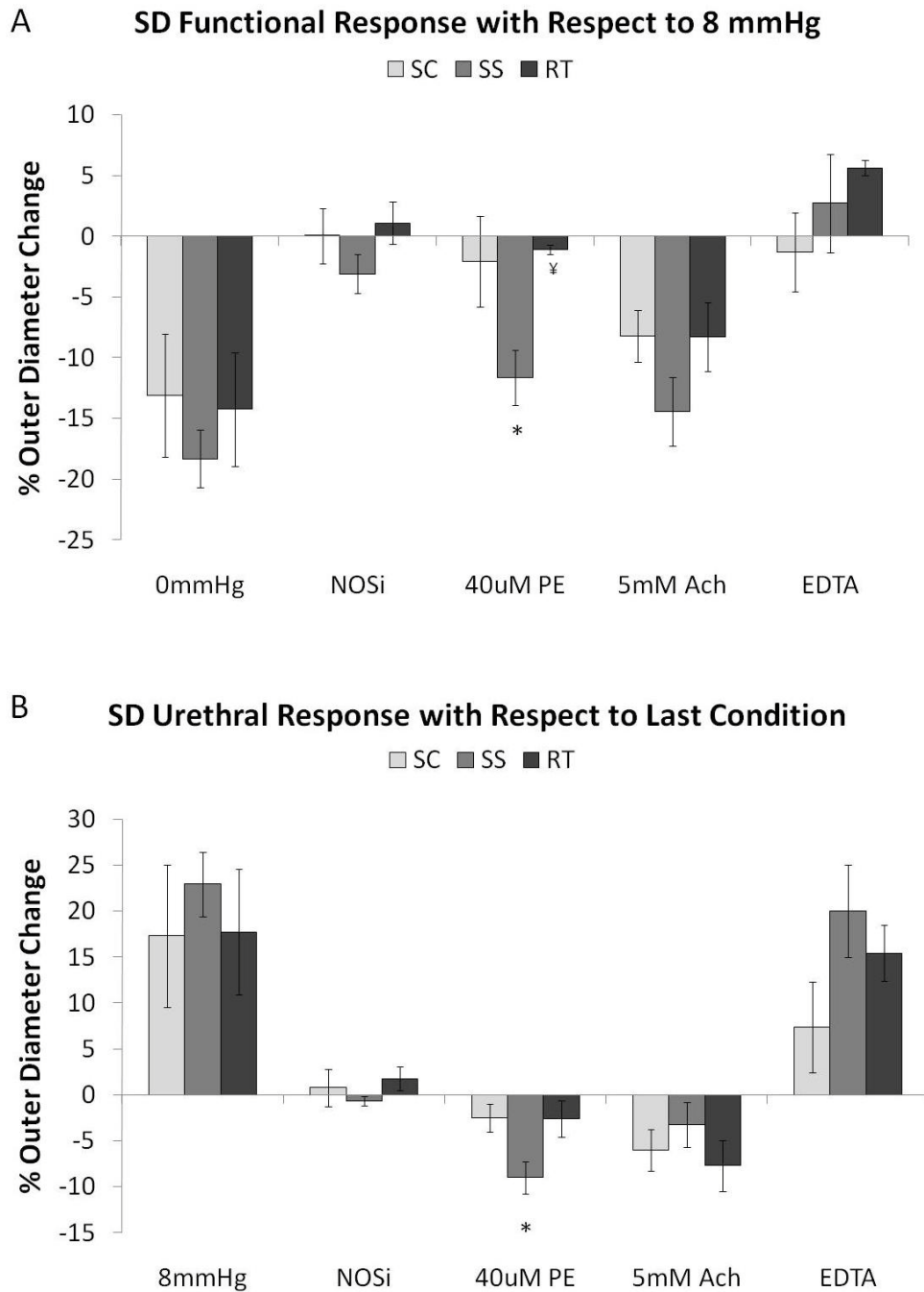


**Figure 7.5** Outer diameter change of the middle urethra for SD rats of sham continent (SC, n=6), sham SUI (SS, n=6) and rat TEUW (RT, n=4) groups to various agonists and antagonists (NOSi, PE, Ach and EDTA) with respect to 8 mmHg (A) and the equilibrated previous condition (A). Data was measured at 1 Hz with 30 minute equilibrations at each condition. Outer diameter measurements were normalized to the initial outer diameter at 0 mmHg. Values shown as average  $\pm$  SEM. \*,<sup>‡</sup>p<0.05 compared to SC.

## 7.2.2 Assessment of Ex-Vivo Mechanical Properties and Composition for Lewis Rats

### 7.2.2.1 Ex-vivo mechanical testing

Pressure-diameter curves showed a left to right gradient from treatment to control groups in the proximal and middle portions of the urethra under both baseline (**Figure 7.6**) and passive (**Figure 7.7**) conditions, indicating an increase a lower compliance in treatment groups. The rat TEUW curve lying to the left of the control groups indicates that it is less compliant than both the sham SUI and sham continent groups in both the proximal and middle portions. Both baseline (**Figure 7.8**) and passive (**Figure 7.9**) step-wise compliance curves show the greatest difference between groups occurs at low pressures (0, 2 and 4 mmHg).

SC rats have the greatest proximal compliance at all pressure ranges in both the baseline (**Figure 7.10A**) and passive (**Figure 7.11A**) states. The proximal urethra of the SC group was significantly more compliance than the RT group at the overall pressure (0-20 mmHg) range in the baseline state (**Figure 7.10A**) and at both the low (0-6 mmHg) and overall ranges in the passive state (**Figure 7.11A**). Middle urethral compliance values were highest in the SS group at low and overall pressure ranges in both baseline (**Figure 7.10B**) and passive (**Figure 7.11B**) conditions, but the SC group was significantly greater than both the SS and RT groups at high (12-20 mHg) pressures in the baseline state (**Figure 7.10B**). Distal urethral compliance is greatest in the SS group at low and overall pressures, but in SC at middle and high pressures in the baseline state (**Figure 7.10C**). The RT compliance is most similar to that of the SC group at both low and overall pressure ranges in the baseline state (**Figure 7.10C**) and middle and high pressures in the passive state (**Figure 7.11C**). Distal passive compliance decreases from SC to RT in both low and overall pressure ranges (**Figure 7.11C**), similar to passive proximal compliance.

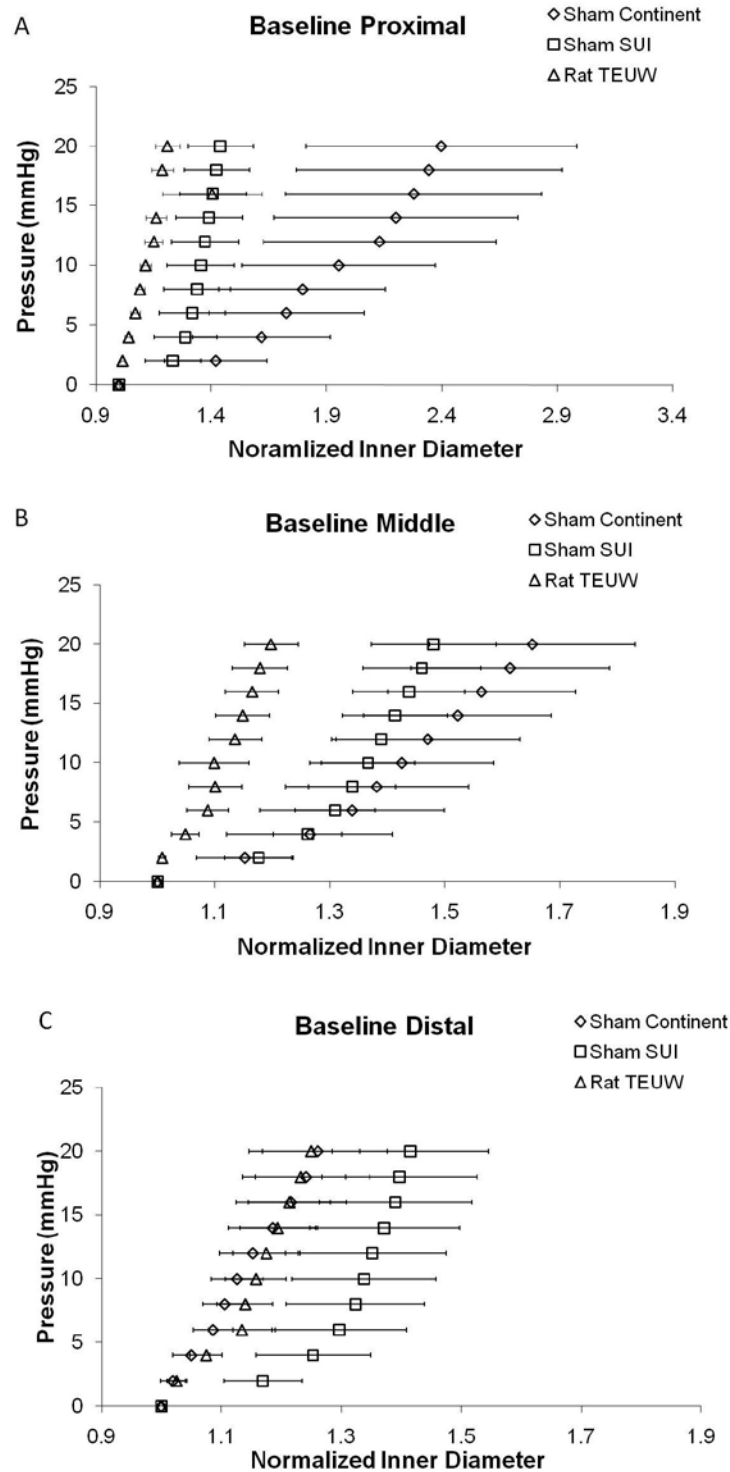


**Figure 7.6** Baseline pressure-diameter curves for the proximal, middle and distal urethra of sham continent (SC; n=5), sham SUI (SS; n=6) and rat TEUW (RT; n=7) groups. Data shown as average  $\pm$  SEM.

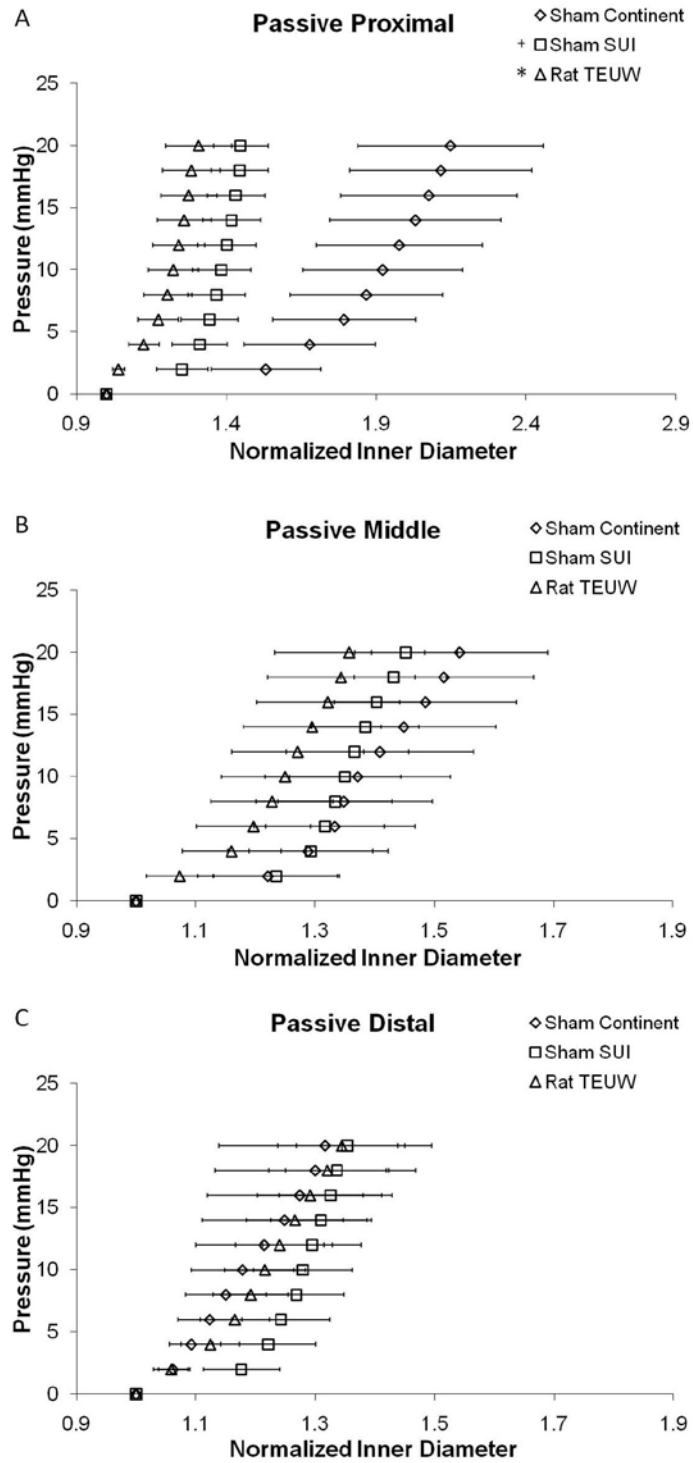


**Figure 7.7** Passive pressure-diameter curves for the proximal, middle and distal urethra of sham continent (SC; n=5), sham SUI (SS; n=6) and rat TEUW (RT; n=7) groups. Data shown as average  $\pm$  SEM, \*,<sup>†</sup>p<0.05 compared to Sham Continent.

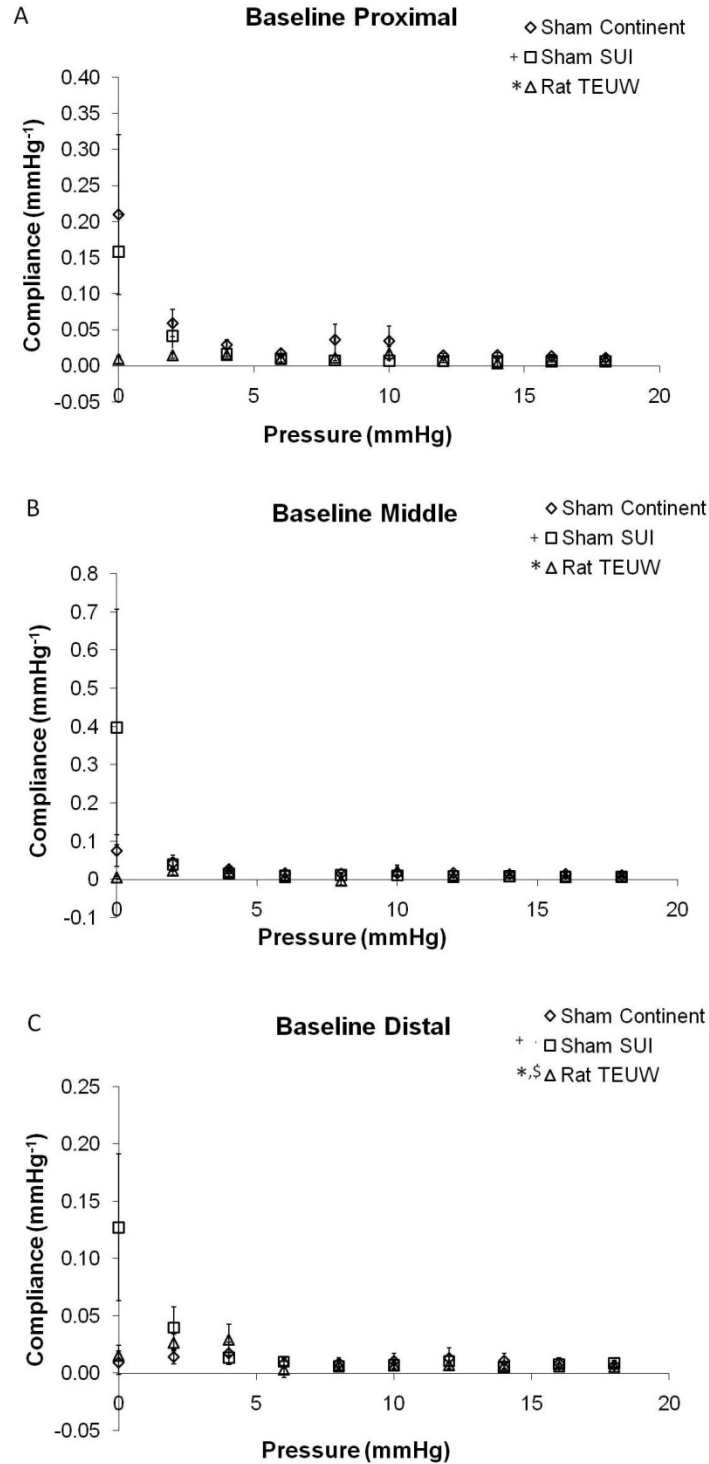


**Figure 7.8** Baseline step-wise compliance curves for the proximal, middle and distal urethra of sham continent (SC; n=5), sham SUI (SS; n=6) and rat TEUW (RT; n=7) groups. Data shown as average  $\pm$  SEM,  $^{*+}$ p<0.05 compared to Sham Continent and  $^{\$}$ p<0.05 compared to Sham SUI at the designated pressure.

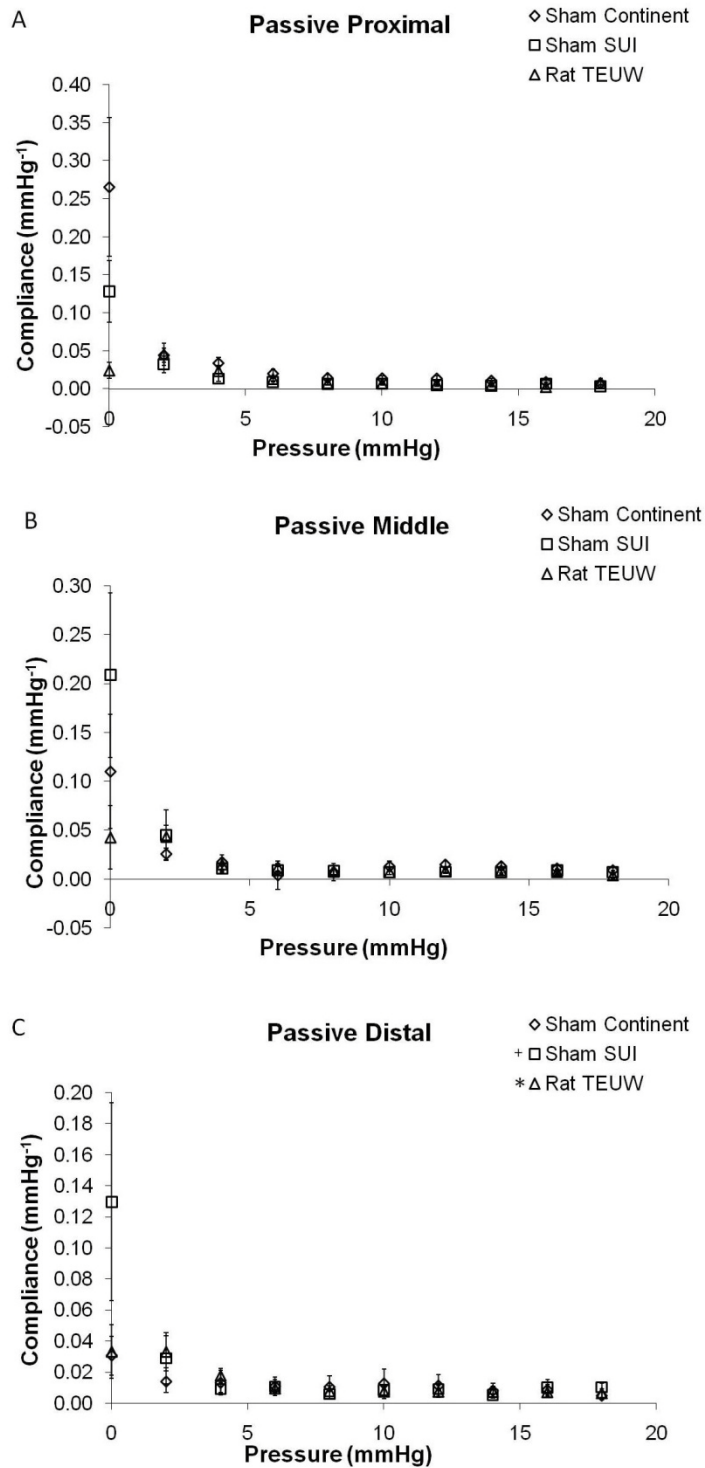


**Figure 7.9** Passive step-wise compliance curves for the proximal, middle and distal urethra of sham continent (SC; n=5), sham SUI (SS; n=6) and rat TEUW (RT; n=7) groups. Data shown as average  $\pm$  SEM, \*,<sup>+</sup>p<0.05 compared to Sham Continent at the designated pressure.

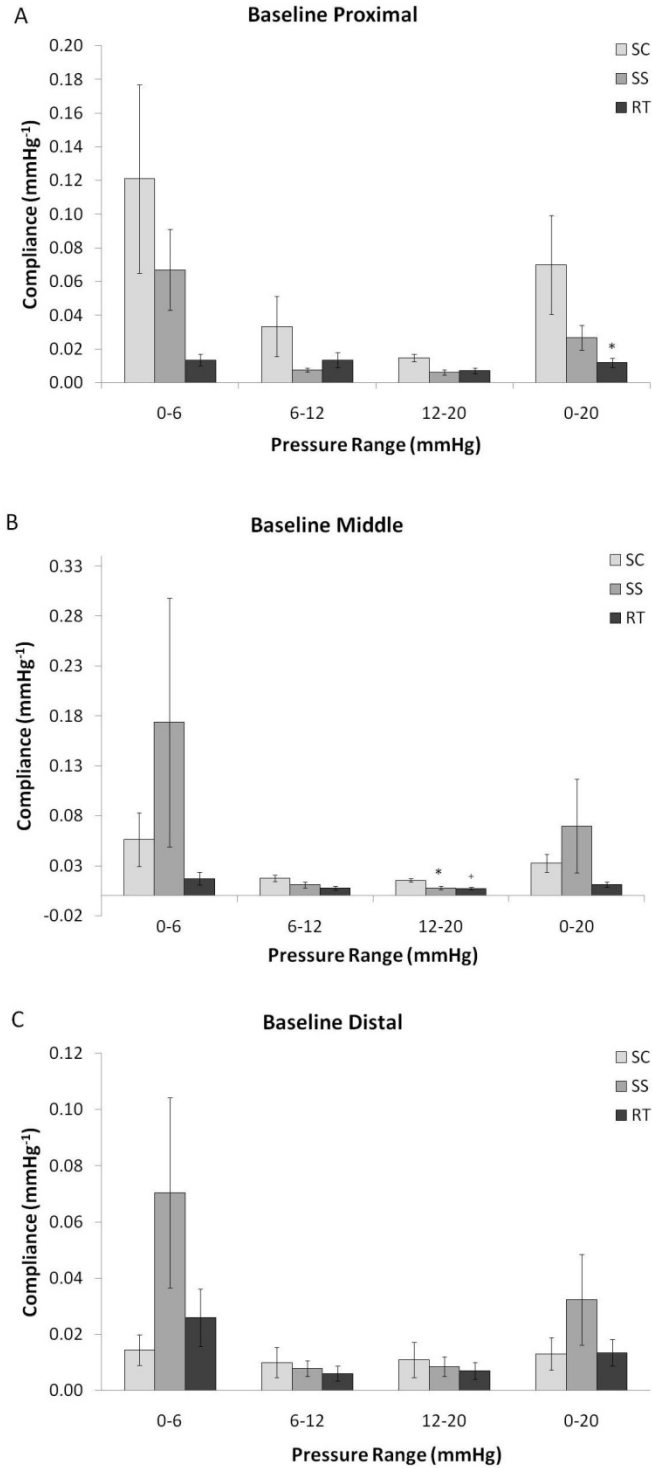


**Figure 7.10** Baseline compliance values for the proximal, middle and distal urethra of sham continent (SC; n=5), sham SUI (SS; n=6) and rat TEUW (RT; n=7) groups. Data shown as average  $\pm$  SEM, \*, <sup>+</sup>p<0.05 compared to Sham Continent.

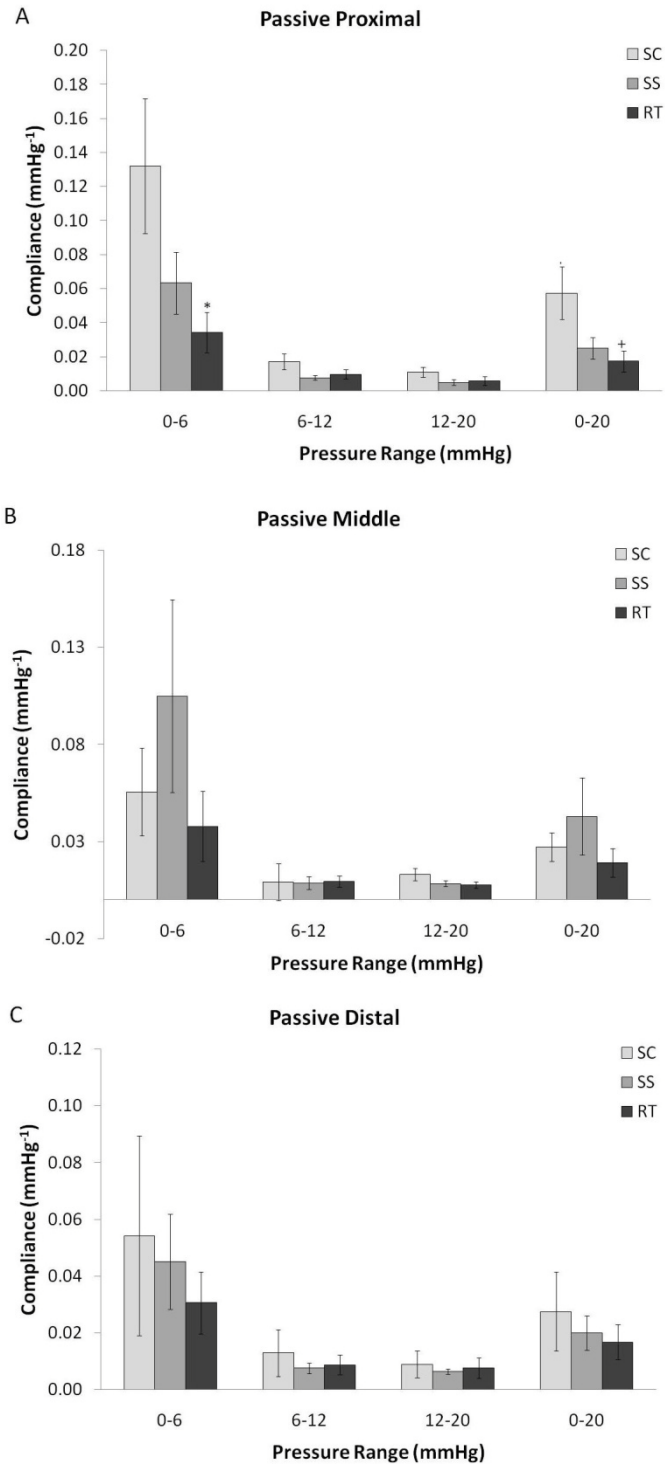


**Figure 7.11** Passive compliance values for the proximal, middle and distal urethra of sham continent (SC; n=5), sham SUI (SS; n=6) and rat TEUW (RT; n=7) groups. Data shown as average  $\pm$  SEM, \*,<sup>+</sup>p<0.05 compared to Sham Continent.

Beta stiffness values calculated over the entire pressure range (0 to 20 mmHg), show SC animals to have the lowest stiffness in all three urethral portions in both the baseline and passive states (**Figure 7.12**). SS animals had the greatest stiffness in middle urethra in both the baseline (**Figure 7.12A**) and passive (**Figure 7.12B**) states and in the baseline proximal portion. RT stiffness values tended to fall between the SC and SS values in the proximal and middle portions of the urethra, indicating that it may be returning the urethra to healthy values. However, RT values were slightly higher than both SS and SC groups in the distal portion in both baseline and passive states.

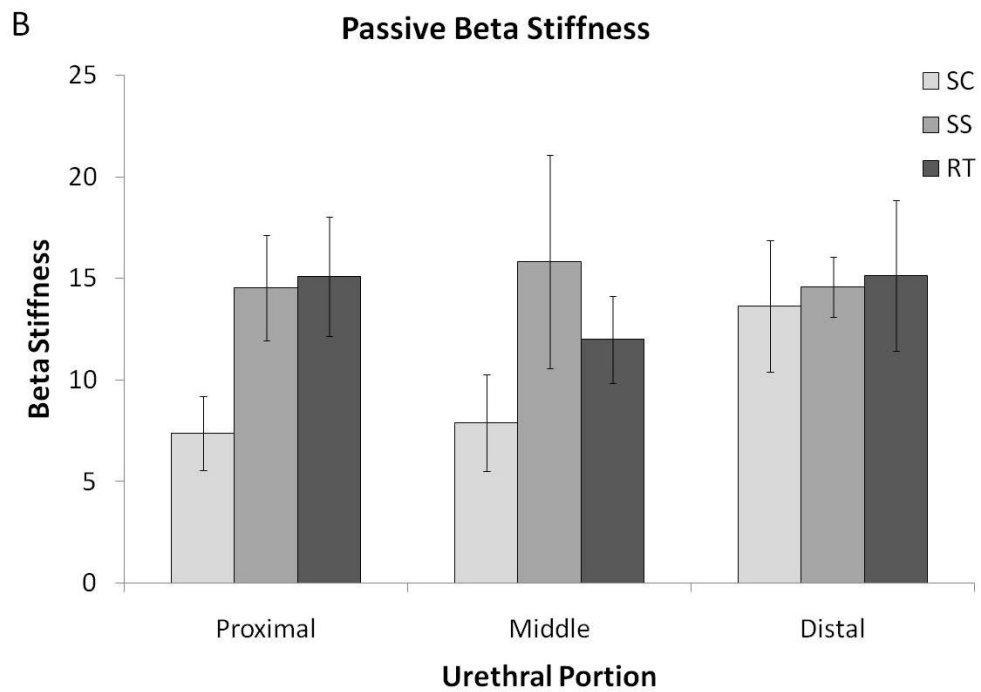
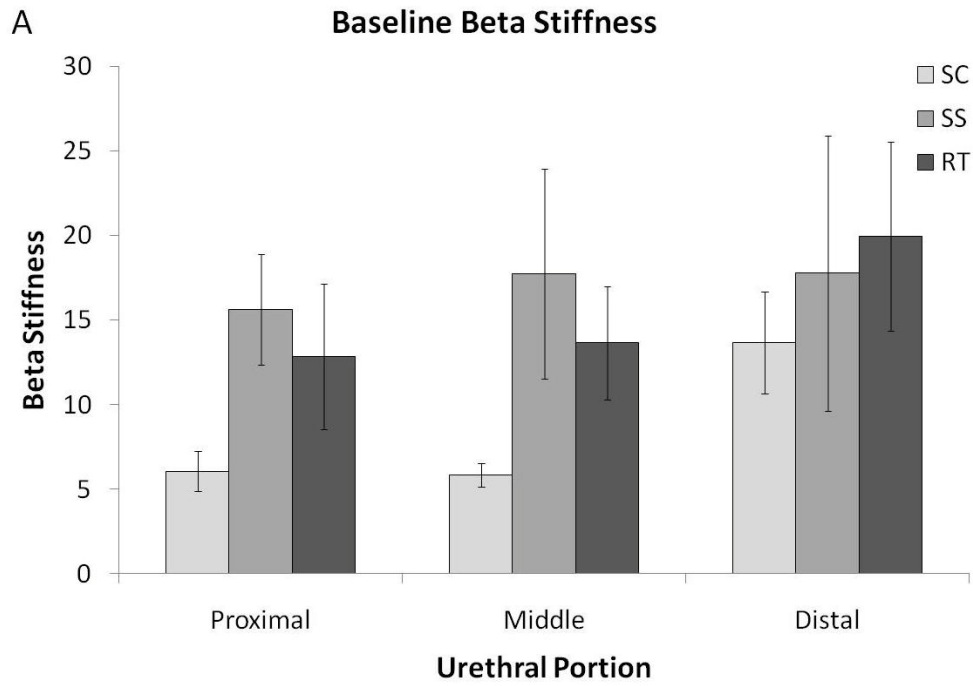


**Figure 7.12** Baseline and passive beta stiffness values for the proximal, middle and distal urethra of sham continent (SC; n=5), sham SUI (SS; n=6) and rat TEUW (RT; n=7) groups. Values shown as average  $\pm$  SEM.

### 7.2.2.2 Histology

Trichrome staining indicated a large degree of muscle (red staining) in both the proximal and middle portions of all three groups, with a greater degree of collagen (blue/green staining) in the distal portions (**Figure 7.13**). The rat TEUW appeared to be completely degraded and/or remodeled, as the fibrin, which typically stains red/pink (recall **Figure 6.12**), was no longer visible and had been replaced by a layer of collagen on the vaginal side of the proximal urethra (**Figure 7.13**).

PSR staining, which shows the maturity of collagen fibers, showed a strong red signal, indicative of mature and oriented collagen fibers, throughout most of the proximal and middle urethral cross-sections, with more yellow to green staining, indicative of immature and less oriented collagen fibers, in the distal portion (**Figure 7.14**). The area surrounding the proximal urethra in the RT group shows a strong yellow staining where the TEUW had been placed. The middle portion of the RT group qualitatively has a larger amount of green and yellow staining than both the SC and SS groups, although there appears to be more in the SS group than the SC group, indicating that both the SS and RT groups have some remodeling occurring in the mid-uerthra.

Smooth muscle alpha actin staining was faint for SC and RT groups, but intense for SS urethral portions (**Figure 7.15**), while the greatest calponin expression occurred in the RT group (**Figure 7.16**). MHC expression was present in all portions of all groups, with some faint positive staining in the area surrounding the proximal portion of the RT group where the TEUW was placed (**Figure 7.17**).

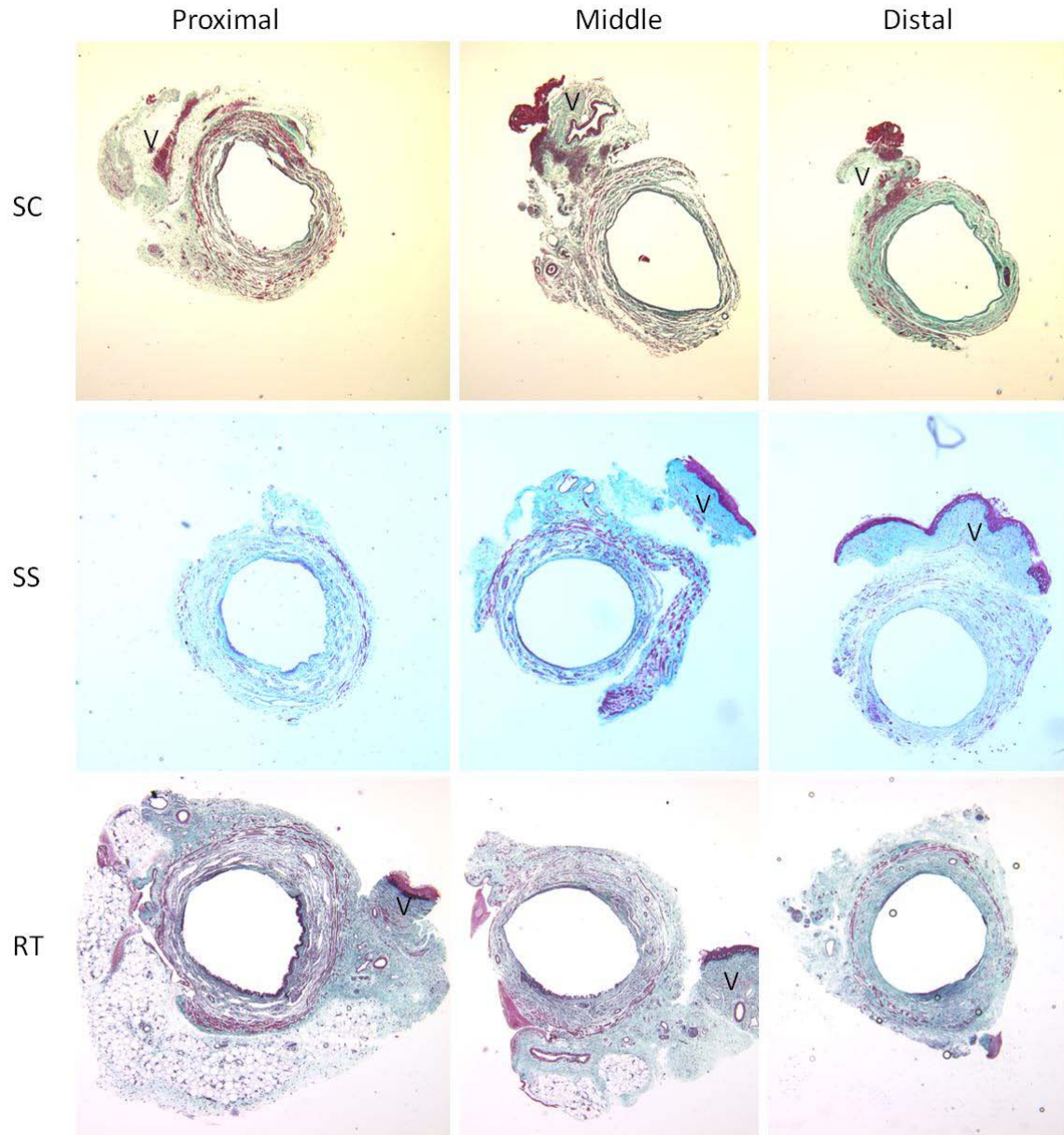


**Figure 7.13** Representative trichrome staining for proximal, middle and distal portions of sham continent (SC), sham SUI (SS) and rat TEUW (RT) urethras. Images taken with a 4x objective. Red = muscle, blue/green = collagen, black = nuclei. The vagina is located with a V, where visible. All images are available in **Appendix H**.

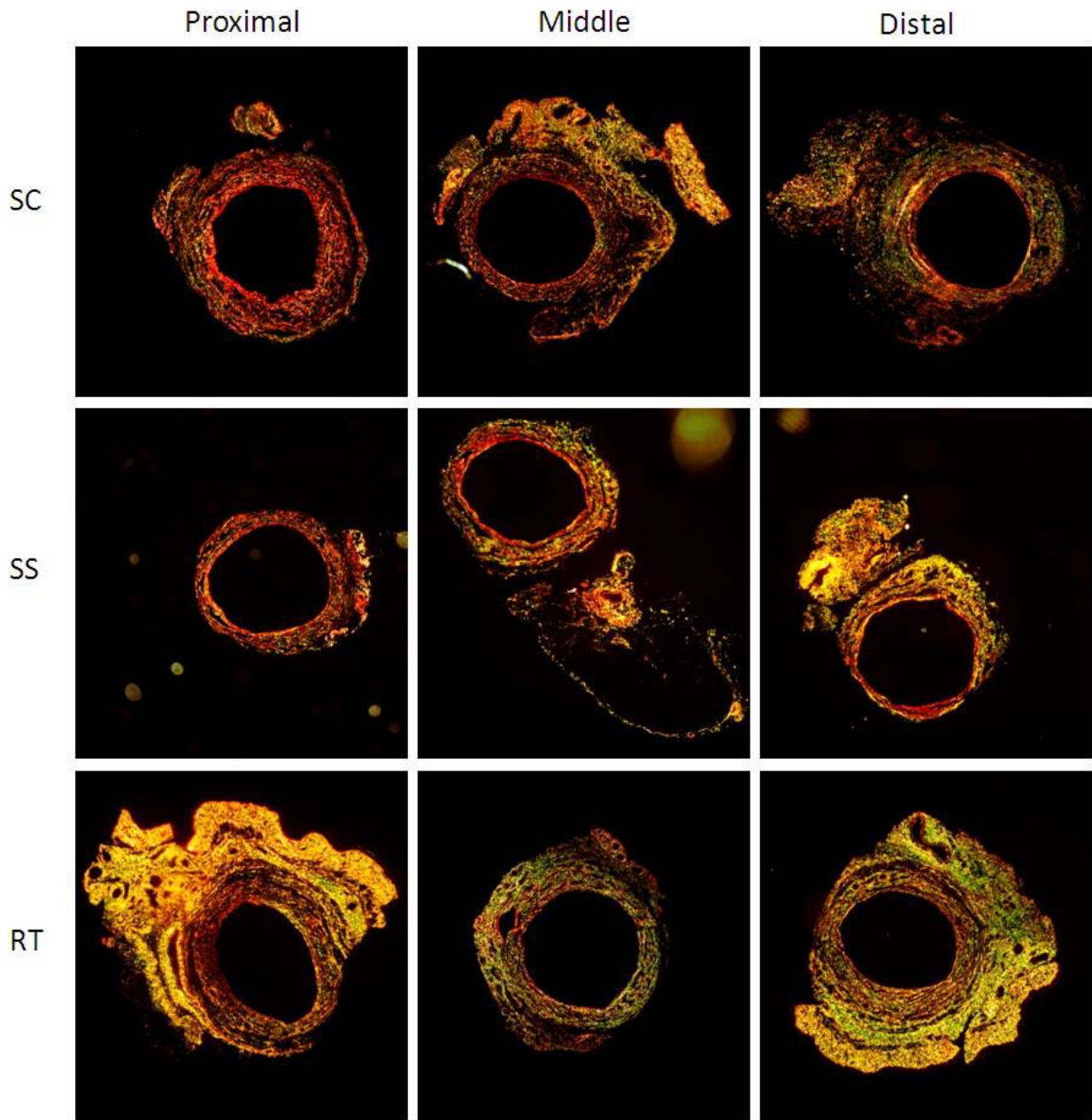


**Figure 7.14** Representative picrosirius red staining for proximal, middle and distal portions of sham continent (SC), sham SUI (SS) and rat TEUW (RT) urethras. Images taken with a 4x objective. Red = mature collagen, green = immature collagen. All images are available in **Appendix H**.

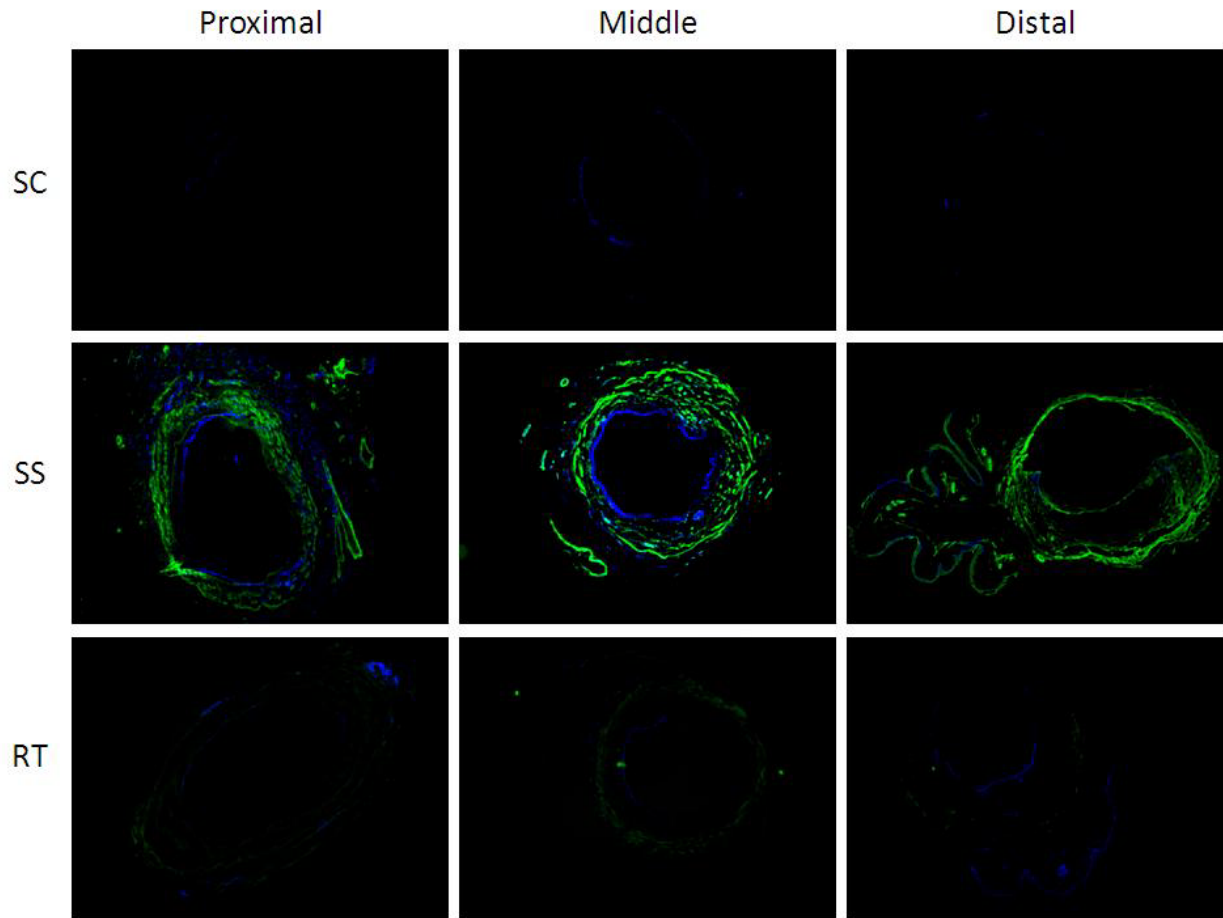


**Figure 7.15** Representative  $\alpha$ -smooth muscle actin staining for proximal, middle and distal portions of sham continent (SC), sham SUI (SS) and rat TEUW (RT) urethras. Images taken with a 4x objective. Green = calponin, blue = nuclei. All images are available in **Appendix H**

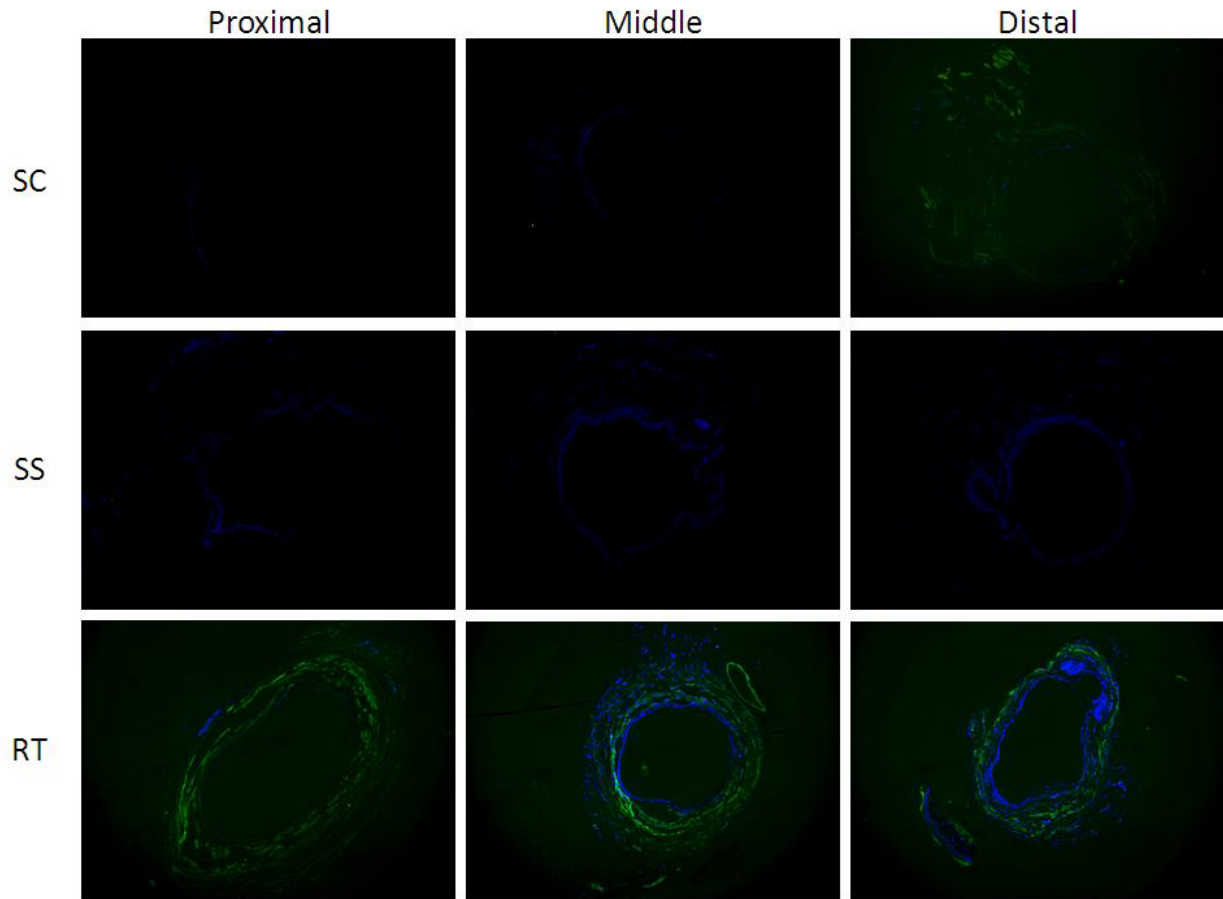


**Figure 7.16** Representative calponin staining for proximal, middle and distal portions of sham continent (SC), sham SUI (SS) and rat TEUW (RT) urethras. Images taken with a 4x objective. Green = calponin, blue = nuclei. All images are available in **Appendix H**

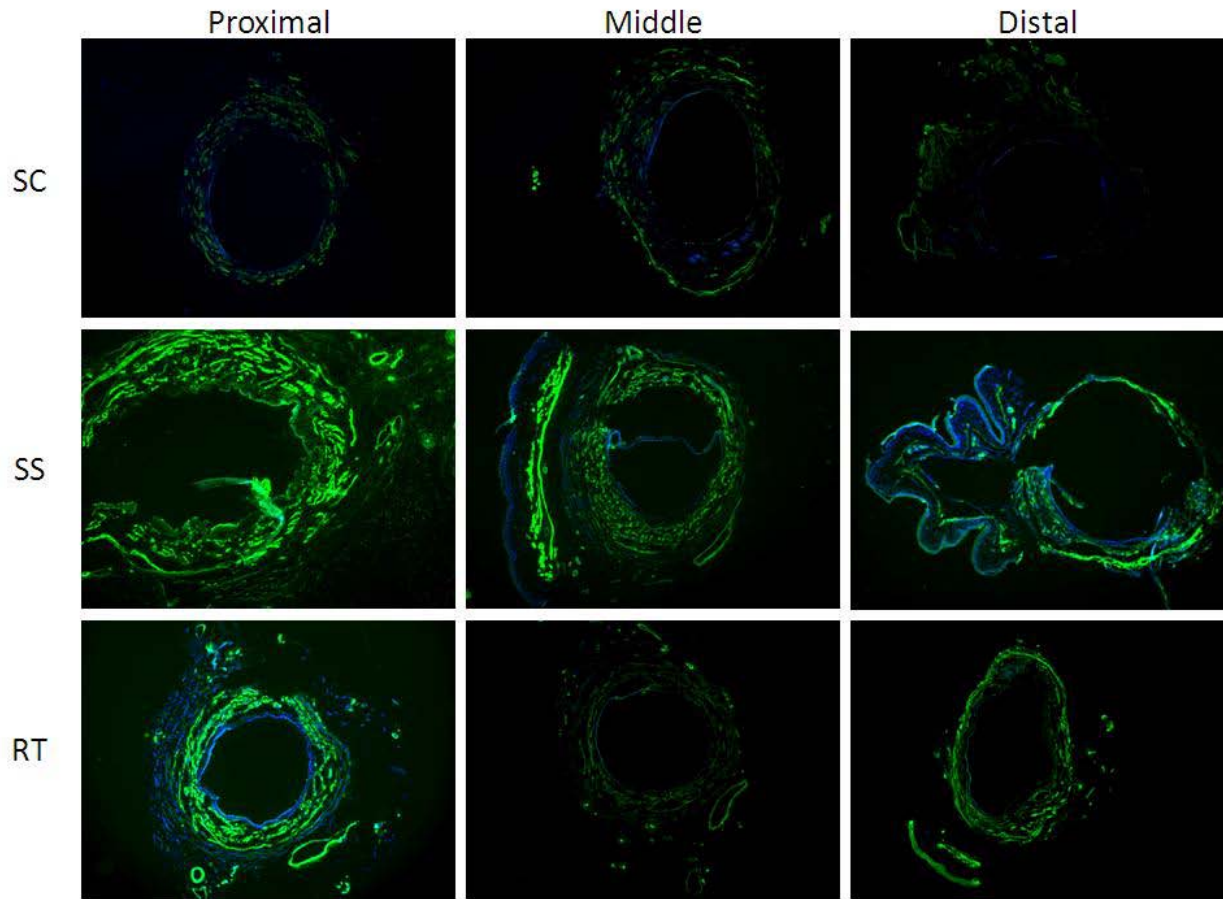
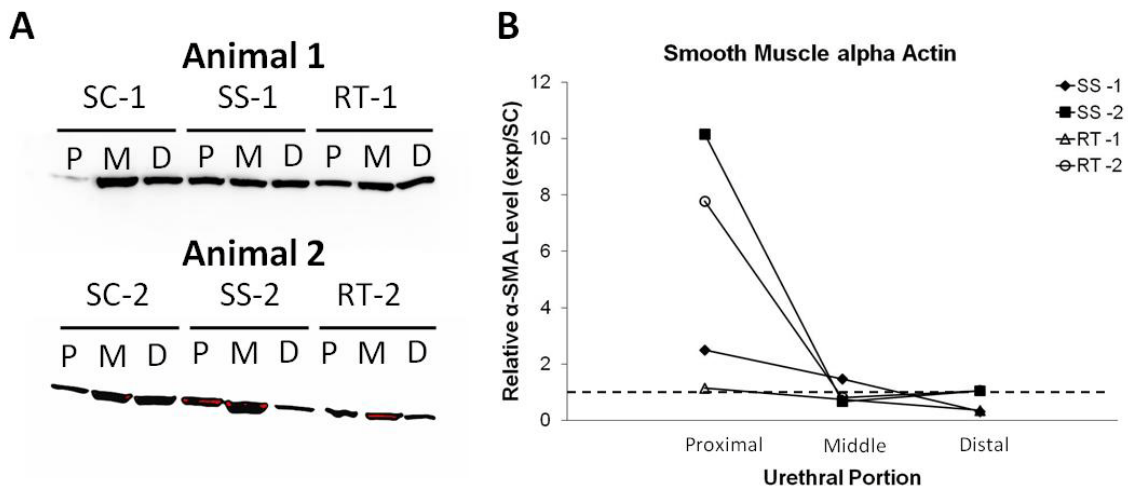


**Figure 7.17** Representative myosin heavy chain staining for proximal, middle and distal portions of sham continent (SC), sham SUI (SS) and rat TEUW (RT) urethras. Images taken with a 4x objective. Green = MHC, blue = nuclei.

All images are available in **Appendix H**

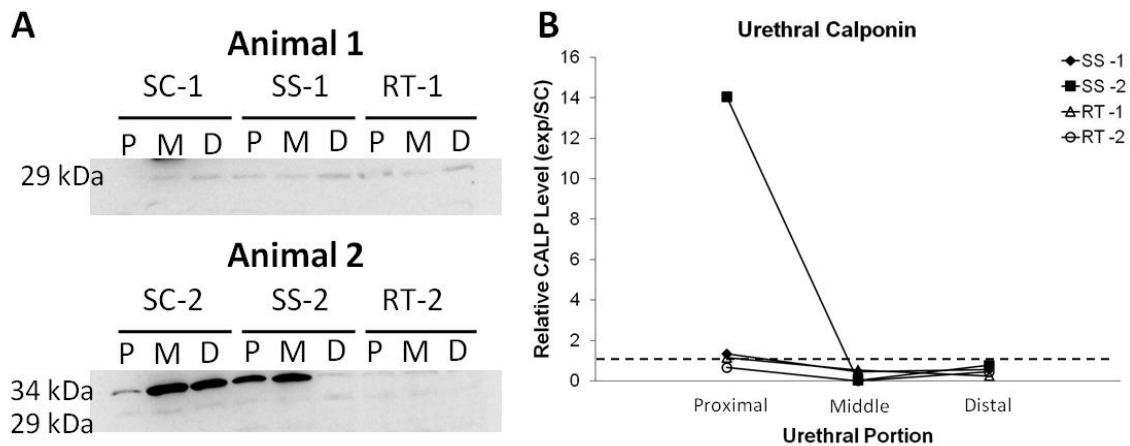
### 7.2.2.3 Western blots

Quantification of  $\alpha$ -SMA western blots (**Figure 7.18A**) shows a decreasing trend from proximal to distal portions in all conditions (**Figure 7.18B**). Between groups, the largest difference is observed in the proximal portion, where sham SUI animals appear to have a greater amount of  $\alpha$ -SMA than those which received a TEUW. This trend is seen for both gels, although at different fold changes. No large difference or consistent trend is seen in  $\alpha$ -SMA within the middle or distal portions.



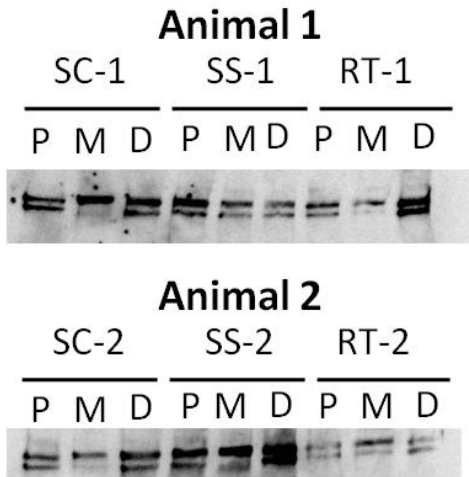
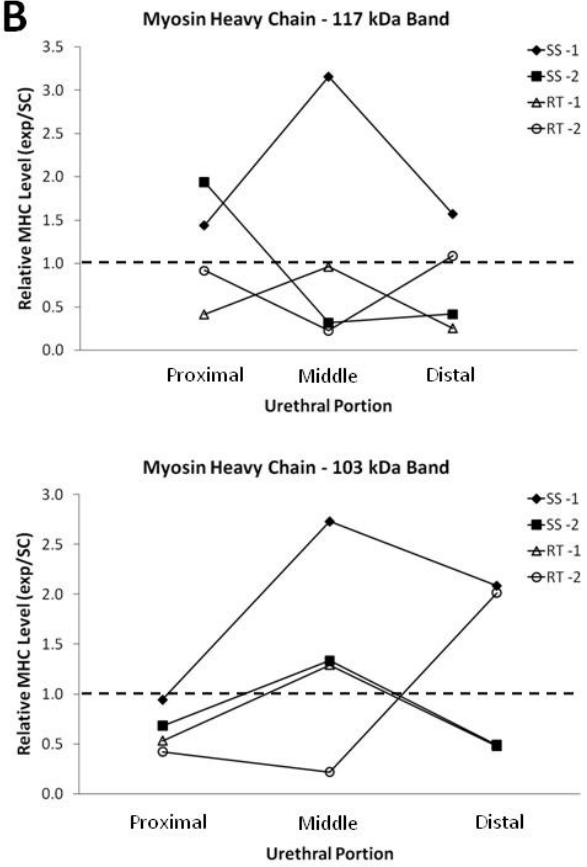
**Figure 7.18** Western blot results for  $\alpha$ -SMA. Blots from  $n=2$  rats per group (A) were quantified by densitometry and reported as changes in  $\alpha$ -SMA levels in urethral portion (P=proximal, M=middle, D=distal) relative to sham continent (SC) animals (B). The dotted line in (B) represents no change.

Calponin (molecular weight in the lower urinary tract is 29 kDa [207]) was weakly expressed compared to h1-calponin (molecular weight of vascular calponin is 34 kDa [208]) (Figure 7.19A). Calponin, like  $\alpha$ -SMA, trends towards decreasing from proximal to distal urethral portions for all conditions. Except for the proximal portion of SS-2, the presence of calponin appears to be relatively consistent in each portion regardless of experimental group (Figure 7.19B), indicating no damage to the SMC component of the urethra by placement of the TEUW. With the exception of SS-2 (Figure 7.19), all proximal urethral portions have unchanged urethral calponin levels relative to SC.



**Figure 7.19** Western blot results for calponin. Blots from n=2 rats per group (A) were quantified by densitometry and reported as changes in calponin levels in urethral portion (P=proximal, M=middle, D=distal) relative to sham continent (SC) animals (B). The dotted line in (B) represents no change.

Myosin heavy chain appears as a doublet (**Figure 7.20A**) with western blotting, with bands at 136 and 121 kDa, as determined by a relative mobility assay (see **Appendix C**). The top band shows a decrease from proximal to middle portions and an increase from middle to distal portions for groups from Animal 2 and the reverse for groups in Animal 1 (**Figure 7.20B**). It appears that the SS animals have a greater amount of MHC than both RT and SC animals for the top band and less than SC for the bottom band, while RT animals have less MHC than SC animals for both bands (**Figure 7.20B**). The bottom band shows an increase in expression from proximal to middle portions and a decrease from middle to distal portions in 75% of the animals (**Figure 7.20B**). The presence of a doublet (at these molecular weights) is thought to be the result of a site-specific enzymatic cleavage of the MHC molecule.

**A****B**

**Figure 7.20** Western blot results for MHC. Blots from n=2 rats per group (A) were quantified by densitometry and reported as changes in MHC levels in urethral portion (P=proximal, M=middle, D=distal) relative to sham continent (SC) animals (B). The dotted line in (B) represents no change.

PGP 9.5, a general neuronal marker, is decreased for the middle portion of both SS (50%) and RT (100%) groups as expected, since they both received bilateral pudendal nerve transections (**Figure 7.21**). We see a trend of SS animals having a greater fold change in PGP 9.5 expression than RT animals. SS animals show an up-regulation of PGP 9.5, indicating an increase in innervation of the proximal portion. RT animals were either unchanged or down-regulated relative to SC controls.

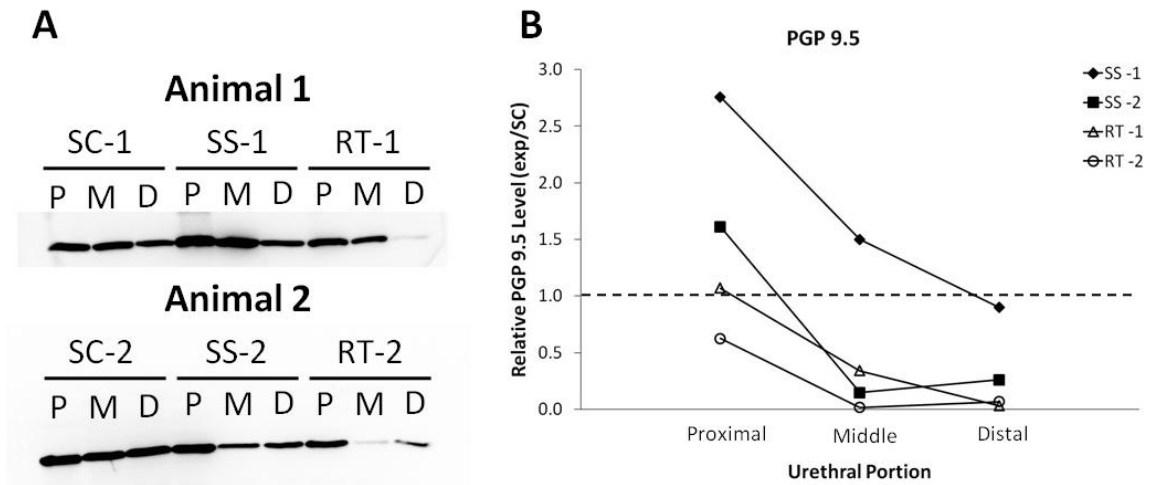


**Figure 7.21** Western blot results for PGP 9.5. Blots from n=2 rats per group (A) were quantified by densitometry and reported as changes in PGP 9.5 levels in urethral portion (P=proximal, M=middle, D=distal) relative to sham continent (SC) animals (B). The dotted line in (B) represents no change.

### 7.3 DISCUSSION

V-LPP was not significantly affected by pudendal nerve transection with or without placement of a TEUW in SD rats (**Figure 7.3**). A trend towards a decreased LPP in both SS and RT groups compared to SC was observed (**Figure 7.3**). Mid-urethral functional response was most similar between SC and RT groups (**Figure 7.5**), with SS animals having a significantly larger contraction than SC (**Figure 7.5A-B**) and RT (**Figure 7.5A**) animals in response to phenylephrine, which causes contraction of smooth muscle. Ex-vivo mechanical testing showed that SS animals had the highest low and overall compliance in the middle and distal urethra (**Figure 7.10** and **Figure 7.11**). TEUW placement provided support to the diseased urethra, decreasing compliance values in the proximal urethra compared to SS and showed downstream effects, producing low and overall compliance values similar to those of control SC animals (**Figure 7.10** and **Figure 7.11**). RT and SS beta stiffness values (**Figure 7.12**) were greater than SC in both the baseline and passive states. However, the RT values were closer to SC values proximal baseline and middle baseline and passive states, when compared to SS values (**Figure 7.12**).

Current treatments for SUI have proven ineffective or result in additional complications [25, 38]. The TEUW approach to treating urethral dysfunction is adapted from cellular therapy such as the injection of muscle derived stem cells, which has shown promising results [80]. The TEUW is designed to provide immediate mechanical support to the urethra via the tubular fibrin matrix, but also provides a cellular therapy as the fibrin degrades, the cells can become incorporated with the native tissue and provide functional support as well. The matrix component of the TEUW limits the migration of cells from the implant area, localizing their effects to the implantation site.

While previous studies have shown that treatments such as the injection of MDSCs increases LPP in a model of ISD [81], our current study shows neither a decrease in LPP with pudendal nerve transection or an increase following treatment with the TEUW (**Figure 7.3**).

Previous studies, including our own work (**Figure 3.1**) have shown that pudendal nerve transection causes a decrease in leak point pressure of SD rats [47, 56, 61]. While damage to the middle urethra was confirmed by the decreased expression of PGP 9.5 seen in the middle and distal portions of the urethra in both SS and RT groups (**Figure 7.21**) there was a lack of response seen in LPP. The absence of a significant decrease in LPP in response to pudendal nerve transection (**Figure 7.3**) could be due to the separation of the proximal portion of the urethra from the vagina, which was performed in all groups. This separation could cause remodeling or scar formation, which may provide support to the urethra and bladder neck preventing leakage. One anatomical study showed that there is a large degree of vascular and neural innervations within the connective tissue between the urethra and the underlying vagina from the bladder neck to the middle urethra [209]. It has been also been reported that SUI treatments involving the separation of these tissues at the proximal urethra, such as sling placement, may worsen a pre-existing condition over time, leading to intrinsic sphincter deficiency [209, 210], which could explain why all of our groups have similar LPP values. Some bladder distension in our model was evident upon urethral isolation which could be due to manipulation of the bladder area during tissue separation. However, it has been reported that urethral denervation can cause bladder distension [58].

SS animals had a larger contractile response to phenylephrine (a smooth muscle contractile agent) than both SC and RT groups (**Figure 7.5**). However, SS urethras contracted less than SC and RT groups in response to the striated muscle agonist, acetylcholine (**Figure**

**7.5B**) when assessing the effects of each individual agent. The increased response of the SS group to PE could be a result of a smooth muscle compensation for the damaged striated sphincter, caused by the nerve transection and evident by the decreased response to Ach (a striated muscle agonist; **Figure 7.5B**) and the decreased expression of PGP 9.5 (**Figure 7.21**) in the middle urethra. This idea of smooth muscle compensation in the SS group is further supported by the increased positive staining of both  $\alpha$ -SMA (**Figure 7.16**) and MHC (**Figure 7.17**) and the greater than one fold increase shown in western blot results for  $\alpha$ -SMA (**Figure 7.18**) and PGP-9.5 (**Figure 7.21**). The RT group has a similar response to both PE and Ach as the SC group (**Figure 7.5B**), as well as PGP 9.5 fold differences close to one (**Figure 7.21B**) indicating that the TEUW is aiding the urethra in maintaining a healthy contractile response and eliminates the need for smooth muscle compensation.

SUI induced by vaginal distension has been reported to increase low pressure proximal compliance in both the baseline and passive states in a rat model [53, 54]. While, our current work indicates that SUI, caused by pudendal nerve transection, causes an increase in low and overall compliance in the middle and distal portions, it also shows a decreased compliance from SC animals in the proximal urethra, and significantly at the middle and high pressure ranges in the middle urethra (**Figure 7.10**). This variability from previously reported compliance values [53, 54] could be largely due to the difference in strain. While our histology was performed on the Lewis urethra, previous studies which focused on the SD urethra [53] qualitatively indicate that the SD rat has a greater muscularity than the Lewis rat in both the proximal and middle portions than the Lewis urethra.

Although we expected changes in the mechanical properties of the middle urethra, since the pudendal nerve innervates the striated sphincter located there (**Section 1.1.2**), we did not

expect to see a decrease in compliance due to pudendal nerve transection. This decrease seen in proximal compliance lends further support to the idea of SMC compensation in the SS group. With the exception of the middle portion in the baseline state, we show minimal differences between all groups at middle and high pressures, which agree with results seen in the vaginal distension model [53, 54]. Although there was no change in V-LPP with placement of the TEUW, it is seen that the TEUW group is less compliant than the SS group at low and overall pressure ranges in all urethral portions (**Figure 7.10** and **Figure 7.11**). This decrease in compliance could be due to the additional layer of collagen surrounding the proximal urethra of the RT group (**Figure 7.13** and **Figure 7.14**). The TEUW also provides urethral compliance values most similar to SC controls at low and overall pressure ranges.

Although we report on changes in MHC in **Figure 7.20**, we expected to see strong banding of the main forms of MHC present in smooth muscle at 200 kDa [211], but instead saw banding at 136 and 121 kDa. These lower molecular weight bands are thought to be the result of a site-specific cleavage of MHC by a particular enzyme. Because we are seeing a doublet, at 136 and 121 kDa, and we used a monoclonal antibody, it is unlikely that these bands are from the same MHC molecule. It is likely that some molecules were cleaved twice (121 kDa), while others were cleaved only once (136 kDa), creating these two particular bands, which still possess the specific sequence that this antibody binds. A thorough literature search did not reveal any reports of MHC at the molecular weights detected here in the rat urethra or anywhere else.

While this work has provided encouraging results which support the TEUW providing both mechanical and functional support to the native urethra, further analyses should be performed. The division of endpoints between two rat strains, which have shown to have different urethral characteristics (**Chapter 3.0**), is the main limitation of this work. Mechanical

testing as well as both histological and protein analyses should be repeated in the SD rat, which is more commonly used in lower urinary tract studies to confirm the trends seen in the Lewis rat. The low n value for protein work (n=2) should be increased to determine if the large degree of variability is consistent in this model. The MHC protein work could be further analyzed by sequencing of the bands or running a more concentrated analysis such as immuno-precipitate. Further analyses should be performed to assess any remodeling, hypoxia or nerve damage that may occur due to tissue separation or TEUW placement by histology. These assessments should be performed on urethras that remained intact with the vagina for better assessment of scar formation and remodeling. Our current isolation method separates these tissues and prevents assessment of scar formation between them. This stripping away of the vagina and possible scar tissue could also explain discrepancies between our in-vivo LPP and ex-vivo mechanical data.

This work provides a novel approach to the treatment of stress urinary incontinence. We have shown that a TEUW composed of fibrin and bone marrow progenitor cells can provide support to the diseased urethra, giving it characteristics more similar to that of a healthy urethra. While further analyses are warranted, we have provided the groundwork for a new, long-term treatment for type-III SUI.

## **8.0 DISCUSSION**

We have developed a novel approach for the treatment of urethral dysfunction with a tissue engineered urethral wrap. To summarize this work, a brief description of each focus area will be followed by a discussion of the clinical relevance. Finally, limitations and future work will be addressed.

### **8.1 SUMMARY OF RESULTS**

#### **8.1.1 The Effects of Disease (Chapter 2.0) and Rat Strain (Chapter 3.0) on Urethral Function**

In order to develop an effective treatment for urethral dysfunction, it is important to understand how the tissue changes in response to various risk factors and to assess it in an appropriate animal model. We evaluated the effects of estrogen deficiency through ovariectomy, denervation of the urethra through bilateral pudendal nerve transection and the effect of in-bred vs out-bred strain on the urethral response of rats. We found that ovariectomy caused a significantly lower middle urethral response to stress and baseline pressure than both control and sham animals, indicating a change in both the striated and smooth muscle components of the urethra and causing SUI in ~63% of Ov animals. This altered urethral response was supported

by ex-vivo mechanical testing, which showed a higher baseline compliance following Ov in both the proximal and middle portions of the urethra, although not significantly. Proximal and middle urethral compliance values were also higher in the passive state of Ov animals, indicating that there may be changes to the urethral ECM in addition to the muscular components. These results indicated that estrogen plays an important role in the continence mechanism and proper urethral function.

Denervation of the urethra assessed in both out-bred (SD) and in-bred (Lewis) rat strains revealed that bilateral pudendal nerve transection significantly decreased LPP in SD rats, but had no effect on Lewis rats. However, Lewis rats had a significantly lower LPP than SD rats. We found that there was a greater contribution of the striated sphincter to the in-vivo maintenance of continence in the SD rat, and a significantly lower UBP in the Lewis rat. Ex-vivo mechanical testing supported the observed in-vivo differences in striated sphincter contribution to continence with higher compliance of the middle urethra in Lewis rats compared to SD rats in both the baseline and passive states and in the Lewis proximal urethra in the passive state. Further evidence of differences in muscular function was seen by a larger diameter change to increased pressure (inability to resist deformation) and lower contractile responses to both smooth (PE) and striated (Ach) muscle agonists of the Lewis middle urethra. Quantification of the cross-sectional muscle components revealed that the Lewis urethra is composed of a greater percentage of smooth muscle, while the SD urethra is composed of a greater percent of striated muscle and has a significantly larger cross-sectional area than the Lewis urethra, showing that the SD urethra has a greater overall muscular component than the Lewis urethra.

### **8.1.2 The Development (Chapters 4.0 and 5.0) and Implementation (Chapter 6.0) of a Novel Bioreactor**

In order for the proposed differentiation studies to progress, we needed to develop a bioreactor for the simultaneous culture of multiple constructs under minimal pressure and flow. We designed and fabricated a compact bioreactor capable of culturing four constructs simultaneously and independently within a standard cell culture incubator and versatile to accommodate various length and inner diameter constructs. The bioreactor was designed for easy monitoring of the environmental culture conditions of each chamber, which remained stable over both 5 and 10 day culture periods. Constructs subjected to bioreactor culture tended to be less compliant than their respective SF controls at middle, high and overall pressure ranges and lower burst pressures. The addition of TGF- $\beta$  resulted in higher compliance values and burst pressures than bioreactor culture without it at both 5 and 10 days. Although no culture condition stimulated collagen production, bioreactor culture with or without TGF- $\beta$  for 5 or 10 days stimulated expression of MHC, a smooth muscle cell contractile marker, indicating differentiation towards a smooth muscle phenotype.

### **8.1.3 Application of a TEUW for Treatment of SUI (Chapter 7.0)**

We demonstrated ex-vivo the feasibility of application and resulting decreased urethral compliance when a TEUW is placed around a denervated urethra. These proof-of-concept studies were followed by an extensive assessment of the in-vivo and ex-vivo effects of implantation of a TEUW in a pudendal nerve transection model of SUI in both SD and Lewis rats, respectively. Denervation of the SS and RT groups was confirmed by a decreased

expression of PGP 9.5 in the middle urethra compared to SC animals by WB. Although there appeared to be no effect of SUI or TEUW placement on SD LPP, SUI altered mid-urethral response to Ach (decreased striated muscle contraction) and significantly to PE (increased smooth muscle contraction) indicating a possible compensation of smooth muscle for the damaged striated muscle. This is supported by an increased expression of  $\alpha$ -SMA in the proximal portion of SS animals compared to both RT and SC groups seen in both IF and WB analyses. Placement of the TEUW maintained urethral responses to PE and Ach at similar levels to controls. TEUW placement provided mechanical support to the Lewis urethra, causing higher beta stiffness values in the proximal and middle urethral portions. However, surgical procedures did cause bladder distension and even stone formation in the ureters and/or bladder. These problems occurred in a small percentage of all experimental groups and are therefore, most likely the result of the separation of the urethra from the underlying vagina. The lack of differences between LPP values could also be a result of this tissue separation, which may cause scar formation. Due to the separation of the urethra from the surrounding tissues for ex-vivo assessment, we were unable to assess if scar tissue had developed.

## **8.2 CLINICAL RELEVANCE**

Urinary incontinence (urge, mixed and stress) is highly predominant in the female population and affects one third of all women in some degree (moderate to severe) [38]. With current treatments being inadequate due to dissipation over time, patient non-compliance or association with additional complications such as vaginal erosion [25, 38], the goal of this research was to develop a long-term, autologous treatment for urethral dysfunctions such as urinary

incontinence. Our results have revealed how risk factors, such as estrogen deficiency and pudendal nerve damage, contribute to dysfunctions such as urinary incontinence. We have shown how ovariectomy and pudendal nerve transection decreased LPP and increased proximal and middle compliance over controls through alterations in both muscle and ECM components. Knowledge of which urethral components are damaged as a result of various factors can aid in the development of both preventative and post-development treatments. These results coincide with previous studies which showed similar damage following vaginal distension [53, 54] and diabetes mellitus [101]. These studies indicate that a treatment which provides both mechanical and functional support to the urethra would be most beneficial.

Our TEUW focused on the use of BMPCs, which can easily be isolated from a bone marrow aspirate of the iliac crest and provide an autologous cell source and minimizing rejection of the implant, and fibrin. Fibrin was chosen as it is a natural biomaterial comprised of fibrinogen and thrombin, which are produced and degraded in the body and can be isolated from the blood, yielding an autologous matrix. The development of a completely autologous treatment, such as the one described here, decreases incidents of rejection and eliminates the need for immunosuppressants, making it more clinically desirable. As both the muscle and ECM can be compromised in urethral dysfunction, the TEUW provides both a structural and cellular component to provide both mechanical and functional support to the urethra. Since fibrin allows cells to freely migrate and produce their own collagen matrix as it degrades [95], the remaining cells and collagen can easily integrate with the ECM surrounding the proximal portion of the native urethra to provide long-term support as indicated by our 3 week in-vivo studies in a rat model. Our TEUW allows for treatment of the urethra while keeping the cells localized to the proximal urethra with matrix, unlike injection therapies [80], which can migrate over time. As

shown in this work, TEUWs that were implanted after 5 days of compaction in spinner flask culture expressed  $\alpha$ -SMA, an early smooth muscle maker. However, for a truly functional therapy, cells within the TEUW should express MHC. Due to the numerous studies which show differentiation towards a smooth muscle phenotype with mechanical and/or chemical stimulation [102-104, 111, 119, 124, 212, 213], we developed and implemented a bioreactor for the differentiation of BMPCs to a smooth muscle phenotype within a tubular structure. Our results indicate that even minimal mechanical stimulation with or without TGF- $\beta$  enhanced differentiation towards a contractile smooth muscle phenotype. Showing that conditioning of these cells can enhance smooth muscle markers and provide cells more capable of providing functional support to the native urethra. Implantation of a functional TEUW would provide an immediate increase to urethral response and thus improve continence.

### **8.3 LIMITATIONS OF METHODOLOGY**

The BMPCs used in this study were composed of a heterogeneous population of cells. Therefore, our reports of the effects of bioreactor culture on the differentiation of these cells may be skewed as the stimulation may have only affected a sub-population of the cells seeded within the constructs. However, we did find that mechanical stimulation with and without TGF- $\beta$  plays an important role in the up-regulation of contractile smooth muscle cell markers and has efficacy for urethral tissue engineering.

A major limitation of most 3-D tissue engineering work is an appropriate assay to detect cell viability and proliferation. Our initial fabrication assays utilized the MTT assay, which measures metabolic activity. However, this assay was designed for monolayer culture and

requires an assumption that all cells have the same metabolic activity. This is a large assumption to make since many things can contribute to an increase or decrease in metabolic activity, making it unrealistic to say that an increased result from MTT is directly proportional to an increase in cell number. Although other assays were investigated including the LIVE/DEAD<sup>®</sup> assay (Invitrogen, Carlsbad, CA), a lactate dehydrogenase (LDH) assay (CytoTox96<sup>®</sup> Non-Radioactive Cytotoxicity Assay, Promega Corporation, Madison, WI) and assessment of cells following fibrinolysis of the constructs, each had its own downfalls. The LIVE/DEAD assay utilizes calcein AM and ethidium homodimer to assess intracellular esterase activity and plasma membrane integrity, respectively, by diffusion of the probes into an un-fixed sample. Therefore, dense tissues prevent adequate diffusion of these molecules to all cells. LDH assays work by measuring the levels of LDH released from cells with compromised cell membranes into the surrounding environment. This assay required a concentration of the ~125mL of media from the bioreactor chambers or spinner flasks, which presented a challenge due to the 15% serum used in our cell culture media. While we also attempted to isolate the cells from the fibrin constructs following culture, the fibrinolysis protocol itself, which involved trypsin, could also lead to cell death, making it difficult to assess if cell numbers were truly based on death during culture. Early studies utilized a pathologist's examination of H&E stained slides, which resulted in no obvious indications of cell death within the constructs. This with the differential expression of smooth muscle cell markers under various culture conditions led us to believe that the cells remained viable throughout culture.

A limitation of our molecular work was our protein assessment through western blots. Due to the time required for ex-vivo testing, we anticipated protein degradation during mechanical assessment. Separate animals were assessed for protein analysis. This increased the

total number of animals, which resulted in a small n value (n=2 per group) for protein analysis. Another limiting factor of our protein assessment was the amount of protein isolated from the urethra. The size of the rat urethra (length = ~25 mm, OD = ~1.25 mm) provides a limited amount of protein. Division of the urethra into proximal, middle and distal portions further decreased our total amount of protein per sample, and it was felt that pooling samples could introduce a large degree of variability. Although we used a strong protease inhibitor cocktail during our protein isolation, our inability to isolate the 200 kDa form of MHC limited our evidence of an increased smooth muscle cell contribution in the SS group. While an extensive literature search provided no evidence of either 121 or 136 kDa isoforms of MHC within the rat urethra, or anywhere else, we are led to believe that these bands are the result of a site-specific enzymatic cleavage of the MHC molecule due to the tight banding observed or non-specific binding of the antibody to other proteins. This enzymatic cleavage may be a result of the surgical dissection of the proximal urethra from the vagina, which activated a wound-healing response. As healing and remodeling activate numerous enzymes, it is possible that it activated some that our protease inhibitor cocktail was not designed to inhibit. Although we were able to isolate a large amount of protein from our bioreactor studies, the large amount of fibrin in the constructs made it challenging to detect the small amount of  $\alpha$ -SMA and MHC that may have been present as in our immunofluorescence results. There was the presence of a ~75 kDa band in the MHC blot, which is also most likely the product of degradation. This inhibited our confirmation of differentiation of the BMPCs to smooth muscle cells within the bioreactor.

Data variability is a large limitation of many studies. We found that the Lewis rat had a large degree of intrinsic variability, creating many trends but little significance in our studies. While the majority of our SD data had very tight error bars, the corresponding Lewis values had

a large degree of variability. Evidence of this is easily observed in the ex-vivo functional testing, where each Lewis urethra tested responded in a different manner. Although increasing n values can reduce variability, a power analysis of pressure-diameter data results in values of n=12 to over 30 in order to show significance. The same variability in ex-vivo data was observed in the ovariectomized animals. Although 10 urethras were tested, the data variability remains large, preventing significance. This variability was also seen in-vivo with only 62.5% of animals becoming incontinent. Although this increased variability with some of our experimental models proved inconvenient for our studies, it is representative of what happens in humans, where not all women develop SUI following menopause. Although not significant in all instances, our work does show several trends, which indicate alterations of urethral characteristics which can provide further insight into appropriate urethral therapies or animal models for urethral studies.

The damage inflicted by the tissue dissection needed for placement of our wrap is a limitation of this treatment. Although other treatments for, such as sling placement or cystocele repair, require the same tissue separation, an increased risk of intrinsic sphincter dysfunction or worsening of perineal neuropathy has been associated with procedures that involve dissection of these tissues [209, 210]. The proximal urethra and vagina are attached by loose connective tissue containing blood vessels and nerve fibers [209], so disruption of this area can cause significant trauma and damage to the vascular and neural innervations of the urethra. Additionally, the separation could cause remodeling, which could result in scar formation, which could contribute to alterations in the urethral properties. All groups in this work assessed animals that had received separation of the tissues. However, they should be compared to untouched animals to determine the effects of the tissue separation on both in-vivo functionality and ex-vivo mechanical properties.

## 8.4 FUTURE WORK

The results of this work have laid the groundwork for continued studies in several areas. First, further assessment of a variety of culture conditions for the differentiation of BMPCs to contractile smooth muscle cells could be performed. While this work focused on the effects of minimal pressure and flow with and without the addition of TGF- $\beta$ , additional studies assessing increased mechanical stimulation may produce a more differentiated phenotype and increase orientation, which could contribute to construct contractility. Previous studies have reported alignment of cells and upregulation of smooth muscle cell markers under rigorous mechanical stimulation with or without growth factors [102-105, 111, 126, 203], indicating that a larger degree of mechanical stimulation via increased intraluminal pressures may cause increased alignment and differentiation, making a more functional TEUW. Although we chose to explore the differentiation potential of TGF- $\beta$  on our BMPCs due to its role in smooth muscle cell differentiation [122-126], other biochemical factors could also be explored. The literature has numerous reports on the differentiating capabilities of a variety of factors including: ascorbic acid [212],  $\beta$ -mercaptoethanol [117, 214], PDGF [119-122] and VEGF [127, 128]. All of which have shown positive results towards the differentiation of cells towards a smooth muscle cell phenotype and may be more effective on the differentiation of the BMPCs used.

Second, although our studies focused on the use of BMPCs, additional work utilizing different cell sources could be performed. One example would be MDSCs, which have already shown much promise for the treatment of SUI when injected directly into the urethra [80, 81]. Utilization of these cells within a TEUW could possibly provide additional benefits as the TEUW could prevent them from migrating away from the injection site. These cells may also be more responsive to mechanical and/or chemical stimulation within the bioreactor.

Third, due to the trends found for altered LPP and mechanical properties following estrogen depletion in virgin rats, it would be interesting to increase n values to see if the trends can become significant. Since, many women experience short term SUI following vaginal delivery, but true onset generally follows menopause [37, 49, 50], an assessment of the role estrogen deficiency on urethral mechanical properties in retired breeders or following vaginal distension would lend insight into the synergistic effects of estrogen and birth trauma on the mechanical characteristics of the urethra and how changes in them can lead to the development and onset of SUI. Such studies could aid in the determination of the role of estrogen in continence compensation following birth trauma and lead to better preventative therapies for SUI.

Fourth, further exploration of the differences between the urethral function of Lewis and SD rats could be explored. Limited explorations of differences in urethral LPP, muscular composition and function have already been performed in this work. Continued studies assessing innervation along the length of the urethra may provide additional insight to the observed differences. Further investigation may determine if the Lewis rat may be an appropriate model for other urethral studies. Measurement of urethral response to agonists at the proximal portion may also indicate a more predominant role of the smooth muscle internal urethral sphincter to continence in the Lewis rat. A comparison of the Lewis urethra to other SUI or lower urinary tract disorder models may support the hypothesis that the Lewis rat could serve as a natural disease model for future studies. Since the Lewis rat has an intrinsically low LPP, higher compliance values and lower muscle contribution, which have been observed in various models of SUI [43, 48, 51, 53, 54, 56], it may be able to serve as a non-surgical model of SUI, upon validation. The low UBP and high baseline compliance of the Lewis urethra indicate

a decreased basal tone, which has been previously reported in a vaginal distension model of SUI [53].

Fifth, effects of the tissue dissection on urethral functional and mechanical properties could be assessed. While preliminary studies comparing SC and untouched controls one week following procedures indicated no severe damage to the urethra following separation, the focus of this work was 3 weeks, which may have allowed enough time for scar formation to alter LPP and mechanical properties of the urethra. Due to the isolation of the urethra for mechanical testing, it was separated from the vagina. Studies assessing the interface between the two tissues could provide evidence for or against scar formation and possibly explain the lack of difference in LPP between experimental groups. If the tissue separation proves to not be detrimental, further studies utilizing constructs cultured within the bioreactor system could be implanted for assessment of further benefits in returning the dysfunctional urethra back to a healthy state.

Lastly, an alternate use for the TEUW could be for the localized delivery of drugs or biological agents to the urethra, or other tubular structures. Fibrin has previously been used for the controlled release of both genes [215] and growth factors [216]. The fabrication method of the TEUW, gelling of a liquid solution during the reaction of fibrinogen and thrombin, makes it ideal for the addition of various agents. During fabrication, additional factors such as drugs, growth factors, microbeads, etc., could be added to the fibrinogen solution prior to the addition of thrombin. Upon implantation, the fibrin would degrade and deliver its contents to the surrounding area. Fibrin gel porosity and fiber size [76], and therefore degradation rate, can be finely tuned by altering the fibrinogen and thrombin concentrations, allowing for a controlled time release of the factor of interest.

## APPENDIX A

### PROPAGATION OF ERROR ASSOCIATED WITH PRESSURE AND OUTER DIAMETER MEASUREMENTS

Previous studies [217, 218] developed the following error analysis. Uncertainty in measured parameters used to calculate quantities must first be assessed in order to assess the propagation of error of the calculated values.

The ex-vivo testing system was set up as described in **Section 2.2.5** with a piece of Penrose drain tube tied to the cannulae. A hydrostatic pressure reservoir filled with water was used to apply each pressure step while outer diameter was read with a He-Ne laser micrometer. This was repeated four times. Values for both pressure and diameter were averaged and standard deviations were calculated. The uncertainty was taken as two standard deviations for 95% confidence limits and given by [217]:

$$\sigma = 2 * 1.96 * \sigma_{\text{measured}} \quad (\text{A. 1})$$

where  $\sigma$  is the uncertainty value and  $\sigma_{\text{measured}}$  is the standard deviation of the measured component (i.e., pressure or outer diameter). The resulting uncertainty values are provided in **Table A.1**.

**Table A.1** Uncertainty values for pressure and diameter measurements used to calculate mechanical characteristics

	Pressure (mmHg)				Diameter (mm)			
	0	6	12	20	0	6	12	20
$\sigma$	0.012	0.038	0.030	0.065	0.008	0.014	0.018	0.018

With the uncertainty values in **Table A.1**, the propagation of error could be calculated for compliance and beta stiffness as follows:

$$\sigma_{\Delta P} = \sqrt{(\sigma_{P_{\max}} + \sigma_{P_{\min}})} \quad (\text{A.2})$$

$$\sigma_{\Delta D} = \sqrt{(\sigma_{D_{\max}} + \sigma_{D_{\min}})} \quad (\text{A.3})$$

$$\% \sigma_{\Delta C} = \sqrt{((\% \sigma_{\Delta D})^2 + (\% \sigma_{\Delta P})^2 + (\% \sigma_{D_{\min}})^2)} \quad (\text{A.4})$$

$$\% \sigma_{P,D} = \sqrt{((\% \sigma_P)^2 + (\% \sigma_D)^2)} \quad (\text{A.5})$$

$$\% \sigma_{\beta} = \sqrt{((\% \sigma_{P,D0\text{mmHg}})^2 + (\% \sigma_{P,D6\text{mmHg}})^2 + (\% \sigma_{P,D12\text{mmHg}})^2 + (\% \sigma_{P,D20\text{mmHg}})^2)} \quad (\text{A.6})$$

Uncertainties were calculated for pressure and diameter differences ( $\sigma_{\Delta P}$ ,  $\sigma_{\Delta D}$ , respectively) using **Equation A.2** and **Equation A.3**. This was calculated for low (0-6 mmHg), middle (6-12 mmHg) and high (12-20 mmHg) pressure compliance values, where  $\sigma_{P_{\max}}$  and  $\sigma_{P_{\min}}$  are the uncertainty values for the maximum and minimum pressures and  $\sigma_{D_{\max}}$  and  $\sigma_{D_{\min}}$  are the maximum and minimum outer diameters in each range. The percentage of error was calculated for each parameter by dividing the uncertainty value by the actual measured difference or measured value (i.e.,  $\% \sigma_{\Delta P} = \% \sigma_{\Delta P} / \Delta P$ ,  $\% \sigma_{\Delta D} = \% \sigma_{\Delta D} / \Delta D$ ). Results for the propagation of error are in **Table A.2**.

**Table A.2** Percentage of propagated error derived from uncertainty values for low, middle and high pressure compliance (C).

Propagation of Error			
$\sigma_{lowC}$	$\sigma_{middleC}$	$\sigma_{highC}$	$\sigma_{\beta}$
1.83%	4.81%	6.38%	0.40%

## APPENDIX B

### WESTERN BLOT IMAGES

#### BIOREACTOR STUDIES

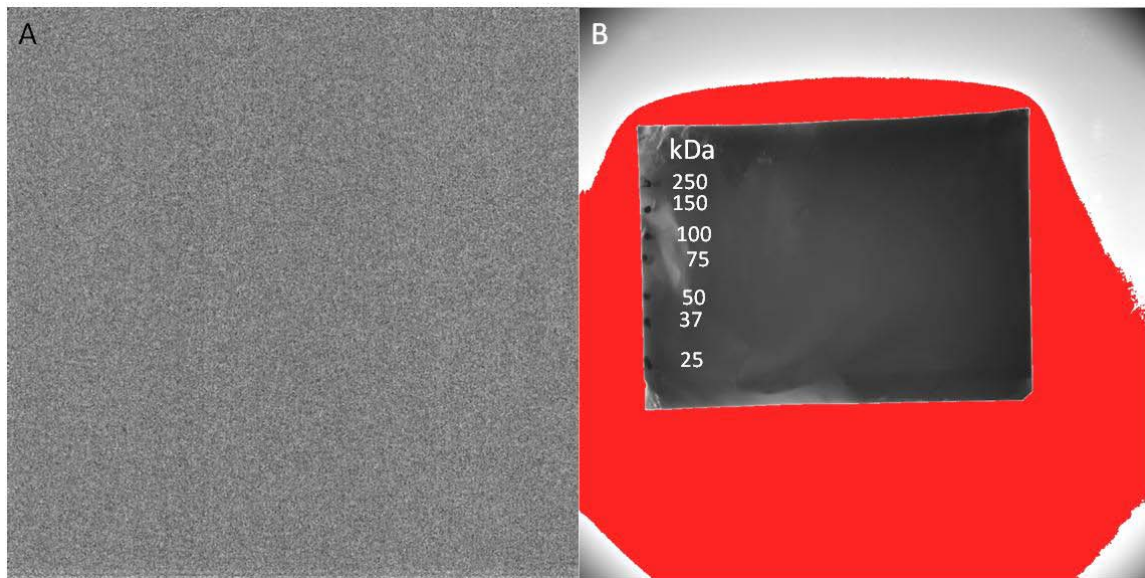


**Figure B.1** Western blot stained for  $\alpha$ -SMA (A) and the white light molecular weight standard (B) for constructs cultured under T0, SF-5 day, SF-10 day, Mo-5 day, MoT-5 day and Mo-10 day culture conditions.

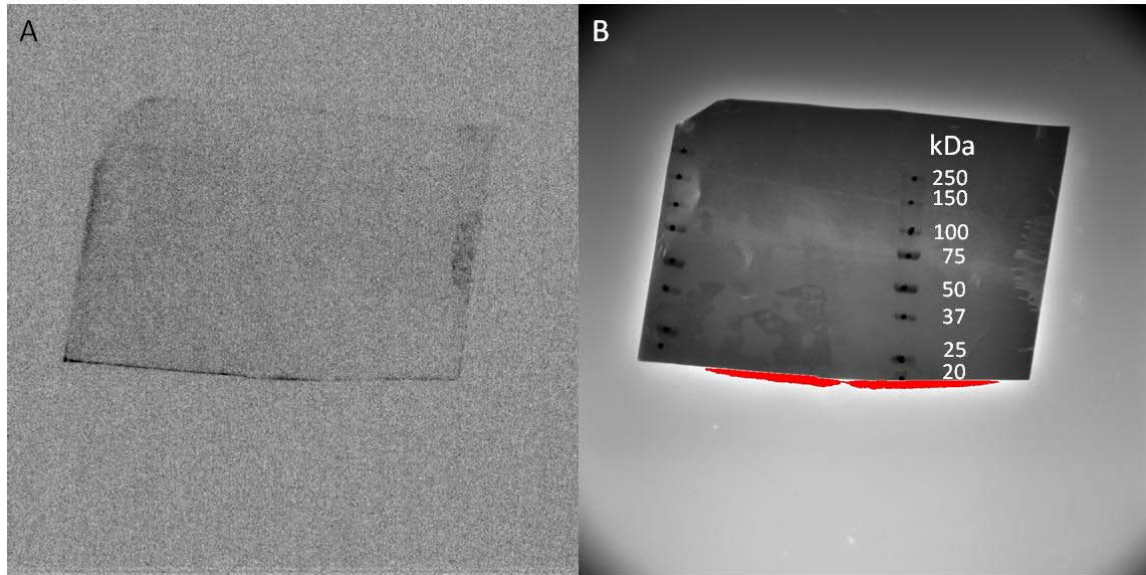


**Figure B.2** Western blot stained for  $\alpha$ -SMA (A) and the white light molecular weight standard (B) for constructs cultured under T0, SF-5 day, SF-10 day, Mo-5 day and MoT-5 day culture conditions.



**Figure B. 3** Western blot stained for CALP (A) and the white light molecular weight standard (B) for constructs cultured under T0, SF-5 day, SF-10 day, Mo-5 day, MoT-5 day and Mo-10 day culture conditions.

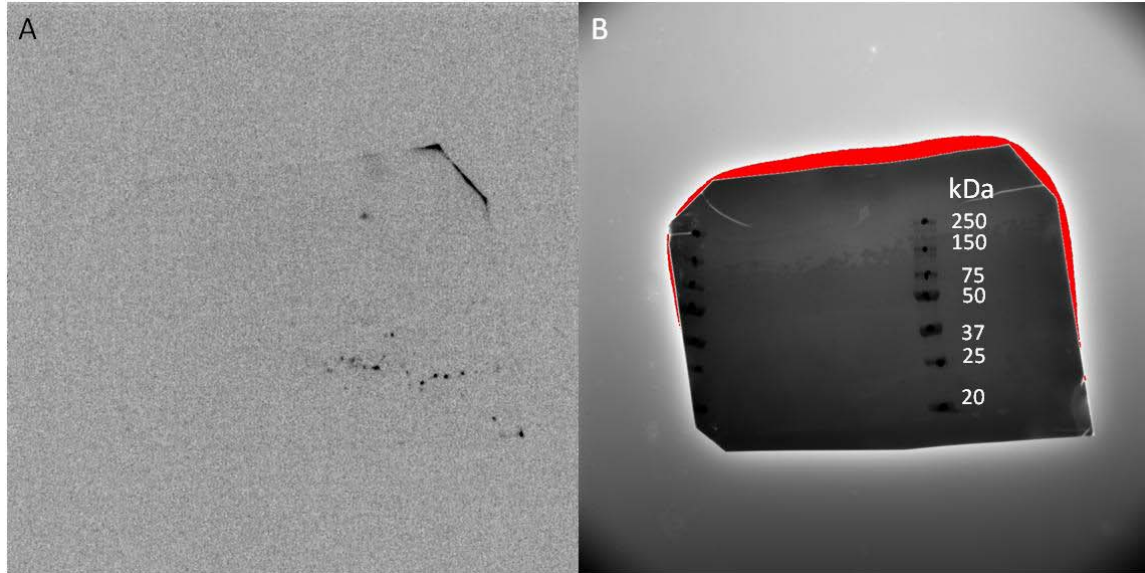


**Figure B.4** Western blot stained for CALP (A) and the white light molecular weight standard (B) for constructs cultured under T0, SF-5 day, SF-10 day, Mo-5 day and MoT-5 day culture conditions.

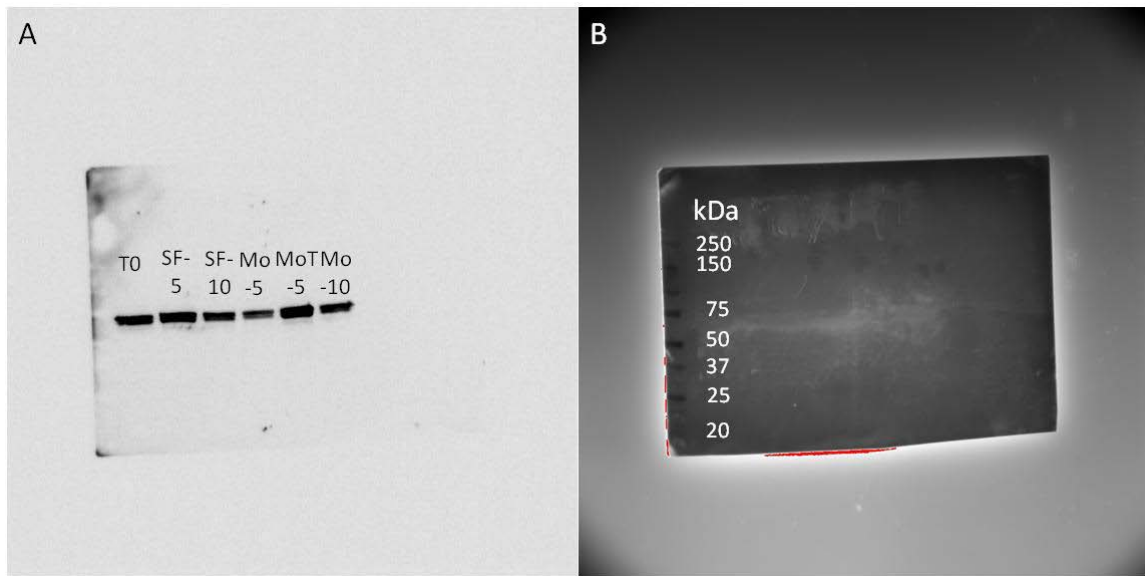


**Figure B.5** Western blot stained for MHC (A) and the white light molecular weight standard (B) for constructs cultured under T0, SF-5 day, SF-10 day, Mo-5 day, MoT-5 day and Mo-10 day culture conditions.

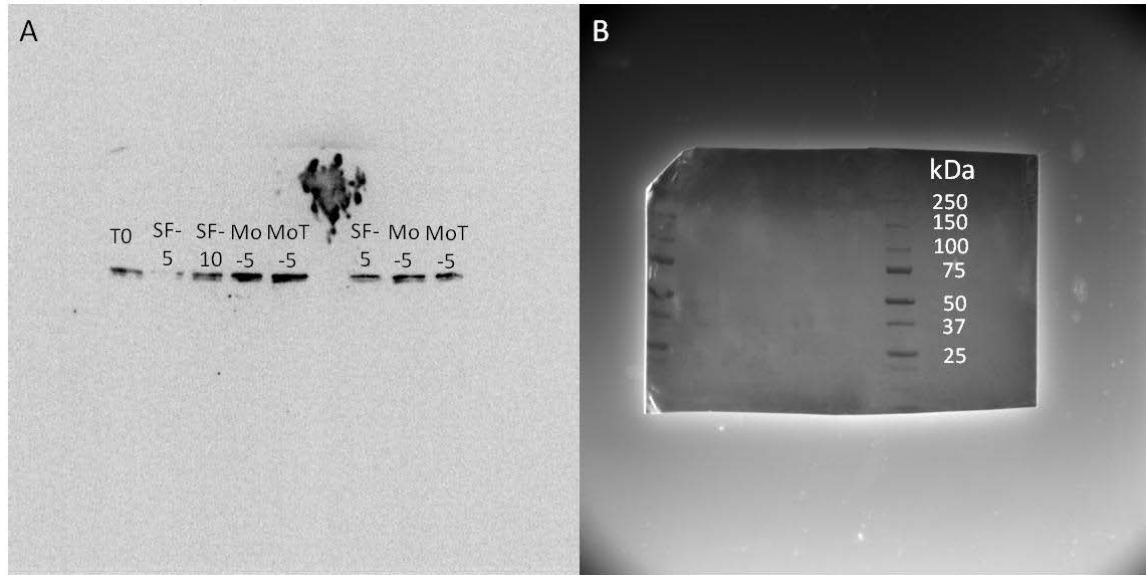


**Figure B.6** Western blot stained for MHC (A) and the white light molecular weight standard (B) for constructs cultured under T0, SF-5 day, SF-10 day, Mo-5 day and MoT-5 day culture conditions.

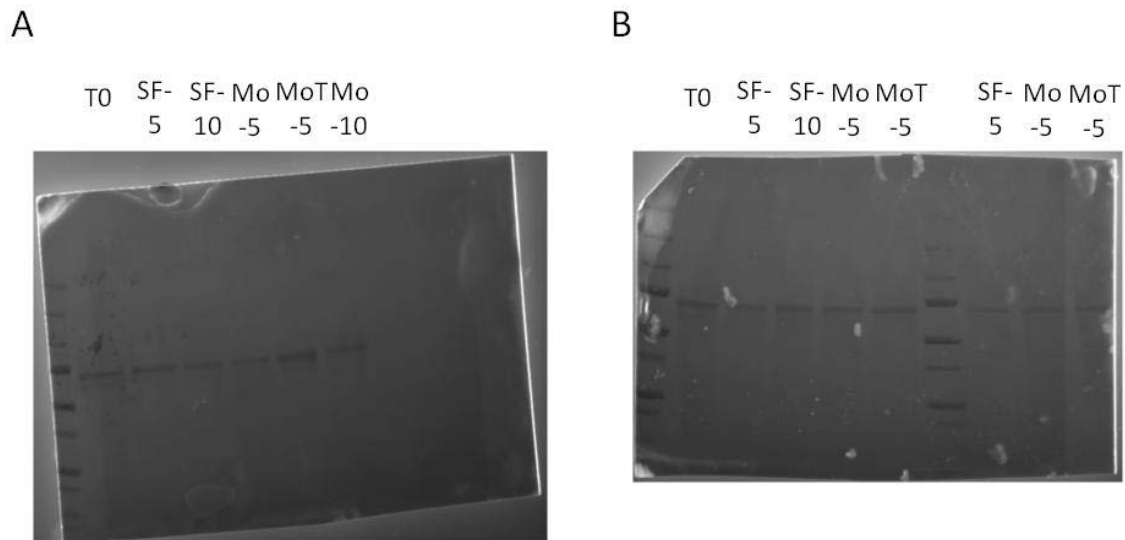
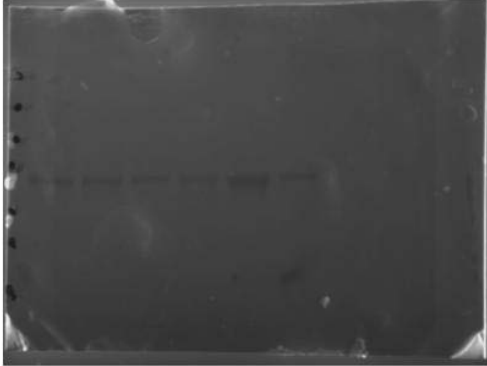


**Figure B.7** Ponceau S stained gels from MHC blots for constructs cultured under T0, SF-5 day, SF-10 day, Mo-5 day, MoT-5 day, and Mo-10 day culture conditions.

A

T0 SF- SF- Mo MoT Mo  
5 10 -5 -5 -10



B

T0 SF- SF- Mo MoT SF- Mo MoT  
5 10 -5 -5 5 -5 -5

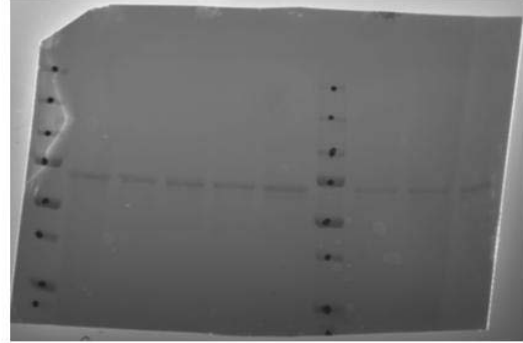
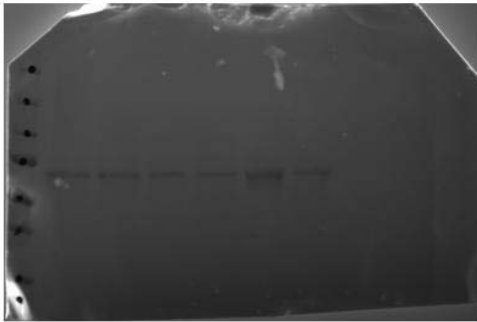


**Figure B.8** Ponceau S stained gels from MHC blots for constructs cultured under T0, SF-5 day, SF-10 day, Mo-5 day, MoT-5 day, and Mo-10 day culture conditions.

A

T0 SF- SF- Mo MoT Mo  
5 10 -5 -5 -10



B

T0 SF- SF- Mo MoT SF- Mo MoT  
5 10 -5 -5 5 -5 -5



**Figure B.9** Ponceau S stained gels from MHC blots for constructs cultured under T0, SF-5 day, SF-10 day, Mo-5 day, MoT-5 day, and Mo-10 day culture conditions.

## IN-VIVO STUDIES

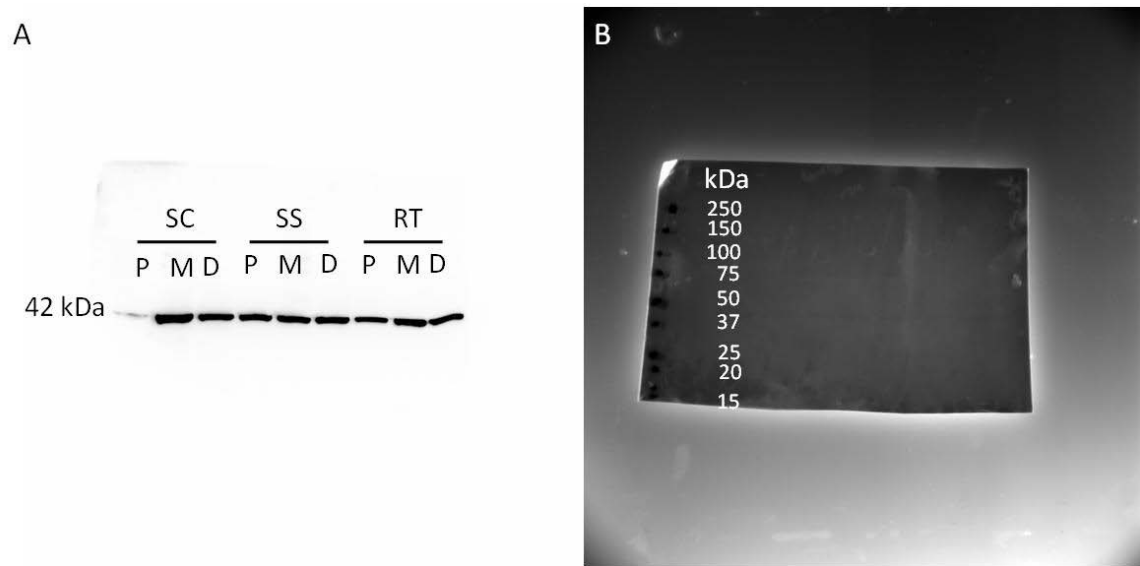


**Figure B.10** Western blot stained for  $\alpha$ -SMA (A) and the white light molecular weight standard (B) for animal-1 of each condition. SC = sham continent, SS = sham SUI, RT = rat TEUW and P, M and D are the proximal, middle and distal portions of the urethra.

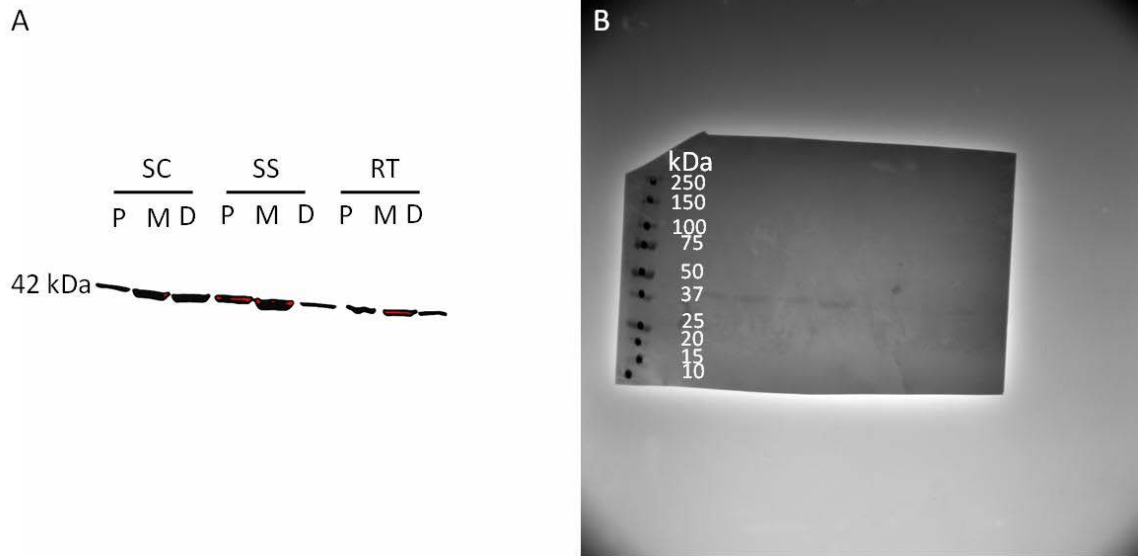


**Figure B.11** Western blot stained for  $\alpha$ -SMA (A) and the white light molecular weight standard (B) for animal-2 of each condition. SC = sham continent, SS = sham SUI, RT = rat TEUW and P, M and D are the proximal, middle and distal portions of the urethra.

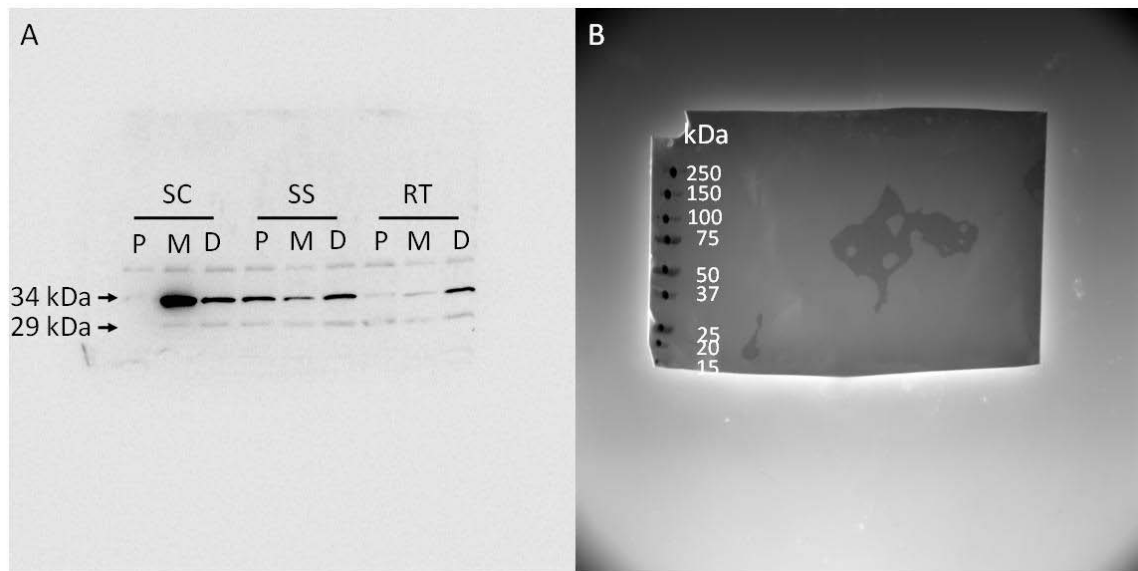


**Figure B.12** Western blot stained for calponin (A) and the white light molecular weight standard (B) for animal-1 of each condition. SC = sham continent, SS = sham SUI, RT = rat TEUW and P, M and D are the proximal, middle and distal portions of the urethra.

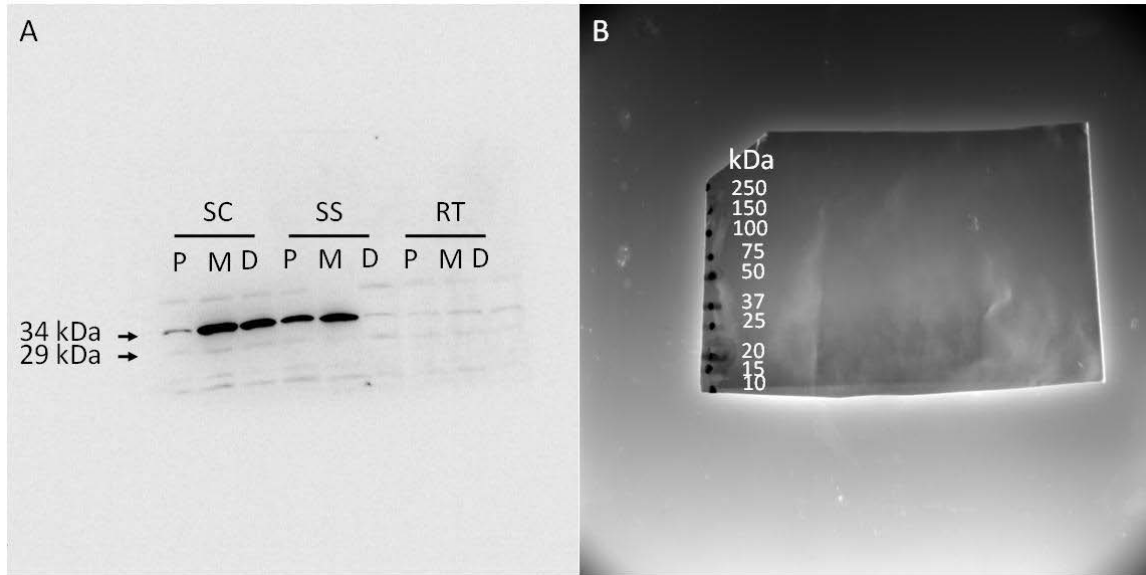


**Figure B.13** Western blot stained for calponin (A) and the white light molecular weight standard (B) for animal-2 of each condition. SC = sham continent, SS = sham SUI, RT = rat TEUW and P, M and D are the proximal, middle and distal portions of the urethra.

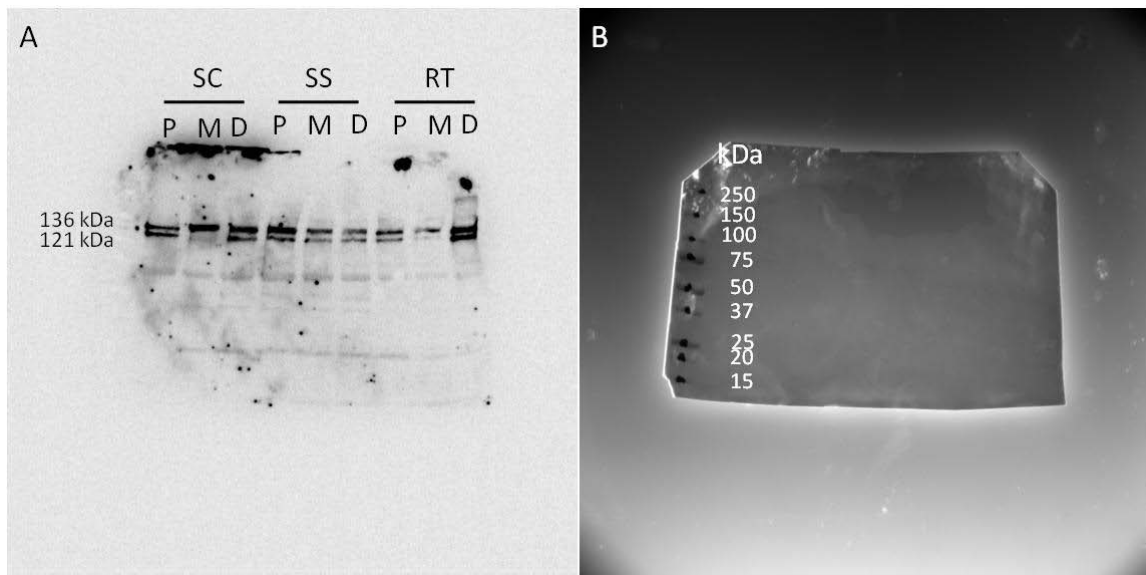


**Figure B.14** Western blot stained for MHC (A) and the white light molecular weight standard (B) for animal-1 of each condition. SC = sham continent, SS = sham SUI, RT = rat TEUW and P, M and D are the proximal, middle and distal portions of the urethra.

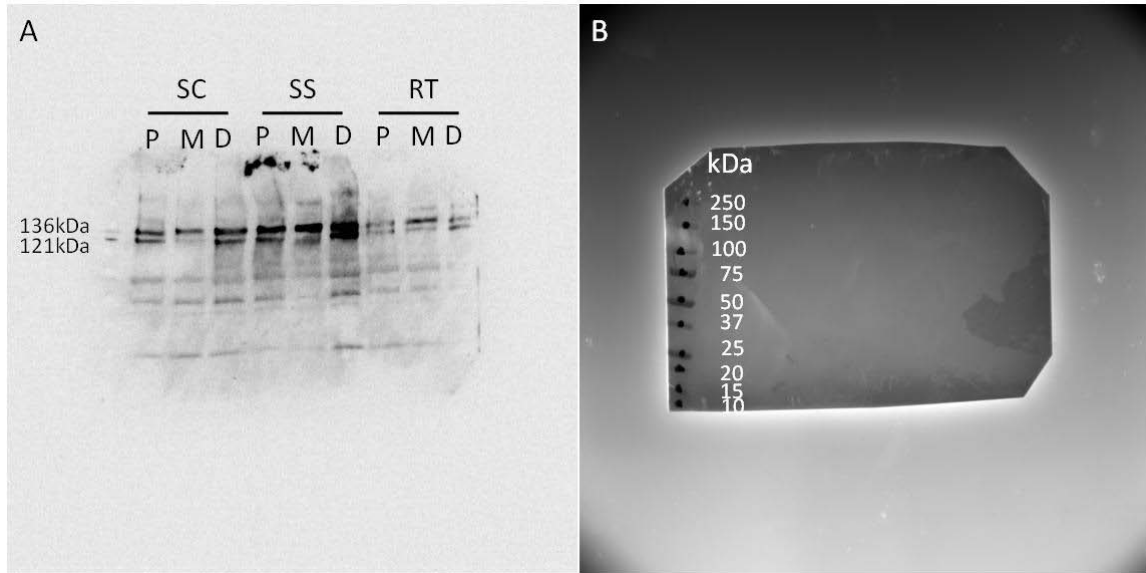


**Figure B.15** Western blot stained for MHC (A) and the white light molecular weight standard (B) for animal-2 of each condition. SC = sham continent, SS = sham SUI, RT = rat TEUW and P, M and D are the proximal, middle and distal portions of the urethra.

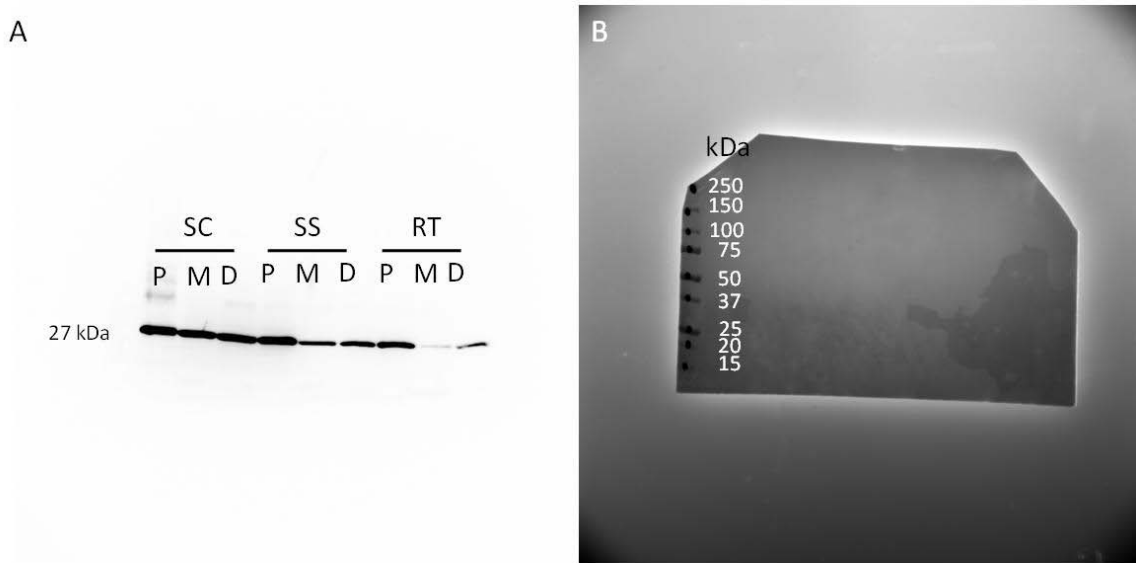


**Figure B.16** Western blot stained for PGP 9.5 (A) and the white light molecular weight standard (B) for animal-1 of each condition. SC = sham continent, SS = sham SUI, RT = rat TEUW and P, M and D are the proximal, middle and distal portions of the urethra.

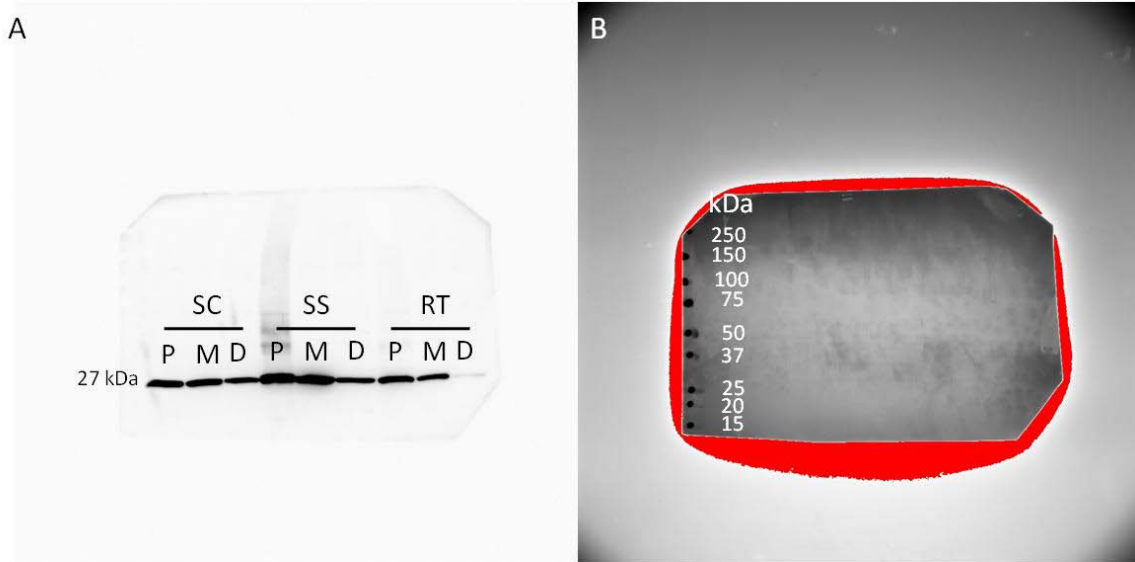


**Figure B.17** Western blot stained for PGP 9.5 (A) and the white light molecular weight standard (B) for animal-2 of each condition. SC = sham continent, SS = sham SUI, RT = rat TEUW and P, M and D are the proximal, middle and distal portions of the urethra.

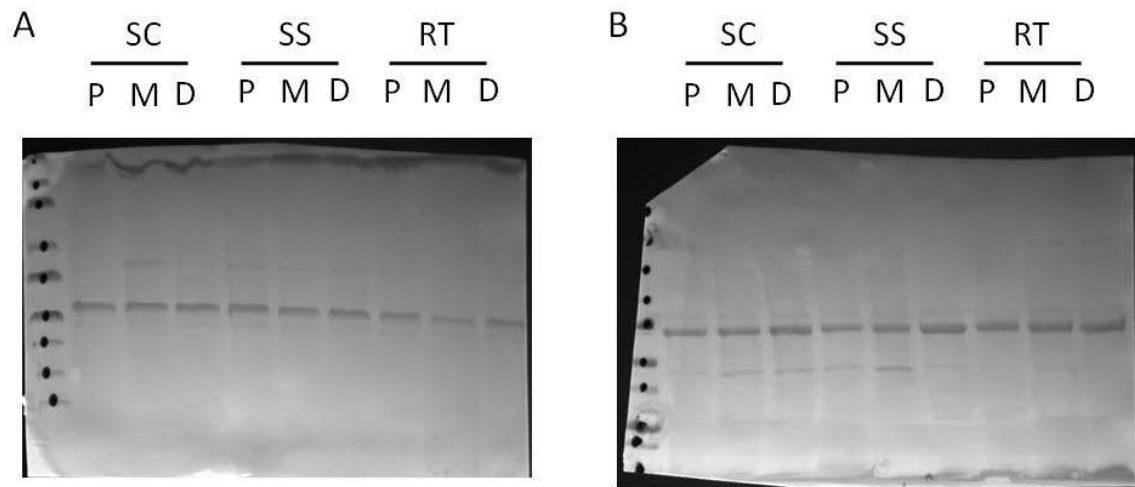


**Figure B.18** Ponceau S stained gels from calponin blots for Animal 1 (A) and Animal 2 (B). SC = sham continent, SS = sham SUI, RT = rat TEUW and P, M and D are the proximal, middle and distal portions of the urethra.

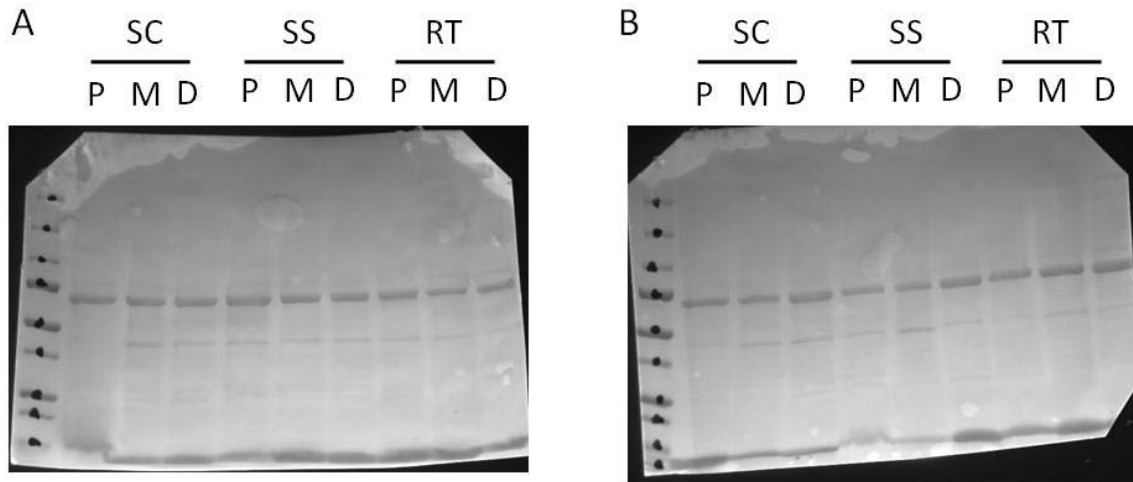


**Figure B.19** Ponceau S stained gels from MHC blots for Animal 1 (A) and Animal 2 (B). SC = sham continent, SS = sham SUI, RT = rat TEUW and P, M and D are the proximal, middle and distal portions of the urethra.

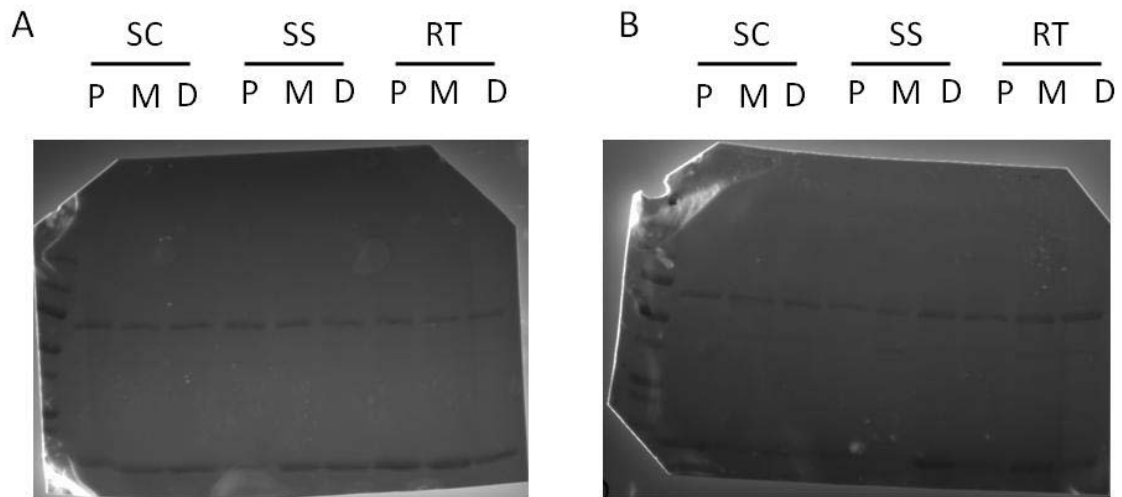


**Figure B.20** Ponceau S stained gels from  $\alpha$ -SMA blots for Animal 1 (A) and Animal 2 (B). SC = sham continent, SS = sham SUI, RT = rat TEUW and P, M and D are the proximal, middle and distal portions of the urethra.

## APPENDIX C

### RELATIVE MOBILITY ASSAY FOR DETERMINATION OF PROTEIN MOLECULAR WEIGHT IN A WESTERN BLOT

Intense banding at unexpected molecular weights was assessed by using relative mobility plot in order to determine the molecular weight of the protein detected according to the methods of Weber *et al.* [219]. Briefly, the distance for a fixed point to the bottom of each molecular weight standard band was measured. The log of the molecular weights for the standards was plotted versus the relative mobility of each standard band through the gel and the equation of the line was found (**Figure C.1**). The distance from the fixed point to the bottom of the band of interest was then measured, and the equation from the standards was used to calculate the molecular weight of the band of interest (**Table C.1** and **Table C.2**). The average across all conditions was calculated for the top and bottom bands in each gel, resulting in molecular weights of 136 kDa and ~121 kDa, respectively (**Table C. 3**).

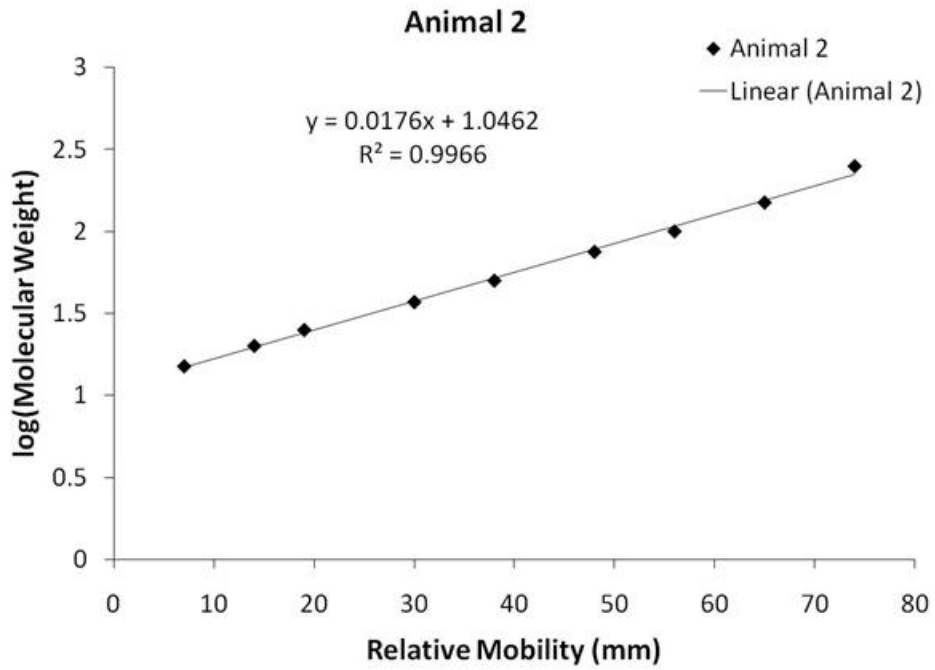
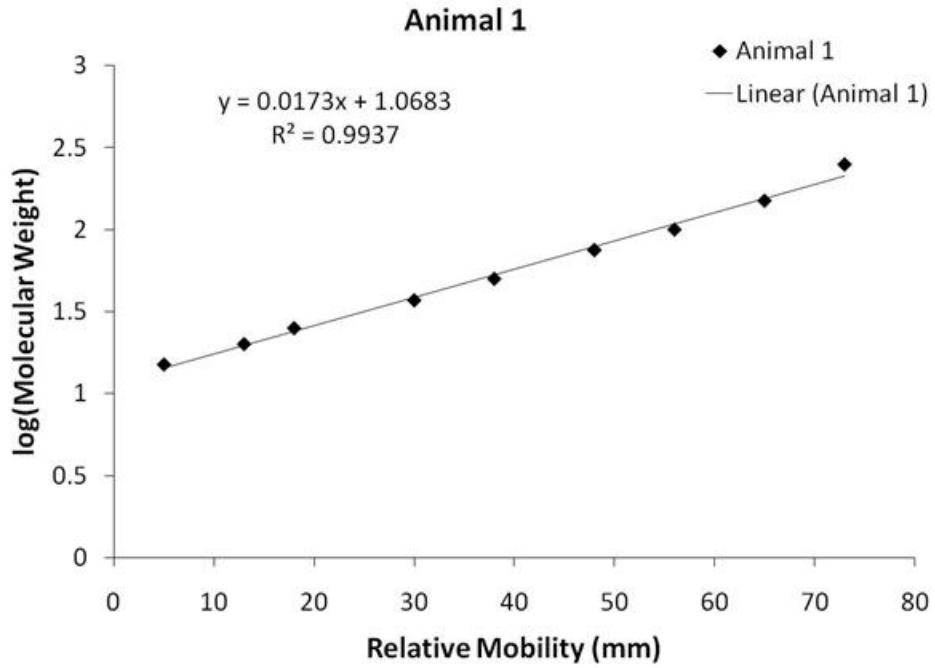


**Figure C.1** Relative mobility plots for two different western blots.

**Table C.1** Relative mobility distances and calculated molecular weights based on standard curves for each gel for the top MHC band seen in in-vivo studies.

<b>Animal -1 Top Band</b>									
	SC-P	SC-M	SC-D	SS-P	SS-M	SS-D	RT-P	RT-M	RT-D
Distance (mm)	61	62	61	62	62	62	62	61	61
MW (kDa)	133	138	133	138	138	138	138	133	133
<b>Animal -2 Top Band</b>									
	SC-P	SC-M	SC-D	SS-P	SS-M	SS-D	RT-P	RT-M	RT-D
Distance (mm)	62	62	62	61	61	62	61	63	62
MW (kDa)	137	137	137	132	132	137	132	143	137

**Table C.2** Relative mobility distances and calculated molecular weights based on standard curves for each gel for the bottom MHC band seen in in-vivo studies.

<b>Animal -1 Bottom Band</b>									
	SC-P	SC-M	SC-D	SS-P	SS-M	SS-D	RT-P	RT-M	RT-D
Distance (mm)	58	60	59	59	59	59	58	59	58
MW (kDa)	133	133	133	133	133	133	133	133	133
<b>Animal -2 Bottom Band</b>									
	SC-P	SC-M	SC-D	SS-P	SS-M	SS-D	RT-P	RT-M	RT-D
Distance (mm)	62	62	62	62	62	62	62	62	62
MW (kDa)	122	122	122	117	117	122	117	122	122

**Table C. 3** Average molecular weight across all conditions of proteins of interest from in-vivo MHC blots.

	<b>Animal-1</b>	<b>Animal-2</b>
	<b>Average M W</b>	<b>Average M W</b>
Top Band	136 kDa	136 kDa
Bottom Band	122 kDa	120 kDa

## APPENDIX D

### ASSESSMENT OF COMPACTION FOR TEUWS

TEUW compaction was calculated as a percentage of the original volume of the construct. Initial TEUW volume and dimensions were determined from the mold dimensions and volume of fibrin-cell solution added to it. Following culture, construct length was measured with calipers, the unloaded diameter by a laser micrometer, and the inner diameter by histology as described in **Section 4.2.5**. The values for construct length, outer diameter and inner diameter following culture can be found in **Table D.1**, **Table D.4** and **Table D.5**, respectively. These values were used to calculate post-culture construct volume (V) as:

$$V_{\text{outer}} = \pi R_o L \quad (\text{D.1})$$

$$V_{\text{inner}} = \pi R_i L \quad (\text{D.2})$$

$$V_{\text{tube}} = \pi R_o^2 L - \pi R_i^2 L \quad (\text{D.3})$$

where  $R_o$  is the outer radius and  $R_i$  is the inner radius and  $L$  is the construct length. If

$$R_i = R_o - t \quad (\text{D.4})$$

where  $t$  is the thickness of the wall (**Table D. 2**), **Equation D.3** simplifies to:

$$V_{\text{tube}} = \pi L(2R_o - t^2) \quad (\text{D.5})$$

To put into terms of inner diameter, we can express  $R_o$  as:

$$R_o = (ID+2t)/2 \quad (D.6)$$

where ID is the inner diameter of the construct. Substituting **Equation D.6** into **Equation D.5**, and allowing  $V_{\text{tube}}$  to equal V, we have:

$$V = \pi L t (ID + t) \quad (D.7)$$

Volumes for all experiments are in **Table D.6**. Compaction [69] as a percentage of the initial volume ( $V_o$ ), which was 5 mL for all constructs, was calculated by **Equation D.8** and can be seen in **Table D.7**.

$$C_m = (V/V_o) * 100 \quad (D.8)$$

**Table D.1** Measured lengths (mm) from constructs seeded with  $0.75 \times 10^6$ ,  $1.00 \times 10^6$  or  $1.25 \times 10^6$  cells/mL and cultured for 3 or 5 days in spinner flask.

Culture	cells/mL	Experiment 1	Experiment 2	Experiment 3	Experiment 4
3 days	$0.75 \times 10^6$	14	17	13	
	$1.00 \times 10^6$	15	17	18	
	$1.25 \times 10^6$	15	17	16	
5 days	$0.75 \times 10^6$	14	16	11	15
	$1.00 \times 10^6$	12	18	14	14
	$1.25 \times 10^6$	12	10	14	12

**Table D. 2** Thickness variability for Experiments 1 and 2. Measured thickness values for each section from each experiment for constructs seeded with  $0.75 \times 10^6$ ,  $1.00 \times 10^6$  or  $1.25 \times 10^6$  cells/mL and cultured for 3 or 5 days in spinner flask.

<b>Experiment 1</b>					
Culture	cells/mL	Section 1	Section 2	Section 3	Section 4
3 days	$0.75 \times 10^6$	$1.2218 \pm 0.0368$	$1.2307 \pm 0.0341$	$1.0884 \pm 0.0253$	$1.0793 \pm 0.0271$
	$1.00 \times 10^6$	$1.2937 \pm 0.0198$	$1.2308 \pm 0.0208$	$1.1782 \pm 0.0101$	$1.3029 \pm 0.0169$
	$1.25 \times 10^6$	$1.0685 \pm 0.0156$	$1.0732 \pm 0.0178$	$1.0616 \pm 0.0171$	$1.0898 \pm 0.0173$
5 days	$0.75 \times 10^6$	$1.0669 \pm 0.0198$	$1.0705 \pm 0.0165$	$1.0524 \pm 0.0172$	$0.9618 \pm 0.0176$
	$1.00 \times 10^6$	$1.1313 \pm 0.0084$	$1.1459 \pm 0.0079$	$1.1194 \pm 0.0271$	$1.1176 \pm 0.0095$
	$1.25 \times 10^6$	$1.1438 \pm 0.0232$	$1.1032 \pm 0.0261$	$1.1187 \pm 0.0266$	$1.1492 \pm 0.0235$
<b>Experiment 2</b>					
Culture	cells/mL	Section 1	Section 2	Section 3	Section 4
3 days	$0.75 \times 10^6$	$1.0185 \pm 0.0287$	$1.0989 \pm 0.0169$	$1.1005 \pm 0.0213$	
	$1.00 \times 10^6$	$0.7453 \pm 0.0079$	$0.6832 \pm 0.0071$		
	$1.25 \times 10^6$	$0.7336 \pm 0.0375$	$0.9584 \pm 0.0394$		
5 days	$0.75 \times 10^6$	$1.0158 \pm 0.0273$	$1.0042 \pm 0.0241$	$1.0575 \pm 0.0290$	
	$1.00 \times 10^6$	$1.1908 \pm 0.0279$	$1.2088 \pm 0.0279$	$1.1348 \pm 0.0378$	
	$1.25 \times 10^6$	$1.1817 \pm 0.0341$	$1.0504 \pm 0.0361$	$1.1450 \pm 0.0547$	

**Table D. 3** Thickness variability for Experiments 3 and 4. Measured thickness values for each section from each experiment for constructs seeded with  $0.75 \times 10^6$ ,  $1.00 \times 10^6$  or  $1.25 \times 10^6$  cells/mL and cultured for 3 or 5 days in spinner flask.

<b>Experiment 3</b>					
Culture	cells/mL	Section 1	Section 2	Section 3	Section 4
3 days	$0.75 \times 10^6$	$0.8561 \pm 0.0387$	$0.9138 \pm 0.337$	$0.8066 \pm 0.374$	
	$1.00 \times 10^6$	$0.7618 \pm 0.0249$	$0.6850 \pm 0.0294$	$0.8221 \pm 0.0266$	
	$1.25 \times 10^6$	$1.1230 \pm 0.0285$	$1.0622 \pm 0.0363$	$0.9587 \pm 0.0440$	
5 days	$0.75 \times 10^6$	$0.8891 \pm 0.0322$	$0.9044 \pm 0.0329$	$0.9344 \pm 0.0334$	$0.8912 \pm 0.0346$
	$1.00 \times 10^6$	$1.0811 \pm 0.0186$	$0.9222 \pm 0.0331$	$1.0221 \pm 0.0388$	
	$1.25 \times 10^6$	$1.0811 \pm 0.0186$	$1.1176 \pm 0.0267$	$1.0185 \pm 0.0356$	
<b>Experiment 4</b>					
Culture	cells/mL	Section 1	Section 2	Section 3	Section 4
5 days	$0.75 \times 10^6$	$0.8640 \pm 0.0159$	$0.8555 \pm 0.0183$	$0.9228 \pm 0.0192$	$0.8833 \pm 0.0125$
	$1.00 \times 10^6$	$0.9101 \pm 0.0093$	$0.8662 \pm 0.0079$	$0.8115 \pm 0.0086$	$0.8210 \pm 0.0090$
	$1.25 \times 10^6$	$0.9235 \pm 0.0173$	$0.9125 \pm 0.0149$	$0.9456 \pm 0.0178$	$0.9051 \pm 0.0147$

**Table D.4** Average measured thickness (mm) values from constructs seeded with  $0.75 \times 10^6$ ,  $1.00 \times 10^6$  or  $1.25 \times 10^6$  cells/mL and cultured for 3 or 5 days in spinner flask.

Culture	cells/mL	Experiment 1	Experiment 2	Experiment 3	Experiment 4
3 days	$0.75 \times 10^6$	1.1551	1.0726	0.8588	
	$1.00 \times 10^6$	1.2514	0.7142	0.7563	
	$1.25 \times 10^6$	1.0733	0.8460	1.0480	
5 days	$0.75 \times 10^6$	1.0379	1.0258	0.9013	0.8805
	$1.00 \times 10^6$	1.1286	1.1781	1.0085	0.8522
	$1.25 \times 10^6$	1.1287	1.1257	1.0724	0.9217

**Table D.5** Calculated inner diameter (mm) values from constructs seeded with  $0.75 \times 10^6$ ,  $1.00 \times 10^6$  or  $1.25 \times 10^6$  cells/mL and cultured for 3 or 5 days in spinner flask.

Culture	cells/mL	Experiment 1	Experiment 2	Experiment 3	Experiment 4
3 days	$0.75 \times 10^6$	0.6469	1.6029	1.2752	
	$1.00 \times 10^6$	0.3187	1.7780	1.5052	
	$1.25 \times 10^6$	1.0019	1.8702	0.5236	
5 days	$0.75 \times 10^6$	0.2658	1.2549	0.4144	0.5687
	$1.00 \times 10^6$	2.7790	0.5239	0.6979	0.7631
	$1.25 \times 10^6$	0.3693	0.4144	0.6482	0.6495

**Table D.6** Calculated volumes ( $\text{mm}^3$ ) from constructs seeded with  $0.75 \times 10^6$ ,  $1.00 \times 10^6$  or  $1.25 \times 10^6$  cells/mL and cultured for 3 or 5 days in spinner flask.

Culture	cells/mL	Experiment 1	Experiment 2	Experiment 3	Experiment 4
3 days	$0.75 \times 10^6$	91.55	153.27	74.85	
	$1.00 \times 10^6$	92.59	95.07	96.72	
	$1.25 \times 10^6$	104.96	122.72	82.79	
5 days	$0.75 \times 10^6$	59.51	117.60	40.98	60.13
	$1.00 \times 10^6$	166.25	113.39	75.69	60.54
	$1.25 \times 10^6$	63.74	54.46	81.15	54.59

**Table D.7** Calculated compaction values from constructs seeded with  $0.75 \times 10^6$ ,  $1.00 \times 10^6$  or  $1.25 \times 10^6$  cells/mL and cultured for 3 or 5 days in spinner flask.

Culture	cells/mL	Experiment 1	Experiment 2	Experiment 3	Experiment 4
3 days	$0.75 \times 10^6$	1.83	3.07	1.50	
	$1.00 \times 10^6$	1.85	1.90	1.93	
	$1.25 \times 10^6$	2.10	2.45	1.66	
5 days	$0.75 \times 10^6$	1.19	2.35	0.82	1.20
	$1.00 \times 10^6$	3.32	2.27	1.51	1.21
	$1.25 \times 10^6$	1.27	1.09	1.62	1.09

## **APPENDIX E**

### **DETERMINATION OF AN ACCEPTABLE RANGE FOR BIOREACTOR ENVIRONMENTAL PARAMETERS**

The acceptable range for pressure measurements was based on the error ( $\pm 2$  mmHg) of the pressure transducers used. Since our ideal pressure was 5 mmHg, the acceptable range was 3 mmHg to 7 mmHg. Acceptable ranges for media parameters were based on readings from control media and previously published work. One chamber of the bioreactor was filled with only media and readings were recorded over a 5 day period as shown in **Table E.1**.

**Table E.1** Recorded values for environmental conditions of control media cultured in the bioreactor for 5 days.

	Day 0	Day 1	Day 2	Day 3	Day 4	Day 5
pH	7.28	7.27	7.30	7.28	7.27	7.29
pCO <sub>2</sub> (mmHg)	37	39	36	38	38	37
pO <sub>2</sub> (mmHg)	150	151	136	138	138	137
HCO <sub>3</sub> <sup>-</sup> (mmol/L)	17	17	17	17	17	17

The acceptable range for pCO<sub>2</sub> was taken as ± 5 mmHg [220], HCO<sub>3</sub><sup>-</sup> as ± 2 mmol/L [220] and pO<sub>2</sub> ± 15 mmHg [220] of average control media readings. These ranges are those generally reported for these parameters in the blood [220], which seemed acceptable for our system as well. The pH range was based on the bicarbonate concentrations as:

$$\text{pH} = \text{pK} + \log \left( \frac{[\text{HCO}_3^-]}{[\text{H}_2\text{CO}_3]} \right) \quad (\text{E.1})$$

where pK = 6.10 and H<sub>2</sub>CO<sub>3</sub> is in equilibrium with CO<sub>2</sub>. Substitutions lead to:

$$\text{pH} = 6.10 + \log \left( \frac{[\text{HCO}_3^-]}{[\text{CO}_2]} \right) \quad (\text{E.2})$$

The solubility coefficient of CO<sub>2</sub> = 0.0301, so we then have:

$$\text{pH} = 6.10 + \log \left( \frac{[\text{HCO}_3^-]}{(0.0301 \cdot [\text{pCO}_2])} \right) \quad (\text{E.3})$$

Therefore, the acceptable ranges for all parameters can be seen in **Table E. 2**.

**Table E. 2** Acceptable range values for pH pCO<sub>2</sub> and HCO<sub>3</sub><sup>-</sup>.

	Low	High
pH	7.22	7.34
pCO <sub>2</sub> (mmHg)	32.5	42.5
pO <sub>2</sub> (mmHg)	126	156
HCO <sub>3</sub> <sup>-</sup> (mmol/L)	15	19

## APPENDIX F

### PRELIMINARY ASSESSMENT OF THE IMPLANTATION OF A TEUW

Preliminary assessments of the effects of a TEUW on LPP and the mechanical and structural properties of the urethra were made at 1 (Lewis and SD rats) and 4 (Lewis rats) weeks following initial procedures according to **Chapter 7.0**. Although rat fibrinogen was the logical matrix choice to reduce rejection by our animal model, implantation of bovine fibrinogen (used in bioreactor work **Chapters 4.0** and **6.0**) was also explored as its use is more economical. In addition to the SC, SS and RT groups listed in **Chapter 7.0** a SUI group, which received only bilateral pudendal nerve transection, and an untouched control (Cont) group were assessed. Animals were assessed for V-LPP, ex-vivo mechanical testing and trichrome staining as described in **Chapter 7.0**

## RESULTS

### Leak Point Pressure

V-LPP values at 1 week (**Figure F.1**) show that SD rats have higher LPP values than Lewis rats for all conditions and significantly for SUI and continent groups. Lewis LPP appears to be independent of experimental condition remaining constant across them. SD control groups receiving tissue separation (SC and SS) have LPP values higher than their non-separated equivalents. SS and RT both appear to have an effect in SD animals, with an n=1 in each group.

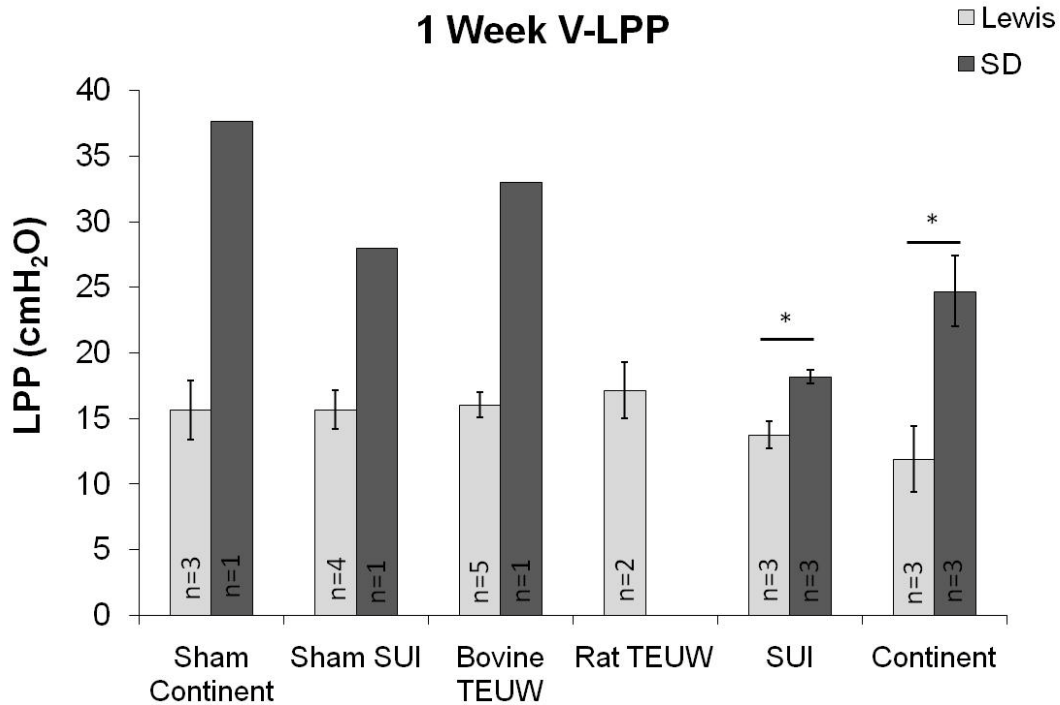


**Figure F.1** One week LPP values for Lewis and SD rats. Values shown as average  $\pm$  SEM. \* $p < 0.05$ .

Assessment of Lewis LPP values across all time points (**Figure F.2**), including the 3 week studies described in **Chapter 7.0** show relatively constant values across all conditions at all time points, with the SUI group having values slightly higher than controls.

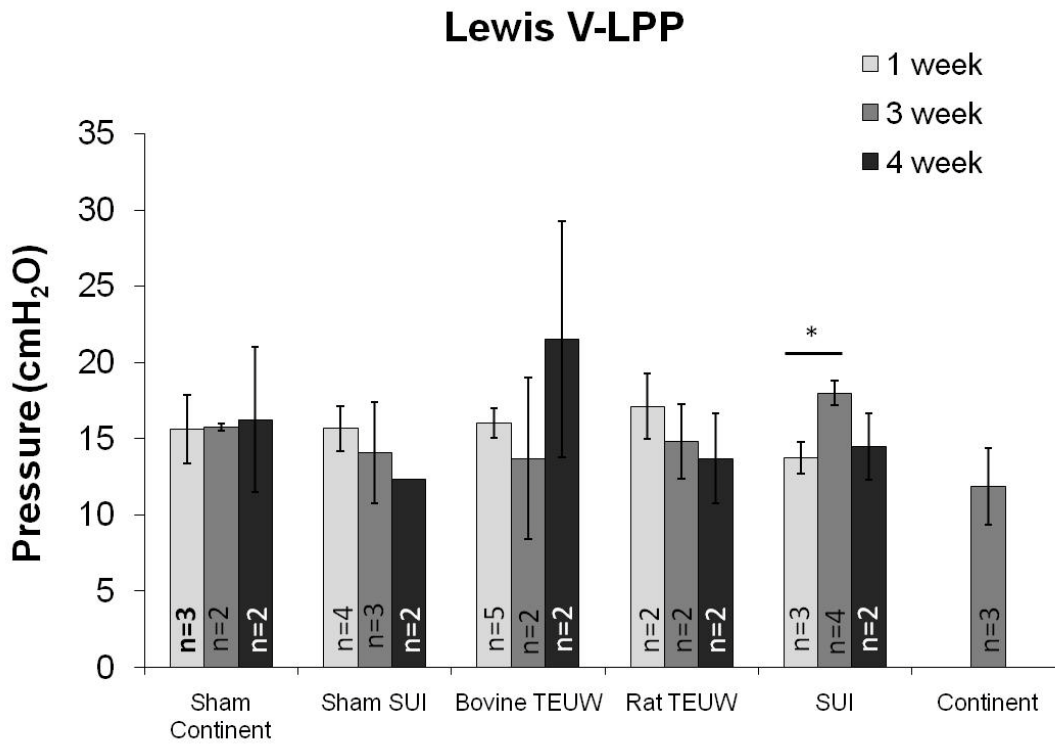


**Figure F.2** Lewis LPP values for 1, 3 and 4 week studies. Values shown as average  $\pm$  SEM. \*p<0.05 and n values are indicated on the bars.

## Ex-Vivo Assessment of One Week Studies

Pressure-diameter curves show that TEUW placement (bovine and/or rat) did have an effect on urethral mechanical properties in both Lewis (**Figure F.4** and **Figure F.5**) and SD (**Figure F.4** and **Figure F.6**) rats. In both strains, the TEUW group(s) had curve shifted to the left of the other conditions in the proximal portion, indicating a decreased compliance due to the wrap. It is also visible that in Lewis rats, SUI caused a shift to the right from Cont, indicative of an increase in compliance, in the proximal portion, while the SD rats showed this shift in the middle portion of the urethra. Lewis SC, SS and RT groups showed little variation at the middle urethra, with all being shifted to the left, indicative of decreased compliance, than Cont. SD rats showed a rightward shift of the SUI curve from other groups in the distal portion, but no other differences, while Lewis rats showed a rightward shift of the RT, SUI and BT curves from Cont, indicating a significant downstream effect.

The trends in compliance for the Lewis (**Figure F.7** and **Figure F.9**) and SD (**Figure F.8** and **Figure F.10**) groups are more easily seen in the stepwise compliance curves. Both Lewis and SD animals showed the greatest spread in data at low pressures, with increased resistance (decreased compliance) with increased pressure. The effects of SUI on proximal (Lewis) and middle (SD) urethral portions appear to be more predominant in the SD rat, with a greater variation between SUI and Cont. TEUWs show little deformation at low pressures, giving support to the native urethra. Distal properties are dependent upon experimental group in the Lewis rat, but only show an increased compliance at 0 mmHg in the SD rat.

Beta stiffness values for Lewis rats (**Figure F.11**), were increased above SUI for SC, SUI and RT groups in the baseline state but similar to SUI in the passive state. SC, BT and SUI groups all had higher beta stiffness values than Cont in SD rats.

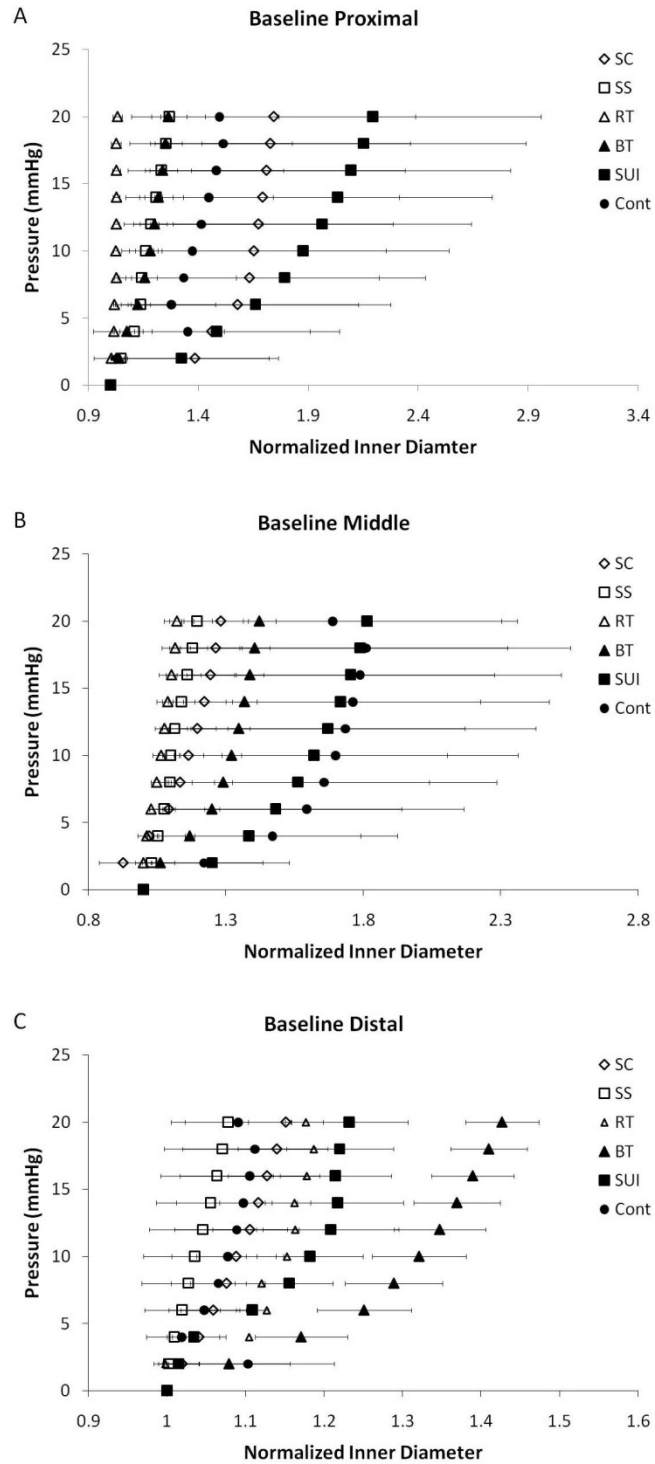


**Figure F. 3** Average baseline pressure-diameter curves for 1 week Lewis studies. SC = sham continent, SS = sham SUI, RT = rat TEUW, BT = bovine TEUW, and Cont = untouched continent. Data shown as average  $\pm$  SEM.

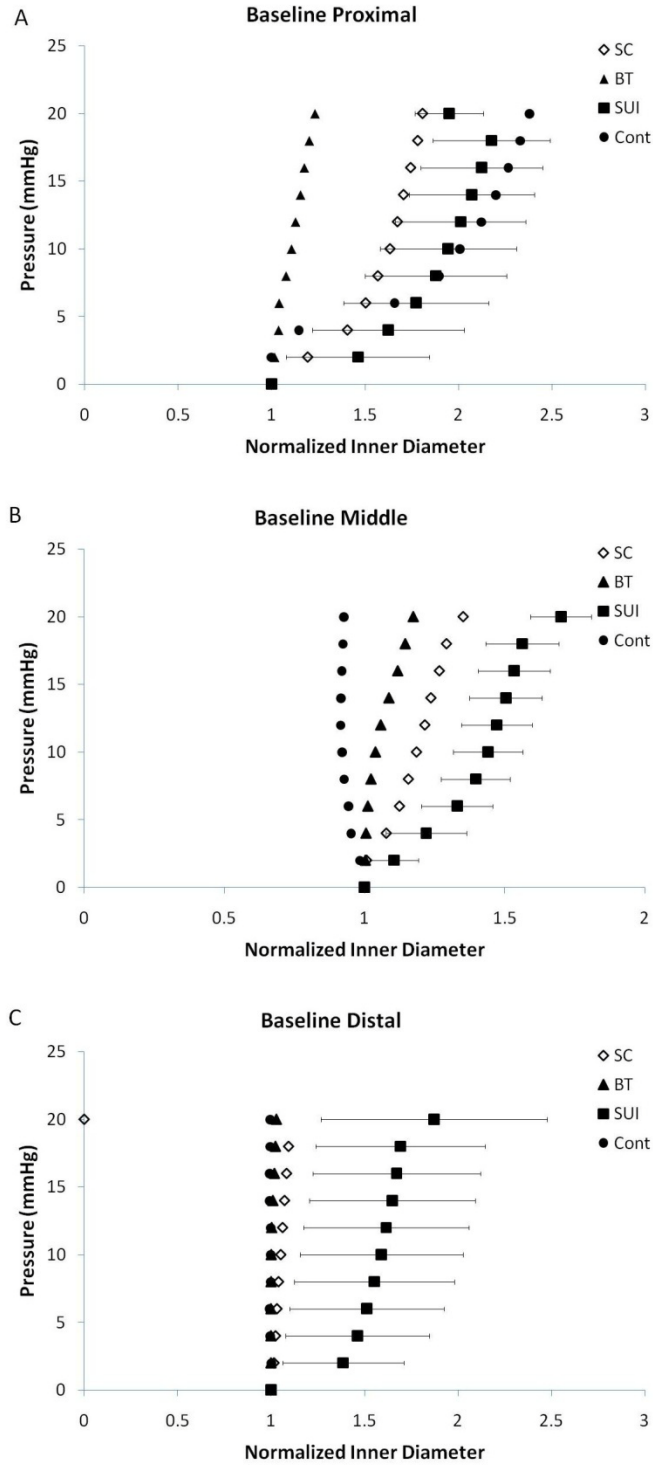


**Figure F.4** Average baseline pressure-diameter curves for 1 week SD studies. SC = sham continent, SS = sham SUI, RT = rat TEUW, BT = bovine TEUW, and Cont = untouched continent. Data shown as average  $\pm$  SEM.

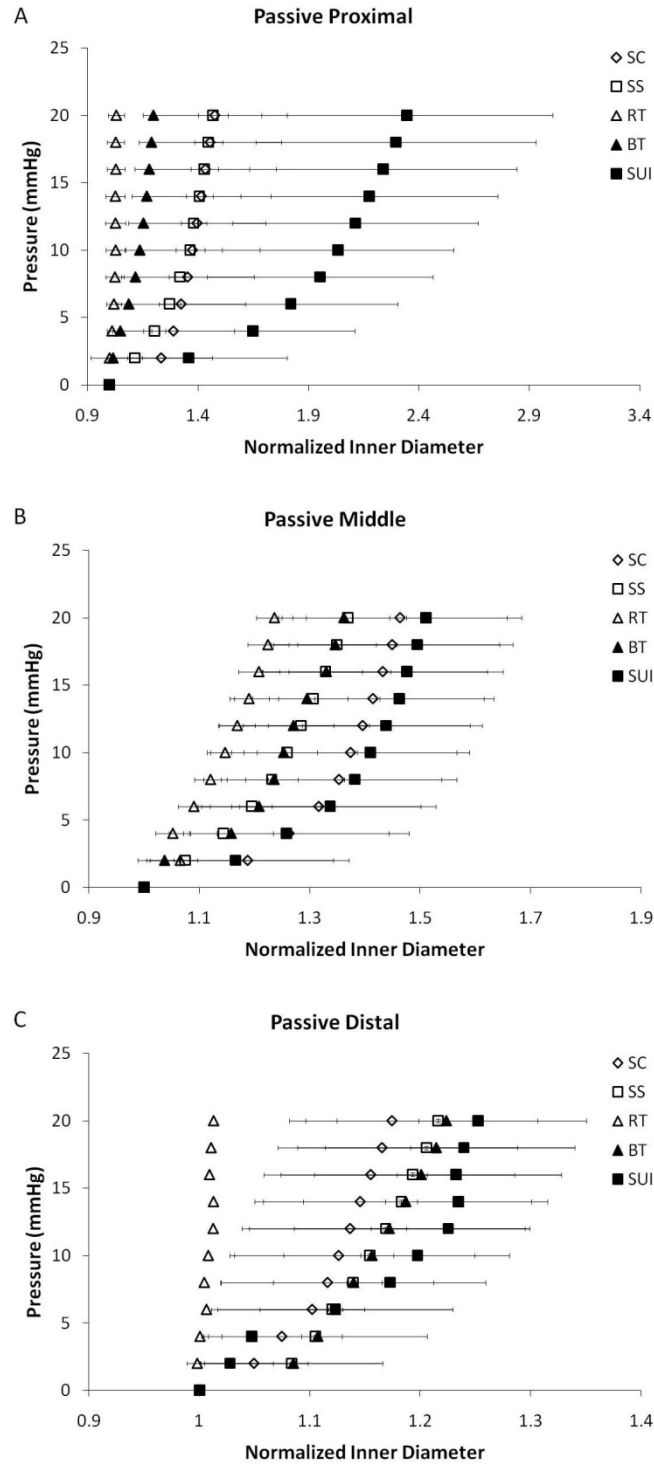


**Figure F.5** Average passive pressure-diameter curves for 1 week Lewis studies. SC = sham continent, SS = sham SUI, RT = rat TEUW, BT = bovine TEUW, and Cont = untouched continent. Data shown as average  $\pm$  SEM.

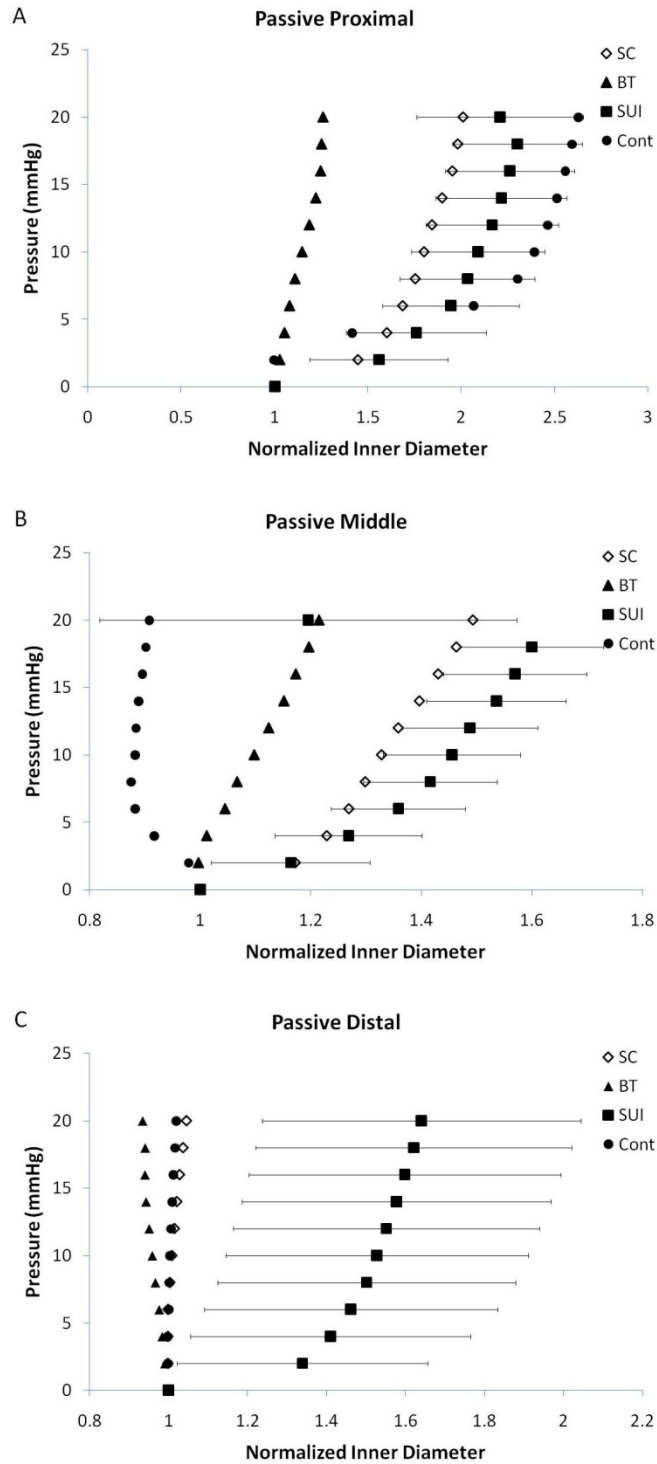


**Figure F.6** Average passive pressure-diameter curves for 1 week SD studies. SC = sham continent, SS = sham SUI, RT = rat TEUW, BT = bovine TEUW, and Cont = untouched continent. Data shown as average  $\pm$  SEM.

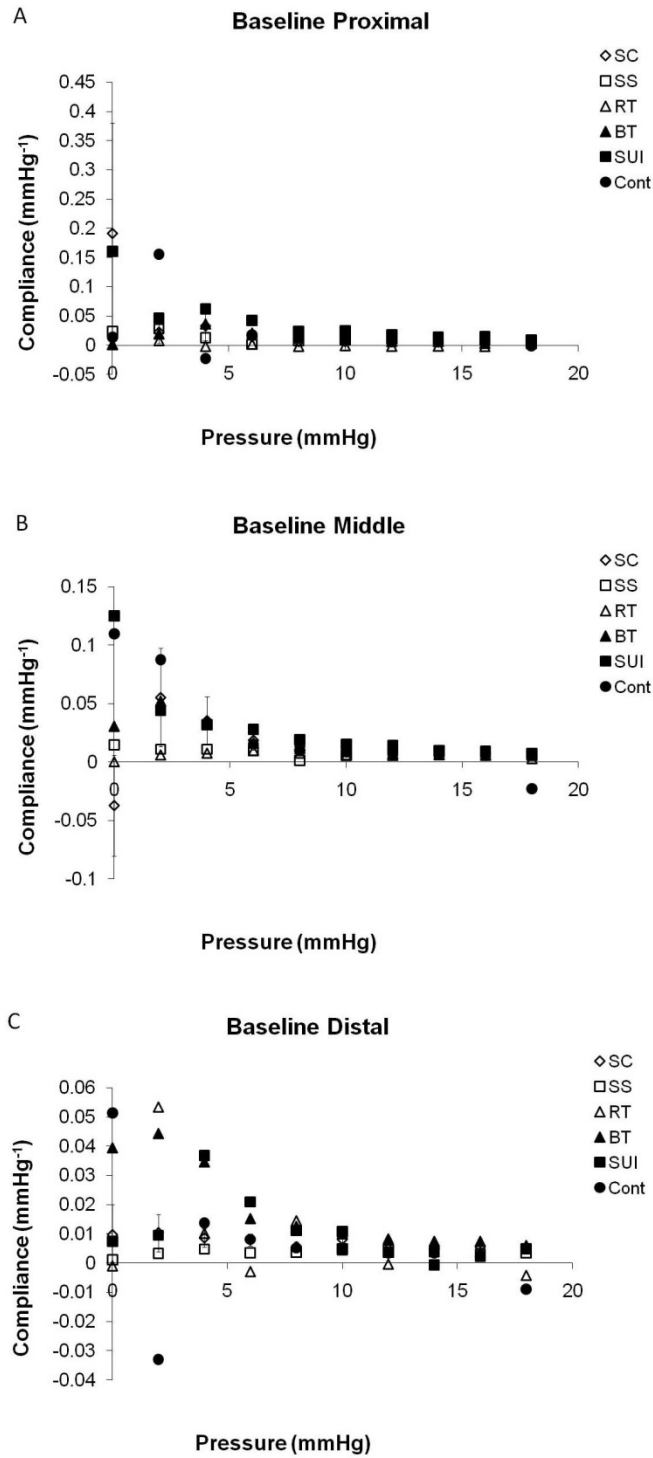


**Figure F.7** Average baseline step-wise compliance curves for 1 week Lewis studies. SC = sham continent, SS = sham SUI, RT = rat TEUW, BT = bovine TEUW, and Cont = untouched continent. Data shown as average  $\pm$  SEM.

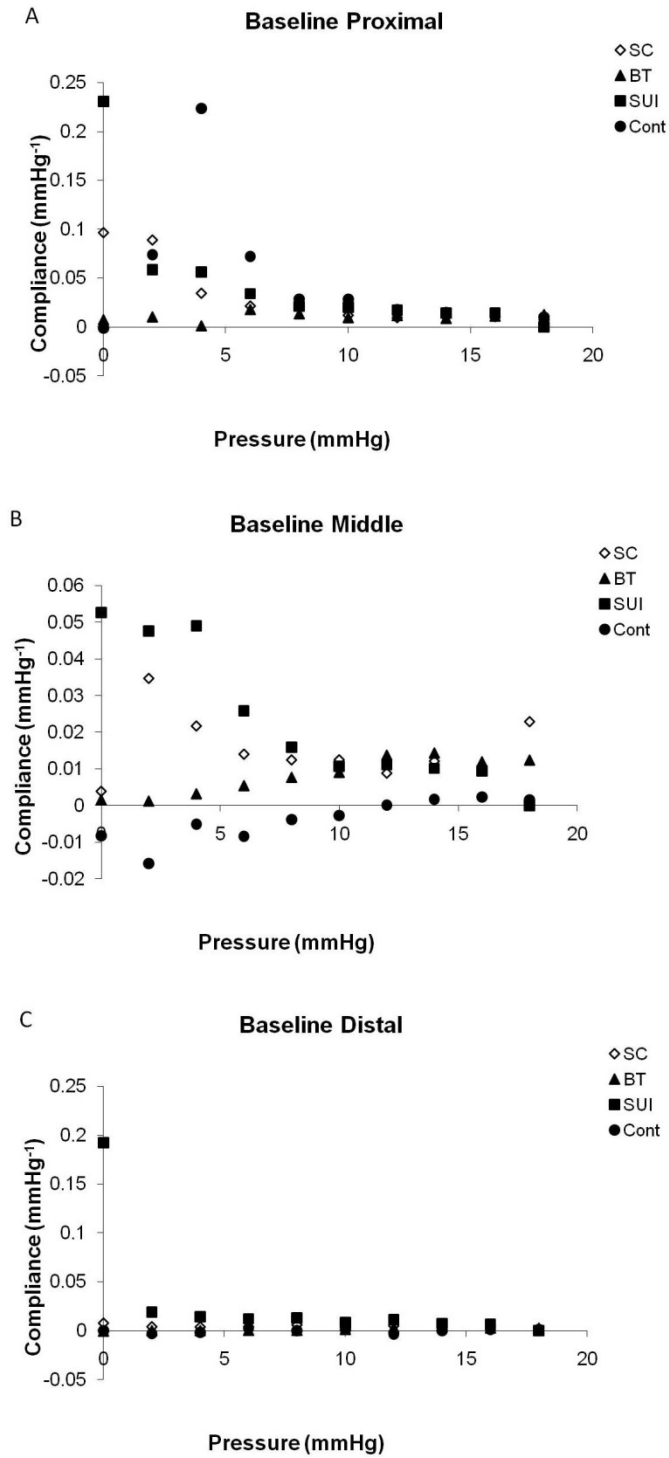


**Figure F.8** Average baseline step-wise compliance curves for 1 week SD studies. SC = sham continent, SS = sham SUI, RT = rat TEUW, BT = bovine TEUW, and Cont = untouched continent. Data shown as average  $\pm$  SEM.

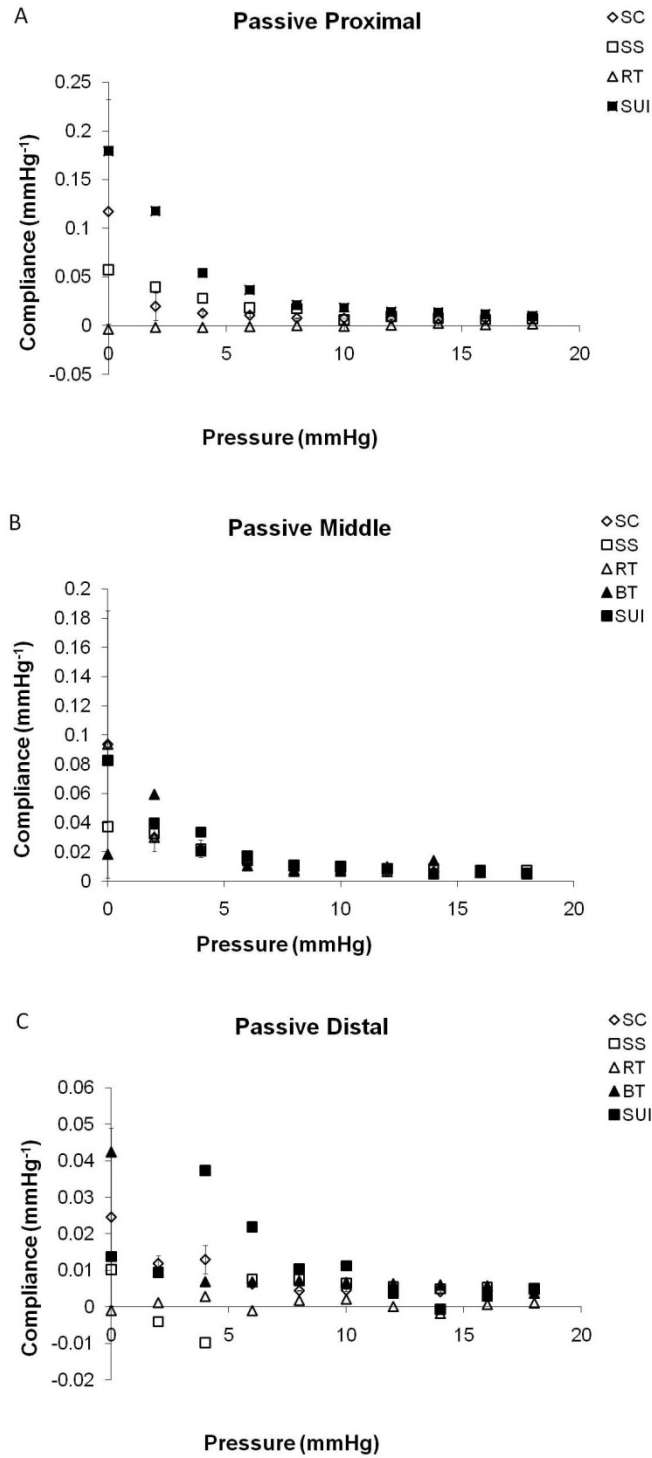


**Figure F.9** Average passive step-wise compliance curves for 1 week Lewis studies. SC = sham continent, SS = sham SUI, RT = rat TEUW, BT = bovine TEUW, and Cont = untouched continent. Data shown as average  $\pm$  SEM.

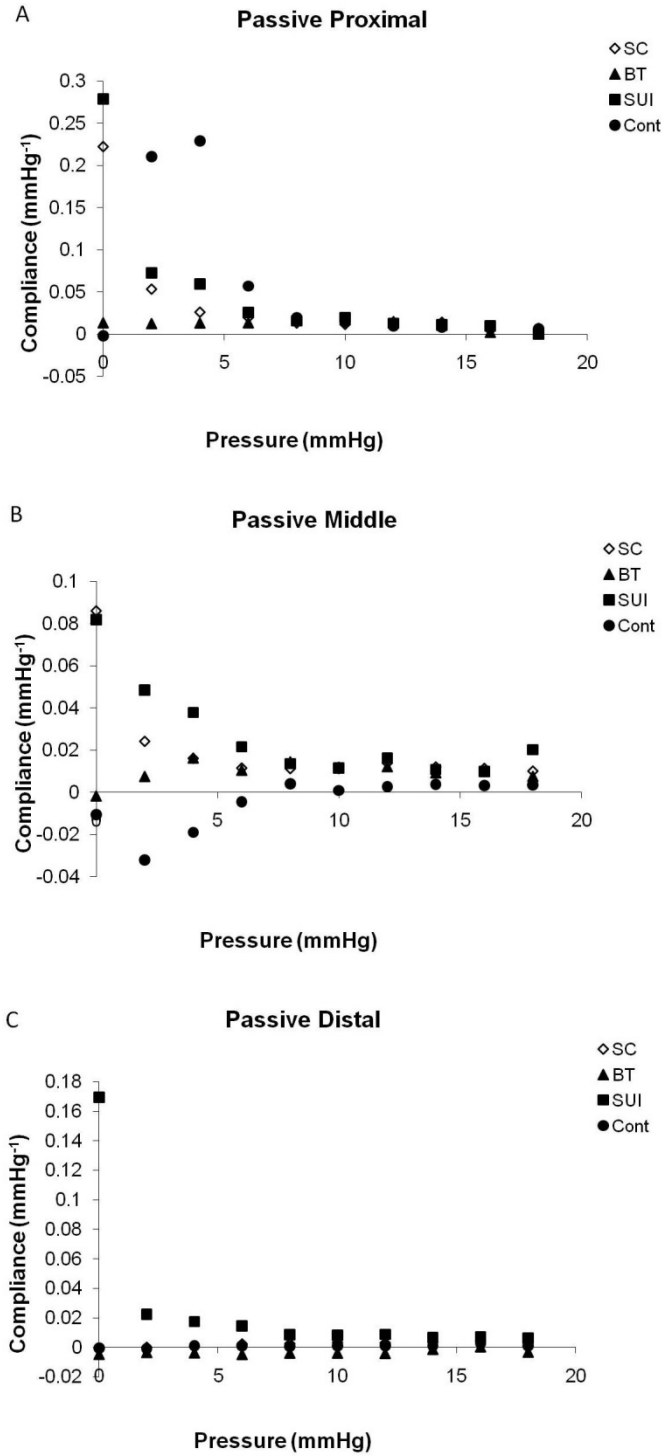


**Figure F.10** Average passive step-wise compliance curves for 1 week SD studies. SC = sham continent, SS = sham SUI, RT = rat TEUW, BT = bovine TEUW, and Cont = untouched continent. Data shown as average  $\pm$  SEM.

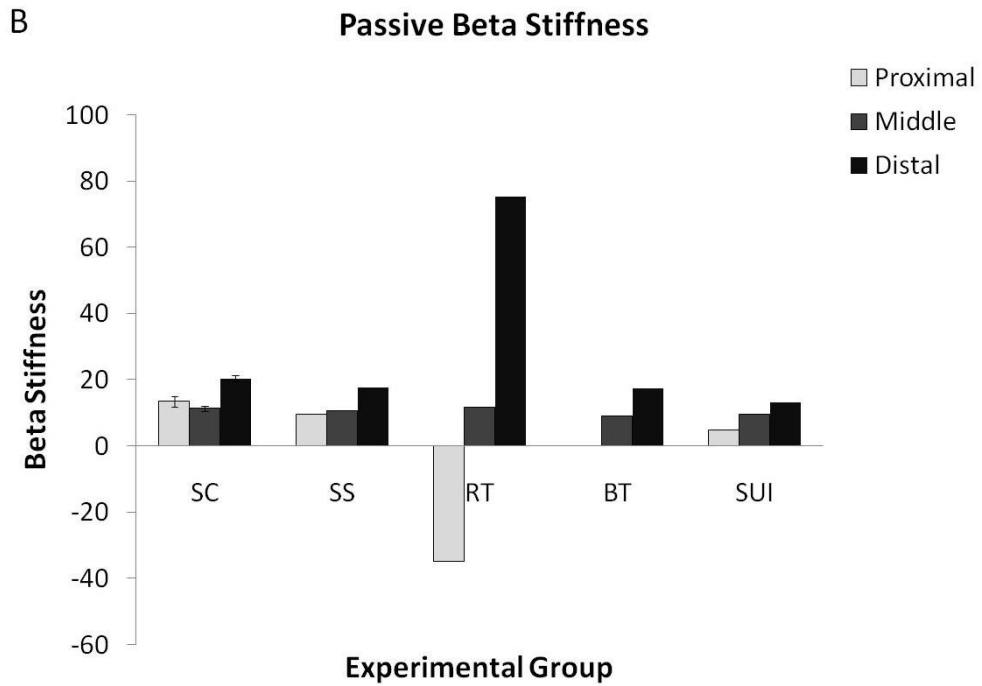
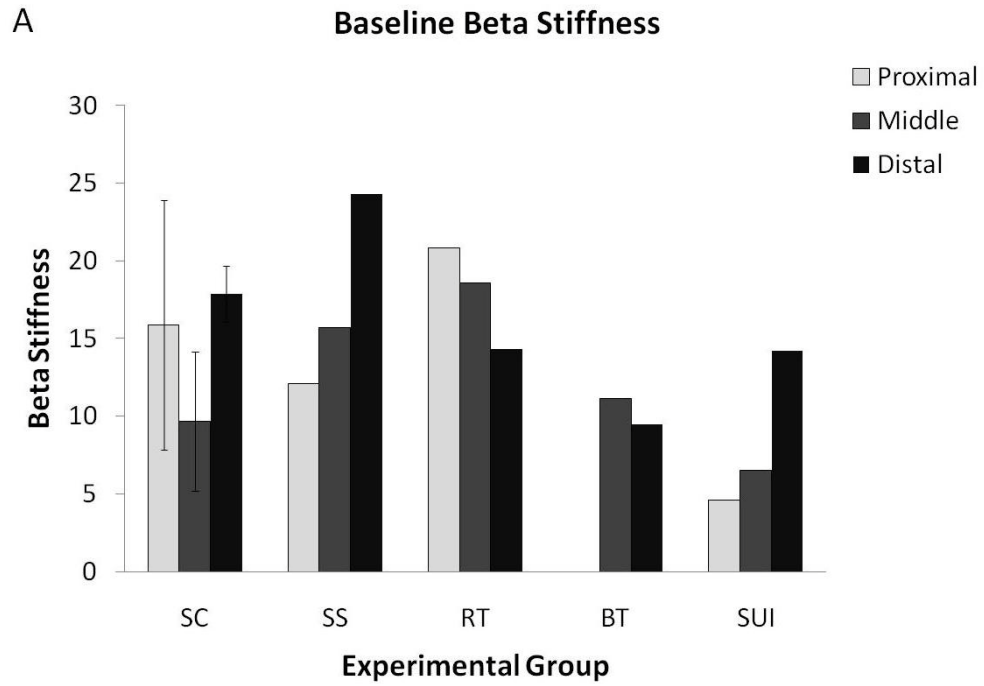


**Figure F.11** Beta stiffness values for 1 week Lewis studies. SC = sham continent, SS = sham SUI, RT = rat TEUW, BT = bovine TEUW, and Cont = untouched continent. Data shown as average  $\pm$  SEM for  $n=2$ , where  $n=1$  for all other groups.

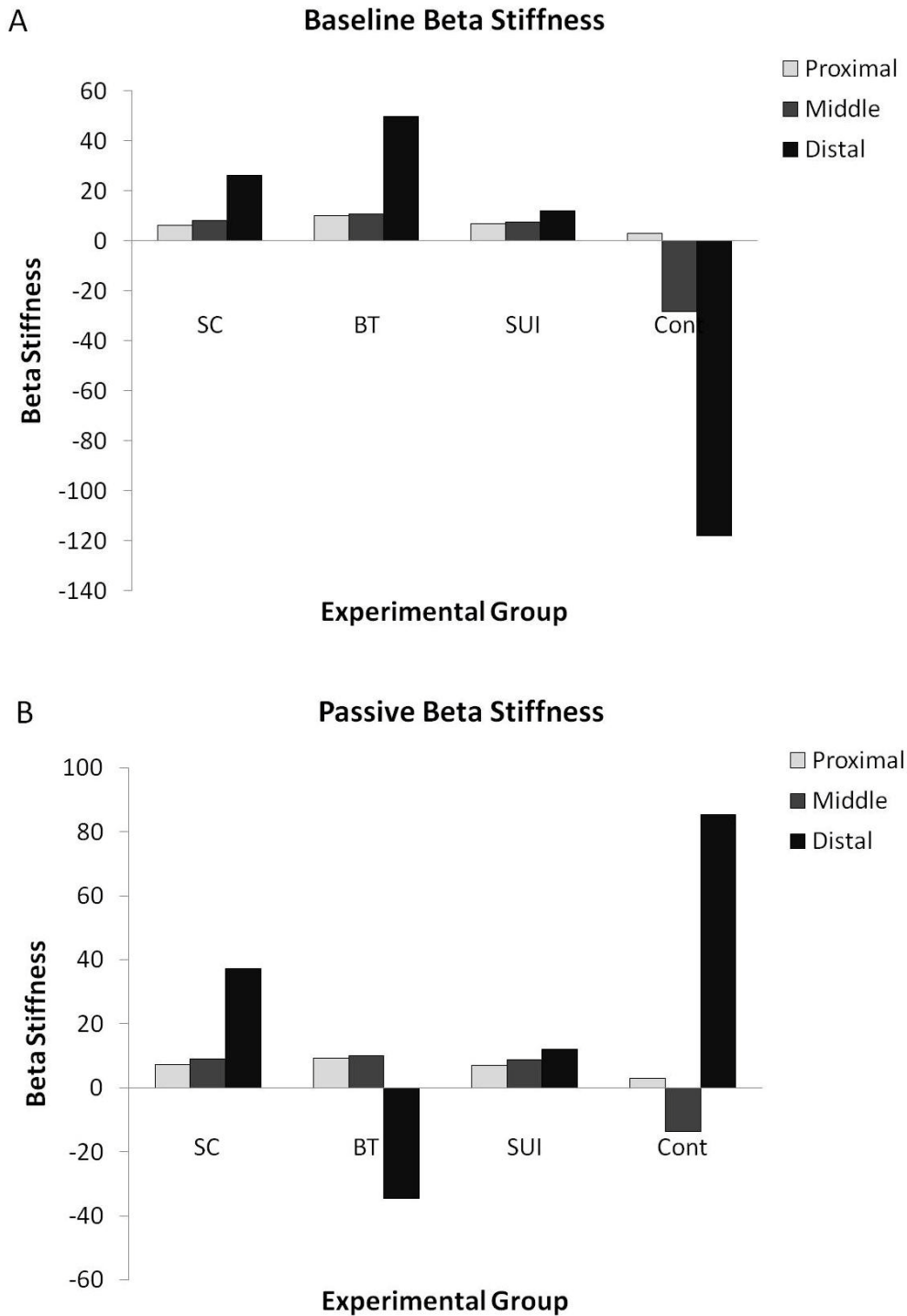


**Figure F.12** Beta stiffness values for 1 week SD studies. SC = sham continent, SS = sham SUI, RT = rat TEUW, BT = bovine TEUW, and Cont = untouched continent. Data shown as average  $\pm$  SEM for  $n=2$ , where  $n=1$  for all other groups.

## **Ex-Vivo Assessment of Four Week Studies**

Four weeks following implantation, TEUWs appear to still be providing support to the proximal urethra, with curves shifted to the left of the others in both the baseline and passive states (**Figure F.13A** and **Figure F.14A**). SC shows a proximal P-D curve similar to Cont animals, however it is shifted to the left of Cont in the middle urethra. SUI shows a middle curve similar to RT in the baseline state (**Figure F.13B**), both of which are shifted to the left of the Cont curve. In the distal urethra, SUI shows the only effect, shifting the curve to the right of all others in both baseline and passive states (**Figure F.13C** and **Figure F.14C**).

Step-wise compliance curves (**Figure F. 15** and **Figure F .16**) show that the greatest spread in data between groups occurs at low pressures (0-6 mmHg), with the highest compliance values generally occurring at 0 and 2 mmHg. These plots more clearly show the lowest compliance in the RT and BT groups in the proximal urethra and the Cont group showing the greatest compliance at low pressures in both the proximal and middle urethra in the baseline state (**Figure F.15A-B**).

Beta stiffness values were similar for all urethral portions in SS and Cont groups in both the baseline and passive states (**Figure F.17**). SC and SUI greatly increased middle stiffness, while RT increased proximal values from Cont. Distal baseline stiffness values appeared independent of experimental group, but SC and RT were much greater than Cont in the passive state.

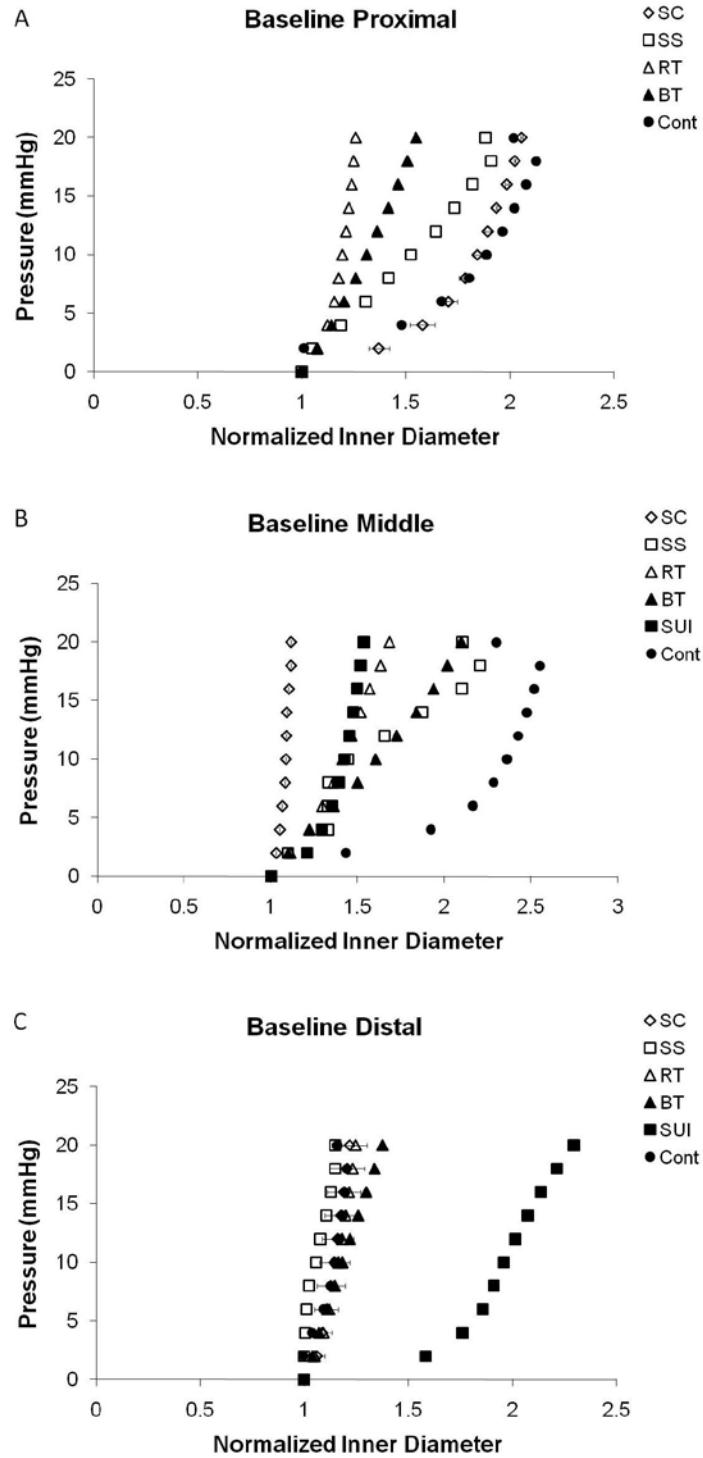


**Figure F.13** Average baseline pressure-diameter curves for 4 week Lewis studies. SC = sham continent, SS = sham SUI, RT = rat TEUW, BT = bovine TEUW, and Cont = untouched continent. Data shown as average  $\pm$  SEM.

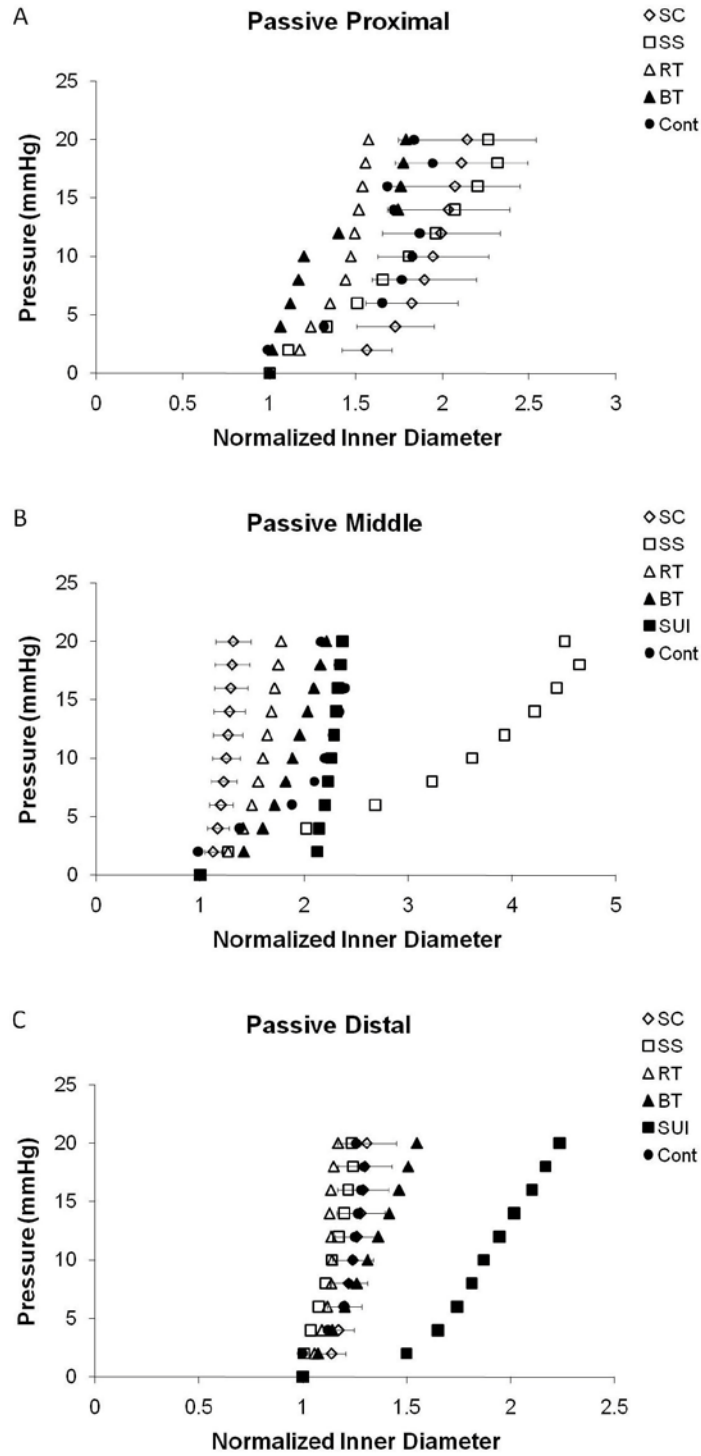


**Figure F.14** Average passive pressure-diameter curves for 4 week Lewis studies. SC = sham continent, SS = sham SUI, RT = rat TEUW, BT = bovine TEUW, and Cont = untouched continent. Data shown as average  $\pm$  SEM for  $n=2$ , where all other groups are  $n=1$ .

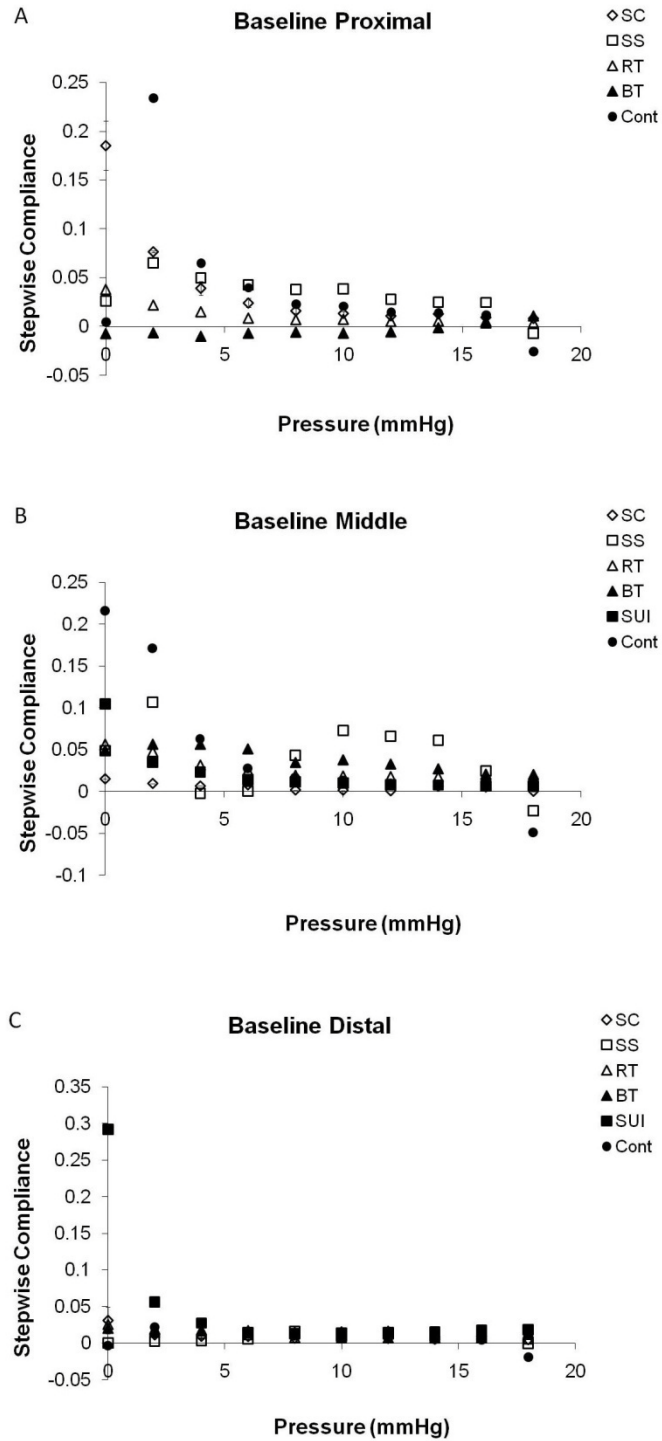


**Figure F.15** Average baseline step-wise compliance curves for 4 week Lewis studies. SC = sham continent, SS = sham SUI, RT = rat TEUW, BT = bovine TEUW, and Cont = untouched continent. Data shown as average  $\pm$  SEM for n=2, where n=1 for all other groups.

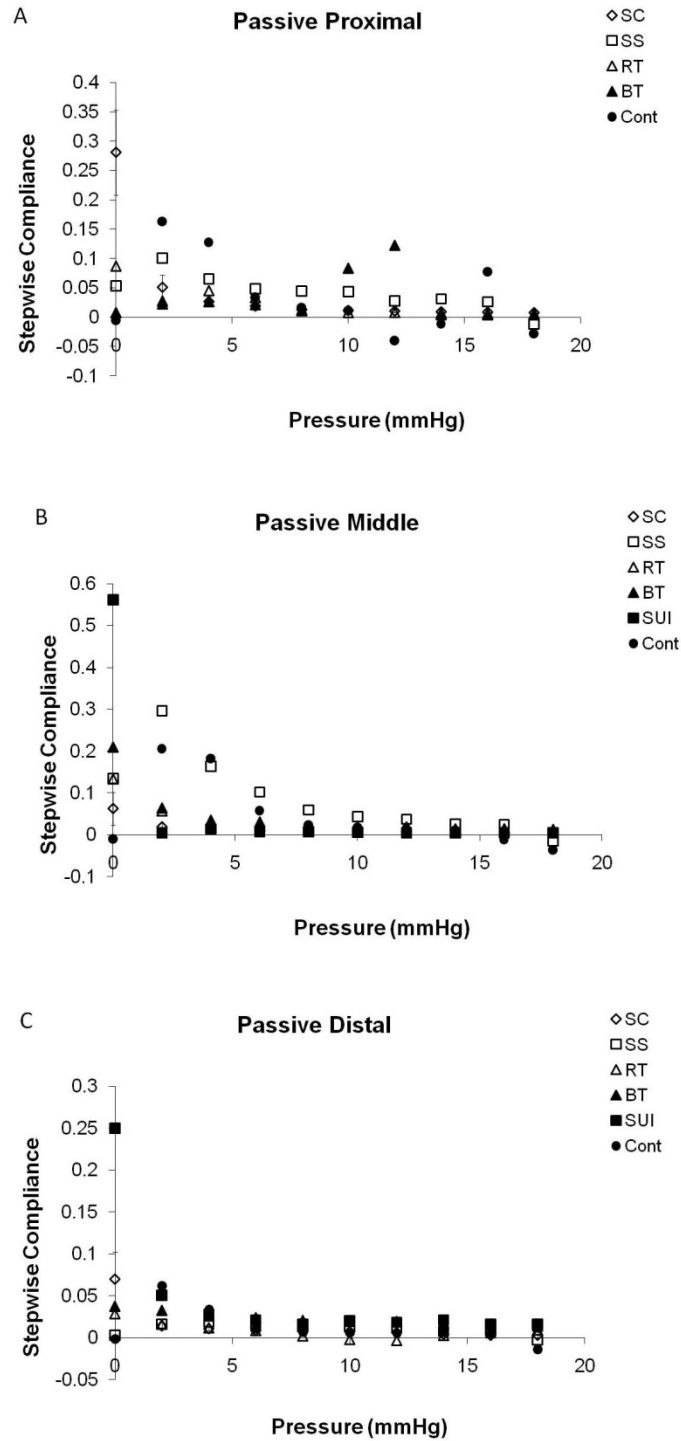


**Figure F.16** Average passive step-wise compliance curves for 4 week Lewis studies. SC = sham continent, SS = sham SUI, RT = rat TEUW, BT = bovine TEUW, and Cont = untouched continent. Data shown as average  $\pm$  SEM for n=2, where n=1 for all other groups.

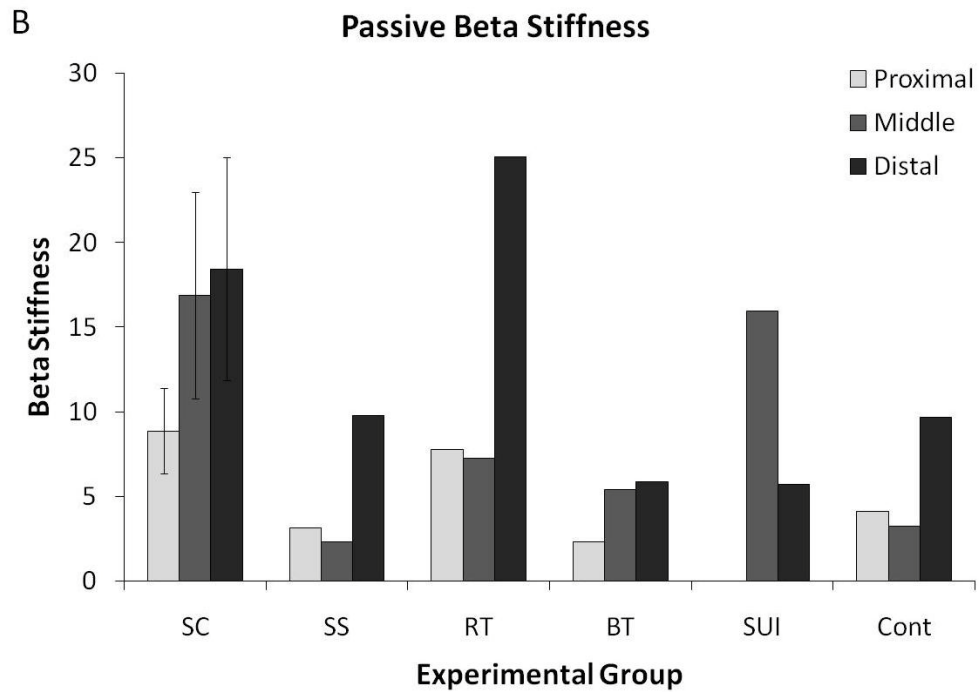
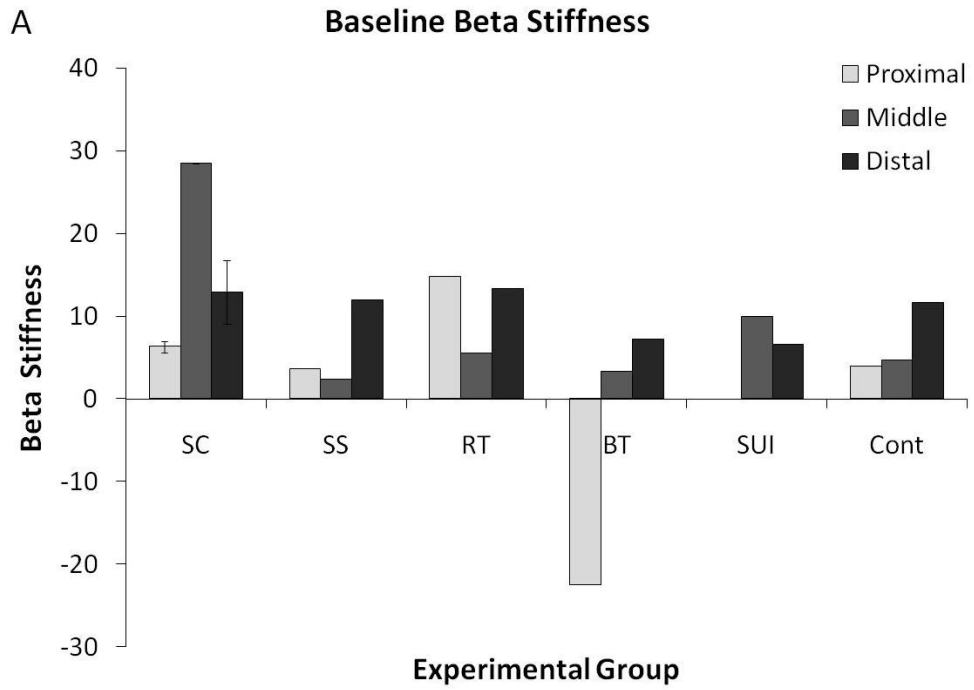


**Figure F.17** Beta stiffness values for 4 week Lewis studies. SC = sham continent, SS = sham SUI, RT = rat TEUW, BT = bovine TEUW, and Cont = untouched continent. Data shown as average  $\pm$  SEM for  $n=2$ , where  $n=1$  for all other groups.

## **Histology**

Histology in the Lewis urethra (**Figure F.18**) showed a large cellular infiltration of the BT at 1 week, but remodeling and collagen production within the RT at the same time point. Both TEUWs degraded over time and were replaced with collagen. By 4 weeks the TEUW had completely degraded. No large variations under other experimental conditions were observed.

## **Summary**

These preliminary studies indicate that SUI, as a result of pudendal nerve transection, affects the urethra of Lewis and SD rats differently. Lewis rats showed no change in LPP values, while SD rats showed a decreased LPP in the presence of SUI. Although Lewis rats showed no changes in LPP over all experimental conditions, SD rats showed an increasing trend in LPP with TEUW treatment, bringing LPP values closer to that of SC controls. Lewis rats also appeared to show more of a proximal urethra response (increased compliance), while SD rats showed a mid-urethral response to SUI. Both groups indicate that TEUW placement provides support to the proximal urethra as seen in the resistance pressure increases. It does appear that separation of the urethra from the vagina may cause increases in urethral resistance due to the increased LPP values of SC, SS and BT groups in the SD model, but the low n value and lack of response seen in Lewis values did not confirm this trend. Histology indicates that rat fibrinogen provides a better remodeling and decreased inflammatory response when compared to bovine fibrinogen and was therefore used for the remaining in-vivo studies.

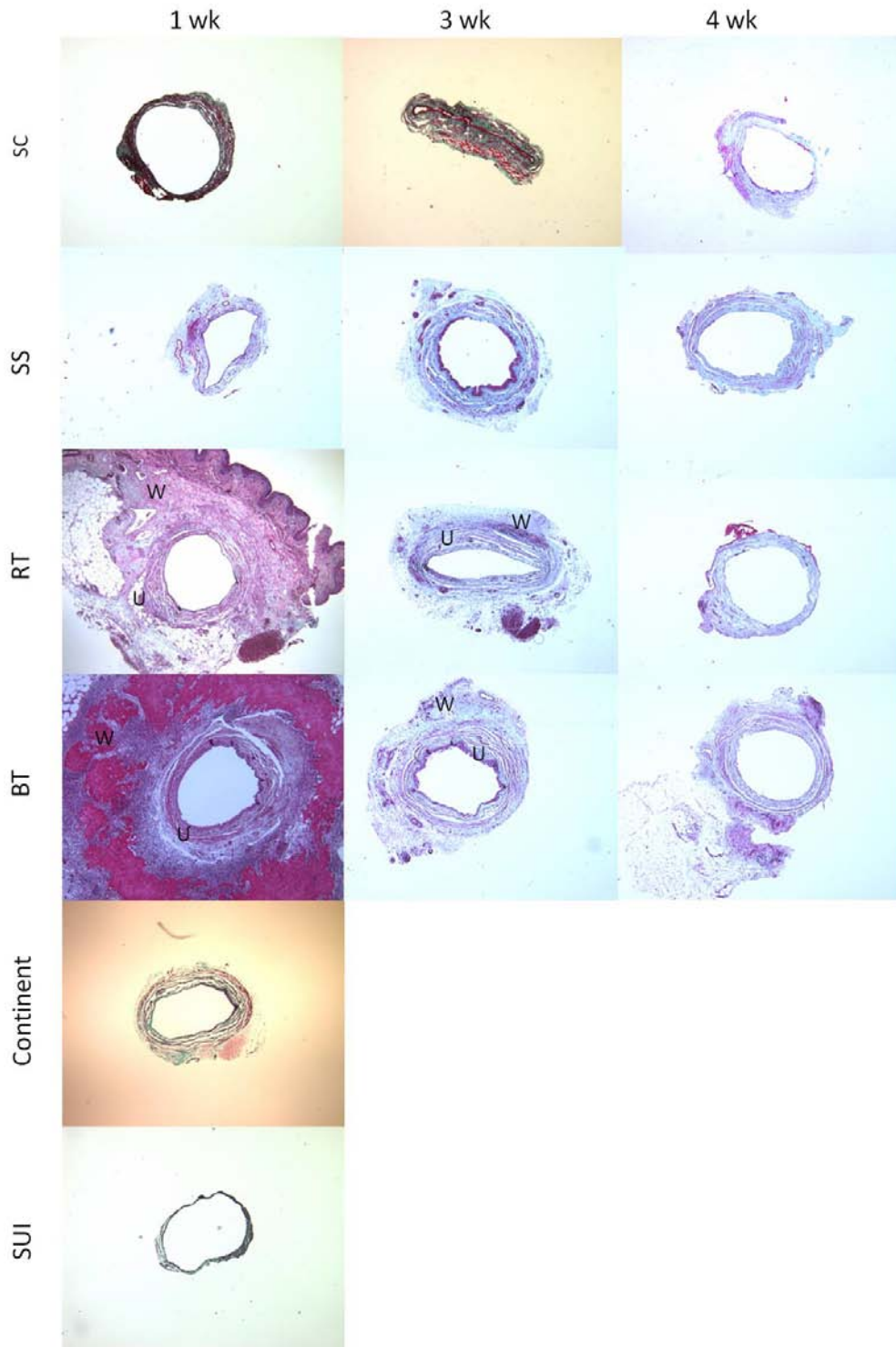


**Figure F.18** Representative trichrome staining of 1, 3, and 4 week Lewis rat studies. SC = sham continent, SS = sham SUI, RT = rat TEUW, BT = bovine TEUW. Red = muscle/fibrin, blue/green = collagen, black = nuclei, where U = urethra and W = TEUW. Images taken with a 4x objective. All images can be found in **Appendix H**.

## APPENDIX G

### IN-VIVO PRESSURE-DIAMETER CURVES

#### 1 WEEK LEWIS BASELINE

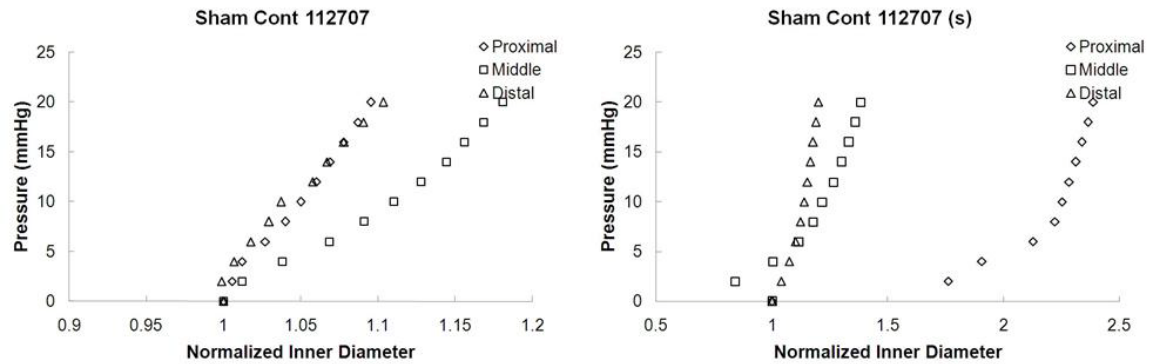
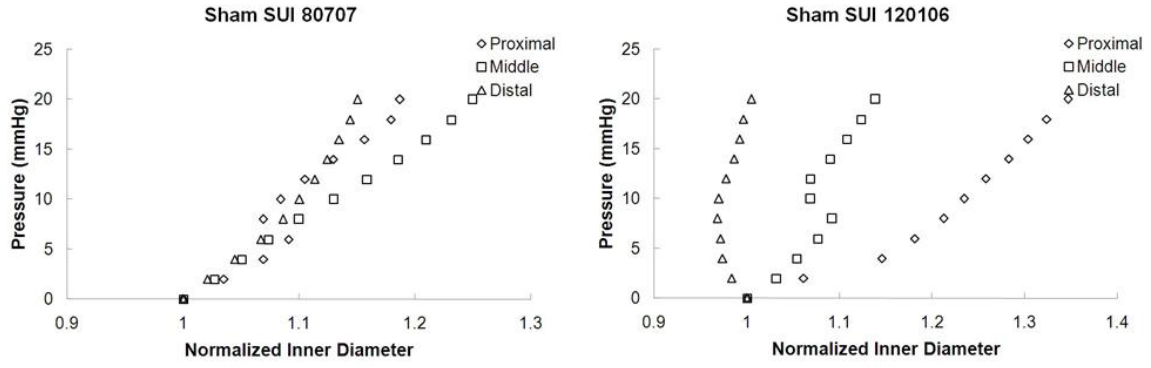
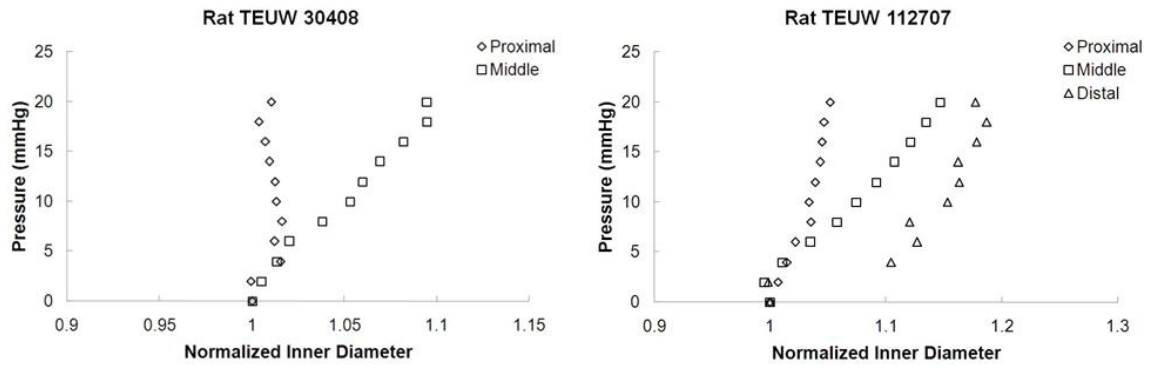


Figure G.1 Baseline pressure-diameter curves for 1 week, Lewis SC proximal, middle and distal segments.



**Figure G.2** Baseline pressure-diameter curves for 1 week, Lewis SS proximal, middle and distal segments.



**Figure G.3** Baseline pressure-diameter curves for 1 week, Lewis RT proximal, middle and distal segments.

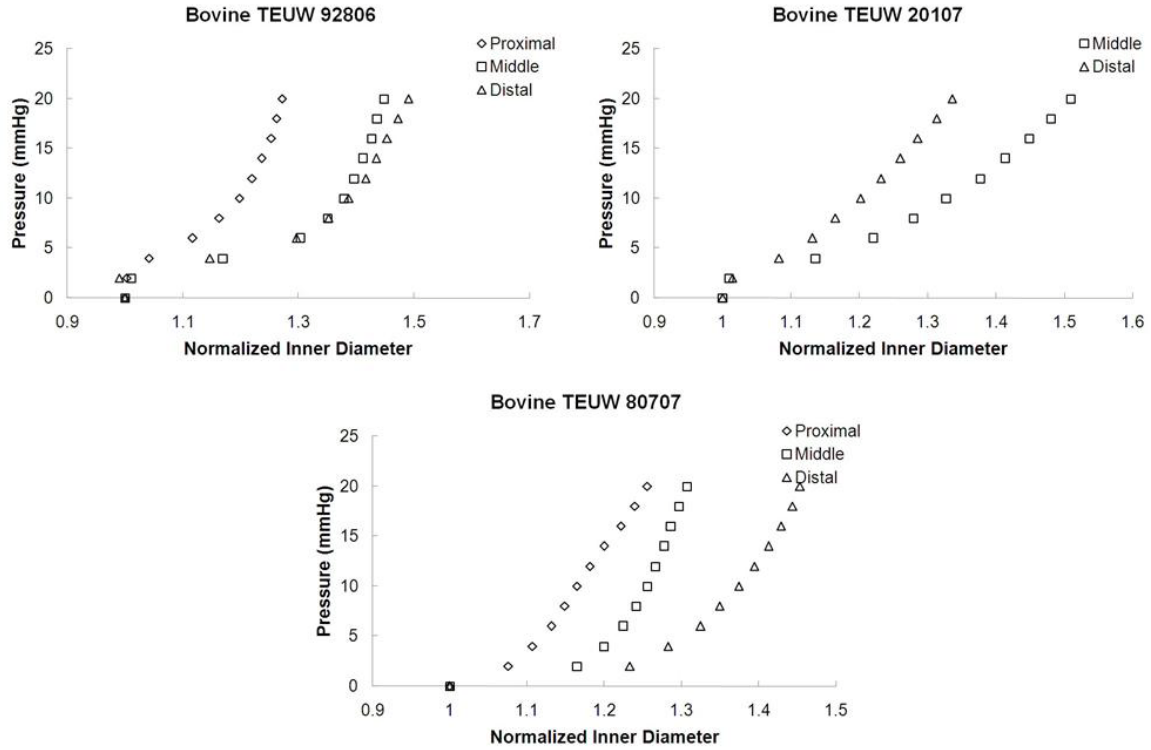


**Figure G.4** Baseline pressure-diameter curves for 1 week, Lewis BT proximal, middle and distal segments.

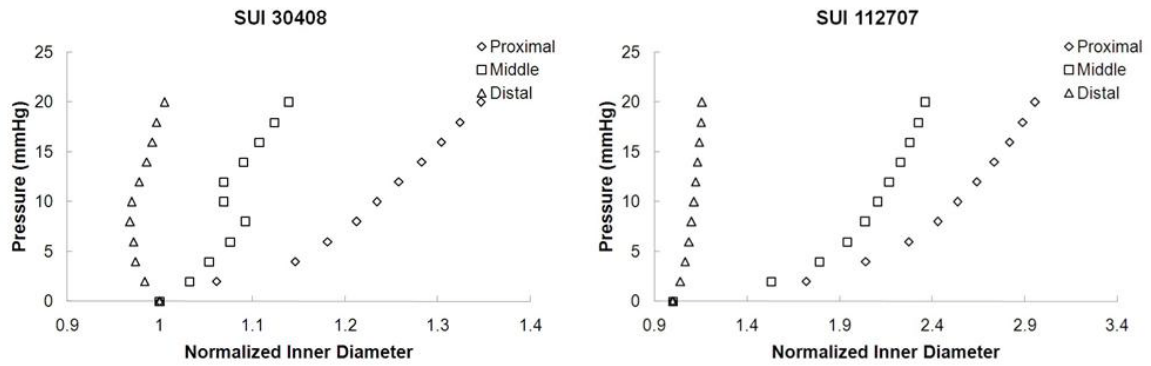


**Figure G.5** Baseline pressure-diameter curves for 1 week, Lewis SUI proximal, middle and distal segments.

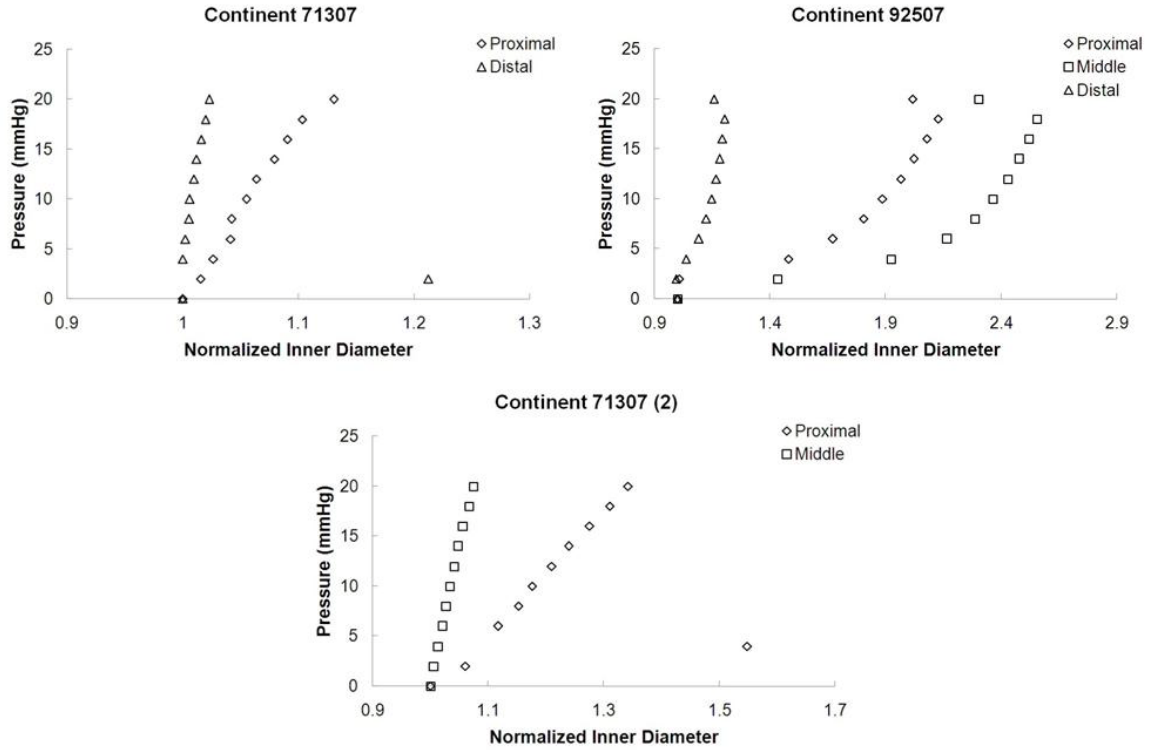


**Figure G.6** Baseline pressure-diameter curves for 1 week, Lewis Cont proximal, middle and distal segments.

### 1 WEEK LEWIS PASSIVE

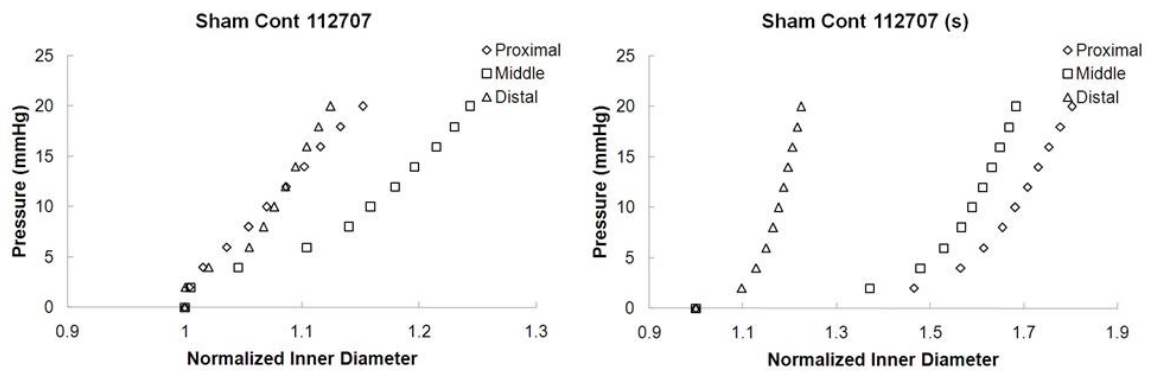


**Figure G. 7** Passive pressure-diameter curves for 1 week, Lewis SC proximal, middle and distal segments.

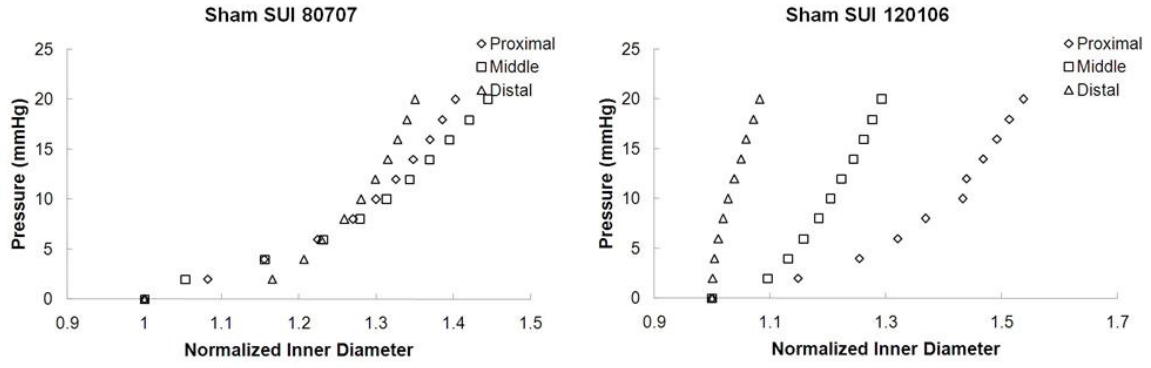


Figure G.8 Passive pressure-diameter curves for 1 week, Lewis SS proximal, middle and distal segments.

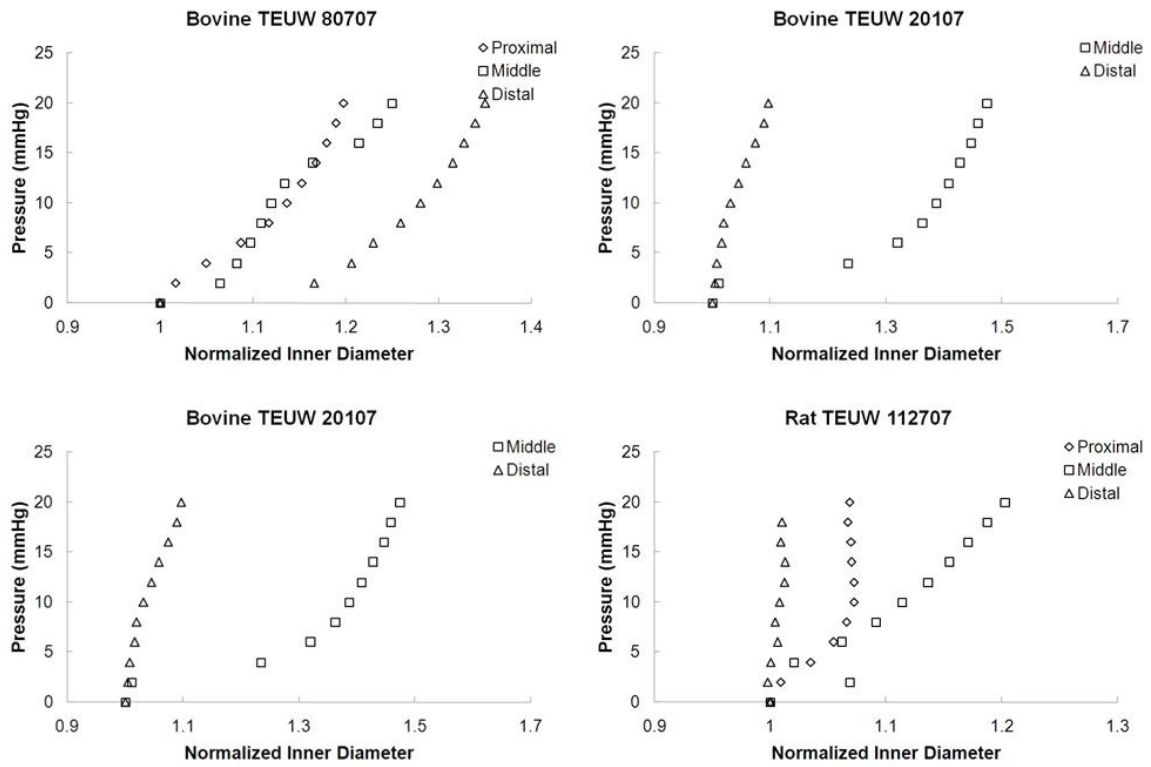


Figure G.9 Passive pressure-diameter curves for 1 week, Lewis RT and BT proximal, middle and distal segments.

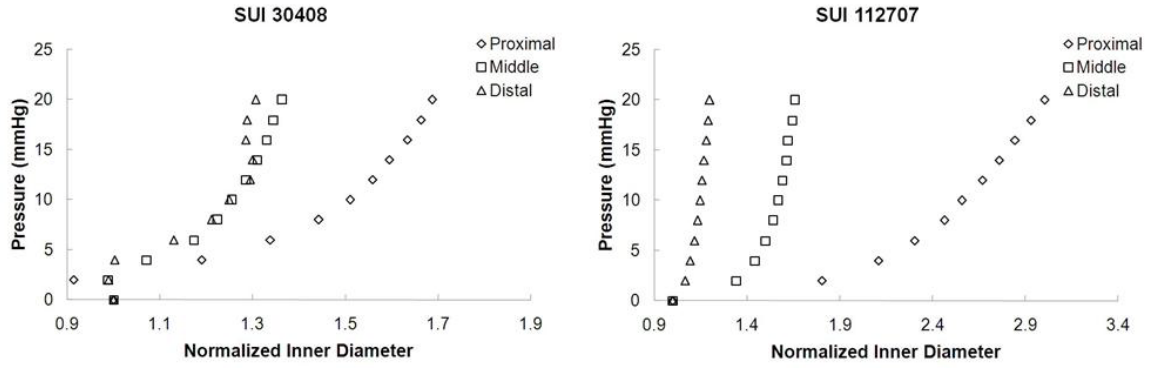


Figure G.10 Passive pressure-diameter curves for 1 week, Lewis SUI proximal, middle and distal segments.

### 1 WEEK SD BASELINE

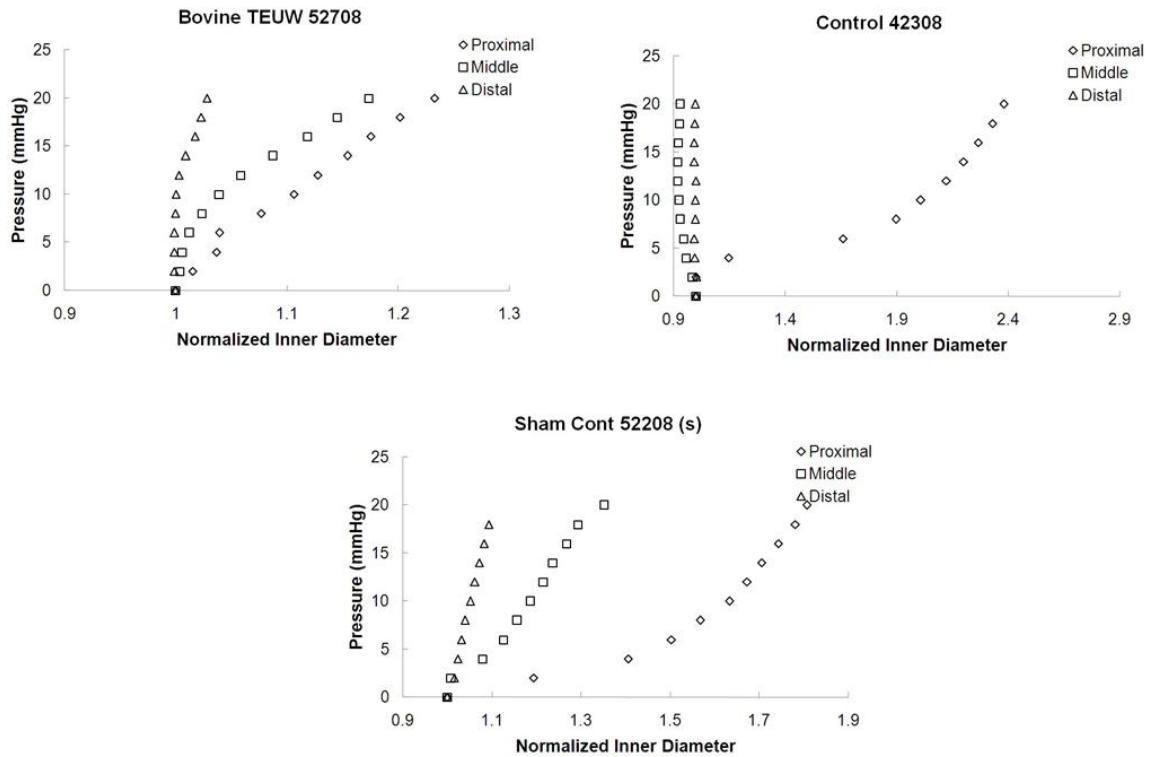


Figure G.11 Baseline pressure-diameter curves for 1 week, SD BT, Cont and SC proximal, middle and distal segments.

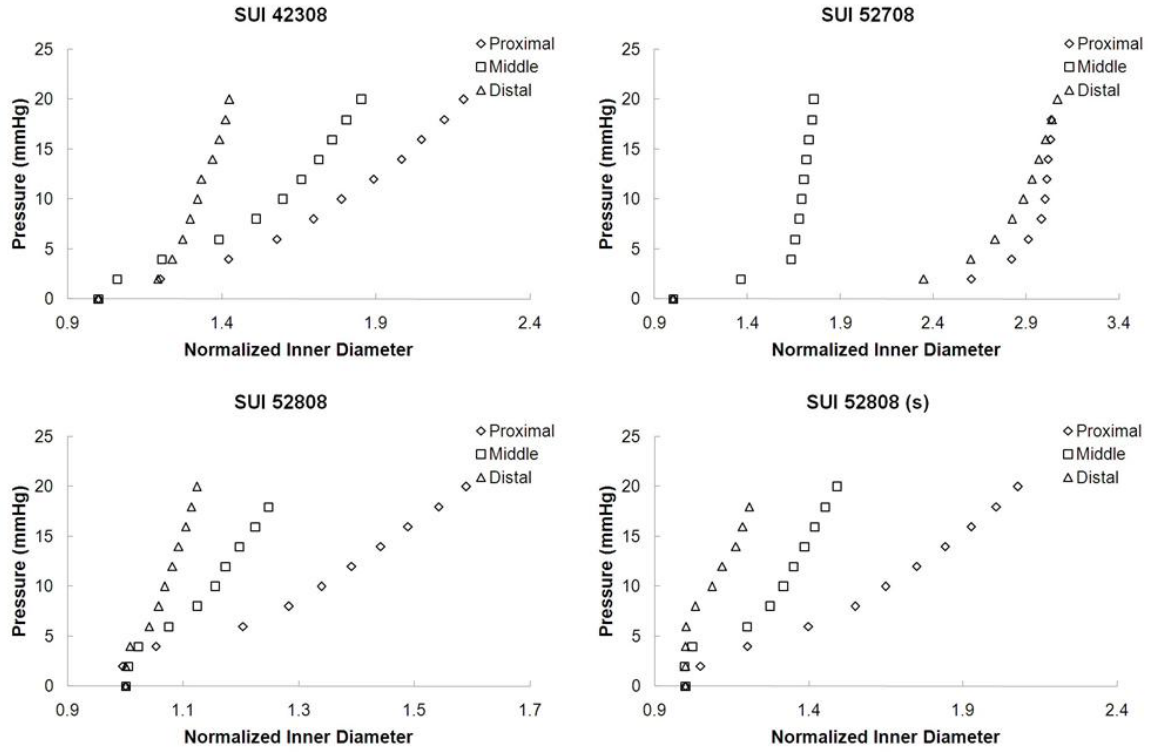
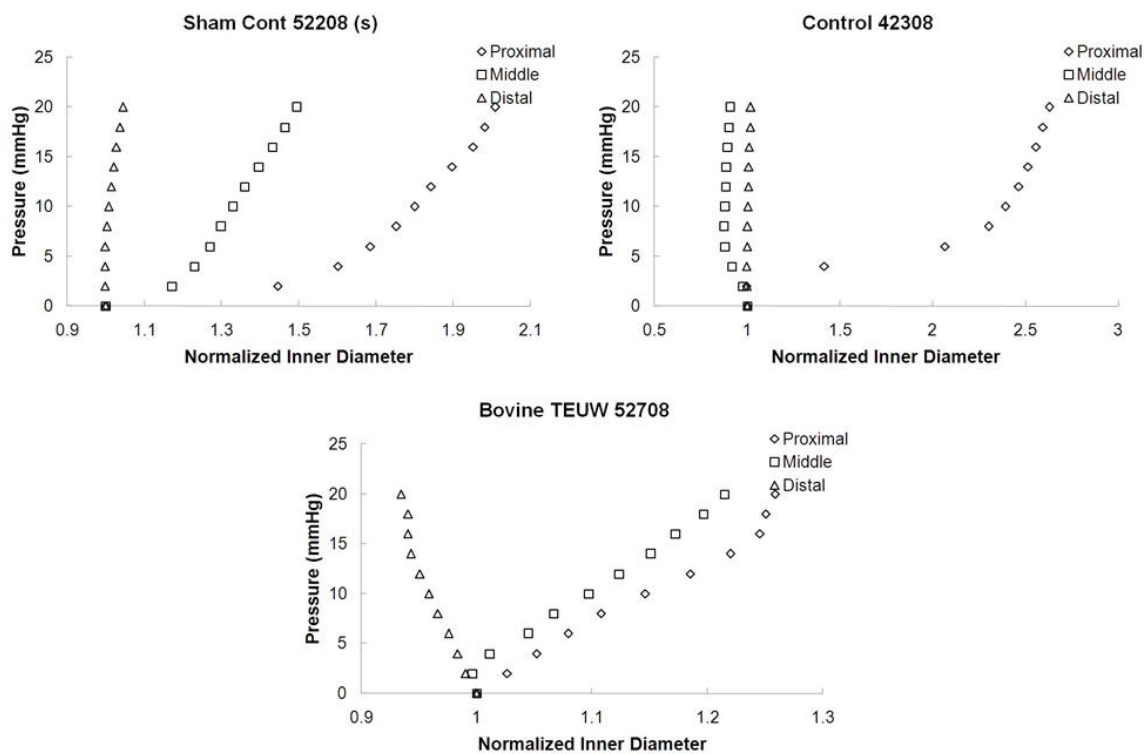


Figure G.12 Baseline pressure-diameter curves for 1 week, SD SUI proximal, middle and distal segments.

# 1 WEEK SD PASSIVE



**Figure G.13** Passive pressure-diameter curves for 1 week, SD SC, Cont and BT proximal, middle and distal segments.

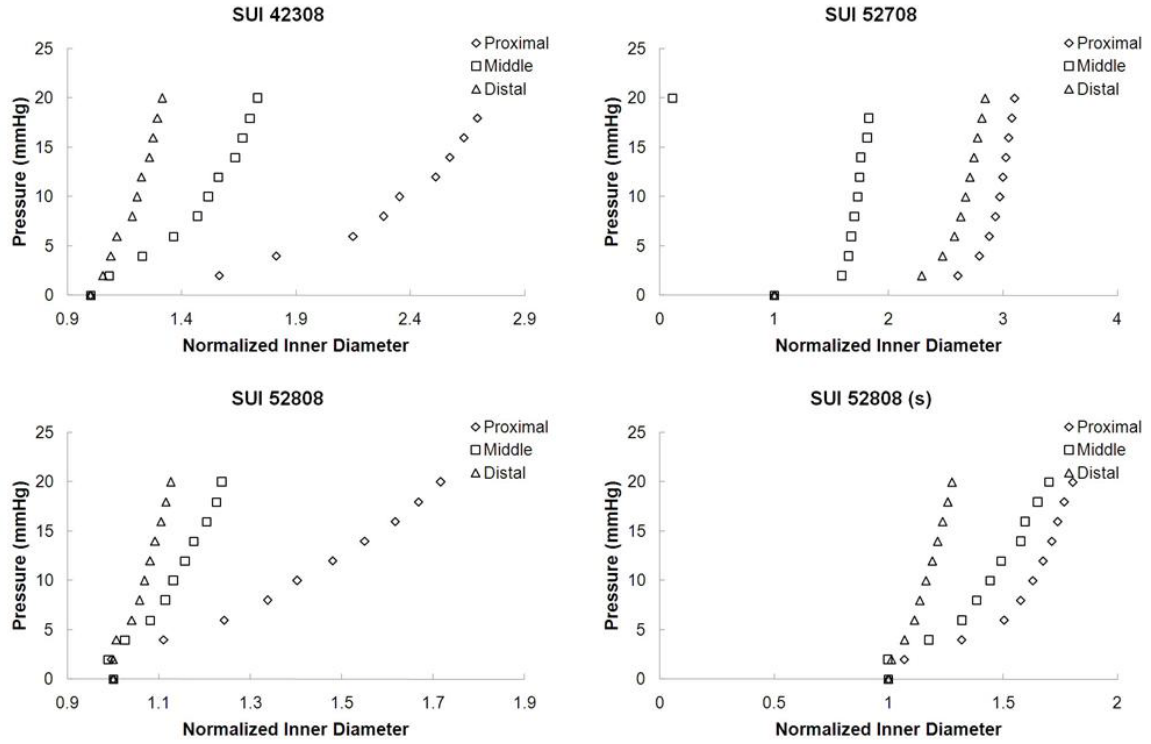


Figure G.14 Passive pressure-diameter curves for 1 week, SD SUI proximal, middle and distal segments.

### 4 WEEK LEWIS BASELINE

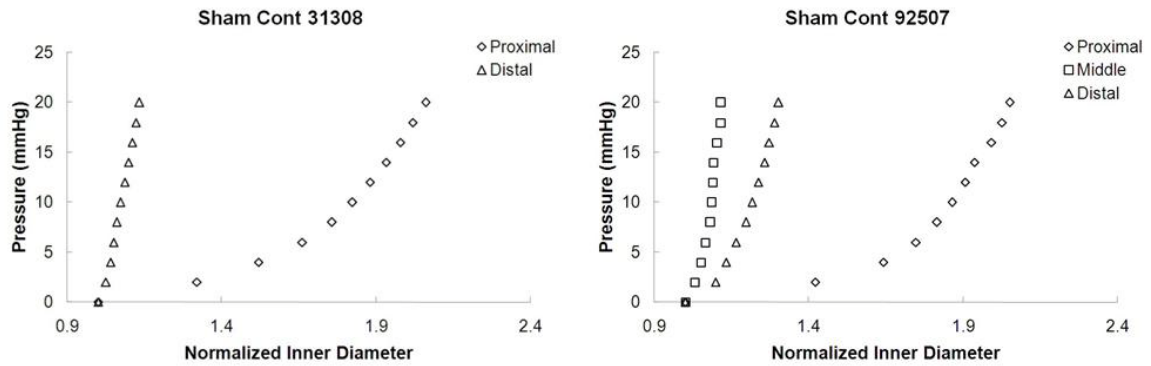
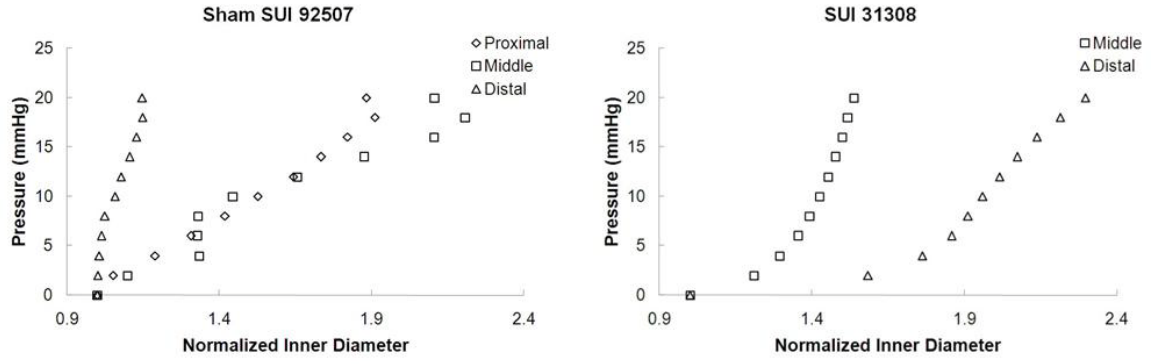
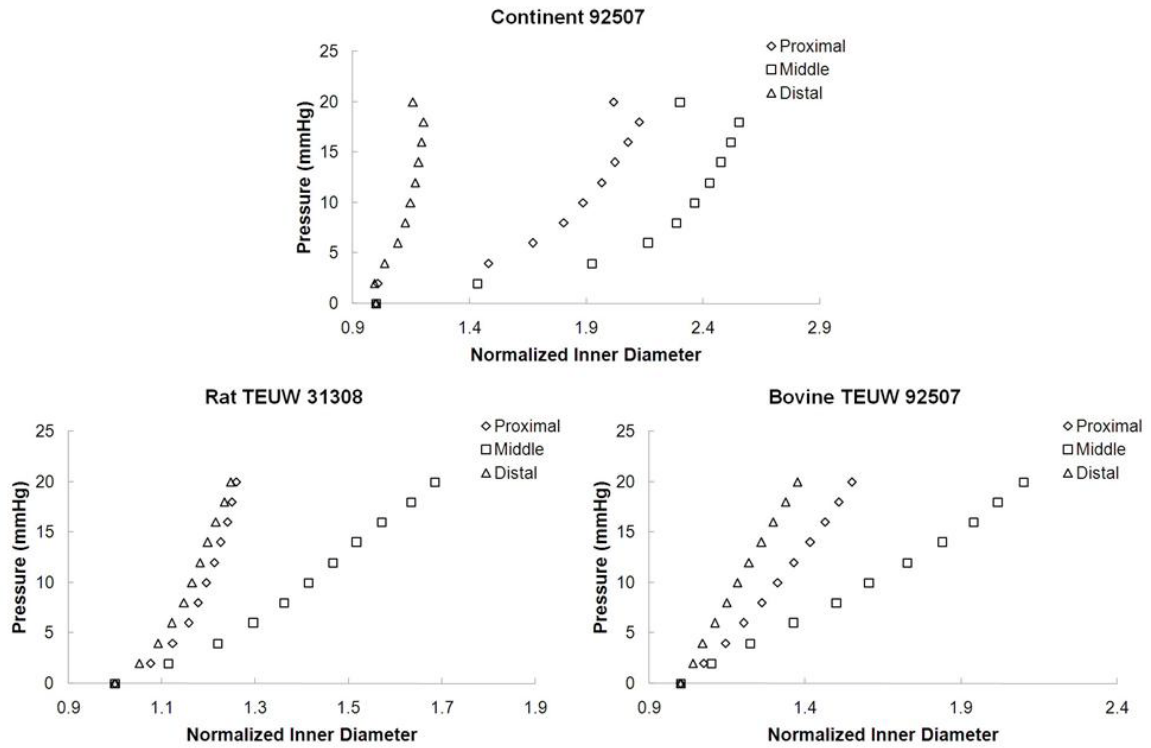


Figure G.15 Baseline pressure-diameter curves for 4 week, Lewis SC proximal, middle and distal segments.



**Figure G.16** Baseline pressure-diameter curves for 4 week, Lewis SS and SUI proximal, middle and distal segments.



**Figure G.17** Baseline pressure-diameter curves for 4 week, Lewis Cont, RT and BT proximal, middle and distal segments.

## 4 WEEK LEWIS PASSIVE

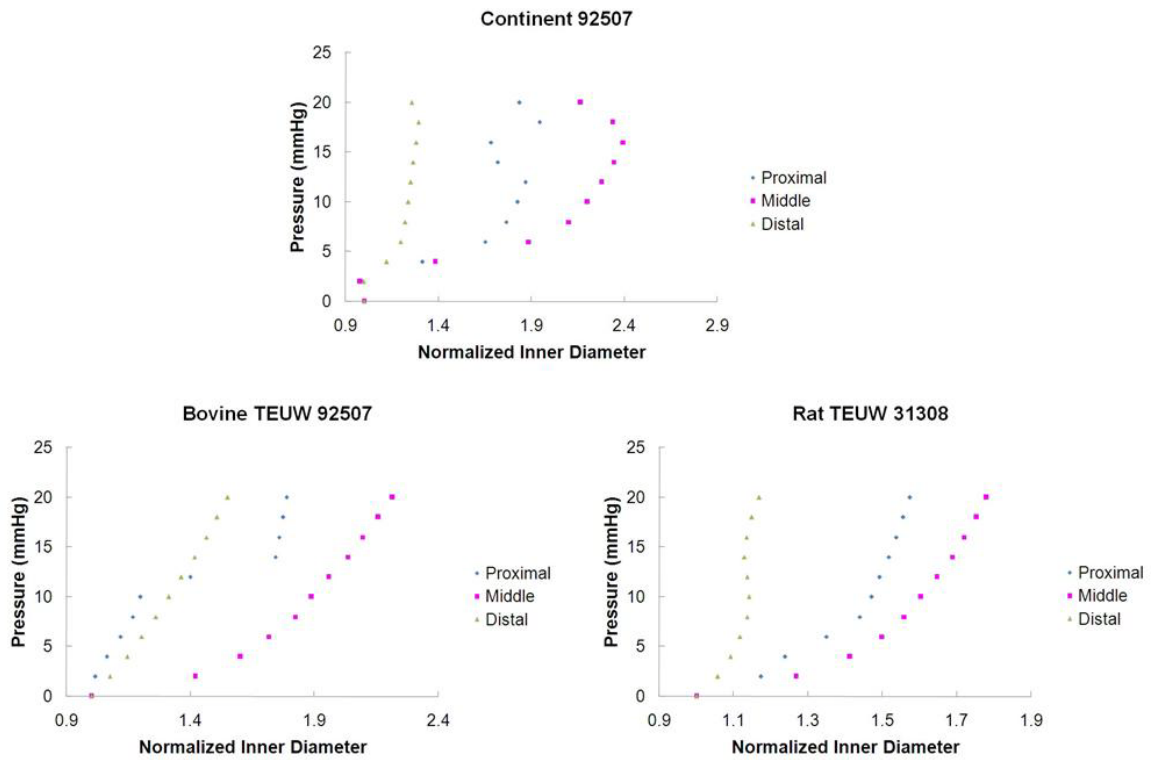


**Figure G.18** Passive pressure-diameter curves for 4 week, Lewis Cont, RT and BT proximal, middle and distal segments.

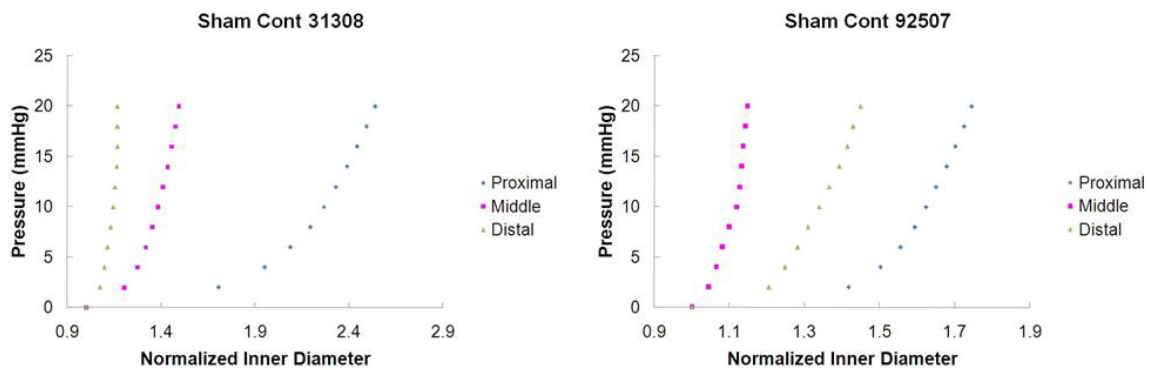


**Figure G.19** Passive pressure-diameter curves for 4 week, Lewis SC proximal, middle and distal segments.

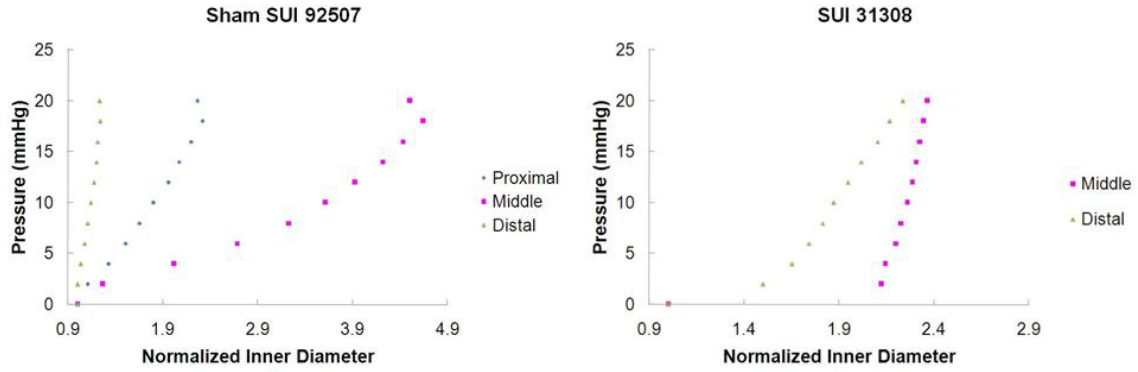


Figure G. 20 Passive pressure-diameter curves for 4 week, Lewis SS and SUI proximal, middle and distal segments.

### 3 WEEK LEWIS BASELINE

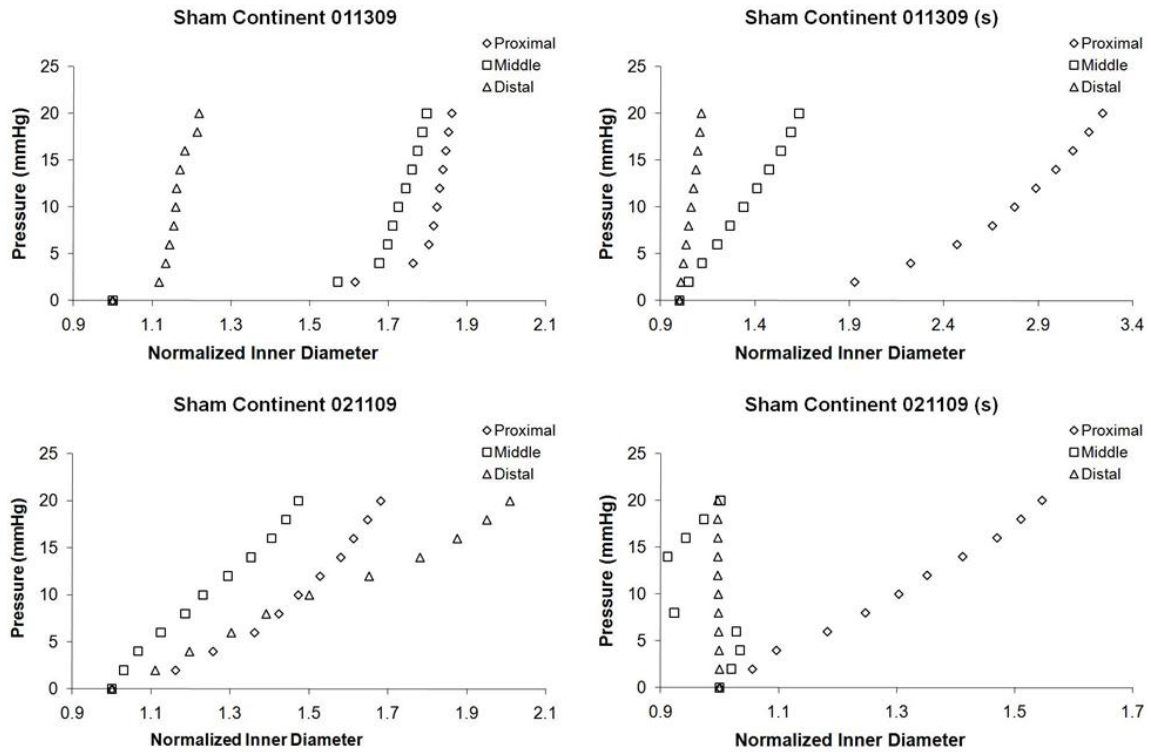


Figure G. 21 Baseline pressure-diameter curves for 3 week, Lewis SC proximal, middle and distal segments.

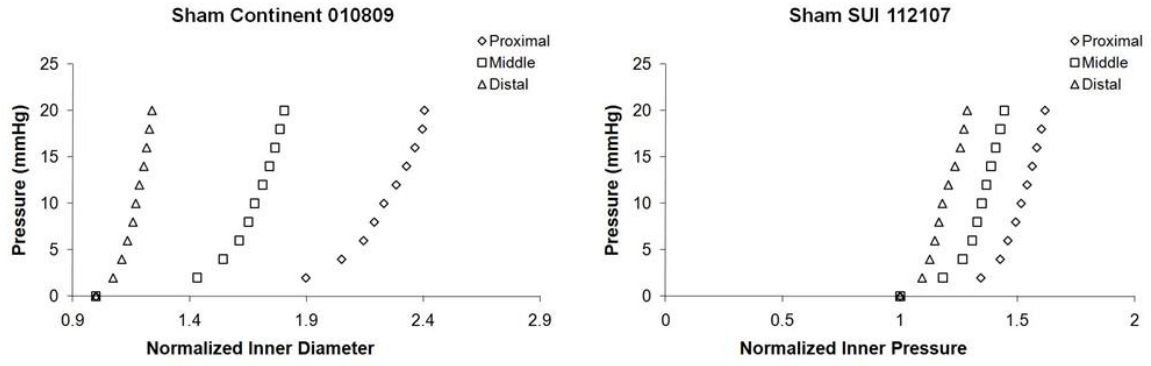


Figure G.22 Baseline pressure-diameter curves for 3 week, Lewis SC and SS proximal, middle and distal segments.

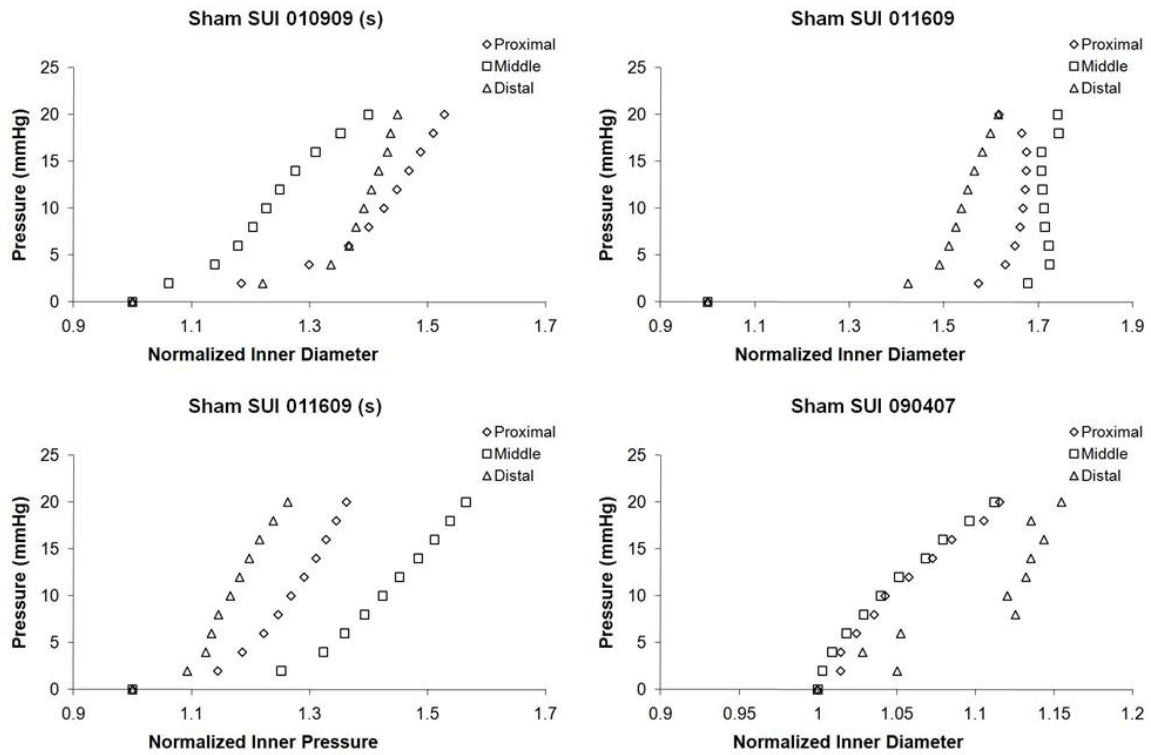
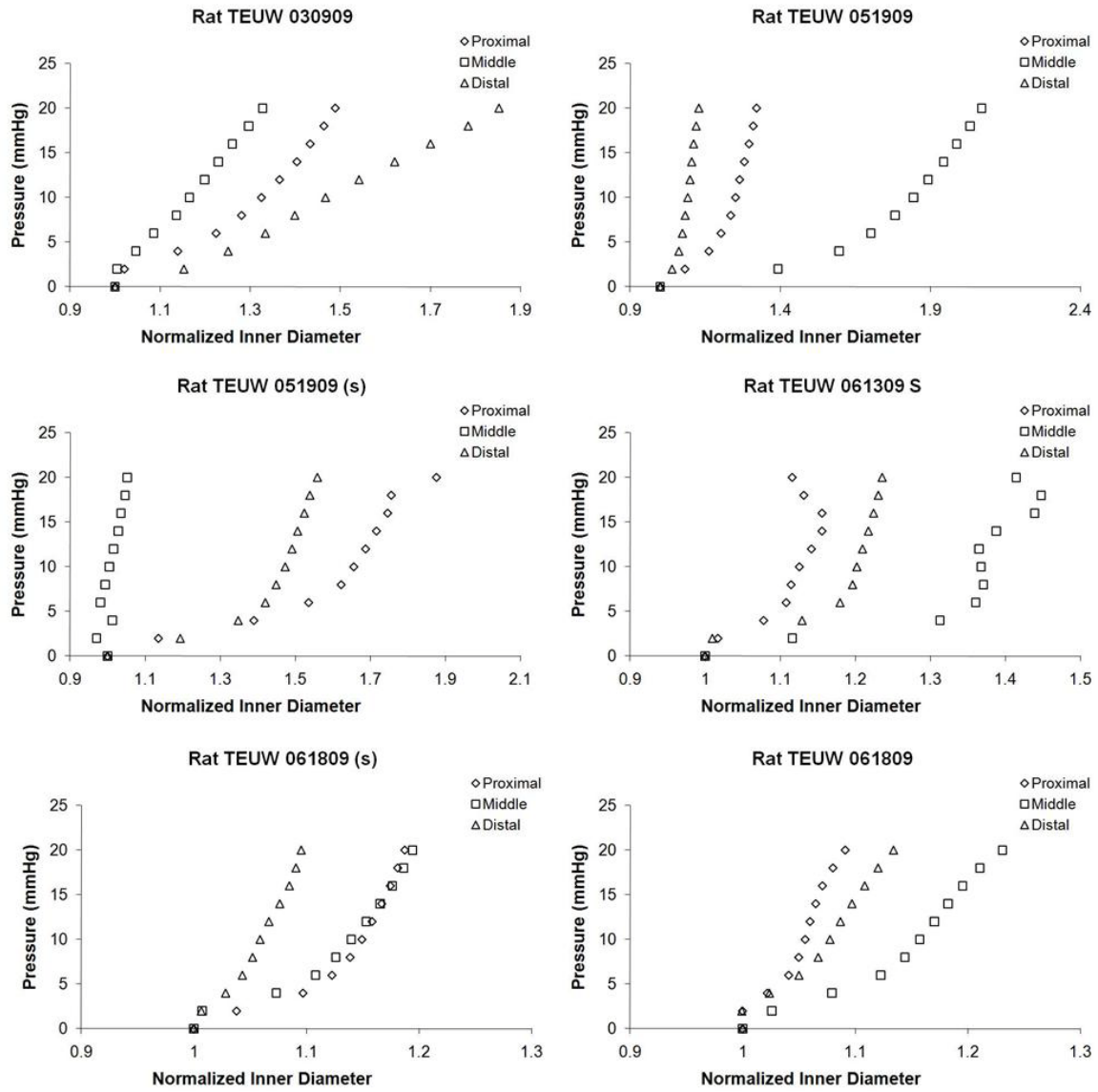


Figure G.23 Baseline pressure-diameter curves for 3 week, Lewis SS proximal, middle and distal segments.



**Figure G.24** Baseline pressure-diameter curves for 3 week, Lewis RT proximal, middle and distal segments.

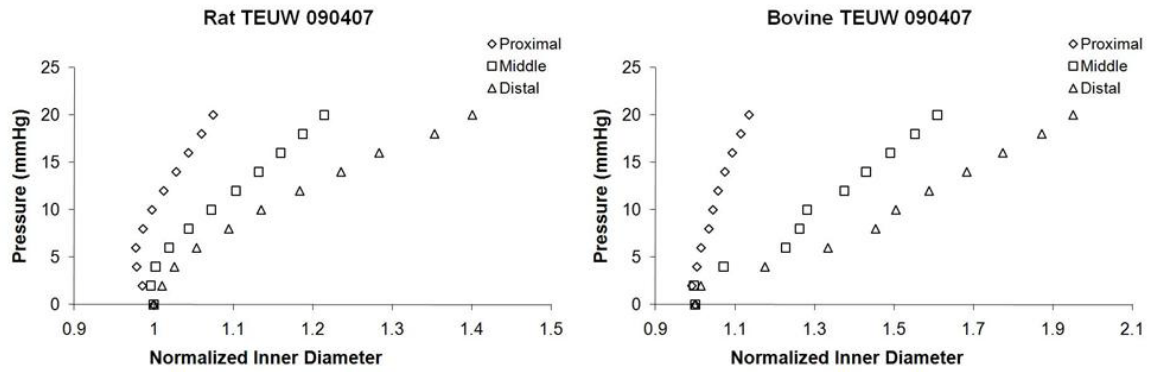


Figure G.25 Baseline pressure-diameter curves for 3 week, Lewis RT and BT proximal, middle and distal segments.

### LEWIS 3 WEEK PASSIVE

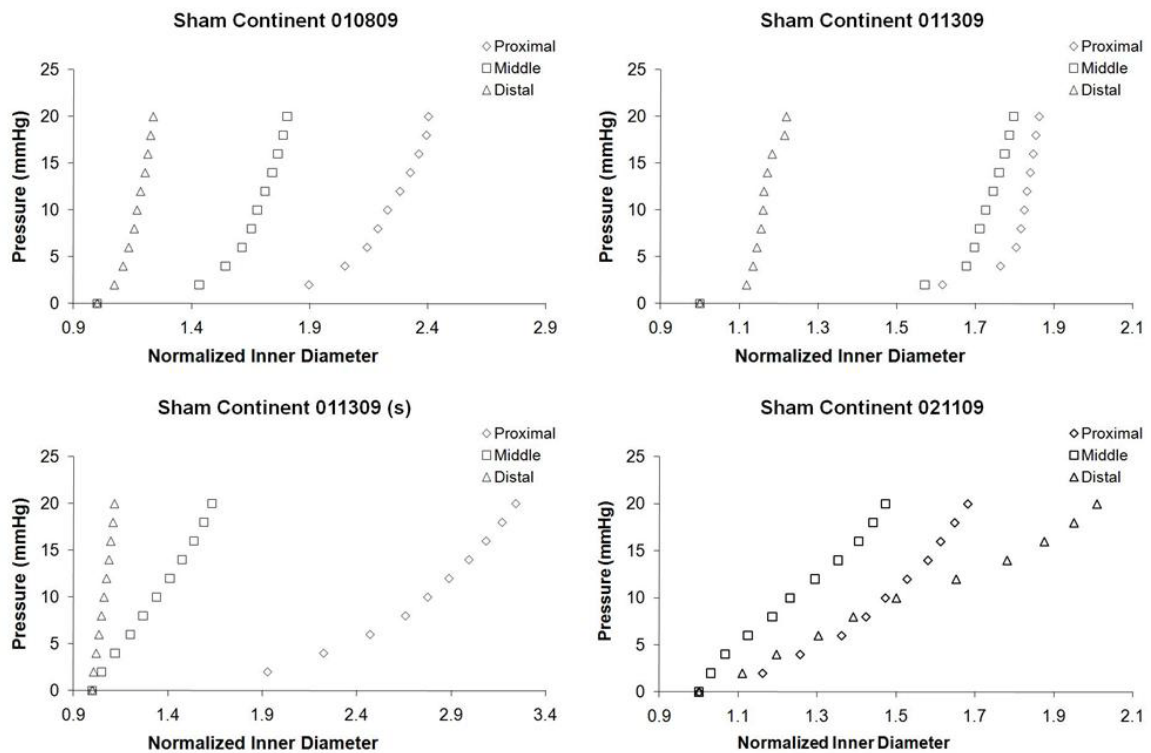
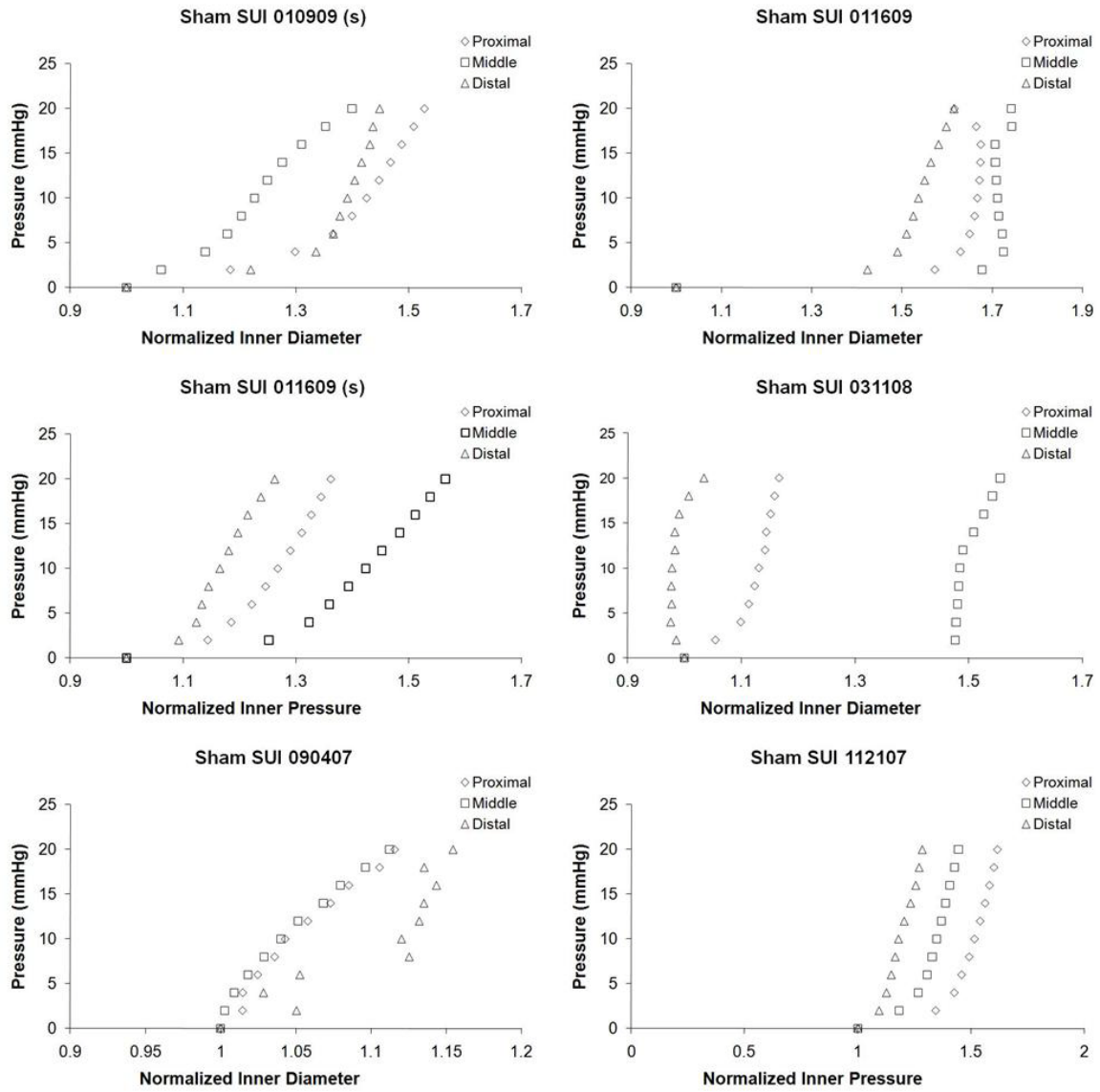


Figure G.26 Passive pressure-diameter curves for 3 week, Lewis SC proximal, middle and distal segments.



**Figure G.27** Passive pressure-diameter curves for 3 week, Lewis SS proximal, middle and distal segments.

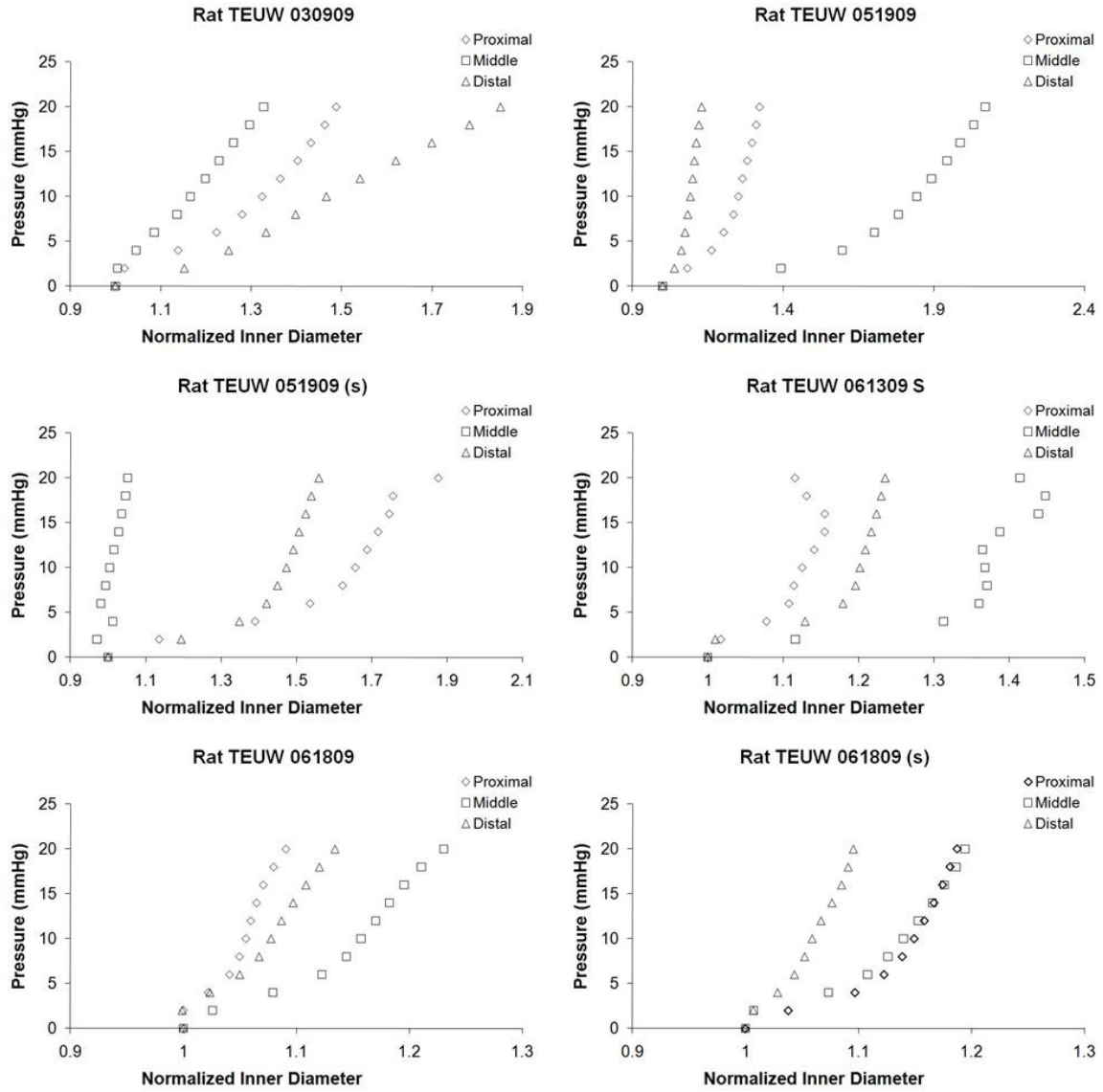


Figure G.28 Passive pressure-diameter curves for 3 week, Lewis RT proximal, middle and distal segments.

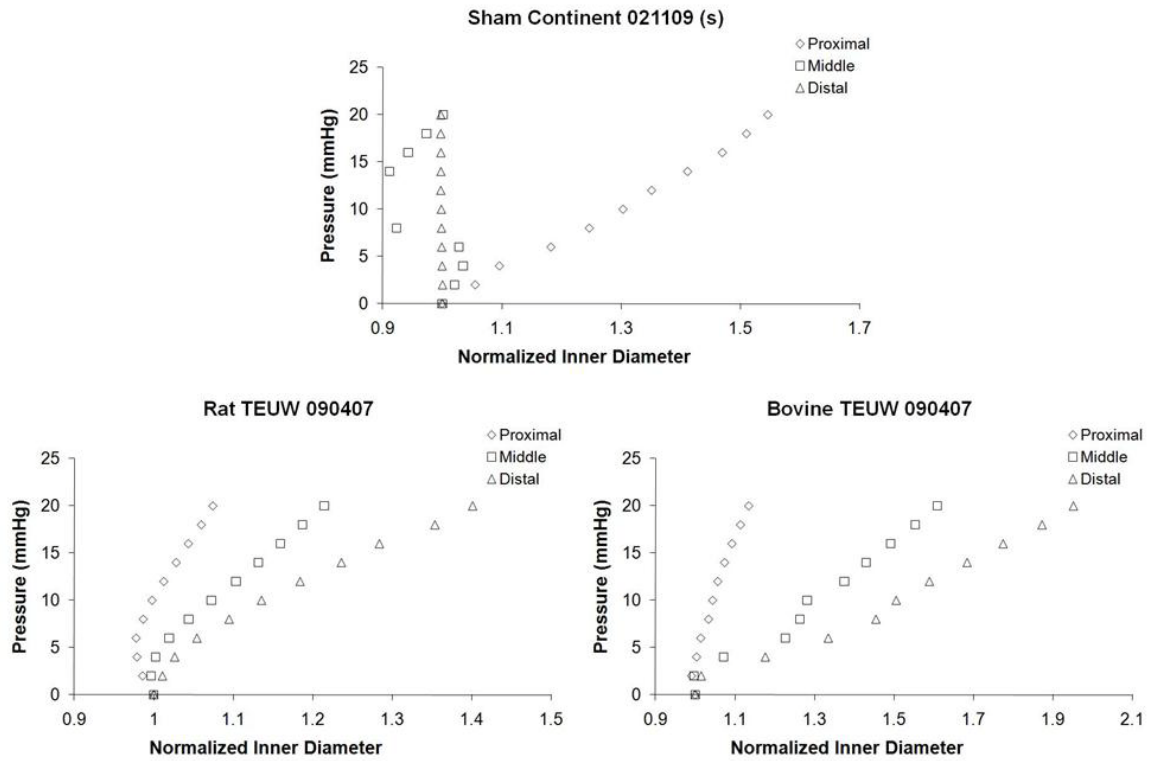


Figure G.29 Passive pressure-diameter curves for 3 week, Lewis SC, RT, BT proximal, middle and distal segments.

### OVARECTOMY BASELINE

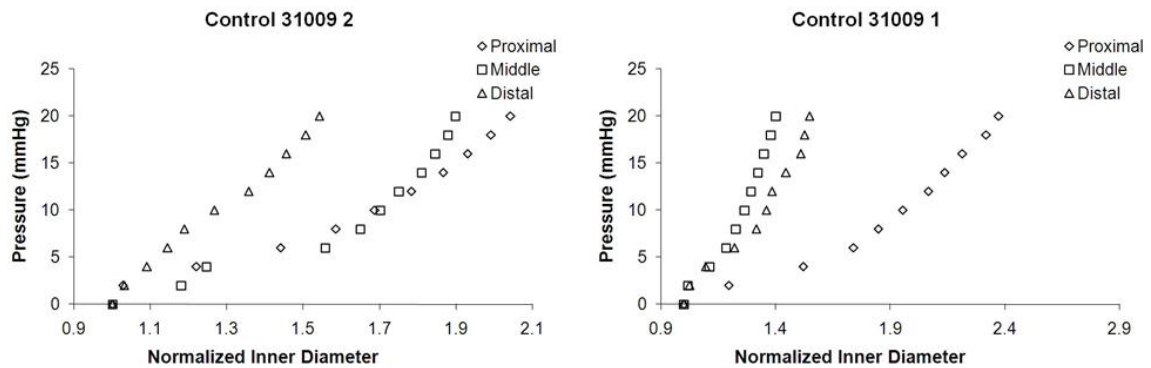
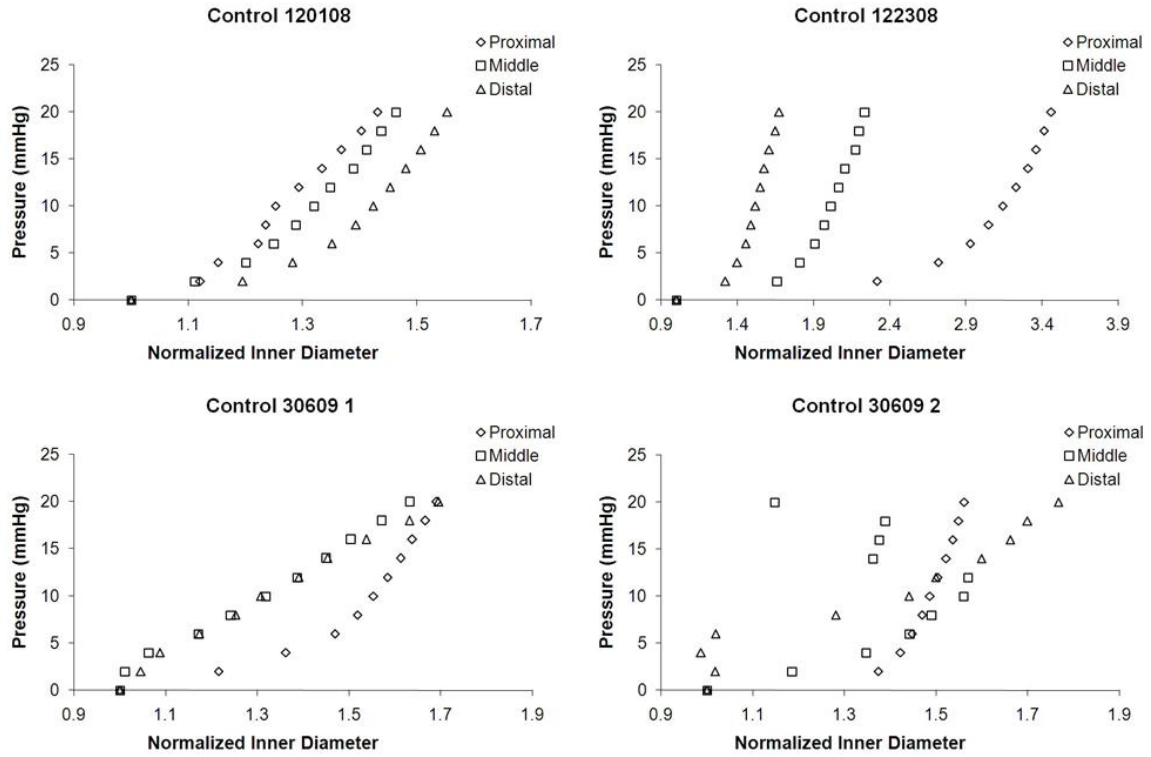
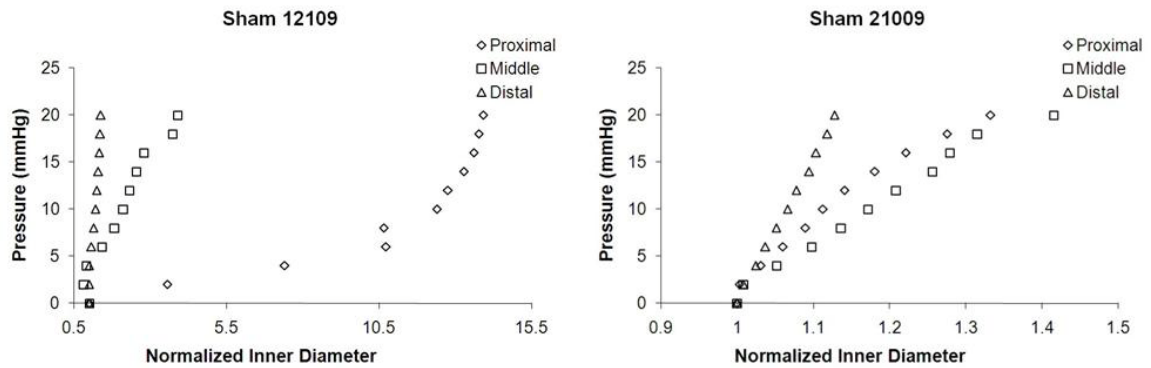


Figure G.30 Baseline pressure-diameter curves for control proximal, middle and distal segments.



**Figure G.31** Baseline pressure-diameter curves for control proximal, middle and distal segments.



**Figure G.32** Baseline pressure-diameter curves for sham Ov proximal, middle and distal segments.

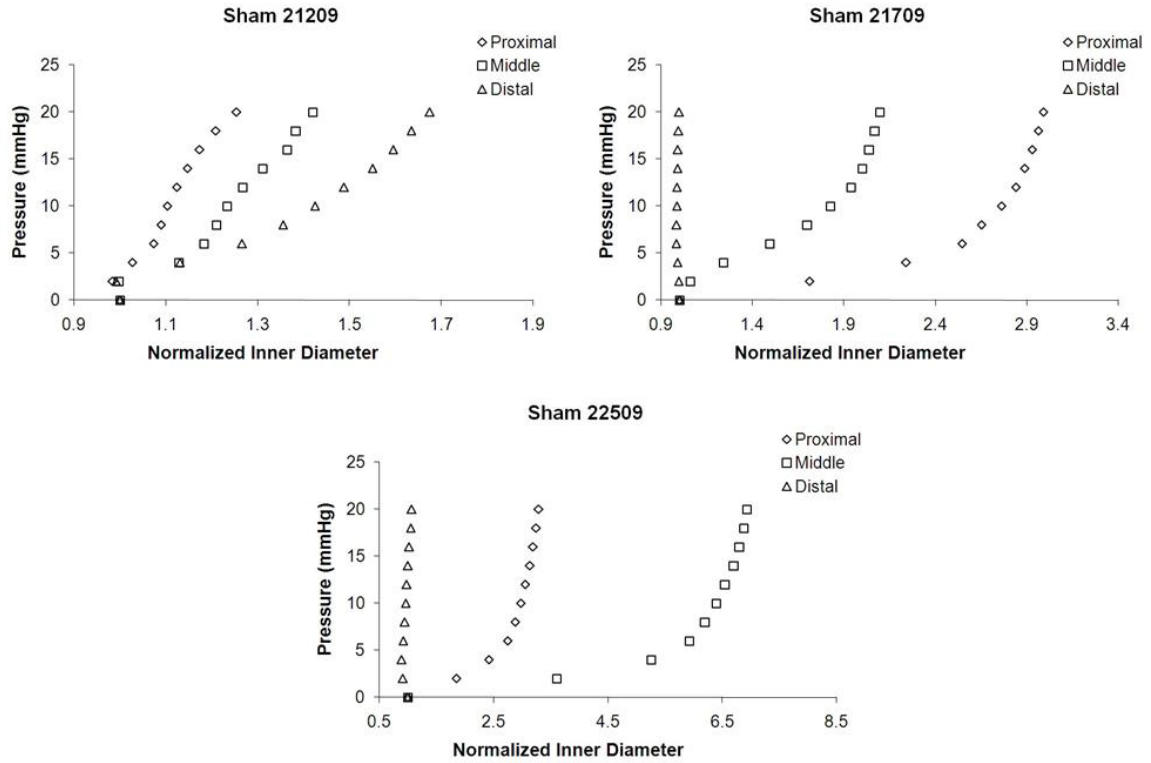


Figure G.33 Baseline pressure-diameter curves for sham Ov proximal, middle and distal segments.

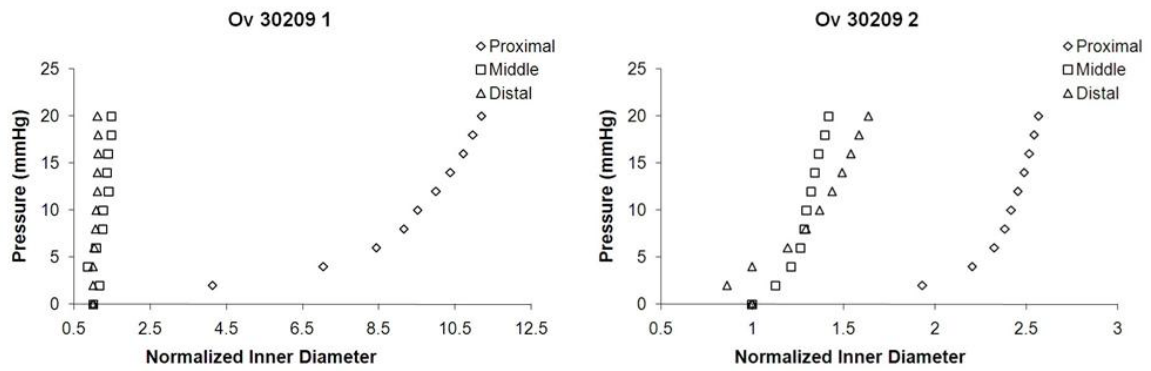


Figure G.34 Baseline pressure-diameter curves for Ov proximal, middle and distal segments.

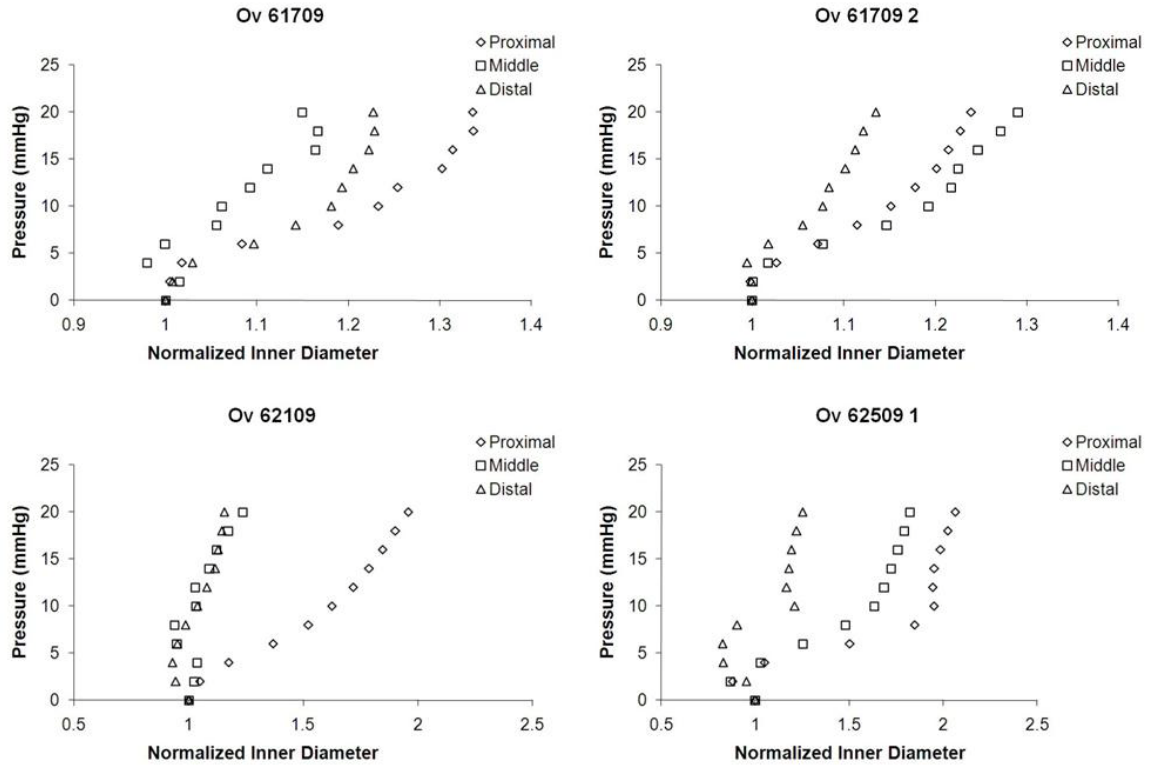


Figure G.35 Baseline pressure-diameter curves for Ov proximal, middle and distal segments.

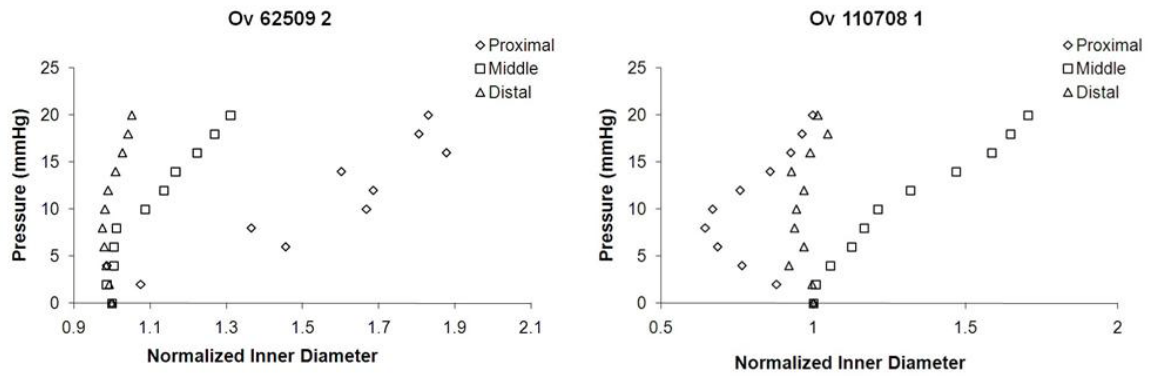


Figure G.36 Baseline pressure-diameter curves for Ov proximal, middle and distal segments.

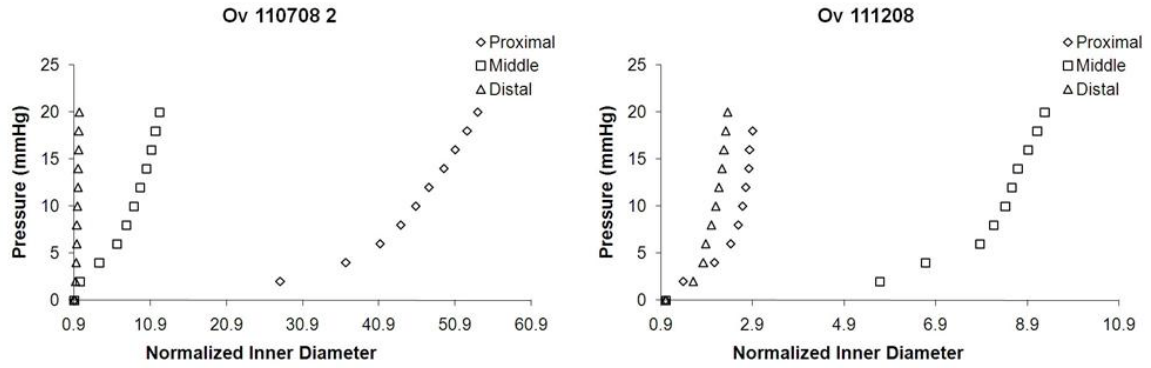


Figure G.37 Baseline pressure-diameter curves for Ov proximal, middle and distal segments.

### OVARECTOMY PASSIVE

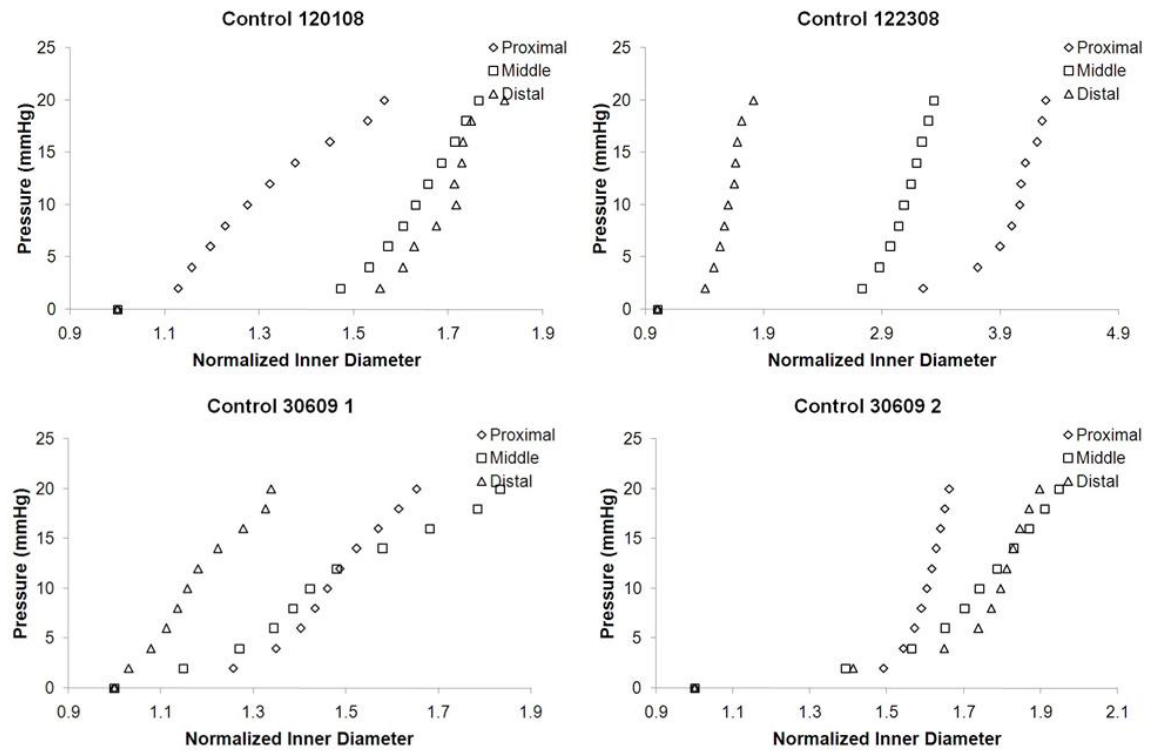


Figure G.38 Passive pressure-diameter curves for control proximal, middle and distal segments.

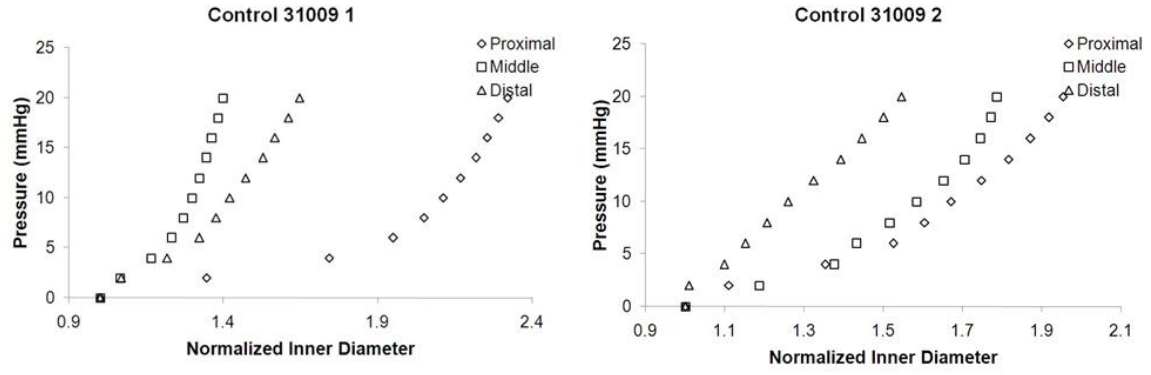


Figure G.39 Passive pressure-diameter curves for control proximal, middle and distal segments.

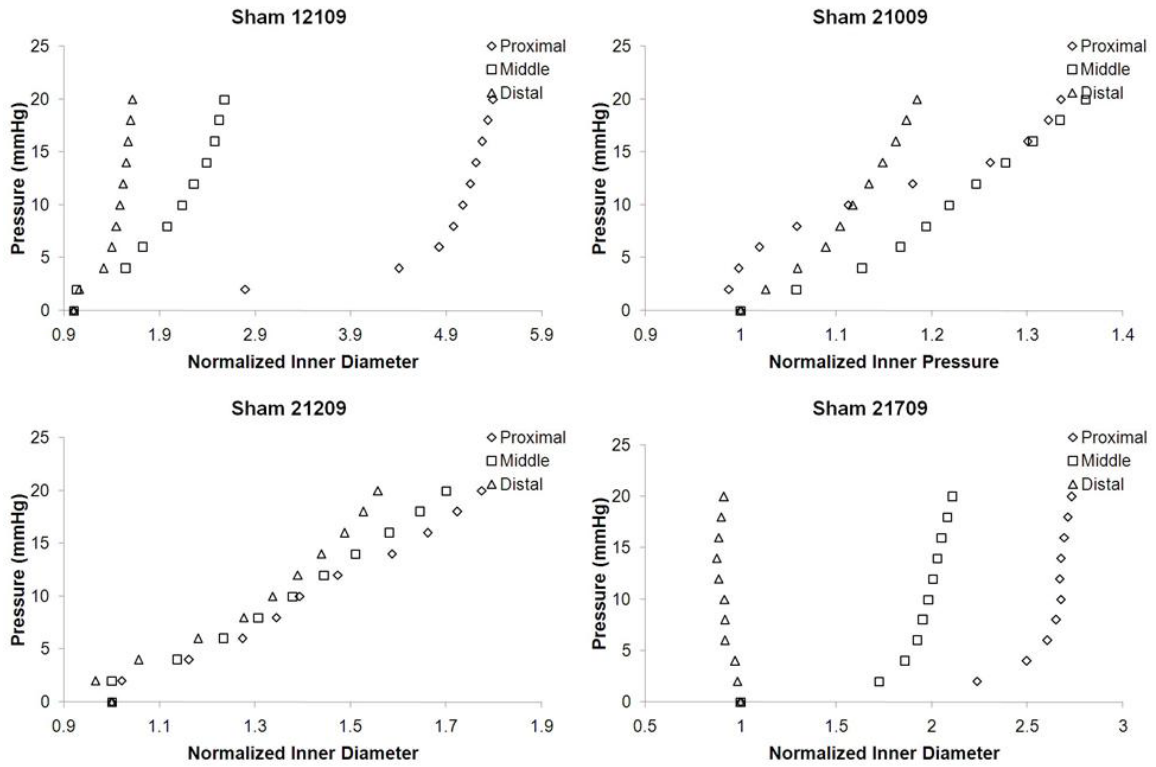


Figure G.40 Passive pressure-diameter curves for sham Ov proximal, middle and distal segments.

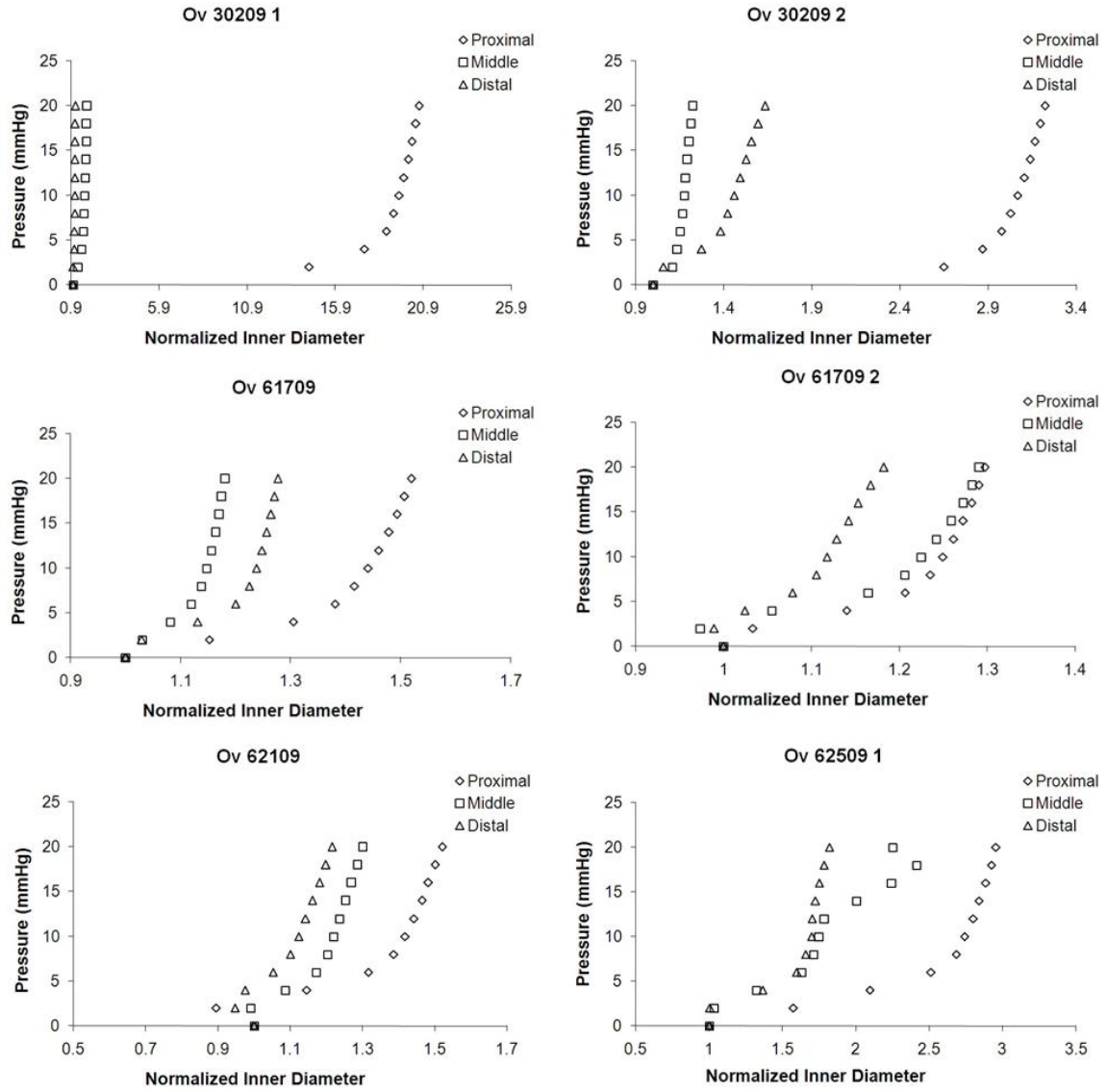


Figure G. 41 Passive pressure-diameter curves for Ov proximal, middle and distal segments.

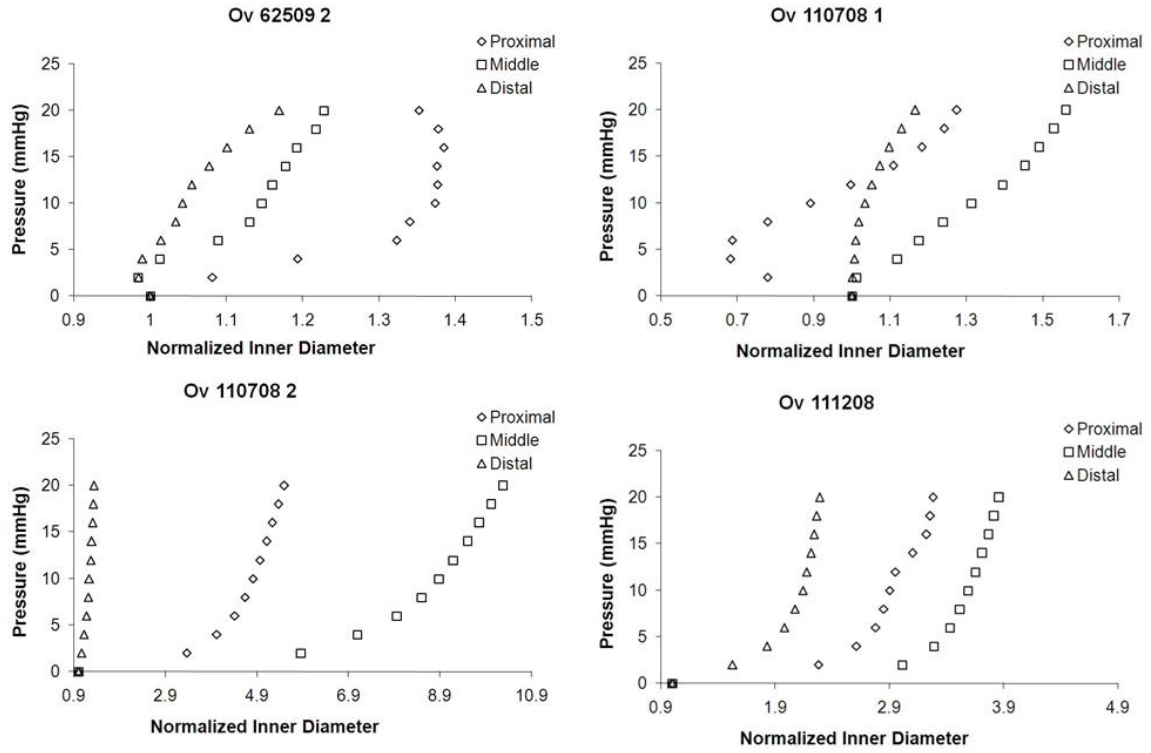


Figure G.42 Passive pressure-diameter curves for Ov proximal, middle and distal segments.

### ALPHABUNGAROTOXIN BASELINE

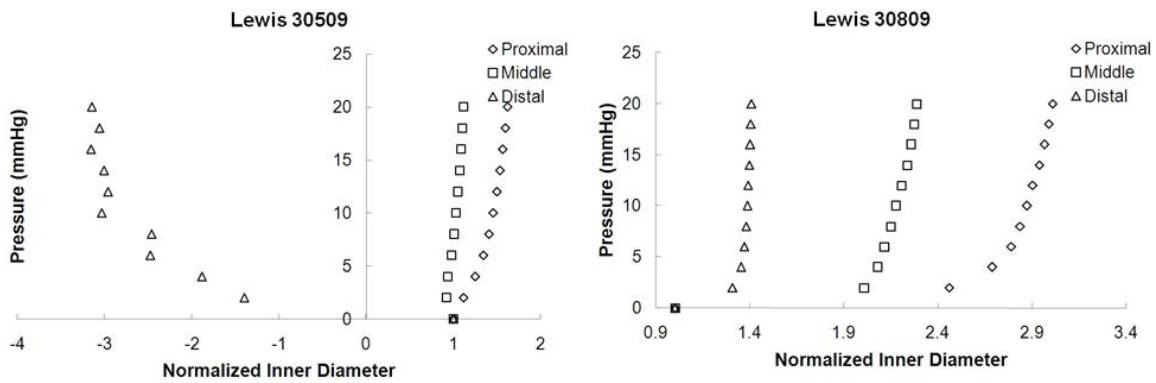


Figure G.43 Baseline pressure-diameter curves for Lewis alphabungarotoxin proximal, middle and distal segments.

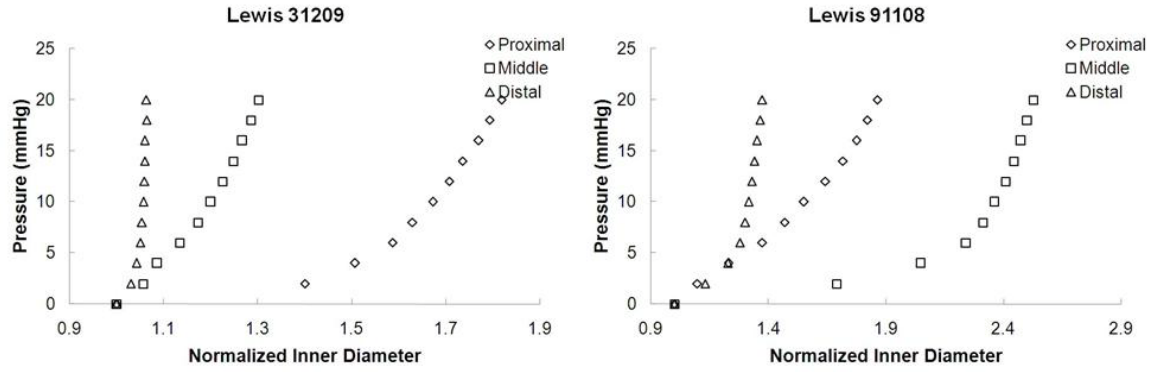


Figure G.44 Baseline pressure-diameter curves for Lewis alphabungarotoxin proximal, middle and distal segments.

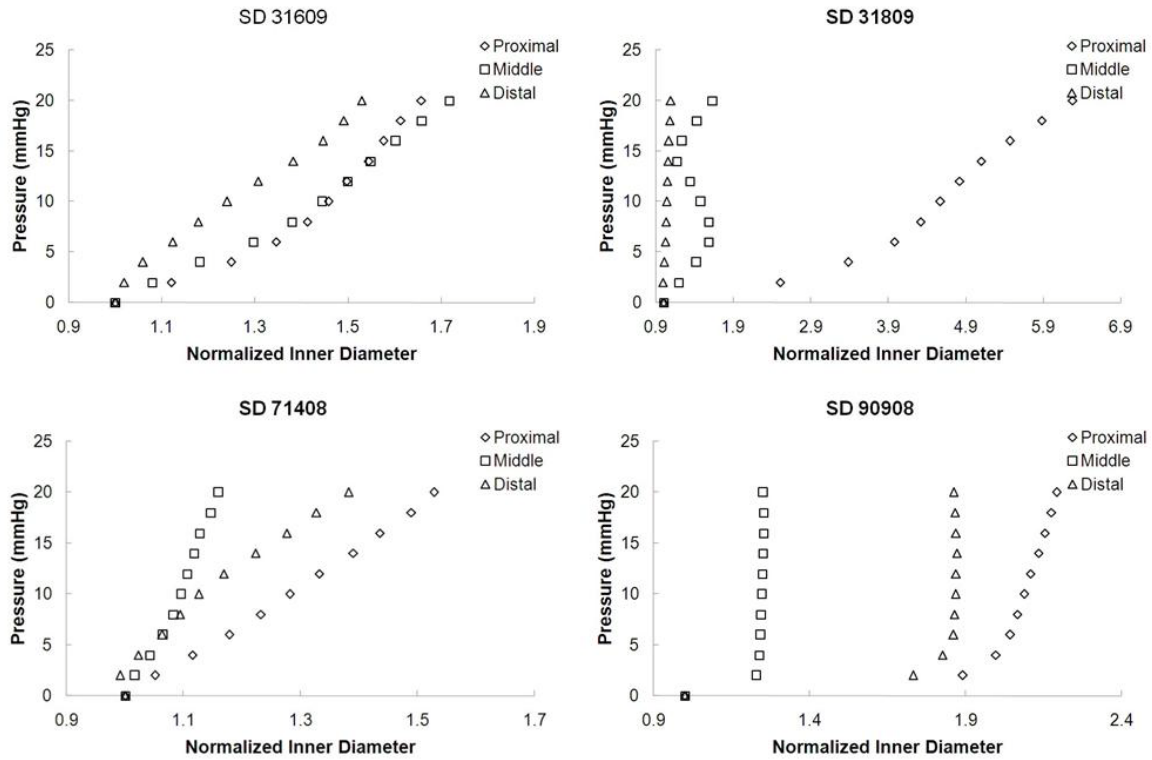
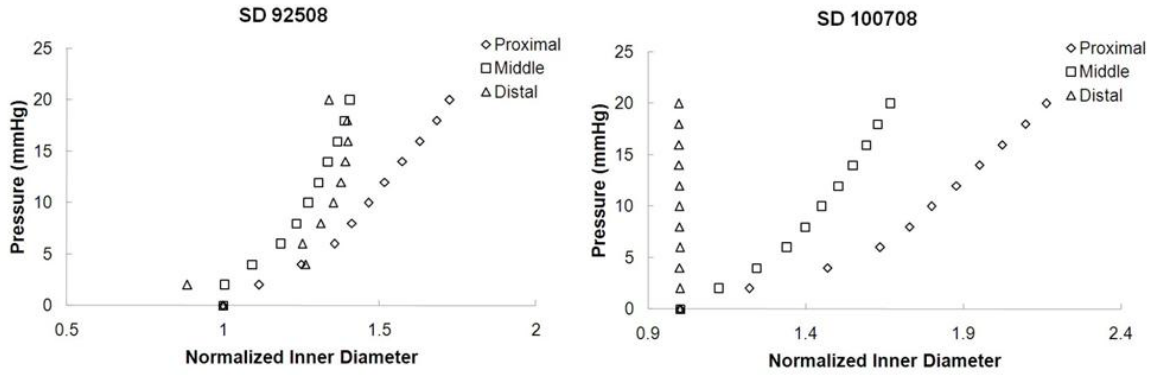
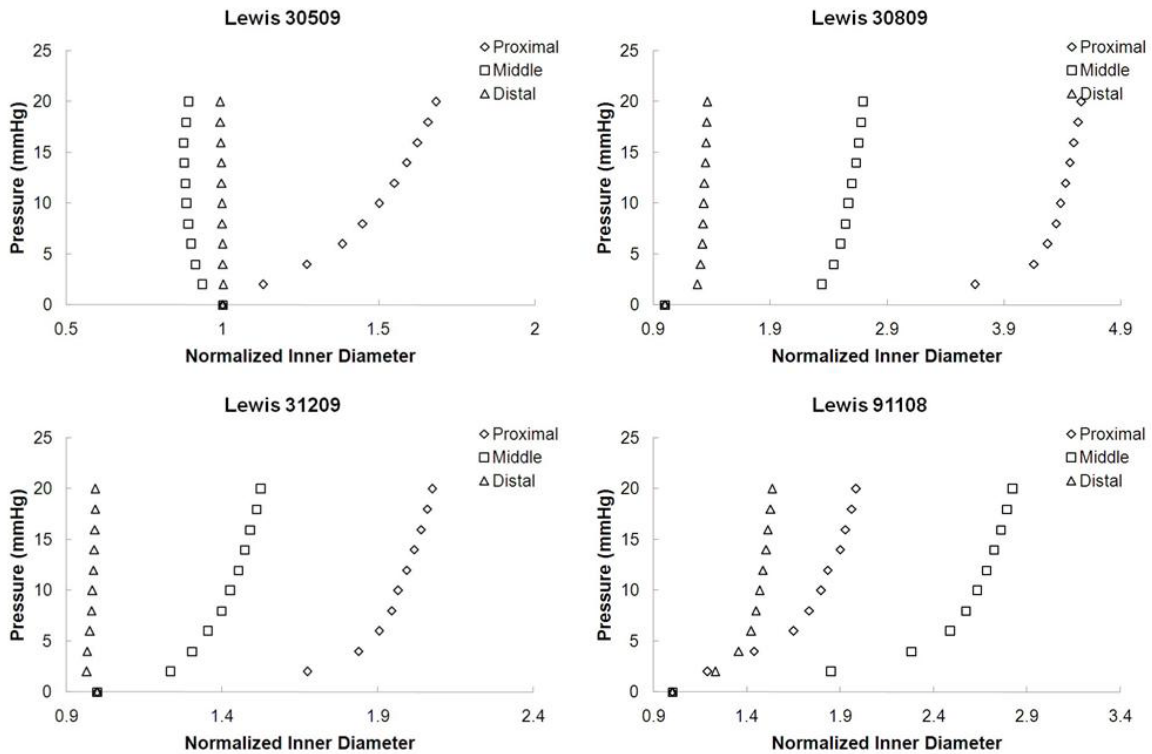


Figure G.45 Baseline pressure-diameter curves for SD alphabungarotoxin proximal, middle and distal segments.



**Figure G.46** Baseline pressure-diameter curves for SD alphabungarotoxin proximal, middle and distal segments.

### ALPHABUNGAROTOXIN PASSIVE



**Figure G. 47** Passive pressure-diameter curves for Lewis alphabungarotoxin proximal, middle and distal segments.

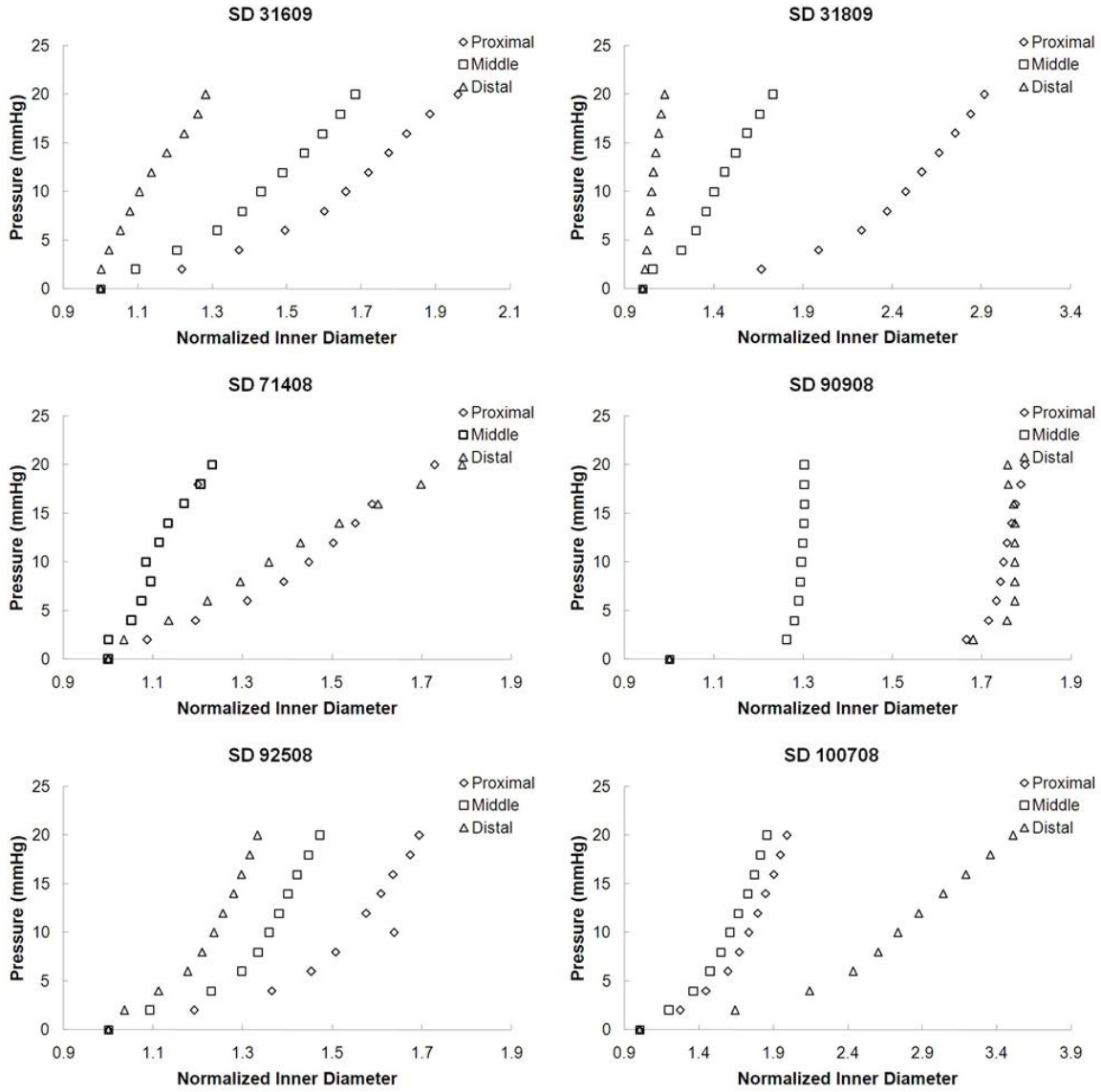


Figure G.48 Passive pressure-diameter curves for SD alphabungarotoxin proximal, middle and distal segments.

### 3 WEEK SD ACTIVE

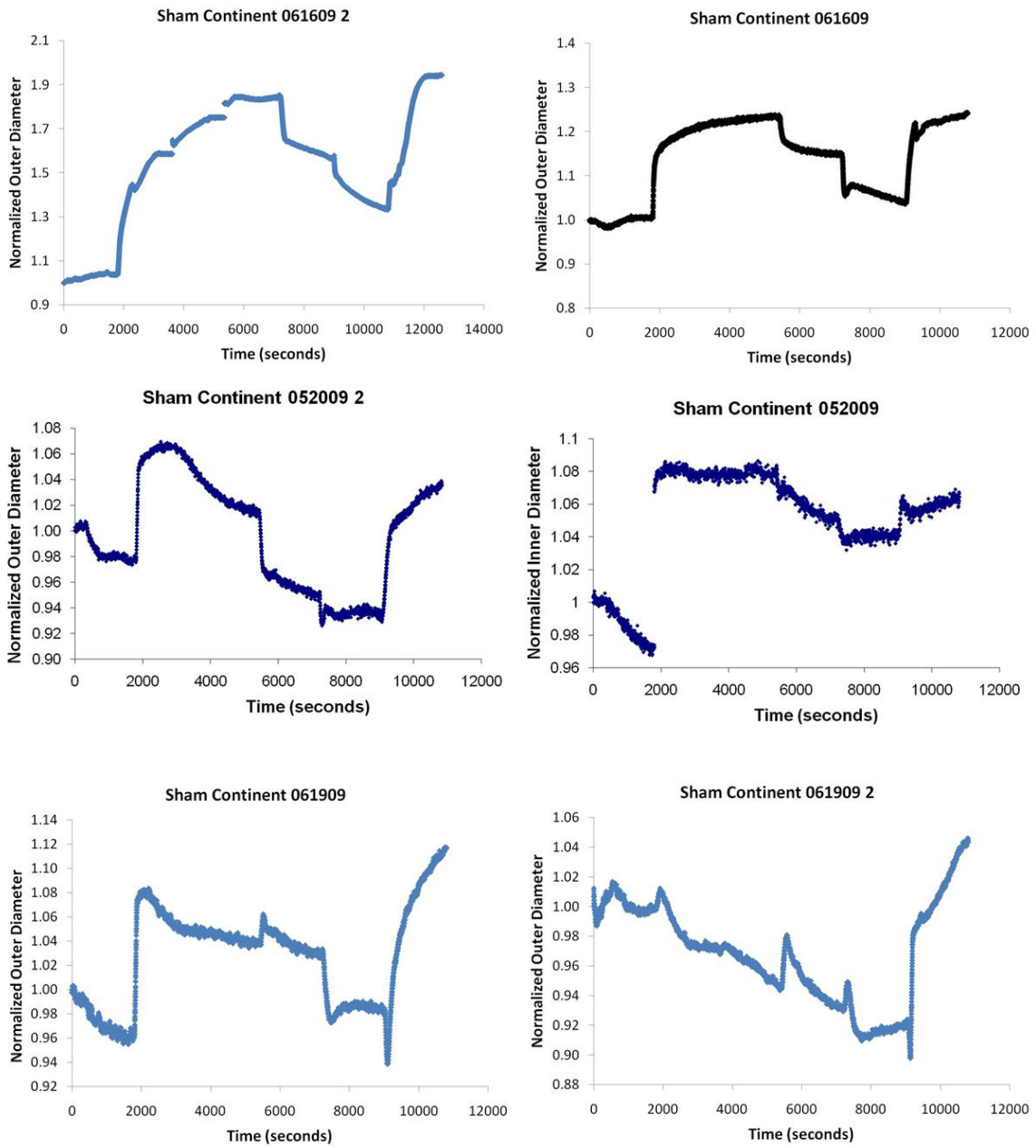


Figure G.49 Active curves for SC middle segment.

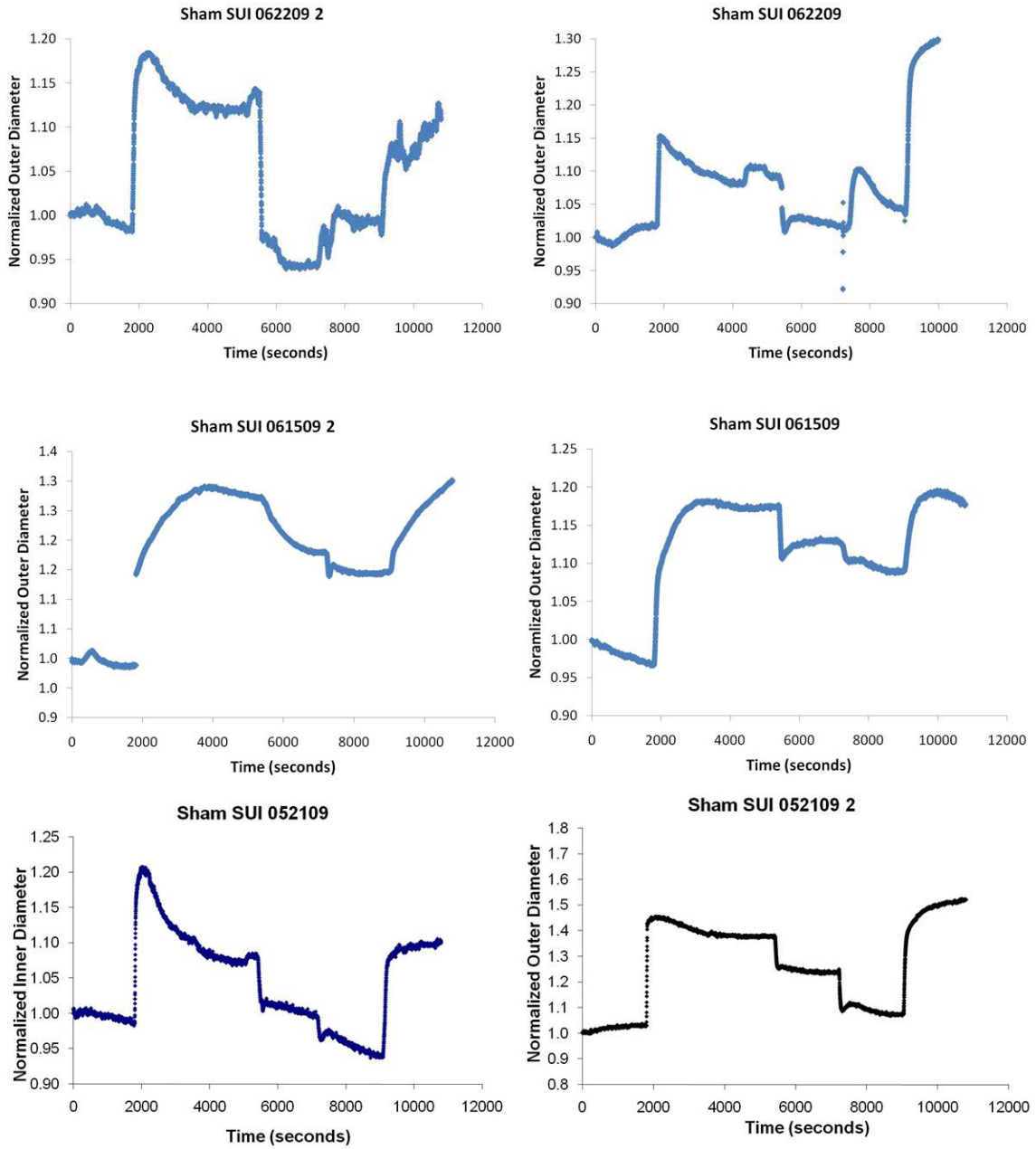
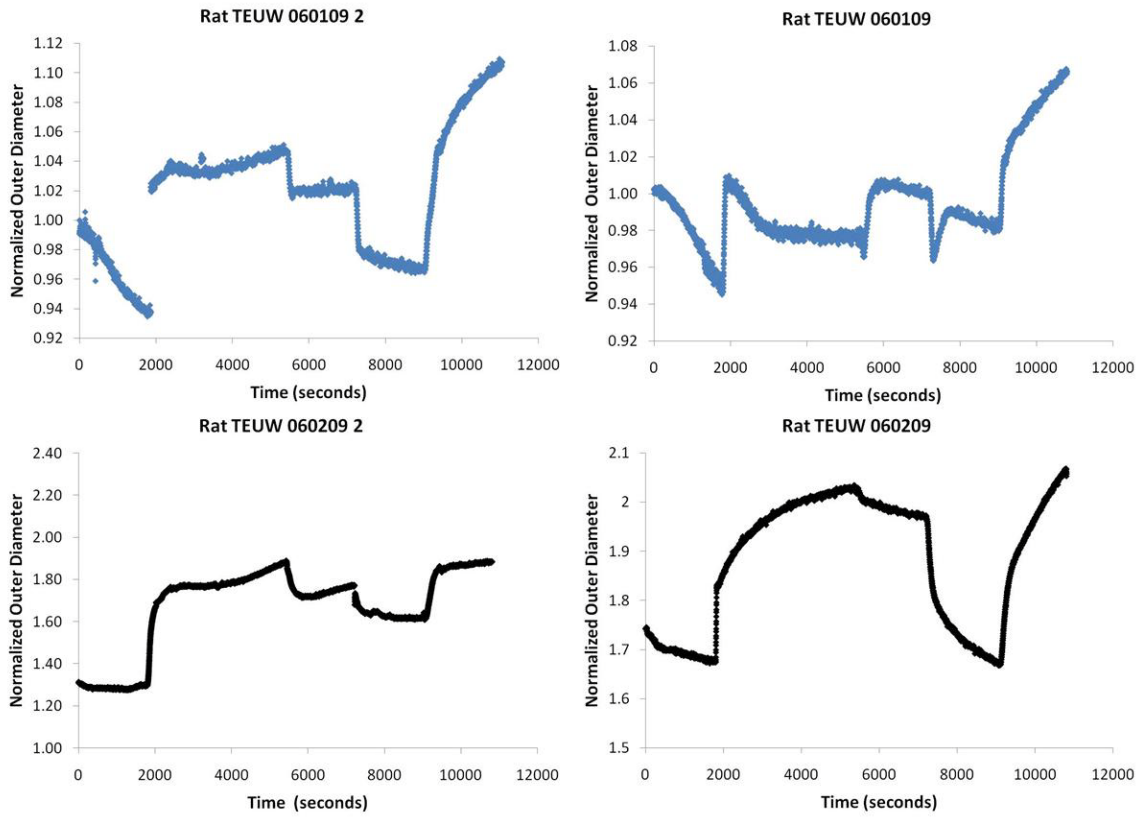


Figure G.50 Active curves for SS middle segment.



**Figure G.51** Active curves for RT middle segment.

**APPENDIX H**

**HISTOLOGY**

**1 WEEK TRICHROME**

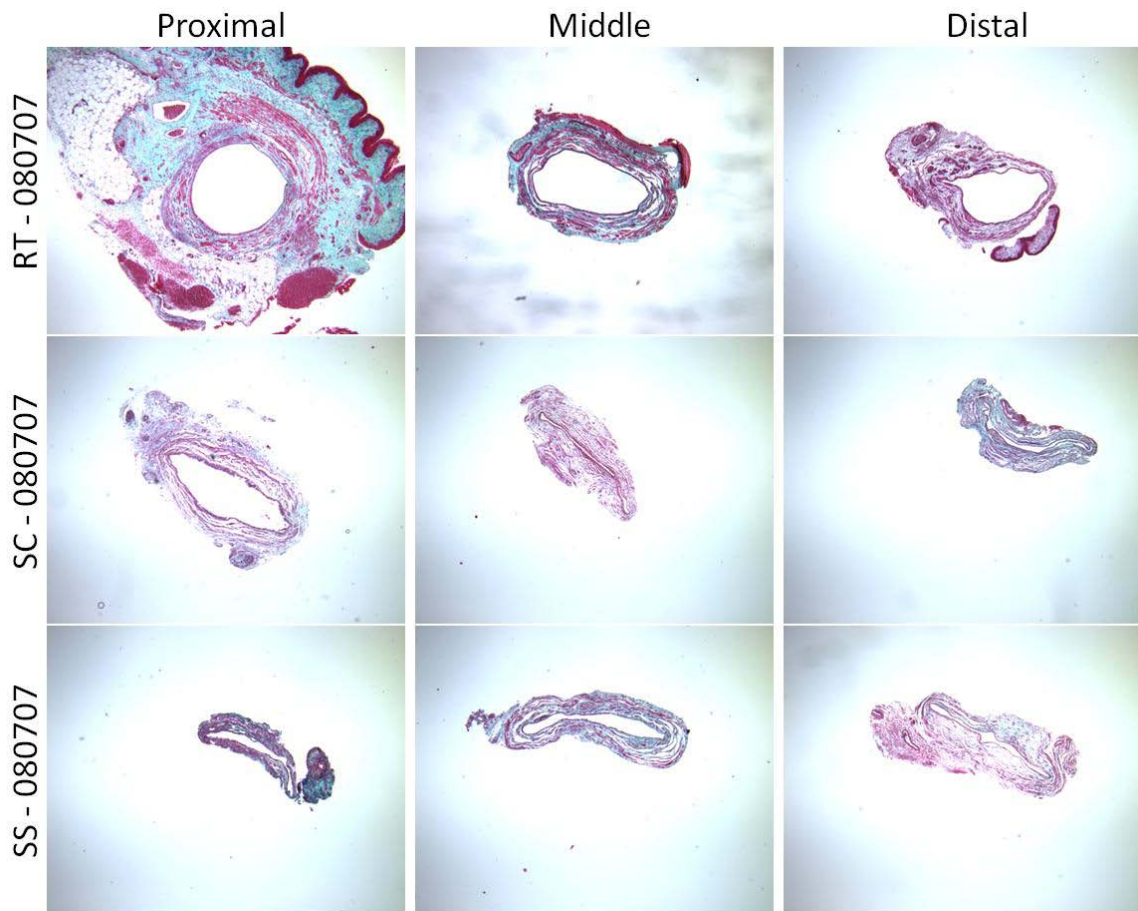


**Figure H.1** Representative Masson's Trichrome for 1 week RT, SC and SS.

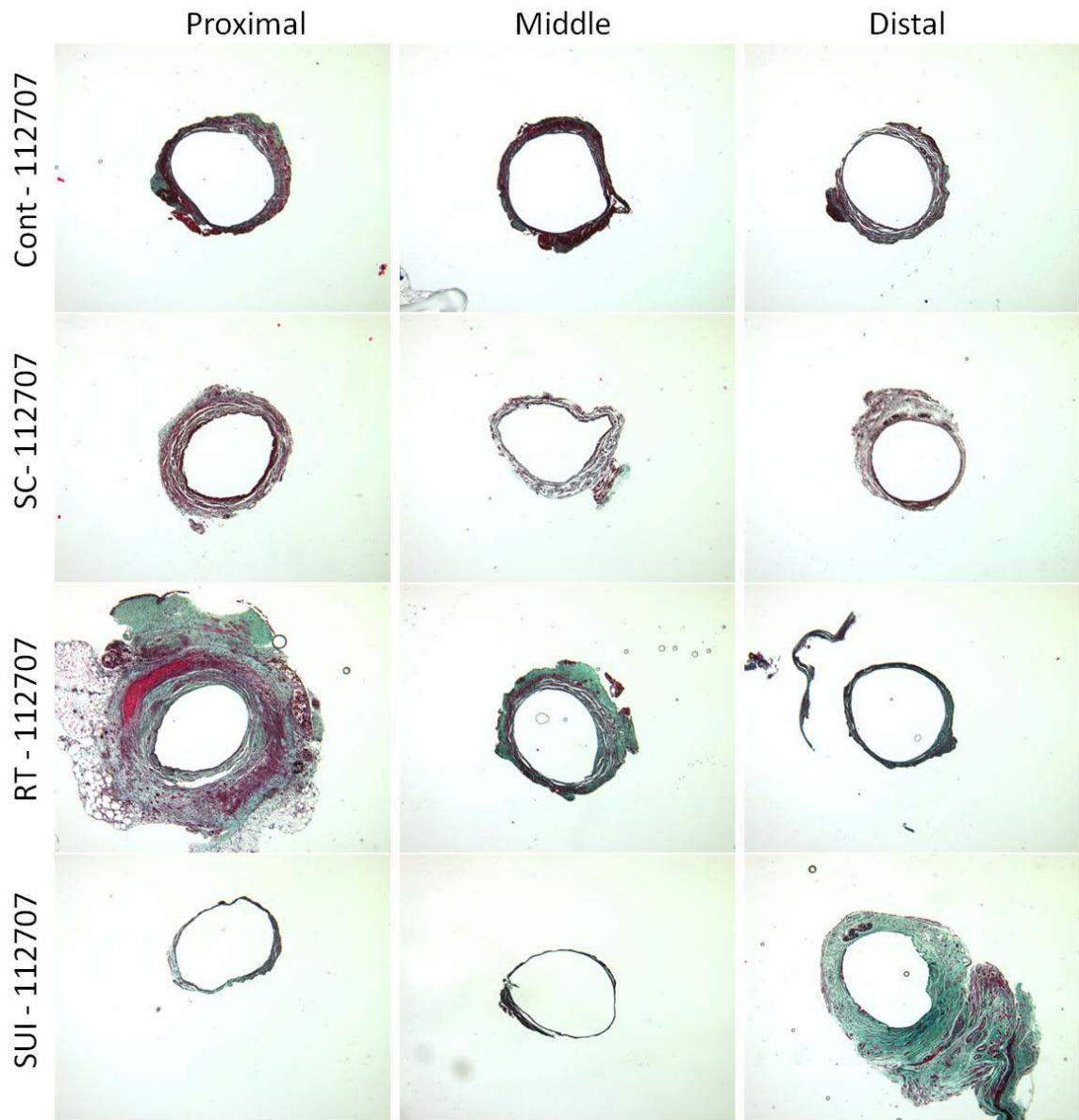


**Figure H.2** Representative Masson's Trichrome for 1 week Lewis Cont, SC, RT and SUI.

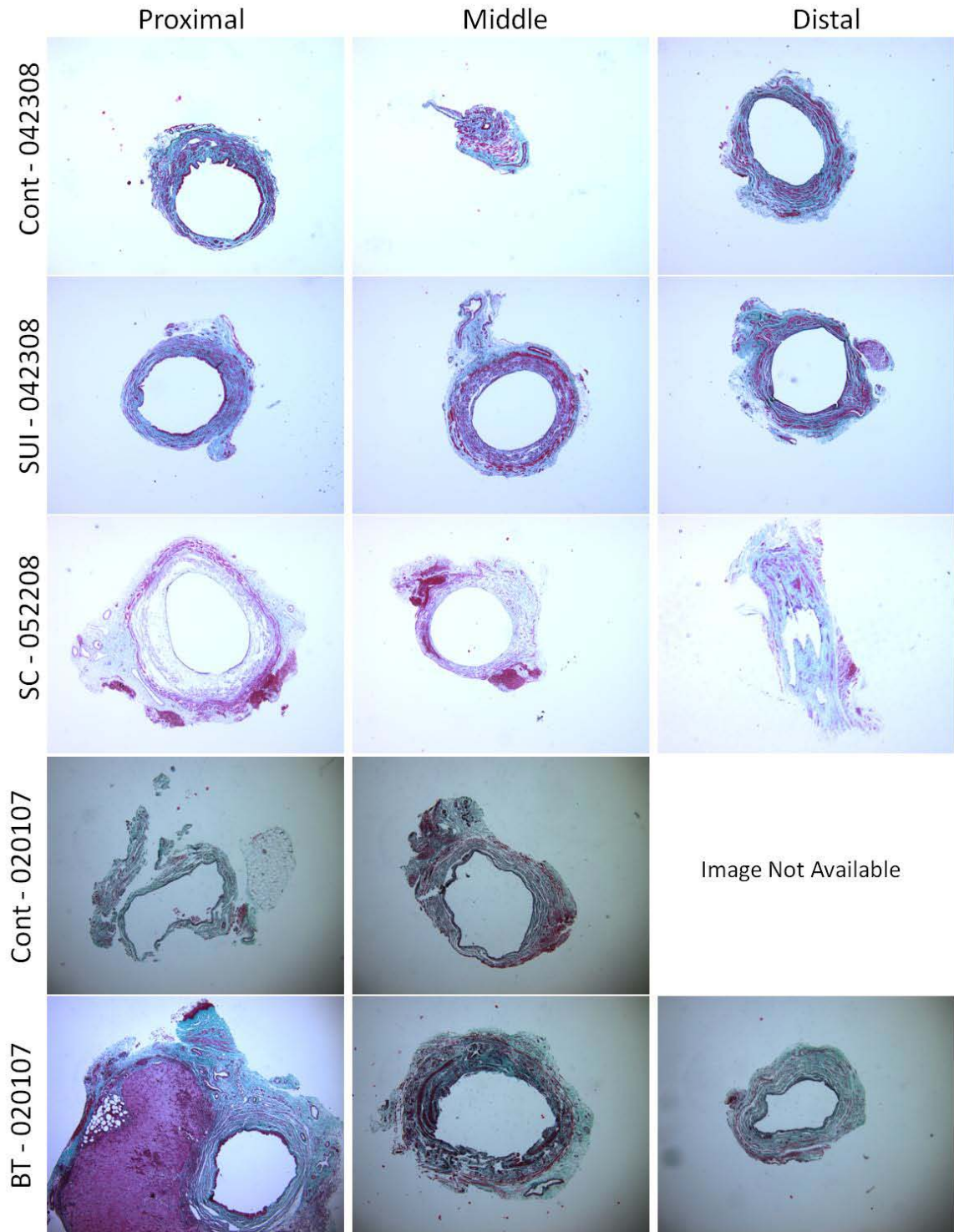


**Figure H. 3** Representative Masson's Trichrome for 1 week Cont, SUI, and BT.

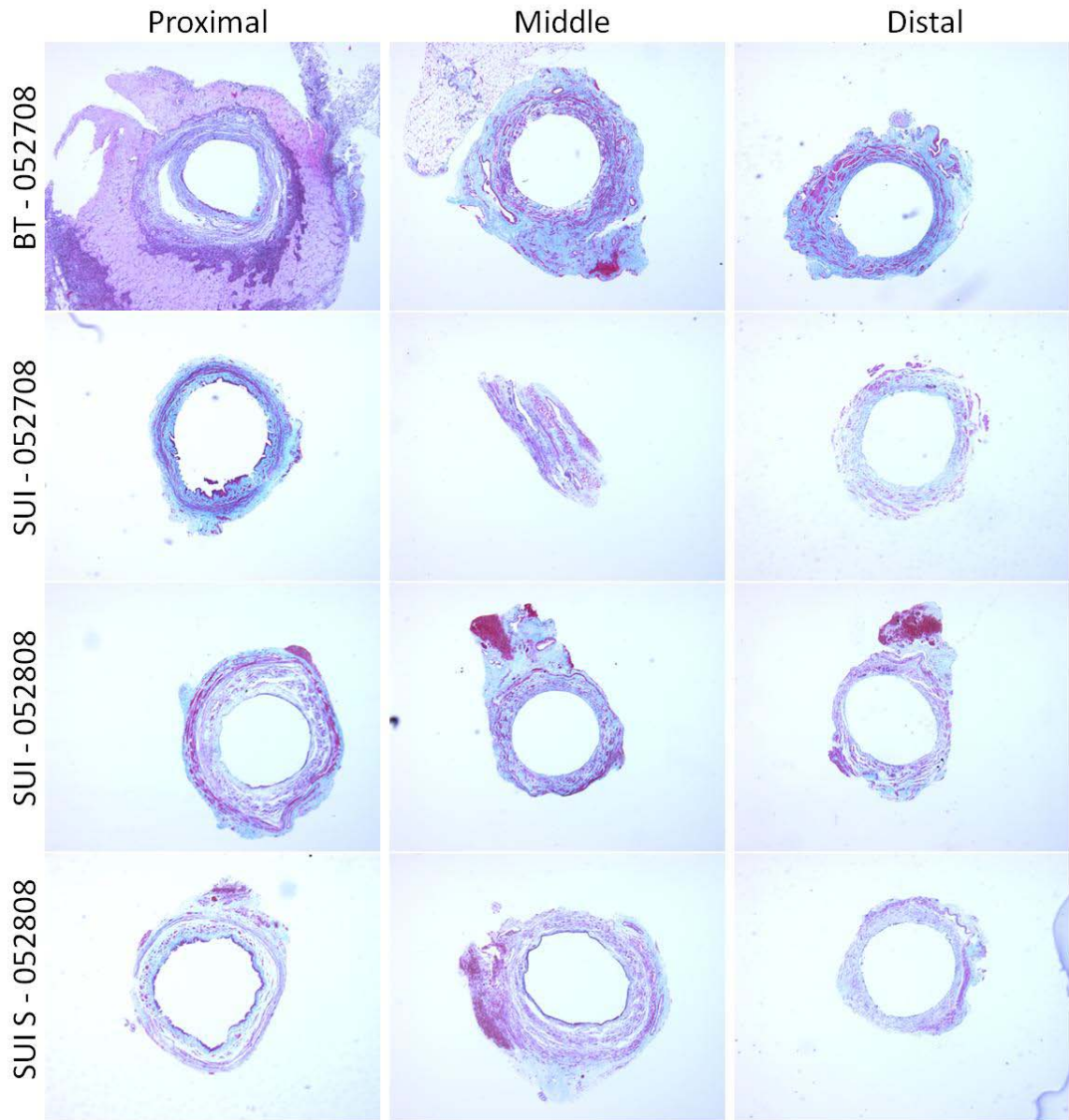


**Figure H. 4** Representative Masson's Trichrome for 1 week BT and SUI.

### 3 WEEK LEWIS TRICHROME

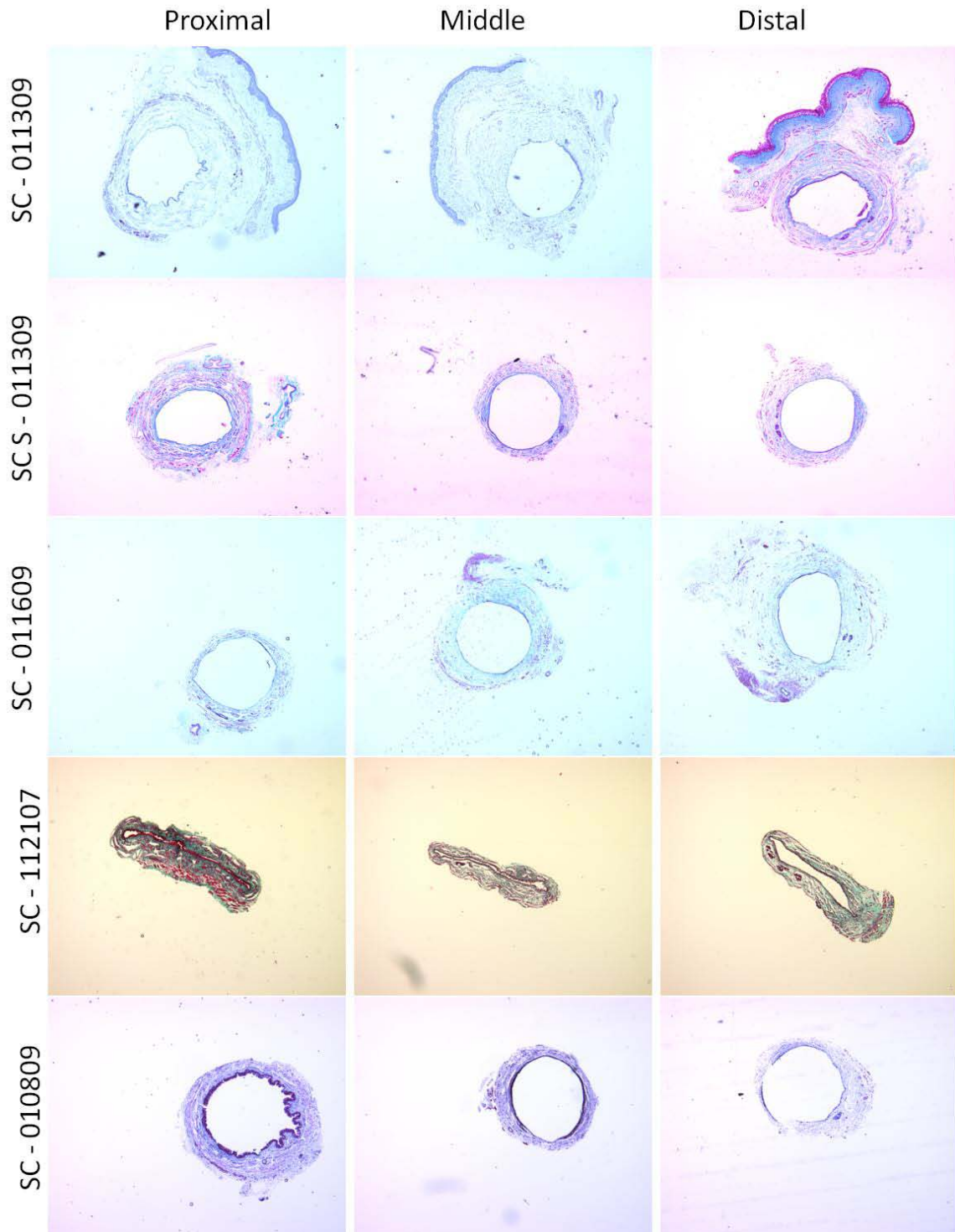


**Figure H.5** Representative Masson's Trichrome for 3 week SC.

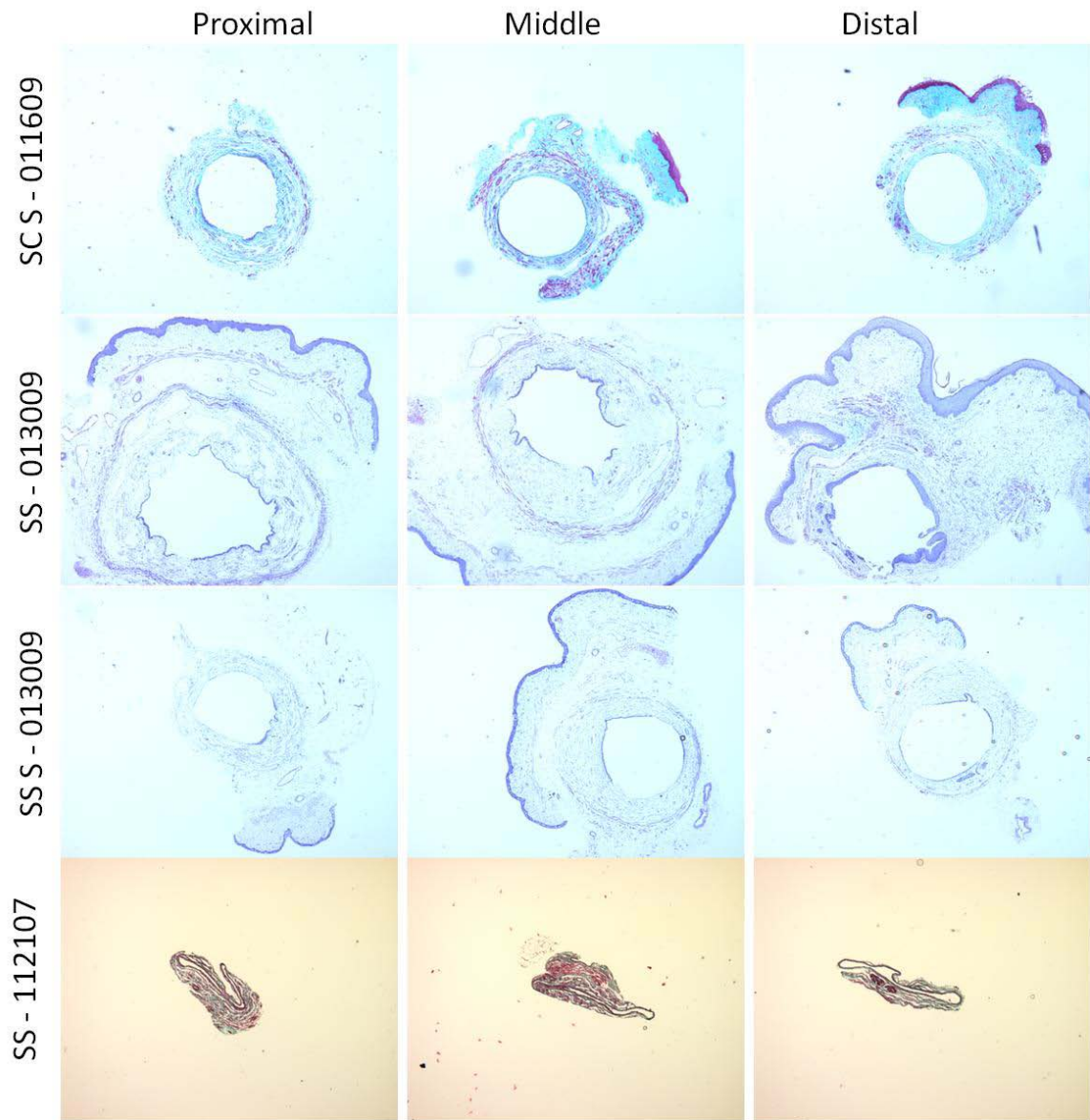


**Figure H.6** Representative Masson's Trichrome for 3 week SC and SS.

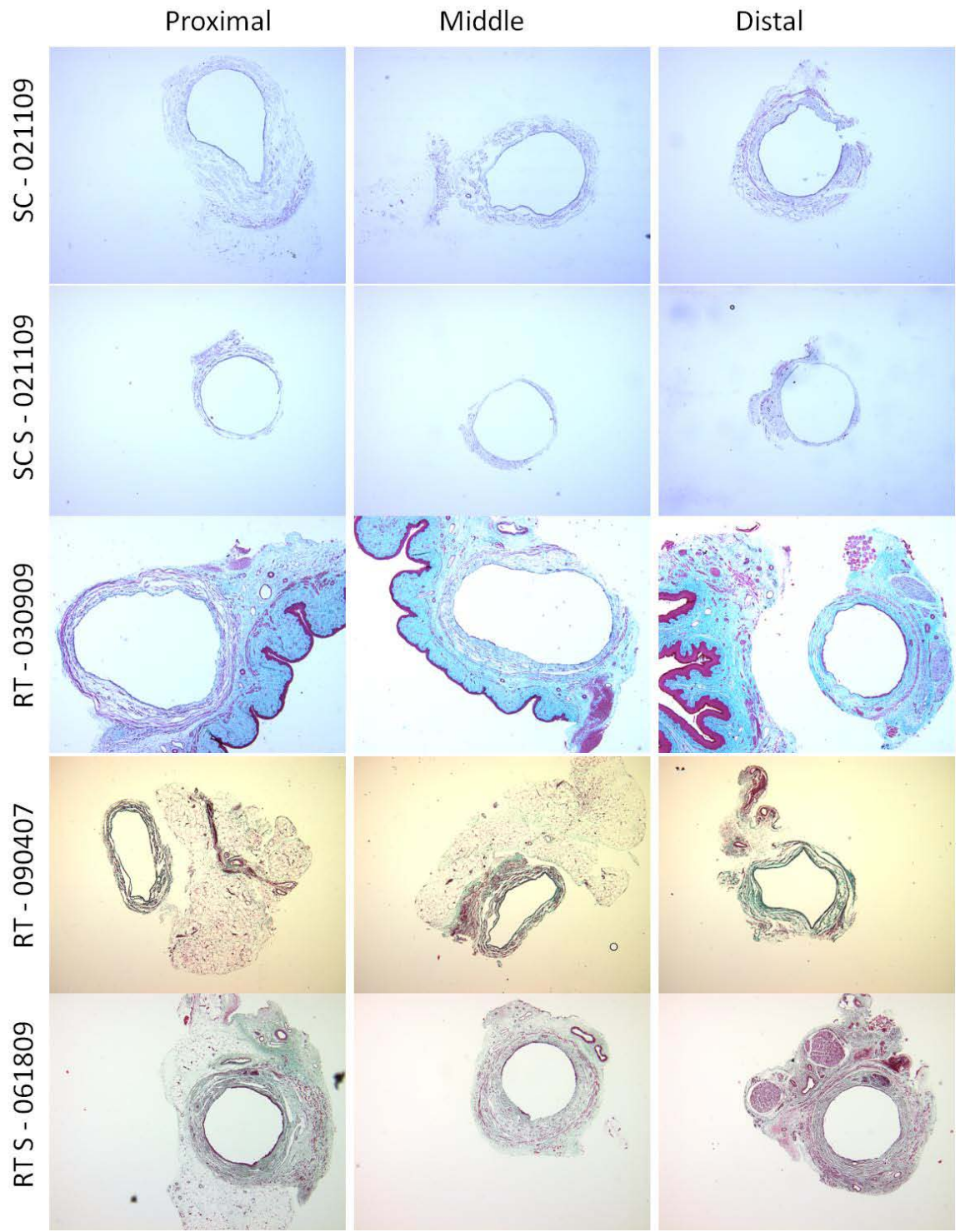


**Figure H.7** Representative Masson's Trichrome for 3 week SC and RT.

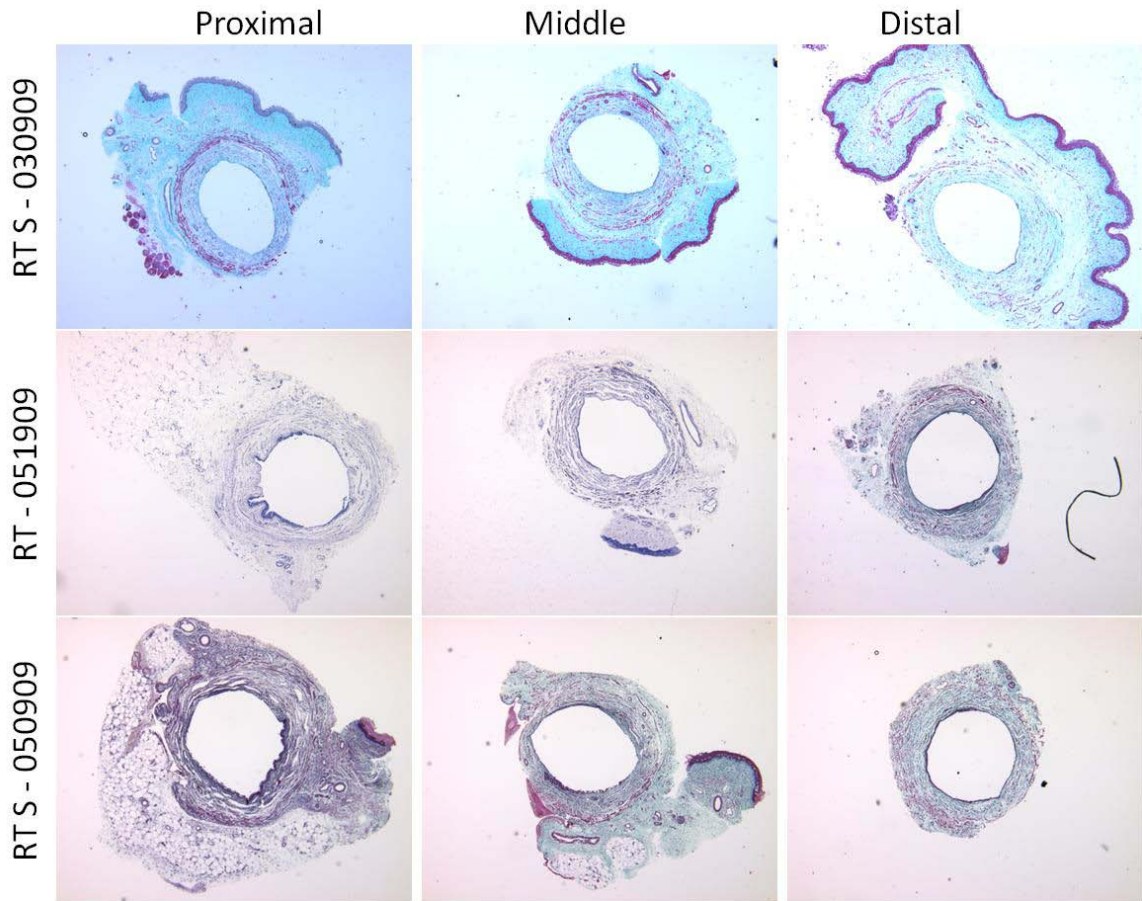


**Figure H.8** Representative Masson's Trichrome for 3 week RT.

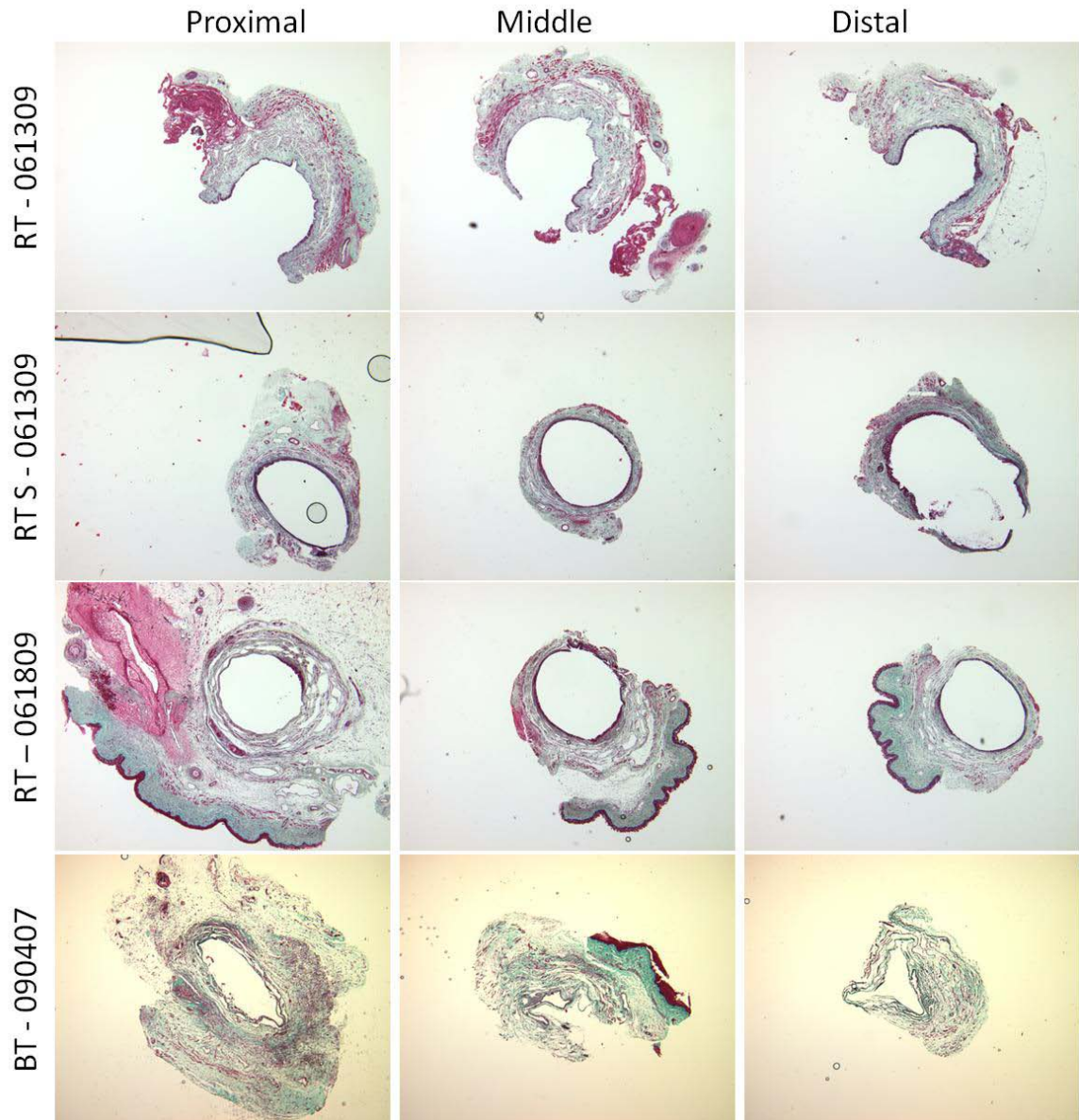


**Figure H.9** Representative Masson's Trichrome for 3 week RT and BT.

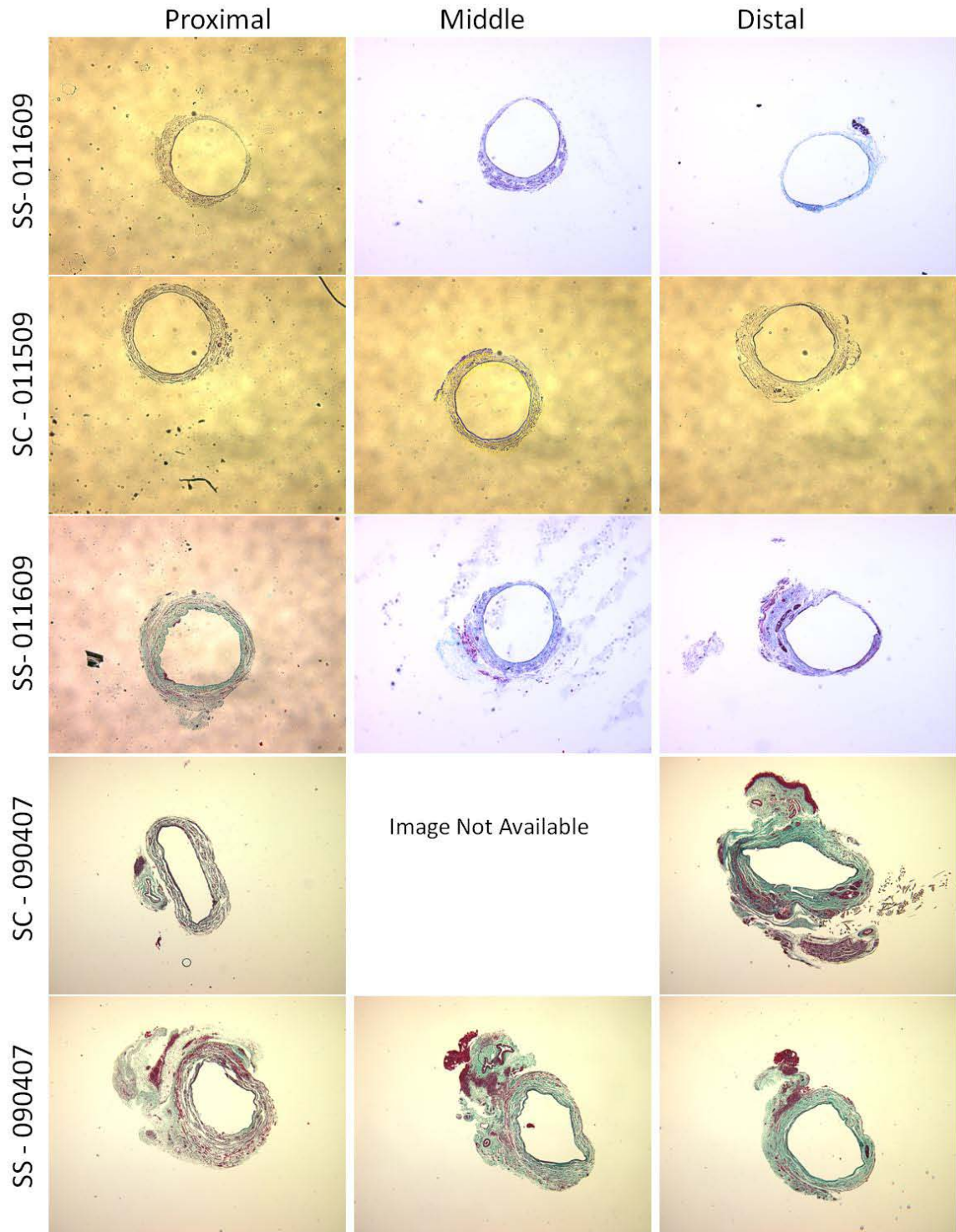


**Figure H.10** Representative Masson's Trichrome for 3 week SC and SS.

### 3 WEEK SD TRICHROME

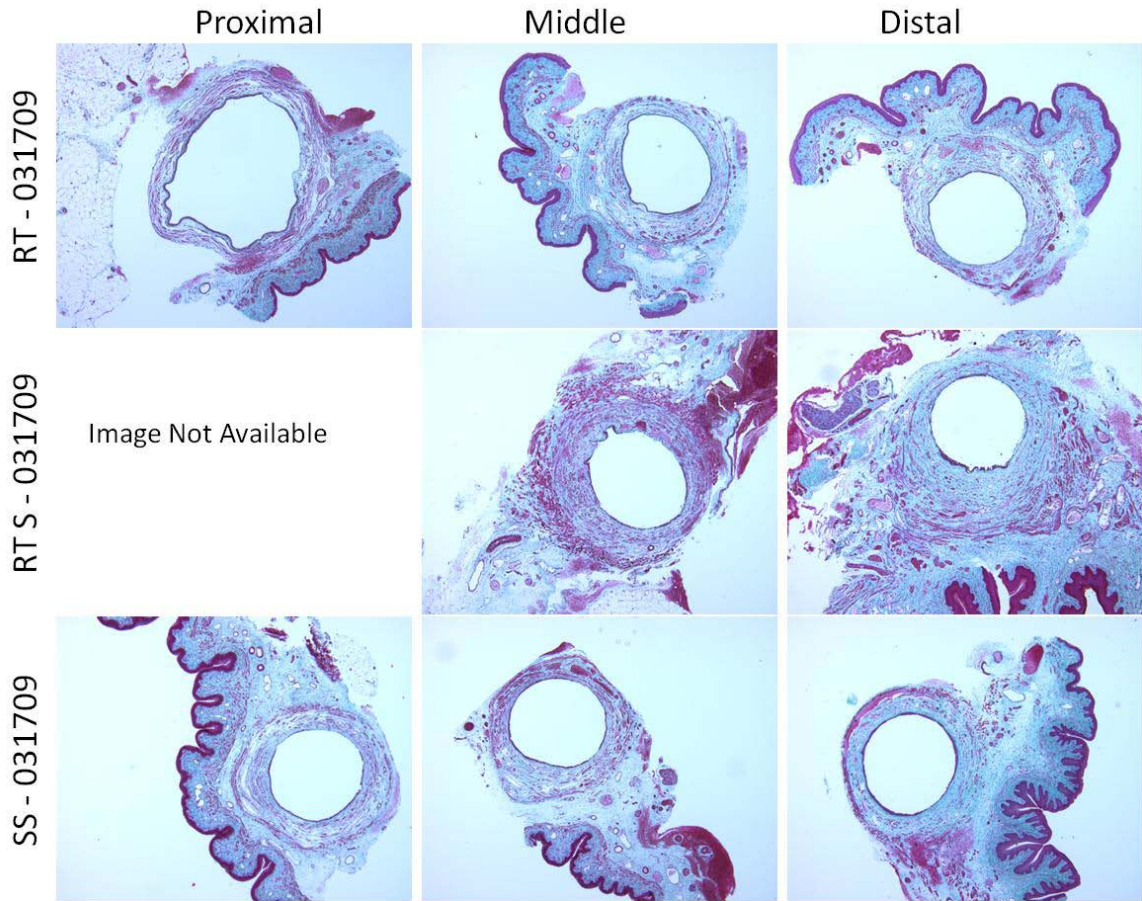


**Figure H.11** Representative Masson's Trichrome for 3 week RT and SS.

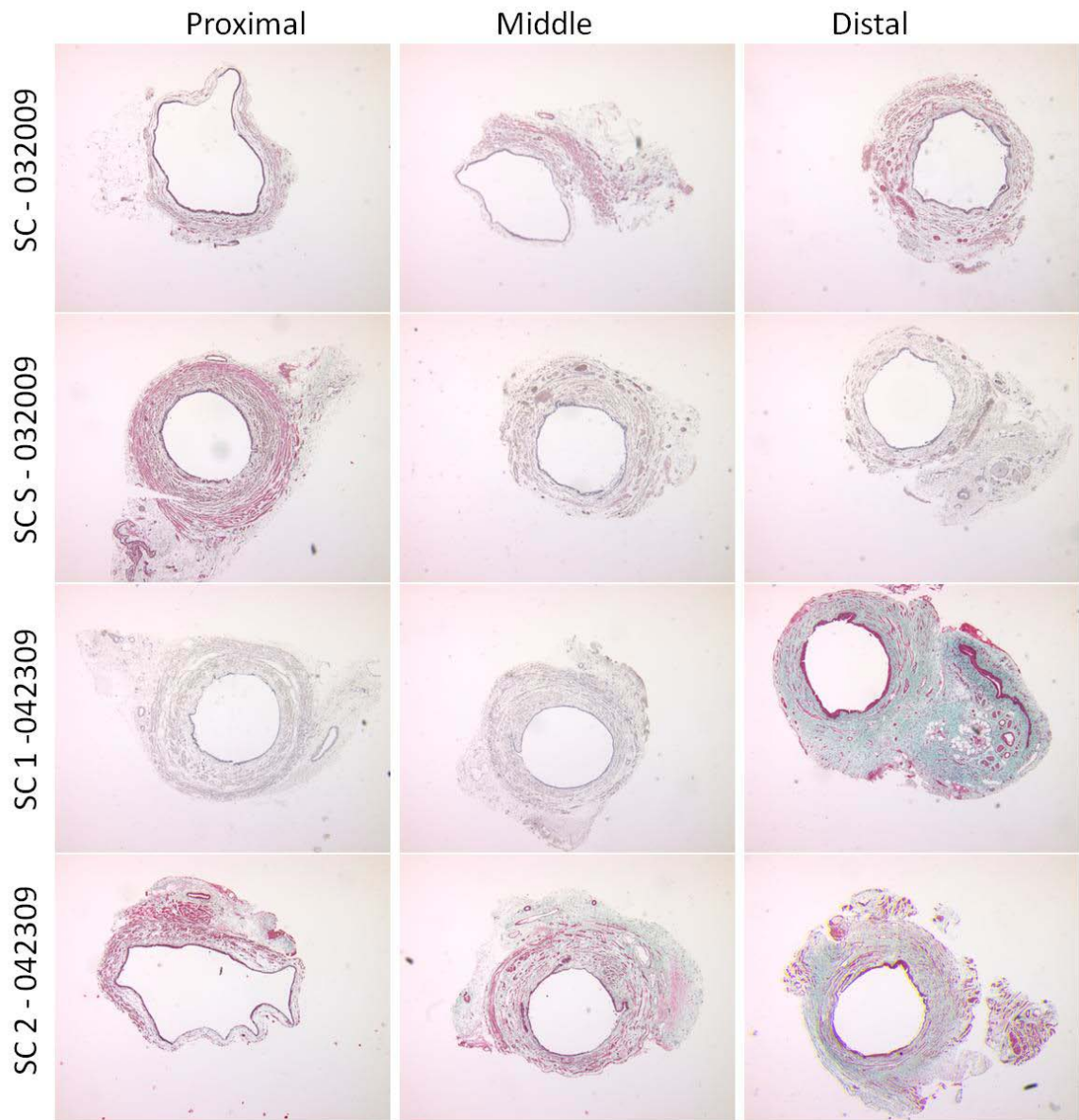


**Figure H.12** Representative Masson's Trichrome for 3 week RT and SS.

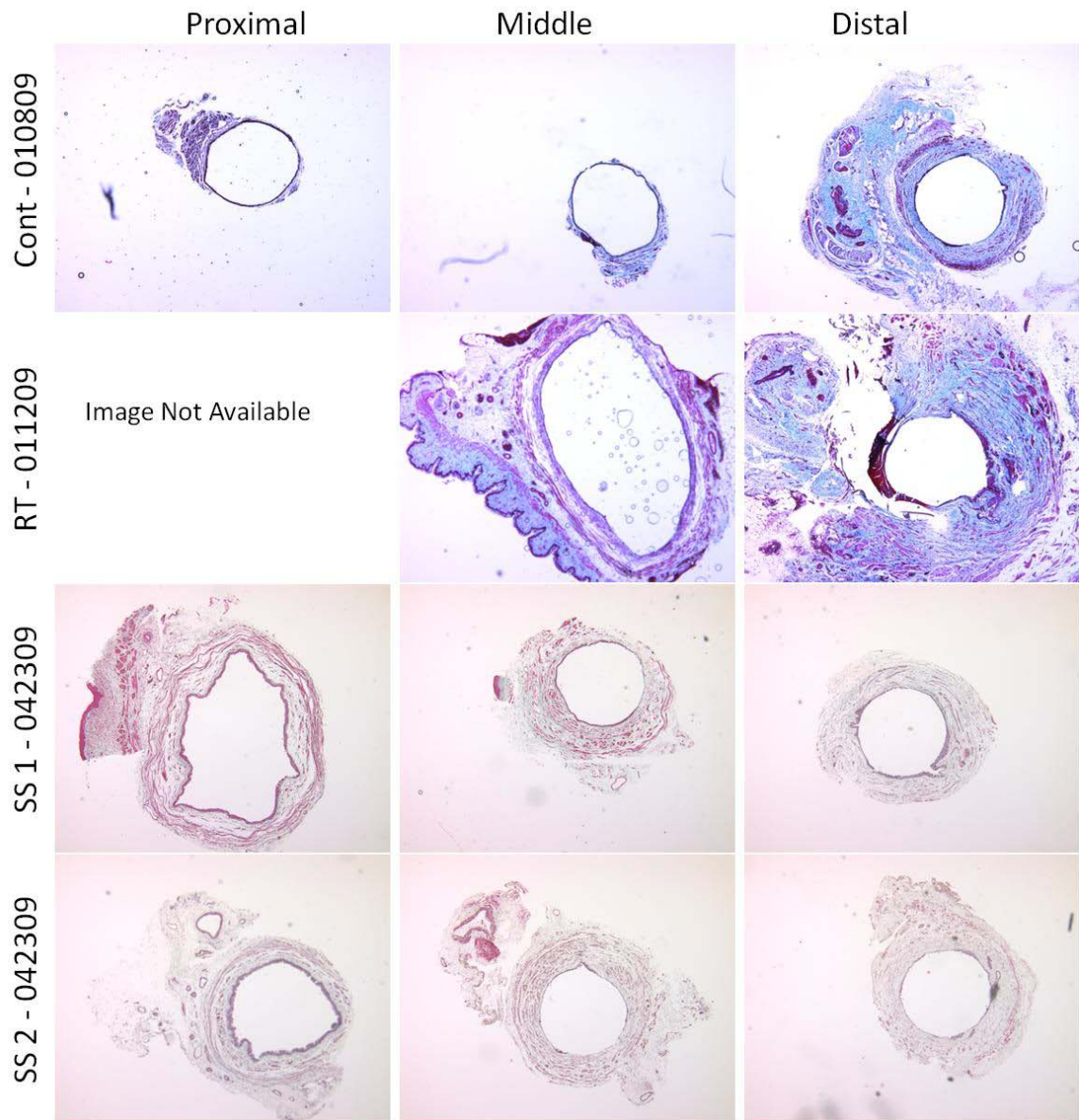


**Figure H.13** Representative Masson's Trichrome for 3 week Cont, RT and SS.

**4 WEEK TRICHROME**

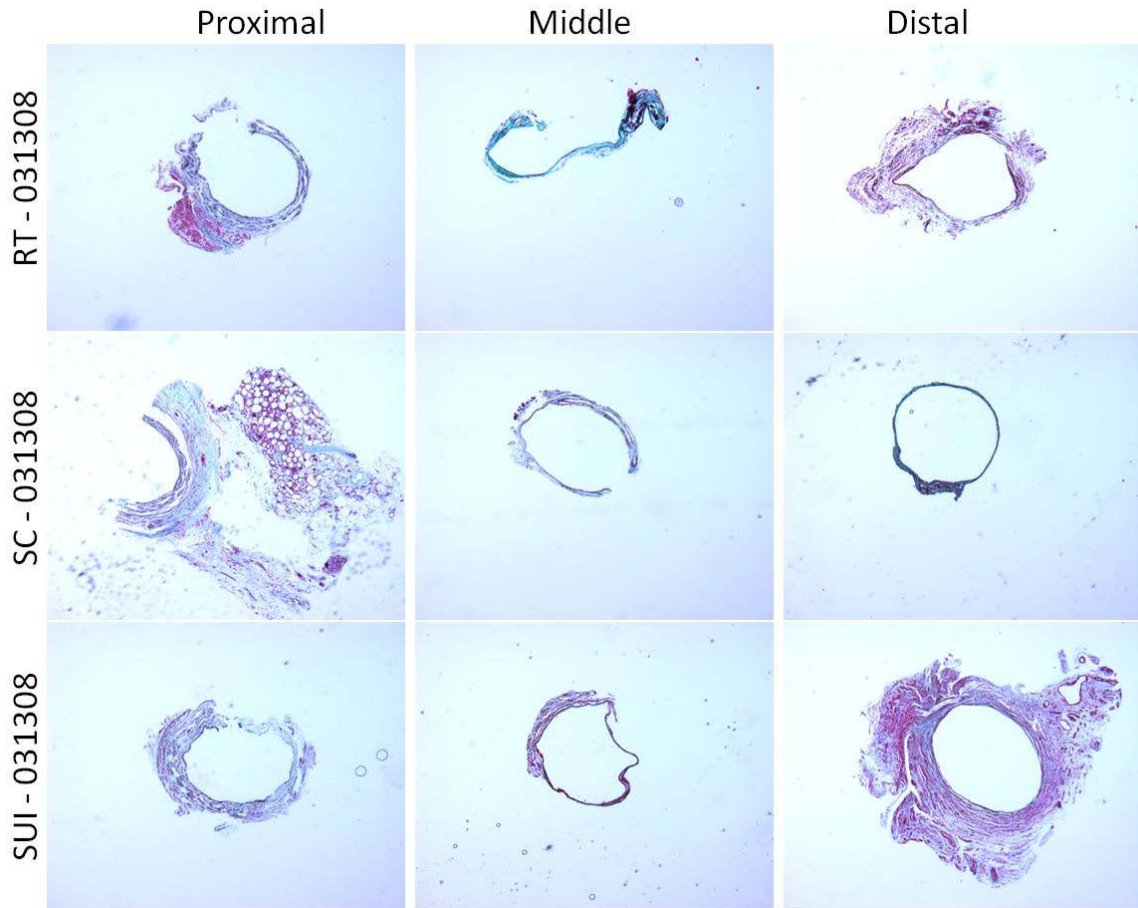


**Figure H.14** Representative Masson's Trichrome for 4 week RT, SC and SUI.

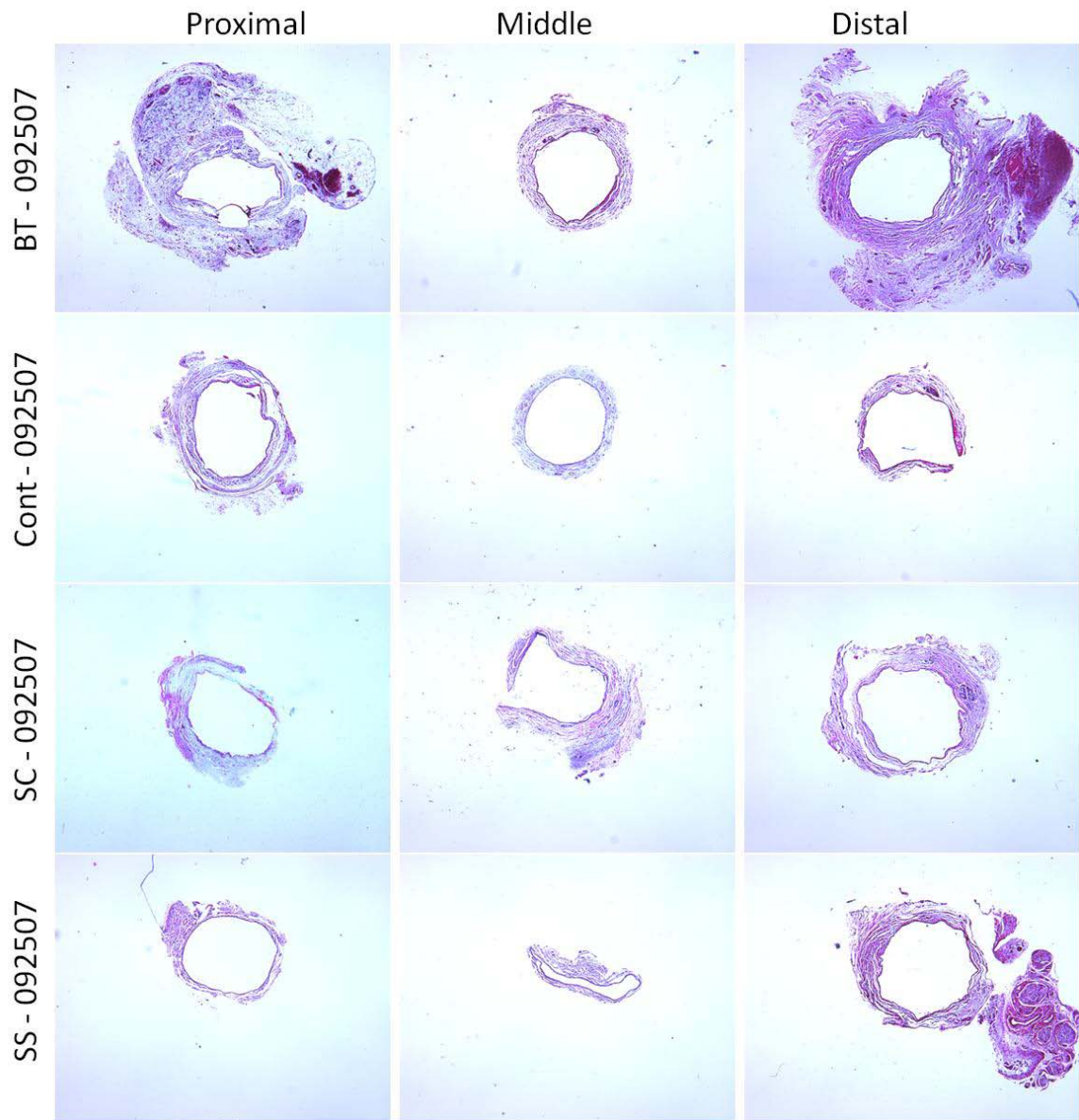


**Figure H.15** Representative Masson's Trichrome for 4 week BT, Cont, SC and SUI.

### 3 WEEK IN-VIVO PICROSIRIUS RED

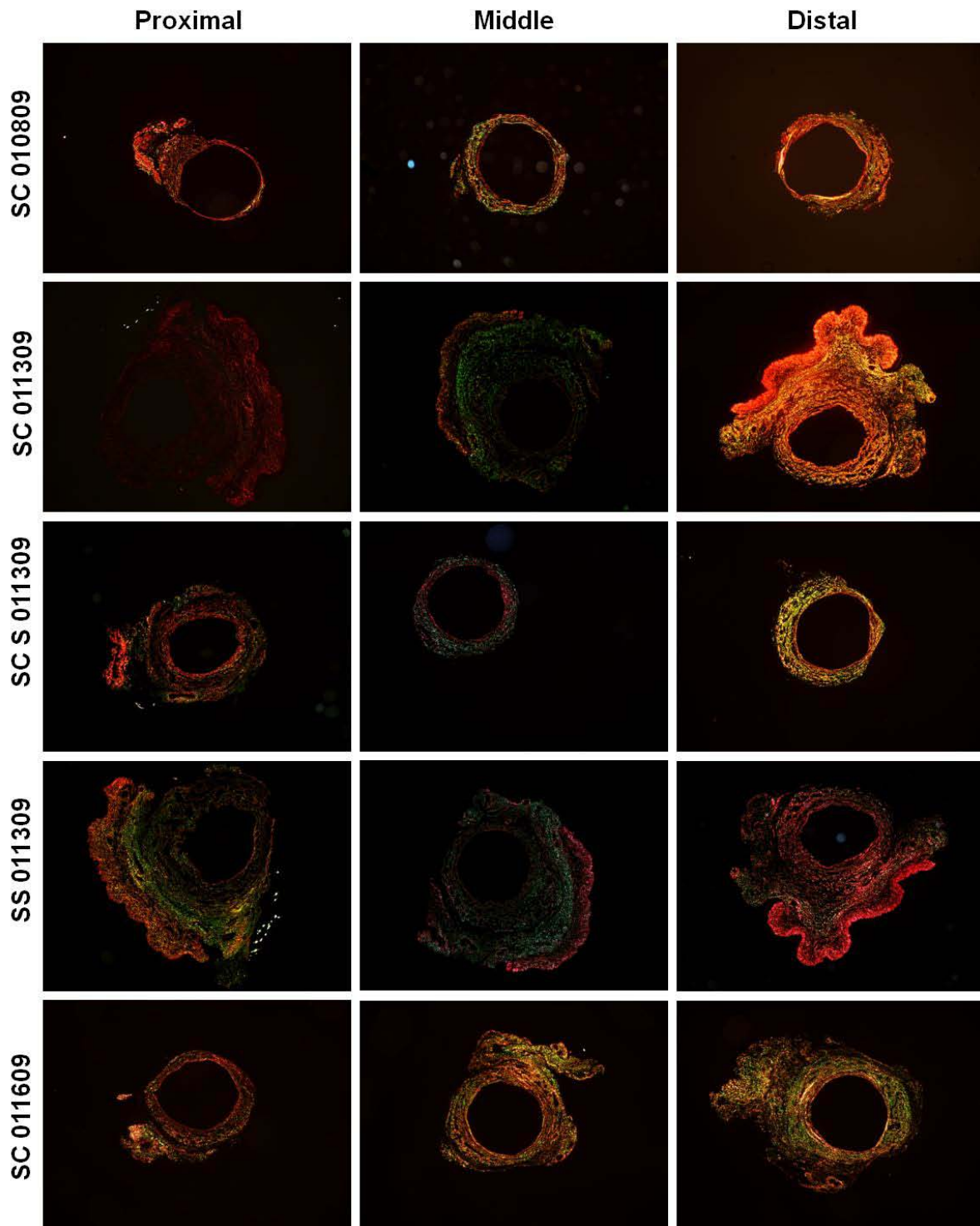


Figure H. 16 Representative PSR for 3 week SC and SS experiments.

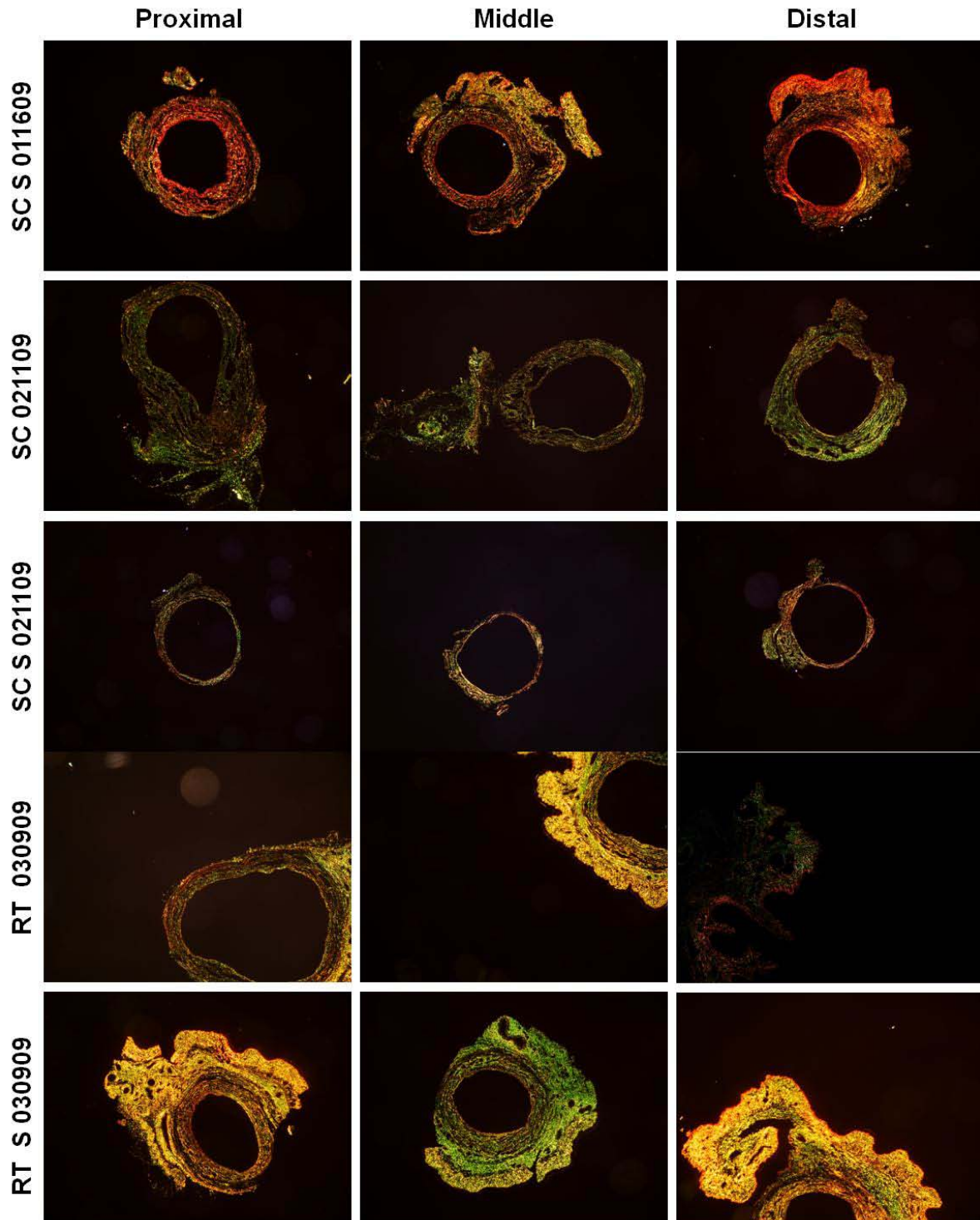


Figure H.17 Representative PSR for 3 week SC and RT experiments.

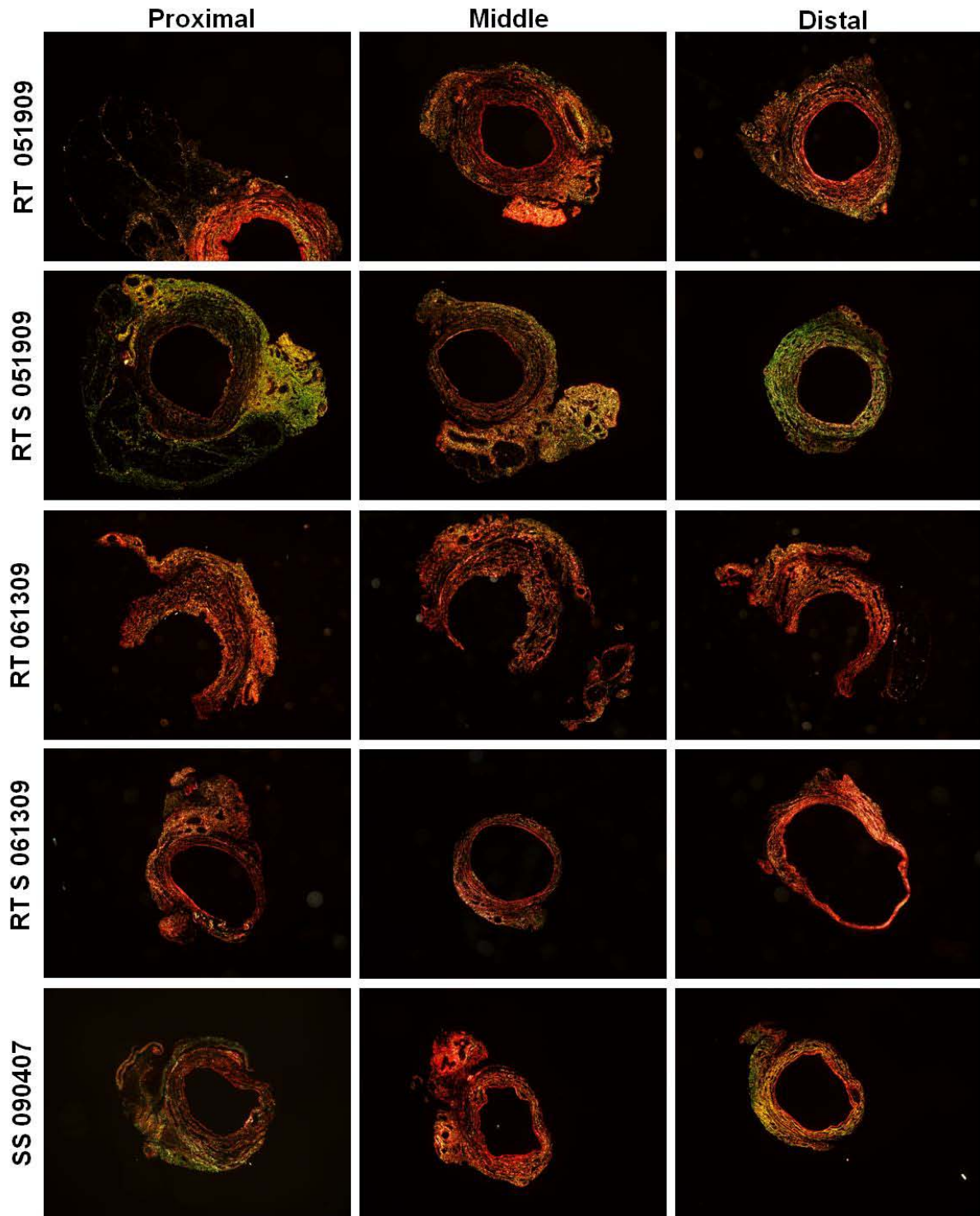


Figure H. 18 Representative PSR for 3 week SS and RT experiments.

## BIOREACTOR IMMUNOFLUORESCENCE

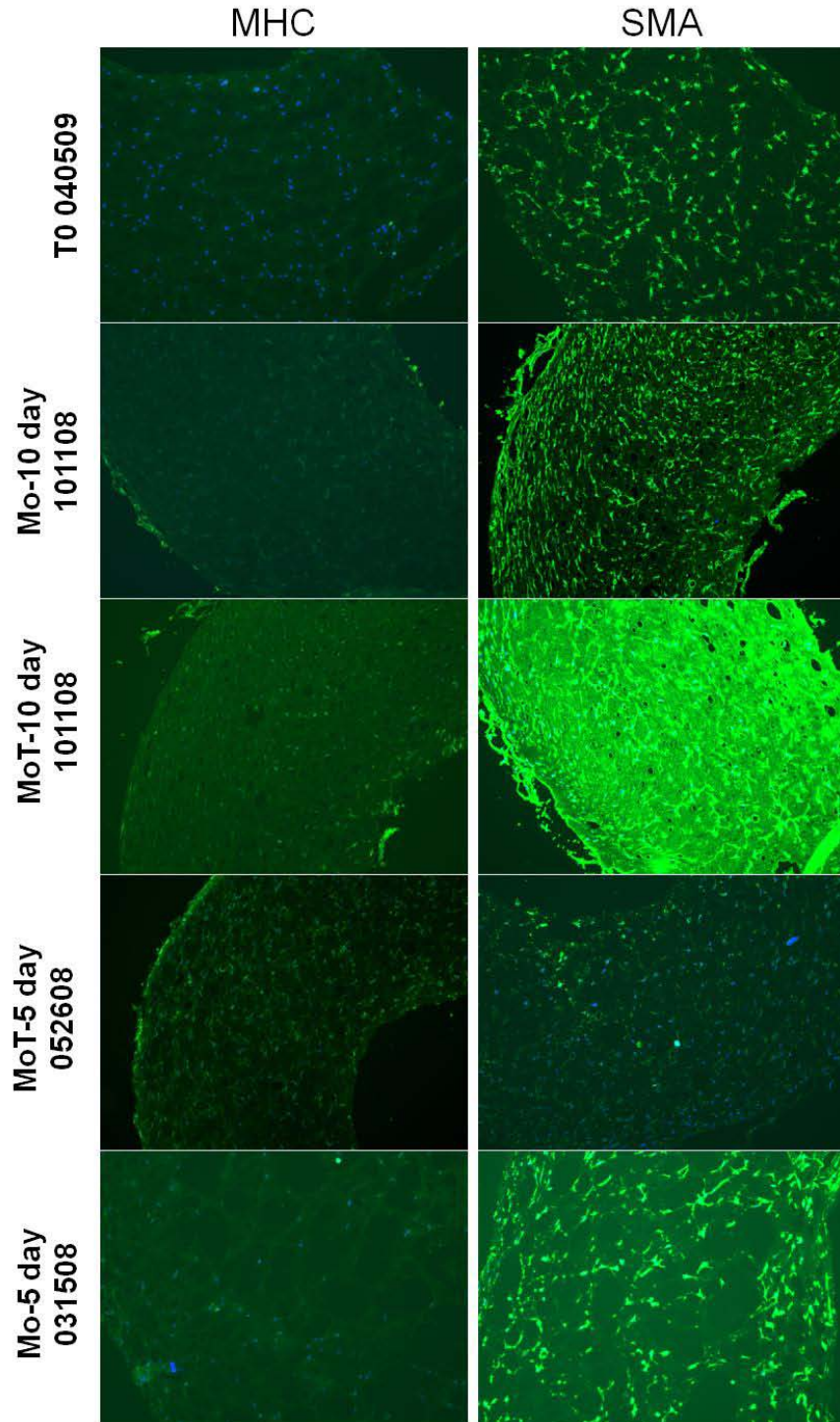
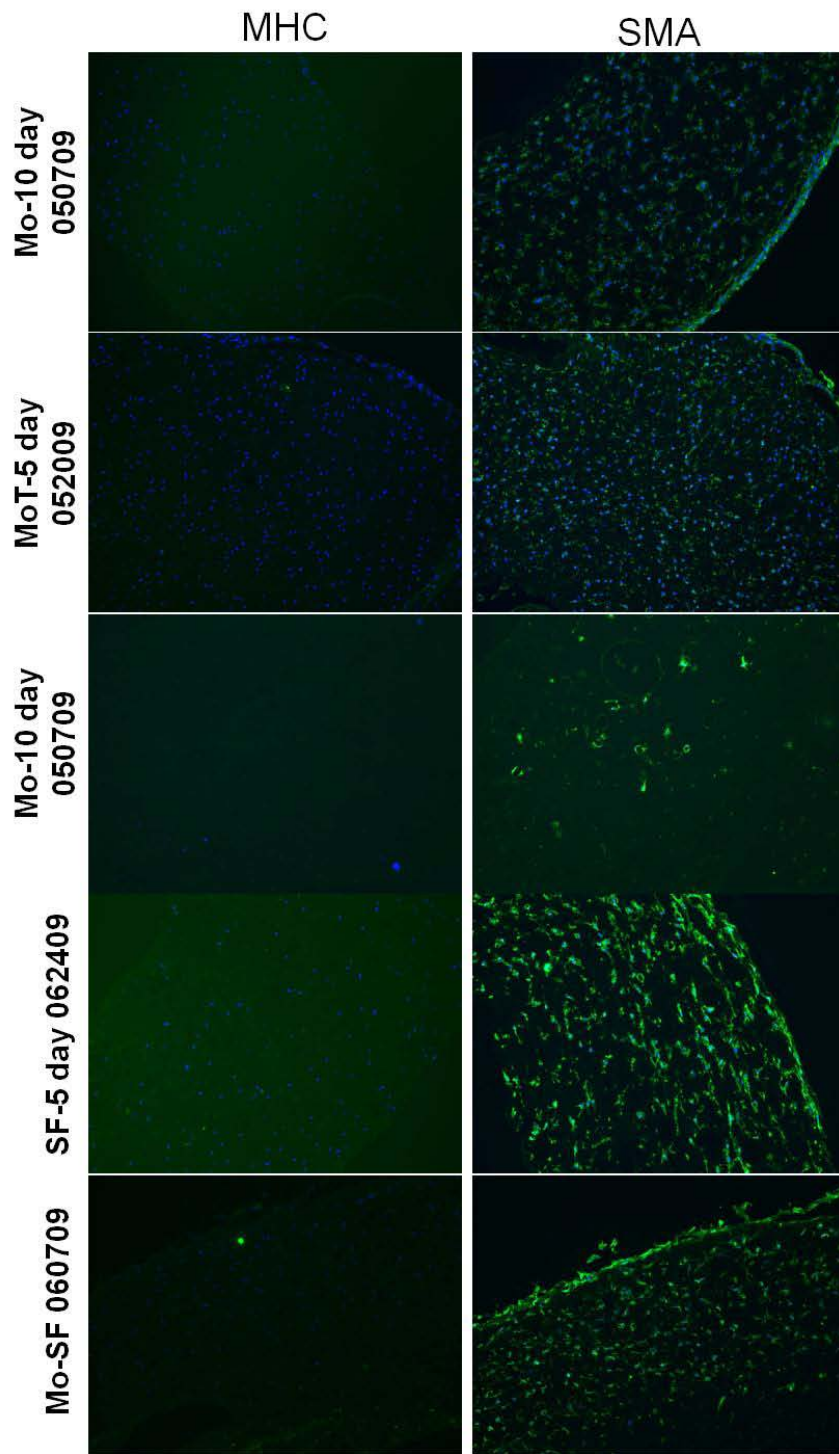


Figure H.19 Representative MHC and SMA staining for Mo, MoT and T0 bioreactor conditions.



**Figure H.20** Representative MHC and SMA staining for Mo, MoT and SF bioreactor conditions.

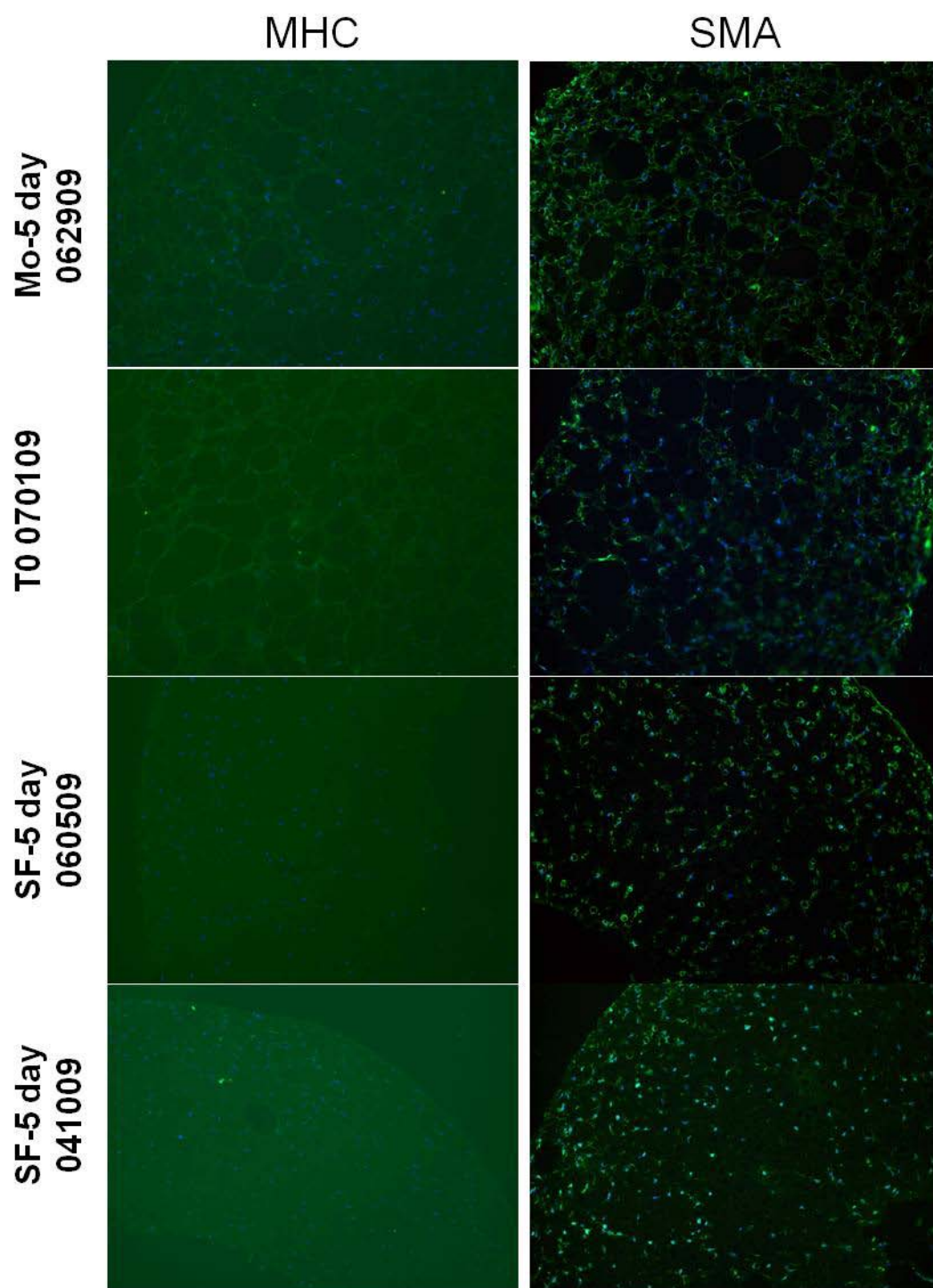


Figure H.21 Representative MHC and SMA staining for Mo, T0 and SF bioreactor conditions.

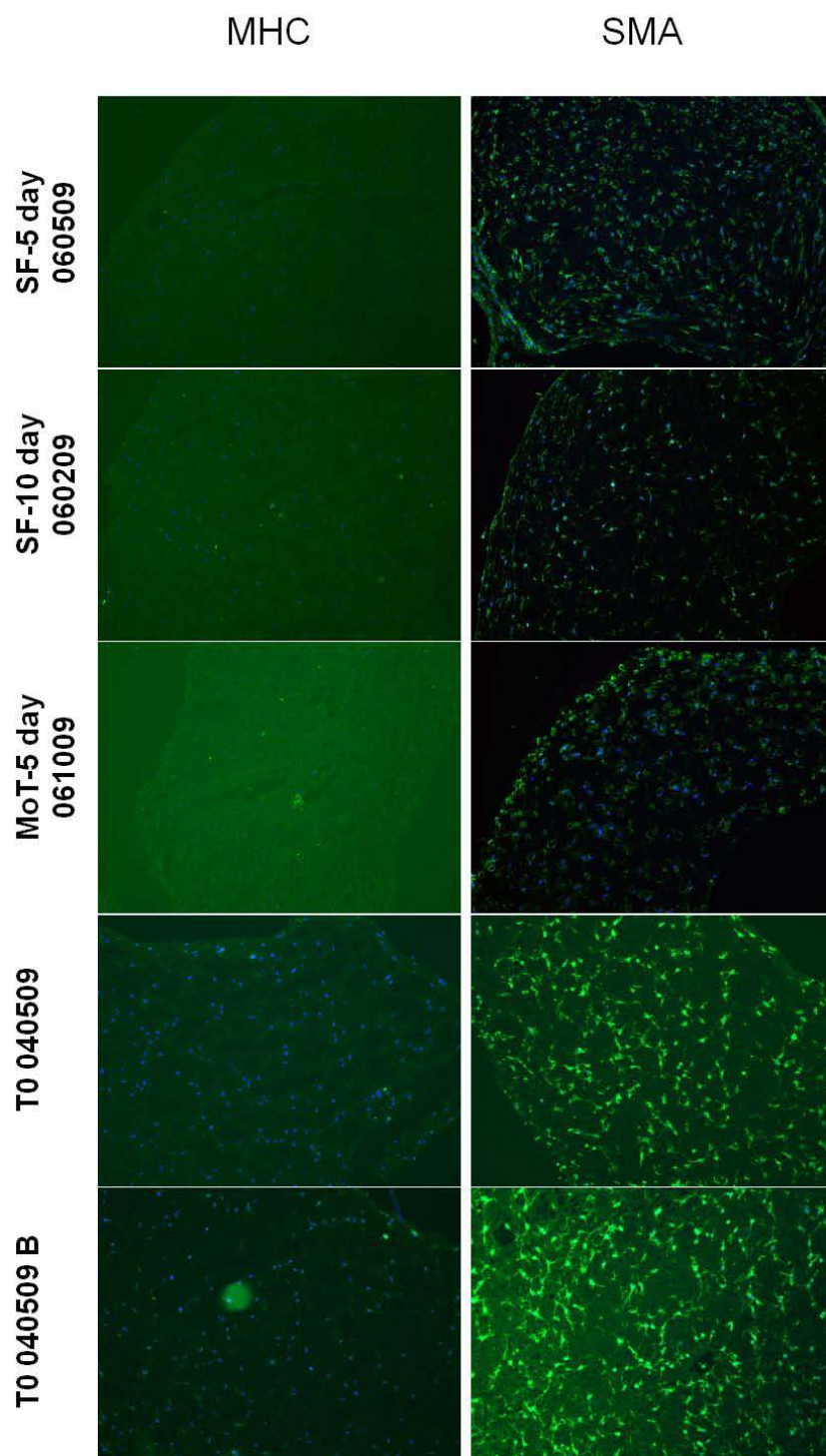


Figure H.22 Representative MHC and SMA staining for MoT, T0 and SF bioreactor conditions.

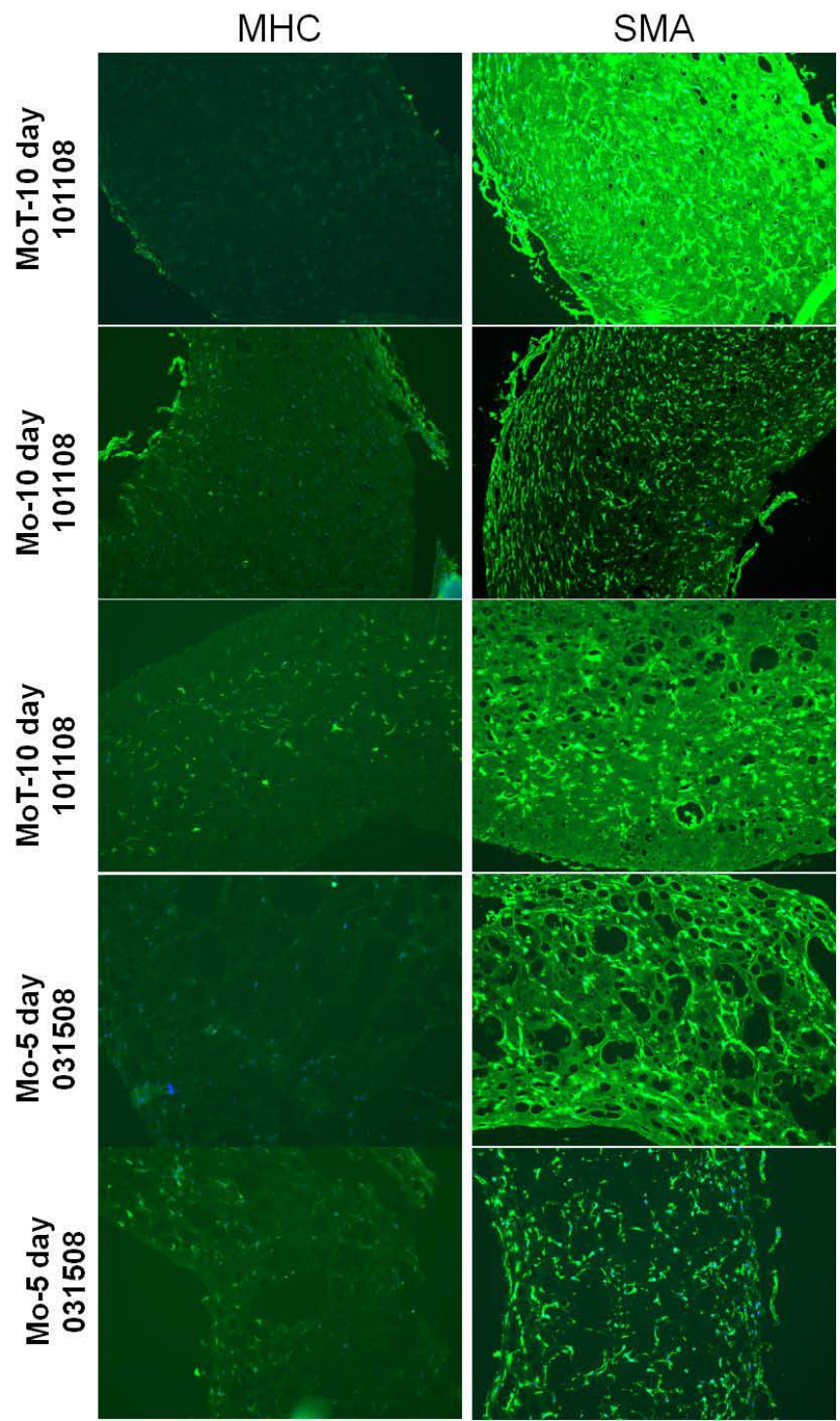


Figure H.23 Representative MHC and SMA staining for Mo and MoT bioreactor conditions.

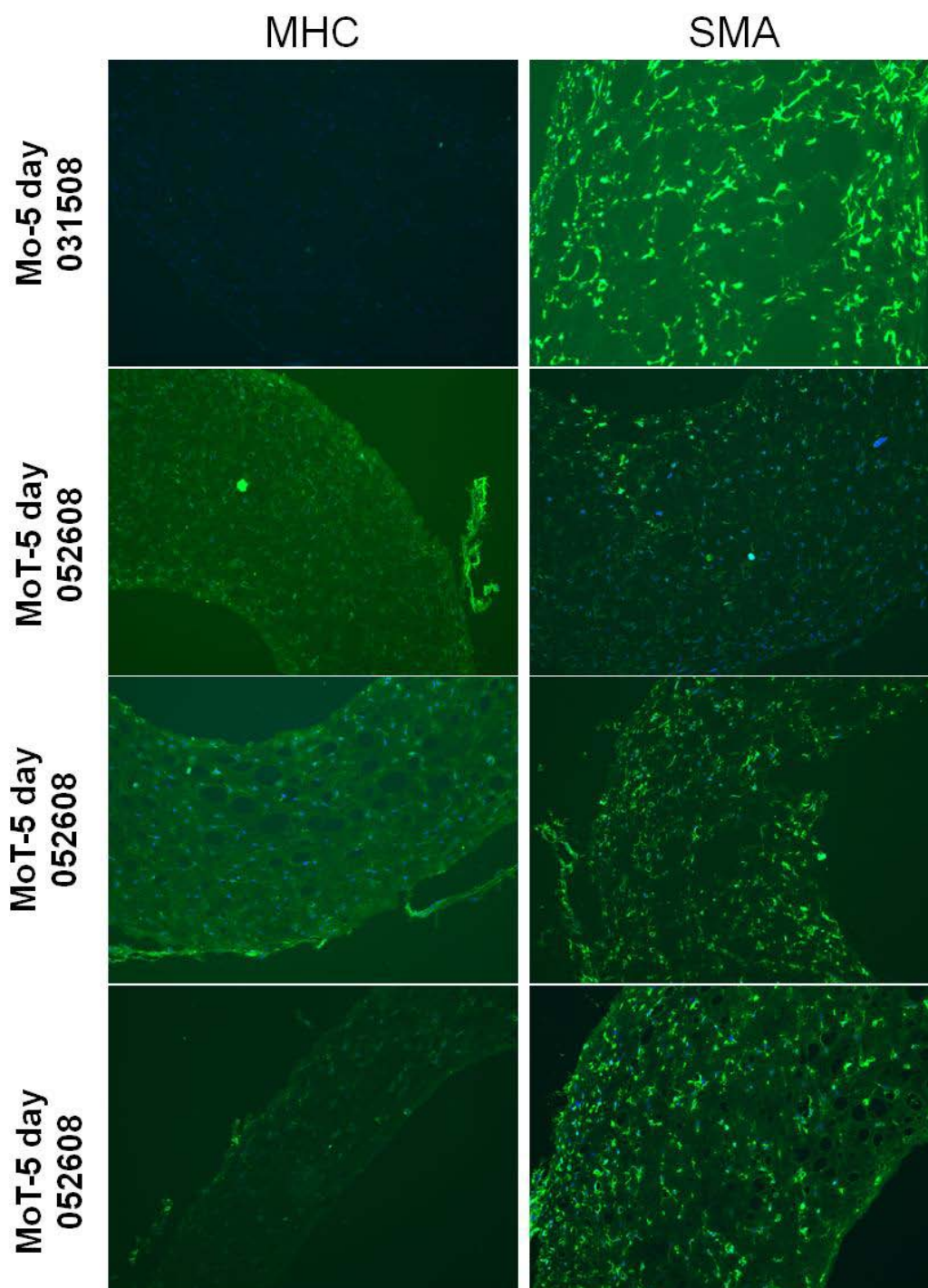


Figure H.24 Representative MHC and SMA staining for Mo and MoT bioreactor conditions.

## IN-VIVO IMMUNOFLUORESCENCE

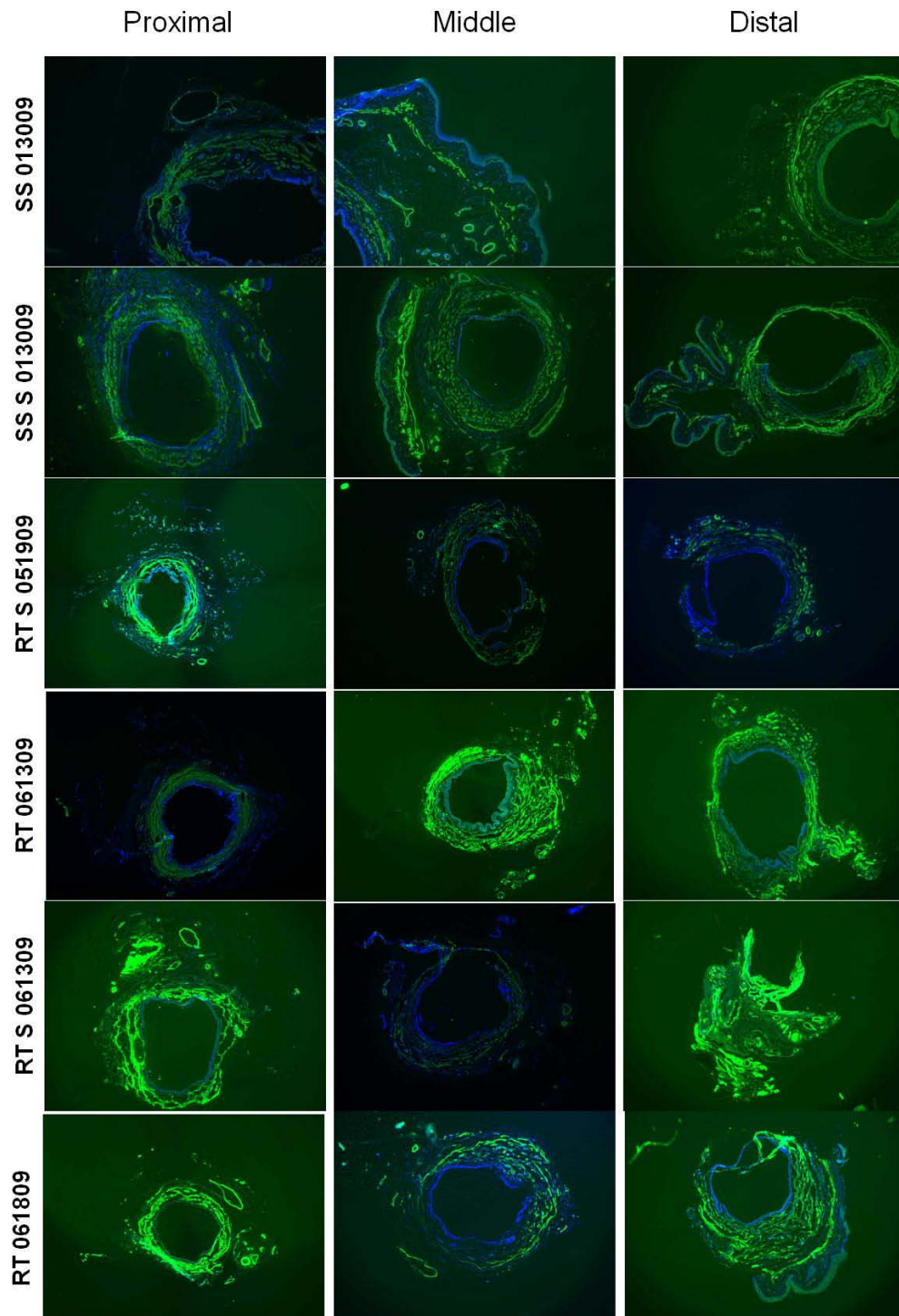
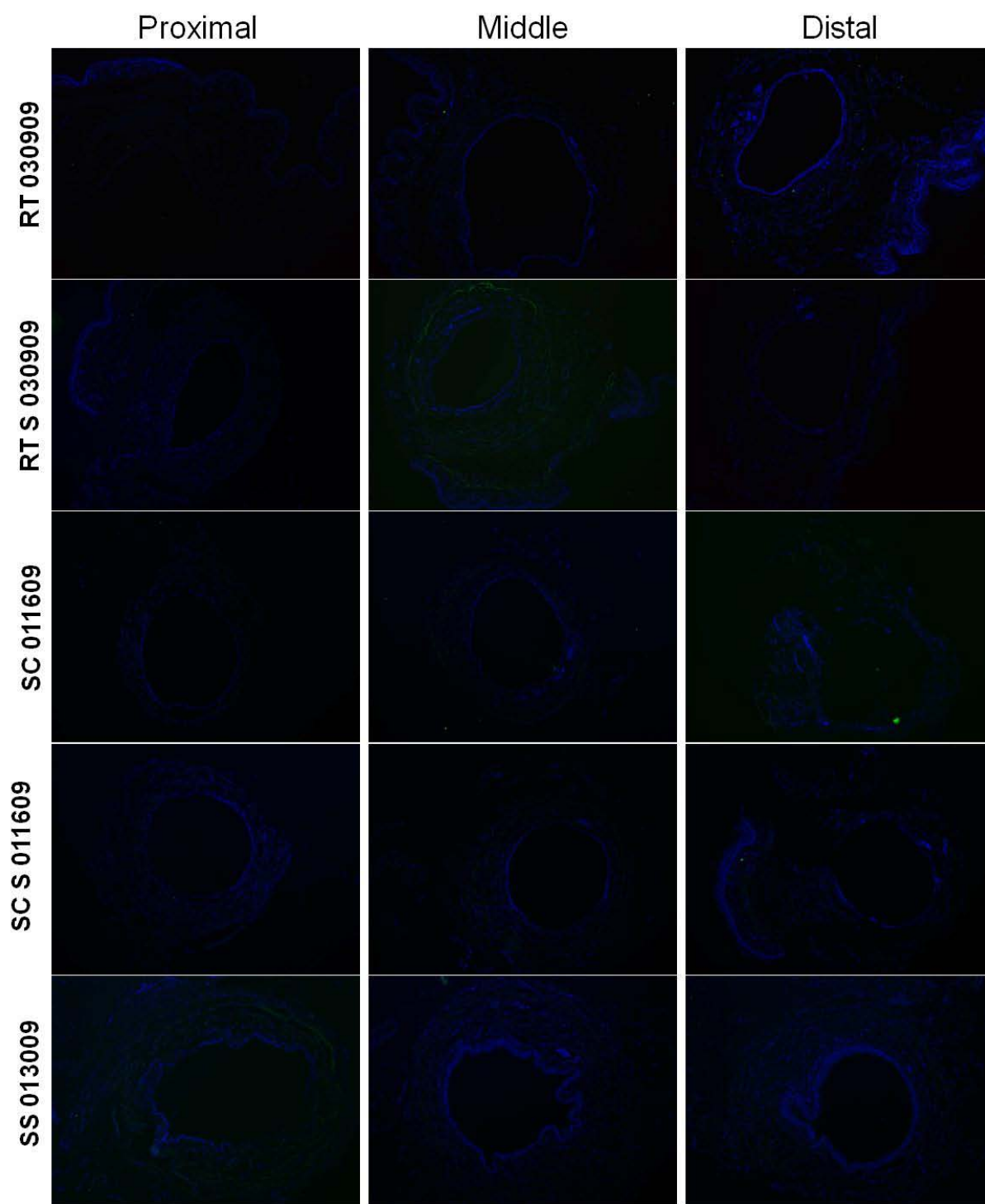


Figure H.25 Representative SMA staining for RT, SC and SS 3 week studies.



**Figure H.26** Representative CALP staining for RT, SC and SS 3 week studies.

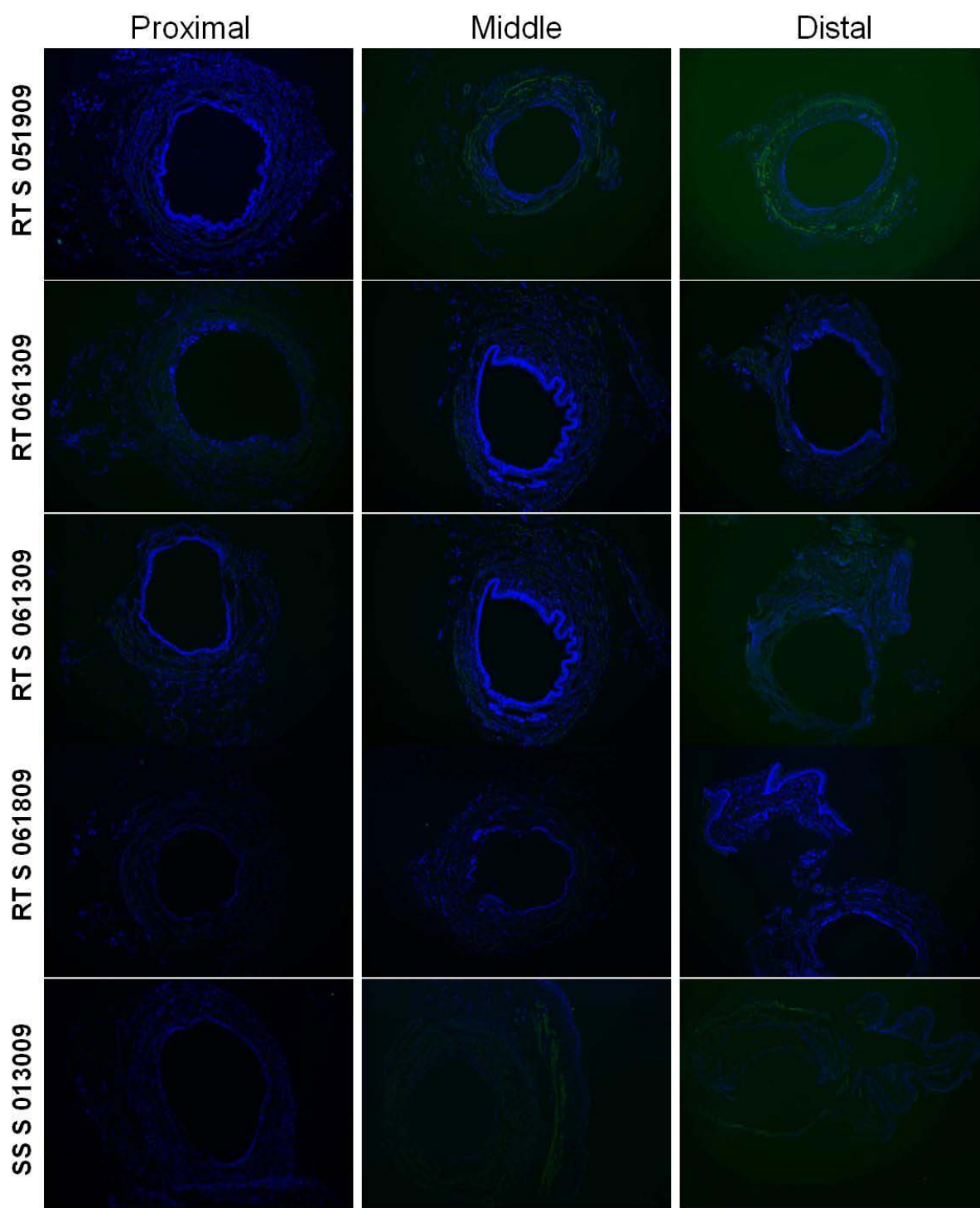


Figure H.27 Representative CALP staining for RT, SC and SS 3 week studies.

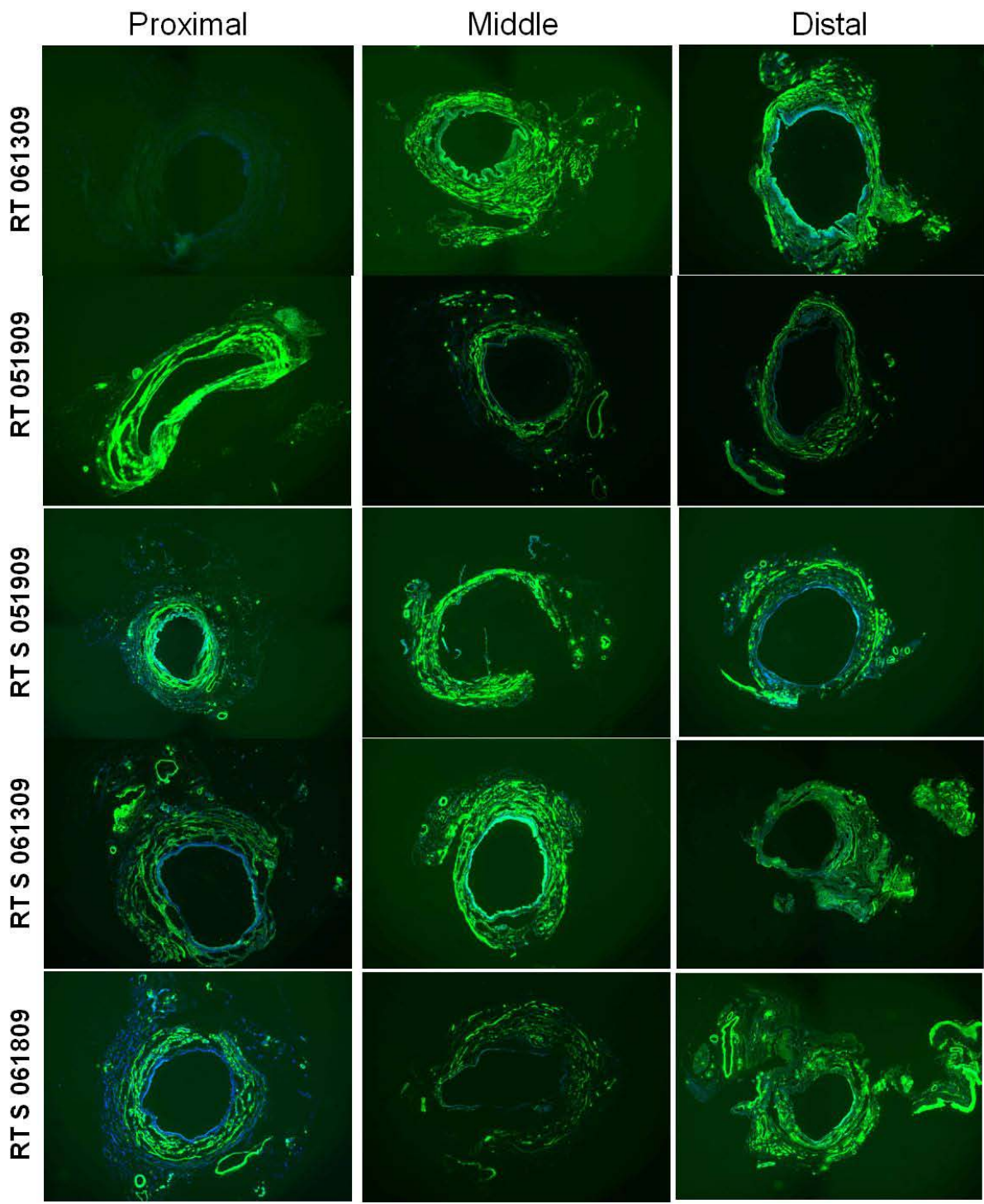
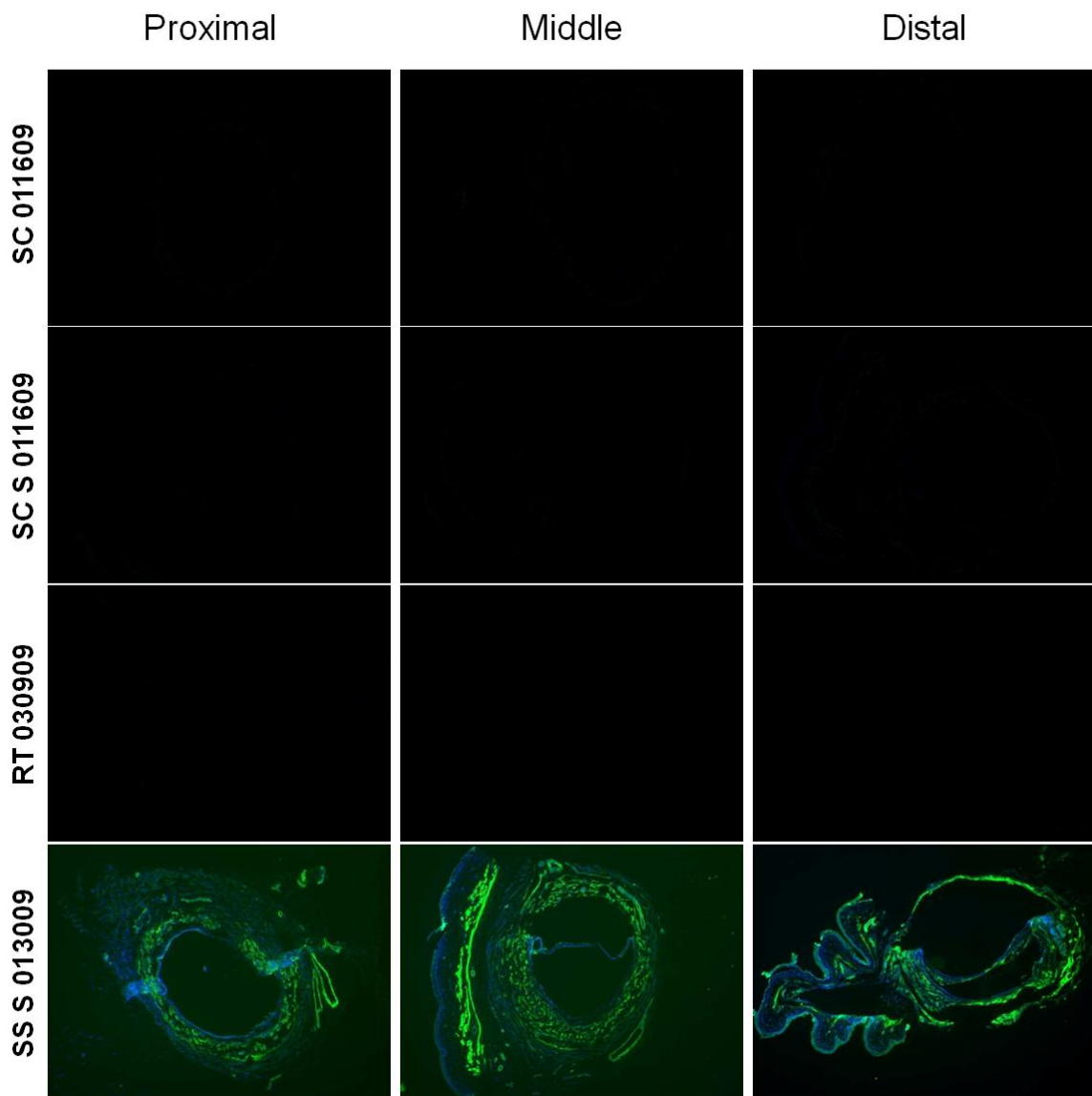


Figure H.28 Representative MHC staining for RT 3 week studies.



**Figure H.29** Representative MHC staining for RT, SC and SS 3 week studies.

## BIBLIOGRAPHY

1. Sui, GP, Rothery, S, Dupont, E, Fry, CH, and Severs, NJ, *Gap junctions and connexin expression in human suburothelial interstitial cells*. BJU Int, 2002. **90**(1): p. 118-129.
2. Resnick, NM and Griffiths, DJ, *Expanding treatment options for stress urinary incontinence in women*. Jama, 2003. **290**(3): p. 395-397.
3. Zinner, N, Ritter, Rogers, Sterling, Arthur *The Mechanism of Micturition*, in *Scientific Foundations of Urology*, D.W.a.G. Chisholm, Editor, William Heinemann Medical Books Ltd.: London. p. 39-51.
4. Buzelin, J, Glemain, P., Minaire, P., *The Physiology of Continence and the Physiopathology of Urinary Incontinence*, in *Societe Internationale D'Urologie Reports: Urinary Incontinence*, A. Steg, Editor. 1992, Churchill Livingstone: New York. p. 13-40.
5. Wei, JT and De Lancey, JO, *Functional anatomy of the pelvic floor and lower urinary tract*. Clin Obstet Gynecol, 2004. **47**(1): p. 3-17.
6. Drake, RL, Vogl, W, and Mitchell, AWM, *Gray's Anatomy for Students*. 2005, Philadelphia: Elsevier Inc. 1058.
7. Saladin, K, *The Urinary System*, in *Anatomy and Physiology The Unity of Form and Function*, K.A. Queck, Editor. 2007, McGraw-Hill: New York. p. 895-927.
8. Wein, AJ, ed. *Campbell-Walsh Urology*. Ninth ed. Vol. 3. 2007, Saunders Elsevier: Philadelphia. 1226.
9. Andersson, KE and Arner, A, *Urinary bladder contraction and relaxation: physiology and pathophysiology*. Physiol Rev, 2004. **84**(3): p. 935-986.
10. Elbadawi, A, *Functional anatomy of the organs of micturition*. Urol Clin North Am, 1996. **23**(2): p. 177-210.
11. deGroat, WC and Booth, AM, *Physiology of the urinary bladder and urethra*. Ann Intern Med, 1980. **92**(2 Pt 2): p. 312-315.

12. Bykova, A, Regirer, S., *Mathematical Models in Urinary System Mechanics*. Fluid Dynamics, 2005. **40**(1): p. 1-19.
13. Haab, F, Sebe, P., Mondet, F., Ciofu, C., *Functional Anatomy of the Bladder and Urethra in Females*, in *The Urinary Sphincter*, J.C.a.E. Schick, Editor. 2001, Marcel Dekker, Inc: New York. p. 15-24.
14. Brading, AF, Teramoto, N, Dass, N, and McCoy, R, *Morphological and physiological characteristics of urethral circular and longitudinal smooth muscle*. Scand J Urol Nephrol Suppl, 2001(207): p. 12-18; discussion 106-125.
15. Brading, AF, *The physiology of the mammalian urinary outflow tract*. Exp Physiol, 1999. **84**(1): p. 215-221.
16. Schafer, W, *Some biomechanical aspects of continence function*. Scand J Urol Nephrol Suppl, 2001(207): p. 44-60; discussion 106-125.
17. Augsburger, HR, *Elastic fibre system of the female canine urethra. Histochemical identification of elastic, elaunin and oxytalan fibres*. Anat Histol Embryol, 1997. **26**(4): p. 297-302.
18. DeLancey, JO, *Structural support of the urethra as it relates to stress urinary incontinence: the hammock hypothesis*. Am J Obstet Gynecol, 1994. **170**(6): p. 1713-1720; discussion 1720-1713.
19. Andersson, PO, Malmgren, A, and Uvelius, B, *Functional responses of different muscle types of the female rat urethra in vitro*. Acta Physiol Scand, 1990. **140**(3): p. 365-372.
20. de Groat, WC, *Integrative control of the lower urinary tract: preclinical perspective*. Br J Pharmacol, 2006. **147 Suppl 2**: p. S25-40.
21. Thor, KB and Donatucci, C, *Central nervous system control of the lower urinary tract: new pharmacological approaches to stress urinary incontinence in women*. J Urol, 2004. **172**(1): p. 27-33.
22. de Groat, WC, Fraser, MO, Yoshiyama, M, Smerin, S, Tai, C, Chancellor, MB, Yoshimura, N, and Roppolo, JR, *Neural control of the urethra*. Scand J Urol Nephrol Suppl, 2001(207): p. 35-43; discussion 106-125.
23. de Groat, WC, *Anatomy of the central neural pathways controlling the lower urinary tract*. Eur Urol, 1998. **34 Suppl 1**: p. 2-5.
24. Sullivan, MP and Yalla, SV, *Physiology of female micturition*. Urol Clin North Am, 2002. **29**(3): p. 499-514, vii.

25. Norton, P and Brubaker, L, *Urinary incontinence in women*. Lancet, 2006. **367**(9504): p. 57-67.
26. Plus, M. *Stress Incontinence*. Medical Encyclopedia [website] 2004 5/4/2004 [cited 2004 8/16/2004]; Available from: <http://www.nlm.nih.gov/medlineplus.htm>.
27. Yokoyama, T, Huard, J., Chancellor, M.B., *Myoblast therapy for stress urinary incontinence and bladder dysfunction*. World J Urol, 2000. **18**: p. 56-61.
28. Donnica, D. *Stress Urinary Incontinence*. DrDonnica.com 2003 [cited 2006 1/30/2006]; Available from: <http://www.drdonnica.com/today/00006954.htm>.
29. Nygaard, IE and Heit, M, *Stress urinary incontinence*. Obstet Gynecol, 2004. **104**(3): p. 607-620.
30. Vecchioli-Scaldazza, C and Morosetti, C, *Urodynamic findings in female patients with urinary incontinence with intrinsic sphincteric deficiency*. Med Sci Monit, 2006. **12**(8): p. CR345-350.
31. Chen, P. *Stress Incontinence*. [website] 2004 May 4, 2004 [cited 2004 August 16]; Medical Encyclopedia]. Available from: [www.nlm.nih.gov/medlineplus/print/ency/article/000891.htm](http://www.nlm.nih.gov/medlineplus/print/ency/article/000891.htm).
32. Lin, AS, Carrier, S, Morgan, DM, and Lue, TF, *Effect of simulated birth trauma on the urinary continence mechanism in the rat*. Urology, 1998. **52**(1): p. 143-151.
33. Trabucco, E, Soderberg, M, Cobellis, L, Torella, M, Bystrom, B, Ekman-Ordeberg, G, Petraglia, F, and Colacurci, N, *Role of proteoglycans in the organization of periurethral connective tissue in women with stress urinary incontinence*. Maturitas, 2007. **58**(4): p. 395-405.
34. Ashton-Miller, JA, Howard, D, and DeLancey, JO, *The functional anatomy of the female pelvic floor and stress continence control system*. Scand J Urol Nephrol Suppl, 2001(207): p. 1-7; discussion 106-125.
35. Damaser, MS, Whitbeck, C, Chichester, P, and Levin, RM, *Effect of vaginal distension on blood flow and hypoxia of urogenital organs of the female rat*. J Appl Physiol, 2005. **98**(5): p. 1884-1890.
36. Hayashi, N, Bella, AJ, Wang, G, Lin, G, Deng, DY, Nunes, L, and Lue, TF, *Effect of Extended-Term Estrogen on Voiding in a Postpartum Ovariectomized Rat Model*. Canadian Urological Association Journal, 2007. **1**(3): p. 256-263.
37. Ahmed, Y, Lin, DL, Ferguson, C, Esparza, N, and Damaser, MS, *Effect of Estrogen on Urethral Function and Nerve Regeneration Following Pudendal Nerve Crush in the Female Rat*. The Journal of Urology, 2006. **175**: p. 1948-1952.

38. Hinoul, P, Roovers, JP, Ombelet, W, and Vanspauwen, R, *Surgical management of urinary stress incontinence in women: A historical and clinical overview*. Eur J Obstet Gynecol Reprod Biol, 2009.
39. Walsh, LP, Zimmern, PE, Pope, N, and Shariat, SF, *Comparison of the Q-tip test and voiding cystourethrogram to assess urethral hypermobility among women enrolled in a randomized clinical trial of surgery for stress urinary incontinence*. J Urol, 2006. **176**(2): p. 646-649; discussion 650.
40. McGuire, EJ, *Pathophysiology of stress urinary incontinence*. Rev Urol, 2004. **6 Suppl 5**: p. S11-17.
41. Lane, TM and Shah, PJR, *Valsalva Leak Point Pressure in the Evaluation of Stress Urinary Incontinence*. Brazilian Journal of Urology, 2000. **26**(4): p. 420-425.
42. Gilleran, JP and Zimmern, P, *An evidence-based approach to the evaluation and management of stress incontinence in women*. Curr Opin Urol, 2005. **15**(4): p. 236-243.
43. Kefer, JC, Liu, G, and Daneshgari, F, *Pubo-Urethral Ligament Transection Causes Stress Urinary Incontinence in the Female Rat: A Novel Animal Model of Stress Urinary Incontinence*. The Journal of Urology, 2008. **179**: p. 775-778.
44. Cannon, TW and Chancellor, MB, *Pharmacotherapy for stress urinary incontinence*. Rev Urol, 2003. **5**(3): p. 135-141.
45. Castro-Diaz, D and Amoros, MA, *Pharmacotherapy for stress urinary incontinence*. Curr Opin Urol, 2005. **15**(4): p. 227-230.
46. Damaser, MS, Broxton-King, C, Ferguson, C, Kim, FJ, and Kerns, JM, *Functional and neuroanatomical effects of vaginal distention and pudendal nerve crush in the female rat*. J Urol, 2003. **170**(3): p. 1027-1031.
47. Hijaz, A, Daneshgari, F, Sievert, KD, and Damaser, MS, *Animal Models of Female Stress Urinary Incontinence*. The Journal of Urology, 2008. **179**: p. 2103-2110.
48. Kamo, I, Kaiho, Y., Canon, T., Chancellor, M.B., de Groat, W.C., Prantil, R.L., Vorp, D.A., Yoshimura, N., *Functional analysis of active urethral closure mechanisms under sneeze-induced stress condition in a rat model of birth trauma*. Journal of Urology, submitted (under revision), 2006.
49. Sievert, KD, Emre Bakircioglu, M, Tsai, T, Dahms, SE, Nunes, L, and Lue, TF, *The effect of simulated birth trauma and/or ovariectomy on rodent continence mechanism. Part I: functional and structural change*. J Urol, 2001. **166**(1): p. 311-317.

50. Ferguson, CL, Lin, DL, Rao, S, and Damaser, MS, *Short-term functional and neuroregenerative response of the urethra to ovariectomy and vaginal distension in female rats*. Int Urogynecol J Pelvic Floor Dysfunct, 2005. **16**(2): p. 119-125.
51. Cannon, TW, Wojcik, EM, Ferguson, CL, Saraga, S, Thomas, C, and Damaser, MS, *Effects of vaginal distension on urethral anatomy and function*. BJU Int, 2002. **90**(4): p. 403-407.
52. Rocha, MA, Sartori, MG, De Jesus Simoes, M, Herrmann, V, Baracat, EC, Rodrigues de Lima, G, and Girao, MJ, *Impact of pregnancy and childbirth on female rats' urethral nerve fibers*. Int Urogynecol J Pelvic Floor Dysfunct, 2007. **18**(12): p. 1453-1458.
53. Prantil, RL, *Biomechanics and Function of the Female Rat Urethra in Stress Urinary Incontinence Induced by Birth Trauma*, in *Bioengineering*. 2007, University of Pittsburgh: Pittsburgh. p. 230.
54. Prantil, RL, Jankowski, RJ, Kaiho, Y, de Groat, WC, Chancellor, MB, Yoshimura, N, and Vorp, DA, *Ex vivo biomechanical properties of the female urethra in a rat model of birth trauma*. Am J Physiol Renal Physiol, 2007. **292**(4): p. F1229-1237.
55. Rodriguez, LV, Chen, S, Jack, GS, de Almeida, F, Lee, KW, and Zhang, R, *New objective measures to quantify stress urinary incontinence in a novel durable animal model of intrinsic sphincter deficiency*. Am J Physiol Regul Integr Comp Physiol, 2005. **288**(5): p. R1332-1338.
56. Ahn, H, Lin, DL, Esparza, N, and Damaser, MS, *Short-term Timecourse of Bilateral Pudendal Nerve Injury on Leak-Point Pressure in Female Rats*. Journal of Rehabilitation Research and Development, 2005. **42**(1): p. 109-114.
57. Rocha, MA, Sartori, MGF, De Jesus Simoes, M, Herrmann, V, Baracat, EC, Rodrigues de Lima, G, and Girao, MJBC, *Impact of pregnancy and childbirth on female rats' urethral nerve fibers*. Int. Urogynecol J, 2007. **18**: p. 1453-1458.
58. Wai, CY, Liehr, P, Tibbals, HF, Sager, M, Schaffer, JI, and Word, RA, *Effect of periurethral denervation on function of the female urethra*. Am J Obstet Gynecol, 2003. **189**(6): p. 1637-1645.
59. Kamo, I, Cannon, TW, Conway, DA, Torimoto, K, Chancellor, MB, de Groat, WC, and Yoshimura, N, *The role of bladder-to-urethral reflexes in urinary continence mechanisms in rats*. Am J Physiol Renal Physiol, 2004. **287**(3): p. F434-441.
60. Yoshimura N, KI, Torimoto K, de Groat W, Chancellor M. *Neural Mechanisms of Tonic and Phasic Urethral Continence Reflexes Preventing Stress Urinary Incontinence*. in *ICS and IUGA 2004 Scientific Programme*. 2004. Paris, France.

61. Peng, CW, Chen, JJ, Chang, HY, de Groat, WC, and Cheng, CL, *External Urethral Sphincter Activity in a Rat Model of Pudendal Nerve Injury*. *Neurourology and Urodynamics*, 2006. **25**: p. 388-396.
62. Cannon, TW, Sweeney, D., Conway, D.A., Kamo, I., Yoshimura, N. and Chancellor, M.B., *A tissue-engineered suburethral sling in an animal model of stress urinary incontinence*. *BJU Int*, 2005. **96**: p. 664-669.
63. Hijaz, A, Bena, J, and Daneshgari, F, *Long-term efficacy of a vaginal sling procedure in a rat model of stress urinary incontinence*. *J Urol*, 2005. **173**(5): p. 1817-1819.
64. Cannon, TW, Lee, JY, Somogyi, G, Pruchnic, R, Smith, CP, Huard, J, and Chancellor, MB, *Improved sphincter contractility after allogenic muscle-derived progenitor cell injection into the denervated rat urethra*. *Urology*, 2003. **62**(5): p. 958-963.
65. Lee, JY, Cannon, T.W., Pruchnic, R., Fraser, M.O., Huard., J., Chancellor, M.B., *The effects of periurethral muscle-derived stem cell injection on leak point pressure in a rat model of stress urinary incontinence*. *Int Urogynecol J*, 2003. **14**: p. 31-37.
66. Lin, G, Shindel, AW, Banie, L, Deng, D, Wang, G, Hayashi, N, Lin, CS, and Lue, TF, *Molecular Mechanisms Related to Parturition-Induced Stress Urinary Incontinence*. *European Urology*, 2009. **55**: p. 1213-1223.
67. Burger, HG, Dudley, EC, Robertson, DM, and Dennerstein, L, *Hormonal Changes in the Menopause Transition*. *Recent Progress in Hormone Research*, 2002. **57**: p. 257-275.
68. Rocha, MA, Sartori, MGF, De Jesus Simoes, M, Herrmann, V, Baracat, EC, Rodrigues de Lima, G, and Girao, MJBC, *Impact of pregnancy and childbirth in the urethra of female rats*. *Int Urogynecol J*, 2007. **18**(645-51).
69. Dass, N, McMurray, G, and Brading, AF, *Elastic fibres in the vesicourethral junction and urethra of the guinea pig: quantification with computerised image analysis*. *J Anat*, 1999. **195 ( Pt 3)**: p. 447-453.
70. Keane, DP, Sims, TJ, Abrams, P, and Bailey, AJ, *Analysis of Collagen Status in Premenopausal Nulliparous Women with Genuine Stress Incontinence*. *Br J Obstet Gynaecol*, 1997. **104**: p. 994-998.
71. Falconer, C, Blomgren, B, Johansson, O, Ulmstem, U, Malmstrom, A, Westergren-Thorsson, G, and Ekman-Ordeberg, G, *Different Organization of Collagen Fibrils in Stress-Incontinent Women of Fertile Age*. *Acta Obstet Gynecol Scand*, 1998. **77**: p. 87-94.
72. Palsson, BO and Bhatia, SN, *Tissue Engineering*. 2004, Upper Saddle River: Pearson Education, Inc. 407.

73. Marra, KG, *Introduction to Tissue Engineering*, I.t.T.E.C. Students, Editor. 2007: Pittsburgh. p. 6.
74. Atala, A, *Tissue engineering and regenerative medicine: concepts for clinical application*. Rejuvenation Res, 2004. 7(1): p. 15-31.
75. Cross, WR, Thomas, DF, and Southgate, J, *Tissue engineering and stem cell research in urology*. BJU Int, 2003. 92(2): p. 165-171.
76. Rowe, SL, Lee, SY, and Stegemann, JP, *Influence of Thrombin Concentration on the Mechanical and Morphological Properties of Cell-seeded Fibrin Hydrogels*. Acta Biomaterials, 2007. 3(1): p. 59-67.
77. Yoo, JJ and Atala, A, *Tissue engineering applications in the genitourinary tract system*. Yonsei Med J, 2000. 41(6): p. 789-802.
78. Park, KD, Kwon, IK, and Kim, YH, *Tissue engineering of urinary organs*. Yonsei Med J, 2000. 41(6): p. 780-788.
79. Atala, A, *Tissue engineering for the replacement of organ function in the genitourinary system*. Am J Transplant, 2004. 4 Suppl 6: p. 58-73.
80. Strasser, H, Berjukow, S, Marksteiner, R, Margreiter, E, Hering, S, Bartsch, G, and Hering, S, *Stem Cell Therapy for Urinary Stress Incontinence*. Experimental Gerontology, 2004. 39: p. 1259-1265.
81. Chermansky, CJ, Tarin, T., Kwon, D., Jankowski, R.J., Cannon, T.W., DeGroat, W.C., Huard, J., Chancellor, M., *Intraurethral Muscle-Derived Cell Injections Increase Leak Point Pressure in a Rat Model of Intrinsic Sphincter Deficiency*. Urology, 2004. 63: p. 780-785.
82. Yokoyama, T, Yoshimura, N., Dhir, R., Qu, Z., Fraser, M., Kumon, H., DeGroat, W., Huard, J., Chancellor, M.B., *Persistence and Survival of Autologous Muscle Derived Cells versus Bovine Collagen as Potential Treatment of Stress Urinary Incontinence*. The Journal of Urology, 2001. 165: p. 271-276.
83. Yokoyama, T, Huard, J., Pruchnic, R., Yoshimura, N., Qu, Z., Cao, B., DeGroat, W., Kumon, H., Chancellor, M.B., *Muscle-Derived Cell Transplantation and Differentiation into Lower Urinary Tract Smooth Muscle*. Urology, 2001. 57(826-831).
84. Yokoyama, T, Pruchnic, R., Lee, J.Y., Chuang, Y., Jumon, H., Yoshimura, N., DeGroat, W., Huard, J., Chancellor, M.B., *Autologous Primary Muscle-Derived Cells Transfer into the Lower Urinary Tract*. Tissue Eng, 2001. 7(4): p. 395-404.

85. Lee, JY, Paik, SY, Yuk, SH, Lee, JH, Ghil, SH, and Lee, SS, *Long term effects of muscle-derived stem cells on leak point pressure and closing pressure in rats with transected pudendal nerves*. Mol Cells, 2004. **18**(3): p. 309-313.
86. Chen, F, Yoo, JJ, and Atala, A, *Experimental and clinical experience using tissue regeneration for urethral reconstruction*. World J Urol, 2000. **18**(1): p. 67-70.
87. Atala, A, *Tissue engineering in urologic surgery*. Urol Clin North Am, 1998. **25**(1): p. 39-50.
88. Lauer, G, Schimming, R, and Frankenschmidt, A, *Intraoral wound closure with tissue-engineered mucosa: new perspectives for urethra reconstruction with buccal mucosa grafts*. Plast Reconstr Surg, 2001. **107**(1): p. 25-33.
89. Atala, A, Guzman, L, and Retik, AB, *A novel inert collagen matrix for hypospadias repair*. J Urol, 1999. **162**(3 Pt 2): p. 1148-1151.
90. Chen, F, Yoo, JJ, and Atala, A, *Acellular collagen matrix as a possible "off the shelf" biomaterial for urethral repair*. Urology, 1999. **54**(3): p. 407-410.
91. De Filippo, R, Yoo, J., Atala, A., *Urethral Replacement Using Cell Seeded Tubularized Collagen Matrices*. The Journal of Urology, 2002. **168**: p. 1789-1793.
92. Atala, A, *Tissue engineering in urology*. Curr Urol Rep, 2001. **2**(1): p. 83-92.
93. Atala, A, *Technology Insight: Applications of Tissue Engineering and Biological Substitues in Urology*. Clinical Practice urology, 2005. **2**(3): p. 143-149.
94. Yao, L, Swartz, DD, Gugino, SF, Russell, JA, and Andreadis, ST, *Fibrin-based tissue-engineered blood vessels: differential effects of biomaterial and culture parameters on mechanical strength and vascular reactivity*. Tissue Eng, 2005. **11**(7-8): p. 991-1003.
95. Huang, YC, Dennis, RG, Larkin, L, and Baar, K, *Rapid formation of functional muscle in vitro using fibrin gels*. J Appl Physiol, 2005. **98**(2): p. 706-713.
96. Swartz, DD, Russell, JA, and Andreadis, ST, *Engineering of Fibrin-based Functional and Implantable Small-diameter Blood Vessels*. American Journal of Physiology Heart Circ. Physiology, 2005. **288**: p. H1451-1460.
97. Cummings, CL, Gawlitta, D, Nerem, RM, and Stegemann, JP, *Properties of engineered vascular constructs made from collagen, fibrin, and collagen-fibrin mixtures*. Biomaterials, 2004. **25**(17): p. 3699-3706.
98. Grassl, ED, Oegema, TR, and Tranquillo, RT, *Fibrin as an alternative biopolymer to type-I collagen for the fabrication of a media equivalent*. J Biomed Mater Res, 2002. **60**(4): p. 607-612.

99. Isenberg, BC, Williams, C, and Tranquillo, RT, *Endothelialization and Flow Conditioning of Fibrin-Based Media-Equivalents*. Ann Biomed Eng, 2006.
100. Ross, JJ and Tranquillo, RT, *ECM gene expression correlates with in vitro tissue growth and development in fibrin gel remodeled by neonatal smooth muscle cells*. Matrix Biol, 2003. **22**(6): p. 477-490.
101. Prantil, RL, *Effects of Diabetes Mellitus on the Biomechanical Properties and Pharmacological Function of the Female Rat Urethra Ex-Vivo*, in *Bioengineering*. 2004, University of Pittsburgh: Pittsburgh. p. 166.
102. Nieponice, A, Maul, TM, Cumer, JM, Soletti, L, and Vorp, DA, *Mechanical stimulation induces morphological and phenotypic changes in bone marrow-derived progenitor cells within a three-dimensional fibrin matrix*. J Biomed Mater Res A, 2007. **81**(3): p. 523-530.
103. Hamilton, DW, Maul, T.M., Vorp, D.A., *Characterization of the Response of Bone Marrow-Derived Progenitor Cells to Cyclic Strain: Implications for Vascular Tissue-Engineering Applications*. Tissue Eng, 2004. **10**(3/4): p. 361-369.
104. Park, JS, Chu, J.S., Cheng, C., Chen, F., Chen, D., Li, S., *Differential Effects of Equiaxial and Uniaxial Strain on Mesenchymal Stem Cells*. Biotechnology and Bioengineering, 2004. **88**(3): p. 359-368.
105. Kobayashi, N, Yasu, T., Ueba, H., Sata, M., Hashimoto, S., Kuroki, M., Saito, M., Kawakami, M., *Mechanical stress promotes the expression of smooth muscle-like properties in marrow stromal cells*. Experimental Hematology, 2004. **32**: p. 1238-1245.
106. Huang, H, Nakayama, Y, Qin, K, Yamamoto, K, Ando, J, Yamashita, J, Itoh, H, Kanda, K, Yaku, H, Okamoto, Y, and Nemoto, Y, *Differentiation from embryonic stem cells to vascular wall cells under in vitro pulsatile flow loading*. J Artif Organs, 2005. **8**(2): p. 110-118.
107. Kim-Kaneyama, JR, Suzuki, W, Ichikawa, K, Ohki, T, Kohno, Y, Sata, M, Nose, K, and Shibamura, M, *Uni-axial stretching regulates intracellular localization of Hic-5 expressed in smooth-muscle cells in vivo*. J Cell Sci, 2005. **118**(Pt 5): p. 937-949.
108. Maul, T, Hamilton, D, and Vorp, D. *Morphologic Changes in Bone Marrow Progenitor Cells Exposed to Cyclic Hydrostatic Pressure Using a Novel Experimental Device*. in *ET2004: Engineering Tissues*. 2004. Hilton Head, SC.
109. Maul, T, Kontos, D, Nieponice, A, and Vorp, D. *Mechanical Stimulation of Bone Marrow Derived Progenitor Cells: A Differential Approach*. in *Regenerate*. 2005. Atlanta, GA.

110. Maul, T, Nieponice, A, and Vorp, D. *Differential Response of Bone Marrow Progenitor Cells to Mechanical Stimulation*. in *Engineered Tissues*. 2005. Hilton Head, SC.
111. Maul, TM, *Mechanobiology of Stem Cells: Implications for Vascular Tissue Engineering*, in *Bioengineering*. 2007, University of Pittsburgh: Pittsburgh. p. 381.
112. Peter, SJ, Liang, CR, Kim, DJ, Widmer, MS, and Mikos, AG, *Osteoblastic phenotype of rat marrow stromal cells cultured in the presence of dexamethasone, beta-glycerolphosphate, and L-ascorbic acid*. *J Cell Biochem*, 1998. **71**(1): p. 55-62.
113. Goldberg, AJ, Lee, DA, Bader, DL, and Bentley, G, *Autologous chondrocyte implantation. Culture in a TGF-beta-containing medium enhances the re-expression of a chondrocytic phenotype in passaged human chondrocytes in pellet culture*. *J Bone Joint Surg Br*, 2005. **87**(1): p. 128-134.
114. Janderova, L, McNeil, M, Murrell, AN, Mynatt, RL, and Smith, SR, *Human mesenchymal stem cells as an in vitro model for human adipogenesis*. *Obes Res*, 2003. **11**(1): p. 65-74.
115. Jia, D and Heersche, JN, *Insulin-like growth factor-1 and -2 stimulate osteoprogenitor proliferation and differentiation and adipocyte formation in cell populations derived from adult rat bone*. *Bone*, 2000. **27**(6): p. 785-794.
116. Kim, SY, Park, SY, Kim, JM, Kim, JW, Kim, MY, Yang, JH, Kim, JO, Choi, KH, Kim, SB, and Ryu, HM, *Differentiation of endothelial cells from human umbilical cord blood AC133(-)CD14(+) cells*. *Ann Hematol*, 2005.
117. Arakawa, E, Hasegawa, K, Yanai, N, Obinata, M, and Matsuda, Y, *A mouse bone marrow stromal cell line, TBR-B, shows inducible expression of smooth muscle-specific genes*. *FEBS Lett*, 2000. **481**(2): p. 193-196.
118. Drab, M, Haller, H, Bychkov, R, Erdmann, B, Lindschau, C, Haase, H, Morano, I, Luft, FC, and Wobus, AM, *From totipotent embryonic stem cells to spontaneously contracting smooth muscle cells: a retinoic acid and db-cAMP in vitro differentiation model*. *FASEB J*, 1997. **11**(11): p. 905-915.
119. Blank, RS and Owens, GK, *Platelet-derived growth factor regulates actin isoform expression and growth state in cultured rat aortic smooth muscle cells*. *J Cell Physiol*, 1990. **142**(3): p. 635-642.
120. Miyata, T, Iizasa, H, Sai, Y, Fujii, J, Terasaki, T, and Nakashima, E, *Platelet-derived growth factor-BB (PDGF-BB) induces differentiation of bone marrow endothelial progenitor cell-derived cell line TR-BME2 into mural cells, and changes the phenotype*. *J Cell Physiol*, 2005. **204**(3): p. 948-955.

121. Ponten, A, Folestad, EB, Pietras, K, and Eriksson, U, *Platelet-derived growth factor D induces cardiac fibrosis and proliferation of vascular smooth muscle cells in heart-specific transgenic mice*. *Circ Res*, 2005. **97**(10): p. 1036-1045.
122. Lee, WC, Rubin, JP, and Marra, KG, *Regulation of alpha-smooth muscle actin protein expression in adipose-derived stem cells*. *Cells Tissues Organs*, 2006. **183**(2): p. 80-86.
123. Sinha, S, Hoofnagle, MH, Kingston, PA, McCanna, ME, and Owens, GK, *Transforming growth factor-beta1 signaling contributes to development of smooth muscle cells from embryonic stem cells*. *Am J Physiol Cell Physiol*, 2004. **287**(6): p. C1560-1568.
124. Chen, S and Lechleider, RJ, *Transforming growth factor-beta-induced differentiation of smooth muscle from a neural crest stem cell line*. *Circ Res*, 2004. **94**(9): p. 1195-1202.
125. Lien, SC, Usami, S, Chien, S, and Chiu, JJ, *Phosphatidylinositol 3-kinase/Akt pathway is involved in transforming growth factor-beta1-induced phenotypic modulation of 10T1/2 cells to smooth muscle cells*. *Cell Signal*, 2006. **18**(8): p. 1270-1278.
126. Lee, WC, Maul, TM, Vorp, DA, Rubin, JP, and Marra, KG, *Effects of uniaxial cyclic strain on adipose-derived stem cell morphology, proliferation, and differentiation*. *Biomech Model Mechanobiol*, 2007. **6**(4): p. 265-273.
127. Wang, Z, Castresana, MR, and Newman, WH, *Reactive oxygen and NF-kappaB in VEGF-induced migration of human vascular smooth muscle cells*. *Biochem Biophys Res Commun*, 2001. **285**(3): p. 669-674.
128. Ishida, A, Murray, J, Saito, Y, Kanthou, C, Benzakour, O, Shibuya, M, and Wijelath, ES, *Expression of vascular endothelial growth factor receptors in smooth muscle cells*. *J Cell Physiol*, 2001. **188**(3): p. 359-368.
129. Broxmeyer, HE, Cooper, S, Li, ZH, Lu, L, Song, HY, Kwon, BS, Warren, RE, and Donner, DB, *Myeloid progenitor cell regulatory effects of vascular endothelial cell growth factor*. *Int J Hematol*, 1995. **62**(4): p. 203-215.
130. Duval, M, Bedard-Goulet, S, Delisle, C, and Gratton, JP, *Vascular endothelial growth factor-dependent down-regulation of Flk-1/KDR involves Cbl-mediated ubiquitination. Consequences on nitric oxide production from endothelial cells*. *J Biol Chem*, 2003. **278**(22): p. 20091-20097.
131. Shah, NM, Groves, AK, and Anderson, DJ, *Alternative neural crest cell fates are instructively promoted by TGFbeta superfamily members*. *Cell*, 1996. **85**(3): p. 331-343.
132. Gong, Z and Niklason, LE, *Small-diameter human vessel wall engineered from bone marrow-derived mesenchymal stem cells (hMSCs)*. *FASEB J*, 2008. **22**(6): p. 1635-1648.

133. Moses, HL and Serra, R, *Regulation of differentiation by TGF-beta*. Curr Opin Genet Dev, 1996. **6**(5): p. 581-586.
134. Yalla, SV and Burros, HM, *Conduit and regional compliance of female canine urethra. Observations during voiding and passive urethral infusion*. Urology, 1974. **4**(2): p. 155-161.
135. Colstrup, H, *Rigidity of the resting female urethra. Part II. Dynamic measurements*. J Urol, 1984. **132**(1): p. 82-86.
136. Colstrup, H, *Rigidity of the resting female urethra. Part I. Static measurements*. J Urol, 1984. **132**(1): p. 78-81.
137. Lose, G and Colstrup, H, *Mechanical properties of the urethra in healthy and stress incontinent females: dynamic measurements in the resting urethra*. J Urol, 1990. **144**(5): p. 1258-1262.
138. Griffiths, D, *The pressure within a collapsed tube, with special reference to urethral pressure*. Phys Med Biol, 1985. **30**(9): p. 951-963.
139. Ward, GH and Hosker, GL, *The anisotropic nature of urethral occlusive forces*. Br J Obstet Gynaecol, 1985. **92**(12): p. 1279-1285.
140. Mayo, ME and Hinman, F, *The effect of urethral lengthening*. Br J Urol, 1973. **45**(6): p. 621-630.
141. Jankowski, RJ, Prantil, RL, Chancellor, MB, de Groat, WC, Huard, J, and Vorp, DA, *Biomechanical characterization of the urethral musculature*. Am J Physiol Renal Physiol, 2006. **290**(5): p. F1127-1134.
142. Jankowski, RJ, Prantil, RL, Fraser, MO, Chancellor, MB, De Groat, WC, Huard, J, and Vorp, DA, *Development of an experimental system for the study of urethral biomechanical function*. Am J Physiol Renal Physiol, 2004. **286**(2): p. F225-232.
143. Jankowski, RJ, Prantil, RL, Chancellor, MB, de Groat, WC, Huard, J, and Vorp, DA, *Biomechanical Characterization of the Urethral Musculature*. Am J Physiol Renal Physiol, 2005.
144. Lachowsky, M and Nappi, RE, *The effects of oestrogen on urogenital health*. Maturitas, 2009. **63**(2): p. 149-151.
145. Rizk, DE, Mensah-Brown, EP, Chandranath, SI, Ahmed, I, Shafiullah, M, Patel, M, Al-Haj, M, and Adem, A, *Effects of ovariectomy and hormone replacement on collagen and blood vessels of the urethral submucosa of rats*. Urol Res, 2003. **31**(3): p. 147-151.

146. Kamo, I, Torimoto, K, Chancellor, MB, de Groat, WC, and Yoshimura, N, *Urethral closure mechanisms under sneeze-induced stress condition in rats: a new animal model for evaluation of stress urinary incontinence*. Am J Physiol Regul Integr Comp Physiol, 2003. **285**(2): p. R356-365.
147. Manzo, J, Vazquez, MI, Cruz, MR, Hernandez, ME, Carrillo, P, and Pacheco, P, *Fertility ratio in male rats: effects after denervation of two pelvic floor muscles*. Physiol Behav, 2000. **68**(5): p. 611-618.
148. Miyazato, M, Kaiho, Y, Kamo, I, Chancellor, MB, Sugaya, K, de Groat, WC, and Yoshimura, N, *Effect of duloxetine, a norepinephrine and serotonin reuptake inhibitor, on sneeze-induced urethral continence reflex in rats*. Am J Physiol Renal Physiol, 2008. **295**(1): p. F264-271.
149. Kitta, T, Miyazato, M, Honda, M, Chancellor, M, Nonomura, K, and Yoshimura, N, *Estrogen deficiency causes an early stage altering of urethral responses during sneeze reflex*, in American Urologic Association. 2009: Chicago, IL.
150. Ahmed, Y, Lin, DL, Ferguson, C, Esparza, N, and Damaser, MS, *Effect of estrogen on urethral function and nerve regeneration following pudendal nerve crush in the female rat*. J Urol, 2006. **175**(5): p. 1948-1952.
151. Smith, PG and Bradshaw, S, *Innervation of the proximal urethra of ovariectomized and estrogen-treated female rats*. Histol Histopathol, 2004. **19**(4): p. 1109-1116.
152. Taggart, MJ, *Smooth muscle excitation-contraction coupling: a role for caveolae and caveolins?* News Physiol Sci, 2001. **16**: p. 61-65.
153. Rizk, DE, Fahim, MA, Hassan, HA, Al-Marzouqi, AH, Ramadan, GA, Al-Kedrah, SS, and Al-Ghafri, LS, *The effect of ovariectomy on biomarkers of urogenital ageing in old versus young adult rats*. Int Urogynecol J Pelvic Floor Dysfunct, 2007. **18**(9): p. 1077-1085.
154. Tsui, KP, Ng, SC, Tee, YT, Yeh, GP, and Chen, GD, *Complications of synthetic graft materials used in suburethral sling procedures*. Int Urogynecol J Pelvic Floor Dysfunct, 2005. **16**(2): p. 165-167.
155. Lorenzo Gomez, MF, Silva Abuin, JM, Garcia Criado, FJ, Geanini Yaguez, A, and Urrutia Avisrorr, M, *[Treatment of stress urinary incontinence with perineal biofeedback by using superficial electrodes]*. Actas Urol Esp, 2008. **32**(6): p. 629-636.
156. Aboushwareb, T and Atala, A, *Stem cells in urology*. Nat Clin Pract Urol, 2008.
157. Lee, JY, Cannon, TW, Pruchnic, R, Fraser, MO, Huard, J, and Chancellor, MB, *The effects of periurethral muscle-derived stem cell injection on leak point pressure in a rat*

- model of stress urinary incontinence*. Int Urogynecol J Pelvic Floor Dysfunct, 2003. **14**(1): p. 31-37; discussion 37.
158. Strasser, H, Berjukow, S, Marksteiner, R, Margreiter, E, Hering, S, Bartsch, G, and Hering, S, *Stem cell therapy for urinary stress incontinence*. Exp Gerontol, 2004. **39**(9): p. 1259-1265.
159. Russell, B, Baumann, M, Heidkamp, MC, and Svanborg, A, *Morphometry of the aging female rat urethra*. Int Urogynecol J Pelvic Floor Dysfunct, 1996. **7**(1): p. 30-36.
160. Woo, LL, Hijaz, A, Pan, HQ, Kuang, M, Rackley, RR, and Damaser, MS, *Simulated childbirth injuries in an inbred rat strain*. Neurourol Urodyn, 2009. **28**(4): p. 356-361.
161. Hijaz, A, Daneshgari, F, Sievert, KD, and Damaser, MS, *Animal models of female stress urinary incontinence*. J Urol, 2008. **179**(6): p. 2103-2110.
162. Peng, CW, Chen, JJ, Chang, HY, de Groat, WC, and Cheng, CL, *External urethral sphincter activity in a rat model of pudendal nerve injury*. Neurourol Urodyn, 2006. **25**(4): p. 388-396.
163. Yoshiyama, M, deGroat, WC, and Fraser, MO, *Influences of external urethral sphincter relaxation induced by alpha-bungarotoxin, a neuromuscular junction blocking agent, on voiding dysfunction in the rat with spinal cord injury*. Urology, 2000. **55**(6): p. 956-960.
164. Smaldone MC, CM, *Bladder or urethra injection of boulinum toxin A injection*. Am J Urol 2005. **3**: p. 1-5.
165. Ahn, H, Lin, DL, Esparza, N, and Damaser, MS, *Short-term timecourse of bilateral pudendal nerve injury on leak-point pressure in female rats*. J Rehabil Res Dev, 2005. **42**(1): p. 109-114.
166. Bakircioglu, ME, Sievert, KD, Lau, A, Lin, CS, and Lue, TF, *The effect of pregnancy and delivery on the function and ultrastructure of the rat bladder and urethra*. BJU Int, 2000. **85**(3): p. 350-361.
167. Torimoto, K, Hirao, Y, Matsuyoshi, H, de Groat, WC, Chancellor, MB, and Yoshimura, N, *alpha1-Adrenergic mechanism in diabetic urethral dysfunction in rats*. J Urol, 2005. **173**(3): p. 1027-1032.
168. Chuang, YC, Fraser, MO, Yu, Y, Beckel, JM, Seki, S, Nakanishi, Y, Yokoyama, H, Chancellor, MB, Yoshimura, N, and de Groat, WC, *Analysis of the afferent limb of the vesicovascular reflex using neurotoxins, resiniferatoxin and capsaicin*. Am J Physiol Regul Integr Comp Physiol, 2001. **281**(4): p. R1302-1310.
169. Ogawa, T, Sasatomi, K, Hiragata, S, Seki, S, Nishizawa, O, Chermansky, CJ, Pflug, BR, Nelson, JB, Chancellor, MB, and Yoshimura, N, *Therapeutic effects of endothelin-A*

- receptor antagonist on bladder overactivity in rats with chronic spinal cord injury.* Urology, 2008. **71**(2): p. 341-345.
170. Banik, RK, Sato, J, Yajima, H, and Mizumura, K, *Differences between the Lewis and Sprague-Dawley rats in chronic inflammation induced norepinephrine sensitivity of cutaneous C-fiber nociceptors.* Neurosci Lett, 2001. **299**(1-2): p. 21-24.
171. Kaminsky, O, Klenerova, V, Stohr, J, Sida, P, and Hynie, S, *Differences in the behaviour of Sprague--Dawley and Lewis rats during repeated passive avoidance procedure: effect of amphetamine.* Pharmacol Res, 2001. **44**(2): p. 117-122.
172. Pill, J, Volkl, A, Hartig, F, and Fahimi, HD, *Differences in the response of Sprague-Dawley and Lewis rats to bezafibrate: the hypolipidemic effect and the induction of peroxisomal enzymes.* Arch Toxicol, 1992. **66**(5): p. 327-333.
173. Chen, Y, DeSautel, M, Anderson, A, Badlani, G, and Kushner, L, *Collagen synthesis is not altered in women with stress urinary incontinence.* Neurourol Urodyn, 2004. **23**(4): p. 367-373.
174. Rocha, MA, Sartori, MG, De Jesus Simoes, M, Herrmann, V, Baracat, EC, Rodrigues de Lima, G, and Girao, MJ, *The impact of pregnancy and childbirth in the urethra of female rats.* Int Urogynecol J Pelvic Floor Dysfunct, 2007. **18**(6): p. 645-651.
175. Furuta, A, Jankowski, RJ, Pruchnic, R, Egawa, S, Yoshimura, N, and Chancellor, MB, *Physiological effects of human muscle-derived stem cell implantation on urethral smooth muscle function.* Int Urogynecol J Pelvic Floor Dysfunct, 2008. **19**(9): p. 1229-1234.
176. Atala, A, *Regenerative medicine and urology.* BJU Int, 2003. **92 Suppl 1**: p. 58-67.
177. Javazon, EH, Colter, DC, Schwarz, EJ, and Prockop, DJ, *Rat marrow stromal cells are more sensitive to plating density and expand more rapidly from single-cell-derived colonies than human marrow stromal cells.* Stem Cells, 2001. **19**(3): p. 219-225.
178. Soletti, L, Hong, Y, Guan, J, Stankus, JJ, El-Kurdi, MS, Wagner, WR, and Vorp, DA, *A bilayered elastomeric scaffold for tissue engineering of small diameter vascular grafts.* Acta Biomater, 2009.
179. Streng, T, Santti, R, and Talo, A, *Similarities and differences in female and male rat voiding.* Neurourol Urodyn, 2002. **21**(2): p. 136-141.
180. Magnan, M, Levesque, P, Gauvin, R, Dube, J, Barrieras, D, El-Hakim, A, and Bolduc, S, *Tissue engineering of a genitourinary tubular tissue graft resistant to suturing and high internal pressures.* Tissue Eng Part A, 2009. **15**(1): p. 197-202.

181. Italiano, G, Abatangelo, G, Jr., Calabro, A, Zanoni, R, Abatangelo, G, Sr., and Passerini-Glazel, G, *Guiding spontaneous tissue regeneration for urethral reconstruction: long-term studies in the rabbit*. Urol Res, 1998. **26**(4): p. 281-284.
182. Swartz, DD, Russell, JA, and Andreadis, ST, *Engineering of fibrin-based functional and implantable small-diameter blood vessels*. Am J Physiol Heart Circ Physiol, 2005. **288**(3): p. H1451-1460.
183. Ng, KW, Leong, DT, and Hutmacher, DW, *The challenge to measure cell proliferation in two and three dimensions*. Tissue Eng, 2005. **11**(1-2): p. 182-191.
184. Portner, R, Nagel-Heyer, S, Goepfert, C, Adamietz, P, and Meenen, NM, *Bioreactor design for tissue engineering*. J Biosci Bioeng, 2005. **100**(3): p. 235-245.
185. Williams, C and Wick, TM, *Perfusion bioreactor for small diameter tissue-engineered arteries*. Tissue Eng, 2004. **10**(5-6): p. 930-941.
186. Corporation, B. *Bose - About ElectroForce*. 2009 [cited 2009 August 22, 2009]; Available from: [http://www.bose.com/controller?event=VIEW\\_STATIC\\_PAGE\\_EVENT&url=/enduratec/index.jsp](http://www.bose.com/controller?event=VIEW_STATIC_PAGE_EVENT&url=/enduratec/index.jsp).
187. Lee, D and Ansell, C, *Emerging Applications for Biomaterials in Tissue Engineering*. 2003, E-Tech Limited: United Kingdom. p. 4.
188. Technologies, TG. *DynaGen Bioreactor Series Overview*. [cited 2009 August 31, 2009]; Available from: <http://www.tissuegrowth.com/powerpoint.cfm>.
189. Chen, HC and Hu, YC, *Bioreactors for tissue engineering*. Biotechnol Lett, 2006. **28**(18): p. 1415-1423.
190. Dennis, RG, Smith, B, Philp, A, Donnelly, K, and Baar, K, *Bioreactors for guiding muscle tissue growth and development*. Adv Biochem Eng Biotechnol, 2009. **112**: p. 39-79.
191. Au-Yeung, KL, Sze, K, Sham, MH, and Chan, BP, *Development of a micromanipulator-based loading device for mechanoregulation study of human mesenchymal stem cells in 3D collagen constructs*. Tissue Eng Part C Methods, 2009.
192. Meyer, U, Buchter, A, Nazer, N, and Wiesmann, HP, *Design and performance of a bioreactor system for mechanically promoted three-dimensional tissue engineering*. Br J Oral Maxillofac Surg, 2006. **44**(2): p. 134-140.
193. Wallis, MC, Yeger, H, Cartwright, L, Shou, Z, Radisic, M, Haig, J, Suoub, M, Antoon, R, and Farhat, WA, *Feasibility study of a novel urinary bladder bioreactor*. Tissue Eng Part A, 2008. **14**(3): p. 339-348.

194. Arrigoni, C, Chitto, A, Mantero, S, and Remuzzi, A, *Rotating versus perfusion bioreactor for the culture of engineered vascular constructs based on hyaluronic acid*. Biotechnol Bioeng, 2008. **100**(5): p. 988-997.
195. Hahn, MS, McHale, MK, Wang, E, Schmedlen, RH, and West, JL, *Physiologic pulsatile flow bioreactor conditioning of poly(ethylene glycol)-based tissue engineered vascular grafts*. Ann Biomed Eng, 2007. **35**(2): p. 190-200.
196. Punchard, MA, Stenson-Cox, C, O'Cearbhaill E, D, Lyons, E, Gundy, S, Murphy, L, Pandit, A, McHugh, PE, and Barron, V, *Endothelial cell response to biomechanical forces under simulated vascular loading conditions*. J Biomech, 2007. **40**(14): p. 3146-3154.
197. Xu, J, Ge, H, Zhou, X, Yang, D, Guo, T, He, J, Li, Q, and Hao, Z, *Tissue-engineered vessel strengthens quickly under physiological deformation: application of a new perfusion bioreactor with machine vision*. J Vasc Res, 2005. **42**(6): p. 503-508.
198. Altman, GH, Lu, HH, Horan, RL, Calabro, T, Ryder, D, Kaplan, DL, Stark, P, Martin, I, Richmond, JC, and Vunjak-Novakovic, G, *Advanced bioreactor with controlled application of multi-dimensional strain for tissue engineering*. J Biomech Eng, 2002. **124**(6): p. 742-749.
199. Prenosil, JE and Villeneuve, PE, *Automated production of cultured epidermal autografts and sub-confluent epidermal autografts in a computer controlled bioreactor*. Biotechnol Bioeng, 1998. **59**(6): p. 679-683.
200. Davisson, T, Sah, RL, and Ratcliffe, A, *Perfusion increases cell content and matrix synthesis in chondrocyte three-dimensional cultures*. Tissue Eng, 2002. **8**(5): p. 807-816.
201. Bancroft, GN, Sikavitsas, VI, and Mikos, AG, *Design of a flow perfusion bioreactor system for bone tissue-engineering applications*. Tissue Eng, 2003. **9**(3): p. 549-554.
202. Maul, TM, Hamilton, DW, Nieponice, A, Soletti, L, and Vorp, DA, *A new experimental system for the extended application of cyclic hydrostatic pressure to cell culture*. J Biomech Eng, 2007. **129**(1): p. 110-116.
203. LoSurdo, JL, *Mechanically- and Biochemically-Induced Differentiation of Bone Marrow Mesenchymal Stem Cells to Smooth Muscle Cells in a Three-Dimensional Fibrin Matrix*, in *Bioengineering*. 2008, University of Pittsburgh: Pittsburgh. p. 127.
204. Grassl, ED, Oegema, TR, and Tranquillo, RT, *A fibrin-based arterial media equivalent*. J Biomed Mater Res A, 2003. **66**(3): p. 550-561.
205. Schlumberger, W, Thie, M, Rauterberg, J, and Robenek, H, *Collagen synthesis in cultured aortic smooth muscle cells. Modulation by collagen lattice culture, transforming*

- growth factor-beta 1, and epidermal growth factor. Arterioscler Thromb*, 1991. **11**(6): p. 1660-1666.
206. Cardozo, L, *New Developments in the Management of Stress Urinary Incontinence*. BJU Int, 2004. **94**(Supplement 1): p. 1-3.
207. Draeger, A, Gimona, M, Stuckert, A, Celis, JE, and Small, JV, *Calponin. Developmental isoforms and a low molecular weight variant*. FEBS Lett, 1991. **291**(1): p. 24-28.
208. Gimona, M, Herzog, M, Vandekerckhove, J, and Small, JV, *Smooth muscle specific expression of calponin*. FEBS Lett, 1990. **274**(1-2): p. 159-162.
209. Ball, TP, Jr., Teichman, JM, Sharkey, FE, Rogenes, VJ, and Adrian, EK, Jr., *Terminal nerve distribution to the urethra and bladder neck: considerations in the management of stress urinary incontinence*. J Urol, 1997. **158**(3 Pt 1): p. 827-829.
210. Zivkovic, F, Tamussino, K, Ralph, G, Schied, G, and Auer-Grumbach, M, *Long-term effects of vaginal dissection on the innervation of the striated urethral sphincter*. Obstet Gynecol, 1996. **87**(2): p. 257-260.
211. Martin, AF, Bhatti, S, and Paul, RJ, *C-terminal isoforms of the myosin heavy chain and smooth muscle function*. Comp Biochem Physiol B Biochem Mol Biol, 1997. **117**(1): p. 3-11.
212. Arakawa, E, Hasegawa, K, Irie, J, Ide, S, Ushiki, J, Yamaguchi, K, Oda, S, and Matsuda, Y, *L-ascorbic acid stimulates expression of smooth muscle-specific markers in smooth muscle cells both in vitro and in vivo*. J Cardiovasc Pharmacol, 2003. **42**(6): p. 745-751.
213. Lee, WCM, T.; Vorp, D.; Rubin, J.P.; Marra K.G. *Smooth Muscle Cell Differentiation of Adipose-derived Stem Cells (ASCs)*. in *Regenerate 2005*. 2005. Atlanta, GA.
214. Okuyama, R, Yanai, N, and Obinata, M, *Differentiation capacity toward mesenchymal cell lineages of bone marrow stromal cells established from temperature-sensitive SV40 T-antigen gene transgenic mouse*. Exp Cell Res, 1995. **218**(2): p. 424-429.
215. Trentin, D, Hall, H, Wechsler, S, and Hubbell, JA, *Peptide-matrix-mediated gene transfer of an oxygen-insensitive hypoxia-inducible factor-1alpha variant for local induction of angiogenesis*. Proc Natl Acad Sci U S A, 2006. **103**(8): p. 2506-2511.
216. Schmoekel, HG, Weber, FE, Schense, JC, Gratz, KW, Schawalder, P, and Hubbell, JA, *Bone repair with a form of BMP-2 engineered for incorporation into fibrin cell ingrowth matrices*. Biotechnol Bioeng, 2005. **89**(3): p. 253-262.
217. Brant, AM, *Hemodynamics and mass transfer aspects of arterial disease*, in *Bioengineering*. 1986, University of Pittsburgh: Pittsburgh. p. 300.

218. Thomas, GB, *Assessing and Presenting Experimental Data*, in *Mechanical Measurements*. 1995, Addison-Wesley Publishing Co.: Reading, MA. p. 45-98.
219. Weber, K and Osborn, M, *The reliability of molecular weight determinations by dodecyl sulfate-polyacrylamide gel electrophoresis*. J Biol Chem, 1969. **244**(16): p. 4406-4412.
220. Speakman, E and Weldy, NJ, eds. *Body Fluids and Electrolytes A Programmed Presentation*. 8 ed. 2002, Mosby, Inc: St. Louis. 135.